Lecture Notes in Civil Engineering

P. V. Timbadiya
Prem Lal Patel
Vijay P. Singh
Vivek L. Manekar *Editors*

Flood Forecasting and Hydraulic Structures

Proceedings of 26th International Conference on Hydraulics, Water Resources and Coastal Engineering (HYDRO 2021)

Springer

Lecture Notes in Civil Engineering

Volume 340

Lecture Notes in Civil Engineering (LNCE) publishes the latest developments in Civil Engineering—quickly, informally and in top quality. Though original research reported in proceedings and post-proceedings represents the core of LNCE, edited volumes of exceptionally high quality and interest may also be considered for publication. Volumes published in LNCE embrace all aspects and subfields of, as well as new challenges in, Civil Engineering. Topics in the series include:

- Construction and Structural Mechanics
- Building Materials
- Concrete, Steel and Timber Structures
- Geotechnical Engineering
- Earthquake Engineering
- Coastal Engineering
- Ocean and Offshore Engineering; Ships and Floating Structures
- Hydraulics, Hydrology and Water Resources Engineering
- Environmental Engineering and Sustainability
- Structural Health and Monitoring
- Surveying and Geographical Information Systems
- Indoor Environments
- Transportation and Traffic
- Risk Analysis
- Safety and Security

To submit a proposal or request further information, please contact the appropriate Springer Editor:

– Pierpaolo Riva at pierpaolo.riva@springer.com (Europe and Americas);
– Swati Meherishi at swati.meherishi@springer.com (Asia—except China, Australia, and New Zealand);
– Wayne Hu at wayne.hu@springer.com (China).

All books in the series now indexed by Scopus and EI Compendex database!

P. V. Timbadiya · Prem Lal Patel · Vijay P. Singh · Vivek L. Manekar
Editors

Flood Forecasting and Hydraulic Structures

Proceedings of 26th International Conference on Hydraulics, Water Resources and Coastal Engineering (HYDRO 2021)

Springer

Editors
P. V. Timbadiya
Department of Civil Engineering
Sardar Vallabhbhai National Institute
of Technology
Surat, India

Prem Lal Patel
Department of Civil Engineering
Sardar Vallabhbhai National Institute
of Technology
Surat, India

Vijay P. Singh
Department of Biological and Agricultural
Engineering, Zachry Department of Civil
and Environmental Engineering
Texas A&M University
College Station, TX, USA

Vivek L. Manekar
Department of Civil Engineering
Sardar Vallabhbhai National Institute
of Technology
Surat, India

ISSN 2366-2557 ISSN 2366-2565 (electronic)
Lecture Notes in Civil Engineering
ISBN 978-981-99-1889-8 ISBN 978-981-99-1890-4 (eBook)
https://doi.org/10.1007/978-981-99-1890-4

This Springer imprint is published by the registered company Springer Nature Singapore Pte Ltd.
The registered company address is: 152 Beach Road, #21-01/04 Gateway East, Singapore 189721, Singapore

Preface

The backbone of any country's economy is agriculture, which is sustained through a proper irrigation system. The development of irrigation systems has a long linkage with the evolution of humankind. There was much evidence readily available in Indian history regarding its existence and growth. It is revealed from the literature that the hydraulic structures not only existed but were well-designed and managed with proper infrastructure. Uneven rainfall distribution is a common feature on a global and local scale. Frequent occurrences of flood and drought events are the by-products of this unevenness. Apart from providing irrigation facilities, the hydraulic structures are also useful for creating hydropower facilities, moderating floods and conversing water for municipal and industrial supplies.

This book is mainly focusing the burning issues related to flood modelling, hydraulic infrastructure and hydropower, including the sub-themes like dam safety and monitoring, rehabilitation of old dams, maintenance of dams including their instrumentation, uncertainty in hydropower development and management, storage and diversion dams including their appurtenant structures, streamflow turbines, canal operation and related structures. Dam safety and monitoring were presented through the studies on non-destructive testing methods, safety against vibrations, in-situ strength parameters, non-invasive diagnostic methods and safety methods against earthquakes. Dam break analysis is presented through the case studies using HEC-RAS 2D modelling and decision-support systems. Flood inundation maps using the hydraulic model and GIS technology, the impact of encroachment of floodplains, and land use land cover are part of this book. The seepage detection techniques like fluorescent dye tracer tests, tracer techniques and logging and tracer study are also reported in this book. Case studies on hydropower generation concerning the potential, risk and uncertainty are also included. The critical aspect concerning to design of various hydraulic structures like auxiliary/additional spillways, plunge pools downstream of a ski-jump bucket, trapezoidal labyrinth weir and chute blocks in stilling basins are included in this book. Besides these, a few interesting studies focus on essential issues like the interlinking of rivers, the role of physical model studies, recent trends in the design of auxiliary/additional spillways and estimation of pressure in a plunge pool. This book will be helpful to the fraternity dealing with the

issues related to water resources in general and hydraulic structure and hydropower projects in particular.

Surat, India — P. V. Timbadiya
Surat, India — Prem Lal Patel
College Station, TX, USA — Vijay P. Singh
Surat, India — Vivek L. Manekar

Acknowledgements

The editors are grateful for the support provided by the technical advisory committee and local organizing committee of the 26th International Conference on Hydraulics, Water Resources and Coastal Engineering (HYDRO 2021) held at Sardar Vallabhbhai National Institute of Technology (SVNIT) Surat during December 23–25, 2021. The editors thank the Indian Society for Hydraulics (ISH) Pune, India, its office bearers and executive council members for their support in conducting the HYDRO 2021 International conference. The editors wish to thank all the authors for their support and contribution to this book. The editors duly acknowledge the timely and sincere efforts of the reviewers in providing their valuable comments and suggestions to maintain the quality of the book. The editors would like to thank the keynote speakers, the session chairs and co-chairs, participants, and student volunteers for their contribution to the successful conduct of the conference. The editors are also thankful to the administrators of Sardar Vallabhbhai National Institute of Technology, Surat (SVNIT), India, for supporting the HYDRO 2021 International Conference. Lastly, the editors are sincerely thankful to the publishing team of Springer Nature for their support and cooperation at various steps since the beginning of the book project.

P. V. Timbadiya
Prem Lal Patel
Vijay P. Singh
Vivek L. Manekar

Contents

About the Editors

P. V. Timbadiya is an Associate Professor in the Water Resources Engineering section, Department of Civil Engineering, Sardar Vallabhbhai National Institute of Technology (SVNIT), Surat, India. He secured his doctoral degree and post-graduation in Water Resources Engineering from SVNIT Surat in 2012 and 2004, respectively. He did his undergraduation in Civil Engineering from Sardar Vallabhbhai Regional College of Engineering Technology (now SVNIT). He has guided three doctoral thesis and 32 master's dissertations. He has more than 110 research papers to his credit, including 30 articles in peer-reviewed journals. He served as Dean (Alumni and Resources Generation), and currently serving as Sectional Head, Water Resources Engineering Section at SVNIT. He played an instrumental role in setting up infrastructure facilities in the Centre of Excellence on 'Water Resources and Flood Management' such as the Experimental Hydraulics Lab, Computational Hydraulics Lab, Water Circulation System and others. He is appointed as 'National Consultant' for Kalpsar Project by Narmada, Water Resources, Water Supply and Kalpsar Department of Government of Gujarat. He is a recipient of 'Best Case Study Award—2015' award by the American Society of Civil Engineers for his publication in the *Journal of Hydrologic Engineering* and 'Young Engineers Award' by the Institution of Engineers (India) in the year 2015. He received 'Prof. R. J. Garde Research Award' for the year 2020 by the Indian Society for Hydraulics. He has awarded DST-SERB Core Research Grant for the project on 'Local Scouring around tandem and staggered bridge piers on Non-uniform mobile bed' in the year 2021. He is active in various professional bodies and organized numerous conferences, workshops and short-term training programmes in his academic career.

Prem Lal Patel is a Professor of Hydraulics and Water Resources in the Department of Civil Engineering, Sardar Vallabhbhai National Institute of Technology (SVNIT), Surat, India. He served as the Deputy Director of SVNIT. He also worked as a Reader in the Civil Engineering Department at Delhi College of Engineering (now DTU) from 1999–2007. He served as an Assistant Executive Engineer in Border Roads Organization (BRO) from 1995–1999. He did his bachelor's in Civil Engineering from Government Engineering College, Rewa, Madhya Pradesh, India, and

then pursued his master's and doctoral degrees in Civil Engineering from the then University of Roorkee, now Indian Institute of Technology Roorkee, India. He has published more than 220 papers in peer-reviewed journals and conferences of repute. He has guided 12 doctoral thesis and 47 master's dissertation so far. He has also served in various academic positions at SVNIT Surat, such as Dean (Academics), Head of Civil Engineering Department, Dean (Research and Consultancy) and Dean (PG). He was also instrumental in setting up a Centre of Excellence (CoE) on 'Water Resources and Flood Management' in the Institute through a research grant from World Bank-sponsored TEQIP-II. He is a recipient of visiting International Fellowship (VIF-2017) 2017 for attending the ASCE EWRI Congress-2017 in Sacramento, California, USA. He is active in various professional bodies and organized numerous conferences, workshops and short-term training programmes in his academic career.

Vijay P. Singh is a University Distinguished Professor, a Regents Professor, and Caroline and William N. Lehrer Distinguished Chair in Water Engineering at Texas A&M University. He received his B.S., M.S., Ph.D. and D.Sc. in engineering. He is a registered professional engineer, a registered professional hydrologist and an Honorary Diplomate of ASCE-AAWRE. He is a Distinguished Member of ASCE, a Distinguished Fellow of AGGS, an Honorary Member of AWRA and a Fellow of EWRI-ASCE, IAH, ISAE, IWRS and IASWC. He has published extensively in the areas of hydrology, irrigation engineering, hydraulics, groundwater, water quality and water resources (more than 1320 journal articles, 31 textbooks, 75 edited reference books, 110 book chapters and 315 conference papers). He has received over 95 national and international awards, including three honorary doctorates. He is a member of 11 international science/engineering academies. He has served as President of the American Institute of Hydrology (AIH), Chair of the Watershed Council of the American Society of Civil Engineers and is currently President of the American Academy of Water Resources Engineers. He has served/serves as editor-in-chief of three journals and two book series and serves on editorial boards of more than 25 journals and three book series. His Google Scholar citations include 64073, h-index: 115 and I10-index: 903.

Vivek. L. Manekar is a Professor in the Department of Civil Engineering and Dean (Planning and Development) at Sardar Vallabhbhai National Institute of Technology (SVNIT), Surat. He worked as Dean (Student Welfare) at SVNIT 'Adjunct Professor' at SCOE, Washim of SGBB University, Amravati. He is a member of the Academic Council (Senate) of the Government College of Engineering, Amravati (an Autonomous Institute of Government of Maharashtra). He was also an Expert Member of the Academic and Selection Board of M. S. University Vadodara. He is working as a member of the State Technical Agency, PMGSY-Gujrat, Government of India. From India, he is one of the members of the Australia India Water Association (AIWA), which is recently formed between the two governments. He has more than 32 years of experience in teaching, research and consultancy in Hydraulics and Water Resources Engineering. He has experience working in different fields of Water Resources Engineering, including management of on-field irrigation systems,

agro-climatic modelling, hydraulic and hydrologic modelling, sediment transport modelling and simulation, flow structure interaction, flood management and impact of changing climate and LULC on water resources. He has many research papers to his credit published in reputed international/national journals and reputed conference proceedings, book chapters, monograph, guided several Ph.D., P.G. dissertations and U.G. projects and completed many consultancy projects and handling of externally funded research projects to his credit.

Impact of Encroachment of Floodplains of Adyar River on Chennai Floods

R. Reshma and S. N. Kuiry

Abstract Floodplains are the natural pathways that accommodate the excess water overtopping the riverbanks during high flow times. However, they have become a zone that causes enormous damage and losses during a flood event, primarily due to floodplain-oriented uncontrolled and unplanned urbanization and developments altering the natural linkage and layout of these regions. The fertile soil, proximity to abundant surface and groundwater sources, and higher land value make them more appealing for human settlements. However, their frequent flooding nature is often overlooked. Earlier studies reveal that a large part of the world's floodplains has disappeared due to haphazard developments, industrialization, and urbanization, this being more prominent in developing nations like India. Most floodplains in the country have been devastated, floodplains of the rivers Adyar, Cooum, Kosathalayar, Yamuna, and Periyar being a few to list. This study assesses the impact of encroachment of floodplains of the Adyar River of the Chennai basin, in India, on the flood flow pattern using Landsat images and hydrologic–hydraulic modeling of the 2015 flood event. The study puts forth a concise idea of the possible flood flow pattern that would have developed during the 2015 flood event if the floodplains were as in 1991 or prior years, unaltered by unnecessary human interventions, depicting the impact of encroachments. The study reveals that the area has undergone rapid urbanization and haphazard encroachments along the Adyar River floodplains resulting in a 188% increase in flood peak and a 48-h reduction in the time to peak of flow. Better late than never—proper floodplain management and strict implementation and execution of floodplain development regulations and guidelines can still be a solution for these impacts and thus reduce the havoc situation and losses created by a flood.

Keywords Floodplain encroachment · Urban flood · Flood modeling · Chennai floods · Hydrologic-hydraulic modeling

R. Reshma (✉) · S. N. Kuiry
Department of Civil Engineering, Indian Institute of Technology Madras, Chennai 600036, India
e-mail: reshmaradhakrishnan094@gmail.com

S. N. Kuiry
e-mail: snkuiry@civil.iitm.ac.in

P. V. Timbadiya et al. (eds.), *Flood Forecasting and Hydraulic Structures*, Lecture Notes in Civil Engineering 340, https://doi.org/10.1007/978-981-99-1890-4_1

1 Introduction

A river overflowing its banks is a natural phenomenon for accommodating the larger flow arising from a heavy downpour or wet season. The relatively flat, low-lying land adjacent on either bank of the river subjected to these frequent inundations is termed as floodplains [1]. The inundation of floodplains is thus a component in the hydrologic cycle similar to other hydrological phenomena. As the overflowing river traverses along the floodplains, the flow deposits the debris and other organic materials it carries, enriching the soil there. The floodplains are mostly shaped and subjected to continuous alterations due to these erosion–deposition processes and water overflow [2]. Fertile soil, water availability, recreational, aesthetic, and industrial value of land—all make it more appealing for human settlement and irrigation. Most of the ancient civilizations had their origin in such fertile floodplains. Besides, floodplains provide a natural mechanism to control floods, slow down the surface runoff, and hence to enrich the replenishment of groundwater reserves, help in maintaining the quality of river water, preserve biodiversity, and maintain the ecological balance [3–5]. However, they have become a zone that causes enormous damage and losses during a flood event. This may be primarily attributed to floodplain-oriented uncontrolled and unplanned urbanization and developments that alter the natural linkage and layout of these regions. Studies reveal that 90% of the floodplains have disappeared due to haphazard developments, industrialization, and urbanization [2].

Construction of hydraulic structures like levees, dams, bridges, etc., across the waterbodies results in the obstruction or diversion of natural flow path leading to a substantial water level rise in the upstream or a high flow to downstream, respectively [5, 6]. Besides, an increase in built-up and paved areas along the floodplains decreases the infiltration rate and hence the storage, increasing the surface runoff and reducing the groundwater augmentation [7]. Floodplain encroachment has a significant impact on the flow dynamics as well. The reduced flow paths and increased imperviousness have led to a rapid rise in the flow velocity and hence a reduction of transit time. Thus, the inundation of floodplains, a natural flood control mechanism, has become a hazard due to anthropogenic interventions, this being more prominent in developing nations like India. The majority of the floodplains in the country have been devastated, owing to the unplanned developments on the banks of many rivers, leaving the surrounding cities flood prone. Most Indian cities are now facing urban floods quite frequently [8]. Thus, there is a high requirement for the assessment and analysis of flood flow dynamics, and mitigation of the flood damages. The process becomes more complicated and tedious when it comes to an urban flood event.

Numerical modeling studies are the primary tools available for the flood modeling and analysis [9]. Hydrologic–hydraulic modeling using different software packages are the most commonly used approach for efficient and accurate flood modeling. A hydrologic model provides the rainfall–runoff response of a catchment considering the various hydro-meteorologic, topographic and geologic characteristics of the catchment. Hydraulic models, on the other hand, route this runoff hydrograph through the river and other channel networks downstream, providing flood dynamics

such as flow velocity, inundation extent, and depth [10]. One-dimensional (1D), two-dimensional (2D), coupled 1D-2D and three-dimensional (3D) models are now available for the purpose. Among these, coupled 1D-2D approach is gaining more popularity these days owing to their ability to replicate the flow dynamics with reasonable accuracy but higher computational efficiency [9, 10]. HEC-HMS, PRMS, SWAT, etc., are the commonly adopted hydrologic models, while HEC-RAS, MIKE Urban, MIKE Flood, Telemac, etc., are some of the hydraulic models in use.

The Chennai Metropolitan Area (CMA), one of the highly urbanized Indian cities, lying along the downstream floodplains of Adyar, Cooum, and Kosathalayar rivers, is considered for the present study to demonstrate the adverse impacts of floodplain encroachment. The city has faced haphazard developments and settlements during the past three decades [8]. Floods that were once in a ten-year event have become more frequent since the 1990s [11]. Though research is being carried out regarding the causes and impacts of urban floods in Chennai under present and future scenarios [12–15], the least attention has been given to the extent and impacts of floodplain encroachment. The objectives of this study are hence to analyze the extent and trend of encroachment over the floodplains of Adyar River of Chennai city during the past three decades, to analyze the natural and the current flood flow evolution pattern in the city, and hence to investigate the influence of floodplain encroachment on the flood flow evolution. Proper floodplain management along with strict implementation and execution of floodplain development regulations and guidelines can still be a solution for these impacts and thus reduce the havoc situation and losses created by a flood.

2 Materials and Methods

The CMA has been facing disastrous flood events almost every year since 2005 [11]. If it was cyclones that generated flood events in the earlier decades, it is the combined effect of climate change, cyclonic series, anthropogenic activities, and its impacts that is causing the floods in recent times. Flood of 2015 is selected for the current study, primarily due to the data availability, also since it was a 1 in 100-year flood event [12], and considering the significant impact the event caused. The research is carried out in four parts—(i) analysis of Land Use Land Cover (LULC) pattern along the floodplains of Adyar River and CMA, (ii) assessment of natural flow path of river overflow in the city, (iii) current flood flow pattern in the city, and (iv) impact analysis of the floodplain encroachment on floodwater movement. The overall methodology adopted for the study is shown in Fig. 1. The procedure adopted is elaborated in the following sections.

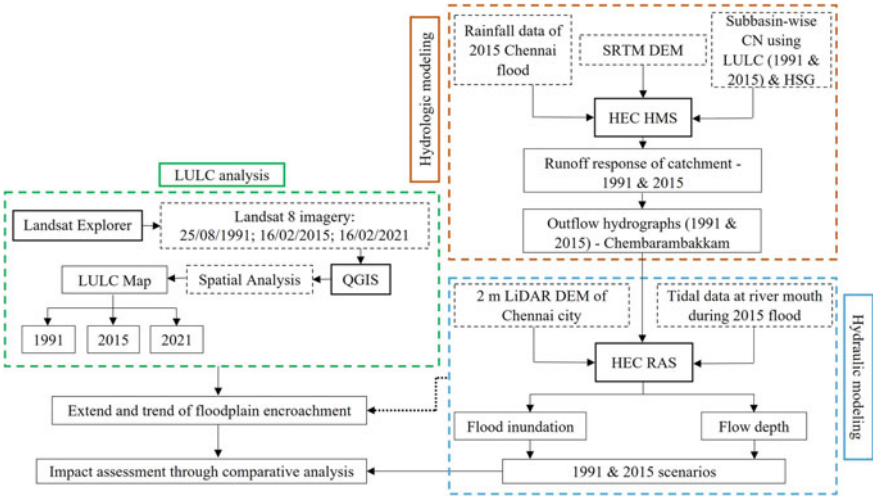

Fig. 1 Methodology flowchart

2.1 Study Area—Chennai City and the Floodplains of the River Adyar

The study focuses on the floodplains of the Adyar River, one of the three major rivers flowing through Chennai (a coastal city lying to the North-Eastern part of Tamil Nadu, India) and the downstream CMA for demonstrating the impact of floodplain encroachment on the flood flow pattern within the city. Chennai, a city of cultural, administrative, and educational value, is the smallest but densely populated city in the state. It falls along 80° 14′ 15.42″ E longitude and 13° 04′ 2.78″ N latitude. On the east, it is surrounded by the Coromandel Coast of the Bay of Bengal, north by Kosathalayar River, and the rest by Thiruvallur and Kancheepuram districts of Tamil Nadu. The city, along with a small portion of these two districts, forms the CMA. CMA as such encompasses two major rivers—Adyar and Cooum, and the third river Kosathalayar flowing along the northern boundary, and five wetlands—Pallikaranai Marsh, Pulicat Lake, Kattupalli Island, Madhavaram-Manali Jheels, and Adyar Estuary Creek. CMA spreads around the downstream of the Adyar and other two rivers—Cooum and Kosathalayar. Hence, any destruction or alteration of their upstream floodplains leads to a disastrous flooding of CMA. Adyar River, a 42.5 km long river, has its origin in Chembarambakkam Lake in Kancheepuram district of Tamil Nadu, and it joins with the Bay of Bengal in Adyar estuary. The river has a total watershed area of 860 km^2 which includes surplus water from ~200 tanks (small water bodies), small streams as well as rainwater runoff that drains off from Chennai city. ~24 km of the river length falls within CMA. The river has been polluted with industrial, municipal, domestic, and construction wastes since the last three decades.

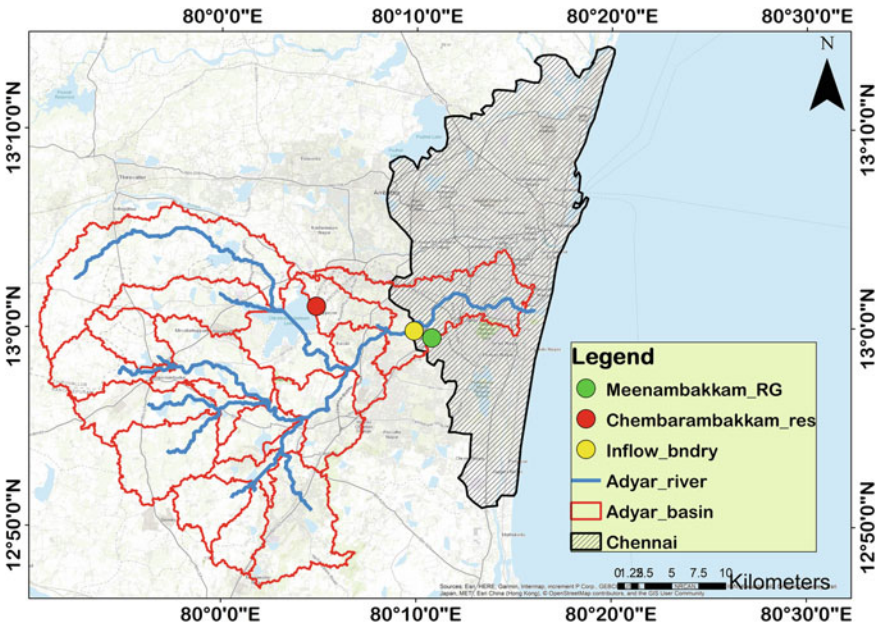

Fig. 2 Study area map

The city has almost flat terrain with minimal green land reserved within Guindy National Park, IIT Madras, and Theosophical Society. Meteorologically the area falls under the hot and humid category with tropical wet and dry climates. The mean annual rainfall received is ~1400 mm, the majority being received during the north-east monsoon extending from September to December. The cyclones forming in the Bay of Bengal also render precipitation in the city. Chennai has turned into a complete urban settlement losing most of its water bodies in the past 50 years. Besides, extensive extraction of water for irrigation and industrialization, sand bar formation at river mouth, and haphazard encroachments of the floodplains of these rivers have made them highly polluted, with very little baseflow. Figure 2 shows the study area with the sub-basins. The yellow dot represents the inflow boundary point adopted for the hydraulic modeling, red dot the Chembarambakkam reservoir, and green dot the Meenambakkam rain gauge station.

2.2 Data Collection

Freely available Shuttle Radar Topography Mission (SRTM) Digital Elevation Models (DEM) of 1 arc-second (30 m) resolution is used for the study. The Landsat 8 imagery (August 25, 1991, February 16, 2015, and February 16, 2021) required for the LULC classification are downloaded from the open-access web-page

Landsat explorer (https://livingatlas2.arcgis.com/landsatexplorer/) powered by Environmental Systems Research Institute (ESRI). Precipitation data at Meenambakkam rain gauge station, reservoir release data at Chembarambakkam, and tidal data at the Adyar River mouth during the 2015 flood event, as used by Devi et al. [12] and Narasimhan et al. [14], is used for the hydrologic and hydraulic model development, validation, and simulation.

2.3 Trend and Extent of Floodplain Encroachment

The trend and extent of the encroachment of the Adyar floodplains are assessed through hydrologic–hydraulic modeling and analysis of LULC variation over the decades. Flood event of 2015 is considered for the simulations.

2.4 LULC Classification and Analysis

Supervised classification of the Landsat 8 imagery is performed using geospatial tools with reference to Google Earth images to generate the required LULC maps of 1991, 2015, and 2021 as shown in Fig. 3. The region of interest is classified into four LULC classes—waterbody, vegetation, built-up, and barren land. The variation of the LULC pattern over the decades is quantified and tabulated as given in Table 1.

2.5 Hydrologic-Hydraulic Modeling

The open-source software packages HEC-HMS and HEC-RAS developed by the United States Army Corps of Engineers (USACE) are adopted for hydrologic and hydraulic modeling, respectively. Meteorological data pertaining to the 2015 Chennai flood and hydrogeological data of the study area is provided as input to the HEC-HMS model to simulate the rainfall–runoff process. Geospatial analysis of the SRTM DEM is performed to derive a sub-basin map of the study area. The area of each sub-basin is computed using geospatial tools. Soil Conservation Services (SCS) curve number loss model [16] is adopted for the quantification of sub-basin losses, and the SCS unit hydrograph model is employed to simulate the direct runoff from each sub-basin. The former works based on the curve number and initial abstraction losses. The sub-basin wise curve number values were assigned based on the hydrologic soil group (HSG) and LULC with reference to Table 2. The HSG of the area was identified as 'D' from the global-scale soil data map available freely at https://swat.tamu.edu/data/india-dataset/. The lag parameter of the SCS unit hydrograph is based on the lag time [17] that depends on the curve number, sub-basin slope, and hydraulic length. All

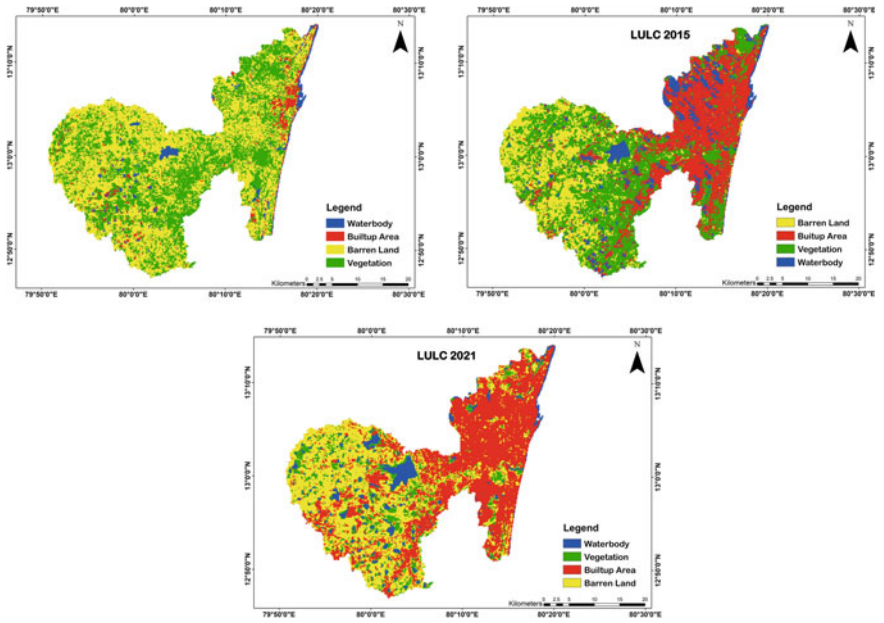

Fig. 3 LULC maps

Table 1 Variation in LULC pattern (in %) through decades

LULC	1991	2015	2021
Vegetation	38.70	38.25	25.72
Built-up area	4.02	30.73	68.28
Barren and	54.35	22.26	0.49
Waterbody	2.93	8.76	5.49

these sub-basin characteristics are extracted using geospatial tools available within HEC-HMS. Channel flow is modeled using the kinematic wave routing model.

The runoff hydrograph at the point of intersection of Adyar sub-basin and CMA is simulated using the HEC-HMS model, and the same is used as input for the hydraulic

Table 2 Curve number adopted for Indian basins [18]

Sl. No.	LULC	Hydrologic soil group			
		A	B	C	D
1	Vegetation	46	58	70	73
2	Built-up area	77	86	91	93
3	Barren land	71	80	85	88
4	Waterbody	100	100	100	100

model. Since the study focuses on the encroachment impact on flood flows within CMA, a 2D unsteady hydraulic modeling is done for the CMA region alone. Flood inundation of the area is simulated with respect to available 2 m × 2 m resolution DEM of the CMA, with building data burned in [12]. The flood hydrograph obtained from the HEC-HMS model is provided as the upstream boundary, while the tidal data at the river mouth is given as the downstream boundary to the 2D area. Manning's roughness coefficient, n of 0.3 $m^{-1/3}$ s, was applied for the study area uniformly [12].

2.6 Impact of Floodplain Encroachment on Floodwater Flow

The floodplain encroachment impact is incorporated in the hydrologic and hydraulic modeling by modifying the parameters—curve number, initial abstraction, lag time, and building data—corresponding to the LULC patterns in 1991 and 2015. The water surface elevation, inundation extent, and flow velocity are recorded for each run. The tidal, reservoir release, and precipitation data corresponding to the 2015 flood event is used for both 1991 and 2015 simulations so as to reproduce the actual impact of the floodplain encroachment. The simulations are run for a period of 44 days (November 01, 2015 to December 14, 2015).

3 Results and Discussions

The generated LULC maps for the years 1991, 2015, and 2021, as shown in Fig. 3, clearly depict the intensity of urbanization and encroachments along the floodplains of the Adyar River. From 1991 to 2015, there was a 26.71% increase in built-up area, while the rate further increased to 37.55% by 2021. In contrast, the barren land reduced by 32.09% in 2015, which has further come down to ~0.5% of the total considered area in 2021. These encroachments over the barren and vegetative covers along the floodplains have a significant impact on the basin characteristics such as perviousness and flow characteristics such as velocity. The entire CMA has now turned into a concrete forest with the least vegetative cover or barren land.

Hydrologic modeling results obtained using HEC-HMS models for 1991 and 2015 scenarios provide a concise picture of the above-stated impact of floodplain encroachment on basin and flow characteristics. Table 3 gives the quantitative representation of the floodplain encroachment impact. There is a sharp increase of 48.13% in the inflow from Adyar floodplains to CMA due to the variation in the LULC pattern. The increase may be primarily attributed to the increase in paved areas adjacent to the river and the reduction in vegetative cover and barren land. Besides, the time to the peak has also reduced sharply by around two days, i.e., for the 1991 scenario, the peak occurs on December 3 at 22:00, while for the 2015 scenario, it is on December 2 at 01:00. This results in the reduction of time available for evacuation and related disaster management measures to be performed during the flood event. Also, the maximum

flow volume at the river mouth during the 1991 scenario is ~1143 cumec (Fig. 4), which is less than the actual carrying capacity (2038 cumec) of the Adyar River. The results thus indicate how anthropogenic activities like unplanned urbanization and developments on floodplains have worsened the flood scenarios.

The flow hydrographs generated at Chembarambakkam are used as the upstream flow boundary for the hydraulic model. The hydrographs obtained for the 1991 and 2015 scenario are shown in Fig. 5. As a 2 m × 2 m resolution DEM was available for the CMA region alone, it was adopted to increase the accuracy of inundation simulations. Also, the hydraulic simulations were performed only for the Adyar floodplain region falling within the CMA to reduce the computational effort. Flood inundation extent map as obtained from hydraulic simulations in HEC-RAS is shown in Fig. 6. While the 1991 flood is more or less confined within the riverbanks and the immediately adjacent floodplains, floodwaters of the 2015 scenario spread onto the surrounding areas, which are highly urbanized, as seen from the LULC map of 2015. Thus, the generated flood inundation maps render a visualization of floodplain encroachment impact on the flood flow pattern.

Table 3 Impact of floodplain encroachment on flood flow pattern

Parameters	1991	2015	Percentage increase
Flow peak at CMA inlet (cumec)	629.7	932.8	48.13
Flow peak at river mouth (cumec)	1142.9	3295.9	188.38
Maximum depth of inundation (m)	9.27	13.54	46.06

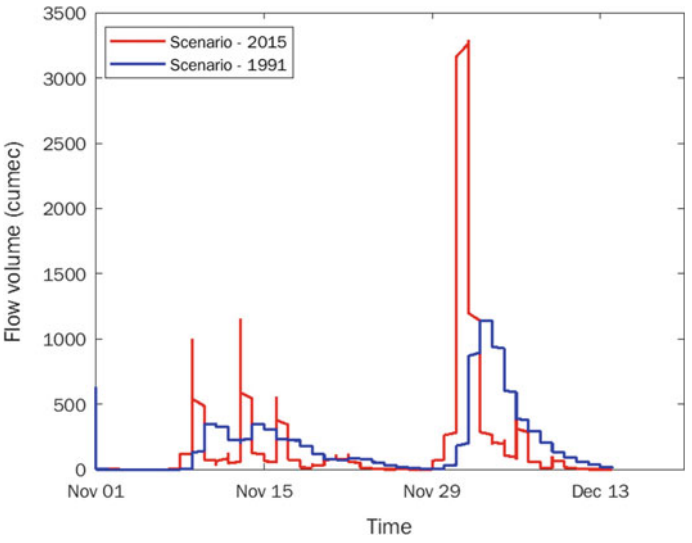

Fig. 4 Outflow at the river mouth

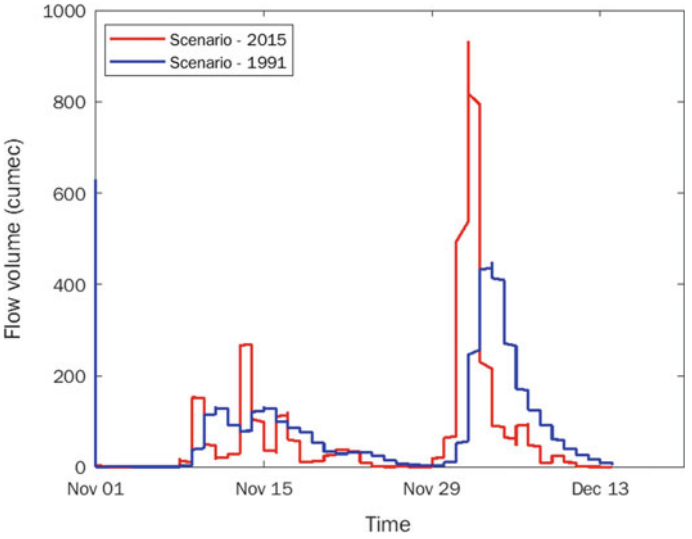

Fig. 5 Total inflow to CMA

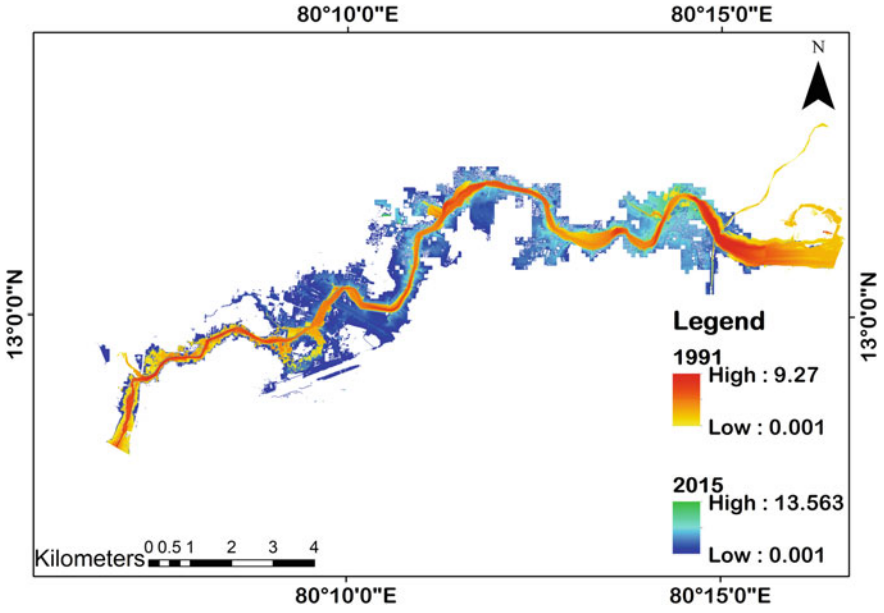

Fig. 6 Flood inundation map—1991 and 2015

The rapid increase in the flood inundation extent suggests the need for better floodplain management and regulations at the earliest. Though flood simulation for the 2021 scenario is not performed to reduce the length of the paper, it can easily be projected from the 1991 and 2015 simulation results. Corresponding to a 26% increase (1991 to 2015) in built-up area along the floodplain, a 48% increase was found in the inflow to the CMA region. This numerical data points to the fact that the 37% increase of urban land from 2015 to 2021 marks a similar drastic increase in the flood inflow to CMA. Also, there is a perilous rise in the depth of inundation owing to the reduced conveyance path for the floodwaters.

4 Conclusion

An impact assessment with respect to the floodplain encroachments along the Adyar River of Chennai is carried out. The study primarily presents a concise idea of the possible flood flow pattern that would have developed during the 2015 flood event if the floodplains were left in 1991 or prior years, unaltered by unnecessary human interventions, thereby depicting the impact of encroachments. The major conclusions arrived at from the study are as follows:

- The study area has undergone rapid urbanization and haphazard encroachments along the floodplains of the Adyar River as a result of which:
  (a) There is an increase of the flood peak by ~188%
  (b) Time to peak of the flood flow has reduced by ~2 days.
- There is a high demand for immediate development and implementation of regulations and guidelines concerning to the developments and constructions in the floodplains.
- Reallocation and rehousing of the current settlements in the near vicinity of the Adyar River is to be done at the earliest.

Acknowledgements The authors acknowledge the effort taken by the National Aeronautics and Space Administration (NASA), ESRI, and Dr. Balaji Narasimhan (IIT Madras), respectively, to render open-source data of DEM, Landsat imagery, and global soil data to the public. The authors are thankful to Devi et al. [12] for providing the necessary precipitation and tidal data required for the current work. The authors are also thankful to Science and Engineering Research Board (SERB), Government of India for necessary funding through the Grant No. EMR/2017/000642.

References

1. Association of State Floodplain Managers [ASFPM] (2008) Natural and beneficial floodplain functions: floodplain management—more than flood loss reduction
2. Tockner K, Stanford JA (2002) Riverine flood plains: present state and future trends. Environ Conserv 29(3):308–330
3. European Environment Agency (2018, 19 Nov) Why should we care about floodplains. Accessed 21 July 2021 https://www.eea.europa.eu/publications/why-should-we-care-about-floodplains
4. Haeuber RA, Michener WK (1998) Natural flood control. Issues Sci Technol 15(1):74–80
5. Hooper PB, Duggin JA (1996) Ecological riverine floodplain zoning: its application to rural floodplain management in the Murray-Darling basin. Land Use Policy 13(2):87–99
6. Townsend PA, Walsh SJ (1998) Modeling floodplain inundation using an integrated GIS with radar and optical remote sensing. Geomorphology 21(3–4):295–312
7. Bhaduri A (2018, 12 Oct) Why floodplains need to be protected. India water portal. https://indiawaterportal.org/articles/sad-state-floodplains
8. Rafiq F, Ahmed S, Ahmad S, Khan AA (2016) Urban floods in India. Int J Sci Eng Res 7(1):721–734
9. Patel DP, Ramirez JA, Srivastava PK et al (2017) Assessment of flood inundation mapping of Surat city by coupled 1D/2D hydrodynamic modeling: a case application of the new HEC-RAS 5. Nat Hazards 89:93–130. https://doi.org/10.1007/s11069-017-2956-6
10. Henonin J, Russo B, Mark O, Gourbesville P (2013) Real-time urban flood forecasting and modelling–a state of the art. J Hydroinf 15(3):717–736
11. Gupta AK, Nair SS (2010) Flood risk and context of land-uses: Chennai city case. J Geogr Region Plann 3(12):365–372
12. Devi NN, Sridharan B, Kuiry SN (2019) Impact of urban sprawl on future flooding in Chennai city, India. J Hydrol 574:486–496
13. Padmanaban R, Bhowmik AK, Cabral P et al (2017) Modeling urban sprawl using remotely sensed data: a case study of Chennai city, Tamil Nadu. Entropy 19(4):163
14. Narasimhan B, Bhallamudi SM, Mondal A, Ghosh S, Mujumdar P (2016) Chennai floods 2015: a rapid assessment. Interdisciplinary Centre for Water Research. IISc. Bangalore
15. Suriya S, Mudgal BV, Nelliyat P (2012) Flood damage assessment of an urban area in Chennai, India, part I: methodology. Nat Hazards 62(2):149–167
16. US Army Corps of Engineers Hydrologic Engineering Centre (US ACE) (March 2000) Hydrologic modeling system—technical reference manual. USACE, USA
17. Costache R (2014) Using GIS techniques for assessing lag time and concentration time in small river basins. Case study: Pecineaga river basin, Romania. Geographia Technica 9(1):31–38
18. Kumar P, Tiwart KN, Pal DK (1991) Establishing SCS runoff curve number from IRS digital data base. J Indian Soc Remote Sens 19(4):245–252

Modeling of Flood Inundation Extent in Data-Scare Regions: The Case Study of Bhavnagar District

Nikunj K. Mangukiya and Bhoomi R. Andharia

Abstract Flood models can be a valuable source of information for flood risk assessments because they predict inundation extents. Due to the impact of climate change, the semi-arid zone of Gujarat is experiencing an increase in annual rainfall. Bhavnagar and the surrounding district received around 521 mm of rain in August 2020, compared to Bhavnagar district's average annual rainfall of 658 mm. The Kalubhar and Ranghola dams in the Bhavnagar district were filled with water, causing high flows in the Kalubhar, Rangholi, Keri, and Ghelo rivers. The flows from these four rivers merge before meeting the Gulf of Khambhat. Despite the lack of data, an attempt has been made in this study to develop a two-dimensional flood model for this region using HEC-RAS v6.0. The study shows that the flood in the region was caused by a high amount of rainfall combined with unplanned development along the coastal line. Based on the simulated results and the difficulties encountered during model development, recommendations and guidelines for resolving the waterlogging problem and reducing the extent of flood inundation for the Bhavnagar coastal region were provided. The study will aid government officials and stakeholders in determining flood prevention measures.

Keywords Flood · HEC-RAS 6.0 · Bhavnagar · Data-scare · Waterlogging

1 Introduction

Floods are a recurrent phenomenon in India [1–3]. Due to varying rainfall and climatic patterns in different parts of India, it has been observed that while some areas are experiencing devastating floods, others are experiencing drought [4, 5]. As a result of global climate change, large-scale floods have occurred across India, including

N. K. Mangukiya · B. R. Andharia (✉)
SMC Division, CSIR—Central Salt and Marine Chemicals Research Institute, Bhavnagar, Gujarat, India
e-mail: brandharia@csmcri.res.in

N. K. Mangukiya
e-mail: nikk.mangukiya@gmail.com

P. V. Timbadiya et al. (eds.), *Flood Forecasting and Hydraulic Structures*, Lecture Notes in Civil Engineering 340, https://doi.org/10.1007/978-981-99-1890-4_2

semi-arid and arid regions [3, 6]. Due to the varied rainfall distribution, places not typically prone to flooding are also severely flooded. There has been a threefold increase in widespread severe rainfall occurrences throughout central and northern India between 1901 and 2020 [7]. Increasing variability in the westerly winds of monsoon, attributed to increasing heat in the Arabian Sea, is responsible for the increase in severe rainfall incidents [8, 9]. These trigger recurring rises of moisture transfer to the subcontinent from the Arabian Sea, leading to intense rainfall of 2–3 days over a large area and inducing flooding. The increase in population and development activities tend to occupy the floodplains, resulting in damage of a more severe nature [10].

India has spent the last few years focusing on developing a reliable early flood warning system [11]. After catastrophic floods in 2015, Chennai became the first city in India to receive an advanced flood warning system in 2019 (https://www.indiawaterportal.org/articles/new-flood-warning-system-chennai). Similarly, in June 2020, Mumbai acquired an integrated flood alert system (IFLOWS) (https://pib.gov.in/PressReleasePage.aspx?PRID=1630928). The Energy and Resources Institute (TERI), in conjunction with the India Meteorological Department (IMD) and the National Disaster Management Authority (NDMA), has created an equivalent flood forecasting system for Guwahati (https://www.teriin.org/press-release/teri-and-ndma-launch-flood-early-warning-system-fews-predict-floods-guwahati). During the monsoon, these flood warning systems can provide area-by-area information on possible flooding. According to the IMD, rainfall data is now being used to determine the total anticipated water accumulation on any river or sub-river basin. Obtaining such information and sharing it with other authorities may also aid in improved flood control. Besides this, many researchers have attempted to develop flood models and early warning systems for small- and large-scale watersheds [3, 12–18]. The accuracy of these flood models is influenced by several factors, including the resolution of the digital elevation map (DEM), the frequency and time interval of observed gauge data, the surveyed geometry, and the topographic characteristics.

Although several hydrodynamic models have been developed and shown the capacity to reproduce flood stages for small- and large-scale watersheds of India, studies for the semi-arid regions in Gujarat state are limited due to data scarcity [3]. Thus, the present study aims to develop a two-dimensional (2D) flood model for the Bhavnagar district. In August 2020, Bhavnagar and the surrounding district received around 521 mm of rainfall within three days, which filled up the region's Kalubhar, Ranghola, and other small check dams. They caused high flows in the Kalubhar, Rangholi, Keri, and Ghelo rivers. The flows from these four rivers merge before meeting the Gulf of Khambhat, which causes waterlogging and inundates the villages along the coastal line. Based on the simulated results and the difficulties encountered during model development, recommendations and guidelines for resolving the waterlogging problem and reducing the extent of flood inundation for the Bhavnagar coastal region were provided. The study will aid government officials and stakeholders in determining flood prevention measures.

2 Study Area and Data Source

Bhavnagar is one of the highly developed localities in Gujarat's Saurashtra region. The district has an area of 9980.9 km^2 between 21° 18′–22° 18′ N and 71° 15′–72° 18′ E in the southern part of Gujarat. It is bounded by the district of Ahmedabad and Surendranagar in the north, Amreli and Rajkot in the west, the Arabian Sea in the south, and the Gulf of Khambhat (Cambay) in the east. The Bhavnagar district has a total population of 2.88 million with a population density of 288 people per km^2, which rise 16.53% in each decade. The district is mainly located in the tropical climate zone with usual dryness, except in the coastal regions. The average annual rainfall in the region is 598.4 mm, most of which is received in India's monsoon season. Numerous small ephemeral streams drain the Bhavnagar region with the easterly and southeasterly flow, namely Shetrunji, Kalubhar, Ghelo, Rangholi, Keri, Melan, Vagad, Padala, Dhantarvadi, Kalbi, Goma, Utavli, Bagad, and Surajvadi. This river dries up in the marshy land near the coastal region. For the present study, the river reaches of Kalubhar, Ghelo, Rangholi, and Keri are considered a study area, as shown in Fig. 1.

The necessary data for the present work were collected from government agencies and open data portals. The digital elevation data with 12.5 m spatial resolution were

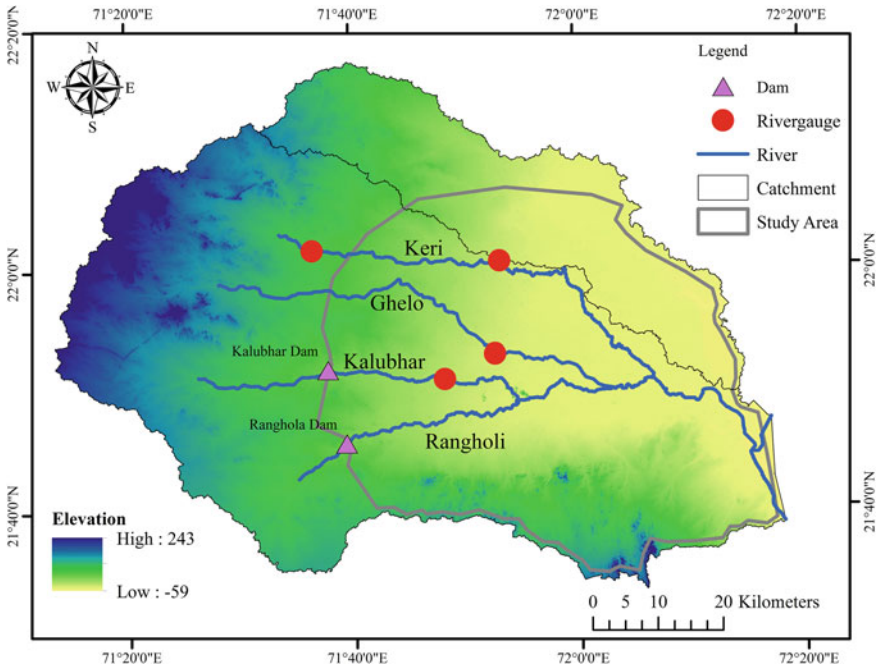

Fig. 1 Index map of the study area showing the locations of gauge stations and river network

obtained from the data portal of the Alaska satellite facility (https://search.asf.alaska.edu/) to extract the geometric properties of the catchment. The land-use land-cover (LULC) data for the region were extracted from the Landsat-8 satellite imageries obtained from the Earth Explorer portal of the United States Geological Survey's (USGS) (https://earthexplorer.usgs.gov/). The discharge data from the Kalubhar and Ranghola dams were collected from the respective dam authorities. The observed gauge data of the river gauging stations were collected from the Bhavnagar Irrigation Circle office.

3 Methodology

Methodology for the present study includes preparing the datasets, developing the hydrodynamic model, and preparing the flood map from the result analysis. Figure 2 represents the methodology flowchart that was followed for the present study.

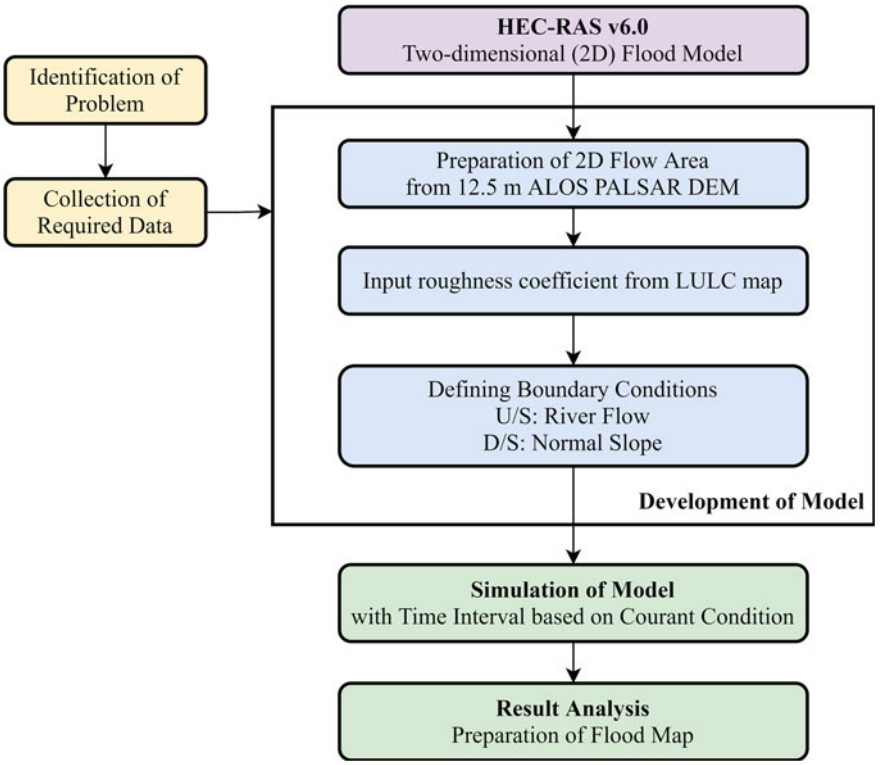

Fig. 2 Flowchart of methodology

3.1 Identification of the Problem

In August 2020, the monsoon remained intense for most of the month over Gujarat. The state has received a whopping 570 mm rainfall against the normal of 203 mm, nearly triple the usual. Moreover, this is the highest monsoon rainfall Gujarat has received in August in at least the last 41 years. In 1979, the state recorded around 600 mm of rainfall. The India Meteorological Department (IMD) has forecasted widespread rains with isolated extremely heavy falls over Gujarat on August 23, 2020 and very heavy falls on August 24, 2020. Owing to the inclement weather, the IMD has issued a red warning (take action) over Gujarat for August 23, followed by an orange alert (be prepared) for August 24. Bhavnagar and surrounding districts such as Amreli, Rajkot, and Botad received intense rainfall for the last week of August 2020 that caused high flows in the Kalubhar, Rangholi, Ghelo, and Keri rivers. The Kalubhar and Ranghola dams of the region were already filled up from the rainfall of July and the beginning of August, forcing the dam authorities to release the water to the downstream area. The rivers of this region are ephemeral and have shallow depths that could not safely pass the dam outflow, causing the flood in the surrounding region. Also, the unplanned development of the coastal area and backflow of tidal water during high tide was responsible for worsening the situation in downstream low-lying villages of Bhavnagar district. The solar salt works and agricultural farms located in the delta region and mouth of the sea were damaged and washed out thoroughly. The flood caused destruction in the form of human deaths, livestock losses, as well as property and infrastructure damage.

3.2 Development of a Two-Dimensional Model

The hydraulic model for the region has been developed using the 2D component of the Hydrologic Engineering Center's River Analysis System (HEC-RAS v6.0). Due to the non-availability of the surveyed topographic data, the Advanced Land Observing Satellite's (ALOS) Phased Array Type L-band Synthetic Aperture Radar's (PALSAR) 12.5 m spatial resolution Digital Elevation Model (DEM) was used in HEC-RAS. After adding DEM data into the RAS Mapper, the 2D flow area was generated with 25 m spatial resolution. The LULC map for the study area was created from Landsat-8 satellite imagery using the "maximum likelihood classification" tool of the ArcGIS Desktop v10.6 software. The results of the LULC map (Fig. 3) were verified using Google Earth Imagery and field visits to the study area. The roughness coefficient for the study area was obtained from the developed LULC map [19] and added to RAS Mapper as Manning's "n" layer (Table 1). The upstream flow boundary conditions were defined upstream of the Rangholi, Kalubhar, Ghelo, and Keri rivers. Releases from the Kalubhar and Ranghola dams were input to upstream flow data for the Kalubhar and Rangholi rivers. The point observation data for the Ghelo and Keri rivers were provided as input to upstream flow data for Ghelo and Keri rivers. The

river meeting point to the Gulf of Khambhat was given as the downstream boundary condition as a normal slope (0.0022) for the river reach for the model. The model was simulated for 190 h (August 30, 2020 to September 6, 2020) with a computation interval of 5 s. The computation interval was decided based on the courant condition for the model stability.

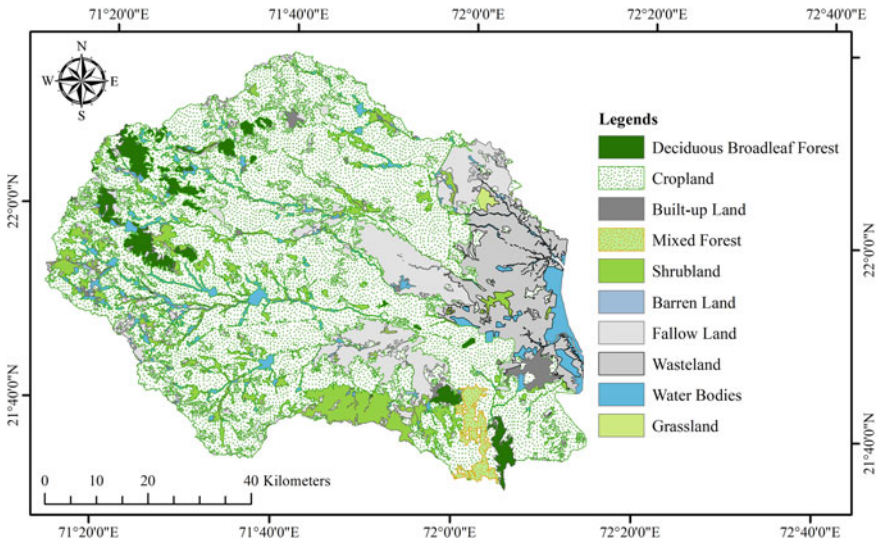

Fig. 3 Land-use land-cover map of the study area

Table 1 Manning's roughness coefficient for different LULC classes [19]

Land-use land-cover	Roughness coefficient
Deciduous forest	0.1
Cropland	0.035
Built-up land	0.03
Mixed forest	0.1
Shrubland	0.05
Barren land	0.03
Fallow land	0.03
Wasteland	0.03
Water bodies	0.035
Grassland	0.05

3.3 Result Analysis and Preparation of Flood Map

HEC-RAS generates result layers in RAS Mapper after successful completion of the simulation. The generated results of water depth and velocity were exported in GIS Format for further analysis. The average and maximum velocity, water depth, and surface elevation were identified from the exported layers and summarized in the result section. The simulated water depth in the river section was compared with the observed water level at the location of the river gauge stations. Finally, the inundated area was measured, and a flood map was prepared.

4 Results Analysis and Suggested Measures

The 2D flood model was successfully simulated using HEC-RAS v6.0, and the results were exported to GIS format for analysis. After adding the result layers in ArcGIS, the point observations were extracted at river gauge stations to compare them with the actual observed data. The comparison of observed and simulated results is shown in Table 2. The simulated water depth and velocity map are shown in Fig. 4. The result shows that the maximum flood depth in the region is 4.89 m, average flood depth is 0.64 m, with a standard deviation of 0.53 m. A total of 850.31 km^2 areas were inundated, among which 161.65 km^2 areas were flooded with a depth of water of more than 1 m. The maximum velocity in the region is 3.5 m s^{-1} with a mean velocity of 0.24 m s^{-1}. As seen from the elevation map of Fig. 1, the ground level for the study area is almost flat, which is the main reason for the low velocity of the water. The comparison of simulated and observed levels is fairly matched. Only the maximum depth of water is compared due to the non-availability of continuous observed stage data.

From the present study, it can be concluded that the open-source data are helpful for the preliminary analysis of the flood situation. For detailed and more accurate flood models, high-resolution surveyed data are required. Present available DEM with 12.5 and 30 m resolution would not be helpful to develop a one-dimensional (1D) flood model as the river width downstream of Bhavnagar district is reducing

Table 2 Observed and simulated water levels

Gauging station	Observed depth of water (max) (m)	Simulated depth of water (max) (m)	Error
Kalubhar @Umarala	2.97	2.8	− 0.17
Ghelo @Vallabhipur	1.8	1.43	− 0.37
Padalio @Muldharai	1.87	1.65	− 0.22

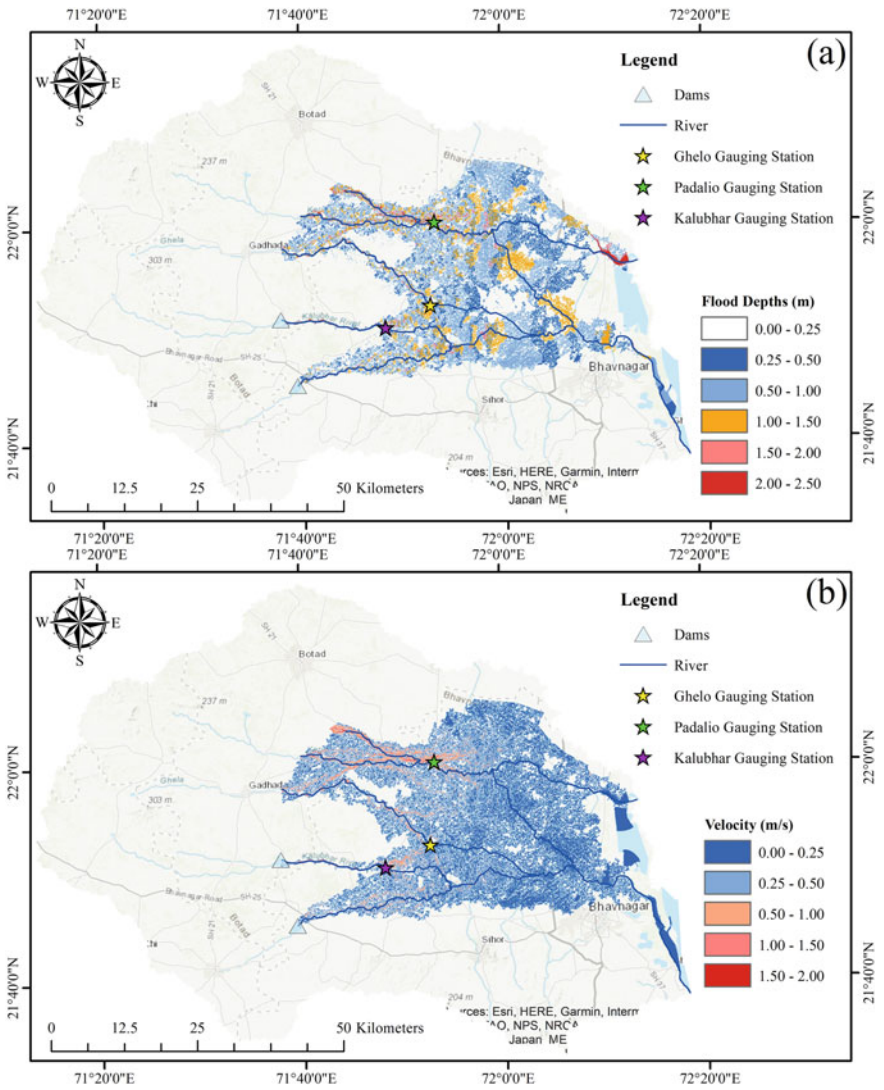

Fig. 4 **(a)** Flood inundation map of the year 2020; and **(b)** Velocity map of flood 2020, for Bhavnagar district

and reaches up to 15–35 m. The Ghelo and Keri rivers are ungauged on the upstream section, and the flow comes directly from the overflowing of small check dams. So, an automatic gauging station is recommended at those check dams to understand and model the real-time flood situation. In the Bhavnagar district, the present gauging stations take the reading at 6 h intervals for observed stage-discharge data. This time interval is very high, and there is a chance of missing the peak stage-discharge data,

which is crucial for flood modeling. So, operating the available gauging stations at 1-h intervals is recommended.

5 Conclusion

In August 2020, Bhavnagar and the surrounding district received around 521 mm of rain compared to the average annual rainfall of 658 mm. This high rainfall caused the high flows in the river Kalubhar, Ghelo, Rangholi, and Keri. The releases from the Kalubhar and Ranghola dam and the low carrying capacity of the downstream river resulted in flood and waterlogging in the coastal region. The unplanned development near the coastal line was responsible for worsening the flood situation. The two-dimensional hydraulic model was developed using HEC-RAS v6.0. The freely available open-source data such as ALOS PALSAR DEM and Landsat-8 satellite imagery were used to overcome the difficulty of unavailable data. The simulated results were fairly matched with the observed maximum water depth. The result shows that the maximum flood depth in the region is 4.89 m, average flood depth is 0.64 m, with a standard deviation of 0.53 m. A total of 850.31 km^2 areas were inundated, among which 161.65 km^2 areas were flooded with a depth of water of more than 1 m. The maximum velocity in the region is 3.5 m s^{-1} with an average velocity of 0.24 m s^{-1}. Based on the simulated results and the difficulties encountered during model development, recommendations and guidelines for resolving the waterlogging problem and reducing the extent of flood inundation for the Bhavnagar coastal region were provided. The study will aid government officials and stakeholders in determining flood prevention measures.

References

1. Mohapatra PK, Singh RD (2003) Flood management in India. Nat Hazards 28:131–143. https://doi.org/10.1023/A:1021178000374
2. Singh RD (2007) Real-time flood forecasting: Indian experience. In: Wheater H, Sorooshian S, Sharma KD (eds) Hydrological modelling in arid and semi-arid areas. Cambridge University Press, Cambridge, pp 139–156
3. Yadav SM, Mangukiya NK (2021) Semi-arid river basin flood: causes, damages, and measures. In: Proceedings of the fifth international conference in ocean engineering (ICOE 2019). Lecture notes in civil engineering, pp 201–212
4. Bhatt CM, Srinivasa Rao G, Manjushree P, Bhanumurthy V (2010) Space based disaster management of 2008 Kosi floods, North Bihar, India. J Indian Soc Remote Sens 38:99–108. https://doi.org/10.1007/s12524-010-0015-9
5. Ramkar P, Yadav SM (2018) Spatiotemporal drought assessment of a semi-arid part of middle Tapi River Basin, India. Int J Disaster Risk Reduct 28:414–426. https://doi.org/10.1016/j.ijdrr.2018.03.025
6. Mangukiya NK, Yadav SM (2022) Integrating 1D and 2D hydrodynamic models for semi-arid river basin flood simulation. Int J Hydrol Sci Technol 14:206–228. https://doi.org/10.1504/IJHST.2021.10035928

7. Roxy MK, Ghosh S, Pathak A et al (2017) A threefold rise in widespread extreme rain events over central India. Nat Commun 8.https://doi.org/10.1038/s41467-017-00744-9
8. Saha K (1974) Some aspects of the Arabian sea summer monsoon. Tellus 26:464–476. https://doi.org/10.1111/j.2153-3490.1974.tb01624.x
9. Schott FA, McCreary JP (2001) The monsoon circulation of the Indian Ocean. Prog Oceanogr 51:1–123. https://doi.org/10.1016/S0079-6611(01)00083-0
10. Uniyal A (2013) Lessons from Kedarnath tragedy of Uttarakhand Himalaya, India. Curr Sci 105:1472–1474. www.jstor.org/stable/24098844
11. Nanditha JS, Mishra V (2021) On the need of ensemble flood forecast in India. Water Secur 12:100086. https://doi.org/10.1016/j.wasec.2021.100086
12. Mehta DJ, Yadav SM (2020) Hydrodynamic simulation of river Ambica for riverbed assessment: a case study of Navsari region. In: Lecture notes in civil engineering, pp 127–140
13. Parhi PK, Sankhua RN, Roy GP (2012) Calibration of channel roughness for Mahanadi river, (India) using HEC-RAS model. J Water Resour Prot 04:847–850. https://doi.org/10.4236/jwarp.2012.410098
14. Patel DP, Ramirez JA, Srivastava PK et al (2017) Assessment of flood inundation mapping of Surat city by coupled 1D/2D hydrodynamic modeling: a case application of the new HEC-RAS 5. Nat Hazards 89:93–130. https://doi.org/10.1007/s11069-017-2956-6
15. Pramanik N, Panda RK, Sen D (2010) One dimensional hydrodynamic modeling of river flow using DEM extracted river cross-sections. Water Resour Manag 24:835–852. https://doi.org/10.1007/s11269-009-9474-6
16. Timbadiya PV, Patel PL, Porey PD (2015) A 1D–2D coupled hydrodynamic model for river flood prediction in a coastal urban floodplain. J Hydrol Eng 20:05014017. https://doi.org/10.1061/(ASCE)HE.1943-5584.0001029
17. Timbadiya PV, Patel PL, Porey PD (2011) Hec-ras based hydrodynamic model in prediction of stages of lower tapi river. ISH J Hydraul Eng 17:110–117. https://doi.org/10.1080/09715010.2011.10515050
18. Vijay R, Sargoankar A, Gupta A (2007) Hydrodynamic simulation of river Yamuna for riverbed assessment: a case study of Delhi region. Environ Monit Assess 130:381–387. https://doi.org/10.1007/s10661-006-9405-4
19. Asante KO, Artan GA, Pervez MS et al (2008) Technical manual for the geospatial stream flow model (GeoSFM)

Hydrodynamic Modelling and Satellite Altimeter-Based Establishment of Virtual Gauging Network in Flood-Prone River Basin

Joshal Kumar Bansal, Pankaj R. Dhote, Vaibhav Garg, and Praveen K. Thakur

Abstract Hydrologic–hydrodynamic modelling has been considered to be an important tool to understand and quantify hydrological processes of the river basins. The scarcity of the in-situ gauging network has made it a challenging task, as these with recent advancement in satellite altimetry, it may play a vital role in establishing the virtual gauges (VG) along the river stretch. In this study, HEC-RAS-based 1D/2D coupled hydrodynamic (HD) model has been set up for the stretch of around 170 km from Boudh to Naraj in the lower Mahanadi River along with two flood-prone tributaries, Kusumi and Rana. Based on the extreme flood events, the model was calibrated for the monsoon season of 2018 and, however, validated for monsoon of 2015 at daily time step. The Nash–Sutcliffe Efficiency (NSE) of 0.83 and root mean square error (RMSE) of 46 cm was estimated between simulated and observed water level (WL) for the calibration and NSE of 0.76 and RMSE of 45 cm during validation. The 04 ground tracks of Jason-2/3 satellite altimeters were identified, which cross the river. The virtual gauging stations were established at these locations to generate the rating curves (RCs) using HD model. The comparison of HD model and altimetry-based water level depicted the NSE and RMSE ranging from 0.76–0.84 to 42–88 cm, respectively. The high agreement between the two showed the potential of satellite altimetry data for the multi-site validation of HD model and constructed RCs at VG stations. This study showed the advantages of the combined use of HD model and satellite altimetry data enabling WL and RCs at multiple virtual locations in addition to existing physical ones. The proposed framework may open

J. K. Bansal
Department of Earth Sciences, Indian Institute of Technology Roorkee, Roorkee, Haridwar 247667, India

P. R. Dhote · V. Garg (✉) · P. K. Thakur
Water Resources Department, Indian Institute of Remote Sensing, Dehradun 248001, India
e-mail: vaibhav@iirs.gov.in

P. R. Dhote
e-mail: pdh@iirs.gov.in

P. K. Thakur
e-mail: praveen@iirs.gov.in

P. V. Timbadiya et al. (eds.), *Flood Forecasting and Hydraulic Structures*, Lecture Notes in Civil Engineering 340, https://doi.org/10.1007/978-981-99-1890-4_3

new perspectives for enhancing flow dynamic studies at a large scale even in remote and poorly gauged basins. Further, upcoming satellite missions like SWOT ensures detailed observations in future as well.

Keywords Hydrodynamic modelling · Satellite altimetry · Rating curves · Virtual gauging station · Mahanadi River

1 Introduction

India and adjacent areas are sensitive to natural disasters such as earthquakes, floods, drought, cyclones, and cloudbursts. The floods are the most frequent and worst occurring natural disasters that cause great damage to life and property, and these most frequent flood calamities in the region are caused by bigger rivers like Mahanadi. The coastal districts of Odisha and especially Mahanadi Delta have been subjected to flood damage concerning the loss of human lives and household animals, property damage, roads and bridges, crops, etc. Statistics mentioned in Beura [2] states that for the years 2003, 2008, 2011, and 2013, and it experienced serious inundations, in addition to several smaller ones and also experienced severe flood events in 2018 and 2020. Increased flood frequencies have led to an increase in more accurate flood studies [18].

Different researchers are widely using the HD modelling approach to study floods that happened over the floodplains [13]. Despite having various advantages of the HD modelling approach, it lacks the fact that it is heavily dependent upon the availability and the quality of bathymetry and gauging data as model parameters (e.g. roughness coefficient) are poorly estimated from the calibration procedure due to the limited availability of in-situ gauging sites over the inland water bodies [12].

This limitation was outgrown with the help of satellite altimetry, as it provides the opportunity to study the river with the limited gauging network [3]. Satellite altimetry missions like Jason-2/3 have shown their potential for water level monitoring of inland water bodies [7]. The generated water surface elevations (WSE) complement the gauge data as it provides spatially distributed WSE data for calibration of distributed non-uniform parameters, especially in the data-sparse region. Satellite altimeters have a high calibration potential for 1D/2D hydraulic models directly connected to WSE. With the satellite altimetry derived WSE, various researches have improved the efficiency of the HD modelling by establishing the virtual gauges.

WSE data derived using satellite altimetry, which is beneficial for the analysis of distributed, uniform parameters [10]. For example, Wilson [16] made its first strive to simulate flood extent and levels of water in 260 km across the Amazon on a wide spatial scale over 22 months, it was found that the RMSE was obtained after a simulation of the water levels and those derived from the simulation of water using SRTM, “Japan Earth Resources Satellite” (JERS)-1 images, gauge observations, and satellite altimetry data, and the main reason for this error was the uncertainty of topographical and altimetry data [17].

The WSE generated with the help of satellite altimetry data is compared with the one generated from HD models with the help of rating curves (RCs) generated within the model. As per Domeneghetti et al. [8], for a certain cross-section (XS), the rating curve or stage-discharge relationship is established through a consequent observation of water depths and interpolated measured discharges. The rating curves are generally used to convert observations of the river stage to release values (discharge). According to Paris et al. [11], RCs depict the hydraulic behaviour of a section of channels and represent the mathematical deployment relationships that hydrographs can define with gauging data and observed knowledge.

In this study, HEC-RAS-based 1D/2D coupled hydrodynamic (HD) model has been set up for the stretch of around 170 km from Boudh to Naraj in the lower Mahanadi River along with two flood-prone tributaries, Kusumi and Rana. The 04 ground tracks of Jason-2/3 (02 from each satellite) multi-mission satellite altimeter were identified, which cross the river. The virtual gauging stations were established at these locations to generate the rating curves (RCs) using HD model.@@ Section 2 describes the approach used to construct RCs using the HD model and extract WL using satellite altimetry data and also the study area's geographical and hydrological description and data used. Section 3 presents and discusses the results that correspond to the set objectives, while Sect. 4 summarizes the work's findings.

2 Study Area and Data Source

2.1 Mahanadi River Basin

Mahanadi, being the eighth largest basin, is 851 km long and have a total catchment area of 139,681.51 km^2 span over considerable parts of Chhattisgarh and Odisha and a comparatively smaller portion of Jharkhand, Maharashtra, and Madhya Pradesh, India. It rises in the Chhattisgarh district of Raipur near Sihawa and passes through Odisha to discharge water into Bengal's Bay ("Basin Details—Mahanadi and Eastern Rivers Organization").The total catchment area it covers is 4.28% of the total geographic area of the country for which agriculture and forest are two of the basin's main land use [1]. The geographical extent of the basin lies between 80° 28′ and 86° 43′ east longitudes and 19° 8′ and 23° 32′ north latitudes [6]. The Mahanadi system is broadly divided onto three distinct sub-basins: (i) Upper Mahanadi (lying mostly in Chhattisgarh region, intercepting the catchment area of 29,796.64 km^2), (ii) Middle Mahanadi (area lying between Hirakund and Tikarpara, intercepting the catchment of 51,895 km^2), and (iii) Lower Mahanadi (area lying between Tikarpara to Mundali, intercepting the catchment area of 57,958.88 km^2). The major area of Hirakund up to Mundali barrage intercepting the catchment area of 48,700 km^2 is mainly accountable for floods in the delta region of Mahanadi [9]. Therefore, the study area is the part of lower Mahanadi sub-basin starting with upstream and downstream gauging stations at Boudh and Naraj (Fig. 1).

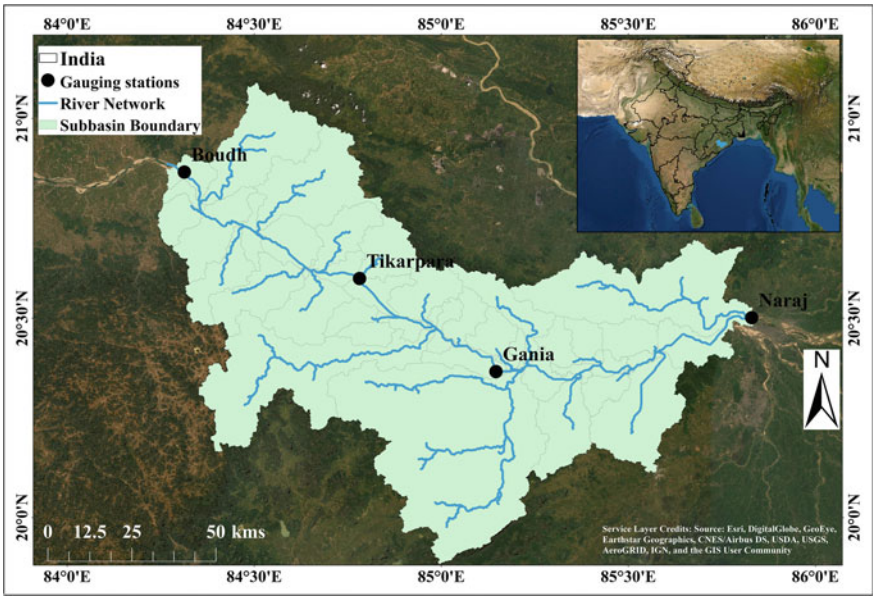

Fig. 1 Study area: lower Mahanadi River basin

Jason-2/3 missions launched by operational agencies: NOAA, CNES, and EUMESAT and lying for the time span of 2008-Present are the follow-up missions for TOPEX/Poseidon, Jason-1. With a temporal resolution of 10 days, it carries dual frequency bands, i.e. "C (5.3 GHz) and Ku (13.6 GHz)" bands. The main objective for Jason missions was to monitor global ocean circulation, discover the tie between the oceans and atmosphere, improve global climate predictions, and to monitor events such as El Niño conditions and ocean eddies. In this study, 04 tracks over Mahanadi River has been identified (02 tracks from each Jason-2 and Jason-3) for the period of 2015–2018.

2.2 Data Used

The stage data and discharge data are required for calibration, and validation of the HD model was obtained from Central Water Commission (CWC), Bhubaneshwar (Odisha) on demand. The gauge data of three stations, namely Boudh, Tikarpara, and Naraj, were provided, and discharge data of Boudh and Tikarpara stations were provided. The surveyed river XS data required to generate the Hybrid XS to correct the geometry of the river profile was obtained from Central Water Commission (CWC), Bhubaneshwar (Odisha), on demand. The XS data for the 18 sites, namely Boudh, Karadi, Dholpur, Harbhanga, Sithalpani, Tikarpara, Kotri, Barmul, Chamundia, Rout

Pada, Pathuria, Kantilo, Padmavati, Baideshwar, Kurumchain, Banki, Kandarpur Ghat, and Naraj, for the year 2018 were provided.

Radiometrically Terrain Corrected (RTC1) ALOS PALSAR DEM with spatial resolution of 12.5 m has been considered in this study. The Alaska Satellite Facility is responsible for the preparation, maintenance, and data availability of this datasets and has been downloaded from Alaska satellite facility Website. The RTC products are prepared by using ALOS PALSAR L1.1 image and a high-resolution DEM like NED13 and medium resolution DEM of SRTM GL1 for the areas with the unavailability of the high resolution of DEM. A SAR image is generated from the down sampling of the DEM and then co-registered with a processed optical image. Further, terrain correction and up-sampling are done for the final product.

The Land Use Land Cover map with global scale 1:250,000 is developed by ISRO Geosphere-Biosphere Program under the National Natural resource Management System (NNRMS) in 2005.

3 Methodology

The entire methodology used in this study is divided into two parts (Fig. 2). The initial part consists of hydrodynamic modelling, in which a water level was simulated by employing standard HEC-RAS model. The second step involves the retrieval of water levels from the multi-mission satellite altimeter like Jason-2/3 using Broadview Radar Altimetry Toolbox.

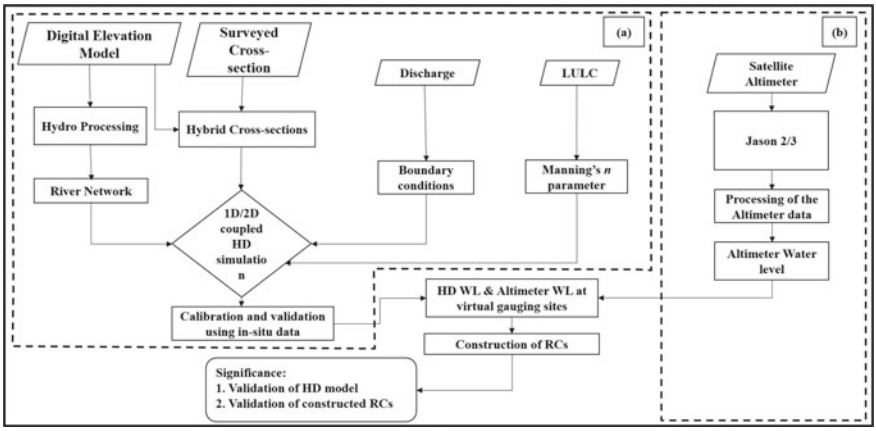

Fig. 2 Flow chart of methodology **a** Methodology used for HD modelling (HEC-RAS) **b** Methodology used for retrieval of WL using multi-mission satellite altimetry data

3.1 HD Model Setup to Construct RCs at Virtual Stations

In this study, HEC-RAS-based HD model that utilizes fully dynamic 1D-2D Saint–Venant equations to solve the river flow of the system over Mahanadi River. The 1D-2D solution techniques are strongly linked with the option of iterating 1D to 2D flow transfer on a one-time step basis. Every step lies in the middle of the 1D and 2D flow elements provides direct feedback. The software was developed for the use of unstructured computer meshes but also structured mesh handling. The structured mesh and unstructured mesh are considered to be the same. The programme assumes that cells are mutually orthogonal (the face between two cells is perpendicular to a line connecting the two cell centres). If orthogonal, certain computations are simplified, and the computation speed is improved. HEC-RAS has a pre-processor for a 2D flow area that transforms cell profiles in detail based on the digital elevation model (DEM) used in the modelling operation. SAR also abbreviated as "Synthetic Aperture Radar" technology-based ALOS PALSAR DEM was used for hydro-processing in ArcGIS tool 10.6.1 to delineate river network and sub-basins of Mahanadi River.

Between Boudh and Naraj, 04 tracks of Jason-2/3 (155, 192 of J2/J3 each) cross the river, as shown in Fig. 3. The points from where tracks of altimeter passes are considered to be as virtual stations (VSs) [7].

The lower Mahanadi River has contribution of eight right bank tributaries (RT1, RT2, RT3, RT4, RT5, RT6, Kusumi and Rana) and six left bank tributaries (LT1, LT2, LT3, LT4, LT5, and LT6). Except for Kusumi and Rana, the HD model was set up

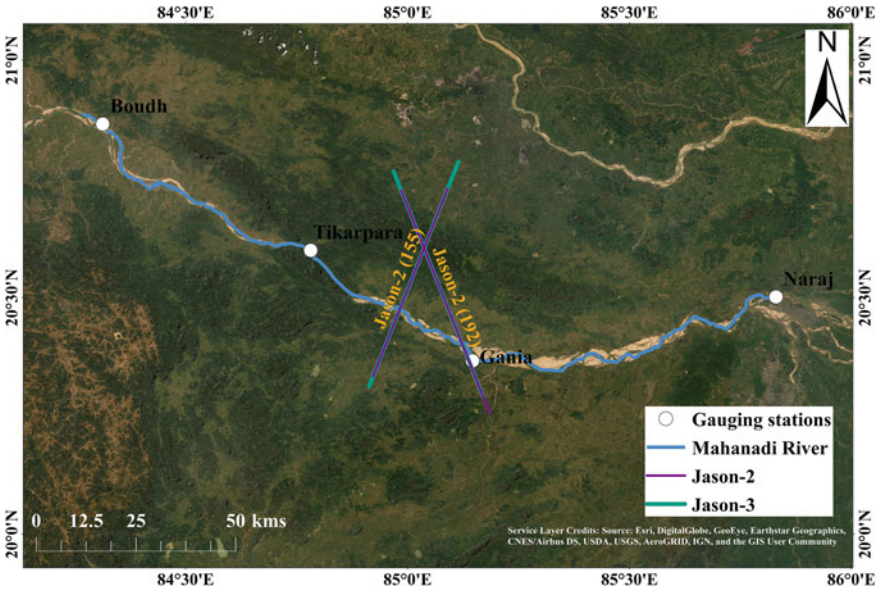

Fig. 3 Jason-2/3 Altimeter passes

for the main Mahanadi River (Boudh to Naraj), with contributions from tributaries treated as lateral inflows during simulation. These two frequently flooding tributaries are modelled as 2D floodplain.

Additional XSs were retrieved from the RTC product of the ALOS PALSAR to increase the density of the river XSs in order to accurately quantify the river's curvature. However, representing the bathymetry for the floodplain topography is quite difficult in comparison to DEM-based illustration. To overcome the challenge, nearest surveyed data were utilized to alter DEM-based XSs in order to keep the conveyance. Finally, in the HD model, Hybrid XSs were utilized. Figure 4 shows the longitudinal geometry of the main channel from Boudh to Naraj, as well as a cross-section at 63,912 m chainage.

The boundary description should be given at the upstream and downstream ends of the network profile. The upstream end should be boundary type as "inflow", whereas the downstream point should be given as normal depth. The flood hydrograph is provided at the upstream end of the main river profile and friction slope is provided as the normal depth at the downstream end, whereas the tributaries which are considered to be as 2-D floodplain have flood hydrograph as a boundary condition at the upstream end of it, and for the downstream end, lateral structures have been provided

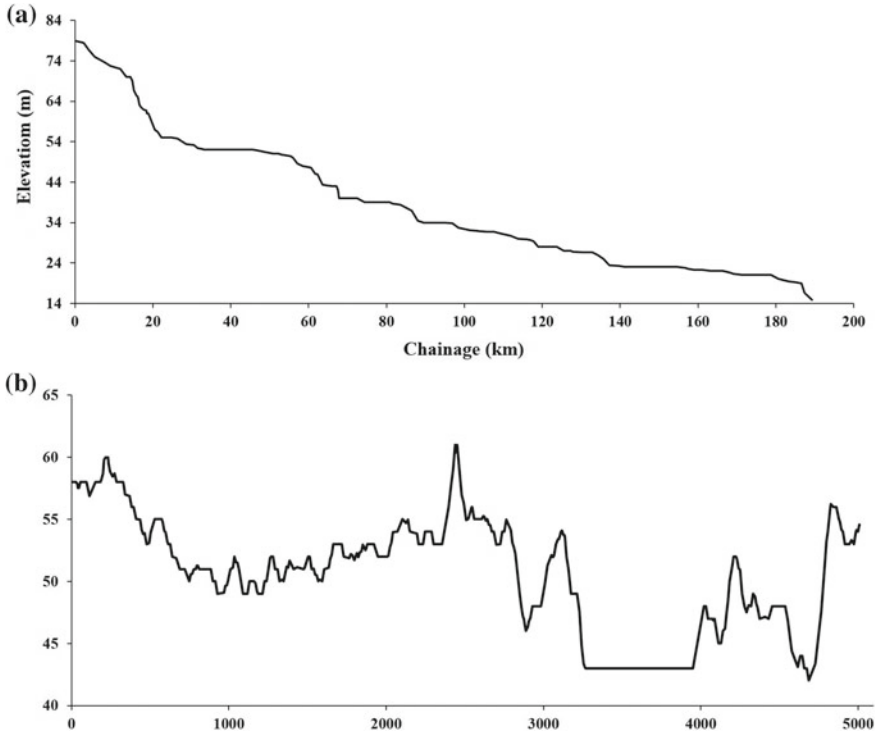

Fig. 4 **a** Main channel longitudinal profile from Boudh to Naraj **b** Hybrid XS at 63,912 m chainage from Boudh river station

which connects the tributaries to the main river. The contribution of the tributaries was provided by giving flow hydrographs calculated using discharge-area ratio method at an internal "lateral inflow" boundary conditions over the river cross-section just upstream of where the lateral inflow will come in (i.e. downstream end of the tributaries). Table 1 represents the details of boundary conditions. As mentioned by Jena et al. [9], most of the floods generated by Mahanadi are due to the contribution of the middle region tributaries, and the hydrometric data generated for tributaries show that the maximum contribution of tributaries is around 21% alongside several small one (Table 2).

The Manning's roughness coefficient (n) is considered to be the most important calibration parameter because it controls the energy losses at every station. ISRO GBP LULC map has been used to generate the Manning's coefficient for different classes. Here, Manning's n for floodplain and main channel is considered to be 0.06 and 0.03 $m^{(-1/3)}$ s.

Table 1 Summary of boundary conditions

Location	Boundary condition type	Data
Boudh (U/S)	External	Discharge time series (cumec)
Naraj (D/S)	External	Normal Depth
Kusumi (U/S)	External	Discharge time series (cumec)
Rana (U/S)	External	Discharge time series (cumec)
Tributaries	Lateral inflow	Discharge time series (cumec)

Table 2 Contribution of tributaries

Tributary	Catchment area (km^2)	Contribution on % using drainage-area ratio method
Rana	499.090	4.96
RT1	102.66	1.18
RT2	288.76	2.87
Kusumi	2117.20	21.07
RT3	1008.68	10.04
RT4	269.21	2.68
RT5	287.39	2.86
RT6	205.47	2.04
LT1	224.94	2.23
LT2	204.94	2.03
LT3	212.57	2.11
LT4	194.89	1.94
LT5	540.18	5.37
LT6	528.27	5.25

Finally, calibration and validation of HD model has been done as mentioned in Sect. 3.1, and rating curves (RCs) have been generated.

3.2 Retrieval of Water Level Using Satellite Altimetry Data

Satellite altimetry is a tool for global surface topography measurement. Radar altimetry was identified as the key technology for supplying essential information on solid ground and ocean dynamics very early on in space technology development [14]. The principle is that a radar wave is released and the returned signal which rebounds off the surface is analysed. Surface height is the difference between the position of the satellite in orbit on the arbitrary referring surface (Earth's centre approximation: reference ellipsoid) and satellite to surface area (the time taken to make the round trip is measured) [5]. Satellite height above a reference ellipsoid represents the altitude of the satellite, and it is defined as the satellite distance concerning an arbitrary reference (e.g. reference ellipsoid). This is conditioned by several constraints such as inclination, air drag, and force of gravity when the satellite's radar altimeter transmits signals to Earth at high frequency and receives echoes from the surface (called as "waveform"). Because the altimeter footprint extends many kilometres, it creates a multi-peak and complicated waveform over large rivers like the Mahanadi due to variable LULC, slopes, and sand bars. The algorithms created for waveform established across ocean are limited in their application due to these constraints. Due to surface characteristics, the return power collected from the water surface within the altimeter footprint remains higher than other features [7].

Retracking algorithms are applied over the VSs identified using the tracks 155 and 192 of both Jason-2/3 to extract the correct waveform. When the leading edge of the target waveform deviates from the tracking gate onboard, retracking methods are performed to the waveform [5]. Because it can compute the midpoint of the leading edge of every waveform if the return power of the leading and trailing edge is in the analysis window, the "off-centre of gravity (Ice-1)" retracking algorithm is used in this work [3, 7]. Water level retrieved from the altimeter contains a lot of disturbances because electromagnetic waves can be decelerated by water vapour or ionization as they move through the atmosphere. The corrections involved due to atmospheric conditions, geophysical condition, and instrumental conditions are applied to generate correct water level [5]. First of all, the water level is estimated using satellite orbit altitude (Alt) and the altimeter range value (R), then retracked range values were applied with the geophysics and atmospheric corrections. It must be pointed out that in this study records of satellite altimetry are referenced to geoid EGM 96. For this purpose, the orthometric height is estimated by taking off the mean elevation of the sea surface as regards the ellipsoid reference Ellipsoid WGS 84 (Eq. 1).

$$H = \mathrm{Alt} - R - (D_{\mathrm{tc}} + W_{\mathrm{tc}} + I_{\mathrm{onc}} + S_{\mathrm{tc}} + P_{\mathrm{tc}}) - \mathrm{MSS}_{\mathrm{ht}} \tag{1}$$

where H: corrected orthometric height; Alt: the satellite altitude from reference ellipsoid; R: the satellite range; D_{tc}: the dry tropospheric correction; W_{tc}: the wet tropospheric correction; I_{onc}: the ionospheric correction; S_{tc}: the solid tide; P_{tc}: the pole tide correction; and MSS_{ht}: the mean sea surface from the reference ellipsoid.

Validation of the HD model and the RCs constructed with the model at the VSs was done using WL time series acquired from four VSs located between Boudh and Naraj.

4 Results and Discussion

Results are divided into two parts: (1) Calibration and validation of HD model; (2) Satellite altimetry observations to validate hydrodynamic model and generated rating curves; results are being presented and discussed.

4.1 Calibration and Validation of the HD Model

For the calibration and validation of the HD model, extreme flood events should be considered, i.e. during the monsoon period of the year 2018 and 2015. So, for the period from 1 July 2018 to 31 October 2018 (daily data), the HD model has been calibrated, and validation is done for the period of 1 July 2015 to 31 October 2015 using water level data procured from CWC, Bhubaneshwar. Manning coefficient (n) was considered to be only variable used to calibrate the HD model. Since the river stretch which is modelled is very long and the process of calibration is provable, n values of the various classes (croplands, settlement areas, forests, and agricultural areas) that fall in the floodplain were constantly maintained [7]. The channel "n" value was varied between 0.03 and 0.04 $m^{-1/3}$ s, and the n value for floodplain values represented by the 2D mesh was varied between 0.04 and 0.1 $m^{-1/3}$ s until a satisfactory match between simulated and observed water levels at Tikarpara station across Mahanadi was found [4, 15]. The analytical index for evaluation of its performance in the calibration and validation stages used is "Nash Sutcliffe Efficiency" (NSE) and root mean square error (RMSE). The ideal "n" value for the river channel and 2D floodplain is considered to be 0.03 and 0.07 $m^{-1/3}$ s, for which the fine understanding between simulated and observed water level is scrutinized. Figure 5 represents a fair match between observed and simulated water levels during calibration (NSE 0.83; RMSE 46 cm) and validation (NSE 0.76; RMSE 45 cm).

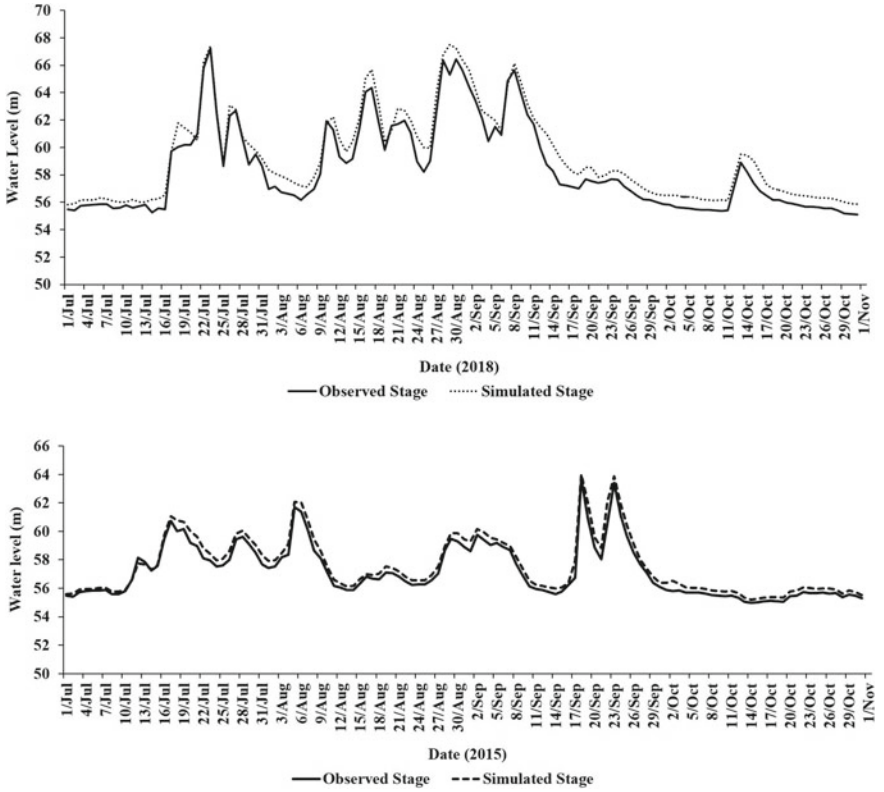

Fig. 5 Calibration and validation of the HD model at Mahanadi station

4.2 Satellite Altimetry Observations to Validate Hydrodynamic Model and Generated Rating Curves

The HD model had originally been calibrated with Mahanadi in-situ data, the comparison on the VS does not only result in multiple sites validation, but the RCs obtained with it are also validated. In this study, an option for verification of the built RCs is provided by the calibrated HD model with in-situ data and the accessibility of altimetry data. It is important to note that if the model is calibrated and the water levels simulated on VSs match the satellite observations, it is assumed that the relationships between the discharged water and the model itself can be reproduced and therefore have a certain confidence in the estimated RCs [7]. Altimeter tracks retrieved from Jason-2/3 over the Mahanadi River provide a good opportunity in conjunction with the existing gauging stations to study water levels at finer intersections. As a result, the simulated WLs at virtual stations were compared to the altimeter data, and RCs were created (Fig. 6). For track 155 situated upstream of Gania, statistics indicated good correlation with NSE of 0.76 and 0.83; RMSE of 42 cm and 60 cm; and NSE

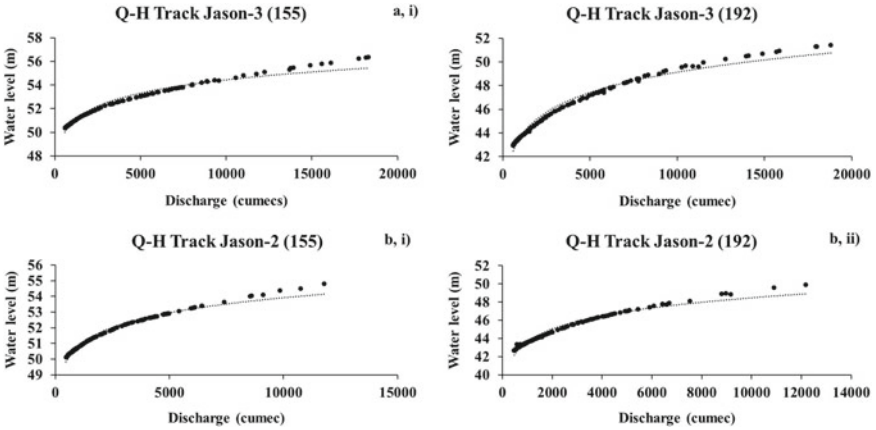

Fig. 6 RCs generated at VSs by means of the HD model run over the period from **a** 1 July 2018 to 31 October 2018 and **b** 1 July 2015 to 31 October 2015

of 0.84 and 0.76; and RMSE of 74 cm and 88 cm for track 192 lying downstream of Gania (Fig. 7). The statistics of the comparison of simulated water level and water level collected from altimeter are shown in Table 3.

RC is a low-cost and rapid method for estimating discharge using water level data. The river gauging network can be expanded thanks to RCs built at VSs. RCs can be used to estimate discharge at VSs and the contribution of various lateral tributaries along the main river because altimetry and HD model predicted water level have a synergistic relationship.

5 Conclusions

In this study, core concepts of hydrodynamic modelling and altimetry have been explored, quantified, and integrated on a spatial scale on the Mahanadi River. The combined 1D/2D HD modelling concepts have been explored as 2D flood modelling capability uses a finite-capacity solution scheme in HEC-RAS. 2D modelling provides a more reliable simulation where the water can surpass and/or breach in many directions by an area behind a levelled system. This study showed the advantages of the combined use of HD model and satellite altimetry data enabling water level and rating curves data at multiple virtual locations in addition to existing physical ones. It could offer up new possibilities for improving flow dynamics studies on a worldwide scale, especially in remote and dense areas where topographic field surveys or river discharge are limited. Forthcoming satellite missions (e.g. SWOT developed by NASA and CNES) ensures detailed observations in future as well.

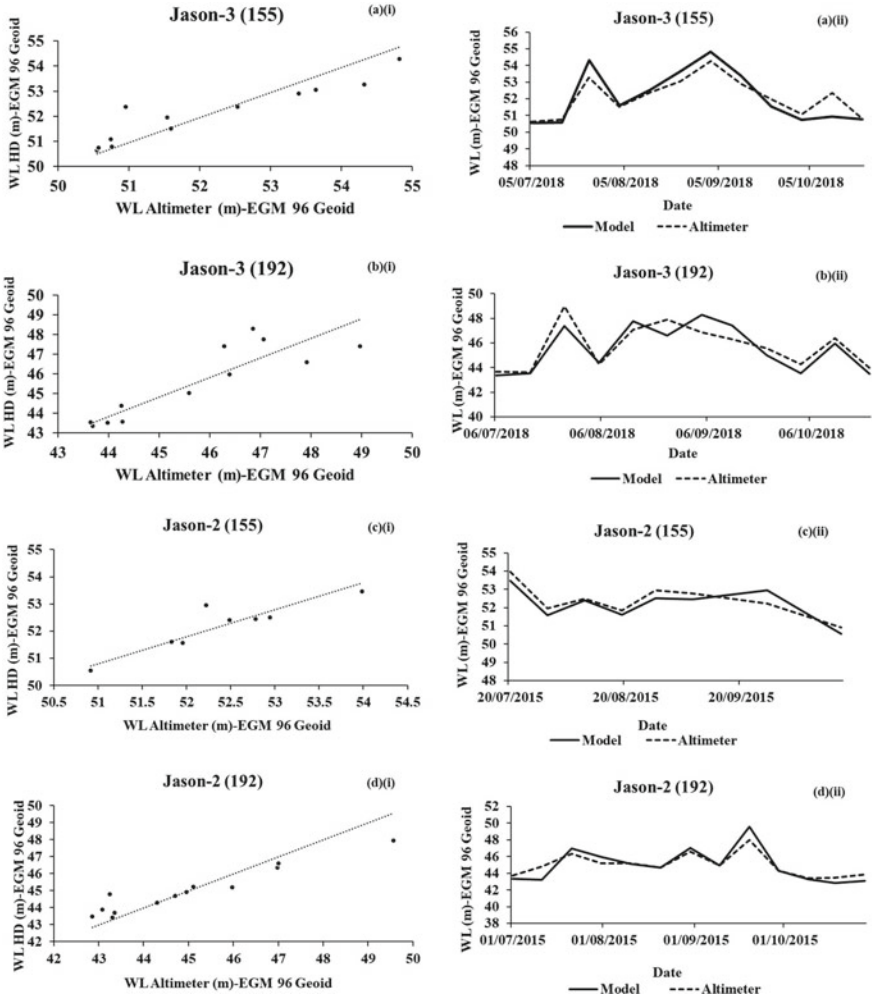

Fig. 7 WL retrieved by the altimeter and the HD model is compared **a** Jason-3 (155) **b** Jason-3 (192) **c** Jason-2 (155) **d** Jason-2 (192)

Table 3 Statistical evaluation for HD model and altimeter data

Satellite	Year	Pass	NSE	RMSE (m)
Jason 2	2018	155	0.76	0.42
Jason 3	2018	192	0.83	0.60
Jason 2	2015	155	0.84	0.74
Jason 3	2015	192	0.76	0.88

Acknowledgements The authors owe special thanks to CWC, Bhubaneshwar, for providing the observational datasets used for the study validation. In addition to it, they extend their gratitude to ESA, CNES, and AVISO to provide the Sentinel-3A/3B, Jason-2/3 and SARAL/AltiKa-based altimeter datasets and Alaska Satellite Facility (ASF) for providing the digital elevation model (DEM).

References

1. Behera, N. K., and Behera, M. D. (2020). Predicting land use and land cover scenario in Indian national river basin: the Ganga. Tropical Ecology, 1–14.
2. Beura D (2018) Floods in Mahanadi River, Odisha. India. Int. J. Eng. Appl. Sci. 2:51–55
3. Chembolu V, Dubey AK, Gupta PK, Dutta S, Singh RP (2019) Application of satellite altimetry in understanding river–wetland flow interactions of Kosi River. J Earth Syst Sci 128(4):1–15
4. Chow VT, Maidment DR, Mays LW, Te Chow V, Maidment DR, L.W.M. (1988) Applied Hydrology. McGraw-Hill Publishers, Singapore
5. CNES and ESA. (2018). How altimetry works – Radar Altimetry Tutorial and Toolbox [WWW Document]. URL http://www.altimetry.info/radar-altimetry-tutorial/how-altimetry-works/ (accessed on 11.01.21).
6. Central Water Commission (2014). Mahanadi Basin Version 2.0 https://indiawris.gov.in/downloads/Mahanadi%20Basin.pdf
7. Dhote PR, Thakur PK, Domeneghetti A, Chouksey A, Garg V, Aggarwal SP, Chauhan P (2021) The use of SARAL/AltiKa altimeter measurements for multi-site hydrodynamic model validation and rating curves estimation: An application to Brahmaputra River. Adv Space Res 68(2):691–702
8. Domeneghetti A, Castellarin A, Brath A (2012) Assessing rating-curve uncertainty and its effects on hydraulic model calibration. Hydrol Earth Syst Sci 16(4):1191–1202
9. Jena PP, Chatterjee C, Pradhan G, Mishra A (2014) Are recent frequent high floods in Mahanadi basin in eastern India due to increase in extreme rainfalls? J Hydrol 517:847–862
10. Jiang L, Madsen H, Bauer-Gottwein P (2019) Simultaneous calibration of multiple hydrodynamic model parameters using satellite altimetry observations of water surface elevation in the Songhua River. Remote Sens Environ 225:229–247
11. Paris A, Dias de Paiva R, Santos da Silva J, Medeiros Moreira D, Calmant S, Garambois PA, Seyler F (2016) Stage-discharge rating curves based on satellite altimetry and modeled discharge in the Amazon basin. Water Resour Res 52(5):3787–3814
12. Shen Y, Liu D, Jiang L, Yin J, Nielsen K, Bauer-Gottwein P, Wang J (2020) On the Contribution of Satellite Altimetry-Derived Water Surface Elevation to Hydrodynamic Model Calibration in the Han River. Remote Sensing 12(24):4087
13. Singh RK, Villuri VGK, Pasupuleti S, Nune R (2020) Hydrodynamic modeling for identifying flood vulnerability zones in lower Damodar River of eastern India. Ain Shams Engineering Journal 11(4):1035–1046
14. Stammer, D., and Cazenave, A. (Eds.). (2017). Satellite altimetry over oceans and land surfaces. CRC press.
15. Subramanya, K. (2013). Engineering hydrology, 4e. Tata McGraw-Hill Education.
16. Wilson, M., Bates, P., Alsdorf, D., Forsberg, B., Horritt, M., Melack, J. and Famiglietti, J. (2007). Modeling large-scale inundation of Amazonian seasonally flooded wetlands. Geophysical Research Letters, 34(15).

17. Yan K, Tarpanelli A, Balint G, Moramarco T, Baldassarre GD (2015) Exploring the potential of SRTM topography and radar altimetry to support flood propagation modeling: Danube case study. J Hydrol Eng 20(2):04014048
18. Zhao, D. (2018). Generating water level time series from satellite altimetry measurements for inland applications (Master's thesis).

Flood Inundation Mapping Using 2D Hydrodynamic Model and GIS Technique for Lower Tapi Basin, India

Theertha Ravi, Shubham M. Jibhakate, and P. V. Timbadiya

Abstract A two-dimensional (2D) hydrodynamic (HD) model is developed for densely populated Surat city, India, located on the bank of the lower Tapi River. Surat city has experienced flooding in the past during the monsoon period due to heavy releases from the Ukai Dam situated 100 km upstream of the city. In the current study, the 2D HD model is developed for the lower Tapi basin (LTB), focusing on Surat city for the past flood that occurred in August 2006. The hourly discharge from the Ukai Dam and tidal levels at the Arabian Sea was used as upstream and downstream boundary conditions, respectively. The distributed floodplain roughness coefficient based on the existing land use land cover (LULC) of the study area is considered across the flood plain. The performance of the model is evaluated against observed water levels along the channel, including maximum flood depth across the flood plain of Surat city and found satisfactory. The developed model will be useful for the local administration in predicting maximum water depth, velocity, and flood duration for various return periods floods of high magnitude and help prioritize the mitigation strategies.

Keywords 2D HD model · Surat city · Lower Tapi River · Ukai Dam · Arabian Sea

T. Ravi (✉) · S. M. Jibhakate · P. V. Timbadiya
Department of Civil Engineering, Sardar Vallabhbhai National Institute of Technology, Surat 395007, India
e-mail: theertha.ravi@gmail.com

S. M. Jibhakate
e-mail: shubhamjibhakate1771@gmail.com

P. V. Timbadiya
e-mail: pvtimbadiya@ced.svnit.ac.in

P. V. Timbadiya et al. (eds.), *Flood Forecasting and Hydraulic Structures*, Lecture Notes in Civil Engineering 340, https://doi.org/10.1007/978-981-99-1890-4_4

1 Introduction

Flood is the most widespread disaster, and it continues to be a problem in many parts of the world. Flooding could create a risk to the community only if the floodplain is occupied and used. As per the technical flood risk management guidelines from https://knowledge.aidr.org.au/resources/handbook-managing-the-floodplain (last accessed on March 15, 2021), intense rainfall in the densely populated areas, increase in industrialization, an illegal settlement in the floodplain, riverbank erosion, and high tide with changing climate are the main reasons behind the flooding. Although structural measures are the traditional approach in the case of flood prevention, engineers worldwide have realized the associated challenges such as the likelihood of failure, new geographical relationships, and performance. Furthermore, new flood concerns arise at a faster rate than structural solutions can be developed. As a result, the idea of flood mitigation is being superseded by the concept of flood risk management, which places a greater emphasis on non-structural solutions [1].

The HD modeling of catastrophic floods for flood-prone areas plays a major role in restricting the number of fatalities and the amount of property damaged. The understanding of past, probabilistic future flood events with information on flood inundation depth, velocity, and duration can lead to likely flood hazard estimation. This can be accomplished by available one-dimensional (1D), two-dimensional (2D), and integrated 1D/2D models [1]. Salimi et al. [2] used a geographic information system and the Hydrologic Engineering Centre's River Analysis System (HEC-RAS) simulation model to determine the extent and level of flooding (GIS). The 1D HEC-RAS model simulated flood water levels along the 79 km Kalu River in Sri Lanka to help limit flood damage. Timbadiya et al. [3] developed, calibrated, and validated a 1D channel model for the lower Tapi River, in the western part of India. 1D channel model in MIKE HYDRO model for the flood-prone tidal river in Southeast Queensland, Australia, developed by Jahandideh-Tehrani et al. [4]. Although 1D modeling approaches, such as for artificial channels, may be beneficial in some cases. When it comes to overflow analysis, they have a lot of drawbacks [5]. In case of overflow from channel embankment, it becomes a 2D phenomenon, making a 1D/2D or 2D model more appropriate. Timbadiya et al. [6] and Patel et al. [7] developed a 1D/2D coupled HD model using MIKE FLOOD and HEC-RAS, respectively, for the year 2006 Surat flood. Mignot et al. [8] used the 2D shallow-water equation for flood modeling and mitigation design in a dense urban area. Quiroga et al. [9] proved the HEC-RAS model's 2D capability by calculating flood depth, flow velocity, and flood duration for the Mamore river flood using the latest HEC-RAS version 5. Farid et al. [10] developed a flood hazard map of Palembang City by using 2D modeling in HEC-RAS. Based on the literature, 1D/2D integrated and 2D HD model was capable of simulating flood events, and a similar approach has been adopted in the current study for simulating the flood in the year 2006 for Surat city, India.

Surat, which is densely populated and located on the lower Tapi River's bank, has previously experienced significant flooding. Rapid urbanization and expansion within the floodplain have exacerbated the problem, particularly in the previous two

decades. The Ukai Dam is a multipurpose dam located 100 km upstream of Surat city completed in 1972, to resolve the irrigation requirement and partial flood control. However, the heavy rainfall in the catchment of Ukai Dam in 2006 led to heavy inflow into the Ukai Dam resulting in a high outflow (peak discharge = 25,780 m^3s^{-1}) from the reservoir. The heavy releases coincide with high tide in the Arabian Sea causes flooding in Surat city in 2006. Thus, the dam hazard analysis for the area downstream of Ukai Dam especially in Surat city is required. The current study was conducted with a focus on Surat city to achieve the following key objectives: (i) development and performance evaluation of 2D HD model using HEC-RAS for lower Tapi basin (LTB) from Ukai Dam to Arabian Sea (ii) development of flood inundation maps based on maximum flood depth and maximum flow velocity.

2 Study Area and Data Source

2.1 Lower Tapi River Basin

The Tapi River, which originates in Madhya Pradesh's Betul region, is India's second-largest west-flowing river and the Indian peninsula's sixth-largest river. It travels through three different states, viz. Madhya Pradesh, Maharashtra, and Gujarat before meeting the Arabian Sea for a total 724 km long stretch [11]. The Tapi basin is divided into three sub-basins as Upper Tapi basin (UTB) (from origin to Hathnur), the Middle Tapi basin (MTB) (Hathnur to Gidhade), and the lower Tapi basin (LTB) (Gidhade to the Sea) [12]. The Ukai Dam multipurpose dam situated about 100 km upstream of Surat was completed in 1972. The Kakrapar weir (Ogee-shaped weir) and the Singanpore weir (broad crested weir) are two inline structures on the study reach, located 22.2 km and 103 km from Ukai Dam, respectively. On lower Tapi (LT), there are four crucial river gauge discharge stations: Kakrapar weir, Mandvi Bridge, Ghala, and Hope Bridge. The tidal wave of the Arabian Sea comes through the main Tapi River channel and continues to influence it until it reaches the Singanpore weir [3]. Surat, one of the most prominent urban centers, located on the bank of LT River, extends on both sides. For administrative purposes, Surat city is divided into seven different zones (See Fig. 1). The detailed index map of the LT River, the location of Ukai Dam, and Surat city are shown in Fig. 1. The locations of stream gauging stations and Ukai Dam are shown in Fig. 2.

The data necessary for the current analysis to develop a 2D HD model of LTB for this study was collected from the central and state government agencies responsible for the measurement and collection of data such as the Central Water Commission (CWC), Surat division; Survey of India (SOI); National Remote Sensing Centre (NRSC), Hyderabad; Surat Municipal Corporation (SMC), Surat; and Surat Irrigation Circle (SIC), Surat. The open source SRTM was DEM downloaded from https://earthexplorer.usgs.gov/ (last accessed on March 15, 2021). Table 1 depicts the type of data, source, and application.

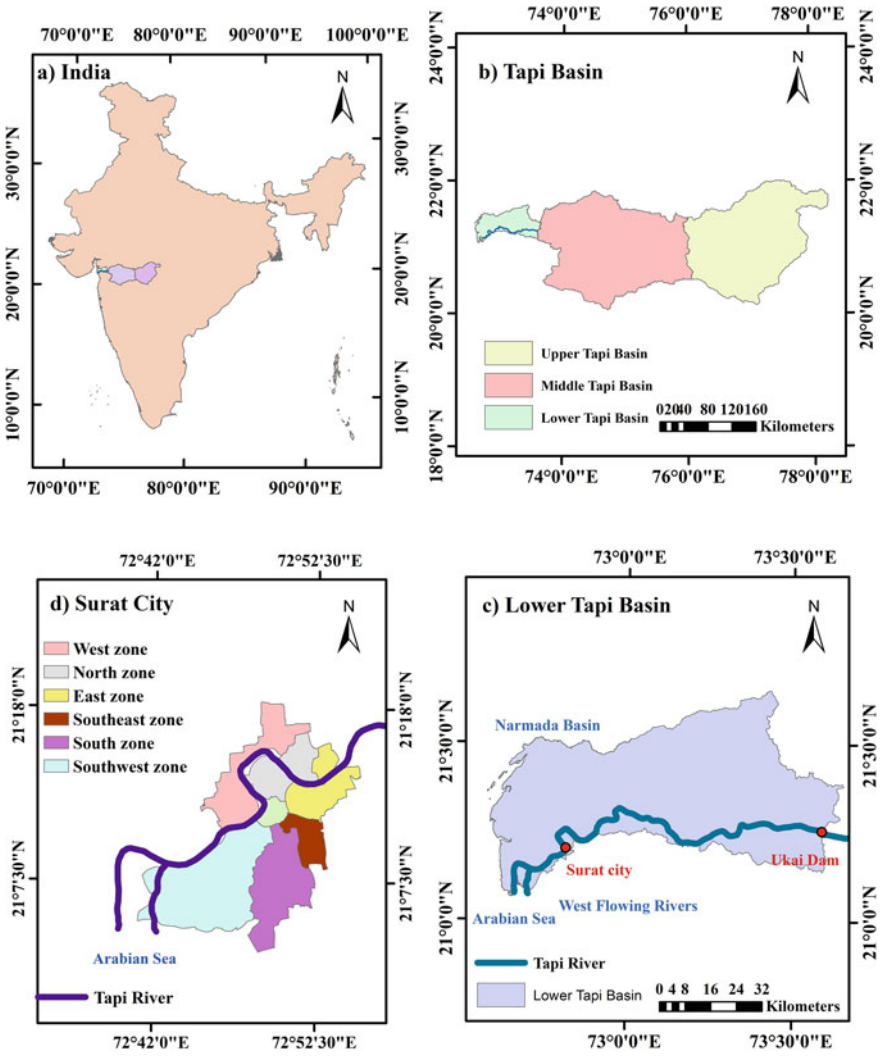

Fig. 1 Index map of the study area

3 Methodology

The detailed methodology adopted in the current study is shown in Fig. 3.

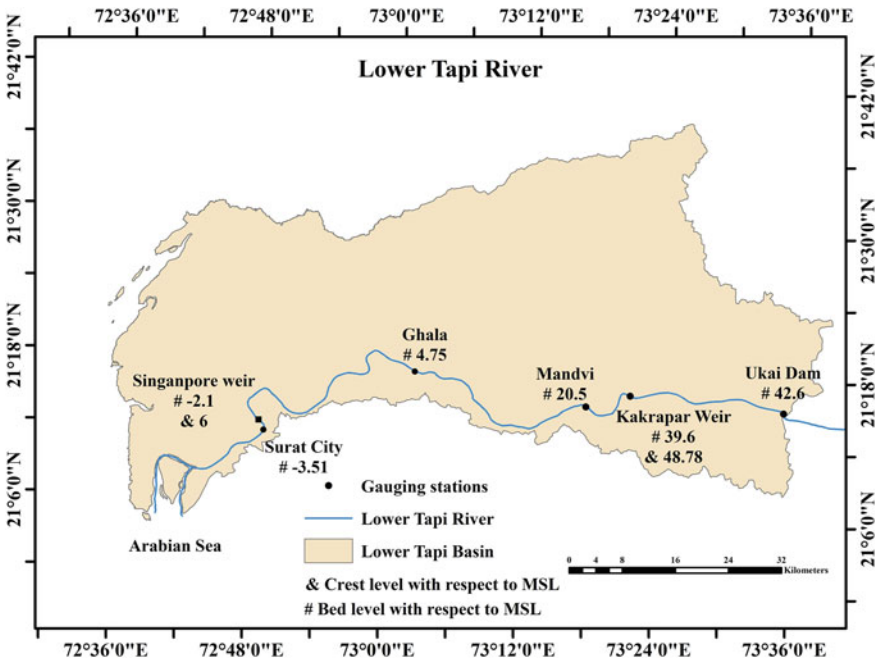

Fig. 2 Stream gauging stations along the lower Tapi River

3.1 Creation of Geometry

The DEM of the study area is created by combining the physically surveyed contour data (from SMC) for Surat city and lower Tapi River, digitized contours from SOI toposheets, and contours generated from SRTM DEM for the remaining area. The SOI contours are not available for the flat area of LTB above Surat city, so we adopted contours from SRTM DEM. All the contours are projected to the same coordinate system. Using the spatial interpolation tool 'Topo to Raster' in ArcGIS10.6.1, the contours (vector) for the LTB from several sources were integrated and transformed to raster. The 2D flow area mesh for the study area is made in RAS Mapper. Specify the coordinate system using ESRI Projection file WGS 1984 UTM Zone 43N. The digital terrain model is created from DEM in RAS Mapper to work on HD properties and the geometry (See Fig. 4) of the 2D flow area. For the LTB, a 2D computation mesh is created. Since Surat city is an urban highly populated area and physically surveyed data with 0.5 m interval contours are available, the study mesh area considered for Surat city is much higher. A near polygon defines this calculation region, and computation cells are generated within the polygon. This indicates that the computing mesh can be made up of a mix of 3, 4, 5, and up to 8 side cells. For LTB, a 50 m $\times$ 50 m computation point spacing was chosen, resulting in a total of 550,054 grid cells. An implicit finite volume approach is used to solve the selected equations.

Table 1 Sources and application of data used

Type of data	Details	Source and year	Application
20 m interval contour	Digitized from SOI toposheet for lower and middle parts of LTB	SOI	To produce DEM
0.5 m interval contour	Physically surveyed for Surat-Hazira twin city	SMC (2007)	To produce DEM
1 m interval contour	Physically surveyed from Ukai Dam to the Arabian Sea	SMC (2007)	To produce DEM
10 m interval contour	Coastal sector of LTB	SRTM (2021)	To produce DEM
Land Use Land Cover (LULC)	Obtained with 56 m resolution updated to 30 m with six classes	NRSC (2006)	To provide appropriate Manning's 'n' value to study area
Hourly discharge data	From Ukai Dam	SIC (2006 flood)	To simulate unsteady flow
Hourly observed water level	Hourly stages at Nehru Bridge	SIC (2006 flood)	To validate the model
Observed tidal water level	Hourly tidal levels including both spring and neap tides at mouth of the sea	SIC (observe between December 6, 2009 and January 5, 2010)	To simulate unsteady flow
Distributed maximum water levels in Surat city	Based on debris marks on walls and communication with locals	SMC (2006 flood)	To validate the model

Readers can refer to 'HEC-RAS, hydraulic reference manual' for more details related to the finite volume approach in software.

3.2 Boundary Conditions

Upstream and downstream boundary conditions are the discharge from the Ukai Dam (outflow hydrograph) and tidal observations (spring tide) synchronized with 2006 flood data in the Arabian Sea (at the mouth of the sea) shown in Fig. 5.

3.3 Hydrodynamic Parameters

Manning's roughness coefficient

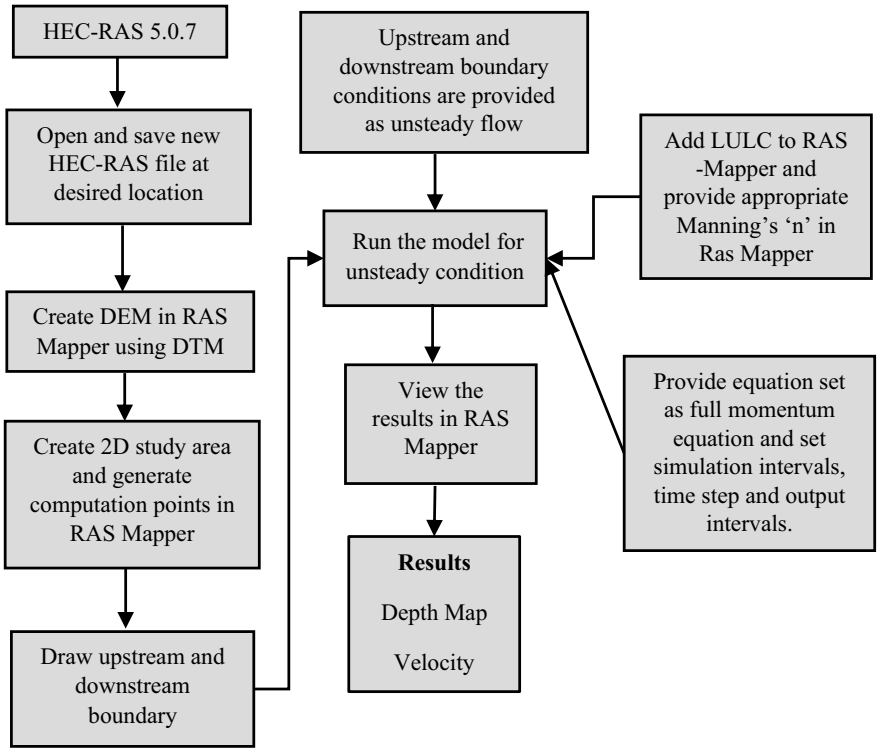

Fig. 3 Methodology adopted in the current study

The NRSC provided a LULC map of the research area with a spatial resolution of 56 m for the year 2006. The resulting LULC has been adjusted with six major land cover types, namely agricultural, fallow, built up, forest, water, and wasteland, at a spatial resolution of 30 m. Table 2 shows Manning's 'n' for various locations based on previous investigations in the Tapi basin [12].

Initial condition

Initial condition time is taken as 1 h, and ramp-up fraction is taken as 0.5. The time steps were determined using the Courant–Friedrichs–Lewy condition [13] to ensure the model's stability:

$$C = \frac{V\Delta T}{\Delta x} \leq 0 \text{ (with maximum } C = 3.0) \tag{1}$$

Or,

$$\Delta T \leq \frac{\Delta x}{V} \text{ (with } C = 1.0) \tag{2}$$

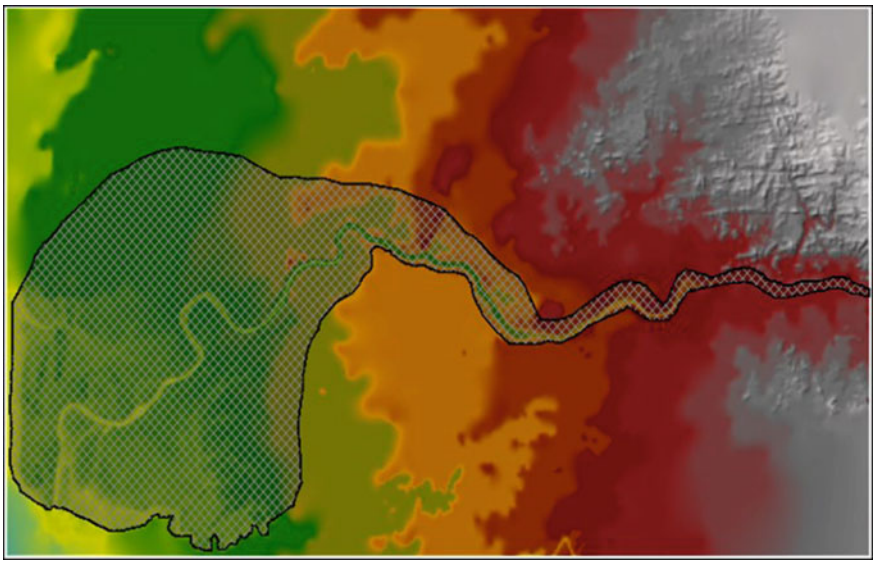

Fig. 4 2D geometry of LTB in HEC-RAS

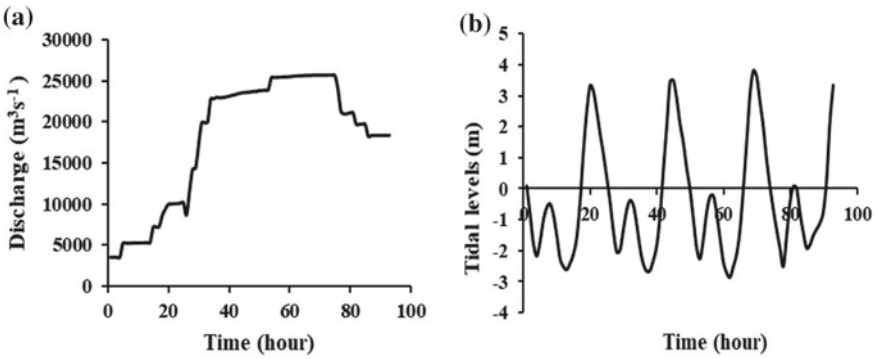

Fig. 5 **a** Outflow hydrograph from Ukai Dam (2006), **b** Tidal levels at the Arabian Sea

Table 2 Manning's 'n' for individual land class

Land cover group	Manning's 'n'
Built up	0.149
Cropland	0.035
Fallow land	0.04
Forestland	0.149
Wasteland	0.035
Waterbody	0.025

C represents Courant number, V represents the flood wave velocity (ms^{-1}), ΔT represents computational time step (s), and Δx represents the average cell size (m) [14]. The river flow velocity near Hope Bridge is estimated to be between 3.5 and 3.0 ms^{-1} based on the observed data [7]. The time step is obtained as 15 s.

3.4 Performance of the Model

The SMC provided observed high flood levels at various sites during the flood event of 2006 in all seven zones of Surat city to test the accuracy of simulated flood depths. Zone by zone, the observed depths were compared to the simulated depths, and RMSE is calculated (Table 3). The observed water level and simulated water level at Nehru Bridge are compared as shown in Fig. 6.

Table 3 Performance of 2D model for highest flood levels in Surat

Zone	RMSE (m)
Central zone	0.661
East zone	1.020
North zone	1.028
Southeast zone	1.785
South zone	1.667
West zone	1.233
Surat city	1

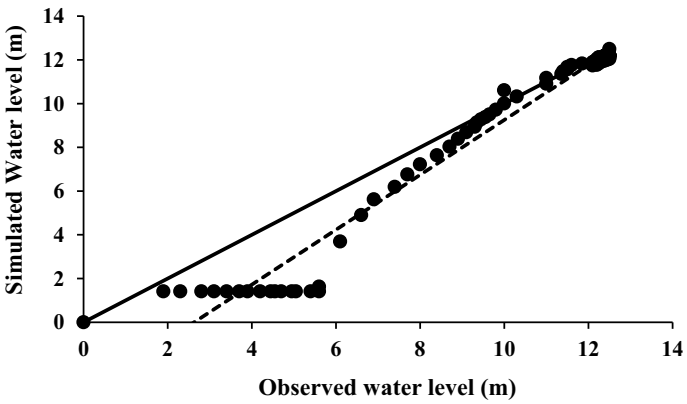

Fig. 6 Comparison of observed water level and simulated water level at Nehru Bridge

4 Results and Discussion

4.1 Flood Wave Propagation Across the LTB Including Surat City

The flood wave propagation across the LTB is shown in Fig. 7. The start of flood event began at 03:00 h on August 7, with a release of 10,069.87 m^3s^{-1}, according to a simulated outcome and Adajan in the west zone is the first place got flooded. The flood inundation maps for the maximum flood depth and maximum flood velocity are shown in Fig. 8; it is evident that 77.53% of Surat city was flooded for the flood of the year 2006. The corresponding zone-wise inundation statistics of Surat city for the flood year 2006 are given in Table 4.

The north zone and Southwest zone are more affected among all other zones. The Southeast zone is the least affected. The north zone is affected by a water depth of more than 3.5 m, whereas a larger area of the west zone and area near Meethi khadi is affected with a water depth of more than 1.5 m. Most of the west zone and north zone have maximum velocity in the range of 0.2–0.6 ms^{-1}.

5 Conclusion

The discharge from the Ukai Dam and the tidal level at the Arabian Sea was used as upstream and downstream boundary conditions, respectively, in the development of a 2D HD model of Surat city for the 2006 flood. A 30 m resolution DEM developed from the data collected from different data sources is used to generate 50 m × 50 m gridded mesh as bathymetry input to HEC-RAS. The flood plain roughness, i.e., Manning's 'n' values are based on the existing LULC of the year 2006, are taken from the past study. The developed model is validated for the maximum flood levels across Surat city, and the model performs satisfactorily. And 77.53% of Surat city got inundated by the flood year 2006. The developed and calibrated model will be useful for the local administration in predicting maximum water depth, velocity, and flood duration during various return periods of floods of high magnitude and help prioritize the mitigation strategies. The dam break analysis of the Ukai Dam and the development of an emergency action plan for the Surat city using a well-calibrated model can be the future scope of the study.

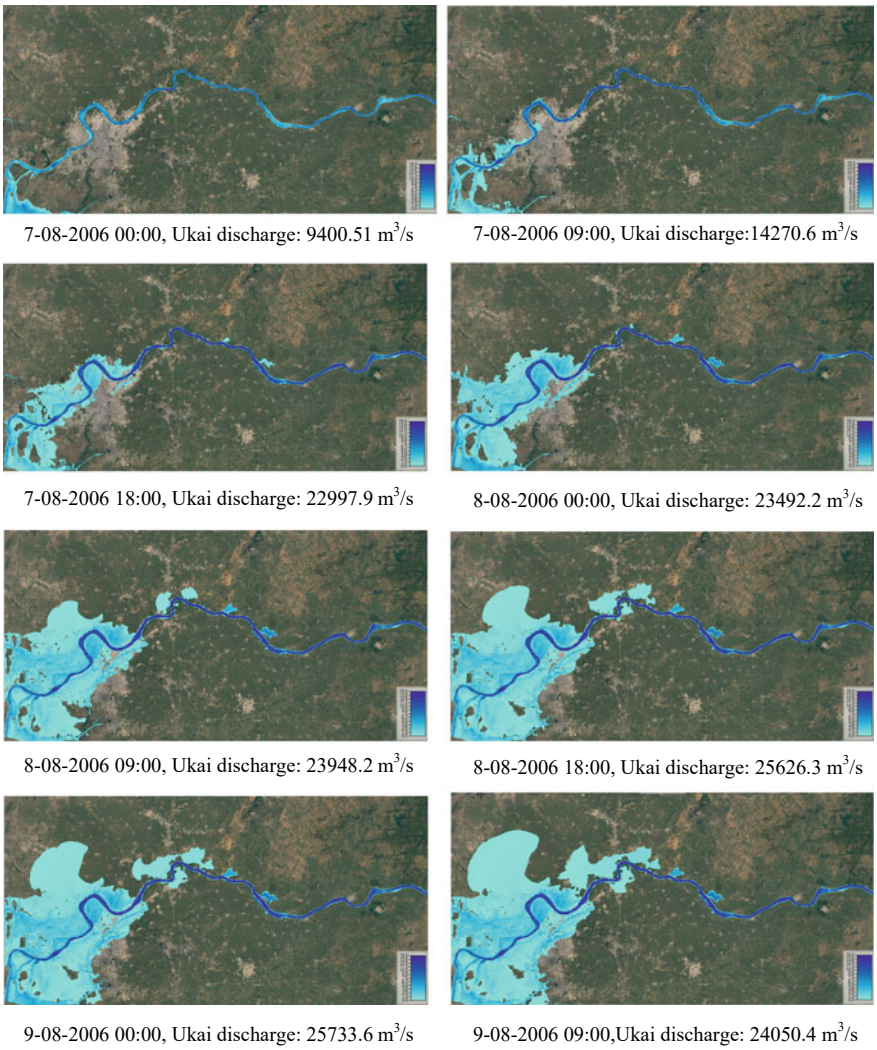

Fig. 7 Simulated flood inundation map of Surat city in 2006 corresponding to the release from Ukai Dam

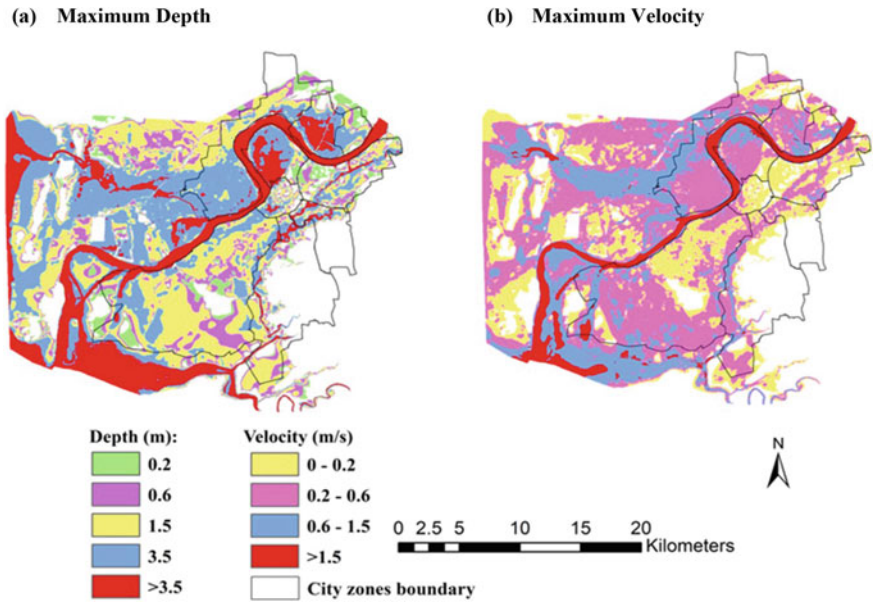

Fig. 8 **a** Flood inundation due to maximum water depth and **b** maximum velocity map for the flood of the year 2006

Table 4 Zone-wise inundation statistics of Surat city for flooding of the year 2006

Zone	No. of cells inundated	Inundated area (km^2)	Area of zone (km^2)	% Inundation
Central zone	7061	6.35	7.78	81.62
East zone	32,070	28.86	33.68	85.68
North zone	33,776	30.39	32.09	94.70
Southeast zone	6214	5.59	18.23	30.66
Southwest zone	111,192	100.07	105.97	94.43
South zone	28,189	25.37	59.75	42.46
West zone	44,597	40.137	47.86	83.86
Total	263,099	236.767	305.36	77.53

Acknowledgements The authors would like to acknowledge CWC Surat; State Water Data Centre (SWDC) Gandhinagar; Ukai Civil Circle, Ukai; (SIC), Surat, SMC, Surat, and NRSC, Hyderabad for providing the required data for the present study. The authors are grateful to the Centre of Excellence (CoE) on 'Water Resources and Flood Management', Sardar Vallabhbhai National Institute of Technology, Surat under TEQIP-II funded by World Bank grant through the Ministry of Education (MoE), Government of India for providing a necessary infrastructural and computational facility for the work.

References

1. Quiroga VM, Popescu IA, Solomatine DP, Bociort L (2013) Cloud and cluster computing in uncertainty analysis of integrated flood models. J Hydroinf 15(1):55–70
2. Salimi S, Ghanbarpour MR, Solaimani K, Ahmadi MZ (2008) Floodplain mapping using hydraulic simulation model in GIS. J Appl Sci 8:660–665
3. Timbadiya PV, Patel PL, Porey PD (2014) One-dimensional hydrodynamic modeling of flooding and stage hydrographs in the lower Tapi River in India. Curr Sci 106(5):708–716
4. Jahandideh-Tehrani M, Helfer F, Zhang H, Jenkins G, Yu Y (2020) Hydrodynamic modelling of a flood-prone tidal river using the 1D model MIKE HYDRO River: calibration and sensitivity analysis. Environ Monit Assess 192:1–18
5. Srinivas K, Werner M, Wright N (2009) Comparing forecast skill of inundation models of differing complexity: the case of Upton upon Severn. Taylor & Francis Group, London, p 25
6. Timbadiya PV, Patel PL, Porey PD (2014) A 1D–2D coupled hydrodynamic model for river flood prediction in a coastal urban floodplain. J Hydrol Eng 20(2):05014017
7. Patel DP, Ramirez JA, Srivastava PK, Bray M, Han D (2017) Assessment of flood inundation mapping of Surat city by coupled 1D/2D hydrodynamic modeling: a case application of the new HEC-RAS 5. Nat Hazards 89(1):93–130
8. Mignot E, Paquier A, Haider S (2006) Modeling floods in a dense urban area using 2D shallow water equations. J Hydrol 327:186–199
9. Quiroga VM, Kure S, Udo K, Mano A (2016) Application of 2D numerical simulation for the analysis of the February 2014 Bolivian Amazonia flood: application of the new HEC-RAS version 5. Ribagua 3(1):25–33
10. Mohammad F, Ayu M, Muhammad SBK (2017) Flood hazard mapping of Palembang City by using 2D model. AIP Conf Proc 1903(1)
11. Gehlot LK, Jibhakate SM, Sharma PJ, Patel PL, Timbadiya PV (2021) Spatio-temporal variability of rainfall indices and their teleconnections with El Niño-Southern oscillation for Tapi Basin, India. Asia Pac J Atmos Sci 57(1):99–118
12. Loliyana VD, Patel PL (2020) A physics-based distributed integrated hydrological model in prediction of the water balance of a semi-arid catchment in India. Environ Model Softw 127:104677
13. Brunner GW (2016a) 2D modeling user's manual. US Army Corps of Engineers, Institute for Water Resources, Hydrologic Engineering Center, pp 1–71
14. Brunner GW (2016b) Combined 1D and 2D modeling with HEC-RAS. US Army Corps of Engineers, Institute for Water Resources, Hydrologic Engineering Center

Unsteady Flood Modelling Using HEC-RAS: Chaliyar River Basin, Kerala

H. B. Shruthi, T. K. Drissia, and Avinash Vasudeo

Abstract Abnormal heavy rainfall in July–August months of 2018 resulted in severe flooding that led to the loss of many lives and damages to properties. Hydraulic simulation models play a vital role in the flood risk management and aid in estimating the flood extent over the flood plain. This paper presents the application of HEC-GeoRAS and HEC-RAS to determine the flood hazard and flood vulnerability of Chaliyar River basin from Kuniyil to Beypore along the 32 km study stretch. The SRTM digital elevation model (DEM) is used to extract the river geometry. Water surface profiles are generated for the unsteady flow simulation and are calibrated using different Manning's values. The result of the analysis indicates the coefficient of determination (R^2) value as 0.99 and 0.76 which indicates a good correlation between the observed and simulated water levels and discharges. Flood inundation maps are developed which identifies the areas at high risk of flooding.

Keywords SRTM DEM · HEC-RAS · HEC-GeoRAS · Flood inundation maps

1 Introduction

Natural calamities are always a threat to humans. Flood is one of the most devastating and frequent natural disaster that claims thousands of lives and causes lot of damages to the properties, communications and transportation all over the world. Flood can be defined as an overflow of water that inundates the land that is normally dry [1]. Flood can occur at irregular intervals that vary in its magnitude, area of extent and duration. Previous studies have shown that rapid urbanization and industrialization

H. B. Shruthi (✉) · A. Vasudeo
Department of Water Resources Engineering, Visveswaraya National Institute of Technology, Nagpur, Maharashtra, India
e-mail: shruthibabu1995@gmail.com

T. K. Drissia
Hydrology and Climatology Research Group, Center for Water Resources and Management, Calicut, India
e-mail: drissia@cwrdm.com

P. V. Timbadiya et al. (eds.), *Flood Forecasting and Hydraulic Structures*, Lecture Notes in Civil Engineering 340, https://doi.org/10.1007/978-981-99-1890-4_5

combined with the climate change fuelled by the greenhouse gases account for a strong tendency towards the extreme precipitation. The extreme weather can lead to the risk of flooding. With the increase in population and developmental activity, there has been a tendency to occupy in the floodplains which resulted in more severe risk over the past few years. With significant increase in risk over the years, there is an urgent need for collaborative, long-term approaches to mitigate the future impacts. This cannot be eradicated but somehow has to be managed. Flood risk management is therefore necessary to reduce the impact of flood events and predict the future flood hazard.

Flood modelling, an advanced method in river engineering stream, is an important tool in the assessment of flood risk, both for flood hazard and flood vulnerability. It is used to define flood warning areas and forecasting the water levels for flood event management [2]. GIS is an integral part of flood modelling to map the flood-prone areas. GIS along with mathematical models has proved to be very effective in flood risk management studies. Hydraulic models help to predict where flooding might occur, how severe it might be and this can assist the planners and policymakers to impose the necessary mitigation measures [3]. Among the many models available, HEC-RAS is a frequently used open-source software. The research aims to study about the Chaliyar, which was one among the severely affected rivers that caused flash floods disrupting the normal life and created havoc in several parts of the district in 2018.

Many flood management studies have been conducted in different parts of the world using different methods. HEC-RAS model was applied to a case study focused on identifying the vulnerable areas which are prone to hydrologic risk is conducted in the Ozana drainage basin, Romania to create management plans for emergency situation [4]. Determination of Manning's value is an influential task in the hydraulics of open channel flow [5].

HEC-RAS 5.0.7 version is used in the present research. It helps in hydraulic modelling with the help of HEC-GeoRAS, which is an extension of the Arc-GIS software to create the geometric file for importing to HEC-RAS. Kerala experienced an unprecedented heavy rainfall from 1/6/2018 to 19/8/2018. Chaliyar River had experienced worst flood in 2018 which led to severe losses and damages. About 600 families lost their homes and farms [6]. The main objective of the study is to analyse the river characteristics and understand the dynamics of Chaliyar River basin, Kerala, from June–August months of 2018 using HEC-RAS software and to generate flood inundation maps of the study area.

2 Study Area and Data Source

2.1 Chaliyar River Basin

Chaliyar River is the fourth longest river in Kerala. It originates in the Western Ghats of Elambari Hills in the Wayanad plateau of Kerala. Chaliyar is also named as Beypore River as it joins the Lakshadweep Sea at Beypore in the downstream. The major portion of the river flows along the northern boundary of Malappuram District (through Nilambur, Mambad, Edavanna, Areacode and Feroke) and a small portion of it flows through Kozhikode District. The location of Chaliyar River is shown in Fig. 1.

Chaliyar River basin in Kerala, India, situated between 11° 30′ N and 11° 10′ N latitudes and 75° 50′ E and 76° 30′ E longitudes fall in the Survey of India (SOI) top sheets 58A and 49M. River is about 169 km in length. The total drainage area of the river covers 2923 km^2 out of which 2535 km^2 lies in Kerala, and the rest 388 km^2 falls in Tamil Nadu. The river has an elevation of 2066 m above the MSL. On an average about 3012 mm rainfall occurs annually in the basin [7]. The important sub-basins of Chaliyar River include Cherupuzha, Kanjirapuzha, Iruvenjipuzha, Chalipuzha, Maruthapuzhza, Punnapuzha, Karimpuzha, Kuthirapuzha and Kuniyil. These constitute Chaliyar River drainage system. Other important tributaries are Kurumanpuzha, Pandipuzha, Maradipuzha and Karakkodupuzha.

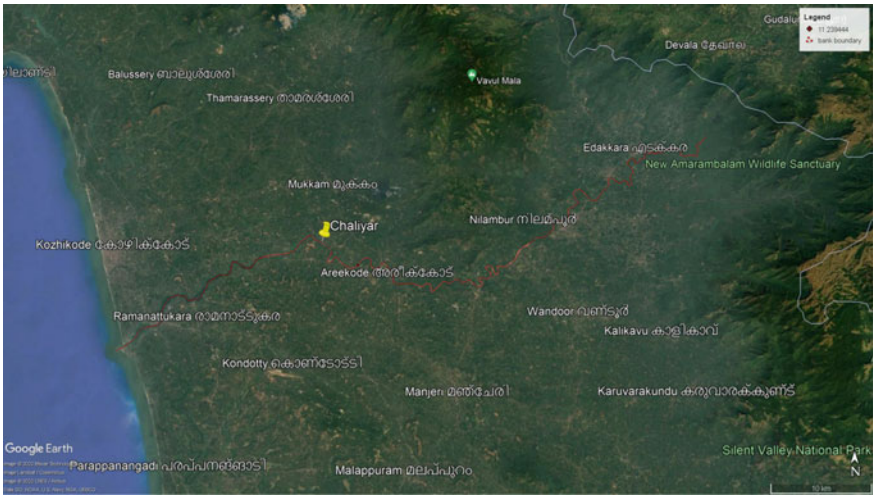

Fig. 1 Location of Chaliyar River. *Source* USGS Earth Explorer

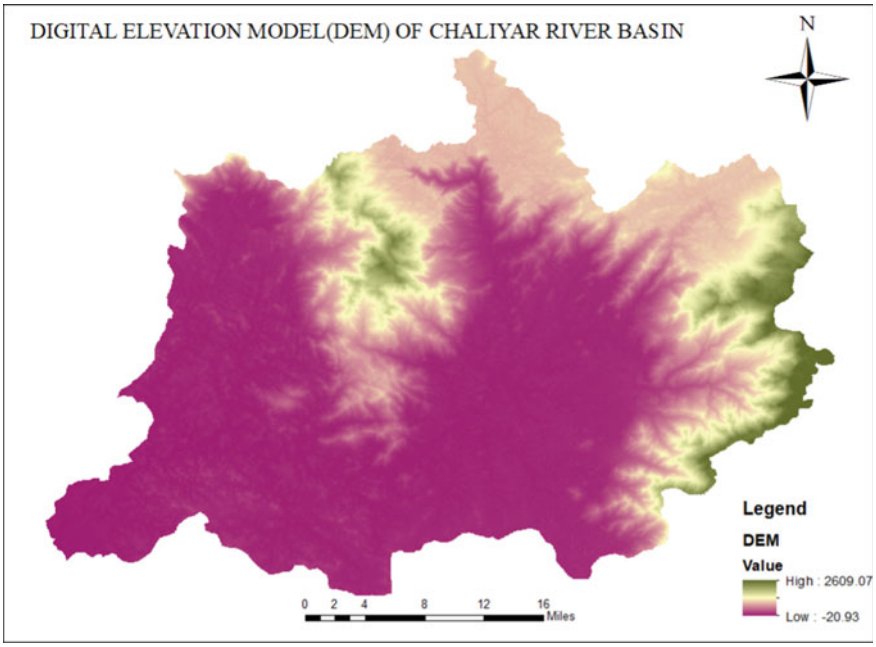

Fig. 2 Digital elevation model of Chaliyar River basin

2.2 Data Used

2.2.1 Digital Elevation Model

Digital elevation model (DEM) is a digital model or 3D representation of topographic surface of the earth. Owing to its reasonable accuracy and free-of-cost availability, a 30 m resolution DEM, which is available from Shuttle Radar Topography Mission (SRTM) has been used to delineate the boundary of the watershed, to define sub-catchment boundaries and a stream network and to analyse the drainage patterns of the watershed. The basic information on the physiographic characteristics, like elevation and slope, were extracted from SRTM DEM downloaded freely from USGS earth explorer. The no data cells or voids in the DEM were filled by interpolating in automatic way using raster functions. The boundary of the study area was used to clip the DEM of the study area as shown in Fig. 2. The elevation of watershed ranges from 20.93 to 2609 m.

2.2.2 Stream Flow Data

In the present study, daily discharge data [8] of Kuniyil gage station has been used for analysing the trend of discharge in the study area. Figure 3 represents the line diagram

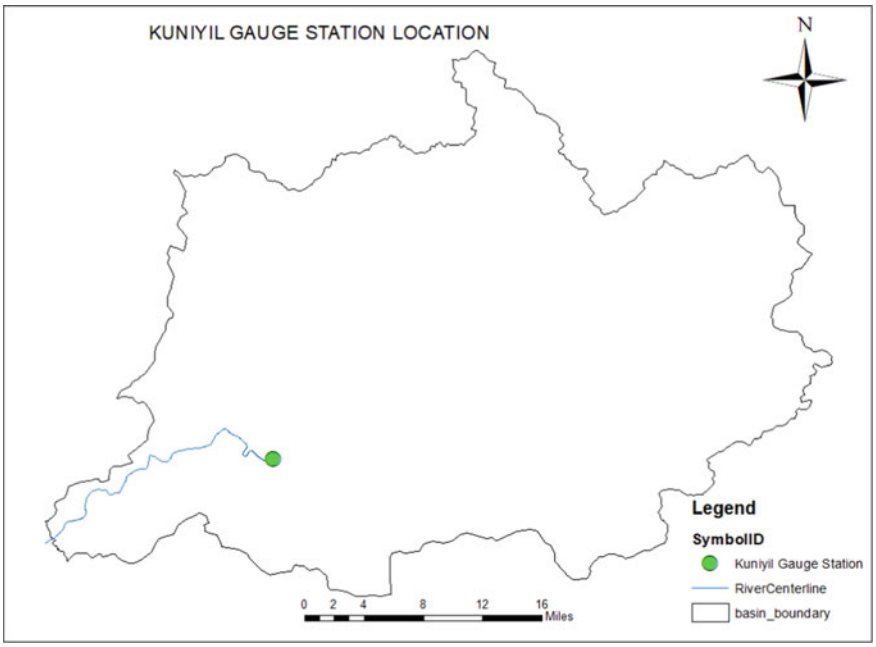

Fig. 3 Line diagram showing Kuniyil gauge station

showing Kuniyil gauge station. Daily stream flow data of Kuniyil gauge station was collected from CWRDM, Calicut. The three monsoon months (June–August) of 2018 were used in the study for hydraulic modelling as majority of annual rainfall in India occurs during this period. From the collected data, a peak flow of 3236 Cumecs was observed in 16 August 2018 and the water level was recorded as 10.16 m as shown in Fig. 4.

3 Methodology

The methodology for developing a flood inundation map for a river includes three main stages: pre-processing, processing and post-processing of data (Fig. 5).

The basic computational procedure is based on an iterative solution of one-dimensional energy equation (Eq. 1) called the standard step method. Water surface profiles are computed from one cross sections to the next by solving the energy equation which is written as follows:

$$Z_2 + Y_2 + \left(a_2 V_2^2\right)/2g = Z_1 + Y_1 + \left(a_1 V_1^2\right)/2g + h_e \quad (1)$$

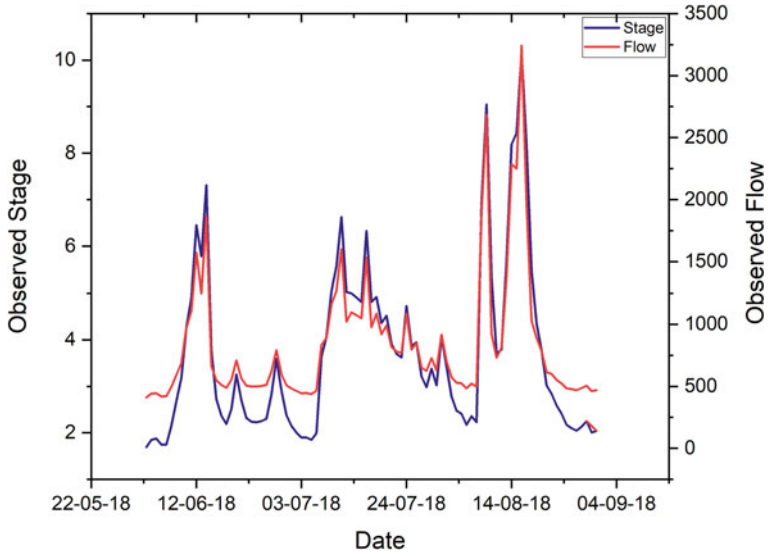

Fig. 4 Graph showing the variation of observed stage and flow values at RS 35,290.29 during June–August 2018

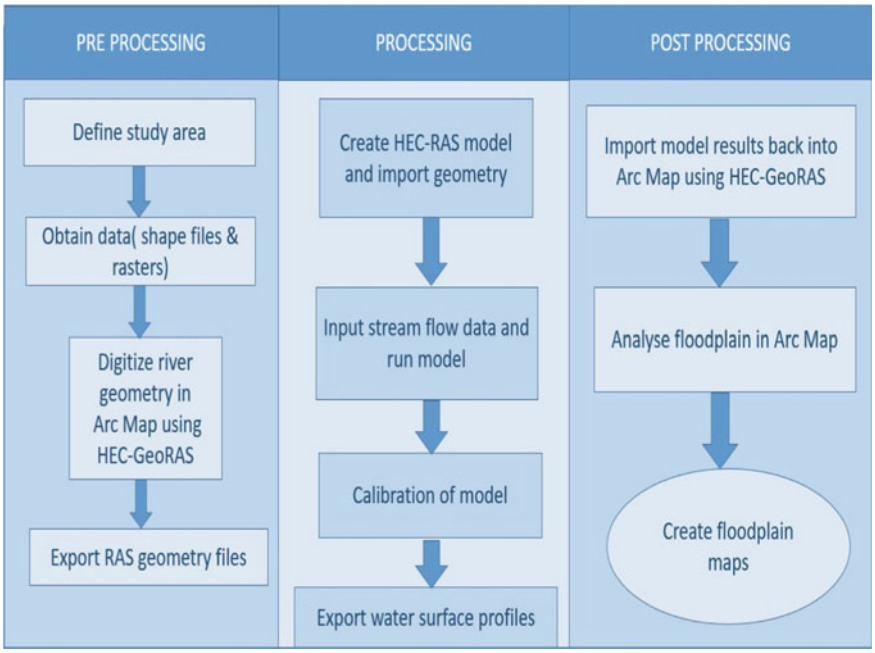

Fig. 5 Methodology involved in the study

where Z_1, Z_2 = elevation of the main channel inverts, Y_1, Y_2 = depth of water at cross sections, V_1, V_2 = average velocities (total discharge/total area), a_1, a_2 = velocity weighing coefficients, g = acceleration due to gravity.

The energy loss term h_e in equation (1) includes friction loss h_f and form loss h_0 [9].

3.1 Development of HEC-RAS Model

The US Army Corps of Engineers' River Analysis System (HEC-RAS) developed by Hydrologic Engineering Centre is an integrated software that helps in performing one-dimensional steady and unsteady, gradually varied flow river hydraulics calculations, sediment transport, mobile bed computations, water quality analysis, water temperature modelling and several hydraulic design computations. It helps in the mixed flow regime analysis, allowing both subcritical and supercritical flow regimes in a single run [9].

Unsteady flow analysis is used in the study. For an unsteady flow simulation in HEC-RAS, a plan is created which comprises of a geometric data and a flow data. Geometric data have been developed by drafting the river schematically along the direction of flow using HEC-GeoRAS, an extension of ARC-GIS. Pre-processing involves the creation of river attribute system layers such as river centreline, river bank lines and river flow path lines. The digitization of river is carried out from the upstream to downstream of the study stretch, i.e. from Kuniyil to Beypore along the 32 km study reach. Flow path lines are drawn at a buffered distance of 1 km from the bank lines. XS cut lines should be perpendicular to the direction of flow and oriented from left to right as shown in Fig. 6. This forms the geometry file which is to be exported into HEC-RAS software for the model execution as shown in Fig. 7.

3.2 Model Execution

The geometry file created in ArcMap was exported into HEC-RAS for the processing stage. One-dimensional unsteady flow is performed. A horizontal coordinate projection within HEC-RAS was established. Geometry data and flow data are the main input parameters needed for the hydraulic simulation. Geometry data includes all the information related to elevation data, cross-sectional data, reach length, bank stations, stream junctions and energy loss coefficients. Flow data comprises of the daily stream flow and water level data of Kuniyil gauge station from June–August (monsoon months) of 2018 as majority of annual rainfall in India occurs during this period. A plan is created which includes the geometry data and flow data.

Stage and discharge hydrograph of Kuniyil gauge station for June–August 2018 is given as the upstream boundary condition as unsteady flow analysis is performed. Missing flows were interpolated automatically in HEC-RAS. Normal depth of 0.01 is

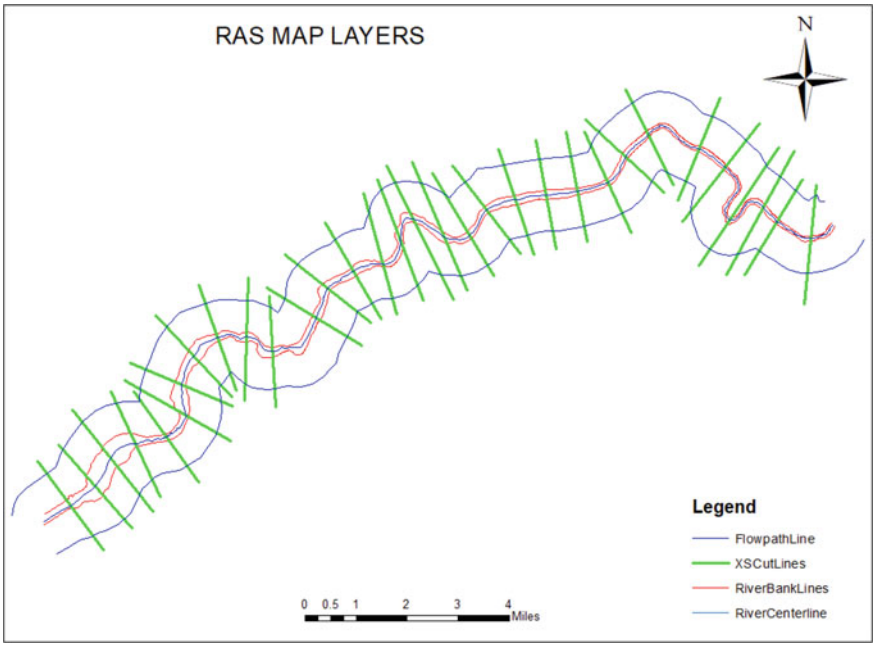

Fig. 6 RAS layers created in ArcMap using HEC-GeoRAS

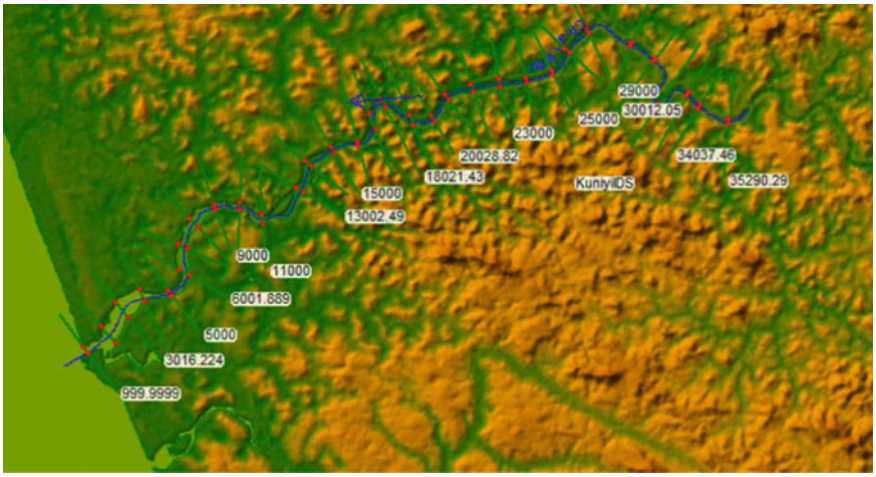

Fig. 7 RAS geometry file imported from HEC-GeoRAS

given as the downstream boundary condition. Flow to be simulated is called a profile. The coefficient of contraction and expansion is given as 0.1 and 0.3, respectively [10].

3.3 Calibration of the Model

High degree of uncertainty exists in floodplain modelling studies due to the complexity in modelling process, parameters and lack of data. As a result, calibration of a river hydraulic model is vital in floodplain management studies. Calibration is the comparison between the observed and simulated values. It helps in checking the accuracy of the model. Manning's roughness coefficient n plays a vital role in the model calibration [11]. Change in Manning's value can affect the stream flow simulation significantly. The major factors affecting the selection of n are (1) type and size of the channel material (2) shape of the channel (3) irregularities of channel (4) vegetation (5) obstructions [12].

HEC-RAS model was calibrated for predicting the discharge and water levels, thereby finding a value of Manning's coefficient for the channel and the banks. The Manning's values were altered continually from 0.02 to 0.085 until the variations between the observed values, and simulated values are within the acceptable limits. It was found that the best match between the measured and simulated flow came at a Manning's value of 0.08 for the channel and 0.085 for the banks. The coefficient of determination (R^2) was evaluated to check the accuracy of the model [5].

4 Results and Discussions

Initially, river lines, riverbanks and flow paths are digitized in Hec-GeoRAS. We generated cross sections at an interval of 1 km throughout the 32 km stretch. The geometric data are then exported to HEC-RAS. For a mixed flow regime both the downstream and upstream boundary conditions are required. Stage and flow hydrograph of Kuniyil station for the period from June to August 2018 are given as the upstream boundary condition and normal depth of 0.01 as downstream boundary conditions. The contraction coefficient is fixed to 0.1, and the coefficient of expansion is fixed to 0.3, respectively. Unsteady flow analysis was performed to get the final output. The flow characteristics like the depth of the river, velocity of flowing river, water surface elevation and flow area can be obtained from the simulated flow in the form of tables and plots. The following section gives the details of the calibration and evaluation of the model.

4.1 Model Calibration and Evaluation

HEC-RAS model was calibrated for predicting the discharge and water levels, thereby finding a value of Manning's coefficient for the channel and the banks. We calibrated the model by altering Manning's coefficient continually from 0.02 to 0.085 until the variations between the observed values and the simulated values were within the acceptable limits. Figure 8 shows the variation of stage and flow values of the calibrated model from June to August 2018 at RS 35,290.29. Maximum flow of 3243.94 Cumecs and stage value of 10.16m are obtained at RS 35,290.29 on 17 August 2018 at the middle downstream of the river. For determining the accuracy of the simulated model, coefficient of determination (R^2) value was evaluated using regression analysis between the observed and simulated values of water levels and discharges as shown in Fig. 9a, b. The coefficient of determination value was found to be 0.99 and 0.76 for the water levels and discharges at Manning's values of 0.08 at the channels and 0.085 at the riverbanks as shown in Table 1. This indicates that the selected Manning's value gives an acceptable match between the observed and simulated data.

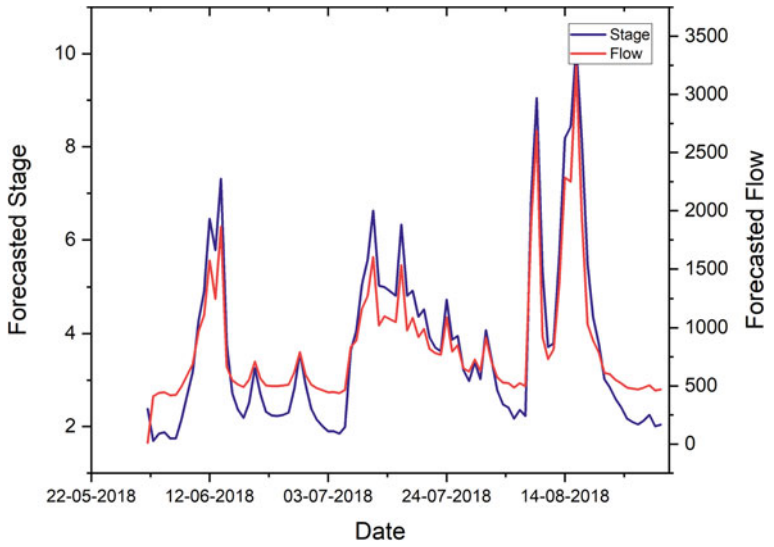

Fig. 8 Graph showing the variation of forecasted stage and flow values at RS 35,290.29 during June–August 2018

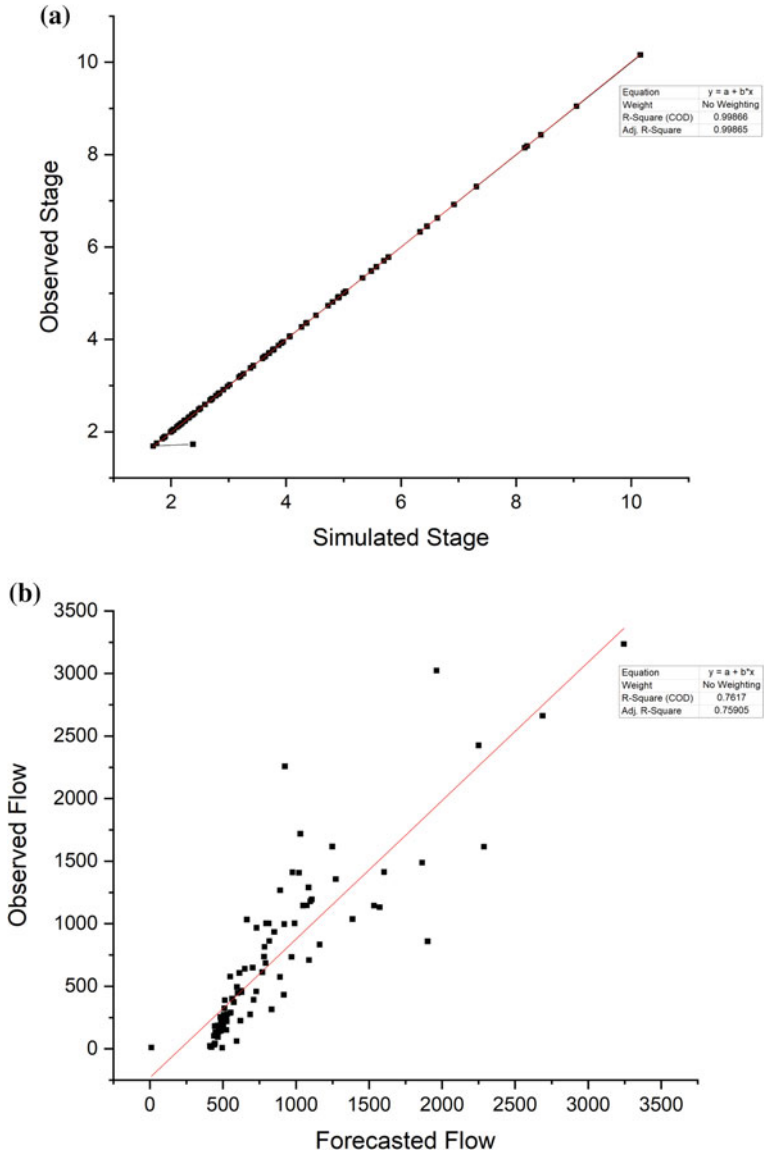

Fig. 9 Observed versus simulated measurements of **a** Water level **b** Discharge from June–August 2018 at RS 35,290.29

Table 1 Evaluation of performance of the model

Simulated flow parameters	Coefficient of determination (R^2)
Discharge	0.76
Water level	0.99

4.2 Flow Characteristics Profiles

Flow characteristics profile plots like flow area profile, water surface elevation profile, depth are plotted for the calibrated results during June–August 2018. Figure 10 represents the distribution of flow areas along the main channel distance on 17 August 2018 as maximum water surface elevation is obtained on that day. Flow area is found to be maximum at the RS 23,000, RS 19,208.23 and RS 12,213 at the middle downstream which is around 14,144 m^2 at a distance of about 22 km from Beypore. Mavoor, Peruvayal and Aayamkulam are likely to be the places which experience maximum flow area. Figure 11 represents the variation of flow along the main channel distance. Maximum flow of 3243.94 Cumecs is observed at RS 35,290.29 at the middle downstream of the river.

The *XYZ* perspective of the simulated inundation boundary of the study reach on 17 August 2018 is shown in Fig. 12.

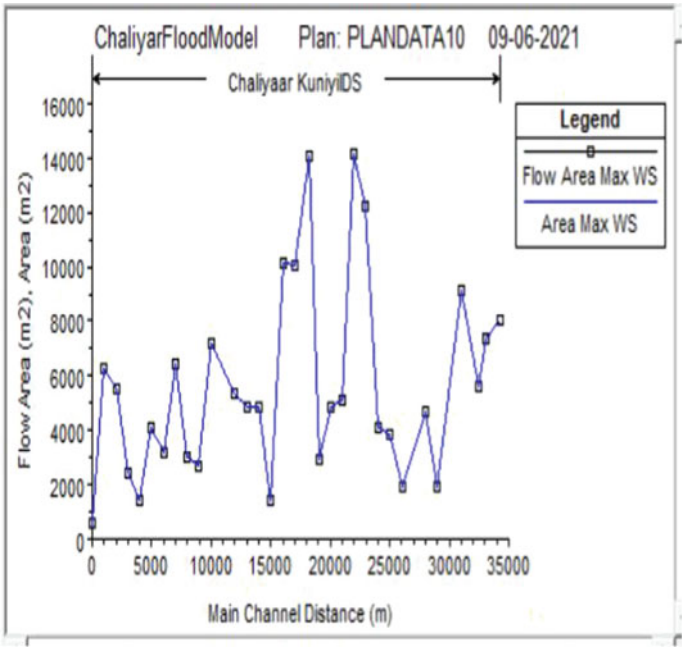

Fig. 10 Flow area profile plot on 17 August 2018

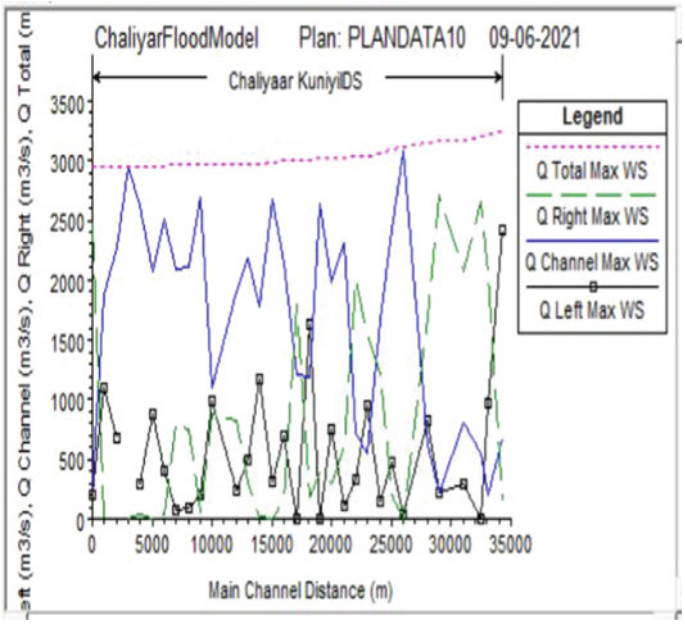

Fig. 11 Flow rate profile plot on 17 August 2018

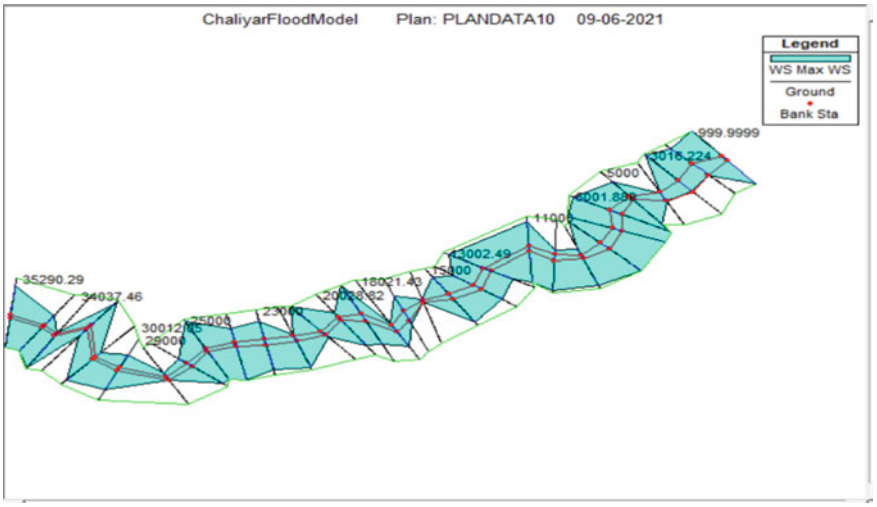

Fig. 12 *X*–*Y*–*Z* water surface profile plot on 17 August 2018

4.3 Floodplain Mapping

One-dimensional HEC-RAS model was set up to generate the water level and stream flow of the study area for the monsoon months from June–August 2018 and are analysed in 2D for preparing the flood inundation maps. The results of HEC-RAS model are viewed on RAS mapper and are exported to HEC-GeoRAS for the generation of flood inundation maps. Model results indicate that maximum value of water surface elevation for all the 32 cross sections and the nearby places were obtained on 17 August 2018. Figure 13 represents the flood inundation boundary showing the places which are severely affected on 17 August 2018 which includes Vazhakkad, Kodiyathur, Kizhupparamba, Mavoor, Vilayil and Cheekode. Table 2 shows the maximum water surface elevation values of the places which are severely affected on 17 August 2018. Figure 14 shows the flood map for maximum water surface elevation of 32 cross sections with the maximum water surface elevation obtained at the RS 35,290.29 at around 10.2 m from the MSL. The collected information from various newspapers of the 2018 flood was found to be same. These same places were flooded in 2018 flood between Beypore and Kuniyil. Table 3 shows the comparison of the observed and simulated water levels and stream flow values at the RS 35,290.29.

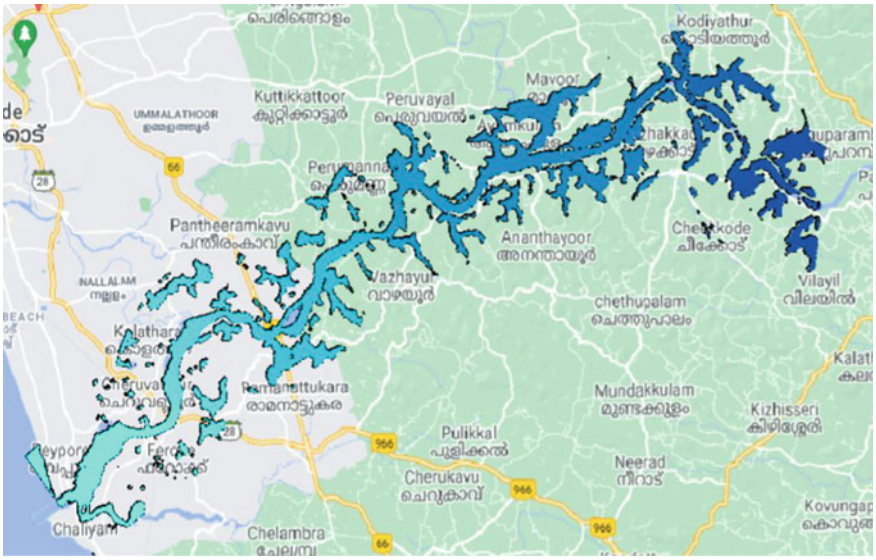

Fig. 13 Flood inundation boundary on 17 August 2018 (view on Google Maps)

Table 2 Water surface elevation values from the simulated model when viewed on RAS mapper

Nearby places that are severely affected	Maximum water surface elevation (m) on 17 August 2018
Kizhupparamba	13.864
Cheekode	13.862
Vilayil	10.152
Kodiyathur	8.862
Vazhakkad	8.845
Mavoor	7.096
Aayamkulam	6.553
Peruvayal	5.785

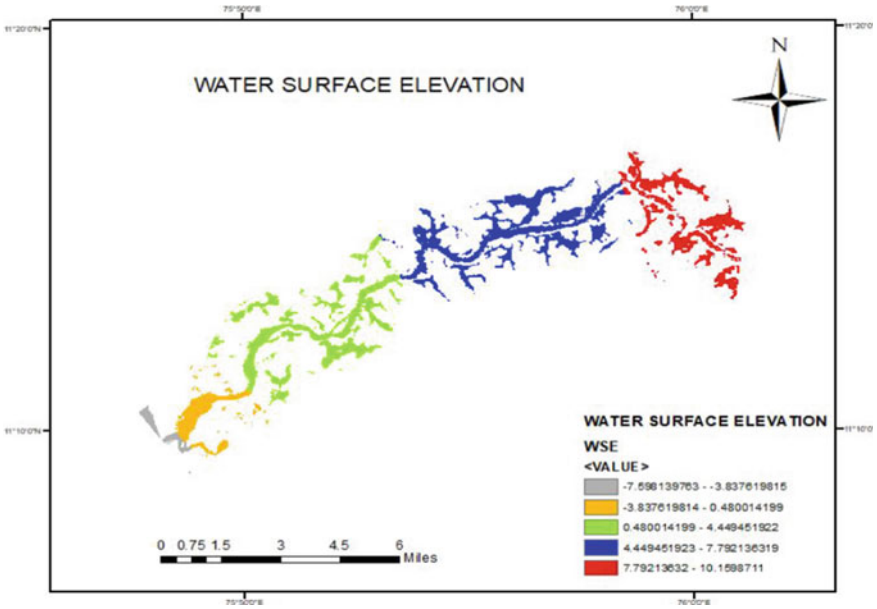

Fig. 14 Flood map showing maximum water surface elevation on 17 August 2018

Table 3 Comparison of observed and simulated water level and stream flow values at RS 35,290.29

Data	Water levels in m	Stream flow in Cumecs	Date of peak value
Observed	10.16	3236	16 August 2018
Simulated	10.16	3243.94	17 August 2018

5 Conclusion

Hydraulic model was developed using HEC-RAS software to analyse the flow characteristics and map the inundated area along the Chaliyar River during June–August months of 2018 between Beypore and Kuniyil. The model was used effectively in simulating water surface elevation and stream flow values for all the 32 cross sections. The maximum value of water surface elevation and stream flow was obtained at RS 35,290.29 on 17 August 2018. The coefficient of determination of the model was evaluated by regression analysis between the observed and simulated water levels and discharges. Coefficient of determination (R^2) value for the model was obtained as 0.99 and 0.76 for water level and discharges at a calibrated value of Manning's constant 0.08 at the channel and 0.085 at the riverbanks. The high values of Manning's coefficient may be due to the medium to dense bushes present in the floodplain [13]. The coefficient of determination was found which tells that the performance of the model is good. Flood inundation maps are prepared that helped to identify the critical areas along the Chaliyar River. The results can be useful for the decision makers and urban planners for flood management and related studies. Some degree of uncertainty exists in the model was not validated in 2D as no historical flood maps were available for the study area. The model strongly suggests the need for more research into methods for validation of this hydraulic model with a good satellite imagery, although the overall calibration results are encouraging and acceptable.

Thus, flood modelling using HEC-RAS provides an effective and efficient method for various hydraulic studies.

Acknowledgements The authors wish to acknowledge the Centre for Water Resources and Management, Calicut, Kerala, for providing technical support and relevant data needed for the successful completion of the research.

References

1. Patel DP, Ramirez JA, Srivastava PK, Bray M, Han D (2017) Assessment of flood inundation mapping of Surat city by coupled 1D/2D hydrodynamic modeling: a case application of the new HEC-RAS 5. Nat Hazards 89(1):93–130. https://doi.org/10.1007/s11069-017-2956-6
2. Mangukiya N, Yadav S (2021) Integrating 1D and 2D hydrodynamic models for semi-arid river basin flood simulation. Int J Hydrol Sci Technol 1(1):1. https://doi.org/10.1504/IJHST.2021.10035928
3. Patel (2016) Floodplain delineation using HEC-RAS model—a case study of Surat city. Modern J Hydrol 6:34–42
4. Iosub M, Enea A, Hapciuc OE, Romanescu G, Minea I (2014) Flood risk assessment for the Ozana river sector corresponding to Leghin village, Romania. In: 14th SGEM GeoConference on water resources. forest, marine and ocean ecosystems, SGEM2014 conference proceedings, ISBN 978-619-7105-13-1/ISSN 1314-2704, June 19–25, Vol 1, pp 315–322
5. Abbas SA, Al-Aboodi AH, Ibrahim HT (2020) Identification of manning's coefficient using HEC-RAS model: upstream Al-Amarah barrage. J Eng 2020:7. Article ID 6450825

6. Riswana KP, Seethara Beegam CR (2019) Tale of tears: development and flood experience of Chaliyar Grama Panchayath, Malappuram. J Compos Theory. ISSN: 0735-6755
7. Anitha AB, Shahul Hameed A, Narasimha Prasad NB (2014) Integrated river basin master plan for Chaliyar. In: International symposium on integrated water resource management CWRDM, Kozhikode, Kerala, India
8. CWC (2018) Daily discharge data. Central water commission, Government of India
9. HEC-RAS User Manuel (2008) Davis version 4.0, US Army Corps of Engineers, Hydrologic Engineering Center, Davis, CA, USA
10. Sunil Kumar P, Varghese KO (2017) Flood modelling of Mangalam river using GIS and HEC-RAS. Int J Adv Res Sci Eng 6(6). ISSN: 2319-8354
11. Ding Y, Jia Y, Wang SSY (2004) Identification of Manning's roughness coefficients in shallow water flows. J Hydraul Eng 130(6):501–510
12. Shamkhi MS, Attab ZS (2018) Estimation of Manning's roughness coefficient for Tigris River by using HEC-RAS model. WASIT J Eng Sci 6(3):90–97
13. Chow's book "Open-Channel Hydraulics" Textbook. USACE (2002) HEC-RAS river analysis system, hydraulic reference manual, U.S Army Corps of Engineers (USACE). Accessed 10th Aug 2015

2D Flood Simulation and Mapping Using Hydraulic Model and GIS Technology

Anant Patel, Neha Keriwala, and S. M. Yadav

Abstract Massive property damage and loss of life have resulted from flooding, which is a common occurrence in many regions of the world, particularly in the developing world. A flood occurs when water from a stream or river overflows its banks and submerges normally dry terrain. Future development and flood mitigation methods rely heavily on understanding flooding behavior and hydraulic features of rivers. The main objective of the research is to simulate the flood event for Lower Narmada River Basin and develop inundation maps. A hydraulic model was utilized in this research to examine a variety of physical variables that are critical to water movement in the river. A digital elevation model (DEM) was used for geometry data generation in ArcGIS, a Geographical Information System (GIS) program, is used to segment the research region for the hydraulic model. Because of this, it makes use of a hydraulic model developed by Hydrologic Engineering Center (HEC-RAS). HEC-GeoRAS is an intermediary module that allows data to be migrated between ArcGIS and HEC-RAS. Flood inundation maps are generated by adding flow data into a model once the necessary geometrical and hydraulic structural data have been gathered and compiled as needed. As a result of hydraulic modeling, flood depth and

A. Patel (✉) · N. Keriwala
Department of Civil Engineering, School of Engineering, Institute of Technology, Nirma University, Ahmedabad, Gujarat 382481, India
e-mail: anant.patel@nirmauni.ac.in; anant.patel14@gmail.com

N. Keriwala
e-mail: keriwalaneha@gmail.com

A. Patel · S. M. Yadav
Department of Civil Engineering, Sardar Vallabhbhai National Institute of Technology, Surat 395007, India
e-mail: smy@ced.svnit.ac.in

P. V. Timbadiya et al. (eds.), *Flood Forecasting and Hydraulic Structures*, Lecture Notes in Civil Engineering 340, https://doi.org/10.1007/978-981-99-1890-4_6

velocity are also determined. It is necessary to consider flood inundation, depth, and velocity statistics in order to identify flood-prone regions. By using the information from this study, we may better prepare for floods by building an embankment, a flood wall, and other flood mitigation measures. Hydrologists and water resources engineers may utilize the results and findings to plan and develop using the HEC-RAS model, which has excellent performance.

Keywords HEC-RAS · Flood · Narmada River · Hydraulic model · DEM

1 Introduction

Natural disasters, such as flash floods, storm surge, and tidal flooding, are an obvious consequence of human interference in the water cycle, a discovery which has had a major impact on planning and research, and the realization that traditional drainage systems aren't adequate for sustainability goals under new social and environmental conditions [1]. In the meaning of "flowing water," the term "flood" may also be used to the intrusion of the tide. A flood is defined as an overflow of water that completely covers territory that is normally dry. Riverine floods, storm runoff floods, cyclonic floods, and meteorological floods all constitute urban floods. The science of hydrology devotes a portion of its curriculum to the study of floods, which are also a major cause for concern in the fields of agriculture, civil engineering, and public health. New standards and architectural principles have been adopted since the 1990s to try to reduce the effect of runoff and floods on cities [1, 2]. Cities face serious risks due to flooding, which have substantial repercussions on society, the economy, and the environment. A few indicators are predicting an increase in these problems. Forecasting channel flows or river levels at different sites is an essential part of flood warning, but the difference between flood forecasting and "flood warning" is the challenge of using these predictions to inform choices about flood alerts.

The increase in urban populations will result in more people being vulnerable to floods. More flooding occurs because it decreases infiltration and allows the hydrological response to occur more quickly, decreasing the natural storage areas [3]. Another important thing is that economic development helps enhance the value of exposed assets. Additionally, severe rainfall is predicted to increase in many areas of the globe [4].

Others concentrate on resilience, while others focus on robustness in flood risk management [5]. Butler et al. [6] proposed a combined strategy for urban water systems that focused on service failure. It included sustainability, resilience, and dependability. We believe that what makes cities resilient in the face of flooding goes beyond the traditional definition. When looking at it from our perspective, we consider "urban flood resilience" to be the ability of an urban system to be able to resist, absorb, accommodate, adapt to, transform, and recover from flooding [7].

The main rainy season in India occurs during the summer monsoon, which lasts from June to September. Indian summer monsoon rainfall (ISMR) forecasting is in

great demand because of the country's large variability, which has a major effect on the economy. Floods often result in huge numbers of people being killed or injured, as well as extensive property damage. To create flood inundation maps for Narmada River in Bharuch, Gujarat, the project's goal is to gather data.

Each year, billions of dollars in infrastructure and property damage are incurred as a result of this natural catastrophe, and hundreds of people are killed. Flood inundation maps can provide the public with accurate information about flood risk, which may help avoid and minimize these dangers and costs.

A digital elevation model (DEM) generated by ArcGIS, a Geographical Information System (GIS) program, is used to segment the research region along the river for the hydraulic model. The hydraulic model is created using HEC-RAS software. HEC-GeoRAS is an intermediary module that allows data to be migrated between ArcGIS and HEC-RAS.

For flood damage estimate maps and flood risk maps, Geographic Information Systems (GIS) are effectively utilized to show the extent of flooding. To predict flood profiles with a particular return time, the GIS must be utilized in conjunction with a hydraulic technique. This program, created by the US Army Corps of Engineers' Hydrologic Engineering Center River Analysis System (HEC-RAS), is extensively used in Europe and the USA. In 1998, it was used for the first time on the Bartin River. Using the River Analysis System (RAS), Hydrologic Engineering Center (HEC) in Davis, California, helped hydraulic engineers better understand channel flow and determine floodplain. Many data input options, hydraulic analysis components, data storage, and administration capabilities as well as graphing and reporting tools are all part of the package. Many government organizations and commercial companies have accepted HEC-RAS because of its advantages, including backing from the US Army Corps of Engineers, ongoing improvements, and acceptance by the general public. It's in the public domain, has undergone peer review, and can be obtained for free by visiting the HEC website. In addition to consultancy services and add-on software, a number of private businesses have registered as recognized "vendors." Some of the malware is also distributed in areas where access to US Army websites is restricted. Hydraulic analysts and scientists should have no problem using the direct download from HEC, which contains comprehensive documentation.

For simulating and calculating water surface profiles in open channels, HEC-RAS is a computer software. Floodplain management and flood insurance studies use HEC-RAS to assess encroachments on floodways. Bridge and culvert design and analysis, levee studies, and channel alteration studies are a few of the other applications. Other modeling techniques are now more generally recognized for dam breach analysis, although it may be utilized. The building of rivers dams may offer significant advantages, such as the provision of drinking water and agricultural water, but the consequences of their collapse might be devastating. They vary significantly based on the area flooded and the number of people who are at danger. Several techniques have been used to model streamflow and floods, including empirical methods, data-driven models [5], system dynamics models, [8, 9] and remote sensing techniques [10]. On flat topography with huge flood extents, 2D models perform better than 1D models if adequate data is provided. In this context, this article provides a

useful methodology for improving the decision support systems by adapting different non-structural mitigation measures techniques especially flood inundation mapping using hydraulic model using GIS technology to meet decision-maker requirements [11, 12]. This chapter focuses on research being conducted for Bharuch, which is situated in the lower basin of the Narmada River. This research will aid in the development of an emergency action plan for the evacuation of the general population, as well as in minimizing property damage.

2 Study Area and Data Source

The Narmada River is an originating in eastern Madhya Pradesh's Anuppur District Shahdol zone called the Narmada Kund, situated near Amarkantak on the Amarkantak Plateau. The river flows from Sonmud to Kapildhara waterfall, where it plunges over a cliff, before continuing on a winding path among the rocks and islands to the ruins of Ramnagar's palace. The river then makes a tight loop to the northwest and heads into Jabalpur. After a 9-m drop into a deep tight channel between magnesium limestone and basalt rocks known as the Marble Rocks in this city, it runs for 3 km in a wide channel. From a height of around 90 m, it is merely squeezed in this channel of 18 m. Ahead of the Arabian Sea's sand dunes The Narmada basin covers 98,796 km^2 and is located between east longitudes of 72° 32′ to 81° 45′ and north latitudes of 21° 20′ to 23°. It is boxed in by the Vindhya and Satpura mountains (Fig. 1).

The Narmada basin covers 98,796 km^2 and is located between east longitudes of 72° 32′ to 81° 45′ and north latitudes of 21° 20′ to 23°. The Narmada-Bharuch-Vadodara basin contains five distinct physiographic zones, with the lower plains including most of these areas. The study region includes the Narmada River's lower basin which covers the 8904 km^2. This lower basin covers the downstream of the Saradar Sarovar Dam. There is important hydraulic structure also available in the downstream of the dam which is Garudeshwar weir. It is the subcontinent's fifth-largest river. It's one of the country's few west-to-east rivers. Through the states of Madhya Pradesh, Maharashtra, and Gujarat it runs its course.

2.1 Methodology

According to several studies, planning may be effective in flood-resilient cities because it makes use of flood risk reduction methods in developing plans and integration can offer a way of resistance to flood impact and building up adaptation to flood risk by never fully avoiding flood. Disaster mitigation formerly relied heavily on development planning [10]. To fight floods, it is possible to take a "hard" strategy like building a levee or a flood dam [11, 13, 14]. These initiatives would make flood defenses stronger and reduce the chance of floods [15]. Similarly, better planning will

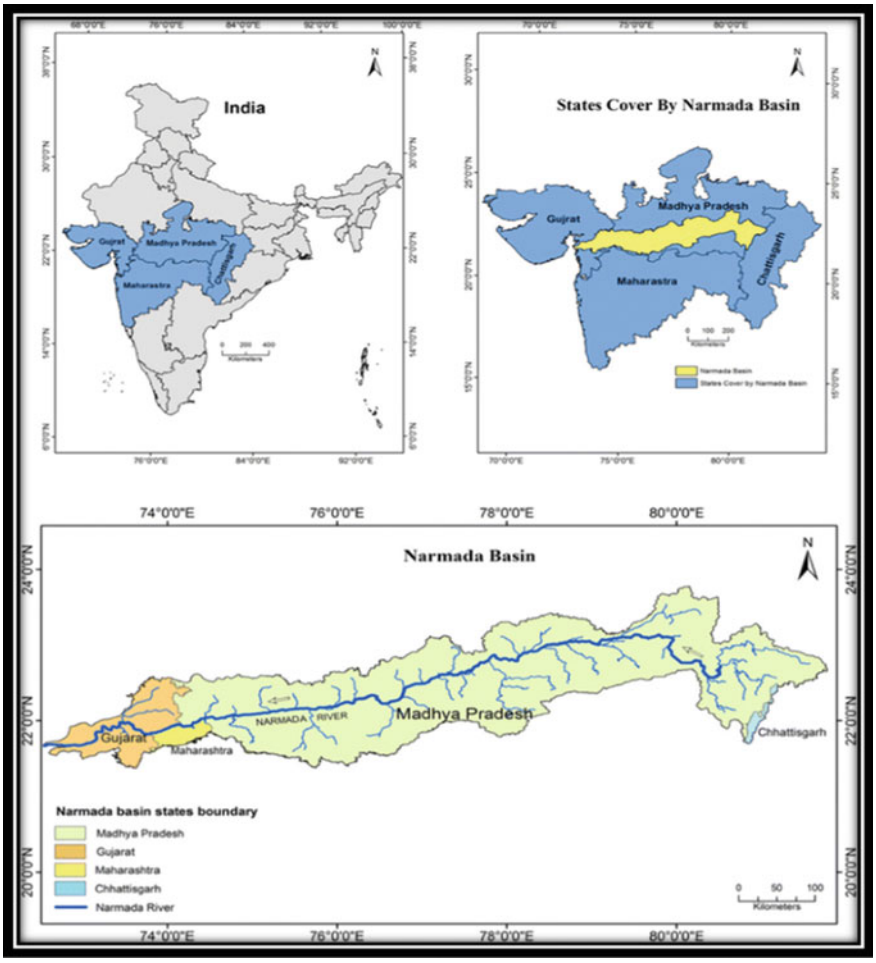

Fig. 1 Study area map of Narmada River Basin

encourage land use management and development control, which will in turn reduce risk [16–18]. The increase in flood protection measures [19] will not decrease flood risks but rather help in resisting the floods. He also believes that protective structural measures, which are included in the resilience concept, weaken resilience by eliminating resistant characteristics [20, 21]. It's possible that advocates of change are motivated by the fact that first, disasters are immitigable, because they are naturally occurring [22, 23] and second, we have long been causing environmental problems through human activities like development, which are long, time-consuming, and expensive to remedy [14, 24, 25].

The problem may be best solved with the whole reform of the existing system [26–28]. Socio-ecological resilience has transformability because it allows for drastic,

Fig. 2 Flowchart of working methodology

systemic adjustments to be made so that a new, more stable, and resilient system may be built to better address future disaster risks [29–31]. It may involve such actions as relocating very toxic zones or rebuilding every facet of the development planning system, including changes to existing development laws and standards and reforms in planning governance [32–34] (Fig. 2).

To alter things, transformation planning involves a large amount of effort, collaboration with all parties, and investment in resources. If existing conditions were really unpleasant, the public would want major changes to rejuvenate the area. The above flow chart shows how we have proceed with the work in the project from collecting data to doing ArcGIS analyses and HEC-RAS model and forming Hydrograph and Flood Inundation Map. Two types of data have been collected during the process: DEM data from ISRO, USGS, or Alos Palsar and hydrological data from different sites were used for the analysis and simulation [35]. DEM image of Alos Palsar was taken for the study as the resolution of DEM is 12 m which is very high compared to other open sources available data.

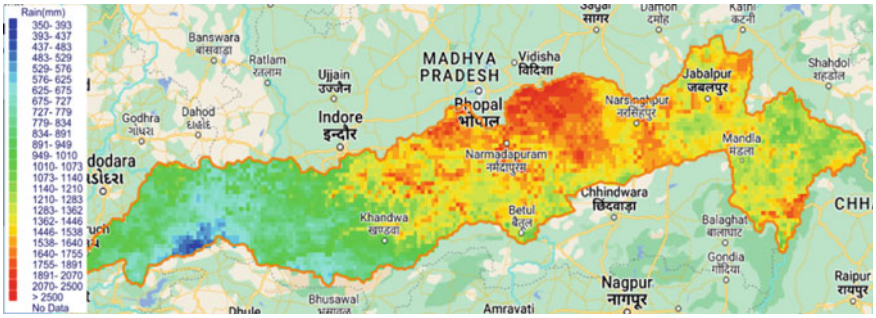

Fig. 3 Average annual rainfall map for Narmada River Basin

3 Rainfall Analysis

Based on the flood events that occurred in the lower basin of the Narmada River during 1994 and 2004, data on rainfall intensity was collected from government sites. The Lower Basin of Narmada River with rainfall map legend can be seen in Fig. 3. The map is sky blue to dark red shade, which shows that rainfall is actually higher in the upper Narmada basin and lower in the lower Narmada basin. Data collected is from the month of June to October, during which maximum rainfall occurred. Data collected is analyzed in the Microsoft Excel and "Line Charts" demographics are created in Excel for both the years. Charts show the normal rainfall in the month of June to October and actual rainfall occurred during these months. In 1994, maximum rainfall occurred on 7th September, and Sardar Sarovar Dam recorded a total discharge of 62,920.03 cumecs. In 2004, maximum rainfall occurred on 2nd August and Sardar Sarovar Dam recorded a total discharge of 56,492.10 cumecs. Rainfall leads to major floods in both years, and major populations near Bharuch were migrated to save location. Flood also caused a lot of property damage in the Bharuch District, surrounding the Narmada River.

As shown in Fig. 4, maximum observed flood from 1970 to 2015 in the Narmada River with the maximum gauge water level reported at the Mandleshwar station in the Narmada River Basin. Figure 5 shows the important flood event hydrograph.

4 HEC-RAS Model

HEC-RAS is a software system developed for usage in an interactive, multitasking environment [36]. The system has a graphical user interface (GUI), distinct analytical components, data storage and administration capabilities, graphics, mapping, and reporting capabilities [37, 38]. The HEC-RAS system includes the following river analysis components: 1D steady flow water surface profile computations; 1D and 2D

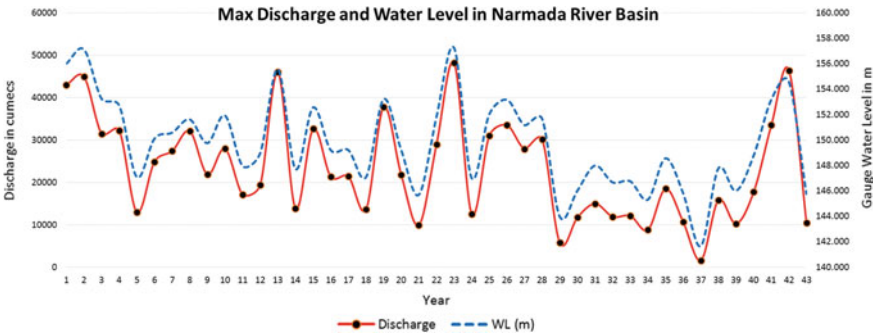

Fig. 4 Historical maximum discharge observed in the Narmada River

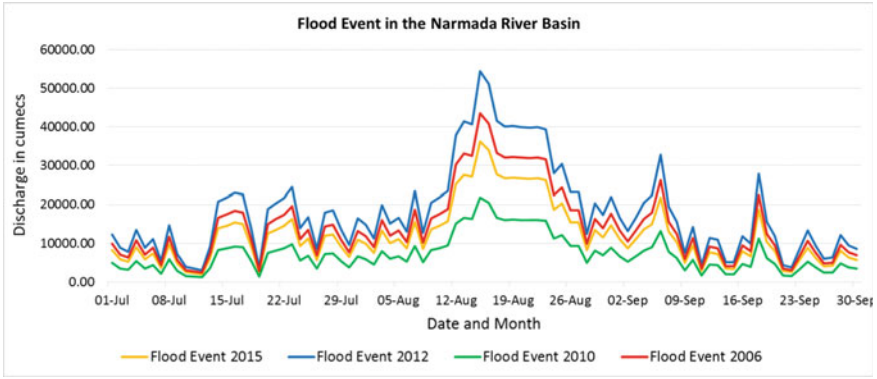

Fig. 5 Observed flood event in Narmada River Basin for year 2015, 2012, 2010, and 2006

unsteady flow simulations; quasi or completely unsteady flow moveable boundary sediment transport computations (1D and 2D); and 1D quality analysis [39–41].

The fact that all four components share the same geometric data representation and geometric and hydraulic computing methods [42, 43] is a crucial factor. In addition to the four river analysis components, the system includes a number of hydraulic design elements that may be activated after the water surface profiles have been calculated. Additionally, HEC-RAS has a comprehensive spatial data integration and mapping system (HEC-RAS Mapper) [44, 45].

HEC-RAS is intended to do one-dimensional and two-dimensional hydraulic computations for a complete network of natural and manmade channels, over-bank/floodplain regions, and levee-protected zones [46]. The following is a description of HEC-primary RAS's capabilities.

In unsteady flow, there are various boundary condition need to add in it. There are two boundary conditions: (i) upstream boundary condition (ii) downstream boundary condition [29, 30].

These are the options for boundary conditions: flow hydrograph, stage hydrograph, stage and flow hydrograph, rating curve, normal depth, lateral inflow hydrograph, uniform lateral inflow hydrograph, groundwater interflow, time series of gate openings, elevation controlled gate, navigation dam, internal boundary stage and/or flow hydrograph, "rules" editor, precipitation [47–49].

Upstream Boundary Condition: Flow hydrograph is taken as an upstream boundary condition for the unsteady flow analysis. Downstream Boundary Condition: Normal depth is taken as a downstream boundary condition for the unsteady flow analysis. Initial Condition: Unsteady flow simulations need users to set up starting conditions in addition to setting up boundary conditions. Flow and stage information at each cross section, as well as the elevations of any storage locations established in the system, are included in the initial conditions. In the unsteady flow data editor, go to the initial circumstances tab to set up your initial conditions. There are two ways for the user to set up the system's initial conditions. It is possible to input flow data for each reach and have the computer do a steady flow backwater run to calculate the stages at each cross section. For storage spaces that are part of the system, the user must additionally input a beginning elevation. This is the most typical way to set up the initial conditions.

Manning's roughness value is 0.030. As the lower Narmada River having clean, straight, full stage, no rifts or deep pools and floodplain. Many researchers have also shown the average value of Manning's roughness coefficient is 0.030 [33, 34, 50].

$$\text{Continuity Equation:} \frac{\partial Q}{\partial x} + \frac{\partial A}{\partial t} = 0$$

$$\text{Momentum Equation:} \frac{1}{A}\frac{\partial Q}{\partial t} + \frac{1}{A}\frac{\partial}{\partial x}\left(\frac{Q^2}{A}\right) + g\frac{\partial y}{\partial x} - g(S_0 - S_f) = 0$$

where

Q—Discharge through the channel,

A—Area of cross section of flow,

y—Depth of flow,

S_0—Channel bottom slope,

S_f—Friction slope (Fig. 6).

5 Results and Discussions

Many big cities situated on the shore, such as Mumbai, Bangkok, Dhaka, and Jakarta, are very vulnerable to floods. For instance, new buildings, installation of infrastructure, and rebuilding of drainage networks in metropolitan environments have all affected how water flows. These areas also get heavy rain during the monsoons. It

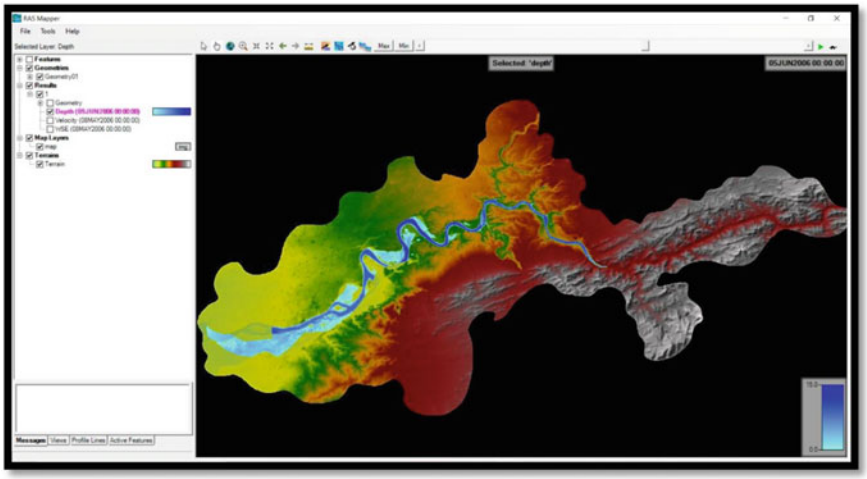

Fig. 6 Unsteady flow simulation in HEC-RAS model

is likely to be hard to execute structural mitigating measures because of resource and space limitations. Flood-proofing and other non-structural methods like better flood warning systems have been discovered to be more beneficial in flood damage reduction. In recent decades, the significant danger of climate-related catastrophe and rising development demands have made it difficult for planning officials to come up with strategies for sustainable growth. There has been a spike in interest in how to create resilience so as to minimize the harm done by natural disasters by strengthening the community's resistance and its capacity to adapt. Although it cannot be completely prevented, catastrophe risk comes from unavoidable natural risks The rainfall and discharge data collected are analyzed and presented in the charts for different years (2015, 2012, 2010, and 2006). These data sets were used for the flood modeling in HEC-RAS software. Satellite DEM data set and Hydraulic data sets were added into the model, unsteady 2-D flow model was run, and based on the results, various analyses were carried out. Fig. 7 shows the various photographs of the obtained results for the lower Narmada River Basin which is the main results of the research.

HEC-RAS model is used for 2D unsteady flood stimulation and hydrographs are prepared of lower Narmada Basin. Inundated area of Bharuch City for the maximum flood is identified, using the compiling HEC-RAS with the Google Earth and Google Map as shown in Fig. 7. Majority of the lower area of the Bharuch City was flooded during the maximum flood simulation event. Figure 8 terrain image shows the maximum flood situation in Narmada River in 2006.

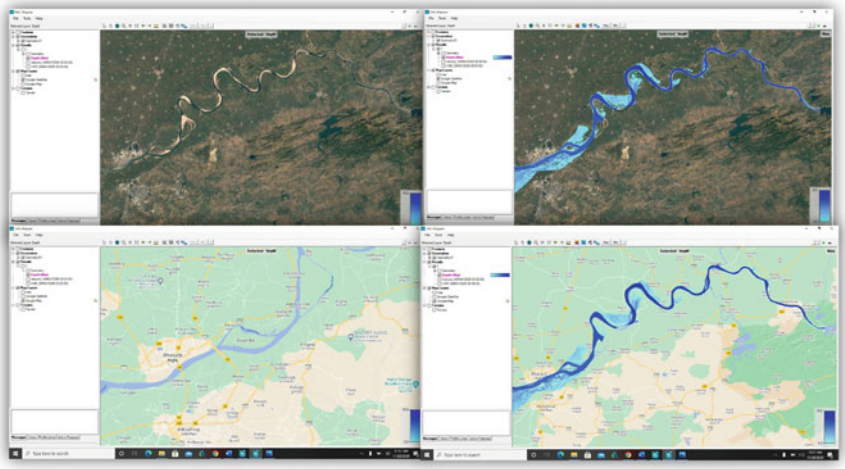

Fig. 7 Flood simulation for the Bharuch City before and after flood scenario

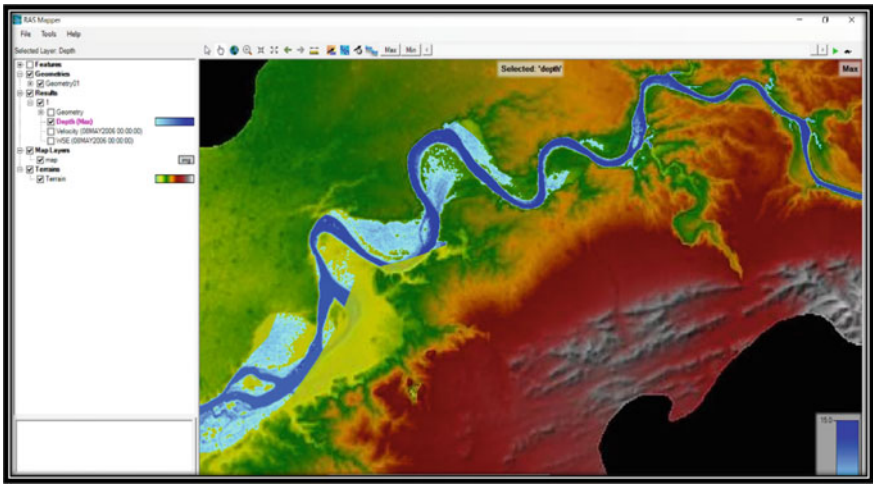

Fig. 8 Simulation of the maximum flood event in the lower Narmada River Basin

6 Conclusion

The results show the maximum flood level that might occur in the study region due to heavy rainfall in upstream area of dam, the downstream of the dam may get flooded if the heavy discharge release from the Sardar Sarovar Dam. This will result in the flooding situation in the Bharuch City. There was a maximum discharge of 69,376.27 m^3/s in the basin. This value's estimation aids in the planning of a civil

engineering structure in the research area. A review of the hydrology of the dam situated at the upstream reach, design of new hydraulic structures in the research region, and appropriate mitigation strategy may all benefit greatly from the above-mentioned findings. Using the flood hydrograph created, HEC-RAS was able to map out the floodplain. This research provided insight into how much flooding could occur in the study region according to the results of the analysis. It is possible to use the velocity curves to estimate the bridge's strength, and how long it will hold up under the most extreme flooding conditions.

Acknowledgements To the Institute of Technology, Nirma University's Department of Civil Engineering, the author expresses gratitude for the opportunity. The author is also grateful to the SWDC, Gandhinagar, CWC-Gandhinagar, and GSDM-Gandhinagar for supplying the necessary data to conduct this research for the Narmada River Basin.

References

1. Admiraal H, Cornaro A (2020) Future cities, resilient cities—the role of underground space in achieving urban resilience. Undergr Space (China) 5(3):223–228. https://doi.org/10.1016/j.undsp.2019.02.001
2. Afriyanie D, Julian MM, Riqqi A, Akbar R, Suroso DSA, Kustiwan I (2020) Re-framing urban green spaces planning for flood protection through socio-ecological resilience in Bandung City, Indonesia. Cities 101(10):102710. https://doi.org/10.1016/j.cities.2020.102710
3. Bardhan R (2017) Integrating rapid assessment of flood proneness into urban planning under data constraints: a fuzzy logic and bricolage approach. Area Dev Policy 2(3):272–293. https://doi.org/10.1080/23792949.2017.1338523
4. Chang H, Pallathadka A, Sauer J, Grimm NB, Zimmerman R, Cheng C, Iwaniec DM, Kim Y, Lloyd R, McPhearson T, Rosenzweig B, Troxler T, Welty C, Brenner R, Herreros-Cantis P (2021) Assessment of urban flood vulnerability using the social-ecological-technological systems framework in six US cities. Sustain Cities Soc 68(February):102786. https://doi.org/10.1016/j.scs.2021.102786
5. Chuang MT, Chen TL, Lin ZH (2020) A review of resilient practice based upon flood vulnerability in New Taipei City, Taiwan. Int J Disaster Risk Red 46(December 2019):101494. https://doi.org/10.1016/j.ijdrr.2020.101494
6. Ciullo A, Viglione A, Castellarin A, Crisci M, Di Baldassarre G (2017) Socio-hydrological modelling of flood-risk dynamics: comparing the resilience of green and technological systems. Hydrol Sci J 62(6):880–891. https://doi.org/10.1080/02626667.2016.1273527
7. Cristiano E, Urru S, Farris S, Ruggiu D, Deidda R, Viola F (2020) Analysis of potential benefits on flood mitigation of a CAM green roof in Mediterranean urban areas. Build Environ 183:107179. https://doi.org/10.1016/j.buildenv.2020.107179
8. Forero-Ortiz E, Martínez-Gomariz E, Cañas Porcuna M (2020) A review of flood impact assessment approaches for underground infrastructures in urban areas: a focus on transport systems. Hydrol Sci J:1943–1955. https://doi.org/10.1080/02626667.2020.1784424
9. Golz S, Schinke R, Naumann T (2015) Assessing the effects of flood resilience technologies on building scale. Urban Water J 12(1):30–43. https://doi.org/10.1080/1573062X.2014.939090
10. González JE, Ramamurthy P, Bornstein RD, Chen F, Bou-Zeid ER, Ghandehari M, Luvall J, Mitra C, Niyogi D (2021) Urban climate and resiliency: a synthesis report of state of the art and future research directions. Urban Clim 38(January). https://doi.org/10.1016/j.uclim.2021.100858

11. Goodchild B, Sharpe R, Hanson C (2018) Between resistance and resilience: a study of flood risk management in the Don catchment area (UK). J Environ Planning Policy Manage 20(4):434–449. https://doi.org/10.1080/1523908X.2018.1433997
12. Gupta K (2007) Urban flood resilience planning and management and lessons for the future: a case study of Mumbai, India. Urban Water J 4(3):183–194. https://doi.org/10.1080/15730620701464141
13. Hammond M, Chen AS, Batica J, Butler D, Djordjević S, Gourbesville P, Manojlović N, Mark O, Veerbeek W (2018) A new flood risk assessment framework for evaluating the effectiveness of policies to improve urban flood resilience. Urban Water J 15(5):427–436. https://doi.org/10.1080/1573062X.2018.1508598
14. Patel SB, Mehta DJ, Yadav SM (2018) One dimensional hydrodynamic flood modelling for Ambica River, South Gujarat. J Emerg Technol Inno Res 5(4):595–601
15. Haruna AI, Oppong RA, Marful AB (2018) Exploring eco-aesthetics for urban green infrastructure development and building resilient cities: a theoretical overview. Cogent Social Sci 4(1):1–18. https://doi.org/10.1080/23311886.2018.1478492
16. Hewawasam V, Matsui K (2020) Equitable resilience in flood prone urban areas in Sri Lanka: a case study in Colombo divisional secretariat division. Glob Environ Chang 62(April):102091. https://doi.org/10.1016/j.gloenvcha.2020.102091
17. Hofmann SZ (2021) 100 Resilient cities program and the role of the Sendai framework and disaster risk reduction for resilient cities. Progr Disaster Sci 11:100189. https://doi.org/10.1016/j.pdisas.2021.100189
18. Khirfan L, El-Shayeb H (2020) Urban climate resilience through socio-ecological planning: a case study in Charlottetown, Prince Edward Island. J Urban 13(2):187–212. https://doi.org/10.1080/17549175.2019.1650801
19. Kim H, Marcouiller DW (2018) Mitigating flood risk and enhancing community resilience to natural disasters: plan quality matters. Environ Hazards 17(5):397–417. https://doi.org/10.1080/17477891.2017.1407743
20. Kim Y, Newman G (2020) Advancing scenario planning through integrating urban growth prediction with future flood risk models. Comput Environ Urban Syst 82(February):101498. https://doi.org/10.1016/j.compenvurbsys.2020.101498
21. Lee K, Chun H, Song J (2018) New strategies for resilient planning in response to climate change for urban development. Procedia Engineering 212(2017):840–846. https://doi.org/10.1016/j.proeng.2018.01.108
22. Lourenço IB, Beleño de Oliveira AK, Marques LS, Quintanilha Barbosa AA, Veról AP, Magalhães PC, Miguez MG (2020) A framework to support flood prevention and mitigation in the landscape and urban planning process regarding water dynamics. J Clean Prod 277. https://doi.org/10.1016/j.jclepro.2020.122983
23. Mehta DJ, Ramani MM, Joshi MM (2013) Application of 1-D HEC-RAS model in design of channels. Methodology 1(7):4–62
24. Kumara YV, Mehtab DJ (2020) Water productivity enhancement through controlling the flood inundation of the surrounding region of Navsari Purna river, India, pp 11–20
25. Mehta DJ, Eslamian S, Prajapati K (2021). Flood modelling for a data-scare semi-arid region using 1-D hydrodynamic model: a case study of Navsari region. Model Earth Syst Environ:1–11
26. Mehta DJ, Yadav SM (2020) Analysis of scour depth in the case of parallel bridges using HEC-RAS. Water Supply 20(8):3419–3432. https://doi.org/10.2166/ws.2020.255
27. Mehta D, Yadav SM, Waikhom S (2013) Geomorphic channel design and analysis using HEC-RAS hydraulic design functions. Paripex Int J Glob Res Anal 2(4):90–93
28. Mehta DJ, Yadav SM (2020) Hydrodynamic simulation of river Ambica for riverbed assessment: a case study of Navsari region. In: Advances in water resources engineering and management. Lecture notes in civil engineering. Springer, Singapore, vol 39, pp 127–140. https://doi.org/10.1007/978-981-13-8181-2_10
29. Mugume SN, Butler D (2017) Evaluation of functional resilience in urban drainage and flood management systems using a global analysis approach. Urban Water J 14(7):727–736. https://doi.org/10.1080/1573062X.2016.1253754

30. Nhamo L, Rwizi L, Mpandeli S, Botai J, Magidi J, Tazvinga H, Sobratee N, Liphadzi S, Naidoo D, Modi AT, Slotow R, Mabhaudhi T (2021) Urban nexus and transformative pathways towards a resilient Gauteng City-region, South Africa. Cities 116:103266. https://doi.org/10.1016/j.cities.2021.103266
31. Patel P, Bablani S, Patel A (2020) Impact assessment of urbanization and industrialization using water quality index on Sabaramati River, Ahmedabad. In: International conference on innovative advancement in engineering and technology (IAET) SSRN Elsevier, pp 1–7. https://doi.org/10.2139/ssrn.3553800
32. Patel A (2018) Design of optimum number of rain gauge network over Sabarmati river basin. i-Manager's J Future Eng Technol 14(1):26–31. https://doi.org/10.26634/jfet.14.1.14207
33. Patel A (2020) Rainfall-runoff modelling and simulation using remote sensing and hydrological model for Banas river, Gujarat, India. In: Advances in water resources engineering and management. Lecture notes in civil engineering. Springer, Singapore, vol 39, pp 153–162. https://doi.org/10.1007/978-981-13-8181-2_12
34. Pandya U, Patel A, Patel D (2017) River cross section delineation from the Google Earth for development of 1D HEC-RAS model–a case of Sabarmati River, Gujarat, India. In: International conference on hydraulics, water resources and coastal engineering, Ahmedabad, India (HYDRO), pp 1–10
35. Keriwala N, Patel A (2022) Impact assessment of tropical cyclone Tauktae on coastal region of Gujarat, India. ECS Trans 107(1):6185
36. Palazzo E (2019) From water sensitive to floodable: defining adaptive urban design for water resilient cities. J Urban Des 24(1):137–157. https://doi.org/10.1080/13574809.2018.1511972
37. Ramkar P, Yadav SM (2021) Flood risk index in data-scarce river basins using the AHP and GIS approach. Nat Hazards 109:1119–1140. https://doi.org/10.1007/s11069-021-04871-x
38. Raška P, Stehlíková M, Rybová K, Aubrechtová T (2019) Managing flood risk in shrinking cities: dilemmas for urban development from the Central European perspective. Water Int 44(5):520–538. https://doi.org/10.1080/02508060.2019.1640955
39. Restemeyer B, Van Den Brink M, Woltjer J (2019) Decentralized implementation of flood resilience measures–a blessing or a curse? Lessons from the Thames Estuary 2100 plan and the Royal Docks regeneration. Plan Pract Res 34(1):62–83. https://doi.org/10.1080/02697459.2018.1546918
40. Restemeyer B, Woltjer J, van den Brink M (2015) A strategy-based framework for assessing the flood resilience of cities—a Hamburg case study. Plan Theory Pract 16(1):45–62. https://doi.org/10.1080/14649357.2014.1000950
41. Shaikh M, Yadav VG, Yadav SM (2018) Simulation of rainfall-runoff event using HEC-HMS model for REL sub-basin, Gujarat, India. Int J Emerg Technol Inno Res 5(4):402–407
42. Shaikh M, Yadav SM, Manekar V (2021, April). Hydraulic modelling of extreme flood event of semi-arid river basin. In: EGU general assembly conference abstracts, pp EGU21-10218
43. Sagathia J, Kotecha N, Patel H, Patel A (2020) Impact assessment of urban flood in Surat city using HEC-HMS and GIS (February 21, 2020). In: International conference on innovative advancement in engineering and technology (IAET). SSRN Elsevier. https://doi.org/10.2139/ssrn.3558360
44. Siekmann T, Siekmann M (2015) Resilient urban drainage—options of an optimized area-management. Urban Water J 12(1):44–51. https://doi.org/10.1080/1573062X.2013.851711
45. Norizan NZA, Hassan N, Yusoff MM (2021) Strengthening flood resilient development in Malaysia through integration of flood risk reduction measures in local plans. Land Use Policy 102(Nov 2020):105178. https://doi.org/10.1016/j.landusepol.2020.105178
46. Singh P, Amekudzi-Kennedy A, Woodall B, Joshi S (2021) Lessons from case studies of flood resilience: institutions and built systems. Transp Res Interdiscip Perspec 9(February):100297. https://doi.org/10.1016/j.trip.2021.100297
47. Yadav SM, Mangukiya NK (2021) Semi-arid river basin flood: causes, damages, and measures. In: Proceedings of the fifth international conference in ocean engineering (ICOE2019), pp 201–212

48. Patel A, Panchal U, Keriwala N (2021) A novel plan for gujarat to mitigate the effect of flood, drought and salinity using interlinking of canal and rivers. In: F-EIR conference on environment concerns and its remediation. Springer, Cham, pp 155–167
49. Patel P, Patel A (2021) Low cost model for desalination of water using solar energy to overcome water scarcity in India. Mater Today: Proc. https://doi.org/10.1016/j.matpr.2021.02.804
50. Patel A, Shah A (2020) Sustainable solution for lake water purification in rural and urban areas. Mater Today: Proc 32:740–745. https://doi.org/10.1016/j.matpr.2020.03.473

Use of Big Data for Flood Assessment Through HEC-RAS Model: A Study of Purna River of Navsari

Azazkhan I. Pathan, P. G. Agnihotri, Dhruvesh Patel, P. J. Gandhi, Cristina Prieto, Usman Mohseni, and Nilesh Patidar

Abstract Big data has recently become popular all around the world. Data generation in each discipline has substantially improved due to the usage of computer systems. Flooding appears to be the most frequently calamity in a tropical country like India. Flooding in urban coastal areas is caused by heavy rainfall, industrialisation, high population density and urbanisation. The Navsari City, Gujarat, India, located near the Arabian Sea coast affected by a disastrous flood in 2004. In this study, the use of big data is implemented to assess the flood using HEC-RAS 2D hydrodynamic modelling. The big data of past floods would be a foundation for the enlargement of the HEC-RAS 2D flood assessment model. Calibration and validation have been performed to ensure the consistency and adequacy of the model. The outcomes of the model depicted that the R^2 of the model was 0.9679 indicating that the observed values are in good agreement with the simulated value. Comparable

Disclaimer: The presentation of material and details in maps used in this chapter does not imply the expression of any opinion whatsoever on the part of the Publisher or Author concerning the legal status of any country, area or territory or of its authorities, or concerning the delimitation of its borders. The depiction and use of boundaries, geographic names and related data shown on maps and included in lists, tables, documents, and databases in this chapter are not warranted to be error free nor do they necessarily imply official endorsement or acceptance by the Publisher or Author.

A. I. Pathan (✉) · P. G. Agnihotri · U. Mohseni · N. Patidar
Department of Civil Engineering, Sardar Vallabhbhai National Institute of Technology, Surat 395007, India
e-mail: pathanazaz02@gmail.com

P. G. Agnihotri
e-mail: pga@ced.svnit.ac.in

D. Patel
Department of Civil Engineering, Pandit Deen Dayal Energy University, School of Technology, Gandhinagar 382426, India

P. J. Gandhi
Bhagvan Mahavir University, Surat 395009, India

C. Prieto
IHCantabria—Instituto de Hidráulica Ambiental de la Universidad de Cantabria, Santander, Spain
e-mail: cristina.prieto@eawag.ch

P. V. Timbadiya et al. (eds.), *Flood Forecasting and Hydraulic Structures*, Lecture Notes in Civil Engineering 340, https://doi.org/10.1007/978-981-99-1890-4_7

to most developed and advanced cities in countries such as the Europe, USA, Japan and China who are exploiting the advantages of big data for assessment of flood, monitoring and mitigation, where as in India, the use of big data for assessing flood is very limited. In the said context, this research work is focussed on the use of big data for flood assessment in Navsari. In this study, we have discussed the needs and applicability of flood assessment through HEC-RAS 2D model across the world's urban coastal areas including Navsari City, accompanied by the important benefits of big data approach.

Keywords Big data · HEC-RAS · Flood · 2D hydrodynamic modelling

1 Introduction

At present, the significance of big data has emerged in the age of computer applications. The historical datasets and their preservation have changed dramatically since the development of the computer system. These are the most crucial elements of the computational structures and frameworks. Furthermore, the requirement for data storage and processing effort has risen with the increased application of computers [1]. Due to advancements in computer storage technology, the last two decades have seen the development of vast amounts of data and its accessibility via numerous search engines, yet this data is not being effectively utilised for the betterment of society. The advent of these events has assisted in the commercialisation of big data becoming more ubiquitous [2]. Because to its tactical and analytical possibilities, big data has rapidly become the subject of corporate and academic research, particularly in terms of generating financial value [3].

Flood is one of the most common natural threats, and it frequently results in significant losses, as well as individual and societal calamities. Asian countries continue to lead the list of countries with the largest number of human deaths and losses. Many Indian cities are located along river banks or along the coast, resulting in flooding [4]. India is the world's most flood-prone country, with 4.84 million people inhabiting in flood-prone areas [5]. Severe flooding, siltation of riverbed, high stream flows, a shift in drainage pattern and other factors are among the primary causes of widespread flooding [6]. Furthermore, climate change will accelerate and intensify the hydrological process, thereby increasing the frequency and intensity of predicted floods [7].

In terms of flood assessment, monitoring and forecasting, big data has been used in just a few research projects throughout the world [1]. The significance of big data in disaster management has shifted. Researchers are currently experiencing one of the most challenging difficulties in dealing with enormous amounts of data generated in disasters [8]. Navsari is one of Gujarat's most populous cities. In the years of 2004, the city was hit by floods. Gujarat's government has 2004 statistics accessible. For the creation of a flood assessment model, the data is a type of big data.

Many hydrodynamic models are currently accessible, each of which describes the benefits, limitations, most recent advancements and future plans [9]. As a consequence, numerical tools were discovered to be significant instruments for identifying flood occurrences, assessing flood risk and determining flood control preparedness [10]. For overflow analysis, the HEC-RAS 2D mode would be more exact. In the Sangam region of Payagraj, India, [11] utilised the HEC-RAS 2D and Global Flood Monitoring System (GFMS) for flood modelling and hazard zone delineation [11]. Quirogaa et al. [12] successfully implemented the new HEC-RAS version 5.0 for assessment of flood hazard and showed the numerical simulation of 2D HEC-RAS model to create flood level, flood degree and flood intensity mapping on the Mamore River [12]. The floodplain region in Bushehr City was found using HEC-RAS unsteady flow with the tide condition [13]. Due to the presence of buildings and other structures in the floodplain, [14] addressed the shallow water model with porosity [14]. Pathan and Agnihotri [15] utilised the HEC-RAS 2D unsteady flow method for identifying the flood inundation in the lower Purna Basin, India [15]. Gallegos et al. [16] showed how to solve two-dimensional shallow water equations utilising a Godunov-type unstructured grid, BreZo and finite volume [16].

Because of the aforementioned research and urban expansion of the Navsari City, it is important to use historical data in the context of big data for developing a flood assessment model using HEC-RAS 2D. This model will aid a variety of institutions, including insurance firms in determining premium amounts and urban municipal governments in developing disaster management and rescue plans. In the light of this expansion and development, the city of Navsari's local government authority should create a big data server as an initial phase in assessing 2D urban coastal floods. Furthermore, the application of remote sensing and GIS techniques was emphasised in this study.

2 Study Area and Data Source

2.1 Navsari City and the Purna River

Purna River is one of the important rivers which originates from the Saputara Hills in Dang District, Gujarat, and flows for 180 km before entering the Arabian Sea coast. It has 2431 km^2 drainage area (CWC 2000–2001). The 2373 km^2 area is utilised by Gujarat, and 58 km^2 area is utilised by Maharashtra State. The Navsari City lies between 72° 42′–73° 30′ E longitude and 20° 32′–21° 05′ N latitude. The location map of the study area is depicted in Fig. 1. Mahuva gauge station is controlled by the Central Water Commission (CWC). Figure 2 shows the hydrological observations of the Purna River at Mahuva station. The city covers the total 2211.97 km^2 geographical area. The city recorded the 1.71 million population as and 88% total literacy rate as per census 2011. Warm weather was recorded between October to May and rainy between June to September. The maximum and minimum temperature were recorded

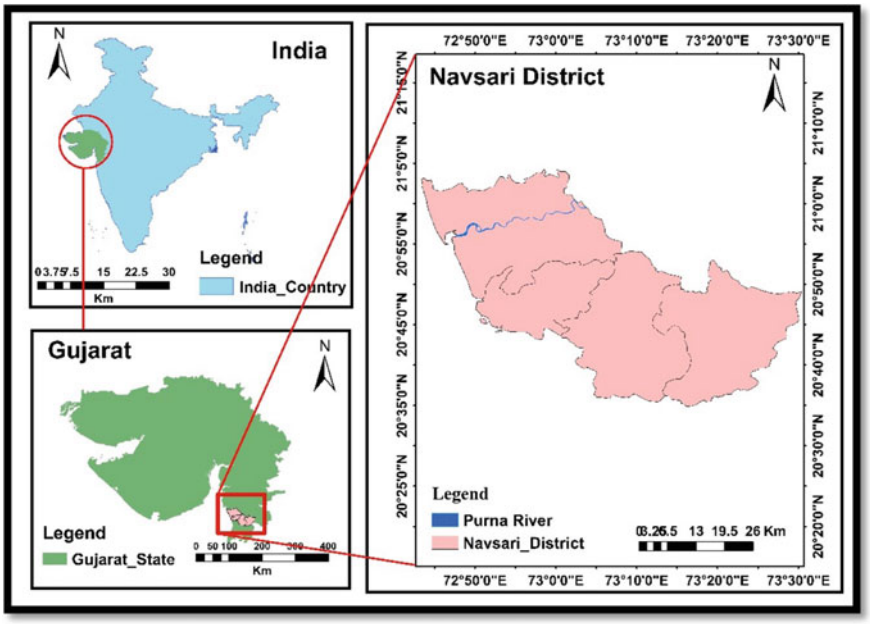

Fig. 1 Index map of study area

as 40 °C and 17 °C, respectively. The average rainfall was observed as 48 inches. The city was hit by devastating floods by 2004-year flood event resulted in significant property damage and fatalities. The backwater impact, climate changes and the heavy rainfall could be the reason for arising floods in the city every year during monsoon.

2.2 Data Used

SRTM DEM was used (https://earthexplorer.usgs.gov/) for 2D HEC-RAS modelling. The soil data for the research area was acquired from the National Bureau of Soil Survey and land use planning (NBSS & LUP). The flood discharge data of the year 2004 was collected from Navsari Irrigation Circle.

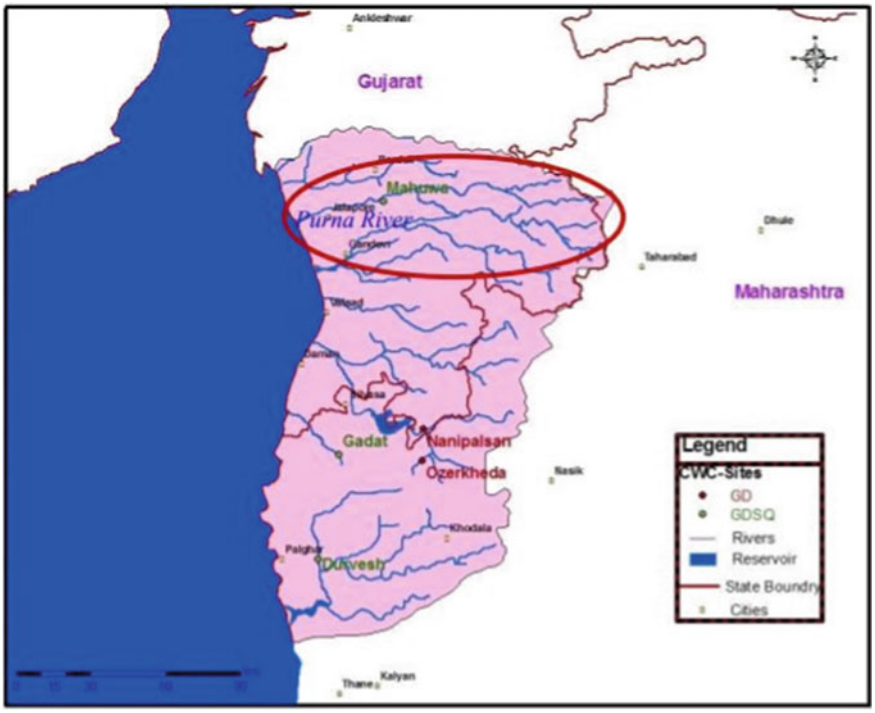

Fig. 2 Hydrological observation of Purna River at Mahuva Gauge station (https://www.cwc.gov.in)

3 Materials and Methods

3.1 Model of Big Data for Flood Assessment

The big data model for flood assessment is describe in this section. The flowchart of the big data model for flood assessment is shown in (Fig. 3). Pre-processing of data is done for cleaning and smoothing to avoid data duplication. All the data are collected using the big data server in the context of Navsari City, where the DEM is obtained from earth explorer, metrological data is collected from State Water Data Centre (SWD) Gandhinagar, Gujarat, past flood discharge and water level data is collected from Navsari irrigation department, soil data was obtained from the NBSS and LUP, the flood extent in terms of water level can be determined through field survey in the city. Following the data collection, flood assessment is to be done using HEC-RAS 2D software in conjunction with big data server. Thereafter, the HEC-RAS results are validated using the field data. The final results derived from the model will be important for the formulation of resilient strategy, emergency action plan to rescue people and decision making to government authorities.

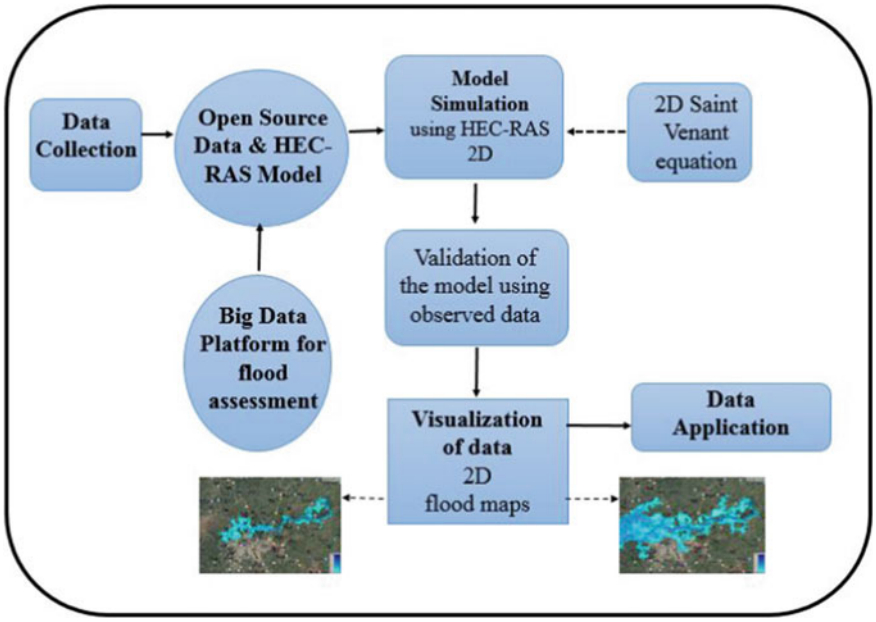

Fig. 3 Flowchart of the methodology

3.2 HEC-RAS 2D Flood Inundation Modelling

The study uses HEC-RAS (2D) open-source datasets to estimate flood inundation of the Purna River in Navsari City. The 2004-year flood event is first reproduced in the model with unstable flow conditions, followed by a flood inundation evaluation. The HEC-RAS model was chosen because to its ease of use and widespread adoption by governments, research institutes and the commercial sector. HEC-RAS 5.0.3 (2D) is utilised to analyse flood inundation in this research study. In flood inundation modelling, Saint Venant equations are used.

HEC-RAS 5.0.3, which solves the 2D diffusion wave equation or the 2D Saint Venant equations, is used to model the flood of 2004 [17].

$$\frac{\partial \xi}{\partial t} + \frac{\partial p}{\partial x} + \frac{\partial q}{\partial x} = 0 \tag{1}$$

$$\frac{\partial p}{\partial t} + \frac{\partial}{\partial x}\left(\frac{p^2}{h}\right) + \frac{\partial}{\partial y}\left(\frac{pq}{h}\right) = -\frac{n^2 pg\sqrt{p^2+q^2}}{h^2} - gh\frac{\partial \xi}{\partial x} + pf + \frac{\partial}{p\partial x}(h\tau_{xx}) + \frac{\partial}{p\partial y}\left(h\tau_{xy}\right) \tag{2}$$

$$\frac{\partial q}{\partial t} + \frac{\partial}{\partial x}\left(\frac{q^2}{h}\right) + \frac{\partial}{\partial y}\left(\frac{pq}{h}\right) = -\frac{n^2 q g\sqrt{p^2+q^2}}{h^2} - gh\frac{\partial \xi}{\partial y} + qf + \frac{\partial}{p\partial y}\left(h\tau_{yy}\right) + \frac{\partial}{p\partial y}\left(h\tau_{xy}\right) \quad (3)$$

where h = depth of water (m), p and q = specific flow in the x- and y-directions $m^2 s^{-1}$, g = gravitational acceleration (m s^{-2}), ζ = surface elevation (m), q = water density (kg m^{-3}), n = Manning resistance, τ_{xx}, τ_{yy}, τ_{xy} are effective shear stress variables, while f represents the Coriolis force (s^{-1}) [18].

For Purna River, the Navsari City, a 2D mesh is first created. For the Purna River in Navsari, the grid of 30 m × 30 m spacing was used. For the simulation of the 2D model, flow hydrograph for August 4, 2004, is used as upstream boundary condition of the Purna River, and downstream boundary condition is given as normal depth at downstream of the river. Because the roughness coefficient is a significant characteristic for the kind of soil, and the primary soil in the research region is silty clay, Manning's coefficient allocated for the simulation of 2D model is 0.035 based on suggestions provided by Chow [19].

To assure the stability of the model, the time steps are computed using the Courant–Friedrichs–Lewy condition [17].

$$C = \frac{V\Delta T}{\Delta x} \leq 1.0 \text{ (with maximum } C = 3.0) \quad (4)$$

$$\Delta T = \frac{\Delta x}{V} \text{ (with maximum } C = 1.0) \quad (5)$$

where C = Courant Number, V = Flood wave velocity m s^{-1}, Δx = Average cell size (m), ΔT = Computational time step (s)

The river flow velocity near Mahuva gauge station ranges from 3.0 to 3.5 m s^{-1}, according to the measured data. This value is defined in Eq. 5 for iteration, and the 30-m grid time step is 15 s. The model is simulated under unsteady flow conditions and the depth of inundation has been calculated.

4 Results and Discussions

The flood of 2004 was simulated for the time period of August 4th 01:00 to August 4th 24:00. The model was allowed to run for a total of 24 h. The arrival of the flood and inundation of key Navsari metropolitan regions were both simulated. Lastly, 2002-year data was used to calibrate the model. In addition, field observed flood data were used to validate the simulated results.

A 2D hydrodynamic simulation was used to simulate the unsteady flow for the flood event of the year 2004 on Purna River. The depth of water is determined by the difference between ground level and equivalent simulation level at the simulation region. The findings of the flood simulation were conducted for the region between the Mahuva gauge station and the Arabian Sea. The data was collected every three hours to determine the flood extent (Fig. 4). According to the outcomes of this simulation, the flood began on August 4th at 02:00 h, with the corresponding discharge of 2011 cumec signalling the start of flood, and the region surrounding by Supa village near Mahuva gauge station get flooded first with an area ranged between 0 and 1.1 km^2, as shown in Fig. 4a. There was no inundation found in rest areas of the city. At 06:00 h, a 4065 cumecs discharge occurred, inundating (1.1–1.3 km^2) areas such as Jalalpore, Limbadi chowk and Radha Krishna society on left side of the river, while the region surrounding by Tavdi Village on the right bank began to be flooded (2.2–2.5 km^2) by the aforementioned discharge, as seen in Fig. 4b. As indicated in Fig. 4c, a massive discharge of 7129 cumecs had swamped the regions and inundated (1.1–3.5 km^2) areas such as Spring Valley Society, Jaysankar Hotel and Party plot by 10:00 h. As a result, on the same day, August 4th, between 11 a.m. and 9 p.m., the regions signifying a rise in flood depth grew fast; subsequently, as shown in Fig. 4d–f, it remained constant and the inundation was observed to be the range between 1.2 and 3.7 km^2. Similarly, in Fig. 5, the areas of submergence have been illustrated with a corresponding discharge and its interval. Because Navsari is located downstream of the Mahuva gauge station, if the discharge surpasses 8836 m^3/sec and the average velocity in the floodplain is 3 to 3.5 m/sec, flooding the whole city may take 11–13 h.

4.1 Calibration and Validation

Using the flood data from 2002, Manning's roughness coefficient, "n", was calibrated. In the present study, Manning's roughness coefficient was calibrated with a single value and many values were then used in the simulations to demonstrate that the findings were acceptable and significant. The numerous single values utilised to calibrate the whole reach for the floods of 2002 are illustrated in Table 1. For the 2002 flood, the HEC-RAS 2D model was used to simulate the water depth for various single roughness coefficients for the Purna River (from Mahuva gauge station to the Arabian Sea). The simulated water depth was compared to the observed water depth at the gauging station to achieve an optimal value for the aforesaid model. For the different Manning's "n" indicated in Table 1**,** RMSE was used to compare simulated and observed water depths [20, 21]. Figure 5 depicts a comparison of simulated and observed water depth (calibration) at the gauging station. The 2004-year flood event was simulated using the calibrated model of HEC-RAS. For Manning's n value equal to 0.035 mentioned in Table 2, the RMSE was utilised to compare the simulated and observed water depths. Figure 5 illustrates the comparison of simulated and observed water depth at gauging station, demonstrating excellent correlation between observed and simulated water depth with a low RMSE value. Moreover,

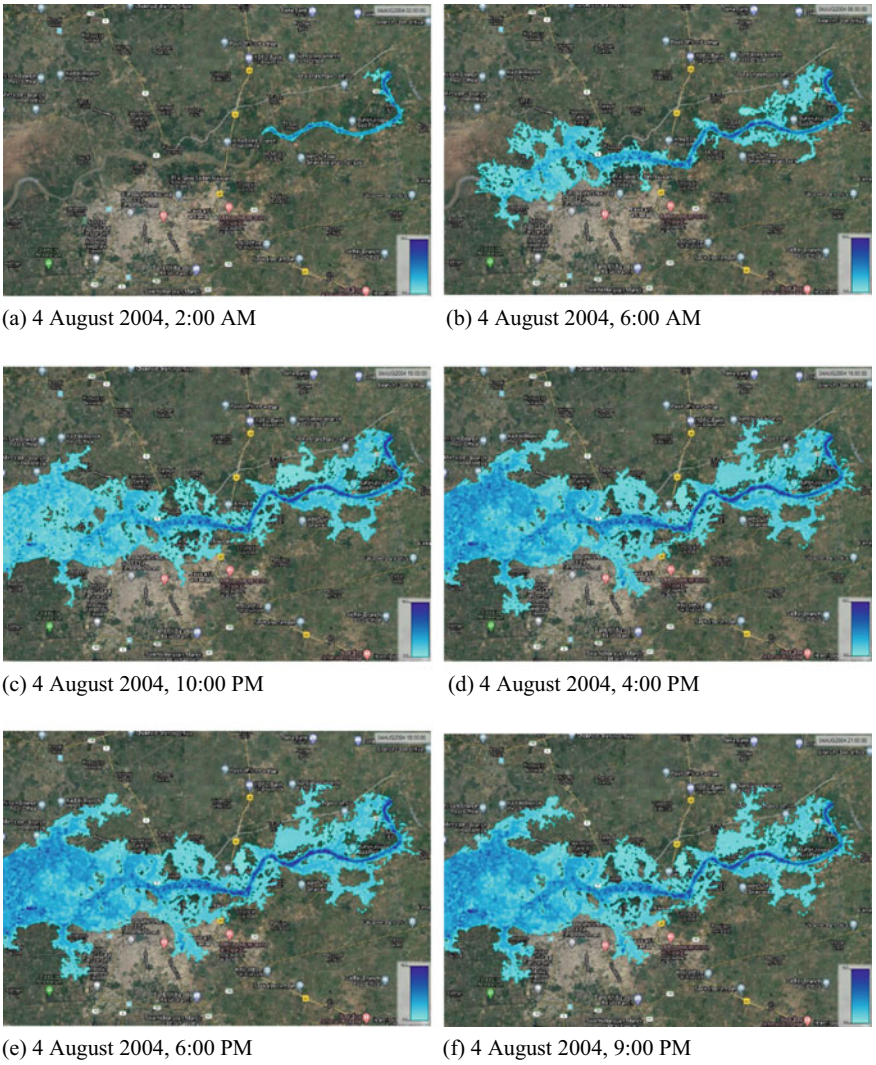

(a) 4 August 2004, 2:00 AM (b) 4 August 2004, 6:00 AM

(c) 4 August 2004, 10:00 PM (d) 4 August 2004, 4:00 PM

(e) 4 August 2004, 6:00 PM (f) 4 August 2004, 9:00 PM

Fig. 4 Simulated flood inundation of Navsari City corresponding to the 2004-year discharge from Mahuva gauge station, SRTM 30 × 30

flood inundation simulation was validated with the observed depth collected from the field survey for the peak flood occurrence (August 4, 2004). High flood level (HFL) marked water levels were collected during the field survey due to lack of data or limitations in the observed flood data of the flood event of 2004. 12 observed high flood level (HFL) marked water levels (i.e. N1–N12) were used to validate the flood inundation simulation of the 2D HEC-RAS model. Figure 7 depicts the actual and simulated water depth profile for the simulated model. The R^2 of the

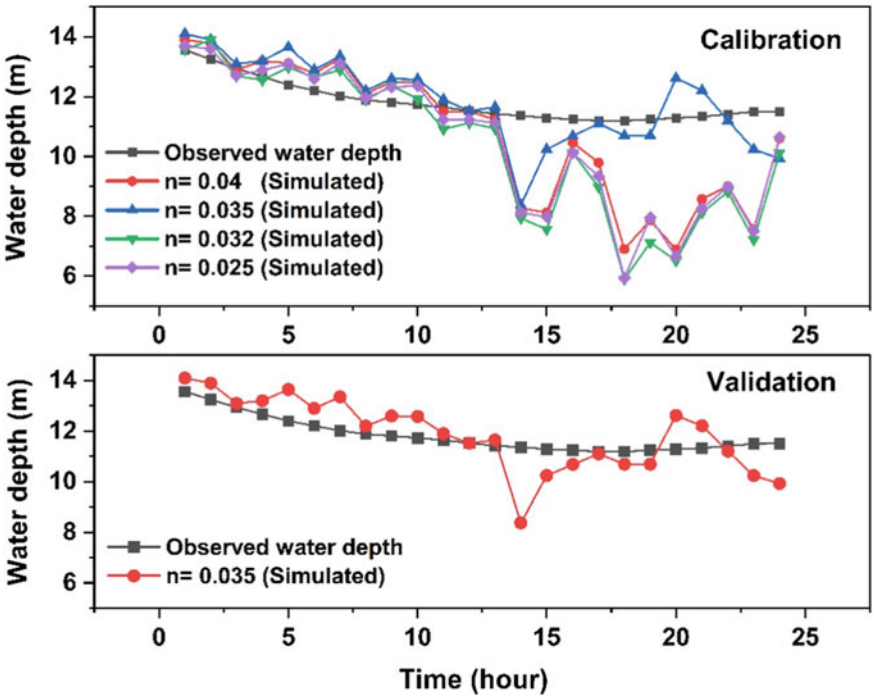

Fig. 5 Observed and simulated water depth at Mahuva gauge station for year 2002 (n = 0.04, 0.035, 0.032, 0.025) calibration and for year 2004 (validation)

connection between simulated and observed water depth was 0.9734 (Fig. 8). The overall findings from the model simulation were identical to the recorded datasets, as shown in Fig. 8. When the simulated outcomes were compared to the observed flood depth, it is found that there is a good correlation. Figure 6 shows the inundation area curve for the Navsari City, illustrating that at peak discharge, low-lying regions such as Viraval, Jalalpore, and the region around railway station were under inundation. As a result, the information may be utilised to appraise mitigating measures for the study area.

Table 1 Calibration of 2D HEC-RAS model at Mahuva Gauging station

Year	Duration of simulation	Roughness coefficient Manning's "n"	RMSE	Gauging station utilised for calibration
2001	July-24, 00 h to July-25, 24 h	0.025 0.032 0.035 0.04	2.2470 2.4160 1.0013 2.092	Mahuva (Calibration)

Table 2 Validation of 2D HEC-RAS model at Mahuva Gauging station

Year	Duration of simulation	Roughness coefficient Manning's "n"	RMSE	Gauging station utilised for calibration
2004	August-3, 00 h to August-4, 24 h.4	0.035	1.3644	Mahuva (Validation)

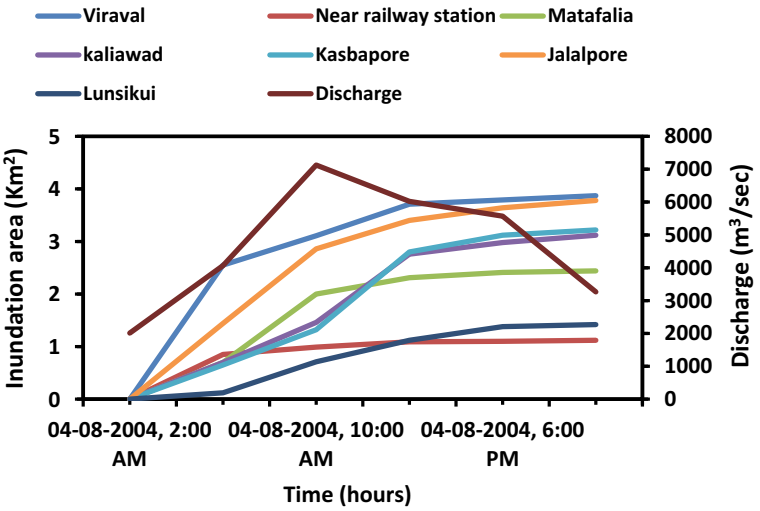

Fig. 6 Discharge–area inundation curve of different area of Navsari City

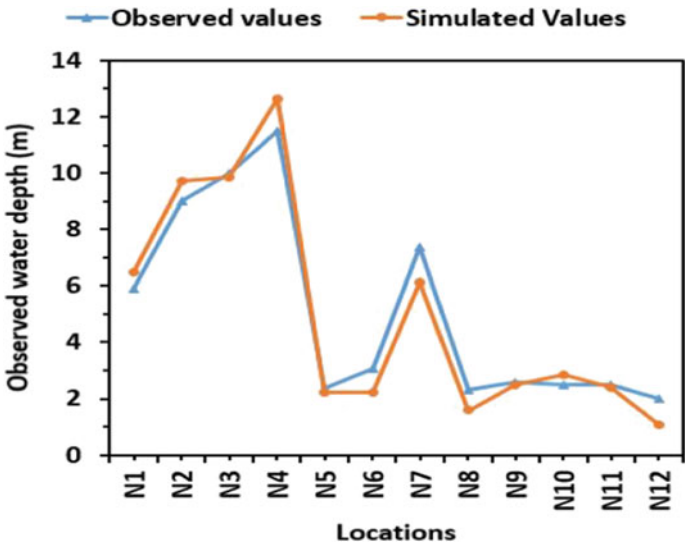

Fig. 7 Observed and simulated depth of water for 30 × 30 m mesh

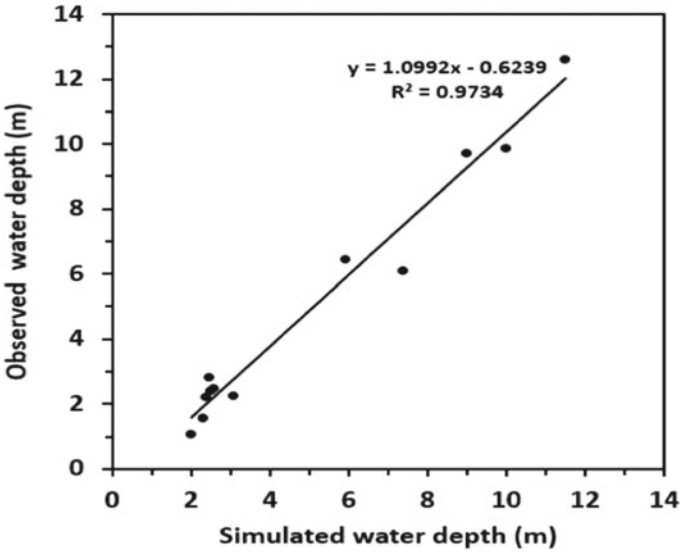

Fig. 8 Regression relationship between simulated and observed water depth for 12 locations

5 Conclusion

Big data has recently become popular all around the world. Data generation in each discipline has substantially improved due to the usage of computer systems. Flooding appears to be the most frequently calamity in a tropical country like India. Flooding in urban coastal areas is caused by heavy rainfall, industrialisation, high population density and urbanisation. The Navsari City, Gujarat, India, located near the Arabian Sea coast affected by a disastrous flood in 2004. In this study, the application of big data has been used to appraise the flood using 2D hydrodynamic modelling in HEC-RAS. The calibration and validation have been accomplished to evaluate the adequacy and stability of the model. The model was validated by comparing simulated depth with the observed water depth. The model outcome showed R^2 (0.9679) values which revealed that the model was more accurate and consistence. Comparable to most developed and advanced cities in countries such as the Europe, USA, Japan and China who are exploiting the advantages of big data for flood assessment, monitoring and mitigation, whereas in India, the use of big data for flood assessment is very limited. In this context, this research work is focussed on the use of big data for flood assessment in Navsari. We have discussed the needs and applicability of flood assessment through HEC-RAS 2D model across the world's urban coastal areas, including Navsari City, accompanied by the important benefits of big data approach.

References

1. Yusoff A, Din NM, Yussof S, Khan S (2015) Big Data analytics for flood information management in Kelantan, Malaysia. 20(20):311–316. https://doi.org/10.1109/SCORED.2015.7449346
2. Provost F, Fawcett T (2013) Data science and its relationship to big data and data-driven decision making. Big Data 1(1):51–59. https://doi.org/10.1089/big.2013.1508
3. Wamba SF, Akter S, Edwards A, Chopin G, Gnanzou D (2015) How "big data" can make big impact: findings from a systematic review and a longitudinal case study. Int J Prod Econ 165:234–246. https://doi.org/10.1016/j.ijpe.2014.12.031
4. Antwi-Boasiako BA (2017) It's beyond my control: the effect of locus of control orientation on disaster insurance adoption. Int J Disaster Risk Reduction 22:297–303. https://doi.org/10.1016/j.ijdrr.2017.02.014
5. Luo T, Maddocks A, Iceland C, Ward P, Winsemius H (2015). World's 15 countries with the most people exposed to river floods
6. Malik A, Abdalla R (2016) Geospatial modeling of the impact of sea level rise on coastal communities: application of Richmond, British Columbia, Canada. Model Earth Syst Environ 2(3):1–17. https://doi.org/10.1007/s40808-016-0199-2
7. Kvočka D, Falconer RA, Bray M (2015) Appropriate model use for predicting elevations and inundation extent for extreme flood events. Nat Hazards 79(3):1791–1808. https://doi.org/10.1007/s11069-015-1926-0
8. Akter S, Wamba SF (2019) Big data and disaster management: a systematic review and agenda for future research. Ann Oper Res 283(1–2):939–959. https://doi.org/10.1007/s10479-017-2584-2
9. Teng J, Jakeman AJ, Vaze J, Croke BF, Dutta D, Kim S (2017) Flood inundation modelling: a review of methods, recent advances and uncertainty analysis. Environ Model Softw 90:201–216. https://doi.org/10.1016/j.envsoft.2017.01.006
10. Bates PD, Dawson RJ, Hall JW, Horritt MS, Nicholls RJ, Wicks J, Hassan M (2005) Simplified two-dimensional numerical modelling of coastal flooding and example applications. Coast Eng 52(9):793–810. https://doi.org/10.1016/j.coastaleng.2005.06.001
11. Kumar N, Kumar M, Sherring A, Suryavanshi S, Ahmad A, Lal D (2020) Applicability of HEC-RAS 2D and GFMS for flood extent mapping: a case study of Sangam area, Prayagraj, India. Model Earth Syst Environ 6:397–405. https://doi.org/10.1007/s40808-019-00687-8
12. Quirogaa VM, Kurea S, Udoa K, Manoa A (2016) Application of 2D numerical simulation for the analysis of the February 2014 Bolivian Amazonia flood: application of the new HEC-RAS version 5. Ribagua 3(1):25–33. https://doi.org/10.1016/j.riba.2015.12.001
13. Hossein A, Javaheri N, Daghigh Y, Tolooiyan A (2006) Simulating of unsteady flow in tidal zones by using HEC-RAS model. Strömungssimulation Im Wasserbau (Flow Simulation in Hydraulic Engineering) 32:57–66. https://doi.org/10.5194/hess-15-2717-2011
14. Soares-Frazão S, Lhomme J, Guinot V, Zech Y (2008) Two-dimensional shallow-water model with porosity for urban flood modelling. J Hydraul Res 46(1):45–64
15. Pathan AKI, Agnihotri PG (2020) 2-D unsteady flow modelling and inundation mapping for Lower Region of Purna Basin using HEC-RAS. Nat Environ Pollut Technol 19(1):277–285
16. Gallegos HA, Schubert JE, Sanders BF (2009) Two-dimensional, high-resolution modeling of urban dam-break flooding: a case study of Baldwin Hills, California. Adv Water Resour 32(8):1323–1335
17. Brunner GW, Piper SS, Jensen MR, Chacon B (2015) Combined 1D and 2D hydraulic modeling within HEC-RAS. In: World environmental and water resources congress 2015: floods, droughts, and ecosystems—proceedings of the 2015 world environmental and water resources congress, pp 1432–1443. https://doi.org/10.1061/9780784479162.141
18. Patel DP, Ramirez JA, Srivastava PK, Bray M, Han D (2017) Assessment of flood inundation mapping of Surat city by coupled 1D/2D hydrodynamic modeling: a case application of the new HEC-RAS 5. Nat Hazards 89(1):93–130. https://doi.org/10.1007/s11069-017-2956-6

19. Chow V (1959) Open channel hydraulics. McGraw-Hill, New York
20. Timbadiya PV, Patel PL, Porey PD (2011) HEC-RAS based hydrodynamic model in prediction of stages of lower Tapi River. ISH J Hydraulic Eng 17(2):110–117
21. Pathan AI, Agnihotri PG, Patel D, Prieto C (2021) Identifying the efficacy of tidal waves on flood assessment study—a case of coastal urban flooding. Arab J Geosci 14(20):1–21

Flood Mitigation in and Around Sangli, Maharashtra, India, by Modification of River Meander Geometry

H. T. Dhumal, S. B. Thakare, S. N. Londhe, Pallavi Gavali, and Mohamed Niyaz

Abstract The Krishna River basin in Western Maharashtra, India, has been facing acute flood problems since 2005. The Krishna River, which originates at Mahabaleshwar in Maharashtra, has a steeper gradient in the initial reach. When the river enters a flatter region after Karad in the Satara District, it travels in a zigzag pattern with many bends and turns with 17 meanders on it. With these meanders with flatter gradients, the river becomes saucer-shaped, which in turn increases flooding and inundation. Straightening and removing the meanders at some places may reduce the channel length and improve the bed gradient, increasing the discharge carrying capacity, which in turn will help to reduce the flood inundation. In this paper, a hydrodynamic analysis with HEC RAS is done with natural river conditions and by removing a meander on the Krishna River, which is just upstream of its confluence with a tributary called Panchganga. The study reveals that removing this meander

H. T. Dhumal (✉)
Water Resources Department, Government of Maharashtra, Pune, India
e-mail: htdhumal@gmail.com

S. B. Thakare
Anantrao Pawar College of Engineering and Research, Pune, India

S. N. Londhe
Department of Civil Engineering, Vishwakarma Institute of Information Technology, Pune 411048, India
e-mail: shreenivas.londhe@viit.ac.in

P. Gavali · M. Niyaz
Centre for Development of Advanced Computing (CDAC), Pune, India
e-mail: pallavig@cdac.in

M. Niyaz
e-mail: niyazj@cdac.in

P. V. Timbadiya et al. (eds.), *Flood Forecasting and Hydraulic Structures*, Lecture Notes in Civil Engineering 340, https://doi.org/10.1007/978-981-99-1890-4_8

helps in flood mitigation. The flood level reduction is 1.29 m at Miraj and 0.45 m at Sangli which are the two majorly affected cities along the banks of the Krishna River in the state of Maharashtra.

Keywords Flood mitigation · Hydrodynamic modelling · Straightening of meanders · Krishna River

1 Introduction

The Krishna River is one of the major rivers in Maharashtra which covers an area of 21,114 km^2, with a length of 282 km within the state. The Krishna River rises in the Sahyadri Hill ranges at Mahabaleshwar and flows through the districts of Satara, Sangli, and Kolhapur in the Indian state of Maharashtra. It mainly flows from the North to the South. The Krishna River has a series of regular sinuous curves, bends, loops, and turns formed by a natural process, called meanders [1]. The experiments show that the erosion and deposition process in river channels initiates meandering [2]. These meanders are formed by adjustments of several variables tending towards the establishment of quasi-equilibrium in river channels [3]. The development and propagation of meanders upstream/downstream happen in heavy floods [4]. The meanders may laterally expand and translate the bend downstream depending on bank erosion coefficient and bank velocities [5]. The reservoirs upstream which in effect changes flood pattern and maximum flood values. These changes have an impact on four major parameters of meanders; the radius of curvature, wavelength, amplitude, and channel length and four indices sinuosity index, radius–wavelength ratio, meander shape index, and meander form index [6]. The discharging capacity of meanders differs from straight channels.

There were heavy rains from the 25 July 2019 to 15August 2019. The rains were widespread. The flood situation in Sangli and Kolhapur districts worsened on August 1 and peaked on August 8, 9, and 10. For more than ten days, nearly 65% of the Sangli and Kolhapur districts were underwater. Crops were submerged for more than ten days. All road and rail communication was disrupted.

The widths of inundation were more on meanders. Earlier researches show that the straightening of the river meander reduces the flow complexity [7], which has an impact on flood plans [8]. The neck cut-offs have effects on the sinuosity of the meanders [9] and increase bank erosion rates [10]. The rivers change their profile and sediment transport equilibrium, and there is little scope for regrowth of meander [11].

The city of Sangli on the banks of the Krishna River is vulnerable to floods. It is necessary to find solutions for the mitigation of these floods. The exact impact of straightening meander on flood stage value reduction has not been studied by anyone in the region. Hence, in this study, the authors have done a hydrodynamic analysis of the Krishna River with floods in 2019 with HEC Ras 6.0. An attempt has been made to straighten the meander at Ghalwad and Shirati lactated downstream of Sangli city,

which was heavily affected during the 2019 floods. The consequential impact on flood stages in and around the city of Sangli was studied and presented.

2 Study Area

The study area includes the Krishna River, which runs 365 kms from Karad in Maharashtra to Almatti in Karnataka. It is situated between the coordinates 17° 59′ 18.8″ N, 73° 38′ 16.7″ E, and 16° 19′ 51.5″ N, 75° 53′ 16.8″ E. The Krishna River has two tributaries: Warna, which is 53 kms long, and Panchganga, which is 94 kms long. The confluence of Warna and Krishna is near Sangli, and the confluence of Panchganga and Krishna is near Rajapur.

The Krishna River basin experienced unprecedented rains from 25 July 2019 to 10August 2019 in the upper reservoir catchments and free catchments areas. The study area is shown in Fig. 1.

The study's focal point is Sangli. All other locations are mentioned in the context of Sangli. Almatti is located 263.912 kms downstream of Sangli. Hippargi is 144.922 kms downstream of Sangli and 118.99 kms upstream of Almatti. Karad is located on the main Krishna River, 102.084 kms upstream of Sangli. All of the distances listed above are along river centre lines. Table 1 shows the distance matrix for the Krishna River.

2.1 Ghalwad Shirati Meander

The Krishna River has many curves and 17 major meanders. The Ghalwad Shirati Meander under consideration is shown in Fig. 2.

According to Fig. 2, this meander is located just upstream of the Panchganga confluence and flows through Ghalwad, Dhavali, Kutwad, Mhaisal, Kanwad, and Hasur, Kavatheguland, and Shirati. The river is 14.93 kms long. If this meander is straightened, it can be connected straight from Ghalwad to Shirati, reducing the length to 4.19 km (a 10.74 km reduction) and the sinuosity index [12] to 3.56.

3 Methodology

An unsteady hydrodynamic flood model is developed in the HEC RAS [13] for the region as explained in 3.2. The analysis is done with two analysis plans, one with natural river geometry and the other with straightening of meander at Ghalwad Shirati. The water levels in and around Sangli city are computed and compared for both plans. The reduction in flood water levels by straightening the meander is analysed, discussed, and presented.

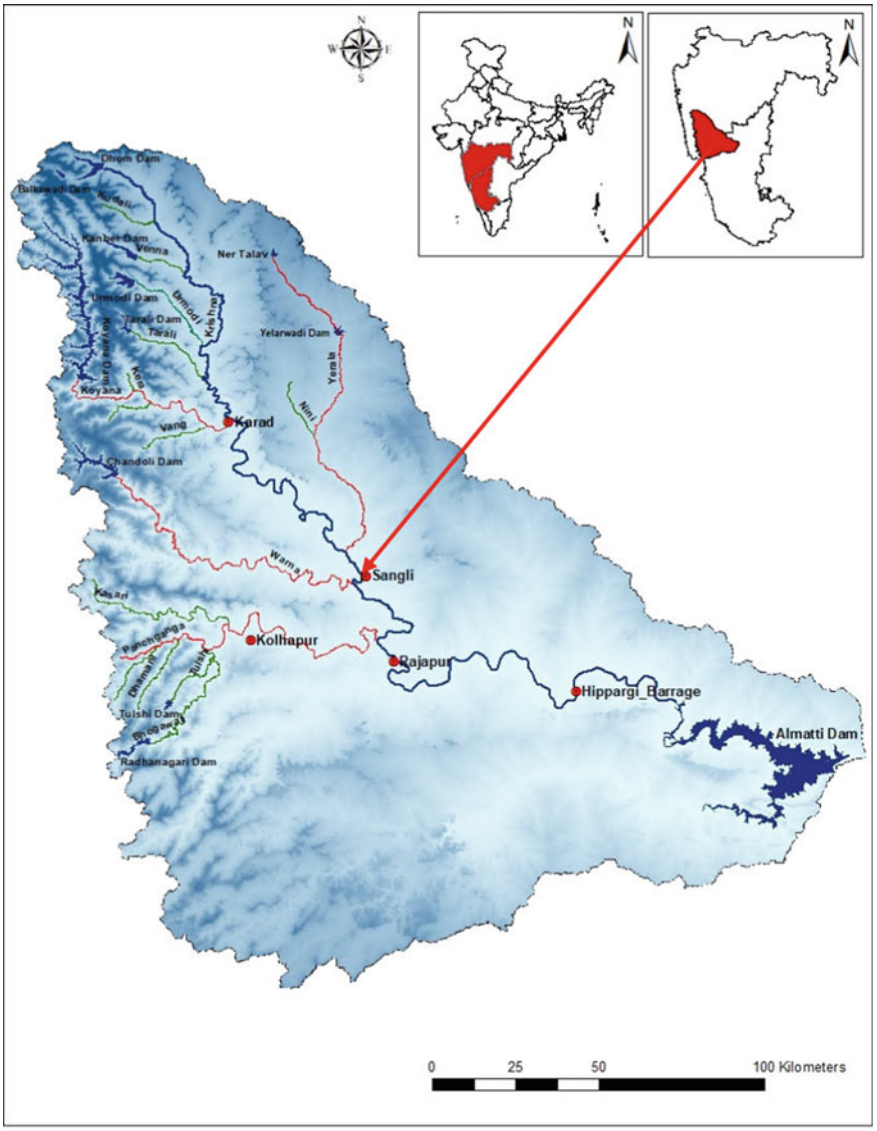

Fig. 1 Study area of the Krishna River basin

3.1 HEC RAS Model for Study Area

HEC RAS is a one-dimensional unsteady flow computer programme developed by the US Army Corps of Engineers' Hydrologic Engineering Centre to model channel flows and hydraulics. HEC RAS includes the RASMAPPER tool, which aids in identifying hotspot areas inundated by floods. This ability to identify inundated hotspot

Table 1 Important locations and their references on the Krishna River

Location		Distance matrix in Km				
Location name	Number in HEC RAS	Karad	Sangli	State Border	Hippargi	Almatti
Karad	502,965	0.00	− 102.08	− 167.74	− 246.54	366.00
Bramhanal	264,370	91.82	− 10.26	− 74.81	− 153.61	273.07
Sangli Irwin	255,405.5	102.08	0.00	− 65.65	− 144.45	263.91
Haripur	259,181	106.96	4.88	− 60.78	− 139.58	259.04
Miraj Arjunwad Bridge	237,688	118.72	16.63	− 49.02	− 127.82	247.28
Ghalwad	229,887	124.63	22.54	− 43.11	− 121.91	241.37
Shirati	166,939	138.76	36.67	− 28.98	− 107.78	227.24
Panchganga Conf	139,243	145.53	43.45	− 22.20	− 101.00	220.46
Rajapur KT weir	108,675	154.76	52.67	− 12.98	− 91.78	211.24
Maharashtra–Karnataka border	70,674	167.74	65.65	0.00	− 78.80	198.26
Hippargi	38,000	246.54	144.45	78.80	0.00	119.46
Almatti	1	366.00	263.91	198.26	119.46	0.00

areas greatly assists decision-makers in mitigating flood effects by implementing appropriate adaptation measures to avoid future floods. The HEC RAS model necessitates the collection of two types of major data: geometrical data and hydrological data.

3.2 Geometrical Data in HEC RAS

The main Krishna River from Karad to Almatti as well as two tributaries Warna and Panchganga has a total length of 544.69 km. Three river reaches on the Krishna River from Karad to Almatti are considered: Karad to Haripur (Warna Confluence), Haripur to Rajapur, and Rajapur to Almatti. Warna and Panchganga are the other two reaches. There are 665 georeferenced cross-sections in total, 170 of which are surveyed by WRD and the remaining 495 are interpolated. RASMAPPER is used to superimpose the geometry on terrain models and Google Maps. As a result, inundation maps and depths can be generated for the actual river channel with curves and meanders. Using USGS 30 m ASTER DEM data, cross-sections beyond surveyed lengths are calculated. Other data such as river geometry, boundary conditions, basin resistance, downstream reach lengths (LOB, channel, ROB), main channel bank stations, data of three junctions, station and elevation coordinates, reach length, channel width at the sections, manning's coefficient and contraction/expansion coefficient, inline structures such as KT weirs, Hippargi barrage, and Almatti dam are included in the

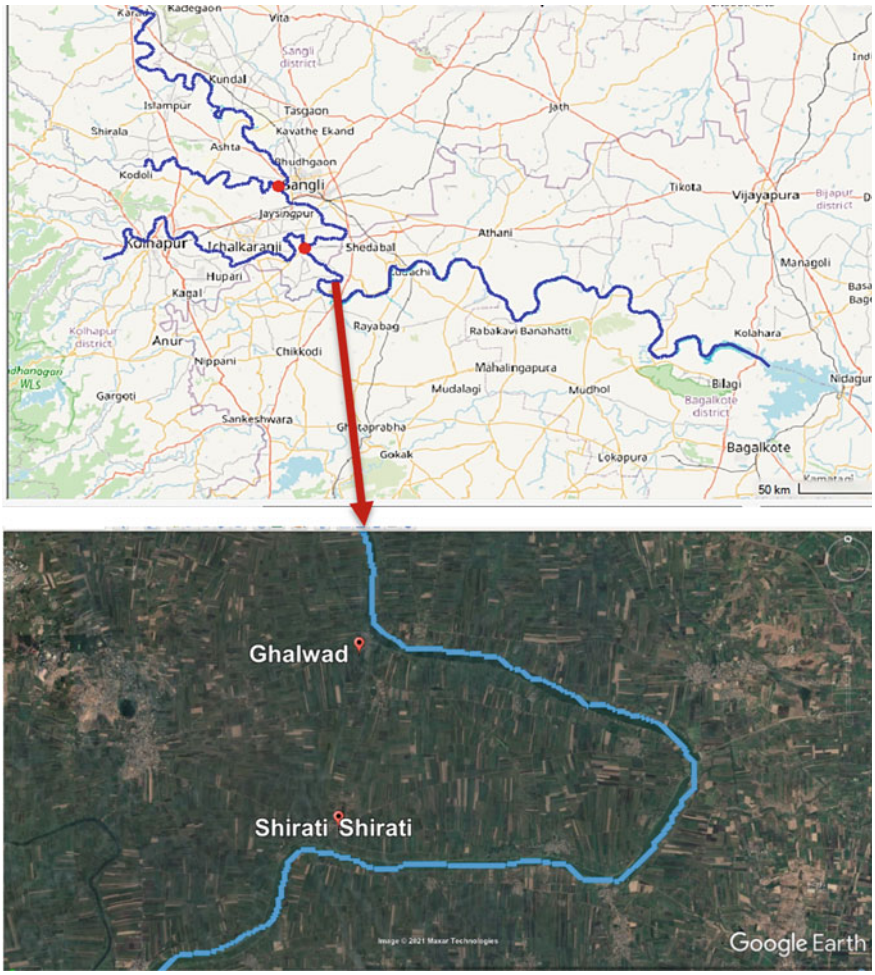

Fig. 2 Ghalwad Shirati meander on Google map

geometric model with specifications and the upstream–downstream length. Figure 3 depicts the geometric model created in HEC RAS.

3.3 Hydrological Data

The hydrological data for the period 25 July 2019 to 17 August 2019 was obtained from the Water Resources Department and used in the HEC RAS model for unsteady flow simulation (as input boundary conditions to the Krishna River). This includes the observed flood hydrograph at Karad, the observed flood hydrograph at Kolhapur's

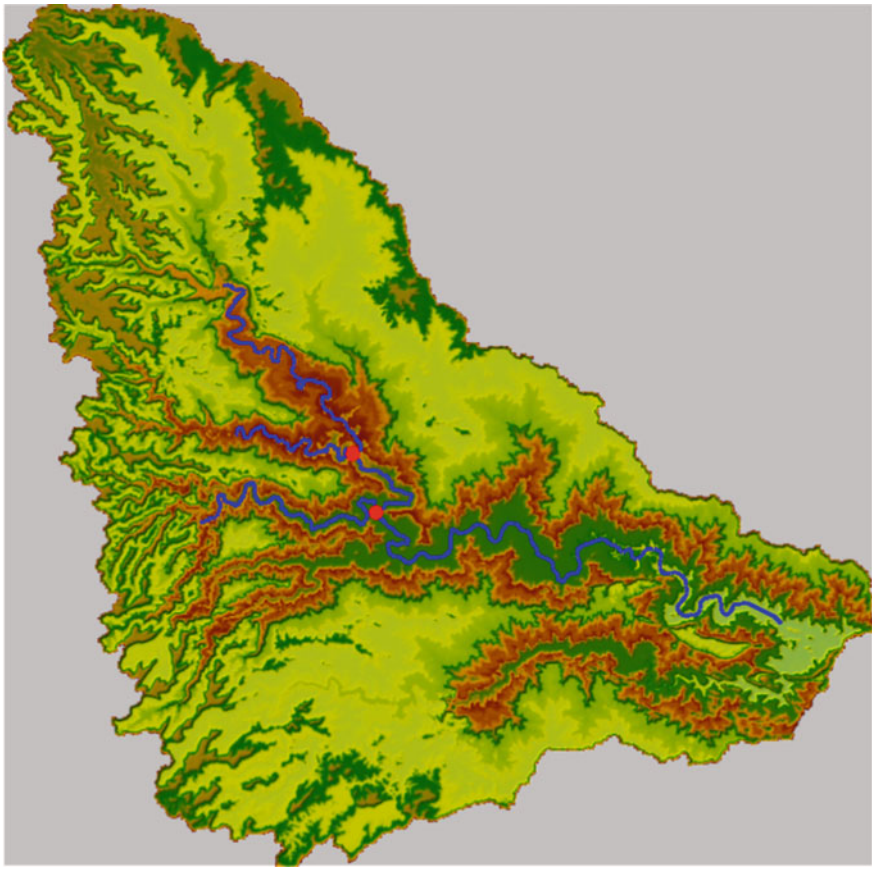

Fig. 3 River geometry with cross-section and associated terrain

Rajaram weir, the uniform lateral hydrograph from Karad to Sangli, Sangli to Rajapur, Rajapur to Hippargi, Hippargi to Almatti, Warna to Krishna confluence, and Kolhapur to Krishna confluence, as well as the observed outflow hydrograph and water levels in the Almatti reservoir as a downstream. For known flood and flood stage values, this hydrodynamic model has been calibrated and validated.

3.4 Analysis

The analysis is done in two analysis plans. In the first plan of analysis, with the geometry and all other conditions mentioned in Sect. 3 above, the unsteady condition of analysis is done for flood hydrographs from 25 July 2019 to 17 August 2019 in a calibrated HEC RAS model. The peak flood stage observed at Irwin bridge, Sangli,

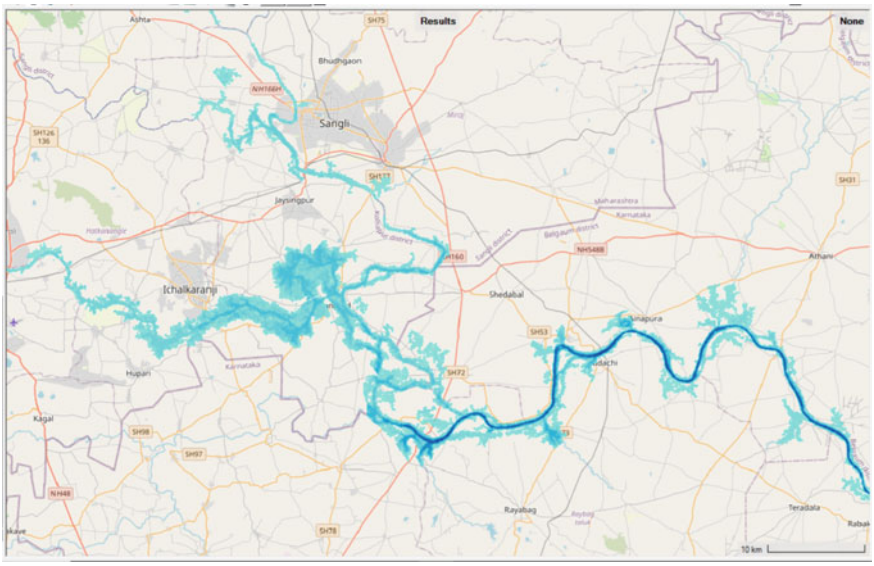

Fig. 4 2D flood inundation map on 9 August 2019 at 04:00 h with natural geometry

is 543.75 m on 9 August 2019 at 04:00 h. A 2D flood inundation map at this instant of time is shown in Fig. 4 which is generated with a tool named RAS Mapper in HEC RAS.

In the second plan of analysis, the Ghalwad Shirati meander is replaced with straight line river geometry hereafter called a straightened meander. For this, the Ghalwad Shirati curved river reach ABC of 14.93 km is replaced by a straight reach AC of 4.19 km in Fig. 5, with all other conditions remaining the same. Both the cross-sections at the start of the meander (Ghalwad) and the end of the meander (Shirati) are surveyed cross-sections. The intermediate cross-sections on the straightened meander are interpolated, with the help of the HEC RAS software.

The straightening of this meander has improved the bed gradients as shown in Table 2.

4 Results and Discussion

4.1 Effect of Straightening of Meander on the Krishna River

The unsteady analysis is done for two plans, one with a natural meander and the other with a straightened meander. The flood stages in and around Sangli are compared for both plans. Two types of water levels are considered here. The first one is on 9 August 2019 when there was a peak flood at Sangli. The second is the maximum

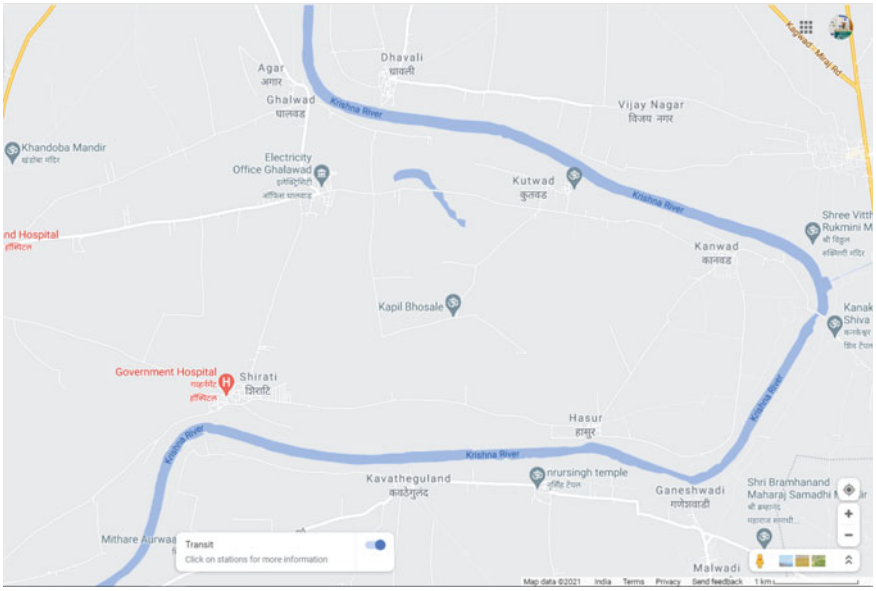

Fig. 5 View of straightened meander at Ghalwad Shirati

Table 2 Original and revised bed gradient

Ground levels in m		Length in km		Bed gradient	
At start	At end	Original	Revised	Original	Revised
522.70	518.33	14.93	4.19	3416.48	958.81

flood value at each location from 25 July to 17 August 2019. The results for both the plans with two flood values (on 9 July and the maximum of the period) are shown in Table 3 with the value of the reduction in flood water level at important locations in and around Sangli.

It can be seen from Table 3 that on 9 August 2019, the straightened meander effect on reduction of the flood level at the start of the meander at Ghalwad is 1.4 m, and the effect is continued on upstream Miraj 1.26 m. Further upstream of Miraj the effect at Sangli KT weir is 0.51 m and 0.47 m at Sangli, the effect is considerable 0.32 m up to Bramhanal, which is 9 km upstream of Sangli and 30 km upstream of the meander. However, there is a slight rise in flood levels downstream of the meander after straightening. The effect of the rise in flood level diminishes at the Maharashtra–Karnataka border. The comparative flood levels in and around Sangli on 9 August are plotted in Fig. 6.

On similar lines, plots of maximum flood levels at various locations with the natural condition and straightened meander are compared in Fig. 7.

Table 3 Water levels in and around Sangli for natural and straightened meander

Location name	Distance from Almatti	Water levels on 9 August in m			Maximum water levels in m		
	In km	Natural condition	Straightened meander	Reduction in level	Natural condition	Straightened meander	Reduction in level
Brahmanal	271.57	545.62	545.3	0.32	545.62	545.3	0.32
	264.90	544.52	544.09	0.43	544.53	544.09	0.44
Sangli Bypass bridge	264.87	544.45	544.01	0.44	544.46	544.01	0.45
	263.91	544.36	543.89	0.47	544.36	543.9	0.46
Irwin bridge	263.89	544.3	543.83	0.47	544.31	543.84	0.47
	263.36	544.23	543.75	0.48	544.24	543.75	0.49
Sangli KT Weir	263.28	543.82	543.31	0.51	543.83	543.32	0.51
	260.01	543.7	543.15	0.55	543.71	543.16	0.55
Warna confluence	259.03	543.7	543.15	0.55	543.71	543.16	0.55
	248.94	542.95	542.19	0.76	542.98	542.21	0.77
Miraj Arjunwad bridge	245.61	542.3	541.04	1.26	542.36	541.08	1.28
Ghalwad	241.37	542.13	540.73	1.4	542.21	540.82	1.39
	234.73	541.28			541.38		
Mhaisal KT Weir	234.69	541.26			541.36		
Shirati	227.23	540.19	540.32	− 0.13	540.58	540.56	0.02
Panchganga confluence	220.46	539.4	539.5	− 0.1	540.14	540.12	0.02
	211.26	538.25	538.36	− 0.11	539.18	539.16	0.02

(continued)

Table 3 (continued)

Location name	Distance from Almatti	Water levels on 9 August in m			Maximum water levels in m		
	In km	Natural condition	Straightened meander	Reduction in level	Natural condition	Straightened meander	Reduction in level
Rajapur KT				0			0
	211.21	538.22	538.33	− 0.11	539.15	539.14	0.01
Maharashtra–Karnataka border	198.26	536.79	536.89	− 0.1	537.86	537.84	0.02

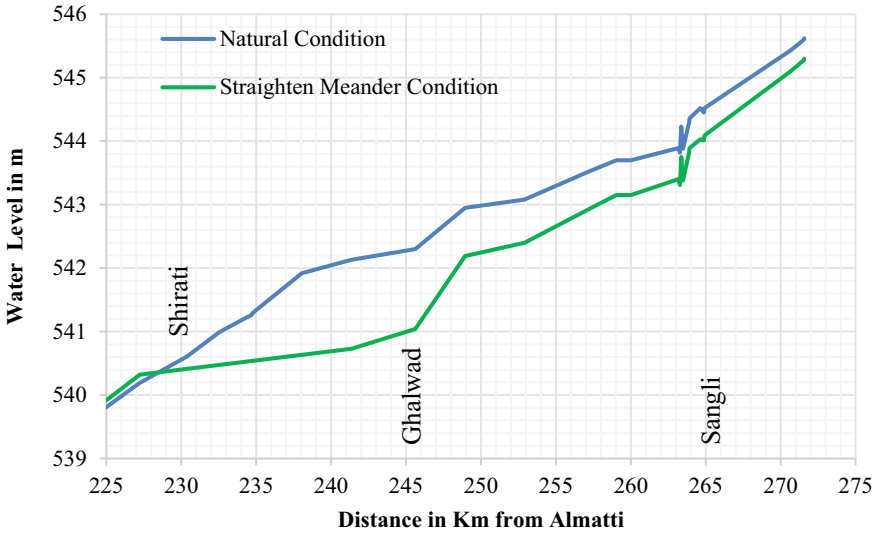

Fig. 6 Water surface profile with natural condition and straightened meander condition of the Krishna River on 9 August 2019

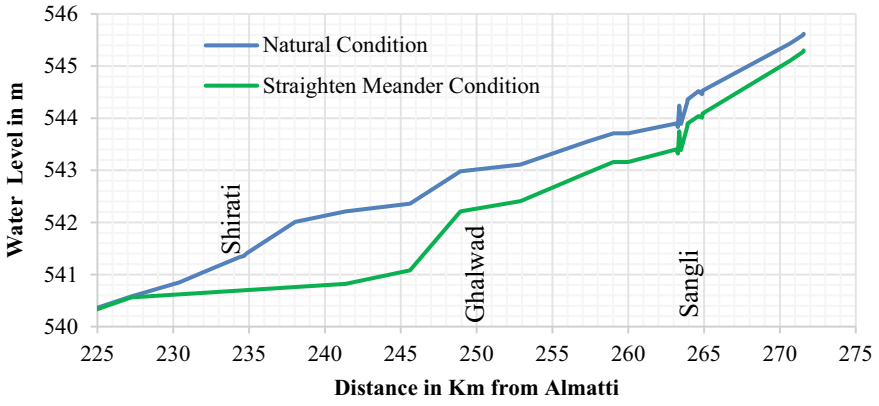

Fig. 7 Maximum water surface profile with natural condition and straightened meander condition in Krishna River

It is seen from Fig. 7 that the effect on maximum flood values is more or less the same as on 9 August 2019. However, in this case, there is no rise downstream of the straightened meander.

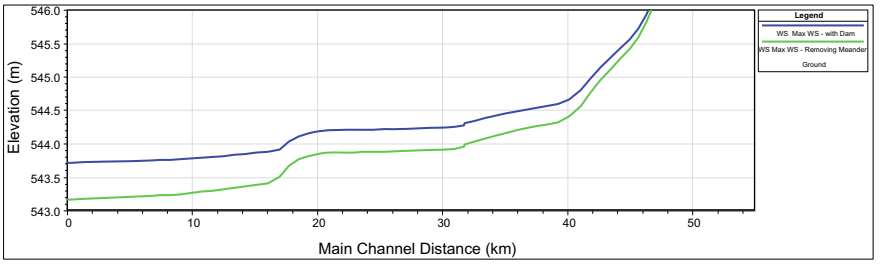

Fig. 8 Maximum water surface profile with natural condition and straightened meander condition in Warna River

4.2 Effect of Straightening of Meander on the Warna River

The confluence of the Warna and Krishna rivers is at Haripur, 3 km downstream of Irwin bridge, Sangli. To study the effect on the Warna river by straightening of meander on the main Krishna River, the direct plot from HEC RAS of these two conditions is shown in Fig. 8

From Fig. 8, it is observed that there is also a positive impact of the straightening of the meander on the Warna River. There is a considerable reduction in flood values up to 40 km.

By removing the meander and straightening, the water level is significantly reduced. Individual meanders must be studied separately, so this cannot be a general conclusion. The feasibility of removing meanders must also be investigated. The combined effect of removing all possible Krishna River meanders may be studied further. The straightening of meanders needs maintenance otherwise river channels will return to their original forms [1]. Other important meanders on the rivers in the study area are tabulated in Table 4.

Table 4 Other important meanders on rivers in the study area

River	Location of meander	Ground levels		Length		Sinuosity
		At start	At end	Original	Straightened	Index
Krishna	Shirgaon-Nagthane	536.26	536.06	7078.2	1010	7.0
Krishna	Khidrapur	515.23	515.02	23,392.8	5811	4.02
Panchganga	Kurundwad	522.4	518.09	13,994.8	2156	6.49
Warna	Danoli	527.53	526.75	4751	2546	1.87

5 Conclusion

On 9 August 2019, the straightened meander effect on the reduction of flood levels at the start of the meander at Ghalwad is 1.4 m, 1.26 m at Miraj, 0.51 m at Sangli KT weir 0.47 mat Sangli and 0.32 m at Bramhanal. A considerable reduction of up to 30 km upstream of the meander is seen. There is a slight rise in flood levels downstream of the meander after straightening which, diminishes at the Maharashtra–Karnataka border. A positive impact of straightening of the meander on the Krishna River is observed on the Warna tributary. There is a considerable reduction in flood values up to 40 km. It is revealed from the study that the straightening of meanders is a helpful structural measure to mitigate floods; however, individual meanders have to be analysed separately. The further combined impact of all meanders may be studied as well.

References

1. Field J, Tambunan B, Floch P (2014) Pyanj river morphology and flood protection [Online]. Available: www.adb.org
2. Yong NS, Mohamad IN, Lee W-K (2018) Experimental study on river meander planform pattern [Online]. Available: www.sciencepubco.com/index.php/IJET
3. Leopold LB, Wolman G (1963) River channel pattern braided, meandering and straight
4. Nagata T, Watanabe Y, Yasuda H, Ito A (2014) Development of a meandering channel caused by the planform shape of the river bank. Earth Surf Dyn 2(1):255–270. https://doi.org/10.5194/esurf-2-255-2014
5. Ashraf FU, Liu X (2013) River meandering prediction: Case studies for four rivers in Texas. In: World environmental and water resources congress 2013: showcasing the future—proceedings of the 2013 congress, pp 2009–2019. https://doi.org/10.1061/9780784412947.197
6. Islam A, Guchhait SK (2017) Analysing the influence of Farakka Barrage project on channel dynamics and meander geometry of Bhagirathi river of West Bengal, India. Arab J Geosci 10(11). https://doi.org/10.1007/s12517-017-3004-2
7. Zhou T, Endreny T (2020) The straightening of a river meander leads to extensive losses in flow complexity and ecosystem services. Water (Switzerland) 12(6). https://doi.org/10.3390/W12061680
8. Bechtol V, Laurian L (2005) Restoring straightened rivers for sustainable flood mitigation. Disaster Prevent Manage: Int J 14(1):6–19. https://doi.org/10.1108/09653560510583806
9. Guo X, Chen D, Parker G (2019) Flow directionality of pristine meandering rivers is embedded in the skewing of high-amplitude bends and neck cutoffs. Proc Natl Acad Sci U S A 116(47):23448–23454. https://doi.org/10.1073/pnas.1910874116
10. Ondruch J et al (2018) Response of channel dynamics to recent meander neck cut-off in a lowland meandering river with artificial training history: the Morava River, Czech Republic. Hydrol Sci J 63(8):1236–1254. https://doi.org/10.1080/02626667.2018.1474218
11. Talbot T, Lapointe M (2002) Modes of response of a gravel bed river to meander straightening: the case of the Sainte-Marguerite River, Saguenay Region, Quebec, Canada. Water Resour Res 38(6):9-1–9-7. https://doi.org/10.1029/2001wr000324

12. García JH (2015) River sinuosity index: geomorphological characterisation (Technical Note) Galician coast view project spatial temporal patterns of river discharges in Spain view project [Online]. Available: https://www.researchgate.net/publication/271529347
13. Brunner GW (2021) HEC-RAS river analysis system user's manual, New York [Online]. Available: www.hec.usace.army.mil

Performance Evaluation of 2D Hydrodynamic Model for Lower Narmada River Basin, India

Madhu Priya Aedla, Shubham M. Jibhakate, and P. V. Timbadiya

Abstract In the current study, a two-dimensional (2D) hydrodynamic (HD) model is developed to investigate the effect of proposed Bhadbhut Barrage on the hydraulics of lower Narmada River, India. The model has been developed for the river stretch of 63 km from Shuklatirth to the Arabian Sea at Gulf of Khambhat. The flood flow, routed from Garudeshwar gauging site to Shuklatirth (ungauged site) using the Muskingum channel (hydrological) routing method, is used as upstream boundary condition, whereas a constant (observed) high tide of 4.69 m above mean sea level is used as a downstream boundary condition in the model. The model is developed for the existing condition, for the flood of year 2006 by considering distributed floodplain roughness coefficient based on land use land cover (LULC) pattern. The performance of the developed model is found satisfactory, against the water level at Golden Bridge, Bharuch, with RMSE of 0.49 m. The calibrated model can be useful to simulate the different scenarios regarding the construction of barrage across lower Narmada River as well as the embankment along the channel and its effect of water level at different locations.

Keywords Lower Narmada basin · Bhadbhut barrage · Two-dimensional hydrodynamic model · Floodplain roughness · Land use land cover

1 Introduction

Floods are the most common and damaging natural hazards in India and other parts of the world. Rainfall, ice melting, structural failure, and other causes can contribute to floods. Due to heavy rainfall, Telangana, Andhra Pradesh, Karnataka, and Maharashtra states experienced floods in October 2020. Forecasting of the floods gives

M. P. Aedla (✉) · S. M. Jibhakate · P. V. Timbadiya
Department of Civil Engineering, Sardar Vallabhbhai National Institute of Technology, Surat, Gujarat 395007, India
e-mail: priyamadhu460@gmail.com

P. V. Timbadiya
e-mail: pvtimbadiya@ced.svnit.ac.in

P. V. Timbadiya et al. (eds.), *Flood Forecasting and Hydraulic Structures*, Lecture Notes in Civil Engineering 340, https://doi.org/10.1007/978-981-99-1890-4_9

sufficient warning to the people and the concerned authorities to take civil defense measures within the time [1]. Many models are employed for flood forecasting and to provide information on flood characteristics. One-dimensional (1D) models, two-dimensional (2D) models, and 1D river flow models linked with 2D floodplain flow (coupled 1D-2D) models have been extensively used for flood estimation, flood hazard, and risk assessment [2]. Despite its ease of use and ability to provide information on bulk flow parameters, 1D models fall short of providing extensive floodplain information. As a result, attempts have been made to represent the 2D models for flow in floodplains [3].

Timbadiya et al. [4] and Patel et al. [5] predicted the water levels using a 1D-2D coupled hydrodynamic model in the lower Tapi River and the Surat City and developed stage-discharge curves to estimate flood levels. Mani et al. [2] and Tansar et al. [3] classified the flooded area as high, medium, and low hazard. Tingsanchali et al. [6]; Masood et al. [7]; Hazarika et al. [8]; and Erena et al. [9] developed two-dimensional hydrodynamic model and prepared flood hazard maps and flood risk maps, which can help in predicting the flood danger ahead of time. Pinho et al. [10] and Ahn et al. [11] developed MIKE 21 hydrodynamic model for Lower Var valley region in France and Lima basin in Portugal and concluded that flexible mesh is more efficient to simulate floods with high spatial resolution. From the past studies, it is evident that the two-dimensional hydrodynamic model is the most promising tool for predicting the water levels corresponding to the flood releases and in fostering the flood inundation maps.

During the monsoon season in India, the Narmada River is notable for recurring floods and flooded heavily in 1818, 1823, 1832, 1854, 1855, 1868, 1878, 1891, 1893, 1894, 1895, 1898, 1907, 1923, 1926, 1937, 1954, 1959, 1961, 1964, 1968, 1970, 1972, 1973, 1984 and 1991 [12]. The Narmada River flows in a deep channel with high banks in Madhya Pradesh, but it expands out and flows as a wide stream with low banks for the rest of its journey down to the Gulf of Khambhat in Gujarat's flat plains [13]. Even moderate floods cannot be avoided due to the Narmada River's low banks downstream of Bharuch to the Gulf of Khambhat. The construction of the proposed Bhadbhut Barrage at Bharuch in lower Narmada River, would have an impact on upstream water levels, especially when floodwater flows through the river. Keeping in view the history of past flood and proposed barrage on river stretch, the major objectives of the current study are (i) to develop a two-dimensional hydrodynamic model for the lower Narmada River from Shuklatirth to the Arabian Sea by considering the effect of tidal level and distributed floodplain roughness (ii) to study the impact of the barrage structure on the water levels.

2 Study Area and Data Collection

2.1 Narmada River Basin

The Narmada River is a major river in Central India and the largest interstate west-flowing River of the Peninsula. It creates the conventional border between South India and North India. The Narmada River originates at Amarkantak Hill in Anuppur District of Madhya Pradesh at an elevation of 1057 m. The Narmada River flows for 1312 km before discharging into the Arabian Sea's Gulf of Khambhat at Bharuch in Gujarat. Out of 41 tributaries, 22 are on the left and 19 on the right, mainly, viz. Barna River, Ganjal River, Chhota Tawa River, Hiran River, and Jamtara River, Kolar Orsang River, Sher River, and Tawa River.

The elongated Narmada basin extends over Madhya Pradesh, Maharashtra, and Gujarat, with a catchment area of 98,796 km^2. Out of total annual rainfall within the basin, 94% of rainfall is recorded during monsoon months (June to October). The basin climate is humid tropical, with sub-humid conditions in the east and semi-arid conditions in the west. The Narmada basin is divided into three sub-basins, (a) Upper Narmada Basin from Origin to Hoshangabad (b) Middle Narmada Basin from Hoshangabad to Sardar Sarovar Dam (c) Lower Narmada Basin from Sardar Sarovar Dam to Arabian Sea.

The present study covers an area of 3423 km^2 from Shuklatirth to the Gulf of Khambhat in the lower Narmada basin, as shown in Fig. 1. The basin area of the current study includes the Ankleshwar, Varga, Bharuch, and Hansot of the Bharuch District. There are four bridges in the study area: Railway Bridge at Bharuch, Golden Bridge upstream of Railway Bridge in Bharuch, and the two road bridges at Zadeshwar. The details of the bridges present in the study reach are tabulated in Table 1. One gauging site is present in the study area at Golden Bridge, Bharuch.

2.2 Data Collection

The details of the input data, viz. topographic, hydrologic, hydraulic, LULC, tidal level, slope of the river data for two-dimensional hydrodynamic modeling of the study area, are described in Table 2.

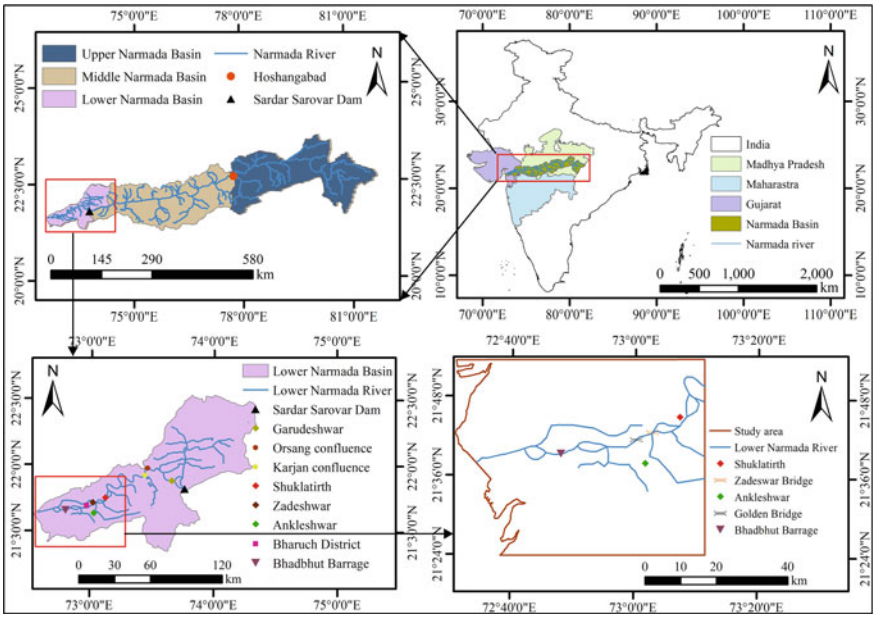

Fig. 1 Index map of Narmada basin and the study area

Table 1 Details of bridges present in the study area

Location	Bridge	Soffit level/ Bottom of girder (m)	Rail/Road level (m)
Zadeshwar	Old road bridge	17.75 m at center 15.73 m at piers	21.25
	New road bridge	18.72 m at center 15.97 m at piers	21.22
Bharuch	Road bridge (Golden Bridge)	16.14	16.79
	Rail bridge	15.26	17.06

3 Methodology

3.1 Hydrologic Channel Routing

Due to the unavailability of hydrologic measurements at Shuklatirth, the flow was routed from the Garudeshwar gauging site to Shuklatirth (ungauged site) using the Muskingum routing method. From the stage-discharge relationship, the inflow hydrograph at Garudeshwar has routed up to Shuklatirth. Tewolde and Smithers [14]; Song et al. [15] applied Muskingum routing method for flood forecasting in ungauged

Table 2 Details of the input data and their source

Types	Data description	Purpose	Source
Topographic data	Contours of the floodplains surveyed at an interval of 0.5 m in the AutoCAD file format Digital Elevation 1 Arc-Second Global data	For mesh generation later creation of Bathymetry	Executive Engineer, PIU-1 (Project Implementation Unit), Gujarat Engineering Research Institute (GERI), Vadodara Shuttle Radar Topography Mission (SRTM) (https://earthexplorer.usgs.gov/)
Hydrologic data	Water level at Garudeshwar and Bharuch for 2006 year	For routing the flood from Garudeshwar to Shuklatirth For calculating RMSE value at Bharuch	Executive Engineer of Central Water Commission for Tapi Division, Surat
Hydraulic data	Location of barrage and bridges	To study the effect of barrage	Central Water Commission for Tapi Division, Surat
Land Use Land Cover (LULC) data	Lower Narmada basin LULC map for 2018 year	For classification of land use land cover into 6 classes	National Remote Sensing Centre (NRSC), Hyderabad
Tidal level	Observed daily tidal levels were synchronized according to the lunar cycle and simulation time period	For downstream boundary condition	National Institute of Ocean Technology (N.I.O.T), Chennai
Slope of the River	Processing Digital Elevation 1 Arc-Second Global data in ArcGIS 10.3	To find longitudinal slope of the Narmada River	Shuttle Radar Topography Mission (SRTM) (https://earthexplorer.usgs.gov/)

basins. The flow characteristics such as depth of flow (y), wetted perimeter (P), hydraulic radius ($R \approx y$, for wide rectangular channel), flow top width ($W = P$, for wide rectangular channel) and average velocity (V_{av}) has utilized to estimate the Muskingum parameters k and x from the empirical relationships given in Table 3.

where Q_p, Q_o, Q_b were the peak, reference, and minimum discharges, obtained from the inflow hydrograph at Garudeshwar. A is the cross-sectional area of flow (m^2), n is Manning's roughness coefficient, S is the longitudinal bed slope (0.0001), V_w is the wave celerity (m/s), and ΔL is the river reach length from Garudeshwar to Shuklatirth (99,607 m). The k and x values will be obtained for different Manning's value using the above empirical relations. The routing interval Δt has been taken as 3 h such that $k > \Delta t > 2kx$ [16] for best results. The flood hydrograph was obtained at Shuklatirth by substituting the values of k and x in the Muskingum Routing Equation (Eq. 9).

Table 3 Empirical equations used to estimate Muskingum parameters k and x [14]

Equations	Eq. No.	Equations	Eq. No.
$Q_o = Q_b + 0.5(Q_p - Q_b)$	(1)	$k = \frac{\Delta L}{V_w}$	(7)
$\mathrm{AR}^{\frac{2}{3}} = \frac{Q_o n}{\sqrt{S}}$	(2)	$x = 0.5 - \frac{Q_o}{2SPV_w \Delta L}$	(8)
$P = 4.76\sqrt{Q_o}$	(3)	$Q_n = C_0 I_n + C_1 I_{n-1} + C_2 Q_{n-1}$	(9)
$y = \left(\frac{Q_o n}{P\sqrt{S}}\right)^{\frac{3}{5}}$	(4)	$C_0 = \frac{-kx+0.5\Delta t}{k-kx+0.5\Delta t}$	(10)
$V_{av} = \frac{1}{n} R^{\frac{2}{3}} \sqrt{S}$	(5)	$C_1 = \frac{kx+0.5\Delta t}{k-kx+0.5\Delta t}$	(11)
$V_w = \frac{5}{3} V_{av}$	(6)	$C_2 = \frac{k-kx-0.5\Delta t}{k-kx+0.5\Delta t}$	(12)

Note Sum of the Muskingum Coefficients, i.e., C_0, C_1, C_2, must be unity

3.2 A Two-Dimensional Hydrodynamic Model in MIKE 21 Flow Model FM

A two-dimensional hydrodynamic modeling approach has been used by a number of researchers to simulate flood flow in floodplains. MIKE 21, a 2D hydrodynamic model developed by the Danish Hydraulic Institute in Denmark, is one of the numerical models. The hydrodynamic module has based on the numerical solution of 2D incompressible Reynolds averaged Navier–Stokes equations using Boussinesq and hydraulic pressure assumptions [17]. The model is made up of equations for continuity, momentum, temperature, salinity, and density. A cell-centered finite volume approach is used to spatially discretize the MIKE 21 FM model equations, which use unstructured grids. The time integration of the shallow water equations has been performed using an explicit method in this model. Because an explicit scheme has a stability constraint, a dynamic time step is used. To ensure model performance and stability, the model specifies the time step for each computing step. In the horizontal plane, MIKE 21 FM uses an unstructured mesh comprising triangles elements. The methodology adopted for the present study as shown in Fig. 2.

3.3 Model Development and Parameterization

The surveyed topographic data and SRTM data were converted into .xyz file format using Arc Map 10.3 and imported into the mesh generator tool in MIKE zero. The arc attributes are specified as one to the land boundary and two to the downstream boundary. The bathymetry at the node points was interpolated using the natural neighborhood method, and the triangular mesh was generated specifying the maximum element area of 5000 m^2 and minimum angle between the element faces of about 28°. The flexible triangular mesh was generated with 1,067,255 mesh elements and 535,625 nodes. The developed bathymetry of the domain is shown in Fig. 3.

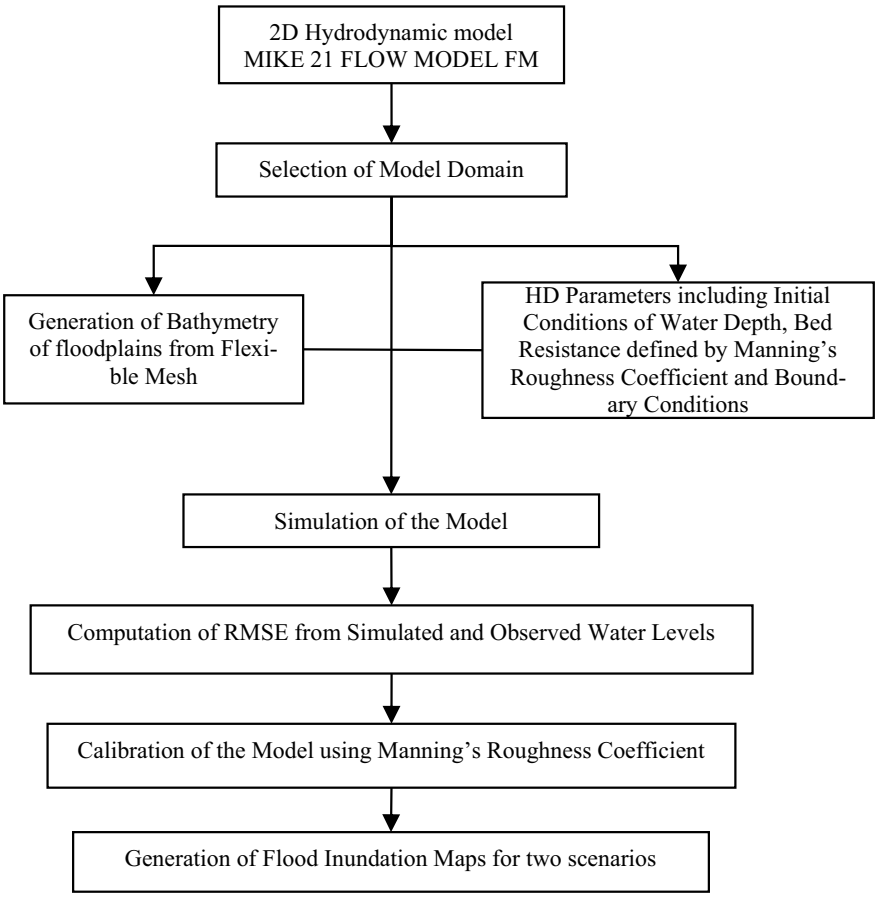

Fig. 2 Methodology adopted for the present study

The time step was taken as 3600 s for the simulation. A lower-order scheme technique was adopted for both time integration and space discretization. The minimum time step of 0.01 s and the maximum time step of 3600 s were chosen to maintain the CFL number smaller than 1.

For the domain area, drying and wetting depths values were given as 0.0025 m and 0.05 m, respectively. Distributed Manning's 'M' values for the entire domain area were taken from the supervised land use land cover (LULC) map of the lower Narmada basin (Table 4 and Fig. 4). A simple source was taken in the discharge varying in time format as the upstream boundary condition.

To avoid instabilities, an initial level for floodplains was dry, and for the river section, water depth was taken as 3.2 m (observed data). A constant high tide level of 4.69 m above mean sea level was given as the downstream boundary condition.

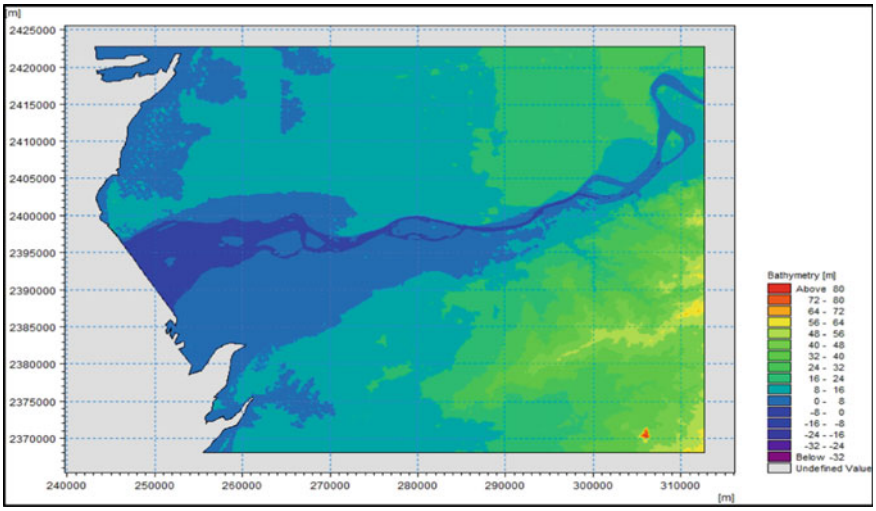

Fig. 3 Bathymetry of the study domain

Table 4 Manning's 'n' and 'M' values for the land use and land cover pattern [18]

Sr. No.	Class	n	M (= 1/n)
1	Water	0.010–0.025	100–40
2	Agriculture	0.035	28.57
3	Fallow	0.040	25
4	Wasteland	0.055	18.18
5	Forest	0.150	6.67
6	Built-up	0.150	6.67

Parameters like wind forcing, ice coverage, infiltration, precipitation–evapotranspiration, tidal potential, and wave radiation stresses were not considered in the model. In MIKE 21 Flow Model FM, the results can be obtained at the desired location as a point, line, and area series. In the present study, model was simulated for the water surface elevation and maximum water depth at Golden Bridge, Zadeshwar Bridge, and proposed Bhadbhut Barrage.

3.4 Calibration of the Developed Model

In the current study, two scenarios: (a) existing condition: without barrage and (b) with barrage gate closed, were considered. The 2D model is simulated for the 2006 flood event considering the first scenario, existing condition: without barrage. The hydrograph for the 2006 flood routed from Garudeshwar to Shuklatirth with a peak

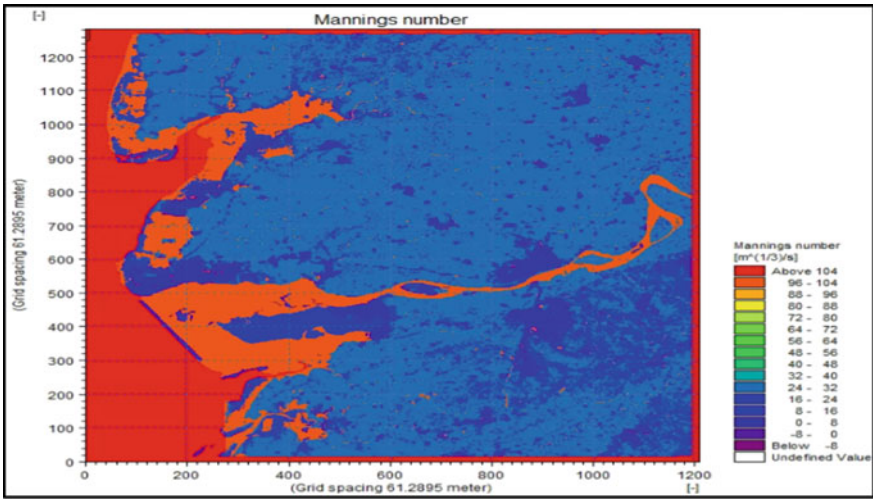

Fig. 4 Spatially distributed Manning's number ($M = 1/n$) across the model domain

discharge of 22,707 m^3/s (on 07-08-2006 at time 18:00:00) used as a source in the model, while a continuous high tide of 4.69 m used as the downstream boundary condition. By trial-and-error method, various combinations of Manning's n value were considered for the flood routing from Garudeshwar to Shuklatirth and for the river stretch from Shuklatirth to Gulf of Khambhat. Simulated and observed water levels at the Golden Bridge, Bharuch, were compared for different trials, and then performance index like root mean square error (RMSE) was computed in Table 5. From Table 5, it can be observed that the simulated water levels have shown good agreement against observed water levels for Manning's roughness coefficient of 0.010 in the river stretch. From Fig. 5, comparisons between observed and simulated water levels were found acceptable.

Table 5 RMSE has computed for the observed and simulated water levels at the Golden Bridge, Bharuch, for different simulation trials of 2006 flood

Sr. No.	Manning's n value for river stretch	Manning's M value for river stretch	RMSE in water levels (m)
1	0.025	40	1.19
2	0.020	50	0.93
3	0.015	66.67	0.68
4	0.010	100	0.49

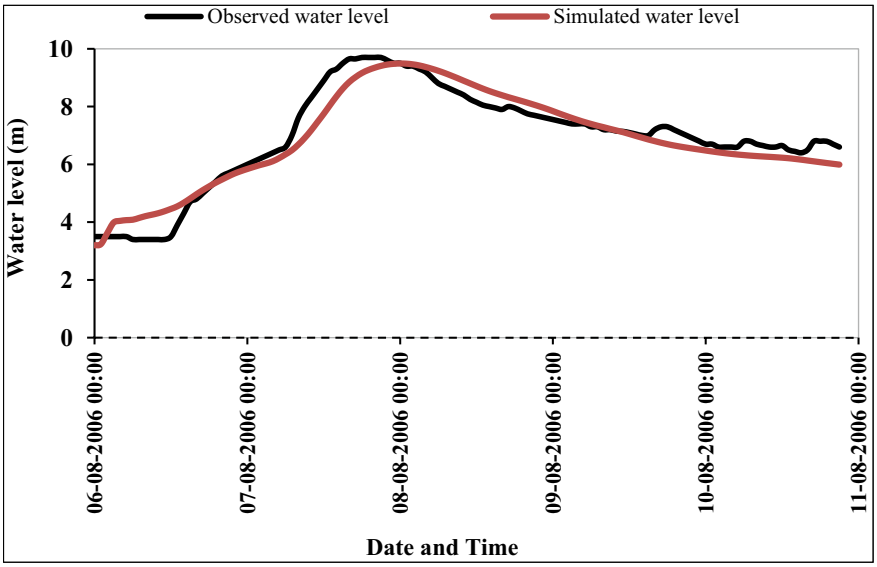

Fig. 5 Comparison of observed and simulated water levels at Golden Bridge

4 Results and Discussions

Along the longitudinal profile of the Narmada River, the water level fluctuations for the 2006 flood event at Zadeshwar Bridge, Golden Bridge, and Bhadbhut Barrage under considered scenarios are given in Table 6. The spatial variation of flood inundation corresponding to the scenarios is shown in Figs. 6 and 7. For both scenarios, most of the floodwater inundates a significant area on the left bank due to low bank height on left side of the Narmada River (Figs. 6 and 7).

Table 6 Water level variations for 2006 flood event considering different scenarios

Scenario No.	Scenario	Maximum water level (m)		
		Zadeshwar bridge	Golden bridge	Bhadbhut barrage
1	Existing condition: without barrage	9.983	9.49	5.082
2	With barrage gate closed	11.084	10.846	10.216

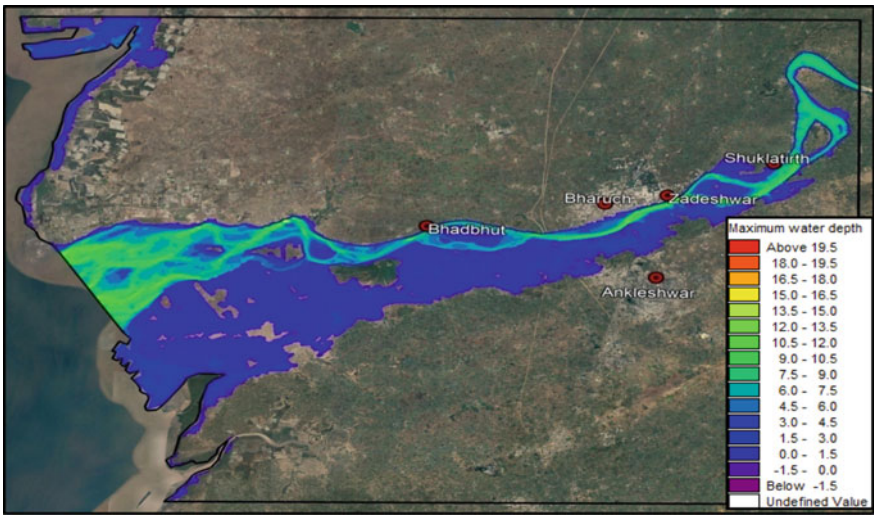

Fig. 6 Spatial variation of flood inundation for scenario 1 existing condition: without barrage 2006 flood

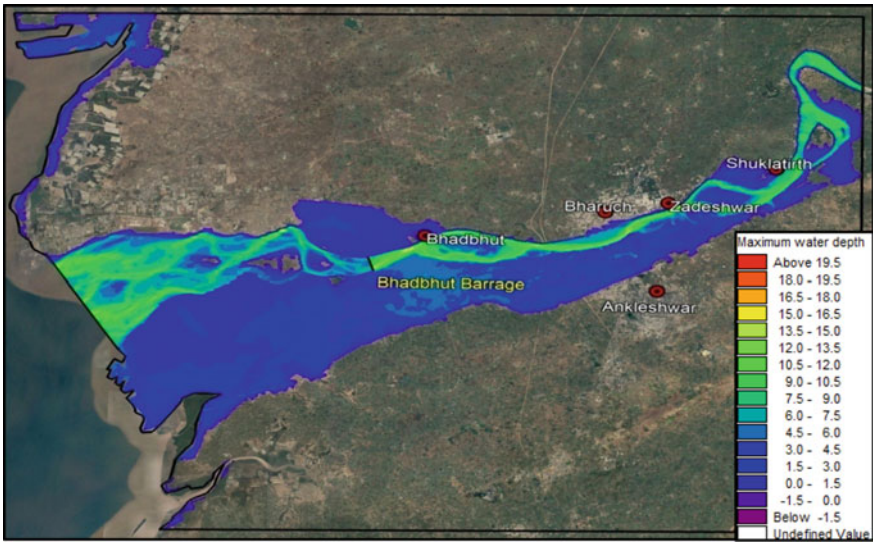

Fig. 7 Spatial variation of flood inundation for scenario 2 with barrage gate closed and no embankments 2006 flood

5 Conclusion

A two-dimensional hydrodynamic model for the lower Narmada River from Shuklatirth to the Arabian Sea was developed by combining physically surveyed and open-source SRTM data, the key conclusions derived from the current study are:

- The Muskingum channel (hydrologic) routing method adopted to route the flow from Garudeshwar to Shuklatirth gauging site situated upstream of model domain. The 2D model was calibrated for 2006 flood using Manning's 'n' = 0.010 for the river stretch and the distributed Manning's 'n' for the floodplain roughness in the 2D model. The model performance was found satisfactory well within the limit.
- For the existing scenario, flood water spilled over the left side bank of the Narmada River due to the low bank levels. The calibrated model also used to simulate barrage closed scenario, results in maximum water level at the Bhadbhut barrage will be beyond the full reservoir level (FRL=7.5 m).
- For both scenarios, maximum water levels are less than the soffit level of the bridges present at Zadeshwar and Bharuch.
- The calibrated model can be used to simulate various scenarios regarding the barrage gate operating conditions and the embankments along the channel.

Acknowledgements The authors would like to acknowledge the infrastructural and computational facility provided by Center of Excellence (CoE) on 'Water Resources and Flood Management,' Sardar Vallabhbhai National Institute of Technology, Surat under TEQIP-II funded by World Bank grant through Ministry of Education (MoE), Government of India for develop a two-dimensional hydrodynamic model in MIKE 21 FLOW MODEL FM. The authors are grateful for Executive Engineer, PIU-1 (Project Implementation Unit), Gujarat Engineering Research Institute (GERI), Vadodara; Central Water Commission (CWC), Surat; National Remote Sensing Centre (NRSC), Hyderabad; National Institute of Ocean Technology (N.I.O.T), Chennai for proving the required data for the present study.

References

1. Rao KH, Rao VV, Dadhwal VK, Behera G, Sharma JR (2011) A distributed model for real-time flood forecasting in the Godavari Basin using space inputs. Int J Disaster Risk Sci 2(3):31–40
2. Mani P, Chatterjee C, Kumar R (2014) Flood hazard assessment with multiparameter approach derived from coupled 1D and 2D hydrodynamic flow model. Nat Hazards 70(2):1553–1574
3. Tansar H, Babur M, Karnchanapaiboon SL (2020) Flood inundation modeling and hazard assessment in Lower Ping River Basin using MIKE FLOOD. Arab J Geosci 13(18):1–6
4. Timbadiya PV, Patel PL, Porey PD (2015) A 1D–2D coupled hydrodynamic model for river flood prediction in a coastal urban floodplain. J Hydrol Eng 20(2):05014017
5. Patel DP, Ramirez JA, Srivastava PK, Bray M, Han D (2017) Assessment of flood inundation mapping of Surat city by coupled 1D/2D hydrodynamic modeling: a case application of the new HEC-RAS 5. Nat Hazards 89(1):93–130
6. Tingsanchali T, Karim MF (2005) Flood hazard and risk analysis in the southwest region of Bangladesh. Hydrol Process: Int J 19(10):2055–2069

7. Masood M, Takeuchi K (2012) Assessment of flood hazard, vulnerability and risk of mid-eastern Dhaka using DEM and 1D hydrodynamic model. Nat Hazards 61(2):757–770
8. Hazarika N, Barman D, Das AK, Sarma AK, Borah SB (2018) Assessing and mapping flood hazard, vulnerability and risk in the Upper Brahmaputra River valley using stakeholders' knowledge and multicriteria evaluation (MCE). J Flood Risk Manage 11:S700–S716
9. Erena SH, Worku H, De Paola F (2018) Flood hazard mapping using FLO-2D and local management strategies of Dire Dawa city, Ethiopia. J Hydrol: Region Stud 19:224–239
10. Pinho J, Ferreira R, Vieira L, Schwanenberg D (2015) Comparison between two hydrodynamic models for flooding simulations at river Lima basin. Water Resour Manage 29(2):431–444
11. Ahn J, Na Y, Park SW (2019) Development of two-dimensional inundation modelling process using MIKE21 model. KSCE J Civ Eng 23(9):3968–3977
12. Rajaguru SN, Gupta A, Kale VS, Mishra S, Ganjoo RK, Ely LL, Enzel Y, Baker VR (1995) Channel form and processes of the flood-dominated Narmada River, India. Earth Surf Process Landforms 20(5):407–421
13. Gupta A, Kale VS, Rajaguru SN (1999) The Narmada River, India, through space and time. Varieties of fluvial form 114-43
14. Tewolde MH, Smithers JC (2006) Flood routing in ungauged catchments using Muskingum methods. Water Sa 32(3):379–388
15. Song XM, Kong FZ, Zhu ZX (2011) Application of Muskingum routing method with variable parameters in ungauged basin. Water Sci Eng 4(1):1–2
16. Subramanya K (2013) Engineering hydrology. McGraw-Hill Education (India) Private Limited, New Delhi
17. DHI (2017) MIKE 21 flow model FM, User manual. Danish Hydraulic Institute, Horsholam, Denmark
18. Loliyana VD, Patel PL (2020) A physics based distributed integrated hydrological model in prediction of water balance of a semi-arid catchment in India. Environ Model Softw 127:104677

UAV (Drone) for Preparation of High-Resolution DEM/DTM—A Case Application of Post Flood Assessment of Dhanera City, Rel River Catchment

Kishanlal Darji, Dhruvesh Patel, Amit Kumar Dubey, Praveen Kumar Gupta, and Raghavendra P. Singh

Abstract Flood assessment in the data scare region is the most challenging task for decision-makers and scientists to estimate the flood catastrophe and flood vulnerability in a flood-prone area. In addition, future preparedness and flood mitigation plan solely depend on the accuracy of the flood assessment after the catastrophic flood. The present case shows state of the art for flood assessment using UAV (drone) techniques. Nowadays, flood assessment is performed using hydrodynamic modeling, where DEM/DTM is the basic input for flood simulation. Dhanera city, Rel River catchment of Banaskantha district, which was affected by the flood in 2015 and 2017, is considered for preparing high-resolution DEM. Phantom 4 Pro RTK and Pix4D software are applied to process the 9222 images across the study reach. The point cloud and high-resolution DEM (3.6 × 3.6 cm) have been extracted from Dhanera city for flood assessment using advanced software techniques. Prepared high-resolution DEM will be utilized for pluvial and fluvial flood assessment through hydrodynamic modeling under unsteady flow conditions. UAV-based high-resolution

K. Darji · D. Patel (✉)
Department of Civil Engineering, Pandit Deendayal Energy University, Gandhinagar 382426, India
e-mail: dhruvesh.patel@sot.pdpu.ac.in

A. K. Dubey · P. K. Gupta
Space Application Centre, Indian Space Research Organization, Ahmedabad 380058, India

R. P. Singh
Indian Institute of Remote Sensing, ISRO, Dehradun 248001, India

P. V. Timbadiya et al. (eds.), *Flood Forecasting and Hydraulic Structures*, Lecture Notes in Civil Engineering 340, https://doi.org/10.1007/978-981-99-1890-4_10

DEM/DTM has been described, and a significant achievement for preparing high-resolution DEM/DTM for flood modeling to improve the decision-making system has been discussed.

Keywords UAV · Flood assessment · Rel River · DEM · Decision-making system

1 Introduction

Flood is an unpreventable natural phenomenon; however, it would be reduced or its effects would be controlled if suitable measures were adopted for flood risk assessment and management. Almost every year, floods of varying magnitude affect some part of the country or the other, which cause massive loss of lives and damage to livelihood systems, property, infrastructure, and public utilities [1, 2]. Gujarat 2017, Kerala 2018, Vadodara 2019, and Bihar 2019 are some recent examples of flooding in India [3]. Therefore, flood assessment is essential to reduce the loss of life and properties. Mainly, it would be assessed using hydrodynamic modeling, i.e., MIKE FLOOD, HEC-RAS, LISSFLOOD, etc.; however, every hydrodynamic model requires a DEM as an input to generate the flood plain in 2D where the flood water will be simulated in flood plain areas. The accuracy of flood assessment and flood risk maps depends on the DEM resolution and input data. DEM is the major input source for building a hydrodynamic modeling. DEM is an array representation of squared cells (pixels) with an elevation value associated to each pixel that can be obtained from contour lines, topographic maps, field surveys, photogrammetry techniques, radar interferometry, and laser altimetry [4]. DEMs contain the elevation of a point on a surface above the mean sea level. DEMs are sometimes referred to as digital terrain model (DTM) or digital surface model (DSM) [5, 6]. Nowadays, much open-source satellite-based DEMs, i.e., ASTER global, SRTM (30 × 30 m), GMTED 2010 (30 arc-second), GMTED 2010 (15 arc-seconds), GMTED 2010 (7.5 arc-seconds), and (ALOS (12.5 × 12.5 m), are available for flood assessment studies [7]; however, low-resolution DEM (generally greater than 30 m) has many vertical inaccuracies, and these DEMs are too old to break the accuracy of estimation of flood hazard in urban area [8, 9].

Recently, unmanned aerial vehicles (UAVs) or unmanned aerial systems (UASs) are the emerging platforms for remote mapping at very high spatial resolution for 3D surveying, earth observation, and monitoring a 3D city mapping. Many cases presented by [10–14] and suggested that UAV-generated very high-resolution DEM can be used for examining the stream characteristics, stream velocity, and floodplain, thereby not only looking and augmenting our scientific understanding of hydrological processes at the (very) small scale but improve the understanding in particular of flood processes. Therefore, the present case approached the preparation of high-resolution DEM/DTM of the flood-prone site at Rel River catchment. The high-resolution DEM for Dhanera city, covering 10 km^2, has been mapped using Phantom 4 Pro RTK UAV and Pix4D software. The 3.6 × 3.6 cm high-resolution DEM has been prepared for

Dhanera city. The prepared DEM will be utilized for flood assessment of Dhanera city at Rel River catchment. This will improve the flood assessment accuracy and the decision-making system. It would also help prepare a robust flood mitigation plan for Dhanera city.

2 Study Area and Data Collection

The study was demonstrated in the Rel River Basin, situated in Banaskantha district, Gujarat, India (Fig. 1). The Rel River originates from the Southern part of the Sundhamata Mountain and meets the Rann of Kachchh in Gujarat. It has two courses. The first course flows from the Sundhamata Mountain to Pachala Dam, Jetpura Dam reaching Bapla and Runi, while the other course mingles in the Kes Pond. Its catchment covers an area of 442 km^2 and lies between 24° 50′ N to 24° 75′ N latitude and 72° 00′ E to 72° 45′ E longitude. The lowest point is near Dhanera taluka and Dhanera city, near the mouth of the Rel River [15]. The Rel River is an ungauged river with the data-scarce region. The river's width is about 280 m and 180 m at the Road Bridge and Railway Bridge, respectively. The river bed slope is about 1 in 500 from U/S of the railway bridge and up to D/S of the causeway location. Rel River has very steep topography in the upper catchment, resulting in the flash flood in the D/S region.

Dhanera city is located in the northern part of Gujarat in the Banaskantha district. This city has the historical inheritance of Mugal and Rajput rulers. It has minimal

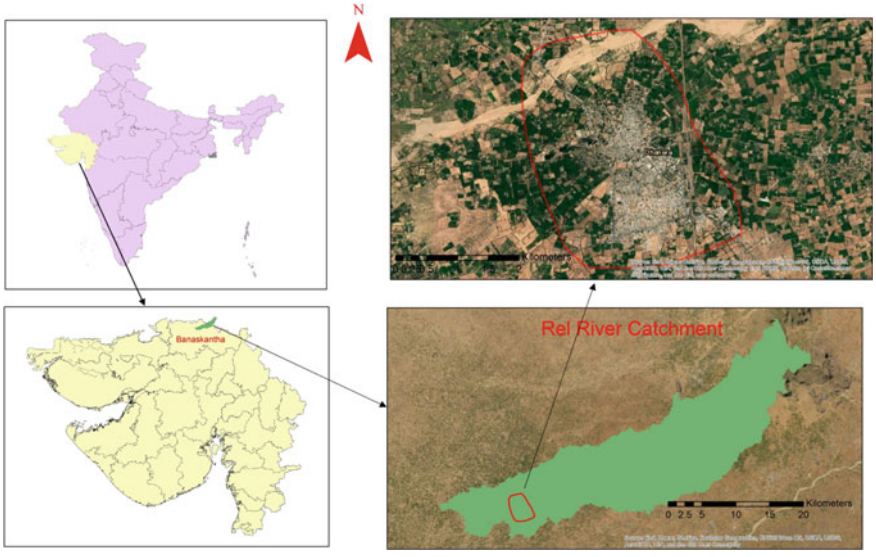

Fig. 1 Location of Dhanera city, Banaskantha district

to moderate rain; hence, it is a dry region. According to 2011 census records, this region's population is 29,578. The principal economic activity is animal husbandry along with agriculture. It covers a 10 km^2 area, including the sub-hubs.

3 Methodology

The method adopted in this research is presented in Fig. 2. UAV is used for mapping and survey purposes, whereas PiX4D is applied to prepare the DEM of Dhanera city. Phantom 4 Professional RTK UAV is used to capture images over Dhanera city. The UAV is consistent with the camera version and has an image width of 5472 px, image height of 3648 px, sensor width of 13.2 mm, sensor height of 8 mm, and focal length of 8.8 mm. The KML file for the region is generated in Fig. 1, where Dhanera has been marked with a red border. It is divided into four zones, and a flight plan is decided. The 7 GCP points are kept in the study region (Fig. 3).

The aerial images are taken with 80% overlap between consecutive images. The flight height is selected at 130 m so that ground sampling distance (GSD) can be 3.56 cm/px. The area covered during the survey is 10 km^2. The RTK module can provide positioning accuracy of 1 cm + 1 ppm (horizontal), 1.5 cm + 1 ppm (vertical). A total of 9222 images is collected for the region. A total of 9222 aerial images were captured using a UAV for the study area. These images were then geo-referenced, and a total 07 number of 3D DGPS points were marked Fig. 3.

Initially, the sample analysis was carried out for 2000 images to check the accuracy and DSM/DTM result. Later, PIX4Dmapper software was used to analyze pictures into digital spatial models. PIX4Dmapper graphic user performs analysis in three stages: Initial processing, point cloud and mesh, and final processing. Pix4Dmapper transforms images into digital spatial models. The seamless DEM has been prepared using cloud process or the desktop photogrammetry platform. In the first stage, a key point's extraction identifies specific features as key points in the images. It involves a fully automatic iterative proprietary algorithm for bundle block adjustment and sparse cloud point generation shown in Fig. 4. Initial processing also generates the initial report, which lets us know about the accuracy of our processing, and it also provides DSM and orthomosaic preview. In the second stage, the point cloud and mesh do the point densification, where additional tie points are created based on the automatic tie points resulting in a densified point cloud. The third stage consists of generating a digital surface model (DSM), which will enable the computation of volumes, ortho mosaics, and reflectance maps. This stage uses inverse distance weighting algorithm (IDW) interpolation for DSM generation (Fig. 5).

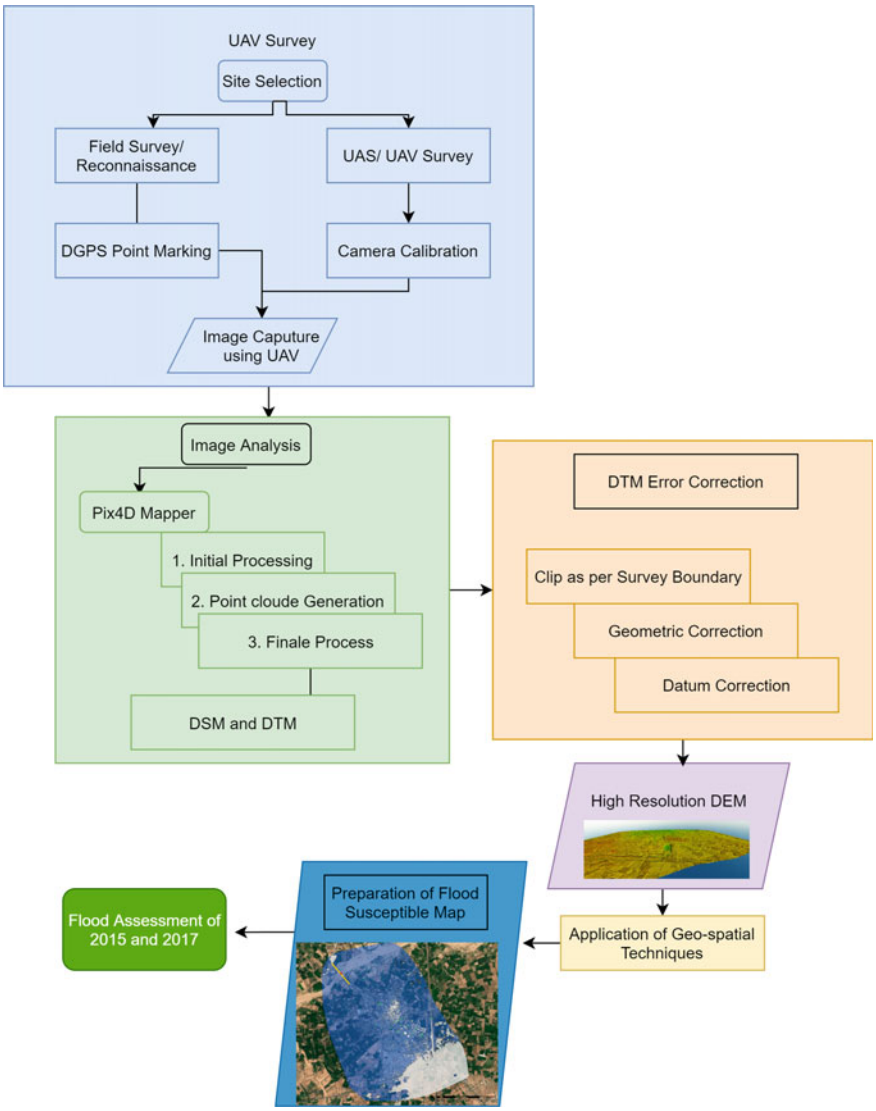

Fig. 2 Methodology chart

3.1 Flood Risk Assessment

This research defines the flood risk based on projected HFL at the Rel River session and UAV-based DEM. Inundation and flood susceptible area by selecting the grid cell of DEM that is lower than the projected HFL and connected to an adjacent flooded

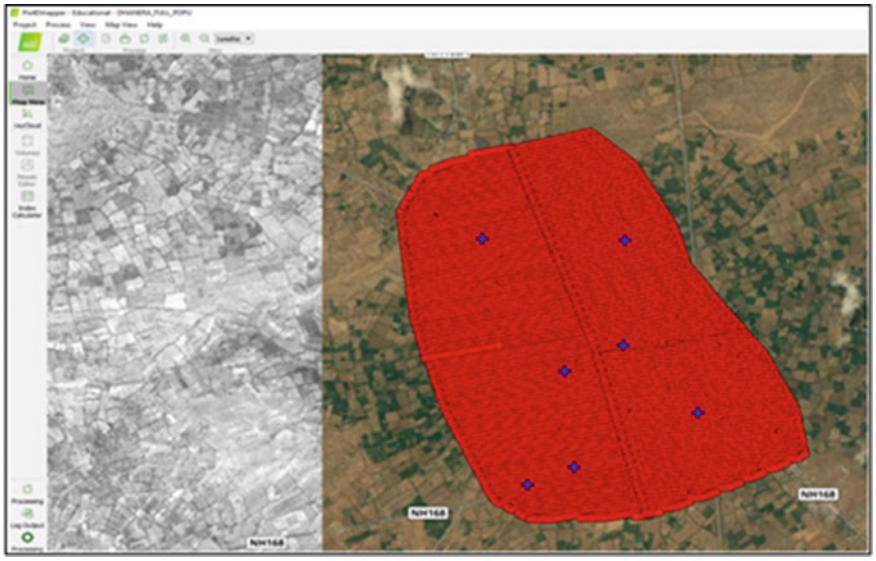

Fig. 3 9222 UAV images along with the location of 07 GCP (Ground Control Points)

Fig. 4 Point cloud and 3D view of Dhanera city

grid cell or open water inundation [16, 17]. Flood risk assessments were performed at different vertical scale levels shown in Figs. 6 and 7.

4 Results

An SFM algorithm is used to restore camera exposure position and generate a sparse point cloud. An MVS algorithm generates the dense point cloud as per the DSM generation method. Flight height, camera pitch, and image overlap are key factors affecting the results, including point cloud and DEM. The processing time in PIX4D

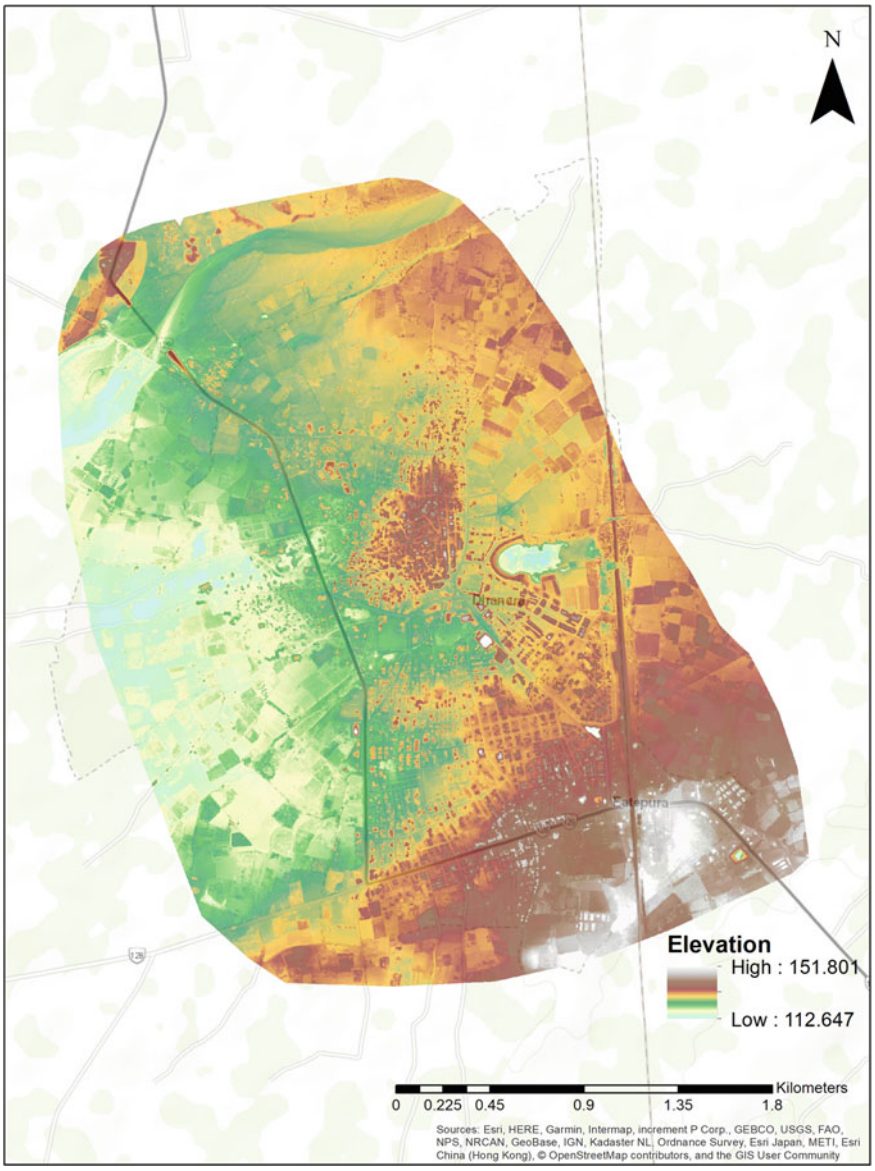

Fig. 5 DTM/DSM of Dhanera city of 3.6 × 3.6 cm

depends on the resolution of images, content, chosen output resolution, and the processor used. This project took about 72 h to process DSM, DTM, and orthomosaic from the 9222 UAV images at 20% overlap. As it was not possible to merge all the UAV images in one go, it was divided into four parts to perform the processing. The

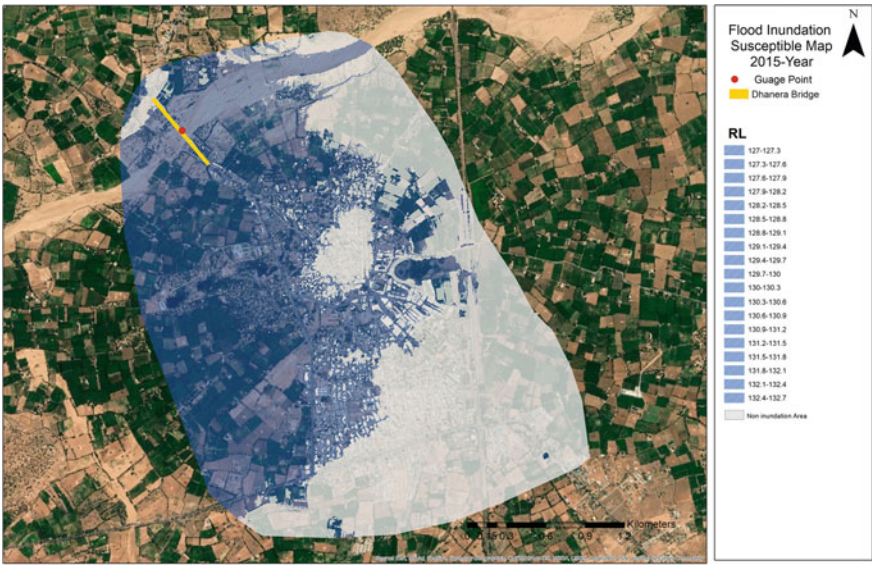

Fig. 6 Flood susceptible map as per flood 2015

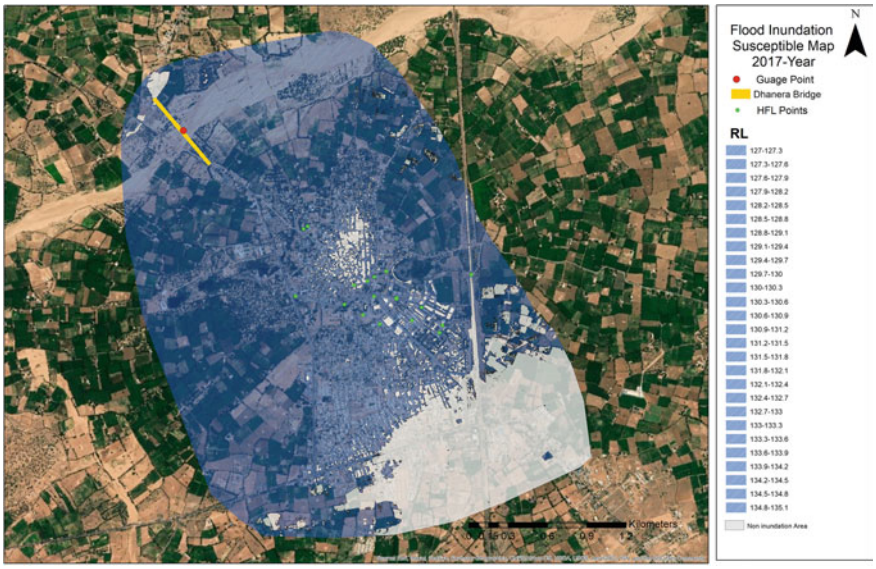

Fig. 7 Flood susceptible map as per flood 2017 along with observed HFL

final images were then mosaicked in a global mapper as a single DEM. The accuracy of the final DEM final obtained was 3.6 cm, as shown in Fig. 5.

4.1 Flood Risk Assessment

The flood inundation maps derived from UAV DEM were showed in Figs. 6 and 7. The flood susceptible at every 0.3 m is indicated. The map shows that the area above RL 135 m (Fig. 7) will be safe and survive under the same flood conditions. Furthermore, the flood susceptible area in 2015 was 54%, whereas in 2017, it is 80%. It shows that the flood inundation has increased by 26% and 2.6 km^2 of Dhanera city. At last, the flood inundation has been compared with the HFL of 2017 at Dhanera city (Fig. 7) and shows a significant correlation with flood susceptible areas. To improve the result, a further hydrodynamic model will be performed to estimate the velocity and flood arrival time at Dhanera city.

5 Discussions

The DEM is a useful source for flood inundation scenario. The present case is an important case study to prepare high-resolution DEM using UAV and PiX4D software. Important points come out from the research.

1. The prepared DEM having more than 25GB in size after the post processiong from PiX4D point clous process, hence, high configuration computer system including RAM, and graphics cards are required to handle the data for flood simulation.
2. A total of 9222 images are captured in a 10 km^2 area of Dhanera city, which needs a 384 h time to mosaic with 80% overlap and process in Pix4D software to produce a high-resolution DEM for study reach. The process is performed with Precision 7820 Tower, Intel (R) Xeon (R) Bronze 3104 CPU @ 1.70 GHz, 32 GB RAM, and a 64-bit operating system.

6 Conclusions

The present case is an important case study to develop a high-resolution UAV-based DEM/DSM for engineering applications. In addition, it would be a cost-effective alternative to produce a high-resolution DEM/DSM instead of costly LIDAR techniques. Prepared DEM/DSM along with river HFL is an essential tool for preparing flood susceptible areas using geo-spatial techniques. It reduces the data deficiency for flood assessment in the data scare region and improves the decision-making system. The study also shows that UAV data have great potential in flood risk assessment

and management, hence applicable for preparing flood resilience plans for urban flood-affected areas in India.

Acknowledgements Corresponding author would like to thank SAC-ISRO for providing the funding support to execute the work under the SARITA project. The author(s) would also like to thank the Survey of India, Irrigation Department, Dhanera Municipal Corporation and R & B department for providing necessary data support to execute the work. First author would like to thank the local police for support during the survey and field executions.

References

1. NDMG (2008) National disaster management guideline
2. NDMP (2019) National disaster management plan
3. Gupta K (2020) Challenges in developing urban flood resilience in India. Philos Trans R Soc A Math Phys Eng Sci 378. https://doi.org/10.1098/rsta.2019.0211
4. Peralvo M, David M (2004) Influence of DEM interpolation methods in drainage analysis. Gis Hydro 4
5. Ajayi OG, Salubi AA, Angbas AF, Odigure MG (2017) Generation of accurate digital elevation models from UAV acquired low percentage overlapping images. Int J Remote Sens 38:3113–3134. https://doi.org/10.1080/01431161.2017.1285085
6. Poon J, Fraser CS, Chunsun Z, Zhang LI, Gruen A (2005) Quality assessment of digital surface models generated from ikonos imagery. Photogramm Rec 20:162–171. https://doi.org/10.1111/j.1477-9730.2005.00312.x
7. Nagesh Kumar D, Shastry AR, Srinivasa Raju K (2020) Delineation of flood-prone areas using modified topographic index for a river basin. H2Open J 3:58–68. https://doi.org/10.2166/h2oj.2020.021
8. Lakshmi SE, Yarrakula K (2018) Review and critical analysis on digital elevation models. Geofizika 35:129–157. https://doi.org/10.15233/gfz.2018.35.7
9. Darji K, Patel D (2020) Creating the high resolution DEM for flood assessment using UAV techniques. In: ISRS-ISG national symposium–2020, p 185
10. Govedarica M, Jakovljević G, Álvarez-Taboada F (2018) Flood risk assessment based on LiDAR and UAV points clouds and DEM. Remote Sens Agric Ecosyst Hydrol XX 10783:66–76. https://doi.org/10.1117/12.2513278
11. Kim K, Davidson J (2015) Unmanned aircraft systems used for disaster management. Transp Res Rec 2532:83–90. https://doi.org/10.3141/2532-10
12. Casado MR, Irvine T, Johnson S, Palma M, Leinster P (2018) The use of unmanned aerial vehicles to estimate direct tangible losses to residential properties from flood events: a case study of cockermouth following the desmond storm. Remote Sens 10:1–21. https://doi.org/10.3390/rs10101548
13. Schumann, Muhlhausen, Andreadis (2019) Rapid mapping of small-scale river-floodplain environments using UAV SfM supports classical theory. Remote Sens 11:982. https://doi.org/10.3390/rs11080982
14. Darji K, Patel D, Dubey AK, Gupta P, Singh R (2021) An approach of satellite and UAS based mosaicked DEM for hydrodynamic modelling—a case of flood assessment of Dhanera City, Gujarat, India. J Geomatics 247–257

15. Memon N, Patel DP, Bhatt N, Patel SB (2020) Integrated framework for flood relief package (FRP) allocation in semiarid region: a case of Rel River flood, Gujarat, India. Nat Hazards 100:279–311. https://doi.org/10.1007/S11069-019-03812-Z
16. Patel DP, Srivastava PK (2014) Application of geo-spatial technique for flood inundation mapping of low lying areas, pp 113–130. https://doi.org/10.1007/978-3-319-05906-8_7
17. Patel DP, Ramirez JA, Srivastava PK, Bray M, Han D (2017) Assessment of flood inundation mapping of Surat city by coupled 1D/2D hydrodynamic modeling: a case application of the new HEC-RAS 5. Nat Hazards 89:93–130. https://doi.org/10.1007/S11069-017-2956-6

Computation of Socio-Economic Vulnerability for Densely Populated Surat City, India

Shubham M. Jibhakate, P. V. Timbadiya, and P. L. Patel

Abstract The Surat city located alongside the banks of the lower Tapi River and at the inference of Arabian Sea. The densely populated Surat city is vulnerable to multiple hazards including extreme rainfall, urban (pluvial) and riverine flooding, tide surge, sea level rise, cyclones as well as human-induced hazard of industrial accidents. The current study focuses on the computation of socio-economic vulnerability of the Surat city area coming under the jurisdiction of the Surat Municipal Corporation (SMC) (area = 326.5 km^2), by considering the risk to the population and asset in the area. The census-based indicators representing socio-economic status are identified for each ward of Surat city; the ward is considered as decision-making unit (DMU). The principal component analysis (PCA) is applied on the indicators for the dimensional reduction as well as to remove the possible co-relation amongst the indicators. Further, the decorrelated data (nearly 75% variability) used as input in the data envelopment analysis (DEA) model to evaluate the vulnerability for each ward. The analysis performed on total 89 wards of the Surat city indicates that the major area within the city is under high to very high vulnerable category specifically densely populated areas. The low to medium vulnerable areas are mostly concentrated over the tail portion South-west zone. The developed socio-economic vulnerability maps will be useful to identify the susceptibility of flood prone Surat city against upcoming

S. M. Jibhakate (✉) · P. V. Timbadiya · P. L. Patel
Department of Civil Engineering, Sardar Vallabhbhai National Institute of Technology Surat, Surat 395007, India
e-mail: shubhamjibhakate1771@gmail.com

P. V. Timbadiya
e-mail: pvtimbadiya@ced.svnit.ac.in

P. L. Patel
e-mail: plpatel@ced.ac.in

P. V. Timbadiya et al. (eds.), *Flood Forecasting and Hydraulic Structures*, Lecture Notes in Civil Engineering 340, https://doi.org/10.1007/978-981-99-1890-4_11

(flood) hazard, planning of mitigation strategies during flood risk assessment and to improve the flood resiliency of the society in near future.

Keywords Surat city · Socio-economic vulnerability · Principal component analysis · Data envelopment analysis

1 Introduction

Vulnerability of any system or region can be define as the degree of sensitivity or susceptibility against the coming hazard and its lack of ability to adapt or react the situation [1, 2]. The devastating effect of natural disaster is not only the function of intensity and magnitude of disastrous event but also the level of vulnerability of society [3]; higher the vulnerable society, high will be the risk. Therefore, while planning the disaster management strategies, reduction in the risk of any society or region can be accomplished by reducing the vulnerability. There are different, direct (physical, economic, ecological) and indirect (socio-economic) indirect dimensions of the vulnerability. However, the highly sensitive dimension of socio-economic vulnerability is overlooked during the disaster management strategies [4].

Natural disasters cause physical damage and psychological trauma to the society; therefore, for better understanding it is necessary to consider socio-economic aspect of the vulnerability. The social aspect of vulnerability by considering the census (2001 and 2011)-based indicators over India, influencing hydro-climatic risk of the country, was analysed by Vittal et al. [3]. Jha and Gundimeda [5] assessed indicator-based flood vulnerability at district level for Bihar state. The topographic vulnerability in combination with (census) indicator-based socio-economic vulnerability for flood risk forecasting in Kerela studied by Tripathy [6]. The socio-economic vulnerability evaluated at the lowest administrative (village) level for Jagatsinghpur district in Mahanadi River basin of Odisha; the vulnerability was combined with flood hazard maps obtained from hydrodynamic model to identify individual contribution of vulnerability in flood risk using bivariate approach by Mohanty et al. [4]. The disaster vulnerability for densely populated coastal urban area (Mumbai city) at ward level is analysed by Sherly et al. [7]. They mention coastal urban regions are highly susceptible against the multiple (riverine, urban, extreme rainfall, cyclones, tide surge and sea level rise) hazard; therefore, a comprehensive vulnerability assessment is need of time for the coastal cities specifically in flood prone areas.

Surat is a densely populated city, situated on the bank of Lower Tapi River. It is nearly 100 km downstream of Ukai multipurpose reservoir and 20 km upstream of Tapi River mouth, where river meets to Arabian Sea. It is the second largest city and administrative capital of Gujarat state. The city experiences major floods in the year 1994, 1998 and 2006 due to heavy release from Ukai Dam after commencement of the dam in 1972. The situation is worsened due tide surge. Apart from riverine flood, the city is susceptible to urban flooding (year 2013), cyclones generated in

Arabian Sea and extreme rainfall due to climate change. The increasing daily rainfall intensity is observed over the lower Tapi basin which can aggravate the riverine, urban flooding situation in the region [8]. Keeping in view the importance of Surat city and its susceptibility to natural disaster events, a comprehensive vulnerability assessment is needed. However, the current study focuses on analysing the socio-economic dimension of vulnerability related to the capability of a community or population to cope up with the (flood) hazard. The major objectives of the current study are: (i) compute the socio-economic vulnerability of each ward of Surat city using (2011) census-based indicators and (ii) sensitivity analysis of considered socio-economic vulnerability indicators.

2 Study Area and Data Source

The densely populated Surat city is the eighth largest city in country extended on both side of Lower Tapi Riverbank close to Arabian Sea. Surat is major industrial and commercial centre famous for textile trade, diamond cutting-polishing business and lately establish itself in information technology sector. Due to continuous growth and employment opportunity in the city, the migration of people from various part of country has been observed. Surat having total population of 44,66,826 spread over the area of 326.52 km^2 (census 2011) under the jurisdiction of Surat Municipal Corporation (SMC) with population density of 13,680 person/km^2. For the better administrative purposes, the city is divided into seven zones and further divided into 101 wards. The climate of the city is pleasant during monsoon with average annual rainfall of 1143 mm. The temperature during summer varies from 37.78 °C to 44.44 °C with mean humidity of 60%, and during winter, it ranges 10–15.5 °C. The wards map of the Surat city with population density is shown in Fig. 1. In the current study, 13 small sizes nearby wards in Randher region (west zone) combine as single ward, so total 101 wards reduced to 89 Nos. Other details of the wars of Surat city can be accessed through https://www.suratmunicipal.gov.in/TheCity/Demographics.

The data representing social and economic status of the Surat city were downloaded from census of India website (censusindia.gov.in) for year 2011 and SMC website (www.suratmunicipal.gov.in).

3 Methodology

The socio-economic vulnerability of Surat city is evaluated using the framework shown in Fig. 2.

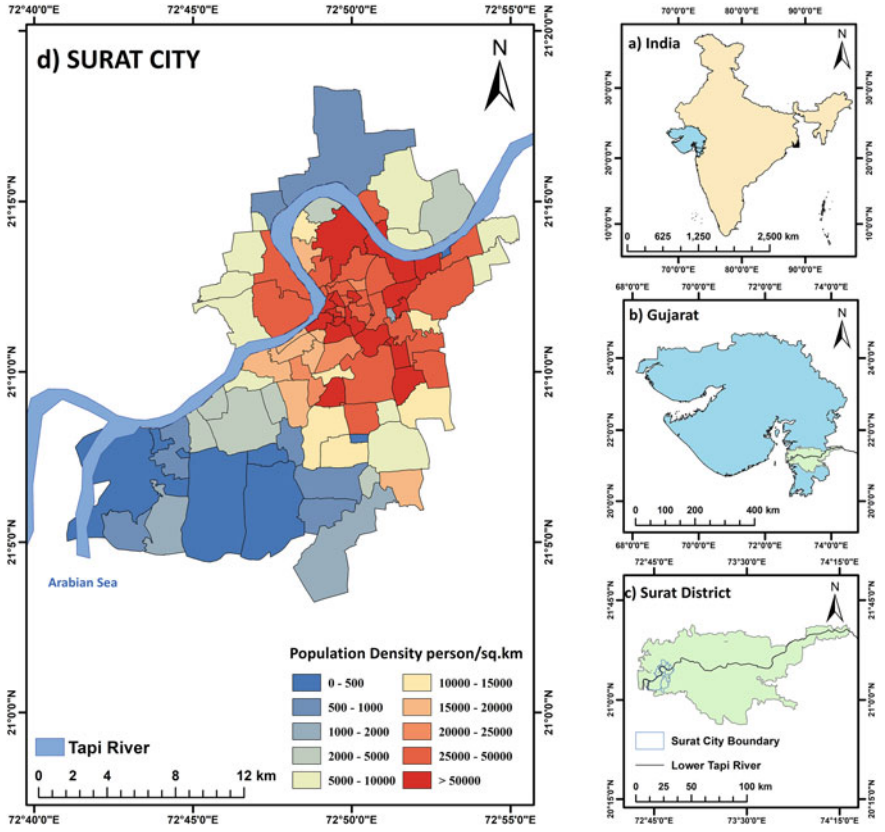

Fig. 1 Index map of the Surat city

3.1 Identification of Indicators

A total of 20 indicators representing social and economic status [7] of the Surat city were identified from 2011 census data for each ward of Surat city. The indicators are further classified into positive (increase vulnerability) and negative (decrease vulnerability) indicators. The selected indicators along with corresponding reasoning are shown in Table 1. In order to compare the indicators with different units, the indicators are standardized (dimensionless) between 0 and 1. The standardization is performed by using Eqs. 1 and 2 [9].

$$A_i^{\text{std}} = \frac{A_i - A^{\min}}{A^{\max} - A^{\min}} \quad \text{for positive indicators} \tag{1}$$

$$A_i^{\text{std}} = \frac{A^{\max} - A_i}{A^{\max} - A^{\min}} \quad \text{for negative indicators} \tag{2}$$

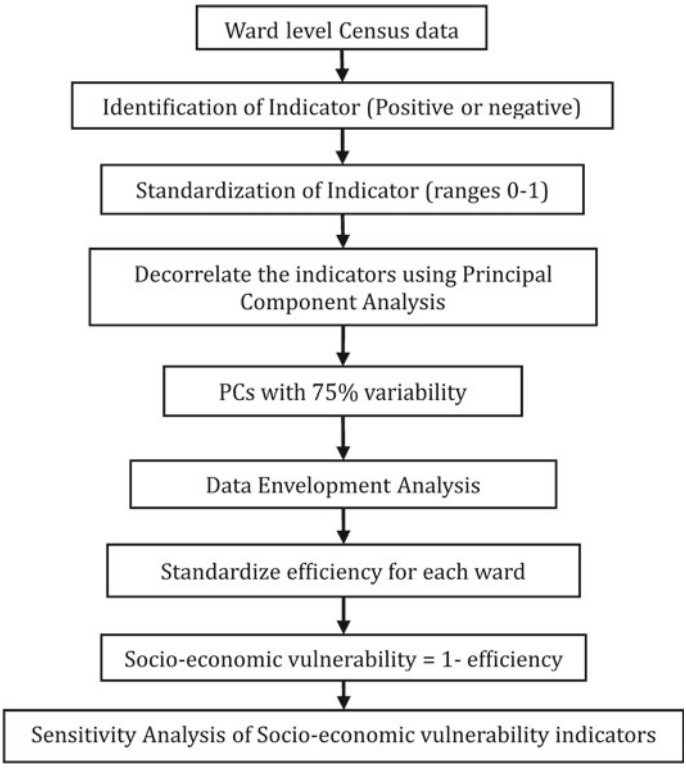

Fig. 2 Flow chart of the methodology adopted in the current study

Here, A_i^{std} = Standardize vulnerability indicator for *i*th ward

A_i = Vulnerability indicator for *i*th ward

$A^{\max}$ = Maximum value of vulnerability indicator amongst all the ward

$A^{\min}$ = Minimum value of vulnerability indicator amongst all the ward.

3.2 Principal Component Analysis (PCA)

Principal component analysis (PCA) is a statistical tool used to decorrelate and dimensional reduction of the standardize dataset. PCA converts the correlated indicators into uncorrelated set of components, called principal components (PCs). It follows orthogonal linear transformation in order to capture the maximum variation close to original dataset. The first PC holds maximum possible variation followed by other subsequent PCs to retain the maximum possible variability. PCs totally depend on the covariance matrix of indicators $[A_i^{\text{std}}]^{J\times K}$ in which J is the total number of

Table 1 List of socio-economic indicators

Indicators	Influence on the socio-economic vulnerability	Justification
No. of households	Positive	More number of household having more habitats and economic dependence hence increases the vulnerability during flood
Total population	Positive	Larger population leads to increase exposure to flood hazard
Total female population	Positive	Majority of the female population devoted to household activities and less exposure to educational and social activities
Population in the age group < 6 year	Positive	Required special attention during evacuation and depends on the adults for their care and needs during disaster
Population SC + ST	Positive	It is the weaker economic section of the society categorized under backward community
Population SC + ST Female	Positive	Backward community and women tend to have more responsivity in taking care of the family
Population illiterate	Positive	Tend to have less employable skill and less access to the information regarding the hazard or risk during flood
Population illiterate female	Positive	They find more difficult to follow the evacuation warning or guidelines during taking care of their family during disaster
Slum households	Positive	House conditions are depleted (kaccha house), leaving in unsensitized area and more susceptible against the flood
Slum populations	Positive	Already susceptible category will lead to more exposure of the people
Marginal workers population	Positive	They are having temporary jobs, mostly landless labours (low financial stability)
Non-workers population	Positive	These population will depend on the other adult family member and more susceptible against copping the disaster effect
Location of drinking water source (Away) (%)	Positive	The away source of drinking water has huge impact during the flood or other disaster
Number of households without latrine and drainage facility (%)	Positive	No latrine and drainage facility increase the possibility of spread of diseases during the flood
Total workers population	Negative	Higher working population will have higher resilience against the flood

(continued)

Table 1 (continued)

Indicators	Influence on the socio-economic vulnerability	Justification
Total workers population Female	Negative	The resiliency of the family increases with the more working female population
Population literate	Negative	Higher literacy tends to enhance the knowledge of the society pertaining to cop up with the flood
Population literate female	Negative	Increases the resiliency of the family due to access to the knowledge and warnings during to flood
Household with good house condition (%)	Negative	The impact of the flood will be less on good house condition
Drinking water from treated source (%)	Negative	Availability of drinking water from treated source will help families to cope with (diseases) during flood

total number of wards and K is the total number of indicators in the current study. It resulted into $K \times 1$ eigen values and $K \times K$ eigen vector (called as loadings) and variance explained by each PCs. The number of PCs explaining more than (>) 75% of variance are used in the further analysis.

3.3 Data Envelopment Analysis (DEA)

The data envelopment analysis (DEA) a non-parametric aggregation technique widely accepted for evaluating the relative efficiency amongst decision-making units (DMUs) [4, 7, 10], in the current study ward is consider as DMU. It is the frontier estimation which optimize each observation (indicator) associate with DMUs. The efficiency of the DEA model is highly reduced when the number of observations (indicators) is less than the DMUs; also, the results from DEA are sensitive to the selected input and output [7]. In the current study, popular Banker, Charnes, Cooper (BCC) model is adopted. The PCs explaining more than 75% of variability are given as input to DEA [6]. It is considered that the vulnerability of any system represents the state before occurrence of hazard and unity: (1) a dummy output is assign in DEA. The socio-economic vulnerability for each ward is computed by subtracting the efficiency obtained from DEA. Lower the efficiency, higher the vulnerability for the respective ward. In the current study, two PCs with 75% variability given as input to DEA. For the detailed stepwise explanation of DEA readers can refer to Sahana et al. [11]. The vulnerability is discretized into five classes from very low to very high (see Fig. 3).

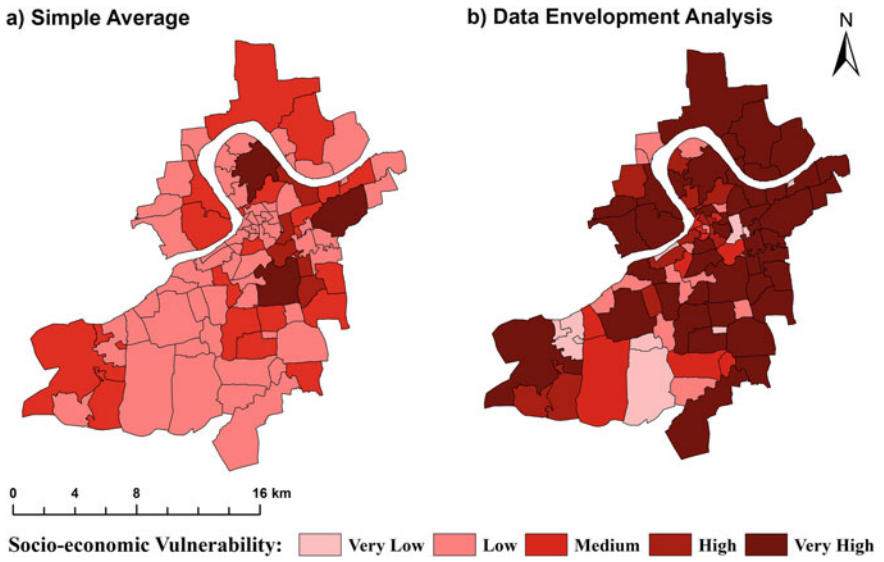

Fig. 3 Socio-economic vulnerability using **a** simple averaging, **b** data envelopment analysis for Surat city, India

3.4 Sensitivity of the Indicators in Vulnerability Influence

The selection of indicators affects the assessment of socio-economic vulnerability. The sensitivity of selected socio-economic vulnerability indicators is evaluated using the Map removal technique [11, 12] given by Eq. 3. The map removal technique is one variable at a time type of sensitivity analysis.

$$S = \sum_{i} w_i |R(V_i) - R(V_{\_i})|. \tag{3}$$

S is the sensitivity of particular indicator considered (removed) while performing sensitivity analysis. w_i is the weightage assign to the location (DMU or ward) considered 0 in the current study. $R(V_i)$ and $R(V_{\_i})$ are the ranks of unperturbed and perturbed vulnerability of the wards i. Higher the value of S for removed indicator, more will be the sensitivity.

4 Results and Discussion

The socio-economic vulnerability for each ward of Surat city has been initially evaluated by simple averaging method. It is found that 28 out of 89 wards (44.43% area) of the Surat city are under medium to very high vulnerable class, whereas only 8 wards

(10% area) of city under high to very high category shown in Fig. 3a. The averaging is the simplest method, but it treats all the indicators equally. It can underestimate or overestimate any of the importance or less important indicator with each other. The PCA-DEA aggregation technique optimizes each indicator with objective of quantifying the discrete piecewise frontier estimation overcome the equal weightage limitation of simple averaging. Analysing with DEA, 66 out of 89 wards (85% of area) of the Surat city under medium to very high vulnerable category (see Fig. 3b). A total of 44 wards spread over 66% area of Surat city are under very high class. It is specifically concentrated over area with high population density. The low to medium vulnerable areas are mostly concentrated over the tail portion South-west zone of which larger area belongs to agricultural land with low population density.

The sensitivity of selected indicators in DEA is computed by using map removal technique. It is found that, tap water from treated source during disaster followed by slum households, slum population are more sensitive and signifies their importance in socio-economic vulnerability of Surat city (See Fig. 4). However, household with good condition and total working population are more resilient during the disaster. The outcome of socio-economic vulnerability (DEA-based) and sensitivity of indicators will be helpful for the local administration to plan the mitigation strategies.

5 Conclusions

The socio-economic vulnerability for each ward of Surat city using census-based indicators subject to multiple hazard (specifically flood) has been evaluated using DEA (frontier estimation) technique. Out of total 89 wards, 66 fall under medium to very high vulnerable category which approximately 85% the city area, concentrated over densely populated part, whereas areas with low population density fall under low vulnerable class. Amongst the indicators considered in the analysis, tap water from treated source and good house condition are found to be the most sensitive and resilient indicators, respectively. The developed socio-economic vulnerability maps will be useful to identify the susceptibility of flood prone Surat city against upcoming (flood) hazard, planning of mitigation strategies during flood risk assessment and to improve the flood resiliency of the society in near future.

In the current socio-economic vulnerability study of Surat city, 20 indicators have been considered, and the indicators can be increased with availability of data. Also, the analysis of vulnerability by considering existing critical infrastructure, land use exposure can be taken as the future scope of the current study.

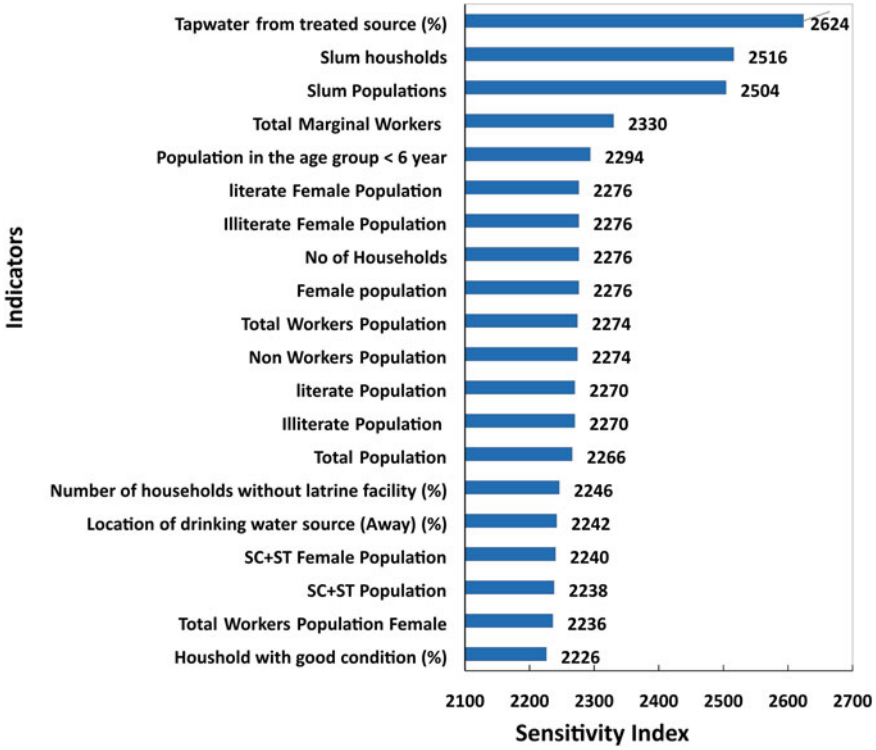

Fig. 4 Sensitivity analysis of indicators used in DEA (map removal technique)

Acknowledgements The authors would like to acknowledge the financial support received from Indian National Committee on Climate Change (INCCC), Ministry of Jal Shakti, Department of Water Resources, River Development and Ganga Rejuvenation, Government of India for funding this research. The authors appreciate the infrastructural and necessary infrastructural facility provided by Centre of Excellence (CoE) on Water Resources and Flood Management, TEQIP-II, Ministry of Human Resources Development (MHRD), Government of India, for conducting the study reported in this paper. We thank Dr. Sahana V, Researcher-Water Risk Modeler, International Water Management Institute, Delhi, India for aiding in the current study.

References

1. Zachos LG, Swann CT, Altinakar MS, McGrath MZ, Thomas D (2016) Flood vulnerability indices and emergency management planning in the Yazoo Basin, Mississippi. Int J Disaster Risk Reduction 18:89–99
2. Eini M, Kaboli HS, Rashidian M, Hedayat H (2020) Hazard and vulnerability in urban flood risk mapping: machine learning techniques and considering the role of urban districts. Int J Disaster Risk Reduction 50:101687

3. Vittal H, Karmakar S, Ghosh S, Murtugudde R (2020) A comprehensive India-wide social vulnerability analysis: highlighting its influence on hydro-climatic risk. Environ Res Lett 15(1):014005
4. Mohanty MP, Vittal H, Yadav V, Ghosh S, Rao GS, Karmakar S (2020) A new bivariate risk classifier for flood management considering hazard and socio-economic dimensions. J Environ Manage 255:109733
5. Jha RK, Gundimeda H (2019) An integrated assessment of vulnerability to floods using composite index—a district level analysis for Bihar, India. Int J Disaster Risk Reduction 35:101074
6. Tripathy SS, Vittal H, Karmakar S, Ghosh S (2020) Flood risk forecasting at weather to medium range incorporating weather model, topography, socio-economic information and land use exposure. Adv Water Resour 146:103785
7. Sherly MA, Karmakar S, Parthasarathy D, Chan T, Rau C (2015) Disaster vulnerability mapping for a densely populated coastal urban area: an application to Mumbai, India. Ann Assoc Am Geogr 105(6):1198–1220
8. Gehlot LK, Jibhakate SM, Sharma PJ, Patel PL, Timbadiya PV (2021) Spatio-temporal variability of rainfall indices and their teleconnections with El Niño-Southern oscillation for Tapi Basin, India. Asia Pac J Atmos Sci 57(1):99–118
9. Karmakar S, Simonovic SP, Peck A, Black J (2010) An information system for risk-vulnerability assessment to flood. J Geogr Inf Syst 2(03):129
10. Charnes A, Cooper WW, Rhodes E (1978) Measuring the efficiency of decision making units. Eur J Oper Res 2(6):429–444
11. Sahana V, Mondal A, Sreekumar P (2021) Drought vulnerability and risk assessment in India: sensitivity analysis and comparison of aggregation techniques. J Environ Manage 299:113689
12. Lodwick WA, Monson W, Svoboda L (1990) Attribute error and sensitivity analysis of map operations in geographical information systems: suitability analysis. Int J Geogr Inf Syst 4(4):413–428

Two Dimensional Flood Inundation Mapping Under Overtopping Failure of Umrar Dam—Effect of Terrain Resolution and Sensitivity Analysis

Santosh K. Sasanapuri, Mahendra K. Choudhary, and Tej R. Nayak

Abstract In this study, a hypothetical dam break analysis is carried out at Umrar Dam, Madhya Pradesh, India to map the extent of flood and sensitivity analysis is conducted to find out the impact of dam break parameters on water depth and water velocity at four locations on the downstream side of the dam. An overtopping failure mode is selected based on the type of dam and historical failures of the dam. Different regression equations are used to estimate dam break parameters. The Hydrological Engineering Centre's River Analysis System 2D (HEC-RAS 2D) model was used to model and analyze the dam break flood based on the parameters of the dam break. To determine the effect of terrain resolution on the extent of flood inundation, the differential global positioning system (DGPS) was used to generate the following three different resolution terrains: SRTM-30 m, ALOS PALSAR 12.5 m, and 8 m resolution DEM. The terrain with high resolution (8 m) gave the maximum inundation area of 4.383 km^2 which is 13.84% higher when compared with the low-resolution DEM of 30 m cell size. The effect of this dam failure is very high inundating 9 villages on the downstream fully or partially within 1.5 h of dam break failure with a maximum inundation depth of 16 m. The sensitivity analysis conducted by varying the dam break parameters (dam break bottom width, side slopes, break formation time) by

S. K. Sasanapuri (✉) · M. K. Choudhary
Department of Civil Engineering, Maulana Azad National Institute of Technology, Bhopal 462003, India
e-mail: sasanapuri.santosh@gmail.com

M. K. Choudhary
e-mail: mkchouhary@manit.ac.in

T. R. Nayak
Scientist 'F' and Head, Regional Centre, National Institute of Hydrology, Bhopal 462016, India

P. V. Timbadiya et al. (eds.), *Flood Forecasting and Hydraulic Structures*, Lecture Notes in Civil Engineering 340, https://doi.org/10.1007/978-981-99-1890-4_12

± 25%, + 50%, + 75% showed that their impact on water depth and water velocity is minimal on downstream side and limiting to only immediate downstream area, concluding that the dam break parameters estimated using the regression equations developed by Froehlich DC (2008) are optimum. However, the results at 0.4 km downstream of dam site shows that the water depth and water velocity values increase with the dam break bottom width.

Keywords Overtopping failure · Flood inundation modelling · HEC-RAS 2D · SRTM-30m · ALOS PALSAR 12.5m · DGPS survey · Sensitivity analysis

1 Introduction

Dams are one of the most important structures constructed across streams or rivers to store the water in the reservoir. Basic purpose of a dam is to store and release water for domestic water supply, industrial use, irrigation, hydro-power generation, navigation, etc., and whenever there is a demand. During flood, the dam can serve as protection for towns and cities downstream of the dam along the river. In addition to the dams' many benefits and uses, flash floods caused by sudden dam failure or sudden water release through gates often result in the loss of life and severe property damage in the downstream area.

The sudden failure of dam can be defined as formation of an opening in the body of the dam. When there is a sudden failure of dam or an opening is formed in the body of the dam, all the water stored in the reservoir flows downstream uncontrollably resulting into flash flood. Mainly, the dams are classified into two types based on the construction material used are concrete dams and embankment dams. These dams can be further classified into sub-categories based on the shape and how they are constructed. The main cause for concrete dam failures is foundation failure. The embankment dam breach failures can be classified into two types: (a) overtopping and (b) piping failures. The overtopping failure is occurred when the water level in the reservoir rises and the body of dam starts to fail from the top leading to an opening in the body of dam. The piping failure is occurred when the water seepages through the body of the dam and in the prolonged time it leads to formation of an opening. Out of these two failures, overtopping failure is more dangerous because the time required for the formation of an opening is less compared with the piping failure.

Even with the advanced engineering technology and high construction quality over the years, 100% guarantee for the safety of the dam is not possible and number of accidents occurred over the years. There have been around 200 dam failures in the twentieth century worldwide, with notable consequences. These failures resulted in several disasters in the downstream side of the dam in terms of both casualties and loss of infrastructure. The cause of the dam breach failure depends on type of dam, age of the dam, natural disasters, and manmade errors. The age of the dam is directly related to the risk of failure.

Because of this, dam break analysis is one of the important tasks for the estimation of downstream water depth, water velocities, warning time available for the evacuation of downstream population to avoid hazard situation during flash flood resulting from dam break. There are so many hydraulic models available in the market for conducting dam break analysis. From the literature review on hydraulic models available for the dam break analysis and flood inundation mapping, it was found that HEC-RAS is more reliable for conducting dam break analysis and flood mapping [1]. The dam break analysis results of HEC-RAS, DAMBRK, and MIKE11 found that the results obtained from HEC-RAS are much closer to observed values [2]. The HEC-GeoRAS extension in ArcGIS along with HEC-RAS for dam break analysis and the results obtained are reliable [3]. Due to its high accuracy and capacity for simulating various rivers and canals, the Hydrologic Engineering Centre River Analysis System (HEC-RAS) was chosen to carry out this study. The most recent version of HEC-RAS software can simulate two-dimensional (2D) flow, in contrast to earlier versions that could only simulate one-dimensional (1D) flow [4]. According to [5] and [6], 1D flood models cannot simulate flood wave side diffusion since they study flows that are presumed to occur in a longitudinal direction, such as rivers and confined channels. In order to simulate the range of floods that 1D models cannot provide, 2D models are used to simulate the floodplain region. This is based on the idea that perpendicular water movement cannot be omitted [5].

There are three purposes of this study. They are (a) possible dam break simulation of Umrar Dam for overtopping failure state; (b) identify the impact of terrain resolution on the flood inundation area; (c) carry out a sensitivity analysis on dam breach parameters and observe the variation of water surface elevation and maximum water velocity.

2 Study Area and Data Source

2.1 Study Area

The study area lies on the Umaria River stretch as shown in the Fig. 1. It covers a distance of 14 km from Umrar Dam to the confluence of Umrar River with the Narshara River. The Narshara River joins Son River which is a tributary of Ganga River, therefore Umrar river comes in Ganga Basin. This stretch lies in Umrar District of Madhya Pradesh, India. Umaria is the largest city in Umrar district, at a distance of 7 km from the Umrar Dam. The dam is located at 23°29′37.18″ N and 80°49′24.17″ E. The construction of the dam was started in 1977 and completed in 1978. It is an earthen dam having 995 m long earthen embankment dam. The width of the dam at top is 5 m and the height of the dam is 21.852 m. The maximum water level capacity of dam is 23.316 MCM at an elevation of 504.72 m. The dead storage level is 481.28 m. The top bank level of the dam is increased from 506.86 m to 507.08 m.

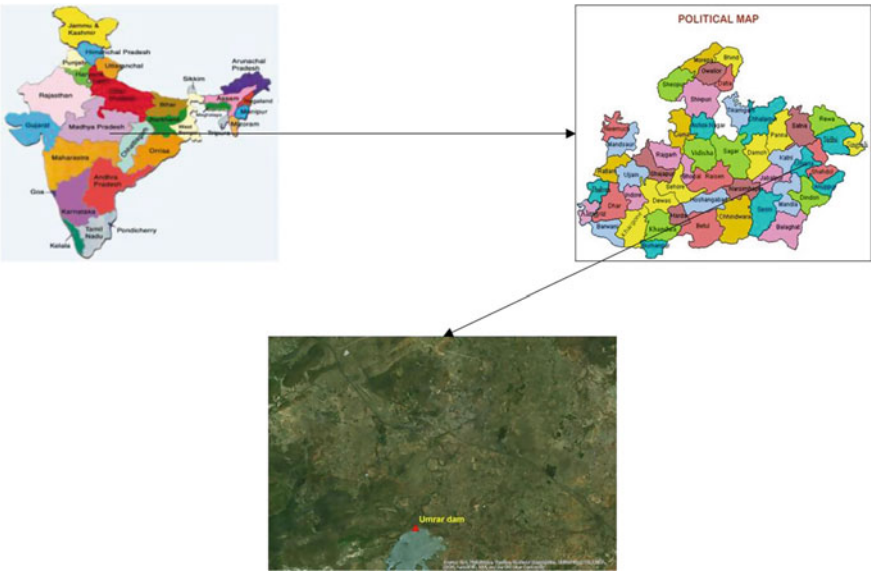

Fig. 1 Index map of the study area

The average rainfall of the Tapi Basin has been reported to be 815.7 mm. From the global maps of the Köppen–Geiger climate classification, at spatial resolution of 0.5° for the period 1951–2000, it is found out that nearly 48.5% of the basin area is classified as semi-arid region (BSh), while remaining 51.5% region experiences sub-humid climate (tropical dry savannah—As, and tropical wet savannah—Aw).

2.2 Data Used

2.2.1 Toposheet and LISS III Data—LULC Mapping

For the proper delineation land use land cover (LULC) map for the downstream area of the Umrar Dam, remote sensing data were obtained, such as 23.5 m Linear Imaging Self—Scanning Sensor III (LISS III) data was acquired for the month of August 2013. The reason for acquiring data for the August month is all the agricultural fields will be at full scale in agriculture and it helps in proper identification of agricultural fields from the barren lands. The LISS III data can be downloaded from https://bhuvan-app3.nrsc.gov.in/data/download. Along with the satellite data, the toposheet for the area is also acquired for the proper mapping of all the villages presented in the study area. A total of four classes were identified from the LULC map and they are agriculture, water bodies, settlements, and forest. Out of these four classes agriculture

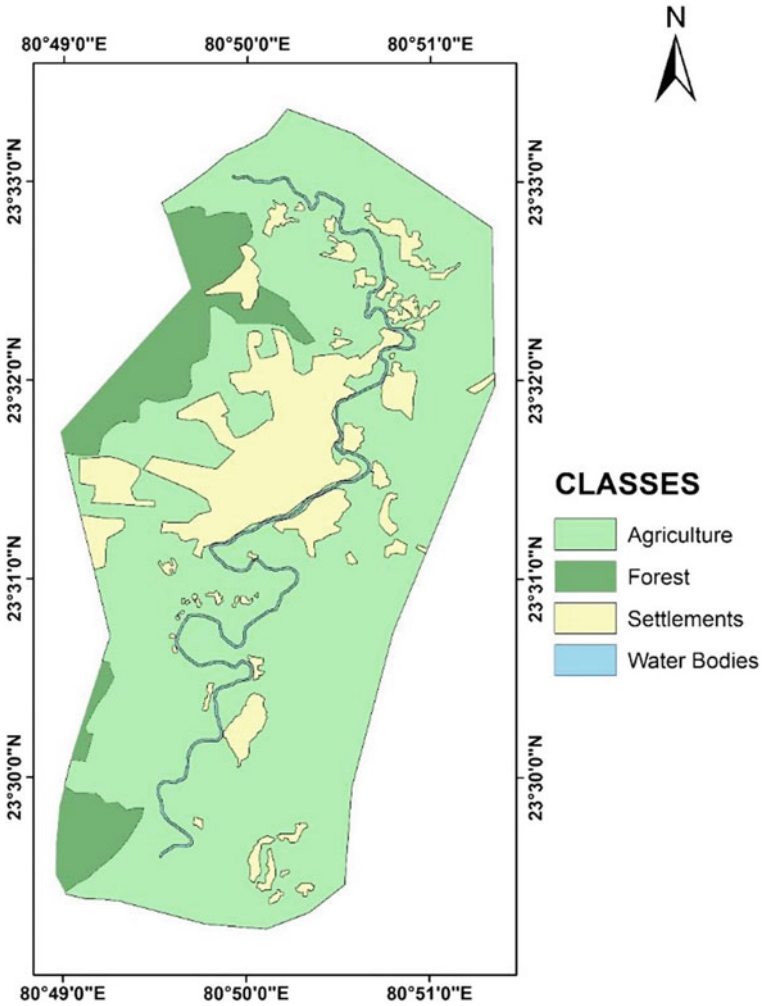

Fig. 2 Land use land cover of the study domain

contributes for an area of 70.15% of the total area. The next highest occupied class is settlements with 19.16%. The LULC of the study area is shown in Fig. 2.

2.3 River Cross-Sections

River cross-sections are important for accurate flood modelling through a river. A differential global positioning systems (DGPS) survey was conducted by National Institute of Hydrology (NIH), Regional Centre, Bhopal for the estimation of river

Fig. 3 River cross-sections on downstream of Umrar Dam

cross-sections elevations and the same data was obtained from NIH, Regional Centre, Bhopal. The survey was conducted at 19 different important cross sections of the Umrar River within a span of 14 km at locations shown in Fig. 3. These surveyed cross-sections are used along digital elevation model (DEM) for improving the river geometry for dam break flood modelling.

2.4 Digital Elevation Model

For this study, two different DEMs were used. The first one is a digital elevation model of the Shuttle Radar Topography Mission (SRTM) with a 30 m resolution that may be downloaded from earthexplorer.usgs.gov. The second one can be downloaded from Alaska Satellite Facility and is called Advanced Land Observing Satellite Phased Array Type L-band Synthetic Aperture Radar (ALOS PALSAR), digital elevation model with 12.5 m resolution. The ALOS PALSAR DEM requires pre-processing of vertical datum. This can be done with the geoid. By combining both the ALOS PALSAR and the DGPS surveyed data, a new DEM was generated of 8 m resolution

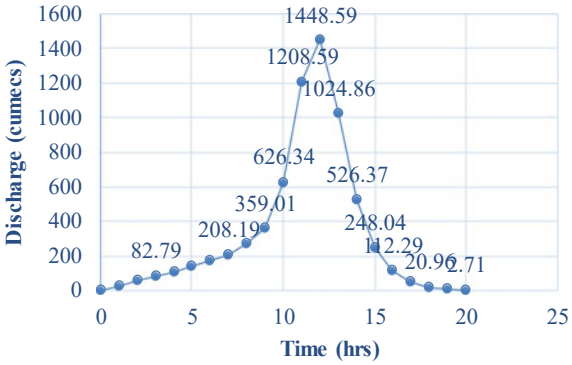

Fig. 4 Lateral inflow flood hydrograph

using the kriging method. These three DEMs were used in this study to identify the impact of terrain resolution on the flood inundation extent.

2.5 Digital Elevation Model

The lateral inflow flood hydrograph for the Umrar Reservoir was provided by Madhya Pradesh Water Resources Department, Bhopal. The flood hydrograph is used as inlet boundary condition into the reservoir. The flood hydrograph shown in Fig. 4 is the design flood hydrograph of Umrar Dam. The flood hydrograph has peak value of 1448.59 m^3/s.

The elevation storage curve for the Umrar Reservoir was provided by Madhya Pradesh Water Resources Department, Bhopal. In HEC-RAS software, the storage data can be entered as area times depth method or elevation versus capacity curve. In the above two methods, elevation versus capacity method is most accurate one. Hence, elevation storage curve is important for using HEC-RAS model. Figure 5 gives the elevation storage curve of Umrar Reservoir from full reservoir level (FRL) to top bank level (TBL).

3 Methodology

3.1 DEM Correction

In surveying and mapping, a datum is a point, line, or surface that serves as a reference. The coordinates on any map are determined using a geodetic datum, which is a mathematical representation of the Earth. A datum is the Earth's mathematical model, to put it simply. Every coordinate uses a specific collection of numbers to describe the size and shape of the Earth. When creating their maps and surveys, several nations

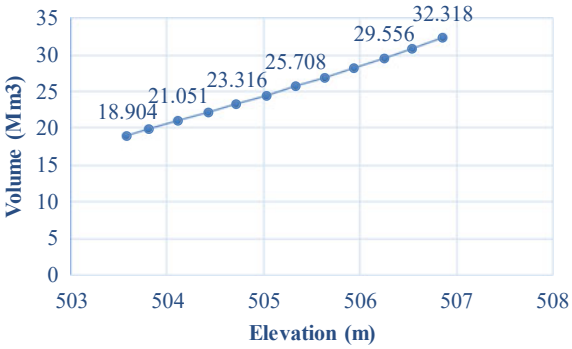

Fig. 5 Elevation storage curve of Umrar Reservoir

utilize their own datum, or local datum. Datum comes in two varieties: a vertical datum for elevation and a horizontal datum for position. Although nearly all maps and charts use mean sea level as their height, they may use any of the more than a hundred distinct horizontal position datum. On a map, there may occasionally be more than one grid. Each grid typically corresponds to a separate datum.

The equipotential surface of the Earth's gravitational field called the Geoid best approximates the average sea level around the world using least squares. The geoid is a depiction of what the Earth would look like if the sea were to cover it. In contrast to the idealized geometric shape of a reference ellipsoid, the geoid is frequently referred to as the genuine physical figure of the Earth. If the oceans were in equilibrium, at rest (relative to the spinning Earth), and extended across the continents, then that equipotential surface would exactly coincide with the mean ocean surface of the Earth (such as with very narrow canals). Contrary to the reference ellipsoid, a mathematically idealized representation of the real Earth, the geoid surface is uneven, yet it is still noticeably smoother than the real Earth's surface. The ALOS PULSAR DEM was corrected for the DGPS surveyed data using krigging method in ArcGIS with an output cell size of 8 m. Figure 6 shows the flowchart for the DEM correction with the surveyed data.

3.2 Dam Breach Parameter Estimation

There are several methods and softwares are available for the estimation of dam break parameters for different types of dams. Based on the availability, literature, suitability for the type of dam, and accuracy, Froehlich DC [7] method was chosen for the estimation of dam break parameters of Umrar Dam. Based on the incorporation of new data, Dr. Froehlich DC revised his breach equations in 2008. Dr. Froehlich DC created a set of equations to estimate average breach width, side slopes, and failure time using 74 earthen, zoned earthen, earthen with a core wall (i.e. clay), and rockfill datasets [8].

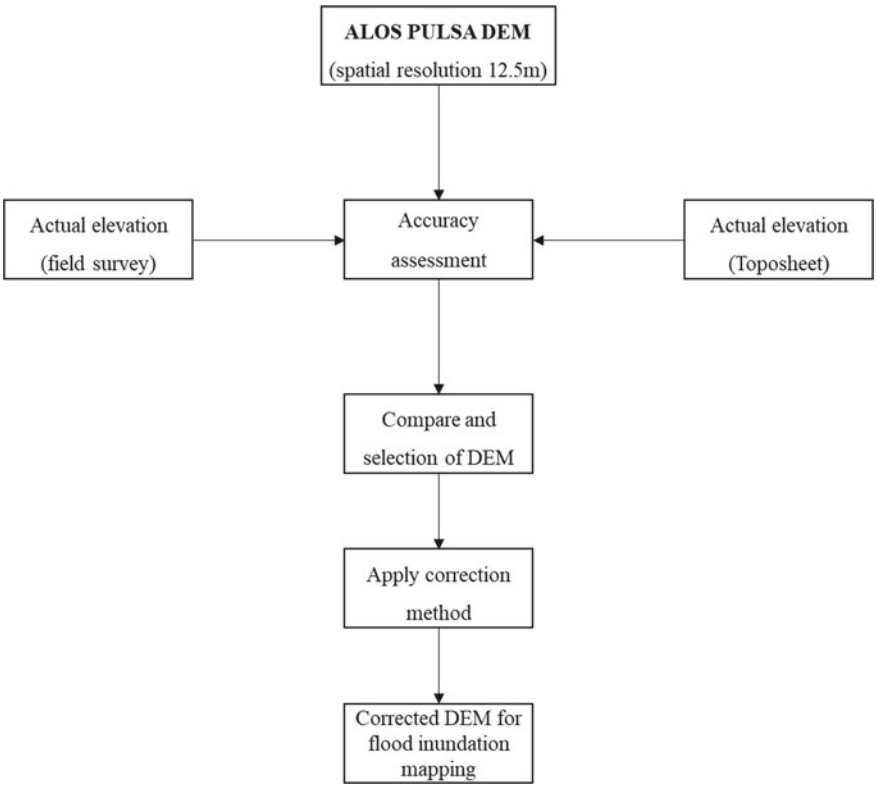

Fig. 6 Flowchart for correction of DEM

Bavg = 0.27 Ko Vw0.32 hb0.04

tf = 63.2 $\sqrt{}$Vw/*g*hb2

Bavg = Average breach width (m)

Ko = Constant (1.3 for overtopping and 1.0 for piping)

Vw = Reservoir volume at time of failure (m^3)

hb = Height of final breach

g = Gravitational acceleration

tf = Breach formation time (s)

Froehlich DC 2008 paper states that the average side slopes should be:

1.0 H:1V Overtopping failures
0.7 H:1 V Otherwise (i.e. piping/seepage)

4 Results and Discussions

The downstream area of the Umrar Dam is densely populated with 9 villages which includes major city like Umaria, connected with 11 bridges across the river which includes a railway bridge.

Table 1 gives the maximum depth and minimum arrival time of the flash flood resulting from the overtopping failure of dam at the villages on the downstream of the dam. Table 2 gives the maximum depth and minimum arrival time at the bridges on the downstream of the dam due to overtopping failure of the Umrar Dam. Khalesar village is receiving maximum depth of water of 14.195 m at a distance of 5.6 km from the Umrar Dam. The inundation area for high resolution terrain modified using DGPS surveyed data of 8 m cell size gives an area of 4.383 km^2, also Pulsar DEM of 12.5 m cell size is 4.190 km^2 and for SRTM DEM of 30 m cell size is 3.776 km^2. The inundation boundaries of three different DEMs were shown in Fig. 7.

4.1 Sub-Basin Wise Rainfall Distribution

A sensitivity analysis was conducted by varying the dam breach parameters by – 25%, + 25%, + 50%, + 75%. Breach bottom width, side slope and breach formation time are varied, and at four places downstream of the dam the maximum water surface elevations and maximum velocity are observed. Table 3 gives the sensitivity analysis results for ± 25% and Table 4 gives the results for + 50% and + 75%.

Table 1 Maximum depth and minimum arrival time at different villages on the downstream

Priority order	Village name	Distance from Umrar Dam (km)	Maximum depth (m)	Minimum arrival time (HH:MM:SS)
1	Mahori	0.4	5.51	0:12:30
2	Mahori	1.5	10.10	0:20:30
3	Amliyatola	4.1	10.01	0:32:30
4	Khalesar	5.6	14.19	0:37:30
5	Umaria	6.9	12.21	0:42:00
6	Lalpur	8.8	11.03	0:58:00
7	Ghaghari	10.3	6.78	1:07:30
8	Bhangha	11.5	8.04	1:14:00
9	Loharganj	13.5	4.95	1:32:00

Table 2 Maximum depth and minimum arrival time at different bridges on the downstream

Bridge ID	Bridge location	Distance from Umrar Dam (in km)	Overtopping failure	
			Maximum depth (m)	Minimum arrival time (HH:MM:SS)
Bridge 1	Near Mahori	1.5	8.03	0:20:30
Bridge 2	Near Mahori	2	4.55	0:24:00
Bridge 3	Near Mahori	2.3	6.66	0:24:00
Bridge 4	Between Amliyatola and Khalesar	5.6	6.31	0:38:00
Bridge 5	Railway Bridge between Umariya and Khalesar	7	4.35	0:51:30
Bridge 6	Between Umaria and Khalesar	7.5	7.73	0:52:30
Bridge 7	Between Umaria and Khalesar	7.7	1.43	0:57:00
Bridge 8	Between Umaria and Lalpur	8.5	6.17	0:57:30
Bridge 9	Between Umaria and Lalpur	8.8	10.32	0:59:00
Bridge 10	Between Umaria and Ghaghari ara>	10.3	5.03	1:07:00
Bridge 11	Between Bhangha and Loharganj	13.4	3.21	1:32:00

5 Conclusions

The following conclusions are derived from the foregoing study:

- The above Table 1 gives that all the 9 villages are receiving flood with a minimum depth of 4.955 m.
- The village named Khalesar was receiving maximum water depth of 14.195 m.
- In this study, three types of DEMs were used and the results show that high resolution DEM gave the maximum area of inundation with an area of 4.383 km^2.
- The sensitivity analysis of dam breach parameters shows not much variation in the WSE and velocities. At a distance of 0.4 km downstream of the dam site shows that, as the dam breach bottom width values are increasing the WSE and velocity values are increasing.

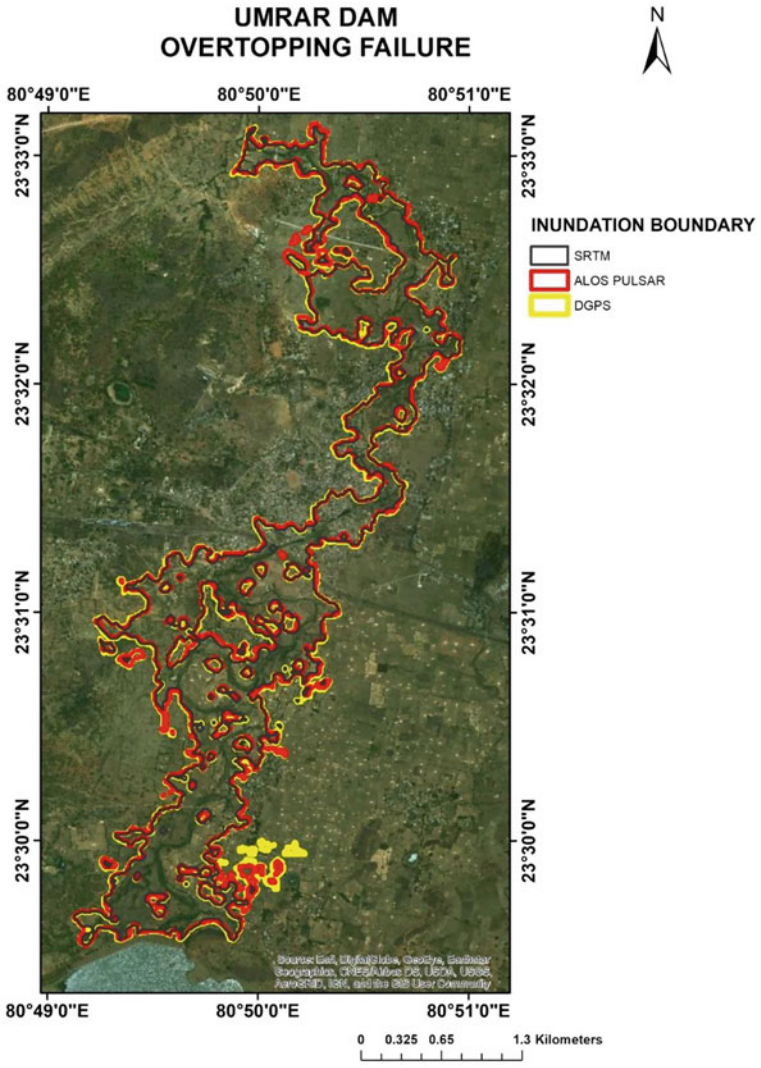

Fig. 7 Inundation boundaries for different DEM resolutions

Table 3 Dam break sensitivity analysis 1 (± 25%)

Location	Distance from dam (km)	Break without adjustment		Adjusted breach width			
				Decrease 25%		Increase 25%	
		WSE (m)	Velocity (m/s)	WSE (m)	Velocity (m/s)	WSE (m)	Velocity (m/s)
Mahori	0.4	469.63	2.67	469.55	2.53	469.70	2.78
Railway bridge b/w Umaria and khalesar	7	458.92	8.49	458.82	8.37	458.82	8.41
Bridhe b/w Umaria and Lalpur	8.5	453.43	5.66	453.29	5.54	453.27	5.54
Loharganj	13.5	437.61	1.97	437.58	1.93	437.58	1.93

Adjusted breach side slopes				Adjusted breach formation time			
Decrease 25%		Increase 25%		Decrease 25%		Increase 25%	
WSE (m)	Velocity (m/s)	WSE (m)	Velocity (m/s)	WSE (m)	Velocity (m/s)	WSE (m)	Velocity (m/s)
469.57	2.57	469.69	2.77	469.72	2.82	469.57	2.56
458.82	8.37	458.80	8.39	458.82	8.42	458.82	8.36
453.29	5.56	453.25	5.58	453.27	5.60	453.28	5.52
437.58	1.93	437.58	1.93	437.58	1.93	437.58	1.93

Table 4 Dam break sensitivity analysis 2 and 3 (+50% & 75%)

Location	Distance from dam (km)	Break without adjustment		Adjusted breach width			
				Increase 50%		Increase 75%	
		WSE (m)	Velocity (m/s)	WSE (m)	Velocity (m/s)	WSE (m)	Velocity (m/s)
Mahori	0.4	469.63	2.67	469.76	2.89	469.81	2.99
Railway bridge b/w Umaria and khalesar	7	458.92	8.49	458.82	8.44	458.83	8.47
Bridhe b/w Umaria and Lalpur	8.5	453.43	5.66	453.27	5.58	453.28	5.62
Loharganj	13.5	437.61	1.97	437.58	1.93	437.59	1.93

Adjusted breach side slopes				Adjusted breach formation time			
Increase 50%		Increase 75%		Increase 50%		Increase 75%	
WSE (m)	Velocity (m/s)	WSE (m)	Velocity (m/s)	WSE (m)	Velocity (m/s)	WSE (m)	Velocity (m/s)
469.75	2.88	469.81	2.98	469.53	2.49	469.49	2.43
458.80	8.41	458.79	8.42	458.83	8.38	458.85	8.38
453.24	5.53	453.23	5.59	453.30	5.59	453.33	5.59
437.58	1.93	437.58	1.93	437.58	1.94	437.58	1.94

Acknowledgements The authors would like to acknowledge Madhya Pradesh Water Resources Department and National Institute of Hydrology for providing the Umrar Dam, Umrar Reservoir, and DGPS surveyed data.

References

1. Kumar S, Jaswal A, Pandey A, Sharma N (2017) Literature review of dam break studies and inundation mapping using hydraulic models and GIS. Int Res J Sci Technol 4(5):55–61
2. Aravind V, Muthiah P, Rai NN (2017) Performance analysis of three dam failure analysis modules. In: Third national dam safety conference at IIT Roorkee
3. Balogun O, Ganiyu H (2016) Study and analysis of ASA river hypothetical dam break using HEC-RAS. Niger J Technol 36(1):315–321. https://doi.org/10.4314/njt.v36i1.39
4. Xiong Y (2011) A dam break analysis using HEC-RAS. J Water Resour Prot 03(06):370–379
5. Dasallas L, Kim Y, An H (2019) Case study of HEC-RAS 1D–2D coupling simulation: 2002 Baeksan flood event in Korea. Water 11(10):2048
6. Teng J, Jakeman A, Vaze J, Croke B, Dutta D, Kim S (2017) Flood inundation modelling: a review of methods, recent advances and uncertainty analysis. Environ Model Softw 90:201–216
7. Froehlich DC (2008) Embankment dam breach parameters and their uncertainties. J Hydraul Eng 134(12):1708–1721
8. Joshi MM, Shahapure SS (2017) Two dimensional dam break flow study using HEC-RAS for Ujjani Dam. Int J Eng Technol 9(4):2923–2928

Dam Break Flood Inundation Mapping of Umrar Dam Using HEC-RAS

Bikram Prasad, H. L. Tiwari, and Sunny Gupta

Abstract Flood inundation mapping can assist with municipal and urban growth planning, disaster management, flood insurance rates, and ecological studies. Both the ability to forecast the behavior of the stream in question for various recurrence interval storm events and the ability to interpret the forecasted results into a plan-view extent of flooding are required for mapping a flood plain. Dam break was modeled and analyzed using the HEC-RAS model based on the dam breach parameters. The Hydrologic Engineering Center River Analysis System (HEC-RAS) can simulate flood events and generate water surface profiles along the length of a stream model. Using the companion GIS tool, HEC-GeoRAS, those water surface profiles can be easily converted to flood inundation maps. The type of dam and the dam's historical failures is used to select an overtopping failure mode. Different regression equations were used to estimate breach parameters, and the final breach parameters for the dam were chosen, which were derived by Froehlich. In this study, two different types of DEMs were used: first, an Advanced Land Observing Satellite (ALOS) The Phased Array Type L-band Synthetic Aperture Radar (PALSAR) DEM with a resolution of 12.5 m, and second, an Shuttle Radar Topography Mission (SRTM) DEM with a resolution of 30 m. Both DEMs were compared, and it was discovered that the inundation area is larger for higher resolution. Finally, the downstream inundation area is calculated, and outflow hydrographs at key sites are exported to ArcGIS from the RAS mapper in HEC-RAS for analysis. The maximum depth map, maximum velocity map, maximum water surface elevation map, and minimum flood wave arrival time map were created for various bridges along the river on the downstream side of the dam.

B. Prasad (✉)
Civil Engineering Department, Bansal Institute of Science and Technology, Bhopal, India
e-mail: bikram2010@gmail.com

H. L. Tiwari
Civil Engineering Department, MANIT, Bhopal, India

S. Gupta
Water Resource Engineering, MANIT, Bhopal, India

P. V. Timbadiya et al. (eds.), *Flood Forecasting and Hydraulic Structures*, Lecture Notes in Civil Engineering 340, https://doi.org/10.1007/978-981-99-1890-4_13

Keywords Flood inundation mapping · HEC-RAS · ALOS PALSAR · SRTM · DEM · GIS · HEC-GeoRAS

1 Introduction

1.1 Flood Inundation Mapping

Flood inundation mapping is a beneficial tool for engineers, planners, and authority's corporations in municipal and concrete boom planning, emergency reaction plans, flood coverage rates, and ecological studies. Decision makers can higher allocate sources to put together for emergencies and enhance standard first-class of existence with the aid of using knowledge the quantity of flooding and floodwater inundation. The River Analysis System (HEC-RAS) of the Hydrologic Engineering Center is a software program bundle; this is well-appropriate for growing flood inundation maps for a lot of applications. An HEC-RAS version may be implemented to each consistent and unsteady flow regimes, in addition to subcritical and supercritical flow regimes. With its associate utilities, HEC-GeoRAS and ArcView, seamless integration with GIS simplifies each version geometry production and output post-processing. As floods and their severe consequences are commonplace in many parts of the world, public, political, and scientific awareness of proper flood protection and management has increased. It is important to assess and manage flooded areas using non-structural techniques for different flood intensities. Previously, several hydrological models were developed to simulate flooding in the catchment area. These models take both land and river currents into account. Also, these models are only used in test tanks or small shallow areas with hypothetical conditions. Few models such as HEC-GeoHMS, HEC-GeoRAS and MIKE BASIN, MIKE11, and MIKEFLOOD are available to simulate floods in a river basin for real flood events, considering the full spatial heterogeneity of the physical topography.

HEC-RAS is a computer program that simulates the flow of water in natural rivers and other channels. The program was one-dimensional before the last update to version 5.0, which means that there is no direct modeling of the hydraulic effect of cross-sectional deformations, bending and other two- and three-dimensional flow aspects. Version 5.0 introduced two-dimensional flow modeling and sediment transfer modeling capabilities. The program was created by the US Department of Defense Army Corps of Engineers to manage the rivers, ports, and other public works under its jurisdiction and has gained widespread acceptance since its release in 1995. The River Analysis System was created by the Hydrologic Engineering Center (HEC) in Davis, California to assist hydraulic engineers with channel flow analysis and floodplain determination. It has numerous data entry components, hydraulic analysis components, data storage, and management capabilities, as well as graphing and reporting capabilities.

1.2 Functions and Applications of HEC-RAS

HEC-RAS can analyze flows in both one and two dimensions. The functions of HEC main RAS are as follows:

1. Calculation of water surface profile in steady flow,
2. Simulation in unsteady flow,
3. Calculations of sediment transport at moving boundaries, and
4. Water quality analysis.

HEC-RAS has numerous applications in and of itself. Among them are

1. Bridge/culvert modeling,
2. Inline structures,
3. Lateral structures,
4. Flood control,
5. Sediment transport and management,
6. Water quality analysis,
7. Flow analysis.

1.3 Brief Literature Review

Alaghmand [1] compared the capabilities of HEC-RAS and MIKE 11 hydraulic models in river flood risk modeling and found that HEC-RAS has higher river flood risk mapping capabilities than MIKE11. Models are compared in four main areas: credibility, available results, model usability, and availability. The maps of river flooding extent and water depth produced by HEC-RAS are more accurate than the maximum flooding estimated by MIKE11.

Amini [2] under overflow and pipeline conditions of Vahdat Dam, Kurdistan, Iran using ArcMAP and HEC-RAS. They found that estimating peak discharge and travel time for dam failures are important factors in assessing risk 8 and providing an emergency plan. This investigation showed that the HEC-RAS software has sufficient capabilities for the dam failure phenomenon.

According to [3], flood mapping is an important tool for municipal and urban growth planning, contingency plans, flood insurance rates, and ecological studies. Mapping a floodplain requires predicting the behavior of the river considered for different storm events at repeat intervals, and the ability to translate the forecast results into a plan view of the extent of the flooding. The flow analysis system and#40; HEC-RAS and #41; In the Hydrologic Engineering Center, you can model flood events and create water surface profiles along the modeled stream. These water surface profiles can be easily converted to flood maps using the companion GIS utility HEC-GeoRAS. This paper will go over the steps needed to conduct a flood inundation mapping study using HEC-RAS, as well as present a case study demonstrating the capabilities of HEC-RAS and HEC-GeoRAS.

Kumar et al. [4], this article describes a study conducted in Prayagraj, India, at the confluence of the Ganga and Yamuna rivers, to develop and understand the methodology to delineate the extent of flooding and to identify different flood hazard zones (Sangam). A proven hydraulic model (HEC-RAS 5.0.7 (2D)) and the Global Flood Monitoring System and #40; GFMSand#41; tools were used in this study. The methodology addresses two shortcomings in flood studies: the ability of the HEC-RAS 2D flood model and GFMS download for 1D and 2D flood modeling, and the development of a methodology to identify different flood hazard zones from the model output.

Gupta et al. [5] used the Center for Hydrological Engineering—Hydrological Modeling System and #40; HEC-HMS & #41; and the Hydrological Engineering Center—River Analysis System y#40; HEC-RAS and #41; as modeling tools to create a runoff and flood assessment model for floodplains for known rainfall. For the spatial analysis of the basin, the model also includes the Aeronautical Reconnaissance Geographic Information System and #40; ARCGISand#41; HEC-GeoRAS and HEC-GeoHMS extensions. HEC-HMS is used for hydrological analysis, and HEC-RAS is used for hydraulic modeling. By forcing the model with forecast rainfall, the flood warning system can generate flood maps ahead of the flood.

Hicks and Peacock [6] most river flood forecasts are currently performed in two steps. First of all, the flood control takes place, which is usually done with hydrological models. With a stationary hydraulic model like HEC-RAS, the resulting flood peaks are converted into water level forecasts. The HEC-RAS model has recently been extended to allow for unsteady flow analyzes, and although the numerical scheme is not robust enough to handle dynamic events (such as ice jam flooding) or supercritical flows, it can guide simple open-water flooding during its water level generates forecasts.

Xiong [7] conducted a dam failure analysis for the Foster Joseph Sayer Dam in the United States using the dam failure and pipe failure tool in HEC-RAS. He also performed a sensitivity analysis by adjusting the nip side slope, total formulation time, nip width, and nip depth by different percentages. He found that failure of the pipeline prolongs elevation of the water surface downstream and prolongs the duration of the hazard. The maximum downstream water surface elevation for PMF has been discovered. The maximum water surface height of did not change with the change in dam failure parameters, based on a sensitivity analysis.

2 Working Methodology

2.1 Data Used

2.1.1 Flood Hydrograph

The National Institute of Hydrology (NIH) Regional Center in Bhopal provided the lateral inflow flood hydrograph of the Umrar Dam. In the HEC-RAS software, this inflow flood hydrograph was used as an inlet boundary condition. The maximum was 1448.59 m^3/s.

2.2 Curve of Elevation Storage

The National Institute of Hydrology (NIH) Regional Center in Bhopal provided the elevation storage data. The HEC-RAS software provides two methods for entering storage area data: the area times depth method and the elevation versus capacity curve method. The elevation versus capacity curve method is the more accurate of the two. As a result, the elevation storage curve is critical input data for the HEC-RAS software.

2.3 Digital Elevation Model (DEM)

A digital elevation model (DEM) is a three-dimensional (3D) computer graphics representation of elevation data used to represent terrain. Digital elevation models are widely used in GIS and are used to create relief maps. DEMs can be obtained from a variety of sources, including the USGS, ALOS PALSAR, BHUVAN, and others, and each DEM has a unique resolution; in this work, I used an ALOS PALSAR DEM with a resolution of 12.5 m.

2.4 Salient Features of Dam

The Dam's distinguishing features have a significant impact on water retention and capacity. These parameters include Mannings roughness coefficient, bed slope, and number of spillways. Any change in these features has a direct impact on the total storage capacity. The Dam's downstream cross-section details are also required for flood inundation studies.

2.5 Methodology for 2D Dam Break Analysis

Step 1: **Entering data in RAS Mapper:** Open HEC-RAS and create new project. Open RAS mapper and define projections for the project. Create new terrain by using the DEM for the area. Then go to map layers and add the Web imagery as ArcGIS World imagery, then go to geometry and add 2D flow area and make the storage area.

Step 2: **Geometric Data Editor**: Open geometric data editor in HEC-RAS and digitize the reservoir and enter the reservoir elevation storage capacity data. Create a mesh of required cell size for the expected flow area. In this study cell size of the mesh is 50 m. A total number of 11,040 cells were created with an average cell size of 4303 m^2. The manning's '*n*' values were taken from CWC guidelines. Then, digitize the dam as SA/2D connection and enter the top elevation (RL 506.663 m) and length of the dam as 995 m. Finally, digitize outlet boundary condition. The outlet boundary condition is frictional bed slope of Umrar River which is 0.00354. Then, go to SA/2D flow area and mention weir width, embankment elevation, and the weir length. Then, go to breach plan data and enter the center station, final bottom width, bottom elevation, left side slope, right side slope, breach weir coefficient, breach formation time, and the bottom elevation.

Step 3: **Editing Unsteady flow data**: Add storage area or reservoir as inlet boundary condition and provide the lateral inflow flood hydrograph as the design flood hydrograph of reservoir also provide the normal depth. The designed peak flood of the Umrar Dam is 478.78 cumecs, and in this study, revised flood hydrograph was used with a peak flood of 1448.59 cumecs. As the TBL of the Umrar Dam was increased from RL 506.86 m to RL 507.08 m, the design flood was revised to 1448.59 cumecs, while FRL and MWL were remained constant. Enter the frictional bed slope of river as the outlet boundary condition. Save the unsteady flow data and close it.

Step 4: **Perform an Unsteady Flow Simulation**: Enter the data like start and end time of the simulation, mention the computational time interval, mapping output interval, etc., and run the simulation.

Step 5: **Viewing of Results in RAS Mapper**: Go to RAS mapper and you can see the results like maximum depth, maximum water surface elevation, maximum velocity, and the minimum flood wave arrival time.

2.6 Methods for Estimation of Dam Break Parameters

The calculation of dam break parameters for various types of dams can be done using a variety of methods and tools. For the estimation of dam break parameters at Umrar dam, methods were chosen based on availability, literature, suitability for the type

Table 1 Dam break parameters estimated

Method	Breach bottom width (m)	Side slopes (H:V)	Breach development time (Hrs.)
[8]	25	0.5	1.02
[9]	90	0.5	0.62
[10]	74	1.18	2.44
[11]	60	1	1

of dam, and accuracy. The four methods for estimating dam break parameters are as follows:

1. Macdonald et al. Formula
2. Froehlich Formula
3. Von Thun & Gillete Formula
4. Xu & Zang Formula.

2.7 Dam Break Parameters

For the estimation of dam break parameters, all four methods listed in the previous page were used. The HEC-RAS programmed and regression equations can also be used to estimate the break parameters. The dam break parameters are calculated using the HEC-RAS software in this project, and they are compared to parameters estimated using regression equations. The conditions of the dam break obtained from the four methods are given in Table 1.

3 Results and Discussion

The lateral inflow flood hydrograph for reservoir was given with start time of 12:00 AM. The dam break occurred at 01:30:00. The computation interval for the model was taken as 6 s, and the mapping output interval was 30 s.

3.1 Flood Hydrograph

The flood hydrographs at the dam site at all the bridges located on the river on downstream side and at the downstream end of the Umar River were observed. The maximum flood at the dam site was occurred at 02:00:00 with a value of 10,265.95m^3/s. The maximum flood value at the downstream end of the river is 3775.77 m^3/s (Fig. 1).

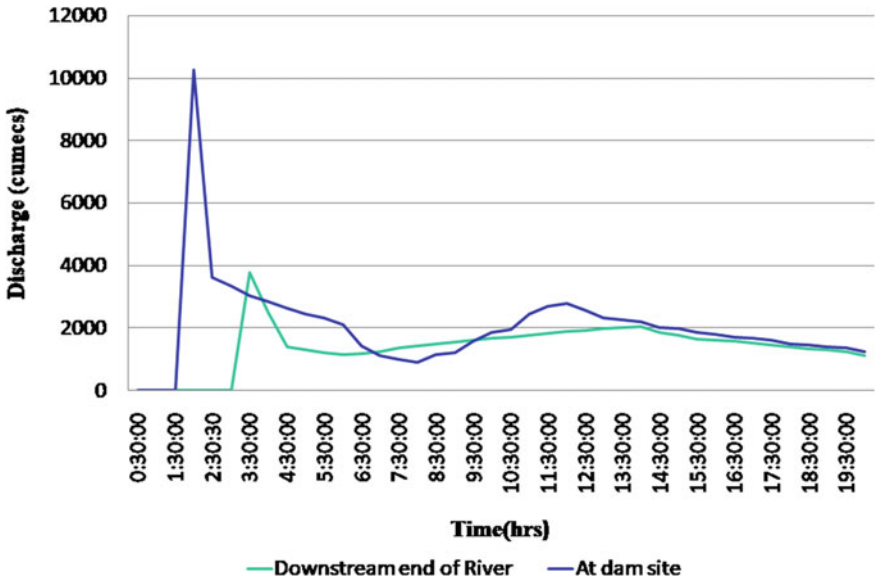

Fig. 1 Flood hydrograph at the downstream end of the river and at the dam site

3.2 Flood Inundation Maps

Maximum depth, maximum velocity, maximum water surface elevations, and minimum flood wave arrival time were used to create flood inundation maps. Layers such as main roads and railway lines, villages, and bridges can be found on all of the maps.

3.3 Maximum Depth

The maximum depth inundation map in Fig. 2 shows the maximum depth at bridges, as well as the total area inundated as a result of the Umrar Dam failure. The maximum depth is 15.353 m.

3.4 Maximum Velocity

The maximum velocity inundation map in Fig. 3 depicts the maximum velocity at bridges, as well as the amount of area flooded as a result of the Umrar Dam's failure. The maximum velocity is 7.43 m/s.

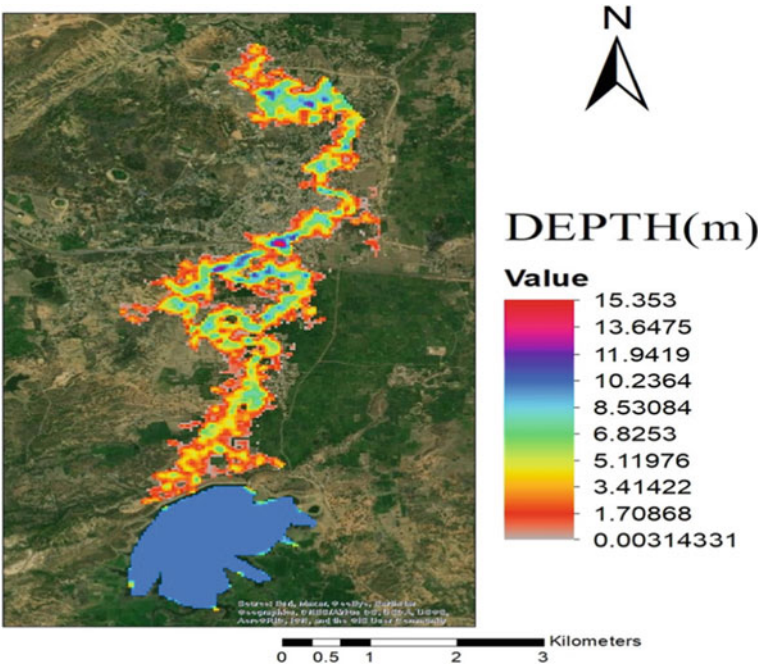

Fig. 2 Maximum depth inundation map from HEC-RAS

3.5 Maximum Water Surface Elevation

The maximum water surface elevations (WSEs) inundation map in Fig. 4 shows the maximum WSE at bridges, as well as the amount of land inundated as a result of the Umrar Dam failure. The maximum water surface elevation being 486 m and the minimum being 425.494 m.

3.6 Minimum Flood Wave Arrival Time

The arrival time inundation map in Fig. 5 shows the time of arrival at bridges, as well as the area inundated as a result of the Umrar Dam's failure.

The minimum flood wave arrival time, maximum velocity, and maximum depth at bridge locations downstream of the Umrar Dam on the Umrar River are listed in the Table 2. Table 2 also included the distance between bridge positions and the Umrar Dam.

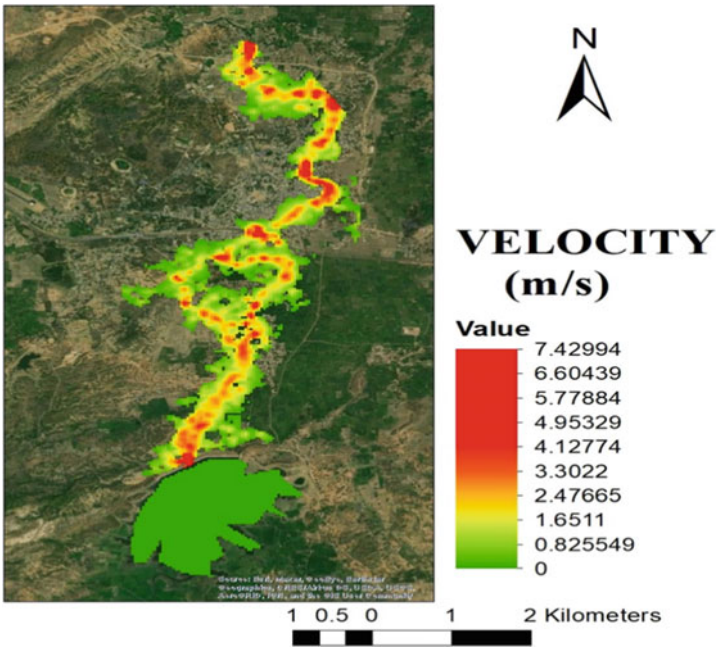

Fig. 3 Maximum velocity inundation map from HEC-RAS

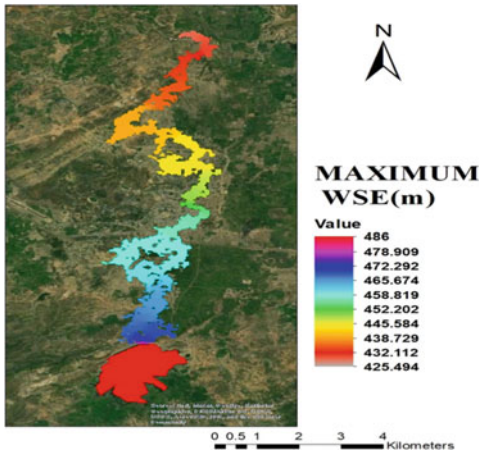

Fig. 4 Maximum water surface elevation

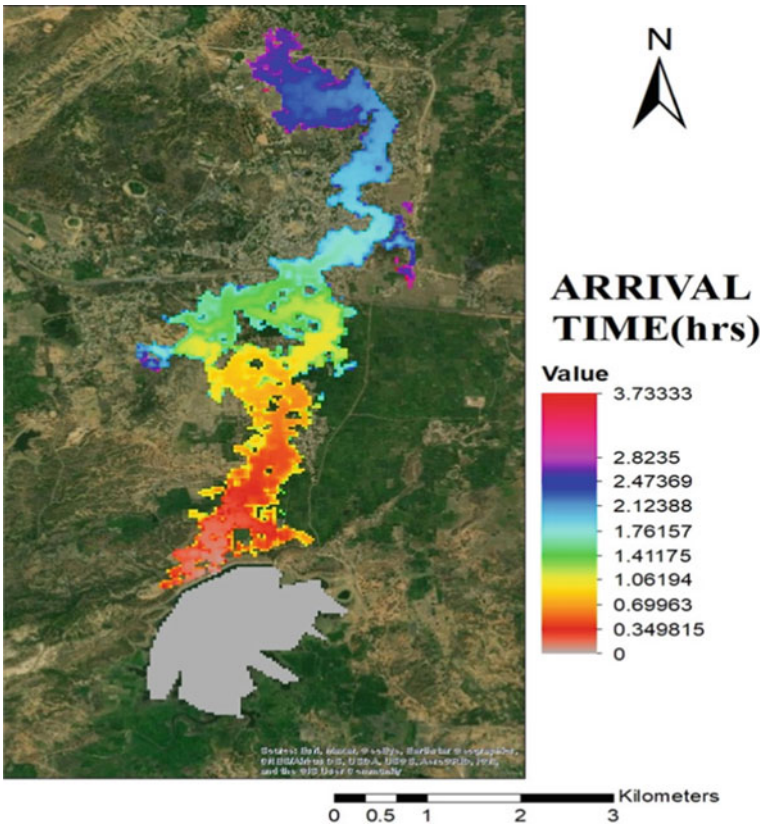

Fig. 5 Maximum flood wave arrival time

Table 2 Maximum depth, maximum velocity, and Min arrival time at bridge locations

Bridge ID	Bridge location	Distance from dam (km)	Max. depth (m)	Max. velocity (m/s)	Min. arrival time (HH:MM)
Bridge 1	Near Mahori	1.5	13.305	4.323	00:16
Bridge 2	Near Mahori	3.197	15.353	4.916	00:31
Bridge 3	Between Amliyatola and Khaleshwar	3.82	8.845	6.659	00:39
Bridge 4	Railway bridge between Umaria and Khaleshwar	4.44	12.356	5.62	00:44
Bridge 5	Between Umaria and Khaleshwar	5.1	11.75	5.75	00:49
Bridge 6	Umaria and Lalpur	6.3	8.61	6.29	00:55
Bridge 7	Between Umaria and Ghaghari	7.12	10.54	6.51	01:01

4 Conclusion

Dam break analysis is one of the most critical aspects of dam safety for both the dam and the people who live downstream on the Umrar River. The flood inundation was exported to ArcGIS from the RAS mapper in HEC-RAS, and the analysis was done in HEC-RAS. The maximum depth map, maximum velocity map, maximum water surface elevation map, and the minimum flood wave arrival time map were generated as results of the analysis. According to the above data, all seven villages are experiencing flooding with a minimum depth of 8.61 m. Khaleshwar village receives maximum depth of 15.335 m. All the seven bridge receives the flood less than one hour of the dam break. The maximum velocity of flood is received by the Amliyatola Village at 6.659 m/s which is at a distance of 3.82 km from the dam. In the study, we used two different DEM's of different resolutions, the results show that as the resolution of the DEM increases, the area of inundation also increases. We used ALOS PALSAR DEM of 12.5 m resolution and SRTM DEM of 30 m resolution, in which we selected the ALOS PALSAR DEM as it has the highest resolution. Therefore, it is recommended that high resolution DEM is preferred for the study.

4.1 Future Scope

1. Compare the results between cross sections obtained from different sources like from Google earth, DEM, and survey data.
2. Compare the results between different DEM resolutions on flooding.
3. Compare the results between the different models used for flood simulation and inundation mapping.
4. Compare the results between different modes of failure like overtopping failure and piping failure.
5. Sensitivity analysis can be done to get more accurate results.

4.2 Limitations of HEC-RAS

1. Terrain resolution. High resolution terrains are required for accurate results.
2. More and authentic data is required for validation in order to obtained good and accurate results.

4.3 Advantages of HEC-RAS

HEC-RAS is a computer program that models water flowing through open channel systems and computes water surface profiles. HEC-RAS finds commercial use in

floodplain management and (flood insurance) studies to evaluate floodway encroachments. HEC-basic RAS's computational procedure for steady flow is based on solving the one-dimensional energy equation. Friction and contraction/expansion are used to calculate energy losses. In situations where the water surface profile changes rapidly, the momentum equation can be used.

Acknowledgements I am grateful to everyone who assisted me during the course of this work, especially Dr. H.L. Tiwari, Associate Professor, MANIT, for their valuable advice and suggestions. I'd also like to thank my parents, colleagues, and friends for their encouragement and support during this difficult time. I am grateful to Almighty for his blessing.

References

1. Alaghmand S, Abdullah Bin R, Abustan I, Eslamian S (2012) Comparision between capabilities of HEC-RAS and MIKE11 hydraulic models in river flood risk modelling (a case study of SungaiKayu Ara River Basin, Malaysia). J Hydrol Sci Technol 2(3):270–291
2. Amini A, Arya A, Eghbalzadeh A, Javan M (2017) Peak flood estimation under overtopping and piping conditions at Vahdat Dam, Kurdistan, Iran. J Geosci
3. Goodell C, Warren C (2006) Flood Inundation Mapping uisngHec-ras. WEST Consultants, 2601 25th St SE, Suite 450, Salem, OR 97302
4. Kumar N, Lal D, Sherring A, Issac RK (2017) Applicability of HEC-RAS and GFMS tools for 1D water surface elevation/flood modelling of the river: a case study of River Yamuna at Allahabad (Sangam), India. J Earth Syst Environ 3(4):1463–1475
5. Gupta R, Thakur R, Parajuli R, Kalra A, Ahmed S (2017) Coupling HEC-RAS and HEC-HMS in precipitation runoff modelling and evaluating flood plain inundation map. World Environmental and Water Resources Congress, Sacramento, California, pp 240–251
6. Hicks F, Peacock T (2005) Suitability of HEC-RAS for flood forecasting. Can Water Resour Assoc 30(2):159–174
7. Xiong Y (2011) Dam break analysis using HEC-RAS. J Water Resour Protect 3:370–379
8. MacDonald TC, Langridge-Monopolis J (1984) Breaching characteristics of dam failures. J Hydraul Eng 110(5):567–586
9. Von Thun JL, Gillette DR (1990) Guidance on breach parameters, unpublished internal document, U.S. Bureau of Reclamation, Denver, Colorado, March 13, 1990, 17 p
10. Zheng N, Tachikawa Y, Takara K (2008) A distributed flood inundation model integrating with rainfall-runoff processes using GIS and remote sensing data. Int Arch Photogram Remote Sens Spatial Inf Sci 37:1513–1518
11. Froehlich DC (2016) Predicting peak discharge from gradually breached embankment dam. J Hydraul Eng 21(11):04016041-1 to 15

A Dam Break Analysis Using HEC-RAS 2D Hydrodynamic Modeling for Decision-Making System

Kishanlal Darji and Dhruvesh Patel

Abstract Flood is the disastrous phenomenon of the nature, especially, when it is associated with large dams. The large dam is constructed for multipurpose use, however the major objective to operate to reduce the flood threat at downstream. In recent climatic uncertainty and extremity, dam operation is the challenging part for flood resilience. In addition, old dams have chances to break under extreme condition. To strengthen the resilience condition and improve the decision-making system, recent state-of-art to utilize a dam break analysis for prior threat detection. This is the case of dam break analysis, it has been developed for Madhuban large dam in Gujarat. The Hydrologic Engineering Center's River Analysis System (HEC-RAS) 5.0.7 version of hydrodynamic model in 2D environment is developed for studies. The digital elevation model, flood hydrograph and elevation capacity curve of dam has been utilized for building the model. The entire approach is simulated under the unsteady flow condition. The water surface elevation, water depth, velocity, arrival time, and inundation maps have been prepared under the guideline of Dam Rehabilitation and Improvement Project (DRIP). Probable future catastrophe has been identified and addressed for future resilience. The case will help to produce the flood mitigation strategies associated with dam break case in Gujarat.

Keywords Dam break analysis · HEC-RAS · Flood · Overtopping failure

Disclaimer: The presentation of material and details in maps used in this chapter does not imply the expression of any opinion whatsoever on the part of the Publisher or Author concerning the legal status of any country, area or territory or of its authorities, or concerning the delimitation of its borders. The depiction and use of boundaries, geographic names and related data shown on maps and included in lists, tables, documents, and databases in this chapter are not warranted to be error free nor do they necessarily imply official endorsement or acceptance by the Publisher or Author.

K. Darji (✉) · D. Patel
Department of Civil Engineering, Pandit Deendayal Energy University, Gandhinagar 382426, India
e-mail: darjikishan1@gmail.com

D. Patel
e-mail: dhruvesh.patel@sot.pdpu.ac.in

P. V. Timbadiya et al. (eds.), *Flood Forecasting and Hydraulic Structures*, Lecture Notes in Civil Engineering 340, https://doi.org/10.1007/978-981-99-1890-4_14

1 Introduction

Approximately 5745 large dams, and several thousand small dams in India, are providing basic social, economic, and ecological services such as flood control, water storage for society, industrial, and agricultural use, river navigation, mining, hydropower generation, industrial waste management, and recreation. However, due to lack of consideration dams have started getting lower priority for maintenance. So, the dams constitute a serious threat to life, property and the environment, due to their potential to fail and cause disastrous flooding. According to [1] Costa reports more than 11,100 people losing their lives due to just three dam failures in the entire world: (1) Vajon dam, Italy (2) Johnstown dam, Pennsylvania, and (3) Machhu II dam, India [2]. In each of these cases, warning signals were not provided to a large number of populations. So, it is required to produce warning signals and emergency action plans of dams to reduce loss of life. The dam offers us a lot of benefits for our society but a result of the floods, caused by the failure of the constructed dams has led to some of the most devastating natural disasters in the last two centuries [3]. Dam break analysis has been carried out in order to investigate the behavior of high floods, as a result of the dam breaking and taking control of the area from flooding. This is very useful for the preparation of an emergency action plan for the evacuation of the people, and the minimized loss of the property [4]. Hurricanes, floods, cannot be avoided, however, by the adoption of appropriate evacuation methods, the losses can be minimized [5, 6]. Particular attention should be paid to effective power management through the development of an emergency evacuation plan to deal damage to a minimum.

Dam failure is generally defined as an incident to, from any structural problems, including accidental releases, or to control the outbreak of the impounded water or the incidents, which could result in the loss of the dam [7]. Different case studies express that dam failure arrives due to several reasons such as flood event, piping/seepage, foundation failure, earthquake, landslide, structural failure, equipment malfunction/failure (such as gates, etc.), upstream dam failure, the rapid drawdown of the pool, sabotage, etc. 25% of all dam failures are due to overflowing. 25% of the earthen dams and 12% of the concrete dams break in link with overtopping [8]. While HEC-RAS hydraulic computation is generally limited to overtopping and piping failure mode, all other failure modes can be simulated with one of these two methods.

The study reviews several literatures in the domain of dam break modeling using HEC-RAS software [3, 9–14]. Dam break modeling involves the prediction of breach parameters (shape, time, and size of failure) and using them to estimate breach outflow hydrograph, which is then routed to downstream of a river reach and then hydrograph at different downstream sections up to the point considered on the river are predicted. The HEC-RAS 2D modeling was toward performing unsteady flow calculations with the intent of determining the outflow hydrograph and peak discharge at various stations and to provide detailed information about a failure such as warning time available, maximum water surface elevation, and velocities at downstream locations.

The HEC-RAS has ability to simulate the break of an inline and lateral structure such as dam and levee [6]. The main aim of this study is to apply HEC-RAS model

for Damanganga dam break analysis based on given geometry data. Dam breach simulation studies may be required for preparing emergency action plan (EAP) to reduce loss of life at a time of failure of the downstream area of Damanganga dam which includes the Sillvassa, Vapi city as well as Vapi industrial area, Daman, and many villages. This paradigm analysis will be very useful to the dam owner to strengthen the decision-making system.

2 Study Area

The Damanganga River is also known as the Dawan River which is located in western part of India. The Damanganga River originates from the Western Ghats range, and it flows west into the Arabian Sea (Fig. 1). This river flows through Gujarat, Maharashtra, Union territory of Daman, and Union Territory of Dadra and Nagar Haveli. The industrial area of Silvassa and Vapi located on the north side of the Damanganga River, and the Daman dominates both sides of the river mouth. Damanganga River has a total of 1813 km^2 catchment area, out of this 376 km^2 in Gujarat, 119 km^2 in U.T. of Dadra, and Nagar haveli, and 1318 km^2 in Maharashtra. The average weighted rainfall of the Damanganga catchment is 2382 mm.

Damanganga reservoir also known as Madhuban dam is the current key project on the Damanganga River located at Madhuban village in Dharampur taluka of Valsad city of Gujarat as shown in Fig. 1. Damanganga reservoir is the inter-state multifunctional project of the Government of Gujarat and Union Territory Daman and Diu and Dadra and Nagar Haveli. Madhuban dam was constructed from 1972 to

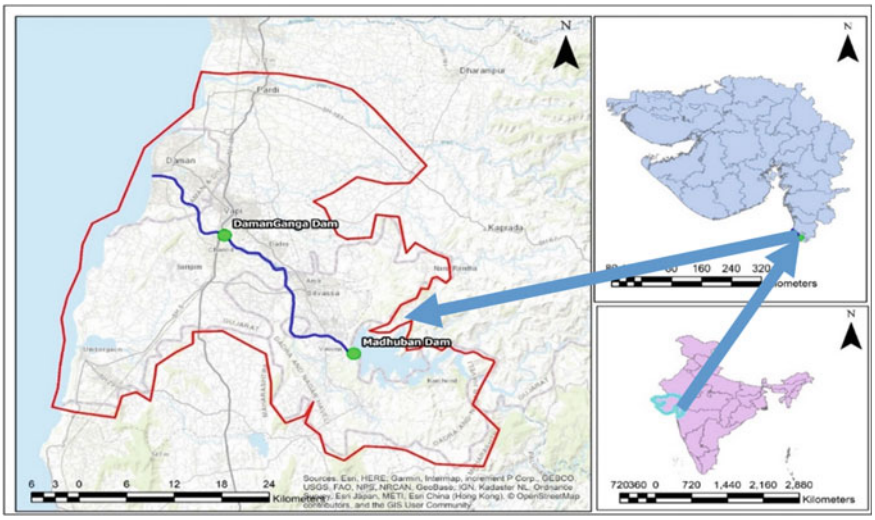

Fig. 1 Location map of the study area

1998. It is a composite dam of saddle dam, earth-fill dams, and masonry. The total length of the Madhuban dam is 2870 m in which 353-m masonry dam, 130-m saddle dam, and 2388-m Earth-fill dam. The maximum height from the deepest foundation level to the top of the roadway is 49.84 m for masonry, 6.3 m for a saddle, and 58.6 m for an earth-fill dam. Madhuban dam was designed up to 9.48 lakh cusecs flood. The gross storage capacity of the dam is 524.86 MM^3 and the live storage capacity is 478 MM^3. The spillway, with a roller bucket for energy dissipation, which is planned to rout a probable maximum flood (PMF) discharge of 7.78 lakh cusecs managed by 10 radial gates each of dimensions 15.55 * 14.02 m.

The 24 villages in U.T. Dadra Nagar Haveli, 112 villages in the Valsad district, and 26 villages in U.T. Daman are irrigated by Damanganga reservoir. The Damanganga reservoir provides 58 million gallons each day for domestic and industrial water demands and also has a minor power plant of capacity 5.6 MW. The budget of the Damanganga reservoir project was distributed between the sharing states as per the Inter-State Agreement of 1992.

3 Data Collection

Meteorological data of the study area were collected from the State Water Data Center (SWDC), flood control cell of Damanganga reservoir (https://swhydrology.gujarat.gov.in), and the Government of Gujarat and Indian Meteorological Department (IMD) (http://www.imd.gov.in/). Thematic maps were prepared from the published literature (https://www.gsi.gov.in/, http://cgwb.gov.in/) of the different agencies in conjunction with the interpretation of the Landsat images, Google Earth images, and SRTM DEM using remote sensing and GIS technology. Salient features and capacity area table of Damanganga reservoir are collected from the Damanganga project division no.1 office.

4 Methodology

The method followed for dam breach analysis is as mentioned as shown in flow chart (Fig. 2).

Required data for model simulation:

- Salient features of Madhuban dam.
- Elevation capacity curve of the Madhuban dam.
- Design flood hydrograph or probable maximum flood as the upstream boundary condition.
- Upstream sectional elevation of a dam.
- Manning's roughness coefficient for a site for a downstream area.

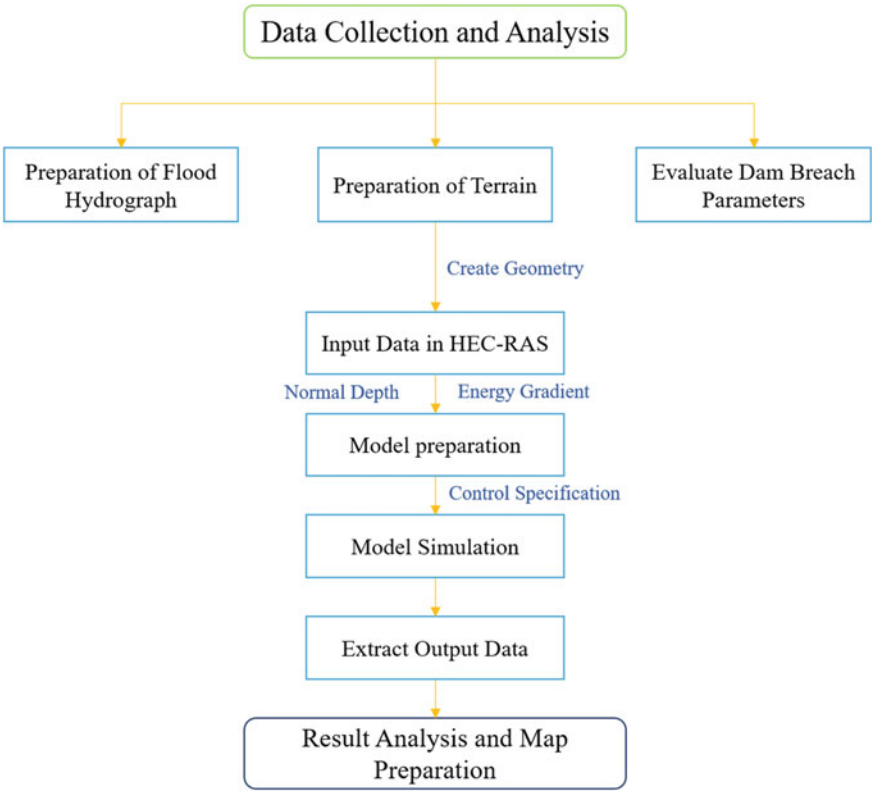

Fig. 2 Methodology flow chart

- The normal depth of the river downstream of Damanganga reservoir.
- Digital elevation model (DEM)—Terrain of the study area.

4.1 Flood Hydrograph

Flood hydrographs are displays that how a basin responds to a period of precipitation. The flood data from the dam, which affects the study area, was obtained from the Flood Cell Department of Madhuban Dam, under the Government of Gujarat for the year 2004 event as shown in Fig. 3.

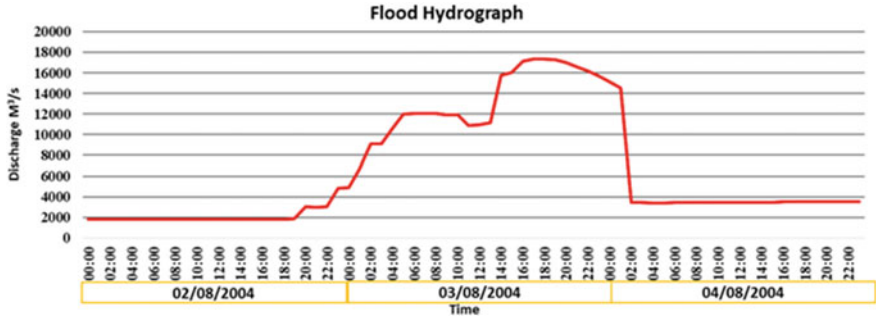

Fig. 3 Flood hydrograph of Madhuban dam of high flood event 2004

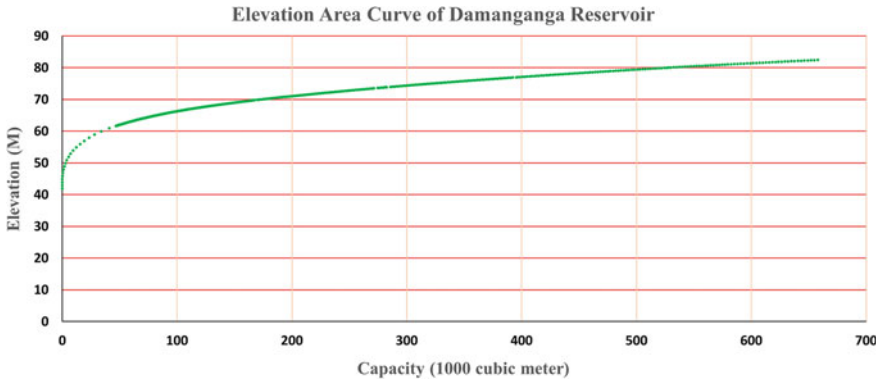

Fig. 4 Elevation capacity curve of Madhuban dam

4.2 Area Capacity Curve

Area capacity curves are generally used for reservoir flood routing, determination surface area of the water, and volume corresponding to each elevation, classification of a reservoir, and distribution of sediments in the reservoir. Elevation capacity curve of Madhuban dam was collected from Damanganga Div. project 1 office which is shown in Fig. 4.

4.3 Estimation of Dam Breach Parameters

It has been shown that the selection of dam breach parameters for dam breach modeling contains the extreme uncertainty of all phases of dam failure modeling and therefore it is necessary to evaluate carefully of dam breach parameters for better understanding and simulating the model.

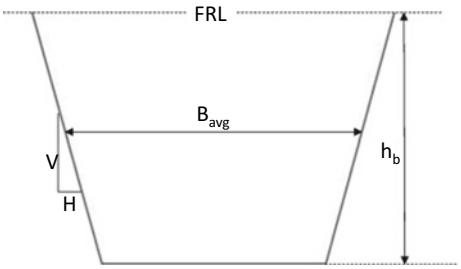

Fig. 5 Cross-section view of breach

There are several methods available for estimating dam breach parameters for use in dam breach simulation. In this study, we have used the Froehlich equation to estimate dam breach parameters which is recommended by Dam Rehabilitation and Improvement Project (DRIP). The Froehlich equation for estimation of Earthen dam breach parameters is [15] (Fig. 5):

$$B_{\text{avg}} = 0.23 \times K_{\text{m}} \times V_{\text{w}}{}^{\frac{1}{3}} \tag{1}$$

where B_{avg} = expected value of average width in meter,

$K_{\text{m}} = 1.0$, for internal erosion failure,

1.5, for failure by overtopping,

$M = 0.6$ for internal erosion failure, and

1.0, for overtopping failure,

where M = expected average breach side-slope ratio.

$$T_{\text{f}} = 60 \times \frac{V_{\text{w}}}{g H_{\text{b}}{}^2}{}^{\frac{1}{2}} \tag{2}$$

where, T_{f} = breach formation time in seconds,

V_{w} = volume of water above breach bottom in M^3, and

H_{b} = height of breach in meters.

4.4 Preparation of Terrain

Terrain preparation for the study area is done by the RAS mapper tool using the digital elevation model as input in the model. The projection of terrain is UTM Zone

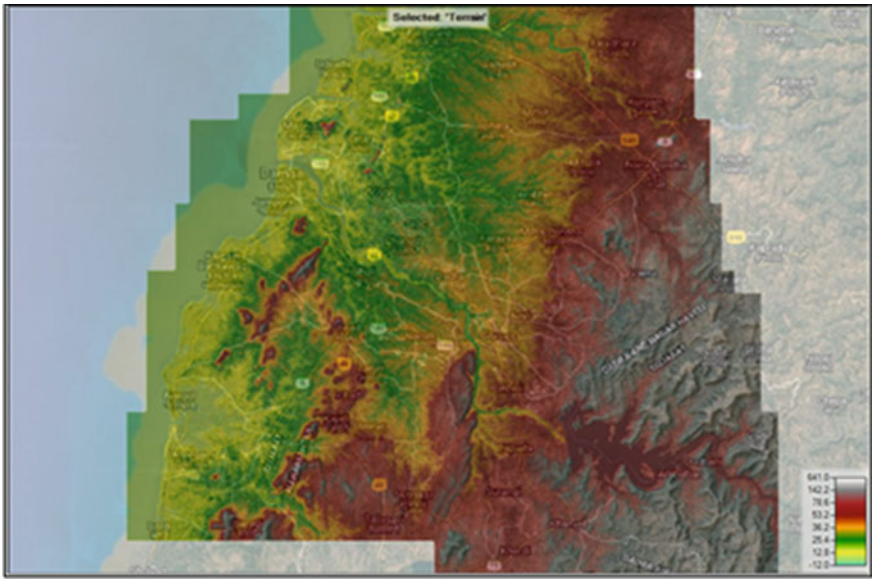

Fig. 6 Terrain of downstream of Madhuban dam

43N as per the study area. Prepared spatial referenced projected terrain is shown in the following Fig. 6.

5 Results and Discussions

HEC-RAS dam breach under unsteady flow condition is performed to simulate the events. The breach parameters are as (1) Breach bottom width is 250 m, (2) Side slope is 1:1 (H: V), and (3) Breach development time is 3.78 h.

After simulation, the dam breach model under unsteady process, flood depth, arrival time, water surface elevation, inundation area, and velocity of flood is extracted. Nearly 238 Km^2 area are under inundation in overtopping flooding condition. This is very useful information for dam wner to prepare an emergency action plan for Damanganga Dam project and reduce the life threating catastrophic event.

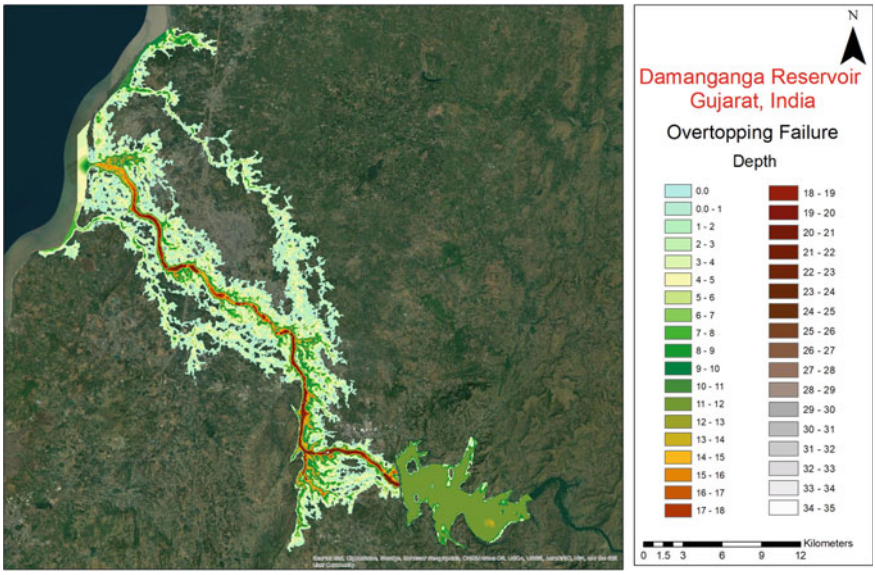

Fig. 7 Water depth map

The basic prepared maps are described as follows:

Depth map: Depth map represents the water depth from ground surface. The Silvassa, Vapi industrial area, northern part of Daman, and low lying area near River is highly vulnerable area due to dense residential and urbanization (Fig. 7).

Water surface elevation: Water surface elevation map indicates the height of the water from mean sea level which is useful to get the RL of water at a particular location (Fig. 8).

Inundation boundary: This map shows that the area of inundation during dam breach condition which is useful for evacuation team (Fig. 9).

Arrival time: Arrival time (hours) signified when the water depth reaches a specified inundation depth. This map is used to find out where to start evacuation of people, so we reduce the loss of life (Fig. 10).

6 Conclusions

Dam break for large dam is the sate-of-the art for flood risk assessment and management using hydrodynamic modeling. Present case of Damanganga reservoir project has a paradigm case analysis for dam break analysis of large dam in Gujarat. The flood depth, water surface elevation, arrival time, and inundation maps are extremely useful

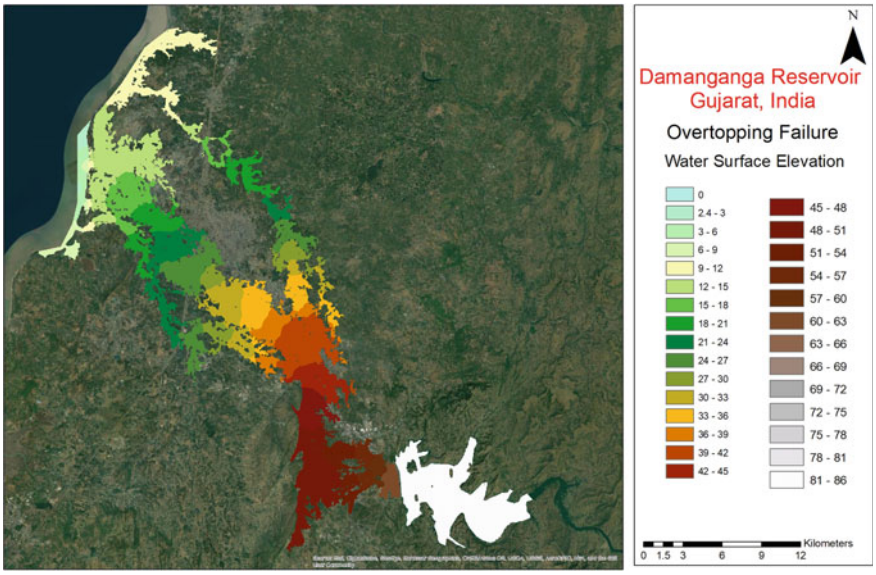

Fig. 8 Water surface elevation map

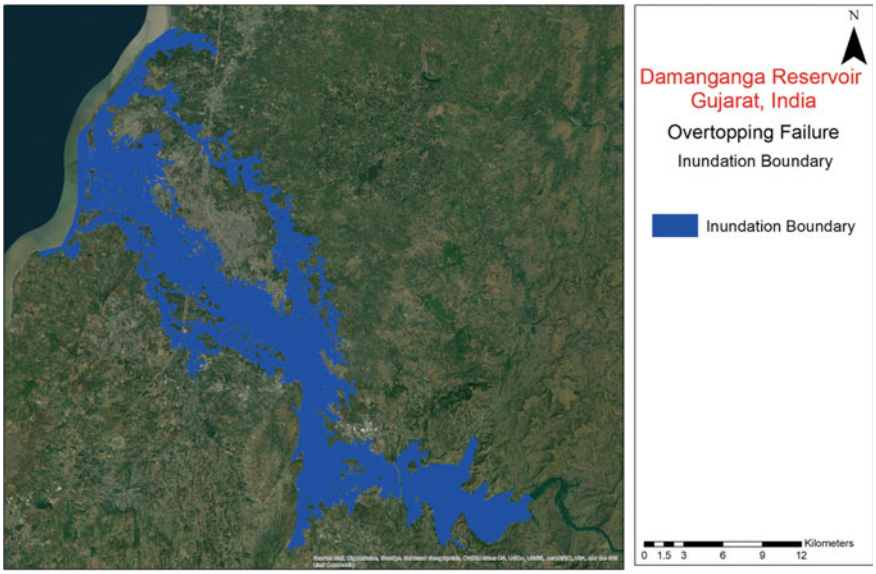

Fig. 9 Inundation boundary map

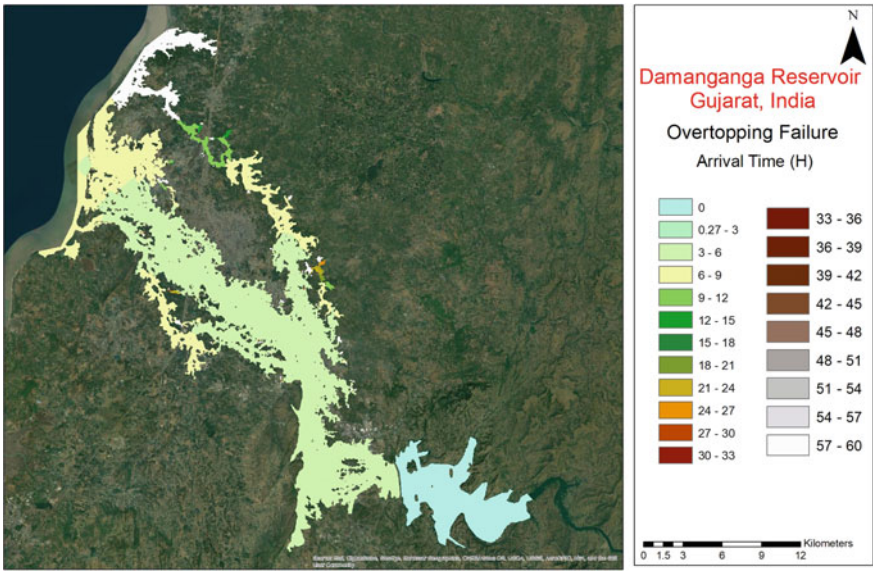

Fig. 10 Arrival time map

to the dam owner to prepare an "emergency action plan" under extreme flooding condition. The result outcomes show that 238 km^2 are under flooded in overtopping flooding condition This is very useful information to dam owner to warn and evacuate the people under any unfavorable condition and reduce the loss of life and properties.

Acknowledgements Author(s) would like to thank Damanganga Project Division No-1, Narmada Water Resources Water Supply and Kalpsar department, GoG, and also would like to thank Survey of India (SOI) to have provided a necessary data support to execute the work. Author(s) would also like to thank Dr. R. P. Singh Scientist-G, Space Applications Center-ISRO, Ahmedabad for supporting technical enhancement to improve the quality of the research work.

References

1. Costa JE (1985) Floods from dam failures. US Geol Surv. https://doi.org/10.3133/OFR85560
2. Wahl TL (1997) Prediction of embankment dam breach parameters. Proc Congr Assoc Hydraul Res 48–53
3. Xiong YF (2011) A dam break analysis using HEC-RAS. J Water Resour Prot 2011:370–379. https://doi.org/10.4236/JWARP.2011.36047
4. Kumar S, Jaswal A, Pandey A (2017) Literature review of dam break studies and inundation mapping using hydraulic models and GIS. Int Res J Eng Technol 4:55–61
5. Darji K, Patel D, Dubey AK, Gupta P, Singh R (2021) An approach of satellite and UAS based Mosaicked DEM for hydrodynamic modelling—a case of flood assessment of Dhanera City, Gujarat, India. J Geomatics 247–257

6. Patel DP, Ramirez JA, Srivastava PK, Bray M, Han D (2017) Assessment of flood inundation mapping of Surat city by coupled 1D/2D hydrodynamic modeling: a case application of the new HEC-RAS 5. Nat Hazards 89:93–130. https://doi.org/10.1007/S11069-017-2956-6
7. Fread DL (1986) Prediction of flood inundation from breached Dams Due to Earthquakes. In: Office of hydrology and national weather service
8. Bobkov SF, Boyarskii VM, Veksler AB, Shvainshtein AM (1999) Main factors when taking into account the discharge capacity of hydro developments for declaring their safety. Hydrotechnical Constr 33:193–200. https://doi.org/10.1007/BF02764506
9. Shahrim MF, Ros FC (2020) Dam break analysis of Temenggor Dam using HEC-RAS. IOP Conf Ser Earth Environ Sci 479:012041. https://doi.org/10.1088/1755-1315/479/1/012041
10. Ramola M, Nayak PC, Basappa V (2021) Dam break analysis using HEC-RAS and flood inundation modelling for Pulichinatala Dam in Andhra Pradesh, India. Indian J Ecol 48:620–626
11. Kilania S, Chahar BR (2019) A dam break analysis using HEC-RAS. World Environ Water Resour Congr 2019 Hydraul Waterw Water Distrib Syst Anal Reston, VA Am Soc Civ Eng 382–389. https://doi.org/10.1061/9780784482353.036
12. Pandya U, Patel DP, Singh SK (2021) A flood assessment of data scarce region using an open-source 2D hydrodynamic modeling and Google Earth Image: a case of Sabarmati flood, India. Arab J Geosci 14(21):1–18. https://doi.org/10.1007/S12517-021-08504-2
13. Pathan AI, Agnihotri PG, Patel D, Prieto C (2021) Identifying the efficacy of tidal waves on flood assessment study—a case of coastal urban flooding. Arab J Geosci 14(20):1–21. https://doi.org/10.1007/S12517-021-08538-6
14. Darji K, Patel D (2020) Creating the high resolution DEM for flood assessment using UAV techniques. In: ISRS-ISG national symposium–2020, p 185
15. Central Water Commission (2019) Guidelines-and-manuals | DRIP—Dam Rehabilitation and Improvement Project

A Sustainable Approach for Flood Mitigation in Kokrajhar, Assam

Sagar Basumatary, Soumen Maji, and Debshri Swargiary

Abstract Kokrajhar town is the headquarter of the Kokrajhar district as well as the headquarter of Bodoland Territorial Region (BTR) of Assam. BTR situated in the foothills of Bhutan and the northern part of the region faces common problems like flash floods, erosion, and crisis of drinking water. Many areas in Kokrajhar town submerge during the month of July–August every year. Prevention of urban flooding in Kokrajhar areas has become an important issue due to the hydrological impact on urban development. In this study, the author tried to investigate the causes behind the flood in the Kokrajhar town every year. Also, sustainable measures for flood mitigation in these areas have been chalked up. By physical survey, it is found that the existing drainage system of the Kokrajhar town is under construction and poorly maintained which led to the accumulation of stormwater or waterlogging. At present, the outfall points of the existing drains are on the Gourang River and the Tarang River through a major canal. Various hydrological factors are analyzed by ArcGIS. The stormwater drainage design works are proposed to be implemented in phases from the intermediate to future design period. A proposal for a drainage network has been made where there is no land available for constructing surface drainage. By monitoring the hydrological impact, the flow capacity of the existing drainage system is analyzed and compared with the proposed design drainage system.

Keywords Urban flooding · Flood mitigation · Kokrajhar · Drainage network · Stormwater

S. Basumatary · S. Maji (✉)
Department of Civil Engineering, Central Institute of Technology Kokrajhar, Kokrajhar, Assam 783370, India
e-mail: s.maji@cit.ac.in

S. Basumatary
e-mail: p19wre1001@cit.ac.in

D. Swargiary
Department of Civil Engineering, National Institute of Technology Jamshedpur, Jamshedpur, Jharkhand 831014, India

P. V. Timbadiya et al. (eds.), *Flood Forecasting and Hydraulic Structures*, Lecture Notes in Civil Engineering 340, https://doi.org/10.1007/978-981-99-1890-4_15

1 Introduction

The Kokrajhar district is bounded on the north by the Himalayan kingdom of Bhutan, Dhubri district on the south, Bongaigaon district on the east, and the Indian state of West Bengal on the west. Kokrajhar is situated in the foothills of Bhutan, and the northern part of the region faces common problems like flash floods, erosion, and crisis of drinking water. Prevention of urban flooding in the Kokrajhar town caused by inadequate drainage systems has become an important issue. As most of the natural ground surface areas are replaced by concrete, and a large number of building structures are constructed that resulted in the surface into impervious land, i.e., the permeability of that area is lost. Tripathi [7] stated that probable reasons for floods for a particular area are changes in catchment characteristics, population growth, climate change, etc. Goyari [3] examined the sustainability of the agricultural sector due to flood damage. He extended that soil erosion is another serious problem due to floods. This study is related to a sustainable environment and flood mitigation in Kokrajhar. The coverage of drains in the Kokrajhar town is not complete.

Thus, it is important to study the situation of the drainage system for Kokrajhar town. Systematic efficient drainage facilities are needed to protect the road and essential structures from damage. The catchment of the Brahmaputra River and the Bhutan River Swrmanga is characterized by very steep hill slopes with coarse soil texture and unstable landmass. This causes high instantaneous runoff and heavy siltation in the tributaries as well as in the channels of the main river. Almost every year, the district gets inundated by floods during monsoon season. The frequent flood affects the groundwater regime of the town with waterlogging problems.

2 Study Area

Kokrajhar district is located on the north bank of the river Brahmaputra. The district lies between 89.46′ E to 90.38′ E longitudes and 26.19″ N to 26.54″ N latitudes. Kokrajhar is an administrative district in the Bodoland Territorial Region of Assam. The average annual rainfall of the district is 1715.7 mm. The Kokrajhar town is bounded by two small rivers, the Gourang River and the Tarang River (Fig. 1).

3 Methodology

Hydrologic and hydraulic analyzes are two major aspects of an efficient drainage design to mitigate urban flooding. Physical and digital survey of whole Kokrajhar town has been conducted. AutoCAD 2016 has been used for digitizing the layout of the existing drainage system and roads (Fig. 2) of Kokrajhar town.

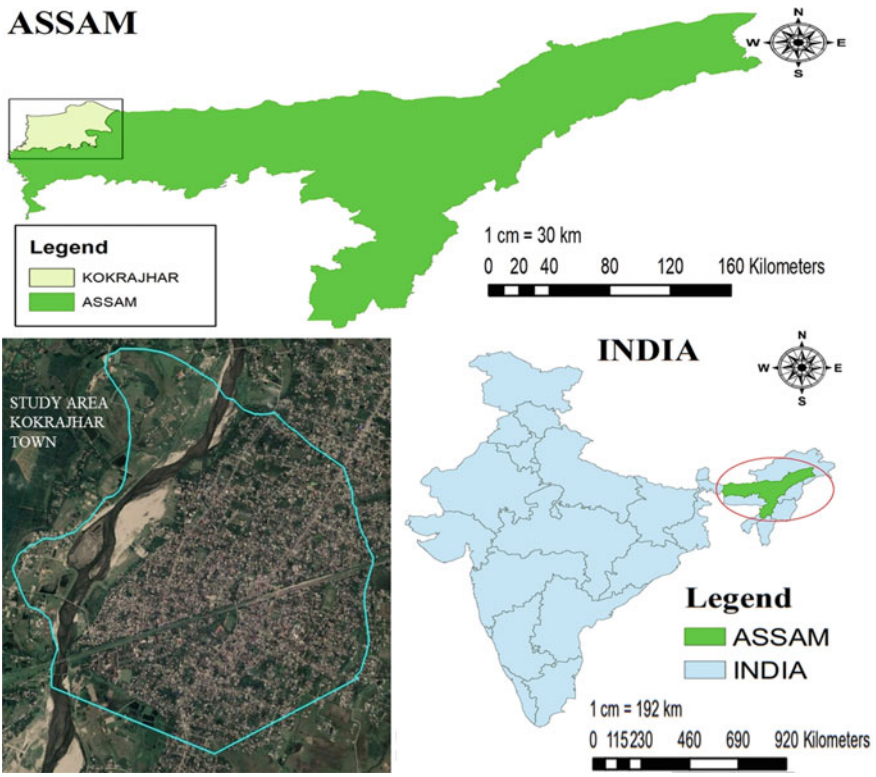

Fig. 1 Geographical location of Kokrajhar Town (*Source* Map of India and Google Earth Pro)

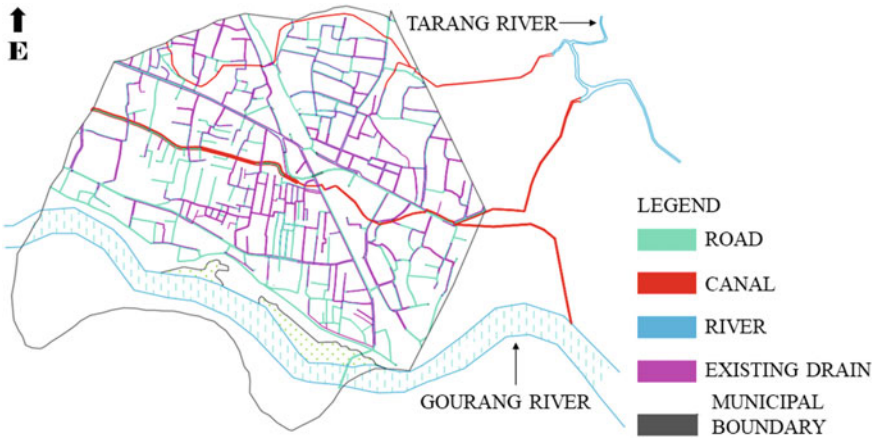

Fig. 2 Kokrajhar town map layout

3.1 Hydrologic Design

Estimates of flood magnitudes as a result of precipitation were analyzed. A common problem in design flood estimation is that different model structures will lead to different estimates of the design flood. Here, the author has tried to overcome this issue with accurate measures.

3.2 Runoff Coefficient

A total of 9 polygons has been identified. Division of study area has been conducted using google pro by ArcGIS 10.8. Catchment surface area is classified as pervious (black) and impervious (green) surface (Fig. 3) using LULC method. The runoff coefficient of each sub polygon area has been calculated.

The weighted equivalent runoff coefficient (C_e) [2] has been calculated $C_e = 0.65$ using the following formula (Eq. 1).

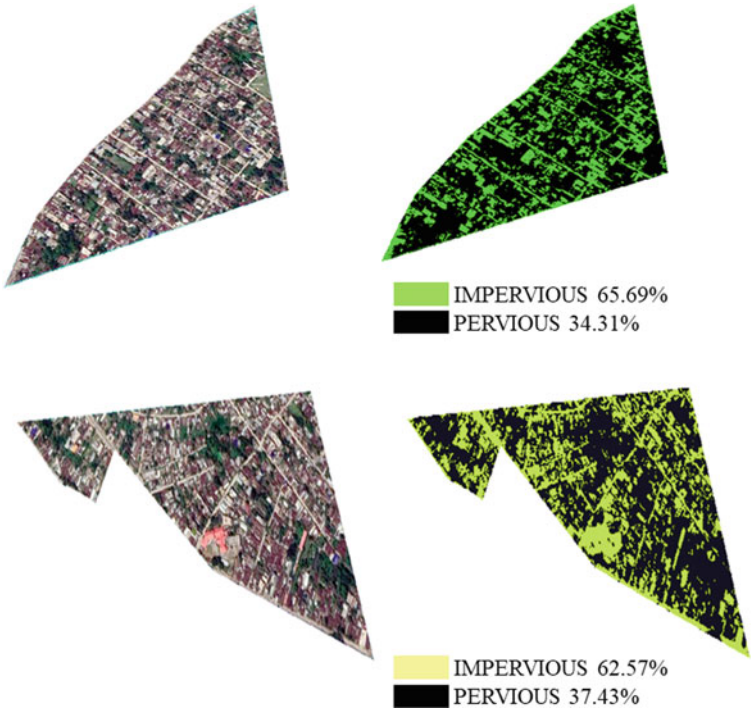

Fig. 3 Image classification on ArcGIS 10.8

$$C_e = \frac{\sum_1^N C_j A_j}{\sum_1^N A_j} \quad (1)$$

where A_j = Areal extent of the sub-area j having a runoff coefficient C_j and N = Number of sub-areas in the catchment.

3.3 Time of Concentration

Kirpich Equation [4] has been used for the calculation of the time of concentration (t_c) and found $t_c = 36.62$ min $= 0.61$ h.

3.4 Rainfall Intensity

Assuming hydrometeorological similarity of the Kokrajhar District and Guwahati, as both being on the North bank of the Brahmaputra River, Intensity–Duration–Frequency (IDF) data of Eastern Zone basin in Guwahati is adopted. For analyzing rainfall characteristics, Rambabu et al. [1] equation was used (Eq. 2).

$$i = (KT^x)/(t_c + a)^n \quad (2)$$

where i is the rainfall intensity in *mm/hr*. T is the return period in years; t_c is the time of concentration in hours; K, a, x, and n are coefficients varying with location. For 10-year return period [6], the calculated rainfall intensity was $(i) = 7.03$ mm*/hr*.

3.5 Discharge

Rational method [6] is a simple technique for estimating a discharge (Eq. 3) from a catchment area. Calculated discharge for few selected polygons has been shown in Table 1.

$$Q = (1/3.6) * C * i * A \quad (3)$$

where,

Q = Design discharge; C = Runoff coefficient; i = Rainfall intensity; A = Catchment drainage area.

Table 1 Discharge calculation (shown for selected few polygons)

Name of the area	Sub-area	C	A (Km^2)	Q (m^3/s)
Polygon 1	A	0.65	0.17	0.22
	B	0.66	0.13	0.16
	C	0.63	0.19	0.23
Polygon 5	A	0.63	0.13	0.16
	B	0.64	0.11	0.14
	C	0.67	0.15	0.20
	D	0.66	0.15	0.20
Polygon 7	A	0.66	0.09	0.12
	B	0.66	0.13	0.17
	C	0.63	0.10	0.13
Polygon 9	A	0.64	0.17	0.21
	B	0.64	0.19	0.23
	C	0.64	0.16	0.20
	D	0.67	0.17	0.22

3.6 Hydraulic Design

Drainage channel geometry and design discharge to carry the runoff of the stormwater are analyzed in this section. The hydraulic parameters required in designing the channels under different flow conditions are estimated by using Manning's formula (Eq. 4) and hydraulically efficient channel section as per the Central Public Health and Environmental Engineering Organization (CPHEEO) manual, Government of India [2]. Design discharge of channel [5] has been calculated by using Eq. 4.

$$Q = (1/n) \times \left(A^{5/3}/P^{2/3}\right) \times S^{1/2} \tag{4}$$

where, Q = Discharge in m^3/s; n = Manning's roughness coefficient; S = Bed gradient of the channel; A = Area of flow cross-section in m^2; P = Wetted Perimeter.

4 Results and Discussion

During surveying the Kokrajhar town, various results related to flood occurrence in Kokrajhar town were noted. The drainage network system of Kokrajhar town is under construction. From Table 1, it is observed that the discharge received from the precipitation is quite more than the conveyance capacity of the existing drainage network. Choked in drain and unrepaired drainage system are the reasons for waterlogging especially in the monsoon session. Poor maintenance of drains leads to damage to the

Fig. 4 Canal blockage and flood in Kokrajhar town

drainage network creating difficulties in the passage of surplus drain water further (Fig. 4). The floods are occurred due to poor drainage and improper solid waste disposal too. A proposed stormwater drainage network (Fig. 5) for the Kokrajhar town in the uncovered drainage area for major flood control has been given.

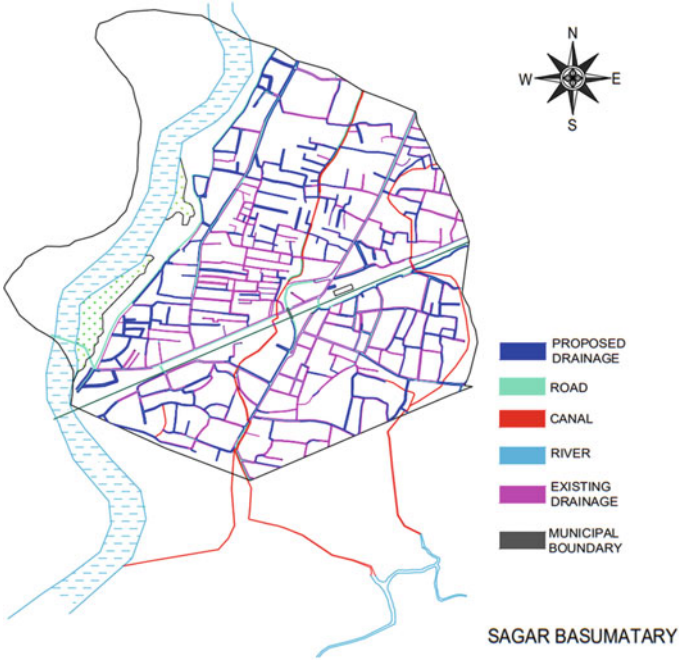

Fig. 5 Proposed drainage network for flood mitigation

5 Conclusion

In this study, probable reasons for flash floods in Kokrajhar especially in every monsoon season was investigated thoroughly. In addition, sustainable environment and drainage system network area in the Kokrajhar town have been studied. Many discontinue drainage networks are observed. Deficiencies in the existing system and lack of disposal arrangement need prompt attention need for upgrading the existing drainage system.

Identification of flood-prone areas, designing, and implementing flood mitigation strategies are required. Hence, a proper drainage system in uncovered areas was suggested to mitigate the adverse effect of flash floods. The following salient points are must indispensable to mention for the flood mitigation:

- Proper solid waste management should be provided by the municipality of Kokrajhar.
- Where there is no land availability to construct a surface drainage, an underground circular RCC Hume pipe drainage is considered with respect to the width of the road.
- Branch drains and major drains are required regular cleaning and maintenance.
- Need to stop the encroachment of the drainage area by illegal constructions.
- De-silting of the existing drainage system should be carried out frequently.
- Under the base line scenario recourse of existing drains to re-design, engineering judgment, etc., would be made for sustainable flood mitigation.
- People's awareness also plays a key role in making the drainage system efficient.

References

1. Babu R, Tejwani KG, Agarwal MC, Bhushan LS (1979) Rainfall-intensity duration return period equations and nomographs of India
2. Central Public Health and Environmental Engineering Organisation (CPHEEO) manual, Government of India (2019) Manual on storm water drainage systems, vol 1
3. Goyari P (2005) Flood damages and sustainability of agriculture in Assam. Econ Polit Wkly, 2723–2729
4. Kirpich ZP (1940) Time of concentration of small agricultural watersheds. J Civ Eng 10(6):362
5. Subramanya K (2009) Flow in open channels. Tata McGraw-Hill Education
6. Subramanya K (2013) Engineering hydrology, 4e. Tata McGraw-Hill Education
7. Tripathi P (2015) Flood disaster in India: an analysis of trend and preparedness. Interdisc J Contemp Res 2(4):91–98

Existence of Swamps and Detention Tanks for Preventing Urban Flood—A Case Study

Ankita Bohidar, Anil Kumar Kar, and Pradip Kumar Das

Abstract The change in land use is going in a faster way in order to accommodate the changes in lifestyle and other socio-economic and infrastructural developments. Rural areas are getting converted to urban areas. The agricultural, barren and other non-productive lands are now used for residential purposes. The basic morphology of land use of an area is under a rapid change. The basic conversion output is a land which was earlier a permeable/semi-permeable area now converted to impermeable or negligibly permeable. Also there is a drastic change in rainfall pattern. The occurrence of short duration and peaky rainfalls is more. These intense rainfalls are the root cause of urban flooding as very less scope of permeability in land is there in urban areas. Few years ago, cities were there with ample scope of drainage of rainwater. But the behavior of same city is different at present era with lot of water logging on the residential and industrial areas. The swamps in the older cities were the places to accommodate the surplus rainwater of the city. These are natural depressions, obviously these also behave naturally. But due to large developments, we are filling these lands in order to be utilized for residential purposes. With the present developments and higher runoff coefficients, the runoff generation is more in an urban area. In order to avoid a probable water logging scenario and to develop a sustainable preventative solution, detention tanks are to be placed for efficient drainage management as well as ground water recharging. The study relates to temporal changes in land use of Bhubaneswar city in connection to the rainfall and corresponding water logging problem in conformity to the temporal variation in temporal land use and land cover.

Keywords Land use · Water logging · Intense rainfalls · Urban drainage · Swamp · Detention tank

A. Bohidar (✉) · A. K. Kar · P. K. Das
Department of Civil Engineering, VSSUT, Burla, Sambalpur 768018, India
e-mail: ankita_bohidar@rediffmail.com

P. K. Das
NIT Rourkela, Rourkela 769001, India

P. V. Timbadiya et al. (eds.), *Flood Forecasting and Hydraulic Structures*, Lecture Notes in Civil Engineering 340, https://doi.org/10.1007/978-981-99-1890-4_16

1 Introduction

The urban population has increased in many folds due to abundance availability of civic amenities, employability, and many more other factors. The migration of people from rural to urban is also a major concern. The per unit of land utilization has increased in urban area as the activities are increased there. So in accommodating these changes, all the cities are not so prepared. The advantages of city life are added with woes related to urban flooding. Urban flooding is a sensitive issue now. The reasons could be many like heavy rain with short duration, improper drainage or absence of water bodies, improper drain construction, poor maintenance and operation of drainage system and water bodies, storage of water in the detention pond and swamps, manmade causes like dumping garbage in open drain, and improper disposal of solid waste.

The peak discharge of this urban flood depends on the intensity and duration of rainfall, the topography and geology of the catchment, its vegetation, and the hydrologic conditions before occurrence of any storm event. Land use and other human activities equally contribute to the peak discharge of these floods.

A number of cities of India and abroad are now facing the urban flood problem. According to State Housing and Urban Development Department and World Bank, about 59% of Bhubaneswar is vulnerable to extreme to moderate urban flood risk. To avoid such disaster, several infrastructural improvements are required. The drainage improvements are very common solutions to it. Besides that retention or detention of urban flood volume in order to minimize the urban flood disasters is also a good attempt. In recent past, also we have seen the role of existing water bodies, where a huge amount of water is being retained. These water bodies are very diversified into different forms from lakes and ponds to swamps/marshes and lagoons as well as mangroves, backwaters, etc., which play an important role in maintaining water balance, avoiding flood, supporting biodiversity and thereby provide food security and livelihoods.

These wetlands/water bodies are gradually getting converted into landed properties or simply used as a dumping ground for sewage and garbage and are receivers of toxic waste. Few observations regarding this are noted subsequently. Delhi Parks and Gardens Society (DPGS) provide data stating over 1000 water bodies in the Capital City of Delhi. However, it was observed that from year 1999 to 2002, around 30% area are untraceable and area 7% reduction in area covered by water bodies. The possession and maintenance of water lie with numerous agencies. With increased awareness about the importance of rejuvenating water bodies to enhance water security in past few years, an initiative has begun in the Capital to revive 201 water bodies [1].

With sustainable drainage, there is more infiltration of rainwater into the soil by slowing the runoff and thus lessen the amount of water in open drains and rivers during heavy rains [2] and help to recover storm water retention capacity. These drainage techniques are more sustainable in long term, to remove the drawbacks caused by urbanization [3]. Dierkes et al. [3] have worked on change of peak flow by

using surface sealing. As compared to traditional drainage techniques, sustainable drainage techniques help to get rid of the rainwater and offer multiple uses playing multiple functions, like implementing rain gardens for improving and beautifying the local surrounding, riverine parks to protect river banks and provide recreational environments [4].

Sustainable drainage helps to create natural condition for the water passage and flood mitigation by using measures like retention/detention ponds. Retention/detention ponds are better sustainable drainage techniques which are effective means of flood control [2]. The design of retention basin within a watershed considering sizing of the network along with its location is cost saving than the traditional methods [5].

Retention and detention ponds improve the water quality, which help with the removal of suspended solids by sedimentation technique, reducing the velocity of water, and thereby retaining a proportion of total suspended solid and other pollutants [6]. Schueler and Helfrich [7] developed an efficient way for removal of suspended solids, by looking into many aspects of detention pond performances. With the use of diverse aquatic plants in the retention/detention, basin removal of pollutants can be improved [4].

According to *Urban Storm Drainage Criteria Manual: Volume 2* [8], detention ponds are storage structures that manage stormwater quantity by reducing peak flows during flood events. The outlet of a detention basin is leveled with the bottom of the basin (having a metal or concrete piece called a riser) so as to finally drain out the water and empty the pond between two storms, whereas retention basins have an outlet or a weir at a upper point so that it retains a permanent level of water [9].

Unregulated urbanization, encroachment of lands, and unplanned construction are the main reasons for urban flooding which are seen in many urban areas in a state. Demarcation of flood zones is required to be done as recommended by researchers [10]. Sreeja et al. [11] developed a cost effective solution by implementing a control strategy for the existing structures at different locations in the drainage network (i.e., by constructing a detention tank in the drainage system for storing excess water during high intensity rainfall and subsequently releasing it to the downstream drainage channel using a flow control mechanism, to optimize the capacity of the drainage system).

According to the observations taken by researchers, the key things create runoff like the changes in land use pattern, surface sealing due to urbanization, occupation of flood plains and obstruction of flood flows, urban heat island effect due to which there is increase in rainfall in and around urban areas, sudden release of water from dams located upstream, and the failure to release water from dams resulting in backwater effect should be taken into consideration. He also suggest construction of storage ponds (like detention ponds) at judiciously selected sites to store water during heavy rainfall and prevent downstream flooding and once the rain stops water can be released.

2 Study Area

The Bhubaneswar City (20.2961° N, 85.8245° E) is the capital city of Odisha (Fig. 1). It is a fast growing city with an area of 422 km^2 and population about 952,587 (Provisional Census 2011; CDP estimates 2011). The climate here is tropical, and the temperature generally varies from 12 °C to 43 °C. Annual rainfall is about 1500 mm. City lies in the eastern coastal plains with an average altitude of 45 m (148 ft) above sea level. The city is bounded by the rivers Daya to the south and the Kuakhai to the east.

2.1 Demography of the City

The population of Bhubaneswar increased to about 131% in the decade 1951–1961. The city registered highest increase in population due to the shift of the Capital of Odisha from Cuttack to Bhubaneswar during the year 1954. Path and Panda [12] reported that the population growth rate of Bhubaneswar city in the next two decades was highest and second highest in India, respectively.

2.2 Land Use and Land Cover of the City

The LULC area for Bhubaneswar is calculated in ArcGIS software in Table 1 (Fig. 2).

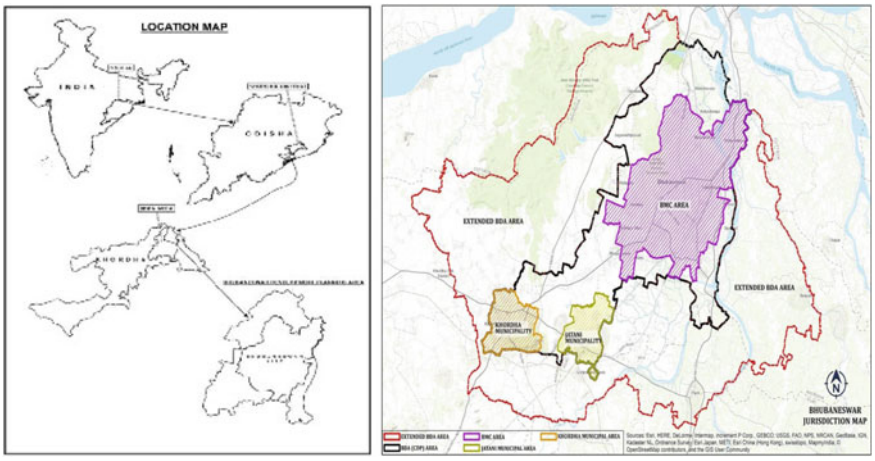

Fig. 1 Study area Bhubaneswar

Table 1 LULC area for Bhubaneswar for three decades

Year	1990	1995	2000	2005	2010	2015	2020
Water body Area (in Km^2)	37.29	33.52	29.14	28.56	25.22	23.51	17.12
Bare land (in Km^2)	18.54	21.22	21.69	25.58	25.76	33.59	42.46
Built-up area (in Km^2)	34.23	37.84	40.55	41.23	45.66	69.66	96.6
Agricultural crop land (in Km^2)	89.17	81.23	77.58	63.35	58.59	49.01	31.61
Vegetational forest land (in Km^2)	74.21	68.24	60.35	50.28	47.42	38.56	22.41

Water bodies are lifeline of major local bodies, and restoration of the same is required where development is faster. The existence of this water bodies is very essential as it can help in prevention of urban flooding or urban drainage, water logging issues, help in fisheries development, hydropower generation, and recreational space for people around local water bodies. The city has 14 major water bodies (including swamps and detention ponds). The Bhubaneswar Municipal Corporation has taken initiative for improvement and strengthening of these water bodies. Besides that constructing rain gardens at public and private places will be useful in storing the flood water.

3 Result and Discussion

The city drainage system contains 10 numbers of natural drains (Fig. 3) which flow west to east and ultimately join Kuakhai river through Gangua nalla. Few structures also act as barrier to the free flowing runoff to the disposing outlet point, i.e., Railway track, Puri-Cuttack highway, and Daya West Canal located on the east of the city. According to Jena and Lohani [13], the flow of the Gangua Nala varies from 8 m^3/s to 60 m^3/s at different locations, and the Gangua Nala receives 107.25 MLD of wastewater from domestic, industrial, and mixed sources. We can further calculate the design discharge of the entire drainage, and using ArcGIS software and DEM maps location of sites having low lying areas are determined and thereby measure like construction of storage structure which can be done to reduce the runoff, few places having water logging are also to be demarcated, and water is to be pumped out. The drains were designated as "Nalas", and 5 drainages passes through the city center covering a catchment area of 40 km^2 and the rest 5 drains covers an area of 44.18 km^2. The wastewater discharged from various drains and the pollution load carried by them is the primary source of pollution for the two rivers Daya and Kuakhai.

The DEM map of Bhubaneswar (Fig. 4) is collected from Bhuvan site. The LULC maps of different year like 2000, 2010, and 2020 are downloaded. Comparative features for water bodies are derived.

To know the spread area of Water bodies in the city of Bhubaneswar, we have generate the normalize difference water index (NDWI) map of Bhubaneswar using

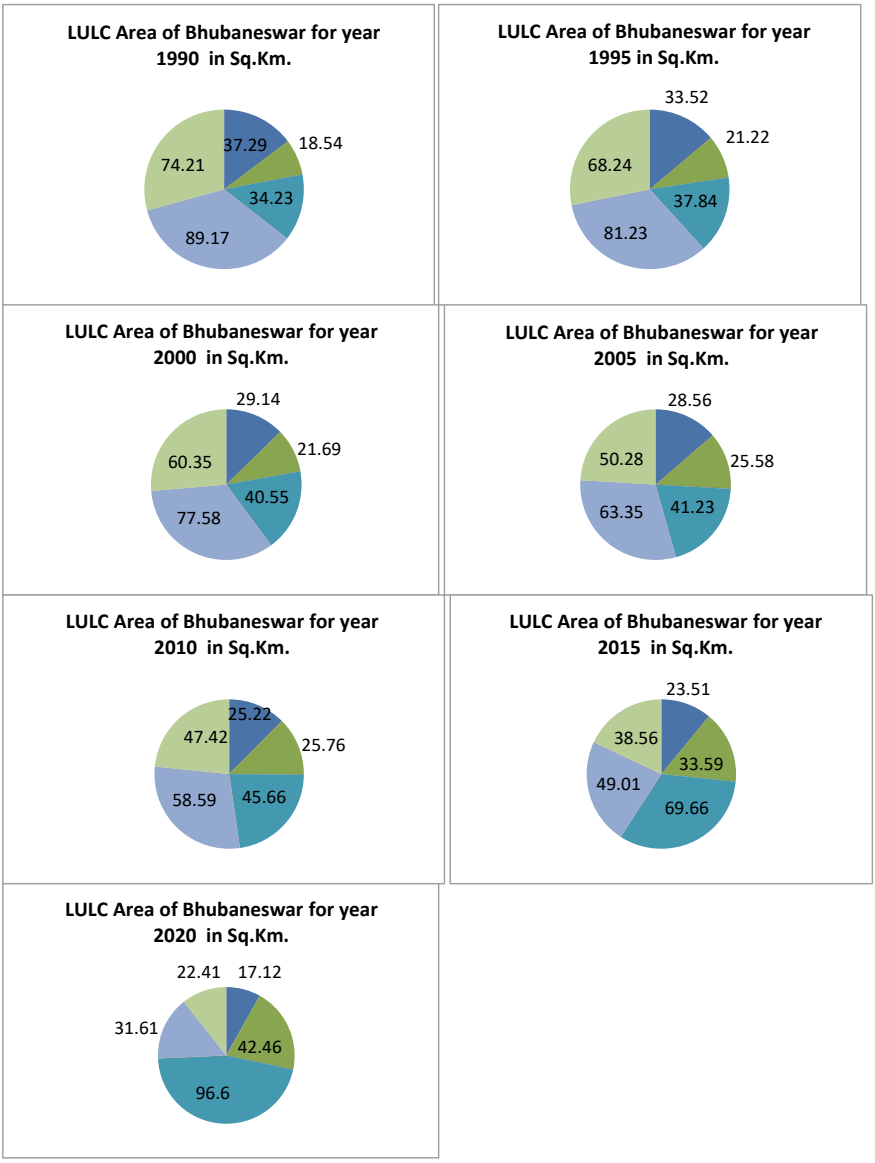

Fig. 2 LULC of Bhubaneswar for last three decades with decrease in area of water bodies shown in blue color

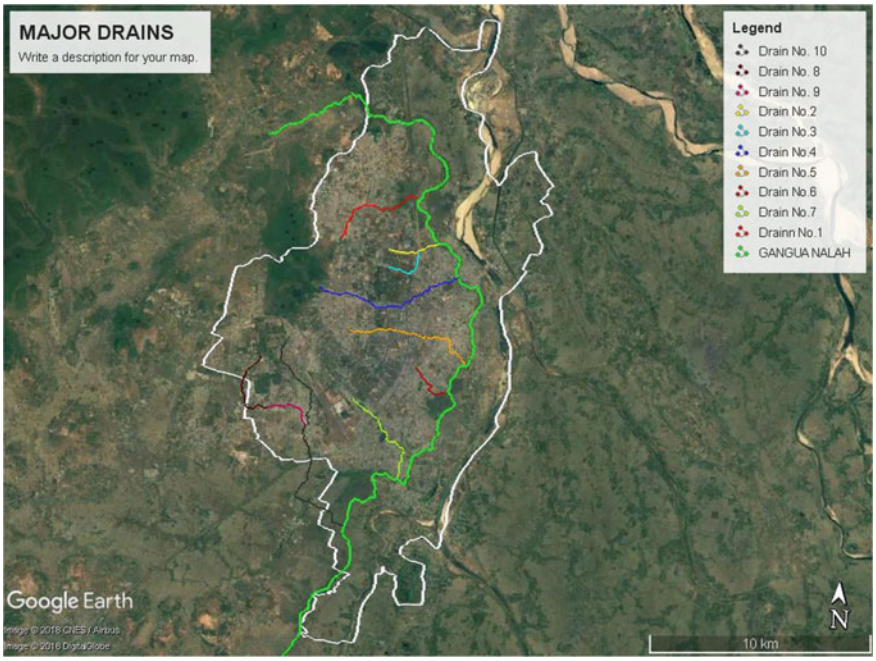

Fig. 3 Natural drains of Bhubaneswar

the satellite data Landsat 4.5, Landsat 7, and Landsat 8 and the shape file of the city was downloaded from USGS and then put as input in ArcGIS (Fig. 5).

It was found that the area of water bodies for three decades as 29.14 km^2 for the year 2000, 25.22 km^2 for year 2010, and 17.12 km^2 for the year 2020. So it is clearly understood that the water bodies are reducing day by day over the years leading to increase in the risk of urban flooding.

It is also possible to construct new water bodies or possible places for detention of water, depressed land, and low and elevated areas by investigating from DEM identifying low lying areas. These low lying areas should be with lesser evacuation as well land acquisition problem.

With data like peak discharge of Bhubaneswar city and the area of water bodies in present scenario, and from the DEM of Bhubaneswar, we can determine major depression zone where area can be calculated from the ArcGIS software and to get the possible space for construction of a detention pond. As a result, when rainfall occurs, a part of storm water can be collected or captured in the detention pond, and hence, the runoff volume generated will be less than the expected. Further, this approach can also increase the scope for ground water recharge. The peak discharge can be calculated by using rational formula taking a reasonable catchment coefficient as well as runoff volume can be calculated by taking the information of LULC as well as the rainfall values. Thus, a flood management can be made by improving the existing water bodies as well as the existing swamp area and water bodies.

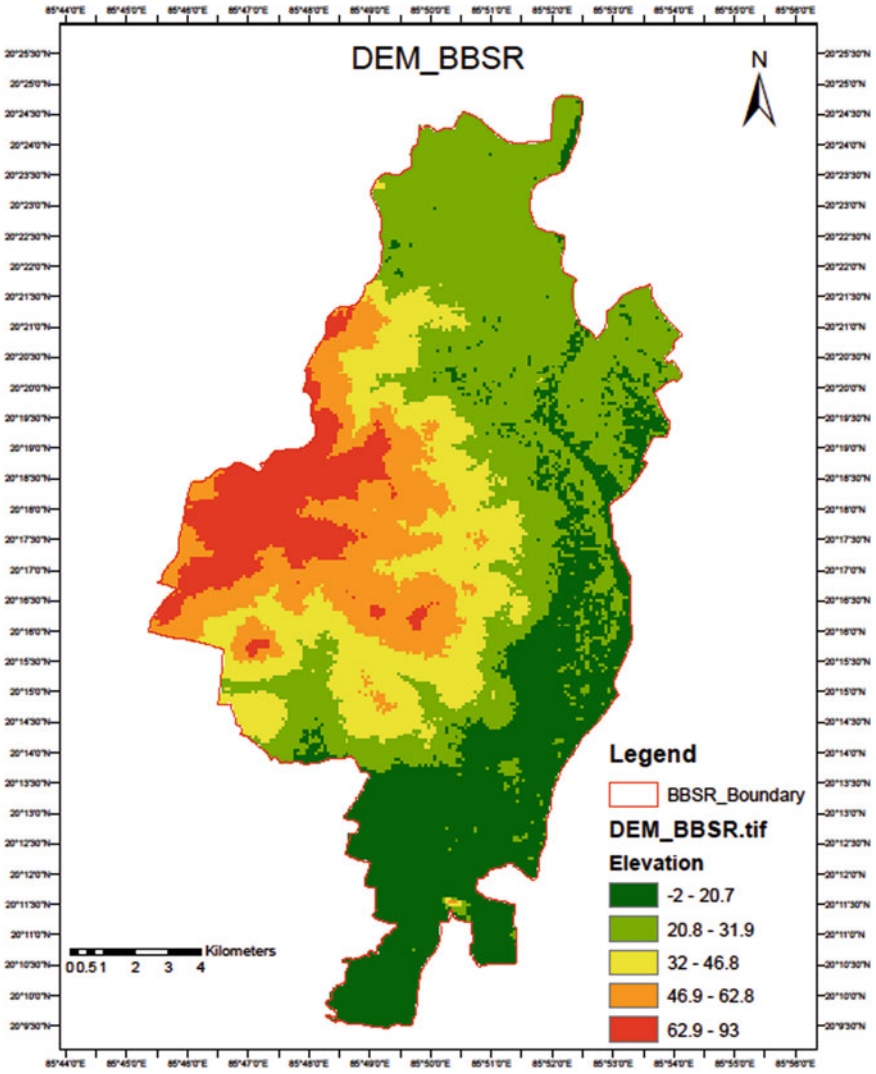

Fig. 4 DEM of Bhubaneswar (*Source* https://earthexplorer.usgs.gov/2017 with resolution 30 m)

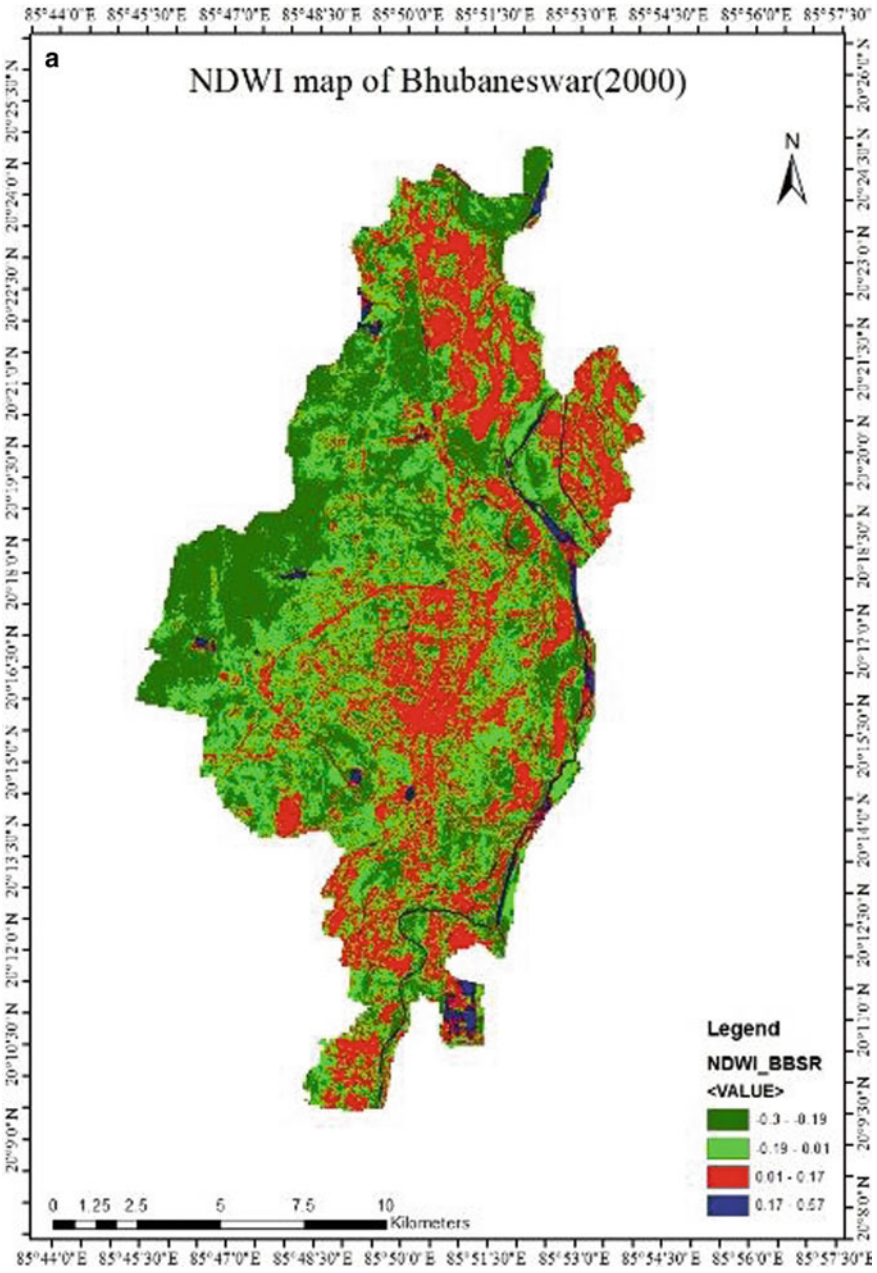

Fig. 5 NDWI maps of Bhubaneswar for the year **a** 2000, **b** 2010, **c** 2020

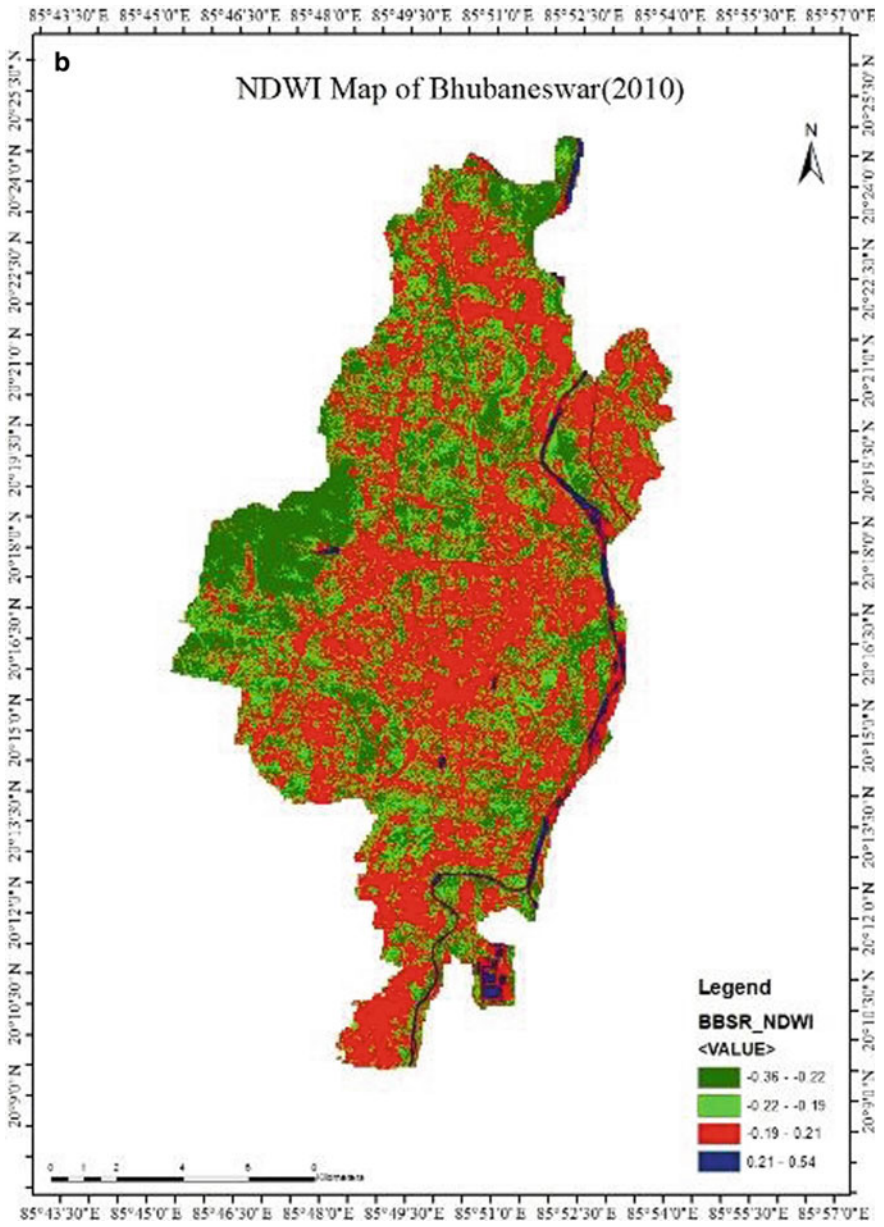

Fig. 5 (continued)

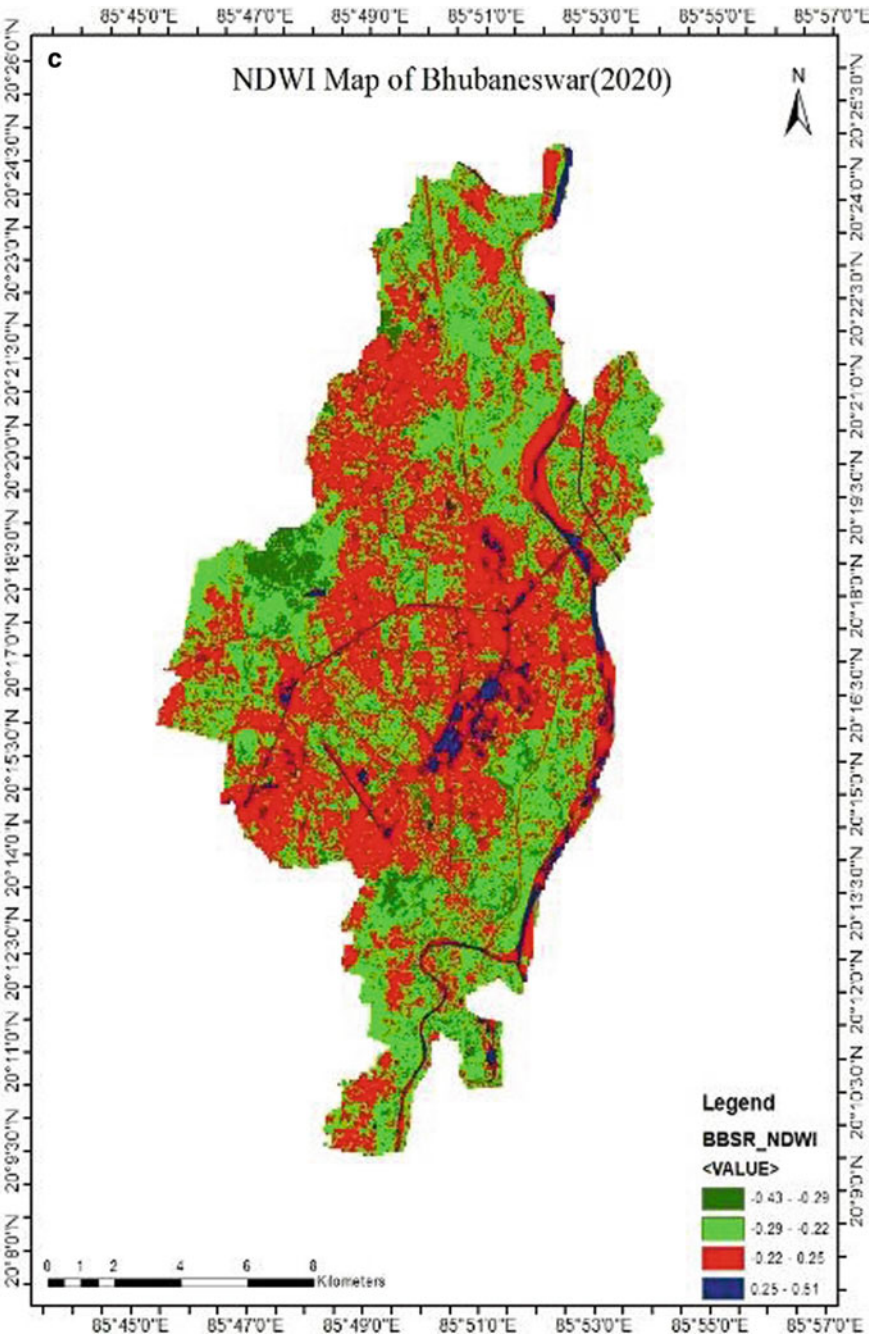

Fig. 5 (continued)

4 Conclusion

Considering the intense rainfall and the changing LULC scenario few important steps may be taken to mitigate the urban flood scenario of the city.

(1) Drains should be properly designed corresponding to the desired return period.
(2) The existing drains to be renovated and wherever necessary its capacity to be increased.
(3) The outfalls of drains to stream and nallahs also to be revisited for early and smooth release of rainwater.
(4) Provision of rainwater harvesting should be initiated from every household.
(5) The swamps and other water bodies need to be renovated to run at their full capacity.
(6) The provision for new water bodies should be made which will be working as a detention tank as well as flood moderator and improving the scope for ground water recharge.

Acknowledgements The authors are grateful to the Bhubaneswar Municipal Corporation and ORSAC, Bhubaneswar for providing data and also grateful to USGS Website for providing satellite images for this study.

References

1. Orissa diaries https://orissadiary.com/odisha-bmc-gears-renovate-14-major-water-bodies-across-city/-15th, May 2017
2. Holman-Dodds JK, Bradley AA, Potter KW (2003) Evaluation of hydrologic benefits of infiltration based urban storm water management. J Am Water Resour Assoc 39(1):205–215
3. Dierkes C, Göbel P, Benze W, Wells J (2000) Next generation water sensitive stormwater management techniques. In: Proceedings of the second national conference on water sensitive urban design
4. Miguez MG, Veról AP, Carneiro PRF (2012) Sustainable drainage systems: an integrated approach, combining hydraulic engineering design, urban land control and river revitalisation aspects. In: Javaid MS (ed) Drainage systems. InTech, Rijeka, Croatia, pp 21–54
5. Travis QB, Mays LW (2008) Optimizing retention basin networks. J Water Resour Plan Manag 134(5):432–439
6. Birch GF, Matthai C, Fazeli MS (2006) Efficiency of a retention/detention basin to remove contaminants from urban stormwater. Urban Water J 3(2):69–77
7. Schueler TR, Helfrich M (1988) Design of extended detention wet pond systems. In: Design of urban runoff quality controls: proceedings of an engineering foundation conference on current practice and design criteria for urban quality control, Potosi, Missouri. ASCE, New York, USA, pp 180–200
8. Urban Storm Drainage Criteria Manual: vol 2 (2016); UDFCD
9. Walker C (2011) Approaches to water sensitive. Urban Des. https://doi.org/10.1016/B978-0-12-812843-5.00013-7
10. Deccan chronicle. https://www.deccanchronicle.com/nation/in-other-news/270721/urban-floods-could-be-prevented-experts.html, 27 July 2021

11. Sreeja P, Gupta K, Mark O (2005) Dynamic modeling of detention tank for flood control in urban drainage system in developing countries. In: Proceedings of 10th international conference on urban drainage, Copenhagen/Denmark, August 2005, pp 21–26
12. Path AC, Panda GK (2012) Modeling urban growth in Indian situation—a case study of Bhubaneswar city. Int J Sci Eng Res (research paper published by IJSER journal). ISSN 2229-5518
13. Jena SK, Lohani TK (2014) Integrated study and quality analysis of surface drainage and sewer water for Bhubaneswar Municipal Corporation, India. Int J Eng Tech Res (IJETR) 2(10). ISSN: 2321-0869

Review on Resilient Spatial Planning Strategies to Reduce Urban Flood Risks

D. G. Patil and S. S. Kashid

Abstract Urban flooding is becoming a global problem due to changes in rainfall distribution patterns and inadequate infrastructure planning. We see many cities are getting flooded every year worldwide, including Pune, Chennai, Mumbai and Kolhapur in India. We carried out a review of research by different researchers with respect to land use–land cover change detection, the impact of urban sprawl in intensifying the flood hazard of the city, rainfall-runoff modeling using different software, effective storm water drainage management and urban planning legislation to control urban floods. We found that significantly less research is carried out to explore how urban planning is linked to urban flooding. Many times, urban flooding is considered as a result of excess rainfall only and effects of urban developments in the watershed are not considered. The traditional flood control measures will include regular corrective actions of local characters based on analysis done after each flooding. New urbanized areas will generate more runoff, and huge funds will be required to improve the working of structures and proper drainage. Still, it will not stop floods completely worldwide. There is a need for metropolitan region development authority at the early stage of city growth to coordinate effectively between different departments and urban local bodies. Hydrological studies of basins need to be carried out while planning for cities through development plan preparation and expansion of city limits considering growth pattern, increase in paved surface area and ultimately its relationship with runoff. Accordingly, stream sizes and networks can be planned for new urbanized scenarios and hydrological conditions. Different reservations should be proposed for urban facilities considering elevations, contours and flood modeling studies. We conclude that improved urban planning practices and newly updated legislations for urban development can control the endemic flooding problem in many cities in future.

Keywords Urban flooding · Rainfall · Urban development and planning · Urbanization · Hydrology · Storm water drainage management

D. G. Patil (✉) · S. S. Kashid
Department of Civil Engineering, Walchand Institute of Technology, Solapur 413006, India
e-mail: dilip.patil@vpkbiet.org

P. V. Timbadiya et al. (eds.), *Flood Forecasting and Hydraulic Structures*, Lecture Notes in Civil Engineering 340, https://doi.org/10.1007/978-981-99-1890-4_17

1 Introduction

Due to growing urbanization, the hydrological processes in a catchment are severely affected, which results in a deteriorating water environment. The natural water balance is disrupted by an increase in impermeable areas. Decreased infiltration raises flood levels even during short-duration, low-intensity rainstorms and leads to higher peak floods. Floods have the potential to greatly increase the costs of mitigation efforts due to the devastation they cause. Urban growth may increase the risk of future flooding due to modifications in local hydrological conditions, an increase in flood exposure as a result of rising population and development of infrastructure in flood-prone areas. As a result, hydrological effects of urbanization should be considered in urban design. We must also consider the impact of the basin's hydrological parameters when making urban development plans, and this can be done by making predictions about future urbanization. The study's findings will aid in the development of policy directives and intervention tactics.

Flooding is a major natural hazard in urban areas, resulting in human casualties as well as material losses. Fluvial flooding occurs when the riverbanks are overtopped by water, whereas pluvial flooding happens when severe rainfall overwhelms the drainage capacity of a small area and causes the river to overflow.

Floods are associated with heavy precipitation. In developing countries, as there is haphazard development which results in flooding during the small intensity of rainfall [1, 2]. People migrate to urban areas in search of job opportunities, construct houses in stream basins, and with urbanization, the frictional resistance to flow of water is reduced which results in more runoff [3, 4]. Also, with changes in climate and a rise in temperature, the intensity of rainfall is increased [5]. Flood inundation mapping and demarcating risk zones will help in flood management policymaking [6]. So, we need to understand the role of urban sprawl and rapid urbanization in increasing flood risk. We will refer to different studies carried out by other researchers for studying the hydrological impact of urban sprawl.

Studies were done on various Indian cities like Chennai [2, 7], Mumbai [6, 8, 9], and Pune [10] revealing that land change results in an increase in runoff in urban areas. If we see the present situation of rainfall in many districts in Maharashtra, the rainfall pattern has changed a lot, and even daily maximum rainfall is also changed (Fig. 1).

A certain part of Pune City is getting flooded almost every year. If we consider one small stream, "*Ambil odha*", which originates in the Katraj area and meets the Mutha River near Dandekar Bridge, it has many encroachments and slum development on the banks, and many unauthorized constructions are carried out. Due to alterations in precipitation patterns and uncontrolled urban development, roads are transforming into streams, causing numerous vehicles and individuals to be carried away by the floodwaters. Rainwater harvesting plays a crucial role in flood control, as well as enhancing infiltration and minimizing runoff, particularly when combined with the presence of open spaces, green areas, and vegetation. Contrary to this, rapid urbanization and increase in paved surface area increase runoff and decrease infiltration,

Fig. 1 Flood in Pune on September 25, 2019, in the southern Katraj area of Pune (Source: https://timesofindia.indiatimes.com/city/pune/how-pune-went-under-water-vehicles-washed-away-infloods/articleshow/71322737.cms)

resulting in low groundwater levels, which is also another problem related to the availability of ground water to some extent for gardening and for purposes other than drinking in urban areas.

At many places, proper drainage facilities are not provided, rivers are narrowed to smaller widths and "nallaha and odhas" are passed through pipes at many places which cannot carry all such flash floods, and so excess water comes on roads as flood and endangers many settlements. There are slums in the riverbed, and waste material is thrown in the riverbed which reduces its carrying capacity. Although the maximum design discharge capacity of Khadakwasla dam is 1 lakh cusecs, Pune gets flooded with 30,000 cusecs discharge only in Mutha River. Considering such flash floods, it is felt necessary to change design parameters to a certain extent for storm water drain sizes and flood level markings (blue line and red line). The effects of rapid haphazard urbanization cannot be neglected in Maharashtra state. Hence, it is required to update the provisions in the "Maharashtra Regional and Town Planning (MRTP) Act 1966" and "Unified Development Control and Promotion Regulations for Maharashtra State" (UDCPR) 2020 accordingly.

In urban areas in many metro cities like Pune and Hyderabad, we are observing haphazard urbanization and narrowing of streams and nallas, which results in converting roads into rivers during flash floods. It is necessary to study the hydrological impacts of changes in land use–land cover and urban sprawl on urban flooding. It is proposed to analyze the haphazard development, change in the land uses, green spaces, open spaces in the study area and study its impact on urban floods by using GIS techniques and temporal RS images. It is also important to carry out a primary survey for knowing the issues and reasons for urban flooding in the study area, and more resilient spatial planning strategies to reduce future flood risks in the urban environment of Pune can be developed.

2 Literature Survey on National and International Scenario

This detailed literature review work is carried out with respect to studies carried out by different researchers for the following steps.

2.1 Studies on Detecting the Change in Land Use–Land Cover (LULC) Using Remote Sensing Images and Related Hydrological Impacts of Urbanization

The rainfall-runoff process is influenced by three prominent watershed parameters like soil permeability, land use–land cover (LULC) change and topographical modifications. The development of the city, human life and infrastructure is affected a lot due to such flooding [11]. The hydrological process is affected due to the effects of change in LULC, which causes urban flooding [10].

People move to urban areas in pursuit of better job prospects, and they change land uses as and when they need them for their activities. The share of the urban population of the world will be 75% in 2050 [6, 12–14]. So, with the change in LULC and demand for urbanization, sufficient land is not available for the expansion of urban drainage infrastructure [15].

Remotely sensed satellite images and toposheets can be used for the evaluation of LULC change [12–14]. Research is required on hydrological impacts of LULC change on the design of drainage infrastructure [16, 17]. Distributed hydrological model was used in six catchments to study changes in peak flow and runoff as a result of LULC change [18].

One of Mumbai, India's watersheds [9] assessed the impact of LULC change on urbanization in terms of geographical and temporal variance. An important part of a city's sustainable growth is to monitor changes in the LULC [19]. Flooding in Mumbai is caused by encroachment on the drainage basin by housing and infrastructural needs [9]. Thus, the appropriate understanding of urbanization, LULC change and surface runoff is necessary to prevent urban flooding.

It was in 2009 that A. Hadeel and colleagues employed remote sensing to inspect, map, and measure the LULC change in the southern part of Basrah province, Iraq, by employing 1:250,000 mapping scale [16]. Landsat TM and ETM+ images were categorized into LULC types: vegetation, sand, urban areas, unused land and water bodies in 1990 and 2003, respectively. The normalized difference built-up index (NDBI) and supervised classification were used to determine the urban boundaries. Over the course of 13 years, they examined various LULC conversions. The urban area has grown by 1.2% annually, from 3299.1 km^2 in 1990 to 3794.9 km^2 in 2003, according to research. Rapid urbanization and rural-to-urban migration have resulted in the conversion of vast areas of forested land into urban development sites. They asserted that RS and GIS are useful for creating LULC maps, which may be used to determine changes over time.

A study in the Lake Tana Basin, northwest Ethiopia, examined the use of RS to identify LULC change [20]. Based on RS data, LULC change detection is a significant tool for water and land resource management, according to the researchers. From 1986 to 2018, agricultural land and residential areas in the basin rose by 15.61% and 8.05%, respectively. As a result, watershed management methods should be implemented to prevent undesired changes in the basin's LULC.

Sergio Ivan Jimenez-Jimenez et al. explored the use of high-resolution RS data and an object-based approach in the appraisal of urban flood damage in 2020. They compared pre- and post-event data using high-resolution satellite and RGB photos from unmanned aerial vehicles (UAVs), DEMs, and object-based image analysis (OBIA) to quickly assess urban flood damage. The Zempoloantongo River flooded Chicahuaxtla, Puebla, Mexico, during Tropical Storm Earl in 2016. With this three-pronged approach, changes can be made before and after the event. Using UAV data, the overall accuracy of automatic classification is 97%. There is no structural damage inspection.

Geospatial analysis was used in 2021 to assess and predict LULC change near the Blue and White Niles in Khartoum, Sudan, due to flood dangers [21]. As a result of the city of Khartoum, Sudan's recent flash floods, they conducted an analysis using RS, GIS, and hydraulic modeling. Over the next three years, the RS–GIS model predicts that waterbodies around BN will shrink by 4.18% and those around WN by 20.35%. Khartoum faces a high risk of flooding. Khartoum's future land and infrastructure management can benefit from this study. To prevent flooding, it is necessary to enhance drainage infrastructure. Flood hazard impacts can be accurately predicted by using RS–GIS approaches. It was revealed that there is flooding in Lagos, Nigeria, due to reduction of bare soil, water bodies and vegetation cover in city [22].

2.2 Studies on Predicting Urbanization

Hybrid approaches for LULC modeling and prediction were used to examine the spatial and temporal dynamics of urban expansion in Nigeria's Lagos Metropolitan Region [23]. Using an integrated "multi-layer perceptron and Markov chain analysis" (MLP-MCA), they were able to map and depict possible future LULC change scenarios in Nigeria's Lagos Metropolitan Area.

A scenario-based urban growth simulation model (SUSM) was created in 2019 by Lakshmi N. Kantakumar and colleagues [24]. This model may be used to analyze the effects of various planning strategies in both geographical and temporal contexts using remote sensing data.

2.3 Impact of Both Urban Sprawl and Climate Change in Intensifying the City's Flood Hazard

Urban sprawl and its impact on sustainable urban development in Morogoro metropolitan municipality, Tanzania, were studied using RS and social media data [25]. Urbanization has a direct effect on the quality of life in cities and on their long-term sustainability. Images were classified using the random forest (RF) approach, and social media usage (Twitter) data was gathered using the Twitter application programming interface (API). Built-up, vegetative, agricultural and water land cover classes were defined by the researchers. A one-mile radius around the city's core was used to locate Twitter users using the Kernel function. The grasslands and forests that once covered the land have been replaced by man-made structures. As a result of the study's social media data, Twitter usage is concentrated in and around the city's central business district, while usage declines further outside of the city.

2.4 Rainfall-Runoff Modeling Using Software Tool "HEC—Hydrologic Modeling System" and to Map Flood Hazard Using HEC—River Analysis System

The combination of GIS and RS with hydrological and hydraulic models is a useful tool for evaluating the influence of LULC on surface runoff [15, 26, 27]. Many urban applications use RS and GIS to develop source data and make decisions [27–29]. It was found that the Adyar River floods more frequently as a result of LULC changes in Chennai, India [2]. Urban planning must incorporate flood hazard management into all aspects of the process. GIS is used by water resource planners and designers to construct an integrated flood model and watershed management spatial decision support system [30–34]. Infrastructural facilities can be prepared using urban flood hazard maps [6, 35].

Although floods cannot be averted, they can be lessened in severity by employing appropriate flood management methods [36]. A new approach to scenario planning called "advanced scenario planning" was investigated [37]. GIS-based artificial neural networks (ANNs) are utilized to estimate future urban expansion scenarios for Tampa, Florida, USA, and NOAA level rise scenarios are used to outline future flood risks based on the current 100-year floodplain.

2.5 Design Parameters for Storm Water Drain Sizes and Flood Level Markings

A case study in So Paulo, Brazil, is called "hydrologic performance assessment of regulated and alternative strategies for flood mitigation: a case study". Conventional and low-impact development (LID) storm water techniques were evaluated in a highly urbanized watershed for their hydrologic performance (10.23 km^2) [38]. Hydrologic–hydrodynamic modeling was suggested to simulate different implementation scenarios. The model was calibrated and validated for the scenario using rainfall data and downstream water level readings from January 2016 to February 2019 (0.77 NSE 0.97). On-site retention tanks at a lot of scale were used to simulate storm water control, which resulted in peak flow reductions of 5% for a 10-year design storm event. Peak flow was reduced by 18% for the same event when the number of property owners required to adhere to the control measures was increased. Using catchment management as a lens, modeling tools can aid in the evaluation and refinement of urban storm water management policies and regulations.

In 2020, Vladimír Hamouz implemented runoff reduction modeling using green and gray roofs in urban areas with PCSWMM (storm water management model) [39]. Proper study and analysis of the effects of runoff in urban areas are required for retrofitting rooftops as green roofs. In the coastal city of Trondheim of Norway, they developed a model of Risvollan with the PCSWMM model. Rooftops in urban areas as green (vegetated) or gray (non-vegetated—expanded clay, detention based) roofs were retrofitted. They measured runoff at the watershed outlet by understanding the detention effect with nine scenarios using three exceedance thresholds. Results showed that 11% of green roof area reduced discharge a lot. So, rooftop detention must be considered to reduce runoff for storm water management.

2.6 Guidelines for Planning and Design of Urban Drainage Systems in Changing LULC Pattern for Inclusion in "Unified Development Control and Promotion Regulations for Maharashtra State 2020" and "Maharashtra Regional and Town Planning Act 1966"

Flood volumes are increased due to more runoff with an increase in rainfall [40]. In urban areas, 90% of rainfall is seen as runoff in urban areas, whereas in countryside rural non-urbanized areas, it is 75%. In urban areas, unauthorized constructions of houses in infrastructures create man-made floods [41]. Floods are induced by anthropogenic activities, which ultimately results in damage of properties [42]. We can compare flood volume before development and after the development of urban watershed to understand hydrological changes for a return period. [43] analyzed

LULC change from 1966 to 2009 using toposheets and RS images for the catchment of Poisar River in Mumbai, India. The watershed's built-up area has increased from 16.64 to 44.08%, while its open space has decreased from 43.09 to 7.38%.

Many times urban flooding is considered the effect of more rainfall, but developments that influence runoff in the watersheds are not considered [44–46]. If we tried to control floods by upgrading drainage system as per our experience with floods on a yearly improvement basis, then it will take much time, and complete flooding will not stop although we invest much money on such repairs. So, we need to change our urban storm water management practices. They studied an urban watershed in Rio de Janeiro/Brazil to demonstrate a multi-criteria index.

In 2020, Hua et al.'s low-impact development (LID) increased infiltration and detention of storm water runoff and conveyed that rapid urbanization has increased urban flooding risks [47]. They carried out simulations to visualize the flood risk under different rainfall scenarios and LID patterns. They observed that for small rainfall conditions, LID reduced runoff in the watershed.

In 2021, Sara Mehryar and Swenja Surminski thought of visionary thinking to control urban floods before development and stressed the importance of good laws related to urban planning considering climate change [48]. They studied 139 laws from 33 countries collected from the "Climate Change Laws of the World and Disaster Law" databases.

In 2020, Adaku Jane Echendu studied that recently flooding situation is observed in a large scale in Port Harcourt city, in Southern Nigeria urban catchments due to climate change and change in rainfall pattern [49]. He urged five urban professionals to look at it from an urban planning perspective. In discussions with planners, he said that urban planners can play important role in controlling urban flooding by some improvement in planning practices. Government should consult planners and work to reduce urban flood risks permanently.

3 Research Gap

3.1 Shortcomings in MRTP Act 1966 from Flooding Points of View

Under procedure of preparation of Development plan of City in Chapter III, Clause 22, it is mentioned that "development plan shall generally indicate the way the use of land in the area of a Planning Authority shall be regulated and indicate the manner in which the development of land therein shall be carried out. It shall provide so far as may be necessary for all or any of the following matters—Clause 22, item j proposals for flood control and prevention of river pollution". So, this is just a general comment about flood control in the area of a Planning Authority or city and hydrological aspects of urban flooding are not considered to the required extent while planning the development in such area.

3.2 Shortcomings in UDCPR 2020

The following points are mentioned in different clauses:

- In point 2.3 (5), it is mentioned that "authority can correct the alignment of Blue and Red flood line on Development Plan/Regional plan where it varies with the said lines given by the Irrigation Department or any other Govt. institutions dealing with the subject, from time to time" but in real practice proper data related to flood is missing and it is not updated with increase in urbanization and people misuse it conveniently for their benefit. So clear demarcation as per hydrological aspects is missing.
- In point 3.1.1 (11), it is mentioned that "Site is not Eligible for Construction of Building if it is within the river and blue flood line of the river (prohibitive zone), unless otherwise specified in these regulations".
- Under general Land development requirements in Chapter III, point 3.1.3 (i) (b), it is mentioned that "Area between blue flood line and red flood line shall be the restrictive zone for the purposes of construction. The construction within this area may be permitted at a height of 0.45 m. above the red flood line level".
- However, people construct retaining walls, construction at greater plinths also obstructs natural discharge of flow and scientific studies, and demarcation of blue and red line is missing.

3.3 Nature of Proposed Work

It is proposed to develop digital elevation model (DEM) and contour maps and marks the alignments of all the streams in the development plan with all its dimensions and geospatial locations and to propose suitable reservations for different public semi-public facilities in accordance with flood control. This work will give proper insight for the planning of stream network on the line and hierarchy of road network in the city area. It will also develop a logic for reservation of land as per the requirement of flood volume generated in nallah, streams considering many combinations and other parameters like blue line, red line, buffer zone and green belt in the vicinity of streams and construction of retaining walls on the banks of streams. Modeling will be done for different patterns of urbanization and runoff conditions to decide sizes of streams. It may pose a need to increase the sizes of streams in the urbanization process, which may be brought forward in the laws of urban development.

3.4 Expected Outcome (Significance and Applications in Town Planning)

A new approach for the planning and design of urban drainage systems will be proposed. Appropriate amendments will be proposed in the development control rules of local authorities [50] and in the act of the Urban Development Department (MRTP Act 1966: Chapter 3, viz. "Preparation, submission and sanction to development plan").

4 Research Methodology

The method consists of data collection, analysis, and interpretation, listed in the following sections.

- Urban sprawl analysis and prediction.
- Flood hazard mapping of the study area using RS and GIS.
- Rainfall-runoff modeling using the HEC-HMS.
- Modifications in urban drainage design policies with respect to sizes of nallas, streams and river system in the development plan of city.

Between 1966 and 2020, there has been an increase in built-up area due to urbanization and a decrease in open space in the overall catchment area. There will be many social benefits of research work. With all these scientific analysis and evaluation, we will design certain processes and lay down standards for drainage through nallas, streams and river system to mitigate risk of riverbank vulnerability, and it will be proposed as amendment in the legislations of town planning department. It will reduce the risk of urban flooding in future. As of now, there are no clear guidelines in MRTP Act 1966 and "Unified Development Control and Promotion Regulations" (UDCPR 2020) about the hydrological aspect's consideration like volume of flood water likely to flow through stream considering increase in runoff due to different coefficients of paved surface and levels of urbanization. So, with this study and calculations, we intend to add some clauses as amendment in these two acts. It may lead to proper consideration of hydrological aspects for planning and design of urban drainage systems. The amendments in laws, if done, may reduce the future urban flood hazards, loss of property and human deaths. Municipal authorities can use flood plain maps and flood hazard maps for disaster and mitigation planning.

5 Conclusions

The studies of urban flooding have been carried out for coastal cities like Chennai and Mumbai for coastal floods, but such scientific study is not carried out for floods in one of the industrial cities and IT hub, i.e., Pune City of Maharashtra**.** Furthermore, it is found that the hydrological aspect is neglected in urban planning (Clause 22 of "Maharashtra Regional and Town Planning Act 1966" and in UDCPR). Hence, it is felt necessary to study the hydrological impacts of changes in land use–land cover and urban sprawl on urban flooding. Accordingly, more resilient spatial planning strategies to reduce future flood risks in urban environments of Pune can be developed, and based on research and calculations, an amendment in the development control rules (in UDCPR 2020) and in the acts of urban planning of state town planning department (MRTP Act 1966 under preparation of development plan) can be proposed.

References

1. Gupta K (2007) Urban flood resilience planning and management and lessons for the future: a case study of Mumbai, India. Urban Water J 4:183–194. https://doi.org/10.1080/15730620701464141
2. Suriya S, Mudgal BV, Nelliyat P (2012) Flood damage assessment of an urban area in Chennai, India, part I: methodology. Nat Hazards 62:149–167. https://doi.org/10.1007/s11069-011-9985-3
3. Olang LO, Fürst J (2011) Effects of land cover change on flood peak discharges and runoff volumes: model estimates for the Nyando River Basin, Kenya. Hydrol Process 25:80–89. https://doi.org/10.1002/hyp.7821
4. Nirupama N, Simonovic SP (2007) Increase of flood risk due to urbanisation: a Canadian example. Nat Hazards 40:25–41. https://doi.org/10.1007/s11069-006-0003-0
5. Wasko C, Sharma A (2017) Global assessment of flood and storm extremes with increased temperatures. Sci Rep 7:1–8. https://doi.org/10.1038/s41598-017-08481-1
6. Zope PE, Eldho TI, Jothiprakash V (2016) Impacts of land use-land cover change and urbanization on flooding: a case study of Oshiwara River Basin in Mumbai, India. CATENA 145:142–154. https://doi.org/10.1016/j.catena.2016.06.009
7. Suriya S, Mudgal BV (2012) Impact of urbanization on flooding: the Thirusoolam sub watershed—a case study. J Hydrol 412–413:210–219. https://doi.org/10.1016/j.jhydrol.2011.05.008
8. Kulkarni AT, Bodke SS, Rao EP, Eldho TI (2014) Hydrologic impact on change in land use/land cover in an urbanizing catchment of Mumbai: a case study. ISH J Hydraul Eng 20:314–323. https://doi.org/10.1080/09715010.2014.902172
9. Zope PE, Eldho TI, Jothiprakash V (2015) Impacts of urbanization on flooding of a coastal urban catchment: a case study of Mumbai City, India. Nat Hazards 75:887–908. https://doi.org/10.1007/s11069-014-1356-4
10. Wagner PD (2013) Impacts of climate change and land use change on the water resources of the Mula and Mutha rivers catchment upstream of Pune, India
11. Hammond MJ, Chen AS, Butler D, Djordjević S, Manojlović N (2013) A framework for flood impact assessment in urban areas. IAHS-AISH Publ 357:41–47
12. Miller SN, Kepner WG, Mehaffey MH, Hernandez M, Miller RC, Goodrich DC, Devonald KK, Heggem DT, Miller WP (2002) Integrating landscape assessment and hydrologic modeling for

land cover change analysis. J Am Water Resour Assoc 38:915–929. https://doi.org/10.1111/j.1752-1688.2002.tb05534.x
13. Seeber C, Hartmann H, Xiang W, King L (2010) Land use change and causes in the Xiangxi catchment, Three Gorges Area derived from multispectral data. J Earth Sci 21:846–855. https://doi.org/10.1007/s12583-010-0136-7
14. Wagner PD, Kumar S, Schneider K (2013) An assessment of land use change impacts on the water resources of the Mula and Mutha Rivers catchment upstream of Pune, India. Hydrol Earth Syst Sci 17:2233–2246. https://doi.org/10.5194/hess-17-2233-2013
15. DeFries R, Eshleman KN (2004) Land-use change and hydrologic processes: a major focus for the future. Hydrol Process 18:2183–2186. https://doi.org/10.1002/hyp.5584
16. Hadeel AS, Jabbar MT, Chen X (2009) Application of remote sensing and GIS to the study of land use/cover change and urbanization expansion in Basrah province, Southern Iraq. Geo-Spatial Inf Sci 12:135–141. https://doi.org/10.1007/s11806-009-0244-7
17. Zope PE, Eldho TI, Jothiprakash V (2016) Development of rainfall intensity duration frequency curves for Mumbai City, India. J Water Resour Prot 08:756–765. https://doi.org/10.4236/jwarp.2016.87061
18. Kalantari Z, Lyon SW, Folkeson L, French HK, Stolte J, Jansson PE, Sassner M (2014) Quantifying the hydrological impact of simulated changes in land use on peak discharge in a small catchment. Sci Total Environ 466–467:741–754. https://doi.org/10.1016/j.scitotenv.2013.07.047
19. Rawat JS, Biswas V, Kumar M (2013) Changes in land use/cover using geospatial techniques: a case study of Ramnagar town area, district Nainital, Uttarakhand, India. Egypt J Remote Sens Sp Sci 16:111–117. https://doi.org/10.1016/j.ejrs.2013.04.002
20. Tewabe D, Fentahun T (2020) Assessing land use and land cover change detection using remote sensing in the Lake Tana Basin, Northwest Ethiopia. Cogent Environ Sci 6. https://doi.org/10.1080/23311843.2020.1778998
21. Abd El-Hamid HT, Kaloop MR, Abdalla EM, Hu JW, Zarzoura F (2021) Assessment and prediction of land-use/land-cover change around Blue Nile and White Nile due to flood hazards in Khartoum, Sudan, based on geospatial analysis. Geomatics Nat Hazards Risk 12:1258–1286. https://doi.org/10.1080/19475705.2021.1923577.
22. Faisal Koko A, Yue W, Abdullahi Abubakar G, Hamed R, Noman Alabsi AA (2021) Analyzing urban growth and land cover change scenario in Lagos, Nigeria using multi-temporal remote sensing data and GIS to mitigate flooding. Geomatics Nat Hazards Risk 12:631–652. https://doi.org/10.1080/19475705.2021.1887940
23. Wang J, Maduako IN (2018) Spatio-temporal urban growth dynamics of Lagos metropolitan region of Nigeria based on Hybrid methods for LULC modeling and prediction. Eur J Remote Sens 51:251–265. https://doi.org/10.1080/22797254.2017.1419831
24. Kantakumar LN, Kumar S, Schneider K (2019) SUSM: a scenario-based urban growth simulation model using remote sensing data. Eur J Remote Sens 52:26–41. https://doi.org/10.1080/22797254.2019.1585209
25. Shao Z, Sumari NS, Portnov A, Ujoh F, Musakwa W, Mandela PJ (2021) Urban sprawl and its impact on sustainable urban development: a combination of remote sensing and social media data. Geo-Spatial Inf Sci 24:241–255. https://doi.org/10.1080/10095020.2020.1787800
26. Hathout S (2002) The use of GIS for monitoring and predicting urban growth in East and West St Paul, Winnipeg, Manitoba, Canada. J Environ Manage 66:229–238. https://doi.org/10.1006/jema.2002.0596
27. Dewan AM, Yamaguchi Y (2009) Land use and land cover change in Greater Dhaka, Bangladesh: using remote sensing to promote sustainable urbanization. Appl Geogr 29:390–401. https://doi.org/10.1016/j.apgeog.2008.12.005
28. Gatrell JD, Jensen RR (2008) Sociospatial applications of remote sensing in urban environments. Geogr Compass 2:728–743. https://doi.org/10.1111/j.1749-8198.2008.00106.x
29. Zeilhofer P, Topanotti VP (2008) GIS and ordination techniques for evaluation of environmental impacts in informal settlements: a case study from Cuiabá, central Brazil. Appl Geogr 28:1–15. https://doi.org/10.1016/j.apgeog.2007.07.009

30. Parkinson J, Tayler K, Mark O (2007) Planning and design of urban drainage systems in informal settlements in developing countries. Urban Water J 4:137–149. https://doi.org/10.1080/15730620701464224
31. Choi JY, Engel BA, Farnsworth RL (2005) Web-based GIS and spatial decision support system for watershed management. J Hydroinformatics 7:165–174. https://doi.org/10.2166/hydro.2005.0014
32. Yan D, Werners SE, Ludwig F, Huang HQ (2015) Hydrological response to climate change: the Pearl River, China under different RCP scenarios. J Hydrol Reg Stud 4:228–245. https://doi.org/10.1016/j.ejrh.2015.06.006
33. Krause P, Boyle DP, Bäse F (2005) Comparison of different efficiency criteria for hydrological model assessment. Adv Geosci 5:89–97. https://doi.org/10.5194/adgeo-5-89-2005
34. Dewan AM, Kumamoto T, Nishigaki M (2006) Flood hazard delineation in Greater Dhaka, Bangladesh using an integrated GIS and remote sensing approach. Geocarto Int 21:33–38. https://doi.org/10.1080/10106040608542381
35. Owrangi AM, Lannigan R, Simonovic SP (2014) Interaction between land-use change, flooding and human health in Metro Vancouver, Canada. Nat Hazards 72:1219–1230. https://doi.org/10.1007/s11069-014-1064-0
36. Mitchell B, Gardner J, Cook R, Veale B (1978) Physical adjustments and institutional arrangements for the urban flood hazard in the grand river watershed, Ontario. Can Water Resour J 3:31–60. https://doi.org/10.4296/cwrj0302031
37. Kim Y, Newman G (2020) Advancing scenario planning through integrating urban growth prediction with future flood risk models. Comput Environ Urban Syst 82:101498. https://doi.org/10.1016/j.compenvurbsys.2020.101498
38. Gomes Calixto K, Wendland EC, Melo D, de CD (2020) Hydrologic performance assessment of regulated and alternative strategies for flood mitigation: a case study in São Paulo, Brazil. Urban Water J 17:481–489. https://doi.org/10.1080/1573062X.2020.1773509
39. Hamouz V, Møller-Pedersen P, Muthanna TM (2020) Modelling runoff reduction through implementation of green and grey roofs in urban catchments using PCSWMM. Urban Water J 17:813–826. https://doi.org/10.1080/1573062X.2020.1828500
40. Campana NA, Tucci CEM (2001) Predicting floods from urban development scenarios: case study of the Diluvio Basin. Urban Water 3:113–114
41. Mohapatra PK, Singh RD (2003) Flood management in India. Nat Hazards 28:131–143. https://doi.org/10.1023/A:1021178000374
42. Istomina MN, Kocharyan AG, Lebedeva IP (2005) Floods: genesis, socioeconomic and environmental impacts. Water Resour 32:349–358. https://doi.org/10.1007/s11268-005-0045-9
43. Zope PE, Eldho TI, Jothiprakash V (2017) Hydrological impacts of land use–land cover change and detention basins on urban flood hazard: a case study of Poisar River basin, Mumbai, India. Nat Hazards 87:1267–1283. https://doi.org/10.1007/s11069-017-2816-4
44. Bertilsson L, Wiklund K, de Moura Tebaldi I, Rezende OM, Veról AP, Miguez MG (2019) Urban flood resilience—a multi-criteria index to integrate flood resilience into urban planning. J Hydrol 573:970–982. https://doi.org/10.1016/j.jhydrol.2018.06.052
45. Miguez MG, Rezende OM, Veról AP (2015) City growth and urban drainage alternatives: sustainability challenge. J Urban Plan Dev 141:04014026. https://doi.org/10.1061/(asce)up.1943-5444.0000219
46. Magro-Filho O, Magro-Érnica N, Queiroz TP, Aranega AM, Garcia IR (2010) Comparative study of 2 software programs for predicting profile changes in Class III patients having double-jaw orthognathic surgery. Am J Orthod Dentofac Orthop 137:2–6. https://doi.org/10.1016/j.ajodo.2009.02.027
47. Hua P, Yang W, Qi X, Jiang S, Xie J, Gu X, Li H, Zhang J, Krebs P (2020) Evaluating the effect of urban flooding reduction strategies in response to design rainfall and low impact development. J Clean Prod 242:118515. https://doi.org/10.1016/j.jclepro.2019.118515
48. Mehryar S, Surminski S (2021) National laws for enhancing flood resilience in the context of climate change: potential and shortcomings. Clim Policy 21:133–151. https://doi.org/10.1080/14693062.2020.1808439

49. Echendu AJ (2020) The impact of flooding on Nigeria's sustainable development goals (SDGs). Ecosyst Heal Sustain 6. https://doi.org/10.1080/20964129.2020.1791735
50. Gokhale K, Shende NR (2020) Unified development control and promotion regulations

Urban Flood Modelling of West Zone of Surat City, India

Jakka Sai Priya, P. V. Timbadiya, Aarti Ghate, and Shubham Jibhakate

Abstract Urbanization has expanded the use of impermeable surfaces, posing issues in dealing with the consequences of climatic changes, such as heavy amounts of precipitation and severity, making cities more vulnerable to urban floods. The study investigates the adequacy of the prevailing storm water drainage network of west zone of Surat city, Gujarat, India. The present study aims to the development of the intensity–duration–frequency curve, rainfall-runoff model, and 1D hydrodynamic model in MIKE+ using the existing topographic and storm water network data of west zone of Surat city. The developed model was used to simulate 2-year and 5-year return period rainfall event in order to determine the maximum discharge at the outlets using the time-area approach. The findings of the study revealed that the current storm water network in west zone of Surat city is insufficient to seamlessly divert the discharge produced by a 5-year return period, 2-h duration rainfall event, necessitating the augmentation of the current network of the west zone, Surat city in the future.

Keywords Storm water network · Surat city · Urban flood · MIKE+ · Time-area method

1 Introduction

As a consequence of global climate change, weather patterns are changing, resulting in more extreme rainfall events occurring over shorter time frames. River floods, urban floods, and coastal floods are the three kinds of floods. Even though urban floods are related with inadequacies in the current drainage system, meteorological parameters such as abrupt rains of higher intensities and minimum duration lead

J. S. Priya (✉) · P. V. Timbadiya · A. Ghate · S. Jibhakate
Department of Civil Engineering, Sardar Vallabhbhai National Institute of Technology, Surat 395007, India
e-mail: saipriya32542@gmail.com

P. V. Timbadiya
e-mail: pvtimbadiya@ced.svnit.ac.in

P. V. Timbadiya et al. (eds.), *Flood Forecasting and Hydraulic Structures*, Lecture Notes in Civil Engineering 340, https://doi.org/10.1007/978-981-99-1890-4_18

to the possibility of this sort of flood. Flooding in metropolitan areas as a result of heavy rain events is a serious issue that is becoming increasingly problematic. A flood occurs when a river reaches an extremely high level, usually when the river overflows its banks and inundates the surrounding area. Human influence in floodplains and catchment areas, such as the erection of dwellings, roadways, canals, and bridges, has a significance on flood severity. Flood routing is a way of calculating the storm hydrograph based on flow data from one or more upstream stations [1]. Approximations of the flow rate or water level at critical points within the channel system will be obtained using a distributed flow routing model based on partial differential equations (the one-dimensional Saint–Venant equations), which permit the rate of flow and water level to be quantified as functions of both area and time, rather than just time, as in lumped models [2].

Abbott and Ionescu [3] developed an implicit six-point finite difference scheme which can be used to solve the 1D hyperbolic dynamic Saint–Venant equations used in MIKE 11, MIKE URBAN, and in latest version MIKE+ for the urban drainage modelling. Vidyapriya et al. [4] developed sewer, canal flow, and overland flow model using MIKE MOUSE engine for the Jafferkhanpet Watershed in Chennai city to simulate 2005 flood event. The simulated flood level at certain important storm drains was somewhat higher than the intended capacity. Bisht et al. [5] designed a cost-effective drainage system for the IIT Kharagpur campus in West Bengal, India, using SWMM and MIKE URBAN models. Khodashenas and Tajbakhsh [6] used MIKE SWMM to simulate and analyze the urban drains of Mashhad's East Eghbal basin that covers 71 km^2. According to the simulation outcomes, 6 urban drainage system conduits had difficulty retaining storm water. Luan et al. [7] used the Mike Urban model to simulate runoff in several situations in Lincheng County, China. The urban pipe drainage networks have been connected to 2D surface flow for overflow simulation. Wang et al. [8] using MIKE URBAN generated a storm water pipe network model for the newly developed future scientific park site in Beijing. Cardoso et al. [9] using MIKE FLOOD and MIKE URBAN created an integrated 1D–2D coupled model of canalized Junca river and relief sewers to anticipate floods in Dafundo, next to the Tagus estuary, Portugal. The findings indicate that sediment accumulation in the canalized river limits river cross-sections, resulting in severe flood levels and rapid wave propagation from D/S to U/S.

The Tapi River is noted for huge floods caused by depressions that originate in the Bay of Bengal and migrate east to west along the river's course, bringing rainfall first in the top catchments and then in the lower catchments, resulting in a worsening of flood magnitude throughout its length. Major floods hit the Lower Tapi River in 1727, 1776, 1782, 1829, 1837, 1872, 1944, 1959, 1968, 1970, 1994, 1998, and 2006 [10]. The Tapi River's flow capacity has been reduced in Surat as a result of increasing urbanization/industrialization and severe encroachment of the floodplain. For instance, a discharge of just 25,780 m^3s^{-1} attained a height of 12.5 m at the Nehru Bridge in Surat city during the flood of 2006, compared to 12.9 m attained by the historically largest flood of discharge of 42,500 m^3s^{-1} in 1968 [10]. Due to a lack of data for modelling, the study did not investigate the association between river water and storm/sewer water in Surat city [11]. According to the analysis of the

Surat flood event of 2006, the west and southwest zones are the most flood-prone, while the east zone is the least [12]. Hence, flooding in metropolitan areas during the rainfall season often creates water logging issues, which not only disrupt people's daily lives but also pose a number of health risks.

Flooding is unavoidable when drainage water systems fail to react to rain event demands, especially when the natural retention capacity is diminishing by the day. Because the repercussions of flooding may be devastating to people, property, and the environment, innovative flood mitigation measures must be researched and implemented. The current study considers the design return period for the west zone of Surat city based on the revised guidelines on storm water drainage systems provided by the central public health and environmental engineering organization [13]. Earlier, the guidelines mentioned the return period for the design storm as once in two years, now as per the revised guidelines, the design storm should be computed for once in five years return period. The scope of the current study is restricted under the assumption of stationarity. The aim of the present study is (1) to develop the intensity–duration–frequency curves for the Surat city. (2) To derive the rainfall hyetograph for different return periods and various storm duration for Surat city. (3) To develop the rainfall-runoff model for the west zone of Surat city using topographic and existing storm water network data in MIKE+. (4) To evaluate the sufficiency of the prevailing storm water drainage network of the west zone of Surat city based on the revised guidelines given in the CPHEEO, 2019 manual [13]. Therefore, effective storm water drainage management may be used to prevent urban floods by determining the correct model from the existing options.

2 Study Area and Data Collection

2.1 Study Area

Surat city in Gujarat state is located in the lower Tapi basin (LTB), 100 km downstream of the Ukai Dam and 19.4 km upstream of the Arabian Sea [14]. Surat is the largest city in Gujarat after Ahmedabad, having a population of 4.5 million during the 2011 census. Surat city at a latitude of 21.112° N and longitude of 72.814° E is situated on the perennial Tapi River and has a 6-km-long coastal belt along the Arabian Sea. Surat city has a tropical climate, with plenty of monsoon rain (about 2500 mm a year). The increasing trend in daily rainfall intensity is observed over the LTB, which can aggravate the flooding situation in LTB and Surat city [15]. It is 13 m above the mean sea level on average. The city comes under Surat Municipal Corporation (SMC) divided into seven different zones, viz. central zone, east zone, west zone, north zone, south zone, southeast zone, and southwest zone. The study area is the west zone (area = 51.279 km^2) with a population of about 4,24,986 according to the 2011 census. The index map of the study area is shown in Fig. 1.

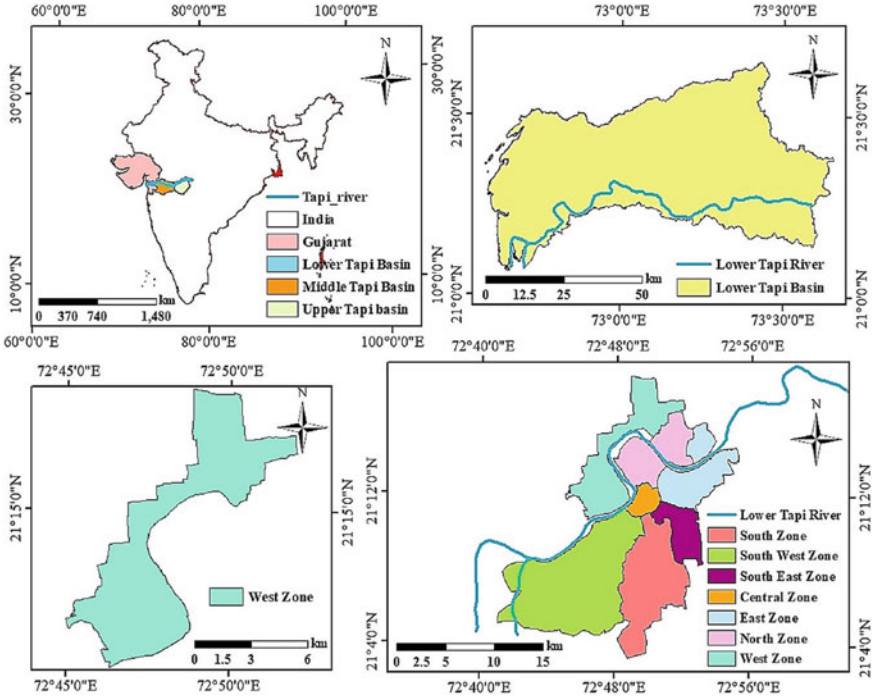

Fig. 1 Index map of study area

2.2 Data Collection

Surat city and its vicinity were physically surveyed by SMC and Surat irrigation circle (SIC), respectively, in the year 2007. SMC delivered zone-by-zone contour maps of Surat city, whereas SIC offered outskirt contour maps in auto-CAD formats. The contour data for this 0.5 m interval is in relation to mean sea level. The contours were used to create a DEM of 10 × 10 m for the current hydrodynamic model. The DEM was created to depict the topography of the catchment using elevation points. For the research region, a categorized land use land cover (LULC) map with a spatial resolution of 56 m of 2018 year was collected from the National Remote Sensing Centre (NRSC), Hyderabad [16]. The acquired LULC map was later categorized into six primary land cover groups, including built-up, cropland, forestland, wasteland, waterbodies, and fallow land at a spatial resolution of 30 m [17, 11]. The daily precipitation data was collected from India Meteorological Department (IMD), Pune. The hydrologic data, referred to as daily rainfall data for the years 1970–2018, were used to establish the model's major input information. Surat Municipal Corporation (SMC) provided data on the storm water pipe network for Surat's west zone, which included 25 auto-CAD designs.

3 Methodology

MIKE+ 1D engine is designed on an implicit finite difference approach for solving fully dynamic, unsteady flow estimates of 1D Saint–Venant equations. MIKE 1D is a numerical software developed by the Danish Hydraulic Institute (DHI) that simulates the hydraulics of water flow via a collecting system network, which may include storm water or waste water networks, natural rivers, as well as the other channels. MIKE+ was used to build a 1D hydrodynamic model of Surat's west zone. As stated in the next paragraphs, the development requires a variety of inputs, including hydrological data, storm water network data, catchment data, including land use and land cover data, and hydrodynamic parameters.

3.1 Hydrological Data

The annual maxima series (AMS) is prepared utilizing the observed daily rainfall information of the Surat city. The AMS is analyzed using generalized extreme value (GEV) distribution. The return levels are computed using the fitted model parameters. The major inputs are prepared for the development of the 1D hydrodynamic model as described in the following sections.

3.2 Intensity Duration Frequency Curve

The intensity duration frequency (IDF) curves for the 2-year and 5-year return periods were constructed employing daily rainfall data of Surat city from 1970 to 2018 using generalized extreme value distribution (GEV), and the shape parameter ($k = -0.051$) of the fitted distribution revealed the data is following the light tail distribution with Type-III family (Weibull) of the GEV distribution [18] and is displayed in Fig. 2.

3.3 Rainfall Hyetograph

Hyetographs for the 2-year return period of 1-h and 2-h storm duration and 5-year return period of 1-h and 2-h storm duration are generated using the intensity and duration data from the developed IDF curve, according to the alternate block technique [2] as shown in Fig. 3.

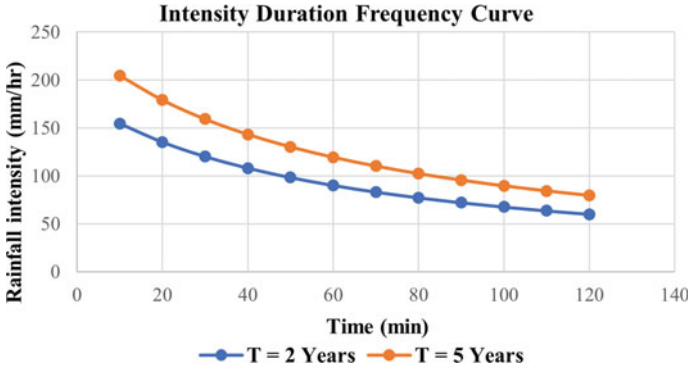

Fig. 2 Intensity curve for 2-year and 5-year return periods

3.4 Mass Curve of Rainfall

Thus, the mass rainfall curve is derived from the hyetograph by plotting cumulative precipitation over time for a 2-year return period of 1-h and 2-h storm length and a 5-year return period of 1-h and 2-h storm duration as shown in Fig. 4. As a result, the mass rainfall curve is used as the primary input to the MIKE+ 1D hydrodynamic model in the form of time series.

3.5 Storm Water Network Data

All auto-CAD drawings acquired from SMC were georeferenced in ArcGIS and the entire network of manholes, and outfalls and pipelines were then manually digitized in MIKE+. The manholes missing ground levels were retrieved from the DEM of the research area supplied. The modelled network consisted of 3035 nodes (manholes) in which 34 are outfalls and 3066 pipes comprised of circular pipes and RCC box drains of varying diameters, totalling 172.81 km in length. The standard manhole was incorporated, which permits flow entry and escape through a 0.25 m manhole cover.

3.6 Catchments

The west zone region was divided into 3007 sub-catchments comprising of total area = 34.26 km^2 (a total area of 34.26 km^2 is modelled out of the actual west zone area of 51.27 km^2, based on the availability of data), and impervious percentages range from 0 to 100%. The hydrological rainfall-runoff modelling method chosen was a time-area approach in the catchment setup field. The time-area technique was chosen

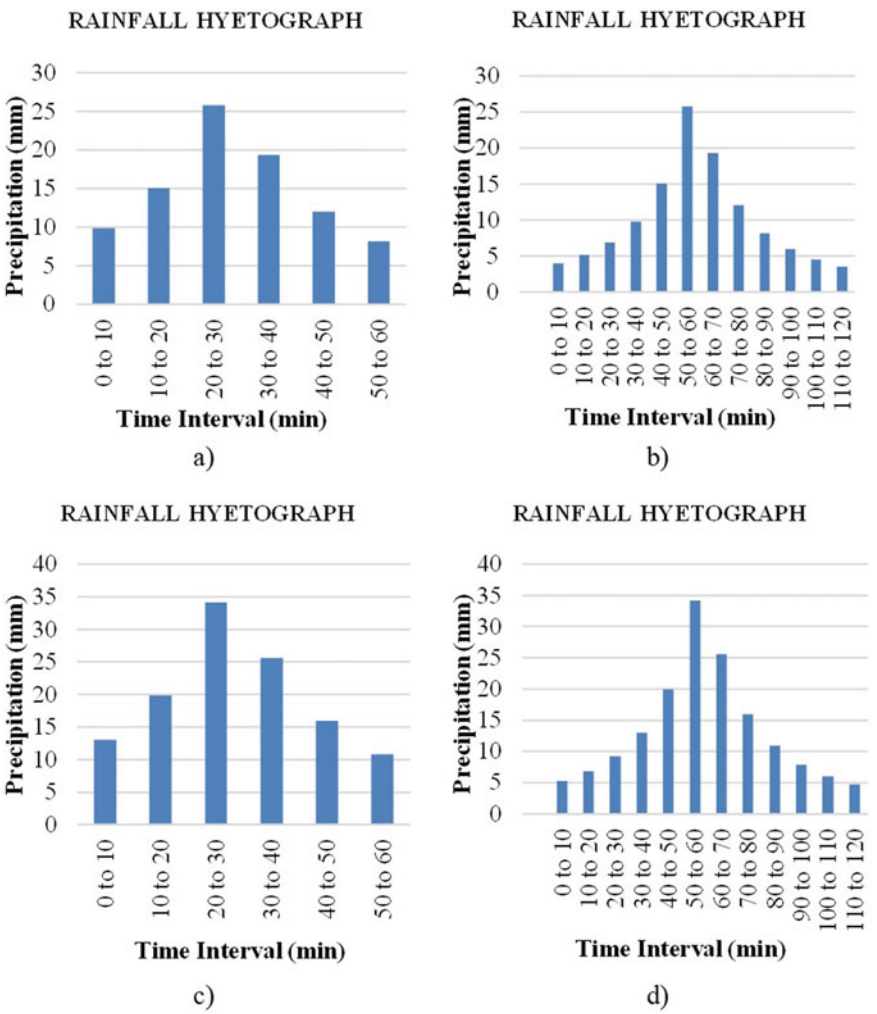

Fig. 3 Rainfall hyetograph for **a** 2-year return period of 1-h storm duration, **b** 2-year return period of 2-h storm duration, **c** 5-year return period of 1-h storm duration, **d** 5-year return period of 2-h storm duration

due to its excellent performance as determined by monitoring data and the absence of more precise information required to calibrate alternative hydrological approaches with a large number of particular parameters.

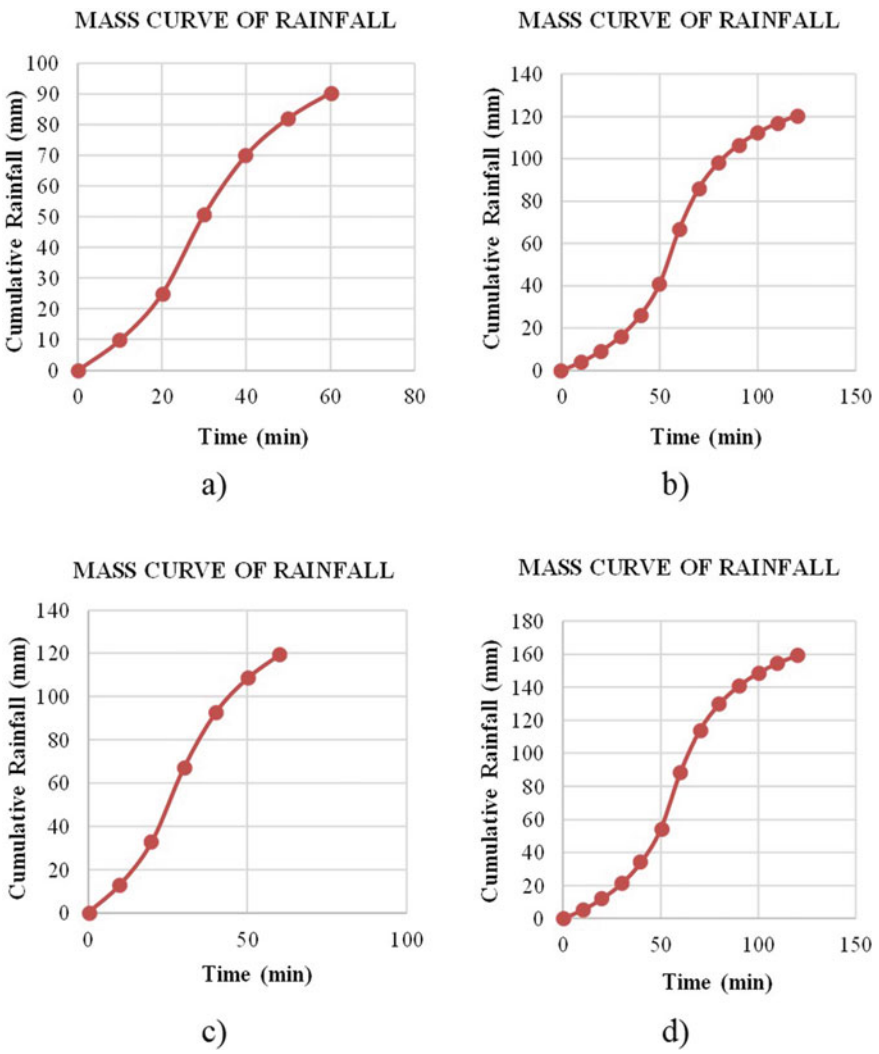

Fig. 4 Mass curve of rainfall for **a** 2-year return period of 1-h storm duration, **b** 2-year return period of 2-h storm duration, **c** 5-year return period of 1-h storm duration, **d** 5-year return period of 2-h storm duration

3.7 Hydrodynamic Parameters

High-order dynamic wave equations are generally suitable for simulating flood flow in the research region. Implicit schemes are inherently stable. The fundamental computational approach is based on solving governing partial differential equations with the well-known six-point implicit finite difference scheme [3].

Selected model parameters were altered in the 1D hydrodynamic model to accomplish reproduction of the real system hydraulic behaviour for the west zone watershed. The following are the parameter values used in unstable flow model simulations:

(i) Conduit's Manning's number (M) = 55.55 [13].
(ii) Minimum design velocity = 0.3 m/sec [13].
(iii) Hydrological reduction factor = 0.9 (MIKE 1D Manual) [19].
(iv) Time step $\Delta t = 1$ s.
(v) Initial loss = 0.6 mm (MIKE 1D Manual) [19].
(vi) Time of concentration (min) is determined using a catchment processing tool.

This urban flood model was used to analyze the storm water network's performance during extreme rainfall conditions and to forecast discharge under various scenarios (return periods) in Surat's west zone.

4 Results and Discussion

The model results can be utilized to assess the flow situations when a different scenario is considered assuming no tidal effect using MIKE+. The maximum discharge results obtained through various simulations at outfalls are as follows.

Total catchment area draining into 34 outfalls is computed as 34.26 km^2, and total length of the storm water pipe network in west zone of Surat city considered is 172.81 km. The maximum total discharge at outlets under 5-year return period of 2-h storm duration is 142.55 m^3/sec, which is more than all the other discharges for various scenario as presented in Table 1. Therefore, the maximum total discharge at the outlets increases with the increase in the return period and increase in the rainfall intensity.

For instance, Fig. 5 presents the comparison between the cumulative flow discharge hydrograph at the outfall Node_1726 for the 2-year return period of 1-h storm duration and the 5-year return period of 1-h storm duration.

The total length of the submerged pipeline increases with the increase in the return period, and the results showing the percentage of the length of the storm water pipe network submerged under various return periods are as follows in Table 2.

Table 1 Maximum discharge at various outfalls under a different scenario

Outfall No	Outfall ID	Area draining (ha)	Length of network (m)	Max Q (m^3/sec) for 1 in 2 year (2-h duration)	Max Q (m^3/sec) for 1 in 5 year (2-h duration)	Max Q (m^3/sec) for 1 in 2 year (1-h duration)	Max Q (m^3/sec) for 1 in 5 year (1-h duration)
Outfall 1	Node_63	197.7	6172	4.9	5.9	4.7	5.7
Outfall 2	Node_45	8.2	2821	0.6	0.8	0.5	0.7
Outfall 3	Node_44	11.7	700	0.04	0.05	0.04	0.05
Outfall 4	Node_41	12.5	2240	0.03	0.06	$1.038e^{-5}$	$1.038e^{-5}$
Outfall 5	Node_37	20.5	651	0.06	0.08	0.06	0.08
Outfall 6	Node_36	115.02	2114	0.4	0.4	0.4	0.4
Outfall 7	Node_35	31.7	1162	1.05	1.2	1.04	1.2
Outfall 8	Node_2949	117.3	9656.5	10.1	11.8	10.04	11.7
Outfall 9	Node_2948	176.7	14,960.3	6.2	6.4	6.2	6.4
Outfall 10	Node_2947	99.9	5022.5	11.6	12.6	11.6	12.6
Outfall 11	Node_2946	55.9	1488	3.1	3.5	3.02	3.4
Outfall 12	Node_2945	124.2	7654.1	9.8	10.5	9.7	10.4
Outfall 13	Node_2149	34.5	2536.5	0.4	0.4	0.4	0.4
Outfall 14	Node_2141	44.7	2768.9	3.9	4.3	3.9	4.3
Outfall 15	Node_2040	9.5	843	2.9	4.1	2.9	4.05
Outfall 16	Node_1937	259.05	14,902.7	5.8	6.1	5.7	6.04
Outfall 17	Node_1862	60.8	7833.9	2.8	2.9	2.7	2.8
Outfall 18	Node_1855	37.5	1950.6	2.5	2.7	2.4	2.7
Outfall 19	Node_18	194.1	5789	1.004	1.3	0.9	1.3

(continued)

Table 1 (continued)

Outfall No	Outfall ID	Area draining (ha)	Length of network (m)	Max Q (m^3/sec) for 1 in 2 year (2-h duration)	Max Q (m^3/sec) for 1 in 5 year (2-h duration)	Max Q (m^3/sec) for 1 in 2 year (1-h duration)	Max Q (m^3/sec) for 1 in 5 year (1-h duration)
Outfall 20	Node_1766	25.8	294	2.8	3.7	2.8	3.7
Outfall 21	Node_1765	7.7	175	0.01	0.01	0.01	0.01
Outfall 22	Node_1764	23.6	329	0.1	0.14	0.1	0.1
Outfall 23	Node_1726	77.4	11,248.1	6.6	7.01	6.5	6.9
Outfall 24	Node_1716	660.2	23,373.3	4.5	4.8	1.72	2.7
Outfall 25	Node_1704	126.5	7943	8.7	9.2	8.6	9.1
Outfall 26	Node_168	91.3	2442.5	4.4	4.6	4.3	4.6
Outfall 27	Node_1672	181.7	2155	3.9	4.2	3.8	4.2
Outfall 28	Node_1663	96.1	3668.3	6.05	6.5	5.9	6.4
Outfall 29	Node_1646	115.5	3618	4.6	4.9	4.5	4.8
Outfall 30	Node_1639	29.8	1328.7	1.6	1.7	1.6	1.7
Outfall 31	Node_1638	6.9	638	1.5	1.8	1.5	1.8
Outfall 32	Node_1637	261.6	19,752.02	9.2	9.7	9.2	9.6
Outfall 33	Node_1632	28.6	1545.1	4.3	4.7	4.4	4.7
Outfall 34	Node_1630	81.9	3036.5	4.2	4.5	4.2	4.5
	Total	3426.07	172,812.52	129.64	142.55	125.33	139.03

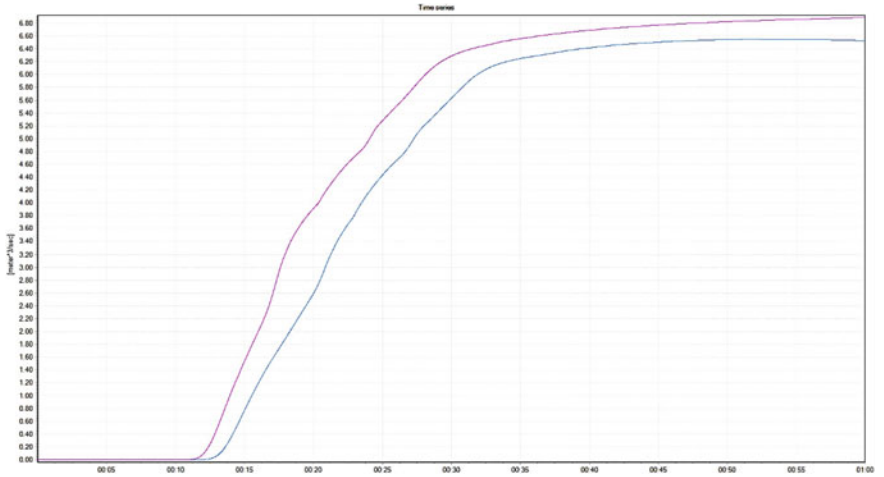

Fig. 5 Cumulative runoff hydrograph at outfall Node_1726 for 2-year and 5-year return period of 1-h storm duration

Table 2 Performance of the storm water pipe network under different scenarios

Scenario	Length of the storm water network (km)	Length of the network (km) in which the water level is higher than the ground levels	Percentage of the length of the pipe under submergence (%)
1 in 2-year (1-h)	172.81	118.56	68.61
1 in 2-year (2-h)	172.81	120.57	69.77
1 in 5-year (1-h)	172.81	122.45	70.85
1 in 5-year (2-h)	172.81	123.22	71.30

5 Conclusions

In the current study, the effectiveness of the storm water network under multiple situations was evaluated. The simulation of different rainfall conditions through a developed 1D hydrodynamic model of the west zone of Surat city resulted in the following conclusions:

- The maximum total discharge at outlets is 129.64 m^3/sec and 142.55 m^3/sec, respectively, for 2-year and 5-year return period rainfall for 2-h duration.
- The existing storm water network is insufficient to take flow generated due to the 5-year return period 2-h rainfall hyetograph.

- Owing to the fact that 71.30% of pipes are submerged due to a 5-year return period of 2-h rainfall, the present storm drainage network in Surat's west zone will need to be augmented in the future to meet the new CPHEEO criteria, 2019.

6 Limitations and Future Scope of the Study

The single LULC map of the year 2018 is considered representative of the study area for the entire rainfall period from 1970 to 2018. Due to the unavailability of observed data at the different junctions, the model is not validated with the field data. The tidal level variations at the outlets of the west zone of Surat city were not considered in the current study. For further research, it would be fascinating to perform a two-dimensional hydrodynamic model of Surat city and surrounding urban-coastal flood plain coupling with a one-dimensional storm network model for simulation of different rainfall scenarios (non-stationary), change in LULC (past and projected) with the variation of tidal level can be considered as future scope of the study. This developed comprehensive model would be helpful for generating a flood risk map, alerting the residents throughout floods, and designing structural flood control measures across the city [20].

Acknowledgements The authors appreciate the infrastructural facility provided by the Centre of Excellence (CoE) on Water Resources and Flood Management, TEQIP-II, for conducting the study reported in this paper. The authors acknowledge the Internet License support of MIKE+ received from MIKE Powered by DHI to carry out the present work. The authors are also thankful to India Meteorological Department (IMD), Central Water Commission (CWC), National Remote Sensing Centre (NRSC) and Surat Municipal Corporation (SMC), Surat Irrigation Circle (SIC) for providing the necessary data to conduct the present study. The authors express their sincere gratitude to the anonymous reviewers for their constructive comments to build the manuscript.

References

1. Subramanya K (2013) Hydraulic machines. Tata McGraw-Hill Education
2. Chow VT, Maidment DR, Mays LW (1988) Applied hydrology. Tata McGraw-Hill Education (India) Private Limited, New Delhi, India
3. Abbott MB, Ionescu F (1967) On the numerical computation of nearly horizontal flows. J Hydraul Res 5(2):97–117
4. Vidyapriya V, Ramalingam M (2012) Flood modelling using MIKE URBAN software: an application to Jafferkhanpet watershed
5. Bisht DS, Chatterjee C, Kalakoti S, Upadhyay P, Sahoo M, Panda A (2016) Modeling urban floods and drainage using SWMM and MIKE URBAN: a case study. Nat Hazards 84(2):749–776
6. Khodashenas SR, Tajbakhsh M (2016) Management of urban drainage system using integrated MIKE SWMM and GIS. J Water Resour Hydraul Eng 5(1):36–45
7. Luan Q, Zhang K, Liu J, Wang D, Ma J (2018) The application of Mike urban model in drainage and waterlogging in Lincheng county, China. Proc Int Assoc Hydrol Sci 379:381–386

8. Wang Y, Luan Q, Wang H, Liu J, Ma J (2019) Risk assessment of rainstorm waterlogging in new district based on MIKE Urban. In: Sustainable development of water resources and hydraulic engineering in China. Springer, Cham, pp 29–40
9. Cardoso MA, Almeida MC, Brito RS, Gomes JL, Beceiro P, Oliveira A (2020) 1d/2D stormwater modelling to support urban flood risk management in estuarine areas: hazard assessment in the Dafundo case study. J Flood Risk Manag 13(4):e12663
10. Timbadiya PV, Patel PL, Porey PD (2014) One-dimensional hydrodynamic modelling of flooding and stage hydrographs in the lower Tapi River in India. Curr Sci 708–16
11. Timbadiya PV, Patel PL, Porey PD (2015) A 1D–2D coupled hydrodynamic model for river flood prediction in a coastal urban floodplain. J Hydrol Eng 20(2):05014017
12. Mehta DJ, Ramani MM, Joshi MM (2013) Application of 1-D HEC-RAS model in design of channels. Methodology 1(7):4–62
13. http://cpheeo.gov.in/cms/manual-on-storm-water-drainage-systems---2019.php
14. Patel DP, Ramirez JA, Srivastava PK, Bray M, Han D (2017) Assessment of flood inundation mapping of Surat city by coupled 1D/2D hydrodynamic modeling: a case application of the new HEC-RAS 5. Nat Hazards 89(1):93–130
15. Gehlot LK, Jibhakate SM, Sharma PJ, Patel PL, Timbadiya PV (2021) Spatio-temporal variability of rainfall indices and their teleconnections with El Niño-Southern oscillation for Tapi Basin, India. Asia Pac J Atmos Sci 57(1):99–118
16. Mohanty MP, Vittal H, Yadav V, Ghosh S, Rao GS, Karmakar S (2020) A new bivariate risk classifier for flood management considering hazard and socio-economic dimensions. J Environ Manage 255:109733
17. Loliyana VD, Patel PL (2020) A physics based distributed integrated hydrological model in prediction of water balance of a semi-arid catchment in India. Environ Model Softw 127:104677
18. Coles S, Bawa J, Trenner L, Dorazio P (2001) An introduction to statistical modeling of extreme values. Springer, London
19. https://manuals.mikepoweredbydhi.help/2020/MIKE_URBAN_Plus.htm
20. https://www.suratmunicipal.gov.in

Effect of Land Use Land Cover Changes on Urban Floods

Himanshu Meena, Vivek L. Manekar, and J. N. Patel

Abstract The flood disasters are responsible for causing huge losses across the globe whether tangible or intangible. The land use land cover (LULC) is one of the most important factors which influences the hydrological processes; thus, it is very much important to evaluate the effects of LULC on the urban floods. The Vadodara City in India is prone to very frequent urban floods and the most disastrous floods happened in 1994, 1996, 2005, 2014 and 2019 in the recent years. The goal of this study is to find out how LULC changes affect the flood of the Vadodara City. In the present study, image classification using ArcGIS has been carried out for accounting for the LULC changes. The LULC image shows the continuous increase in the urban sprawl throughout the Vadodara City. Rainfall-runoff model has been developed using HEC-HMS. For the evaluation of flood-influencing aspects, the current study analyses hydrological parameters using the LULC and curve number.

Keywords Urban floods · LULC · Rainfall-runoff model · Urbanization

H. Meena (✉) · V. L. Manekar · J. N. Patel
Department of Civil Engineering, Sardar Vallabhbhai National Institute of Technology, Surat, Gujarat 395007, India
e-mail: himanshumeena9392@gmail.com

V. L. Manekar
e-mail: vlm@ced.svnit.ac.in

J. N. Patel
e-mail: jnp@ced.svnit.ac.in

P. V. Timbadiya et al. (eds.), *Flood Forecasting and Hydraulic Structures*, Lecture Notes in Civil Engineering 340, https://doi.org/10.1007/978-981-99-1890-4_19

1 Introduction

Over a period of time, rapid and unconstrained population growth, as well as economic and industrial development, have caused increment in the rate of land use land cover (LULC) change, particularly in developing nations. This change has shown great impact on all natural processes including hydrology. The only source of water on the earth is precipitation. LULC is not only affecting the hydrological cycle but seriously affecting the basin response to it. This leads to disasters in the form of floods and water scarcity. Very high rate of change of LULC is noticed throughout the globe because of multiple reasons but primarily due to human intervention with the nature. The current scenario is with huge change in LULC which leads to the global change, through the interaction with ecosystem processes, climate, biogeochemical cycles, biodiversity and even more prominently the human activities [1]. Human activities on earth surface are increasing day by day drastically. Practices of LULC including deforestation, uncontrolled and excessive grazing, increase of agriculture and infrastructure growth. will influence major aspects such as human health, environment quality and natural resources. LULC dynamics identification from the past to the future can be an essential step [2]. The models for analysing and simulating the LULC offer a suitable tool for identifying the spatial pattern and dynamics of land use land cover. It is required to quantify the change in LULC for accounting its effect on the basin response. To note the changes in LULC, it is a herculean task. Today is the era of technology. Remote sensing is the powerful tool which is popularly used for this reason. The satellite images are classified for various classes of land uses to notice the changes.

Predicting water availability in location and time has proven to be a difficult task for the water resources community. Climate extremes (floods and droughts) are also becoming more common as a result of changing climatic conditions around the world [3]. Flood disasters have wreaked havoc on society in both concrete and intangible ways. Previously, any flood disaster management policy was mostly focused on riverine floods that affected wide swaths of rural communities. The city of Vadodara and its administrative district in Gujarat were severely flooded as a result of heavy rainfall in July–August 2019. It is critical to recognize that the causes of urban floods vary, as do the solutions for dealing with them. In the present study, image classification using ArcGIS has been done for the LULC map preparation and rainfall-runoff model using HEC-HMS.

2 Study Area and Methodology

2.1 Study Area and Data Collection

2.1.1 Vadodara City

The study area is Vadodara City, which is situated between 21°49″19′ and 22°48″37′ north latitude and 72°51″05′ and 74°16″55′ east longitude in the Gujarat State of India. Geographic location of study area is shown in Fig. 1. The Vishwamitri River, which runs through the city, is a meandering river with a total length of 70 km and a cross section size ranging from 30 to 60 m. Vadodara is bisected by a 25-km river stretch that runs through the city. In recent years, as the city's urban and industrial growth has accelerated, the Vishwamitri River has been subjected to significant sewage and trash dumping, blocking natural flow and causing flooding and inundation of low-lying areas.

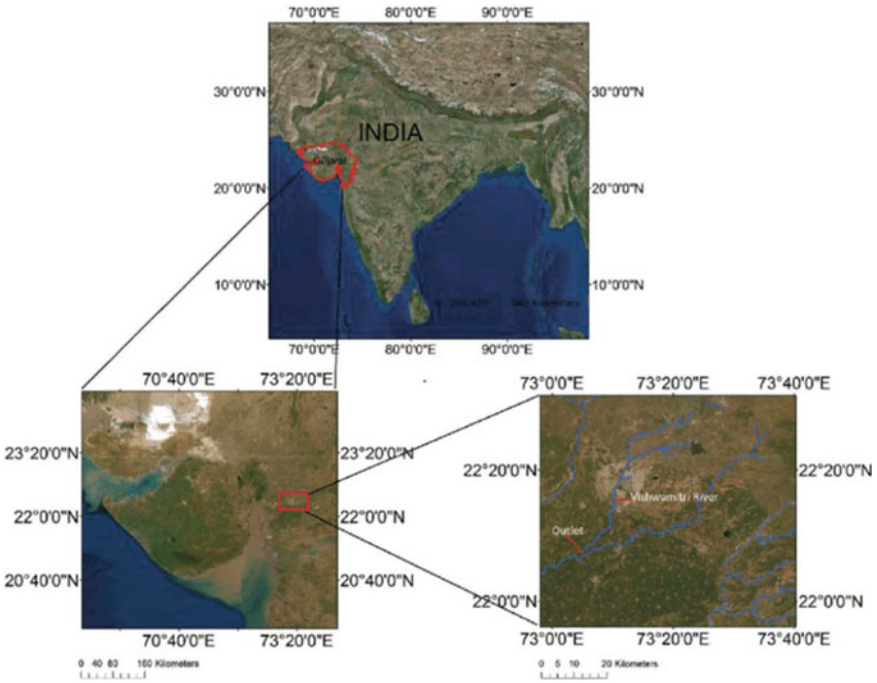

Fig. 1 Geographic location of study area

2.1.2 Data Collection

Bhuvan is a web mapping service that allows users to explore a two-dimensional and three-dimensional representation of the Earth's surface. The browser is precisely made to view India, with maximum resolution. The beta version got launched on August 8, 2009. The digital elevation model (DEM) and Landsat images of Vadodara were downloaded from the website of Bhuvan and United State Geospatial Survey (USGS). The digital soil map was downloaded from FAO soil portal. Data was acquired from the State Water Data Centre in Gandhinagar for the development of the hydraulic model (HEC-HMS).

2.1.3 Basin Delineation

Basins are delineated by the area on the upstream side from a definite outlet point. It can be delineated manually using paper maps, or digitally in the GIS background. Extraction of basin from DEM is required in a variety of environmental studies. The correct delineation also depends on the quality of the DEM and the procedure is accepted. Basin delineation is a main preliminary of hydrologic modelling and watershed. For this study, the basin is delineated in HEC-HMS 4.7.1 software [4]. The technique of delineating watersheds using a digital elevation model is known as terrain pre-processing (DEM). HEC-HMS is used for the delineation of the sub-basins and stream network in DEM [5]. Delineated basin is shown below in Fig. 2. Basin model manager and terrain data manager are used to add required data. In HEC-HMS using GIS tool, the DEM is used to perform set of function, i.e. pre-process sinks, pre-process drainage, identifying streams and delineate elements.

2.2 Preparation of Land Use Land Cover (LULC) Map

2.2.1 Curve Number

The curve number or runoff curve number which is formally known as the soil conservation service or SCS runoff/CN is the parameter used particularly for predicting direct runoff or infiltration from rainfall excess. This number is used to estimate approximately the amount of direct runoff generated from the rainfall over the area.

Satellite imagery with three spectral bands was used for the LULC classification. Built-up area, barren terrain, water body and vegetation were the four land cover types examined in the classification procedure. With the use of ArcGIS 10.8 software, the maximum likelihood supervised classification technique was used, following the strategy provided by the United States Geographical Survey (USGS). The LULC map of the study area is shown in Fig. 3.

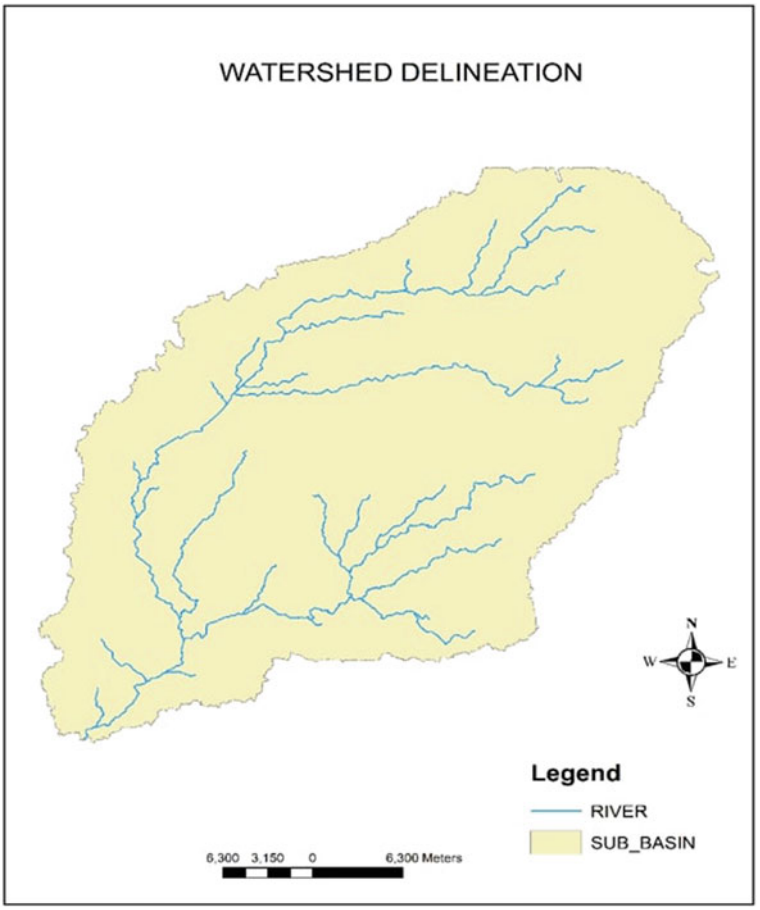

Fig. 2 Delineated basin

2.2.2 HMS Inputs/Parameters

With the help of this function in HEC-HMS, input for transform method, loss method and routing method but no base flow method was taken for this study. In hydrologic parameters, HMS process function was used in which two inputs and three methods were selected like input sub-basin and river, then SCS used for loss method (for calculating excess rainfall from total rainfall) SCS [6] used for transform method (for the conversion of excess rainfall to direct runoff) and lag method for channel routing.

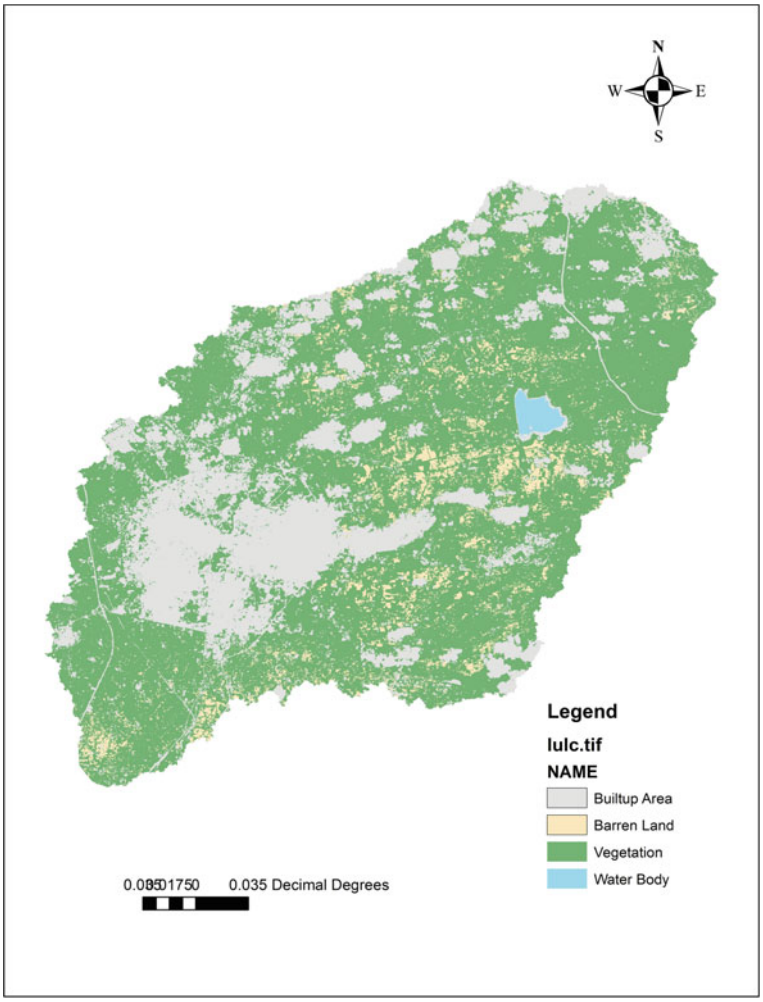

Fig. 3 LULC map

3 Results and Discussions

In the present study, development of hydrological model (rainfall-runoff modelling) is done for the Vadodara Basin with the help of ArcGIS and HEC-HMS and the input parameters are estimated manually as well as generated by the model itself.

Good agreement (correlation coefficient (R2) was observed between the simulated and observed discharge values.

For validation of this model, R2 was 0.73.

For validation of this model, RMSE was 0.40 (Graphs 1 and 2).

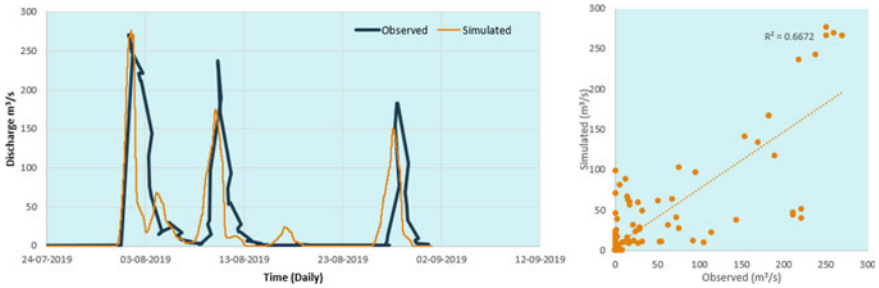

Graph 1 Observed discharges during 2019 were used to calibrate the HEC-HMS model

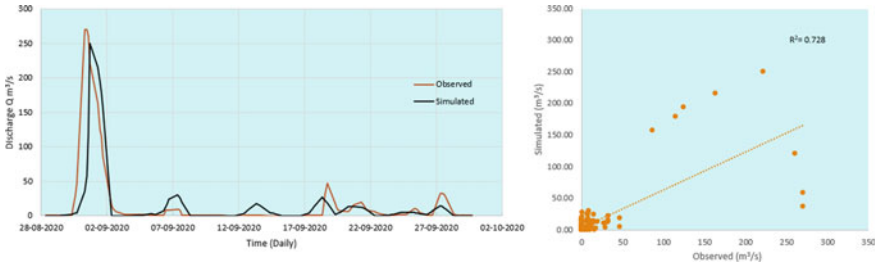

Graph 2 Observed discharges during 2020 were used to validate the calibrated model

4 Conclusions

These following conclusions are drawn from the above research:

- The results of calibration and validation of HMS model have been presented.
- To improve the results of hydrologic model, more sub-basins should be developed to reduce the error caused by using lumped values of parameters. Parameters will remain same for few years only. Thus, more the distributed the model, longer the period for which model will remain valid.
- This model can be integrated with HEC-RAS to develop the flood inundation map for Vadodara Basin.
- Hydrologic model developed for Vadodara Basin can be improved by increasing the number of rain gauge and discharge gauging sites of observations [7].

Acknowledgements The authors are grateful to Gandhinagar's State Water Data Centre (SWDC) for sharing the relevant data for this study.

References

1. Ali M, Khan SJ, Aslam I, Khan Z (2011) Simulation of the impacts of land-use change on surface runoff of Lai Nullah Basin in Islamabad, Pakistan. Landscape Urban Plann 102(4):271–279
2. Rimal B, Zhang L, Keshtkar H, Wang N, Lin Y (2017) Monitoring and modeling of spatiotemporal urban expansion and land-use/land-cover change using integrated Markov chain cellular automata model. ISPRS Int J Geo Inf 6(9):288
3. Trenberth KE (2011) Changes in precipitation with climate change. Climate Res 47(1–2):123–138
4. United States Army Corps of Engineers, Hydrologic Engineering Center USACE-HEC. 2000 Hydrologic modeling system HEC-HMS technical reference manual, Davis, Calif
5. Mokhtari EH, Remini B, Hamoudi SA (2016) Modelling of the rain–flow by hydrological modelling software system HEC-HMS–watershed's case of Wadi Cheliff-Ghrib, Algeria. J Water Land Develop 30(1):87–100
6. SCS U (1972) US department of agriculture soil conservation service: national engineering handbook, section 4, hydrology. US Government Printing Office, Washington, DC
7. Chow VT, Maidment DR, Mays LW (1988) Applied hydrology. McGraw-Hill, New York

Impact of Land Use Changes on Urban Flooding in Patna City

Shashi Ranjan, Imamuddin Mohd Danish, and Vivekanand Singh

Abstract Urban flooding is a serious problem in many regions of the world, and it is a natural calamity that occurs every year. In India, urban flooding is increasing in many cities such as Mumbai, Bengaluru, Delhi, Hyderabad and Patna. Patna city is the congested urban society in Bihar, India. Frequent flooding has been observed in some areas of Patna city due to shrinking of open space, illegal construction, old and chocked drainage system, and lack of waste disposal facilities. Land use affects the urban flooding, and thus, the study of impact of land use on urban flooding is utmost important. In this study, impact of land use changes on urban flooding of Patna city has been studied using Erdas Imagine, ArcGIS, and SCS-CN method during the year 2005–2019. Rainfall data was used to compute antecedent moisture condition, and soil map was used to prepare HSG map. The runoff was computed using the SCS-CN method. The result shows that the change in land use with time affects the curve number and surface runoff. It was found that the built-up area was increased by 22.82% and agriculture land was decreased by 15.48% between 2005 and 2019. During the year 2010–2015, there was a significant change in land use and runoff was increased from 16.8 to 23.72%. This study identified the significant impact of the land use on runoff and consequently on flooding.

Keywords Patna city · Urban flooding · SCS-CN method · ArcGIS

S. Ranjan (✉) · I. M. Danish · V. Singh
Department of Civil Engineering, National Institute of Technology Patna, Patna 800005, India
e-mail: shashi.ce18@nitp.ac.in

I. M. Danish
e-mail: imamuddind.pg19.ce@nitp.ac.in

V. Singh
e-mail: vsingh@nitp.ac.in

P. V. Timbadiya et al. (eds.), *Flood Forecasting and Hydraulic Structures*, Lecture Notes in Civil Engineering 340, https://doi.org/10.1007/978-981-99-1890-4_20

1 Introduction

Flooding is a big concern in many urban areas these days. Every urban settlement suffers from flood as a result of its urbanization (www.youthkiawaaz.com). Patna, capital of Bihar State, is inundated with water after only a few hours of heavy rain, and there appears to be no end in sight. Recently in the year 2019, many residential areas of Patna, including posh colonies like Kankarbagh, Rajendra Nagar, SK Puri, and others, were under five to six feet of storm water due to persistent heavy rainfall and subsequent water logged. Water level did not drop even after rainfall stopped due to clogged and incomplete drainage system (www.hindustantimes.com). A similar case happened in Banglore city in 2016. In a study, it was found that there was the average runoff coefficient increased from 45 to 91% in last 20 years due to impact of land use changes [1].

Patna is rapidly losing its green cover and existing water bodies due to urbanization [2]. The invasion of ponds and wetlands, which may store excess rainwater and regulate water flow, also contributes to the water logging [3]. Expanding Patna is accommodating increased population and regular influx of migrants, resulting in unplanned urbanization and even sabotage of flood plain areas and existing wetlands to make room for the growing population. Various types of depression and low-lying areas that serve as flood absorbers and cushions are filled in and build upon. Flooding in cities has negative social, physical, and economic consequences.

There are various conceptual and physical based hydrological models, which compute runoff from watershed with the occurrence of rainfall events, but this requires large scale of data and is time consuming. SCS-CN technique can be considered as an effective method in combination with remote sensing and GIS [4] for runoff computation. GIS can help in handling with large amount of spatial and non-spatial data in better way than conventional system. It can help in covering large areas for the study, and it is faster and more efficient. SCS-CN method is simple and easy to use for the estimation of runoff from the watershed [5]. This method is based on curve number, which depends of soil type, vegetation, antecedent soil moisture conditions, and land use cover. This method is used widely because of its simplicity, it dependence on one parameter only. For the computation of curve number, land use and hydrological soil group are main factors. It can be used effectively to study the change in surface runoff because of change in land use.

The objective of this study is to investigate the impact of land use and land cover change on urban flooding in Patna city with the help of SCS curve number technique along with remote sensing and ArcGIS.

2 Study Area and Data Used

Patna is the capital of Bihar State and also one of the fastest growing urban city. It is situated on the southern bank of River Ganga. It is bounded by three important rivers, i.e., Ganga in the north, Sone in the west, and Punpun in the east and south. River Gandak is joining River Ganga from the north at Patna. It is large riverine city. It has length of about 35 km and width of 16 to 18 km. Figure 1 shows the study area of Patna Municipal Corporation. The geographical location of Patna is 25°33′22″ to 25°39′20″ N latitude and 85°4′50″ to 85°16′3″ E longitude. It has area of 250 km^2 and elevation of 51 m from MSL. Patna has humid subtropical climate and hottest month is May, with mean maximum temperature of 38.4 °C and mean low temperature of 25.1 °C. Coldest month is January with mean maximum temperature of 22 °C and mean low temperature of 9.3 °C. The average annual rainfall is 1179.5 mm, and about 80% of annual rainfall occurs during monsoon, i.e., from June to September. Soils are mostly sandy loam, with some clay loam with low to high nutrients level [6].

2.1 Data Used

Satellite images of Landsat 5 (for the year 2005 and 2010) and Landsat 8 (for the year 2015 and 2019) were downloaded from USGS Earth Explorer website to prepare land use and land cover map. Soil data was taken from Survey of India (New Delhi) to prepare HSG map. Daily rainfall data was obtained from IMD Patna.

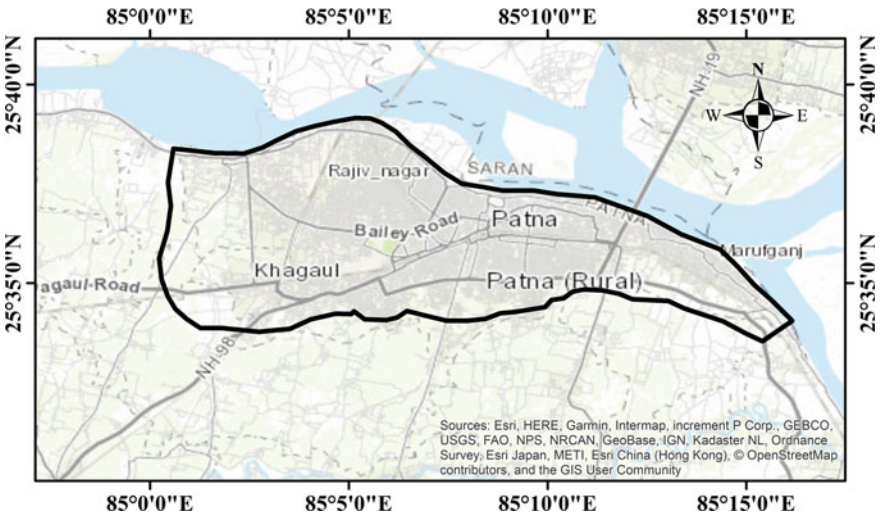

Fig. 1 Study area: urban area under Patna Municipal Corporation

3 Methodology

SCS-CN method is a conceptual method for estimating runoff depth based on storm precipitation developed by Soil Conservation Services of the United States. It is solely dependent on one parameter, the curve number (CN). This approach is used widely in United States and other countries. This method is discussed in details in text book of Subramanya [7] and thus not repeating here. Figure 2 presents the flowchart of the complete methodology.

3.1 Land Use Map Preparation

Satellite images have been downloaded from USGS website and processed in Erdas Imagine 2015 for land use and land cover map for the required year. Images have been automatically georeferenced in Erdas. After extracting the study area, image classification is performed with the help of supervised classification. Land use and cover have been divided into five categories: barren land, vegetation, built-up area, water bodies, and agricultural land. These steps are repeated to prepare land use map for the different time periods, i.e., 2005, 2010, 2015, and 2019.

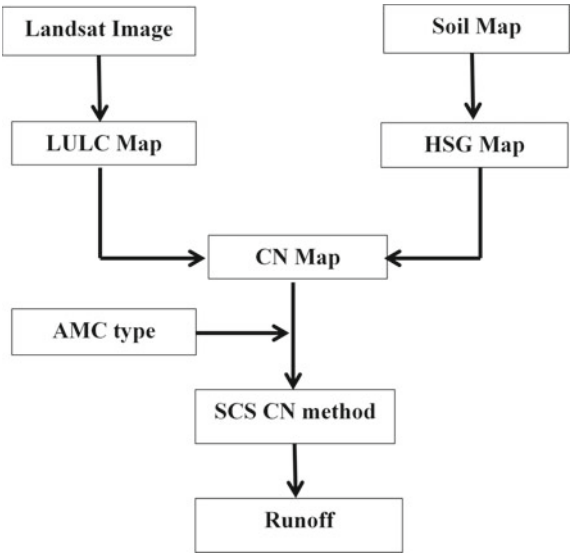

Fig. 2 Flowchart of the methodology

3.2 Hydrologic Soil Group Map Preparation

The soil map was obtained from Soil and Land Use Survey of India (New Delhi) for the preparation of hydrologic soil group (HSG) map. The soil map is extracted according to the study area using the spatial analyst tool's extraction by mask tool.

3.3 Overlaying Land Use and HSG Map

The land use map and HSG map have been integrated to estimate the value of curve number. The attribute table of the integrated map was opened and simplified into the required group according to the land use classification and soil group. Two fields were added in the attribute table, namely area and CN. Area was computed using geometry option, and the value of CN was filled up according to the LULC and HSG group. The average curve number was computed using equation:

$$(\mathrm{CN})_{\mathrm{avg}} = \frac{(\mathrm{CN})_i A_i}{A_{\mathrm{Total}}} \tag{1}$$

where $(\mathrm{CN})_{\mathrm{avg}}$ is the average value of curve number, $(\mathrm{CN})_i$ refers to curve number in ith land use, A_i is the area of a particular class with CN value $(\mathrm{CN})_i$ and A is the total area.

4 Results and Discussions

Table 1 presents the details of the computed values of area in percent and weighted curve number for the different land use and HSG in the year 2005, 2010, 2015, and 2019. The average curve numbers were 86.1, 86.4, 88.0, and 88.7 in the year 2005, 2010, 2015, and 2019, respectively.

4.1 Land Use and Land Cover Mapping

The Landsat images covering the study area were classified for the year 2005, 2010, 2015, and 2019 to obtain the land use and land cover map. Table 2 presents the variation in the land use type at different time intervals. The result shows that there is a major change in the land use type between the period 2010 and 2015. Agriculture land decreased from 44.96 to 31.06 km^2 which is approximately 12%, and built-up area increases from 46.42 to 63.80 km^2, which is 14.28%.

Table 1 Details of the soil classification, hydrological soil group, percentage area, and weighted curve number

Classification	HSG	2005		2010		2015		2019	
		% area	CN	% area	CN	% area	CN	% area	CN
Barren land	B	2.56	86	1.61	86	1.6	86	1.26	86
	C	2.72	91	2.89	91	2.21	91	1.76	91
Water bodies	B	0.79	100	0.79	100	0.71	100	0.8	100
	C	1.5	100	1.15	100	1.4	100	1.29	100
Agriculture	B	13.02	78	13.14	78	11.16	78	10.29	78
	C	27.4	85	25.25	85	14.77	85	13.08	85
Built-up	B	2.76	92	3.36	92	6.67	92	8.26	92
	C	32.93	94	36.14	94	4.63	94	50.99	94
Vegetation	B	3.6	66	3.82	66	2.57	66	2.01	66
	C	12.72	77	11.82	77	11.23	77	10.13	77
Average curve no			86.1		86.4		88		89

Table 2 Land use changes during 2005–2019

Land use type	Area (km^2)				Change in area from 2005 to 2010 (%)	Change in area from 2010 to 2015 (%)	Change in area from 2015 to 2019 (%)	Change in area from 2005 to 2019 (%)
	2005	2010	2015	2019				
Barren land	6.15	5.79	5.33	4.34	(−) 0.28	(−) 0.39	(−) 0.81	− 1.48
Water bodies	6.39	5.68	5.47	5.36	(−) 0.59	(−) 0.17	(−) 0.09	− 0.85
Vegetation	20.4	19	16.2	14.3	(−) 1.67	(−) 1.78	(−) 1.56	− 5.01
Agricultural land	47	45	31.1	28.2	(−) 1.16	(−) 11.94	(−) 2.32	− 15.42
Built-up	42	46.4	63.8	69.7	(+) 3.68	(+) 14.28	(+) 4.86	22.56

Surface runoff was estimated by knowing the AMC type and curve number. Daily runoff was computed using SCS-CN method and daily precipitation for the whole year. The calculation was performed using MS Excel sheet. Figure 3 shows the variation in rainfall and computed runoff for all the study years. In the year 2019, there was heavy rainfall that results maximum runoff in that year, which caused water logging and flooding situation in Patna city.

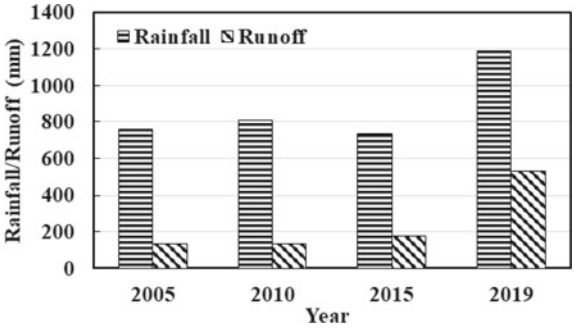

Fig. 3 Variation of rainfall runoff with time

5 Conclusions

The runoff from urban area of Patna has been computed using SCS-CN method. The impact of land use and land cover on urban runoff has also been studied for the year 2005, 2010, 2015, and 2019. The computed curve numbers were 86.06, 86.4, 88.0, and 88.7 for year 2005, 2010, 2015, and 2019, respectively. The built-up area has been increased by 22.82% while the agricultural land decreased by 15.48% between the year 2005 and 2019. The built-up area was 34.38% in 2005, which increased to 38.06 in 2010, then 52.34% in 2015 and 57.20% in 2019. The agricultural land was 38.58% in 2005, which decreased to 37.42% in 2010, then reduced to 25.48% in 2015, and 23.10 in 2019. The major change in land use and land cover takes place between the year 2010 and 2015 with a decrease of 11.94% in agricultural land and an increase of 14.28% in the built-up area. The runoff has also increased from 16.8% in 2010 to 23.72% in 2015. In 2019, the runoff calculated was 44.67% of the total rainfall. This was due to heavy rainfall occurred during this time period causing water logging problems and flooding conditions. The study reveals that the land use change plays an important role in estimating runoff but other conditions like duration of rainfall, intensity of rainfall, and soil condition are also equally important.

References

1. Avinash S, Prasad KL, Reddy GSS, Mukund D (2019) Influence of land use changes on urban flooding: case study of Bangalore City, India. Int J Water Res Eng 5(2):50–61
2. Ahmad MY, Munim N H (2020) Evaluating changes in land use land cover using remote sensing satellite data and GIS (a case study in Patna municipal corporation area) Patna, Bihar. Curr World Environ 15(2)
3. Singh D, Sanjana, Rani R, Nigam B (2014) Water logging and its Implications in Patna municipal corporation. J Res UG PG Stud 6:125–132
4. Al-Juaidi AEM (2018) A simplified GIS-based SCS-CN method for the assessment of land-use change on runoff. Arab J Geosci 11:269
5. Ranjan S, Singh V (2022) HEC-HMS based rainfall-runoff model for Punpun river basin. Water Pract Technol 17(5):986–1001

6. Singh V, Singh A (2017) Variation of temperature and rainfall at Patna. MAUSAM 68:161–168, 551.524.3: 551.577.3 (540.29)
7. Subramanya K (2013) Engineering hydrology, 4th edn. McGraw Hill Education Private Limited, New Delhi

Flood Frequency Analysis of Lower Tapi River Basin: A Case Study of Surat

Vipul Varma, Jinal Pastagia, Darshan Mehta, and Sahita Waikhom

Abstract Flooding is a widespread, recurring, and devastating natural hazard that occurs all over the world. Estimating stream flow has a significant financial impact because it can aid in water resource management and provide protection from water scarcity and potential flood damage. The objective of the study is to carry out a flood frequency analysis of the lower Tapi River Basin, Surat, and to assess which method is more suitable for finding the return period of particular peak discharge. The lower Tapi River Basin is subjected to severe floods during monsoon times. Gumbel's distribution method, Log Pearson Type III (LP3), and Generalized Extreme value probability distribution methods were employed for simulating the future flood discharge scenarios using annual peak flow data (1980–2020), i.e., 41 years from one gauging station (Nehru Bridge) of the lower Tapi River Basin. As a result, a frequency analysis was carried out to correlate the magnitude of occurrences with their frequency of occurrence using a probability distribution. The estimated design floods for different return periods (T_r), such as 2, 10, 25, 50, 100, 150, and 200, were obtained and compared. At a 5% significance level, three goodness of fit tests were used to the fitted distributions: Chi-squared, Kolmogorov–Smirnov, and Anderson–Darling. Based on the above study, it is concluded that Gumbel's Distribution method is more reliable for the lower Tapi Basin compared to the other two methods. Hydrologists, water resources engineers, and floodplain managers will all may benefit from the study's conclusions.

Keywords Flood frequency analysis · Gumbel's distribution method · Log Pearson Type-III distribution method · Peak discharge

V. Varma · J. Pastagia (✉) · D. Mehta (✉) · S. Waikhom
Department of Civil Engineering, Dr. S. & S. S. Ghandhy Government Engineering College, Surat, Surat 395007, India
e-mail: jinal0306@gmail.com

D. Mehta
e-mail: darshanmehta2490@gmail.com; ap_darshan_mehta@gtu.edu.in

P. V. Timbadiya et al. (eds.), *Flood Forecasting and Hydraulic Structures*, Lecture Notes in Civil Engineering 340, https://doi.org/10.1007/978-981-99-1890-4_21

1 Introduction

Flood is defined as overtopping of water from the river and spreads to on dry land. Floods kill more people than other natural calamities [1]. Because comprehensive flood protection is not possible, living with floods and enacting new policies to mitigate their negative consequences are required [2]. Flood underestimating can result in life and property losses. Flood overestimation, on the other hand, results in a waste of money. Hydrologists have been looking for ways to increase the accuracy of flood estimation procedures for a long time [3].

Flood frequency analysis (FFA) is an estimation of the return period of a specific flood peak discharge. Before the analysis of flood frequency, river flow data play important role in the estimation of the return period and to obtain the probability distribution function. Flood discharges of various probabilities are routinely determined using probability distribution functions fitted to maximum flood data [4]. However, selecting the most appropriate probability distribution function is usually controversial. The parameter is obtained from the sample, if any error is recorded data it will pass on the result. Furthermore, uncertainty in the extrapolation of floods predicted by the flood frequency approach is caused by the short length of observed data, outliers, and missing data [5].

The fitting of a probability model to a sample of yearly flood peaks seen during a period of observation for a watershed in a given location is known as flood frequency analysis. The obtained model parameters can then be utilized to predict extreme events with a large recurrence interval. Floodplain management requires accurate flood frequency predictions in order to protect the public, reduce flood-related expenses to government and commercial businesses, build and locate hydraulic structures, and analyze flood-related dangers [6].

Numerous studies on FFA have been conducted in India. In 2019, researchers looked into FFA in the Rapti River Basin. In order to discover the optimum approach for estimating the parameter, they examined the Log Pearson Type-III and Gumbel's Distribution methods. Gumbel's Distribution and Log Pearson Type-III (LP3) were employed as statistical and probability distribution function parameters to determine the frequency association between flood peak discharge and return period. Kolmogorov–Smirnov, Cramer von misses, and Chi-Square goodness of fit (GOF) tests (GEV) are used for evaluating Gumbel's Distribution, Log Pearson Type-III (LP3), and Generalized Extreme Value method. At the Rapti River Basin location, the good-fit study demonstrates that the LP-III approach is more appropriate for flood frequency analysis than Gumbel's method [7].

Flood frequency analysis of lower Tapi Basin at Nehru Bridge site, Surat, is carried out by using the peak discharge of the river from 1980 to 2020. As Surat is situated on the bank of the Tapi River, it faces a flood problem for many years due to the overtopping of water from the river, last most severe flood disaster is seen in 2006. Many agencies are saying that it was a natural disaster but People Committee described the floods as being the result of mismanagement. In the present study, flood

frequency data is analyzed and find out the return period of a particular flood. On the basis of the analysis, the disaster management or mitigation plan is prepared [8].

The Tapi River, which has catchments in Madhya Pradesh, Gujarat, and Maharashtra, is one of India's major west-flowing rivers. The study area receives the majority of its rainfall during the South-West monsoon season, which lasts from June to September. Flooding is widespread in the lower Tapi Basin as a result of excessive rainfall. The regular flooding occurrences that occur in the lower Tapi Basin were thus the basis for choosing this spot. In the case of the 2006 flood, the vulnerability of Surat city to flooding from the Tapi River was the reason for choosing this location. The goal of this study is to calculate the return period for various peak discharges.

2 Study Area and Data Source

2.1 Tapi River Basin

Surat is located on the banks of the Tapi River. The city has a tropical monsoon climate, with summer highs of 44 °C. The annual precipitation runs from 1000 to 1200 mm, with June and September accounting for 90% of the total [8]. 16 km from the city center, the Tapi River empties into the sea. The city has a tidal range of 5–6 m and is located close to the Gulf of Khambhat's mouth. High tides frequently flood the western half of the city.

A large portion of the city is elevated by less than 10 m above sea level. The city has a history of flooding, dating back to 1869 [3]. Prior to the construction of a dam (called Ukai), 94 km upstream of Surat in 1972 to manage repeated floods, the majority of floods in the city were caused by excessive rainfall in the Tapi River's catchment basin, which covers 6% of Gujarat. Between June and October, the watershed area receives 90% of its yearly rainfall, and August is the month with the biggest floods [3]. Heavy rainfall in the catchment region causes a large input of water into the dam's reservoir, which frequently fills up, resulting in large releases from the reservoir, causing flooding in the city (Fig. 1).

The flood of 2006 was the most severe since the Ukai Dam was built in 1971. It engulfed practically the entire city, affecting more than 75% of the people [9] annual peak discharge of the Tapi River at Nehru Bridge gauging station was collected from Surat Municipal Corporation (SMC).

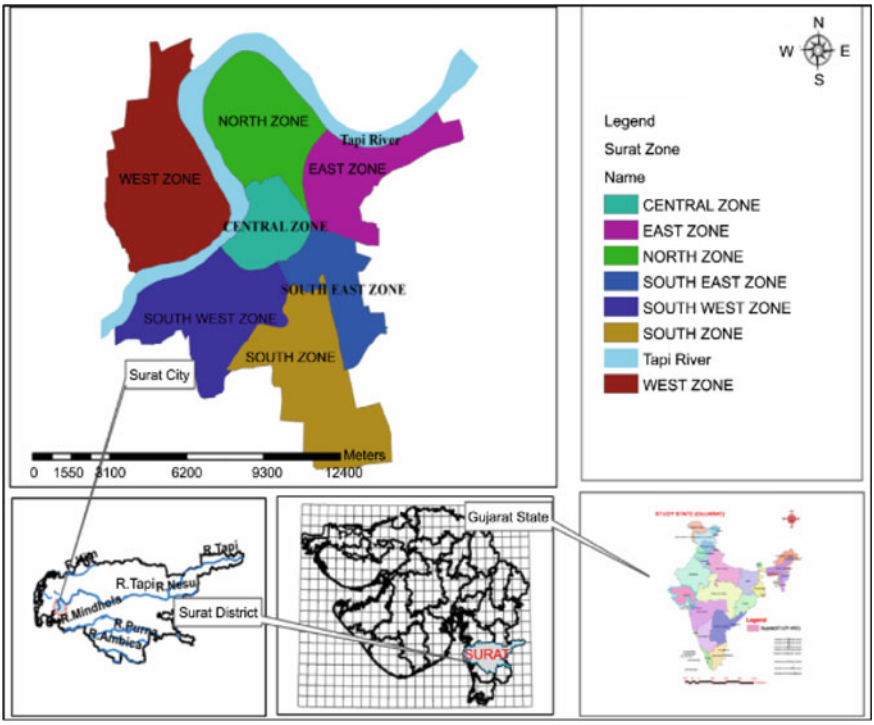

Fig. 1 Map of Surat city zone wise. *Source* Gundaliya et al. and Timbadiya et al. (2015)

3 Methodology

The below mentioned flowchart shows the outline of the methodology for flood frequency analysis.

3.1 Methods of Flood Frequency Analysis (FFA)

The maximum discharge value from the Nehru Bridge, between 1980 and 2020 (41 years) was considered for the FFA by applying the Gumbel's method, Log Pearson Type-III, and Generalized Extreme Value (GEV).

4 Gumbel's Distribution Method

This is a statistical tool for predicting extreme hydrological phenomena like floods (hydrologic study of the channel) [5].

Step I: Annual peak values from 1980 to 2020 are collected.
Step II: Using peak discharge data for 'N' years, the means $\overline{X}$, and standard deviation σ_x are computed using:

$$\overline{X} = \frac{\sum_{i=1}^{n} X}{N} \tag{1}$$

$$\sigma_x = \sqrt{\frac{\sum \left(X - \overline{X}\right)^2}{N - 1}} \tag{2}$$

Step III: Value of Y_n and σ_n is taken as 0.5442 and 1.1436.
Step IV: Using the Weibull equation calculates the return period (T);

Arranging the record from largest to smallest value and assigning the rank first to the highest value (Table 1).

$$T = \frac{N + 1}{m} \tag{3}$$

where

N number of records
m rank assigned to the data after arranging them in descending order of magnitude.

Table 1 Gumbel's extreme value distribution table

N (number of years)	y_n	σ_n	N	y_n	σ_n
10	0.4952	0.9497	65	0.5536	1.1803
15	0.5128	1.0206	70	0.5548	1.1854
20	0.5236	1.0620	75	0.5559	1.1898
25	0.5309	1.0915	80	0.5569	1.1938
30	0.5362	1.1124	85	0.5578	1.1973
35	0.5403	1.1285	90	0.5589	1.2007
40	0.5436	1.1413	95	0.5593	1.2038
45	0.5463	1.1518	100	0.5600	1.2065
50	0.5465	1.1607	200	0.5672	1.2359
55	0.5504	1.1681	500	0.5724	1.2588
60	0.5521	1.1747	1000	0.5745	1.2685

Source AL-Mashidani et al. [4]

Step V: The magnitude of the flood is computed using Eq. 4.

$$X_T = \overline{X} + K_T \sigma_x \tag{4}$$

where

σ_x standard deviation of sample size.
K_T frequency factor which is expressed as,

$$K_T = \frac{Y_T - \overline{Y_n}}{\sigma_n} \tag{5}$$

In which
Y_T Reduced Variate,
Y_n mean of variant y,
σ_n standard deviation.

$$Y_T = -\left[\ln \ln\left(\frac{T-1}{T}\right)\right] \tag{6}$$

4.1 Log Pearson Type-III Distribution Method

This method was adopted by the US Water Resources Council in 1967. To begin, calculate the following after converting the data to logarithms [10].

Step I: Find the log of discharge value.
Step II: Compute mean of log of discharge value (Z).

$$\overline{Z} = \frac{\sum \log x}{N} \tag{7}$$

Step III: Compute the standard deviation of Z

$$\sigma_z = \sqrt{\frac{\sum (Z - \overline{Z})^2}{N-1}} \tag{8}$$

Step IV: Compute the Coefficient of Skewness (C_s)

$$C_s = \frac{N \sum (Z - \overline{Z})^3}{(N-1)(N-2)(\sigma_z)^3} \tag{9}$$

Step V: From the frequency factor (K_Z) table (Table 2) of by applying the value of the Skewness Coefficient, the Log Pearson Type-III distribution calculates the frequency factor for various return periods.
Step VI: Computing Z_T value for different return period by using equation

$$Z_T = \overline{Z} + K_Z \sigma_z \tag{10}$$

Step VII: Compute the peak discharge value for different return period by taking antilog (Z_T).

Table 2 K_Z (frequency factor) value for Log Pearson Type-III distribution

Skew coefficient C_s	Recurrence interval/percent chance of occurrence								
	1.0526	1.25	2	5	10	25	50	100	200
	95	80	50	20	10	4	2	1	0.5
0.70	− 1.423	− 0.857	− 0.116	0.790	1.333	1.967	2.407	2.824	3.223
0.80	− 1.388	− 0.856	− 0.132	0.780	1.336	1.993	2.453	2.891	3.312
0.90	− 1.353	− 0.854	− 0.148	0.769	1.339	2.018	2.498	2.957	3.401
1.00	− 1.317	− 0.852	− 0.164	0.758	1.340	2.043	2.542	3.022	3.489
1.10	− 1.280	− 0.848	− 0.18O	0.745	1.341	2.066	2.585	3.087	3.575
1.20	− 1.243	− 0.844	− 0.195	0.732	1.340	2.087	2.626	3.149	3.661
1.30	− 1.206	− 0.838	− 0.210	0.719	1.339	2.108	2.666	3.211	3.745
1.40	− 1.168	− 0.832	− 0.225	0.705	1.337	2.128	2.706	3.271	3.828
1.50	− 1.131	− 0.825	− 0.240	0.690	1.333	2.146	2.743	3.330	3.910
1.60	− 1.093	− 0.817	− 0.254	0.675	1.329	2.163	2.780	3.388	3.990
1.70	− 1.056	− 0.808	− 0.268	0.660	1.324	2.179	2.815	3.444	4.069
1.80	− 1.020	− 0.799	− 0.282	0.643	1.318	2.193	2.848	3.499	4.147
1.90	− 0.984	− 0.788	− 0.294	0.627	1.310	2.207	2.881	3.553	4.223
2.00	− 0.949	− 0.777	− 0.307	0.609	1.302	2.219	2.912	3.605	4.398
2.10	− 0.914	− 0.765	− 0.319	0.592	1.294	2.230	2.942	3.656	4.372
2.20	− 0.882	− 0.752	− 0.330	0.574	1.284	2.240	2.970	3.705	4.444
2.30	− 0.850	− 0.739	− 0.341	0.555	1.274	2.248	2.997	3.753	4.515
2.40	− 0.819	− 0.725	− 0.351	0.537	1.262	2.256	3.023	3.800	4.584
2.50	− 0.790	− 0.711	− 0.360	0.518	1.250	2.262	3.048	3.845	4.652
2.60	− 0.762	− 0.696	− 0.368	0.499	1.238	2.267	3.071	3.889	4.718
2.70	− 0.736	− 0.681	− 0.376	0.479	1.224	2.272	3.093	3.932	4.783
2.80	− 0.711	− 0.666	− 0.384	0.460	1.210	2.275	3.114	3.973	4.847
2.90	− 0.688	− 0.651	− 0.390	0.440	1.195	2.277	3.134	4.013	4.909
3.00	− 0.665	− 0.636	− 0.396	0.420	1.180	2.278	3.152	4.051	4.970

4.2 Generalized Extreme Value Distribution Method (GEV)

The L-Moments technique is used to compute the Generalized Extreme Value distribution. The data is initially organized in ascending order, and then PWMs are calculated using the following equations: M_{100}, M_{110}, M_{120}, and M_{130} [9].

$$M_{100} = \frac{1}{N}\sum_{i=1}^{n} Q_i \tag{11}$$

$$M_{110} = \frac{1}{N}\sum_{i=1}^{n} \frac{i-1}{N-1} Q_i \tag{12}$$

$$M_{120} = \frac{1}{N}\sum_{i=1}^{n} \frac{(i-1)(i-2)}{(N-1)(N-2)} Q_i \tag{13}$$

$$M_{130} = \frac{1}{N}\sum_{i=1}^{n} \frac{(i-1)(i-2)(i-3)}{(N-1)(N-2)(N-3)} Q_i \tag{14}$$

The sample size is N, the discharge value is Q, and the value's ranking in ascending order is i. The L-moments are then determined according to the following formula [9]:

$$\lambda_1 = L1 = M_{100} \tag{15}$$

$$\lambda_2 = L2 = 2M_{110} - M_{100} \tag{16}$$

$$\lambda_3 = L3 = 6M_{120} - 6M_{110} + M_{100} \tag{17}$$

$$\lambda_4 = L4 = 20M_{130} - 30M_{120} + 12M_{110} - M_{100} \tag{18}$$

Using 19, 20, and 21 equation, coefficient of variation L-CV is derived.

$$\tau_2 = \frac{L2}{L1}(\text{L - CV}) \tag{19}$$

$$\tau_3 = \frac{L3}{L2}(\text{L - Skewness}) \tag{20}$$

$$\tau_4 = \frac{L4}{L2}(\text{L - Kurtosis}) \tag{21}$$

The location parameter (ξ), the scale parameter (α), and the shape parameter (k) are used in the Generalized Extreme Value distribution [11].

$$k = 7.8590\, c + 2.955\, c^2 \tag{22}$$

In which

$$c = \frac{2}{3+\tau} - \frac{\text{Log}\, 2}{\log 3} \tag{23}$$

$$\xi = \lambda_1 - \frac{\alpha\{1 - \Gamma(1+k)\}}{k} \tag{24}$$

$$\alpha = \frac{\lambda_2 k}{\left(1 - 2^{-k}\right)\Gamma(1+k)} \tag{25}$$

where

Γ Function gamma

The following formula is used to calculate the return period discharge:

$$Q_t = \xi + \left(\frac{\alpha}{k}\right)\left\{1 - \left(-\log\frac{(T-1)}{T}\right)^k\right\} \tag{26}$$

Using above equations, GEV is carried out [12]:

Goodness of Fit Tests

Peak discharge datasets of Tapi River at Nehru Bridge site are analyzed using different distribution techniques [13]. Using the goodness of fit tests, we can find the most reliable method. Following are the various tests:

- The Anderson–Darling (AD)
- Kolmogorov–Smirnov (KS)
- Chi-Squared Test

[14] All test statistics were described [14]. The goodness of fit tests was performed with Easyfit (http://www.mathwave.com/easyfit-distribution-fitting.html).

1. ***Anderson–Darling Test***

This test is used to compare an observed CDF to an anticipated CDF. Compared to the KS test, this test gives the tail of the distribution greater weight. The test hypothesis is rejected if the AD statistic is greater than a threshold value of 2.5018 at a specific significance level of 0.05 [15].

2. ***Kolmogorov–Smirnov Test***

This test is calculated using the theoretical and empirical CDFs with the largest vertical distance. The hypothesis is deemed invalid if the KS statistic, like the AD test statistic, exceeds the critical value of 0.1255 at a significance level of 0.05.

The samples are taken from a CDF $F(x)$ model [16]. The following is the test statistic (D):

$$D = \max\left(F(x_i) - \frac{i-1}{n}, \frac{i}{n} - F(x_i)\right) \tag{27}$$

3. ***Chi-Square Test***

This test is used to determine whether a sample fits into a particular distribution. It should be noted that this statistical test has low power and is therefore not very useful [9]. The test is based on binned data, and the quantity of bins (k) is established as follows:

$$k = 1 + \log N \tag{28}$$

The test statistic (x^2) is

$$X_2 = \sum_{i=1}^{k} \frac{(o_i - E_i)^2}{E_i} \tag{29}$$

The Anderson–Darling test, Kolmogorov–Smirnov test, and Chi-squared test, respectively, produced critical values of 2.5018, 0.14355, and 12.592 when the significance level was set to 0.05. The hypothesis is rejected once again if the test statistic exceeds the crucial value [17].

5 Result and Discussions

Climate change has resulted in an increase in the frequency of extreme hydrological events, and as a result of the rapid population growth, excessive socioeconomic activity, and resulting environmental changes in river basin floodplains, the population and assets at risk are now much larger than they were previously. In order to reduce the risk posed by flood hazards, periodic river assessments, especially with regard to their long-term discharge pattern, are highly desirable [7].

A statistical technique for figuring out how rivers behave hydrologically is called flood frequency analysis. The study uses recorded annual peak flow discharge data to calculate statistical information such as mean values, standard deviations, and skewness. The likelihood of various discharges as a function of the frequency of occurrence or the probability of exceeding a threshold is then represented by frequency distributions, which are developed using these statistical characteristics [7].

The average annual flood at Nehru Bridge sites is 8835 (m^3/s) and standard deviation is 7535.37. Table 3 shows the outcome of the various distributions. The entire work is carried out in Microsoft Excel. The graph Figs. 2, 3, and 4 is prepared between peak discharge verses return period. Every graph gives the relation between peak

Table 3 Final outcome showing the return period discharge numbers estimated using three distribution methods

Return period	Nehru Bridge site		
	Gumbel's method	Log Pearson Type-III	GEV
2	7664.32	6405.28	11,707.53
10	20,077.28	20,546.70	23,841.35
25	26,324.93	28,670.78	31,082.66
50	30,959.37	34,710.64	37,019.91
100	35,560.37	40,579.30	43,436.87
150	38,243.12	43,328.09	47,437.74
200	40,144.22	46,263.08	50,395.12

discharge and return period and their coefficient of correlation (R^2). Every method is best fitted in logarithmic regression. Figure 5 gives the comparison of all flood frequency analysis method. GEV gives the maximum discharge value, followed by Log Pearson Type-III and Gumbel's Distribution method, respectively. For the analysis using Gumbel's method, Y_n and S_n value is calibrated from Gumbel's extreme value distribution table (Table 1). In Log Pearson Type-III method, Coefficient of Skewness (C_s) is used to find the frequency factor (K_z) from the frequency factor table (Table 2).

The available discharge data is evaluated in Easyfit software to see if the flood frequency analysis method is best fitted with the best results in terms of return period for discharge data. The three goodness of fit were compared by Easyfit software (Figs. 6 and 7).

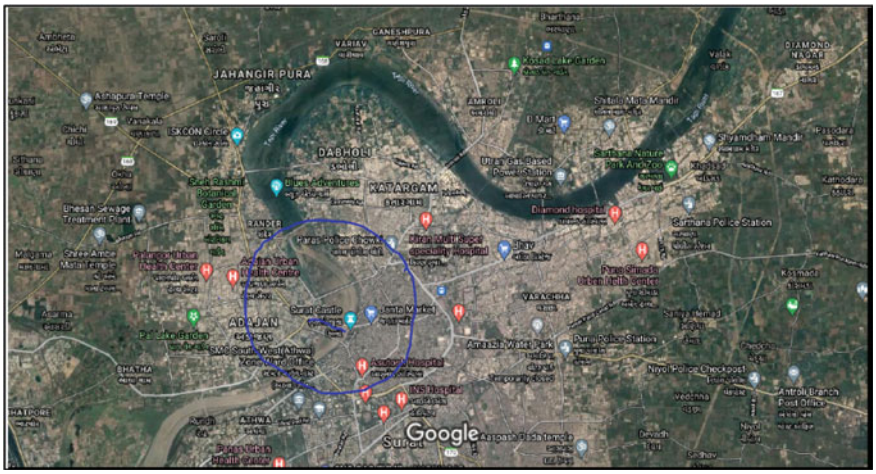

Fig. 2 Map of study area in Google Earth. *Source* www.googleearth.com

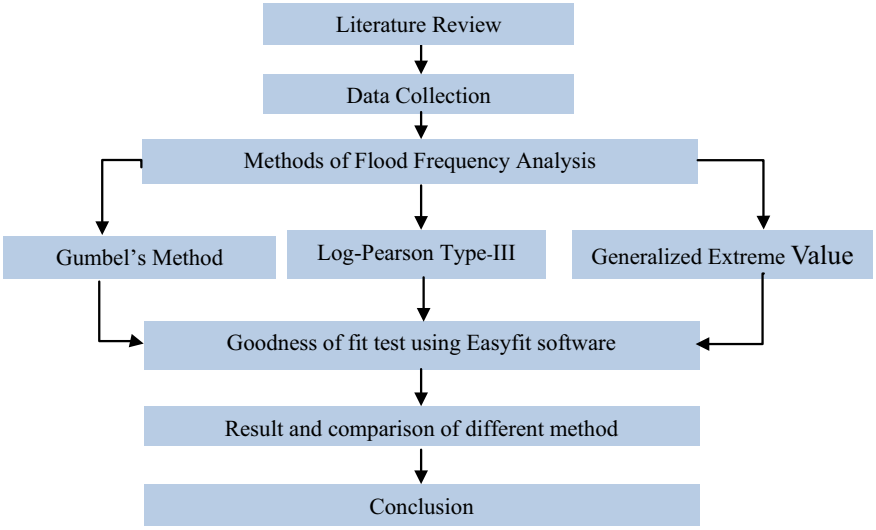

Fig. 3 Flowchart of methodology

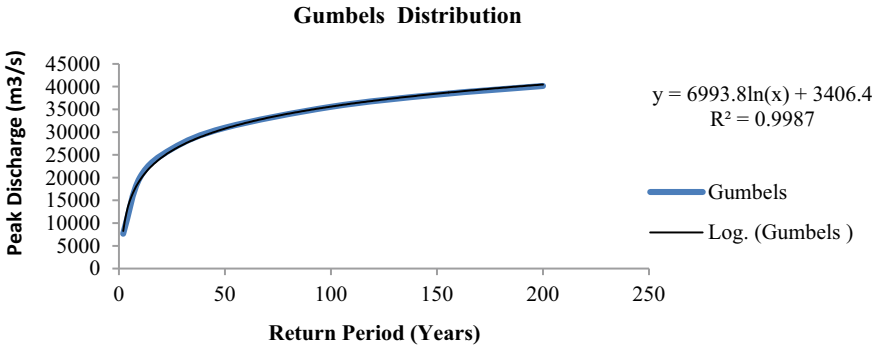

Fig. 4 Peak discharge versus return period (Gumbel's method)

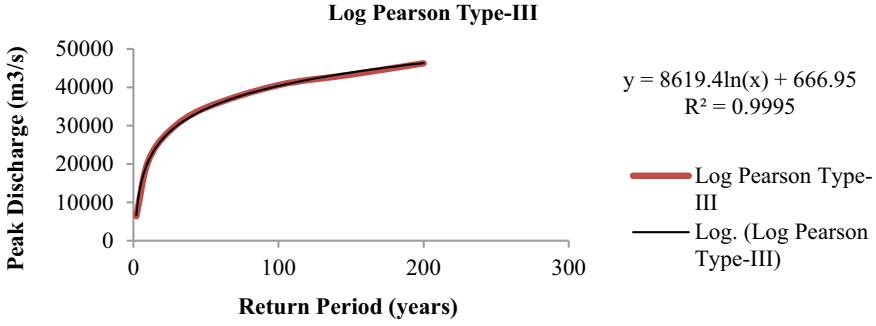

Fig. 5 Peak discharge versus return period (Log Pearson Type-III)

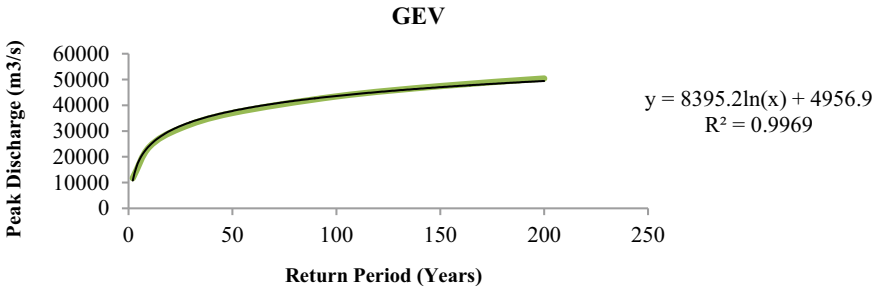

Fig. 6 Peak discharge versus return period (GEV)

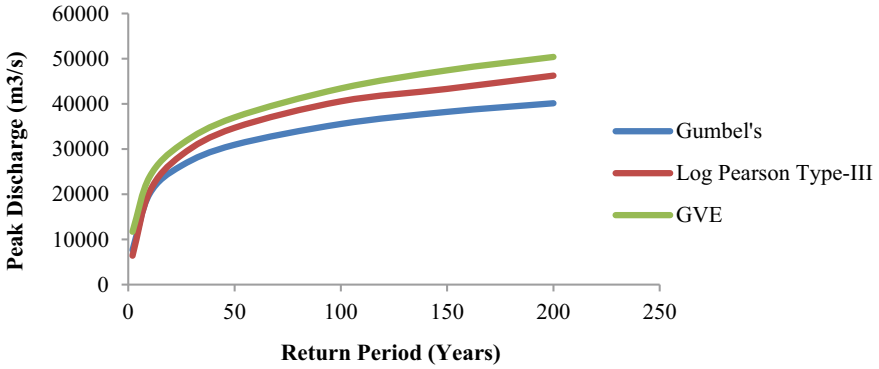

Fig. 7 Graphical representations between peak discharge versus return period of different FFA

The critical value for all three tests at $a = 0.05$, i.e., 95% confidence level, is displayed in the table (Table 4), which distribution will be eliminated from the study depends on this value (Vikash et al. 2016). As we can see that all distribution is accepted with no rejection in easy software goodness fit test. Ranking is given to all the flood frequency analysis method which shows that which method is better fitted in Surat region. As per Kolmogorov–Smirnov, Gumbel's method assigned rank 1, followed by GEV assigned rank 2 and Log Pearson Type-III assigned rank 3.

If we go with Anderson–Darling test rank is assigned 1, 2, and 3 to Gumbel's method, GEV, and Log Pearson Type-III, respectively. From this result, we can say that Gumbel's method and GEV method gave good result in Lower Tapi River Basin, where Log Pearson Type-III gave poor result in lower Tapi Basin.

Cumulative Distribution Function (CDF) and Probability Distribution Function (PDF) of the Lower Tapi Basin are shown in Figs. 8 and 9, respectively shows. Based on the graphical representation it is observed that Gumbel's and GEV distribution is fit best with the observed data while Log Pearson Type-III distribution fit poorly.

As Easyfit software assigned the rank to different test available but in this paper only three test are used and there rank in Easyfit software are given in Table 4.

Table 4 Result of goodness of fit test

Sr. No.	Distribution	Anderson–Darling (critical value at 0.05 = 2.5018)			Kolmogorov–Smirnov (critical value at 0.05 = 0.14355)			Chi-Squared (critical value at 0.05 = 12.592)		
	Nehru Bridge	Statistic	Reject	Rank	Statistic	Reject	Rank	Statistic	Reject	Rank
1	Gumbel's	0.75148	No	1	0.09978	No	1	7.5951	No	1
2	Log Pearson Type-III	1.0541	No	3	0.15439	Yes	3	7.667	No	3
3	GEV	0.7594	No	2	0.11725	No	2	3.8916	No	2

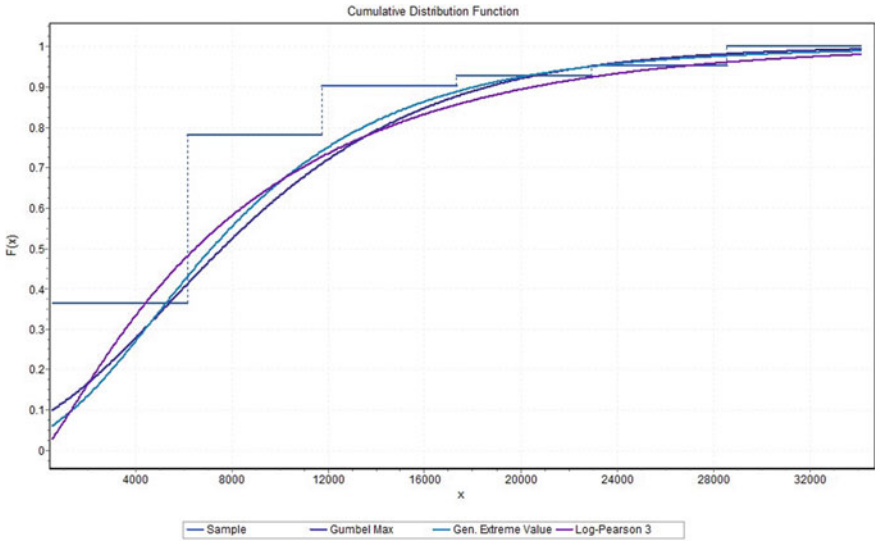

Fig. 8 Cumulative distribution function (goodness of fits test result)

6 Conclusions

The study has been carried out in Lower Tapi Basin using recorded hydrological data at the Nehru Bridge gauging station. Peak discharge data were used for the period of forty-one (41) years which are collected from the gauging station. LP3, GEV, and Gumbel's distribution method were used to carry out flood frequency analysis. For varying return periods of 2, 10, 25, 50, 100, and 200, same methods are also employed to predict the future projected flood discharge in the gauging station. Based on the coefficient of correlation between peak discharge and return periods, the value of R^2 in Gumbel's method, LP3, and GEV is 0.9987, 0.9995, and 0.9969, respectively. From the regression analysis, all three methods are suitable for this region because the coefficient of correlation (R^2) is nearer to 1. The goodness of fit test in Easyfit

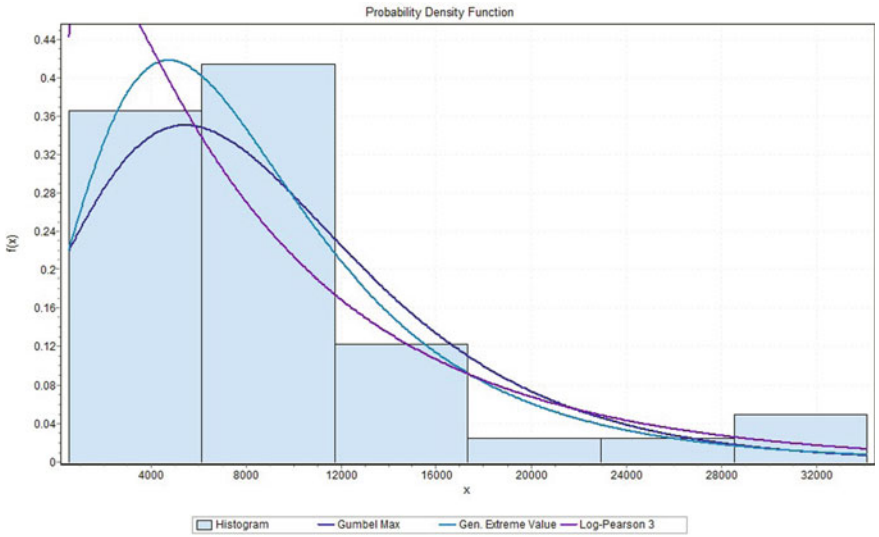

Fig. 9 Probability density function (goodness of fits test result)

software shows that Anderson–Darling and Kolmogorov–Smirnov test assigned the high rank to Gumbel's method and the least rank assigned to Log Pearson Type-III method. Based on the above study, it is concluded that Gumbel's Distribution method is more reliable for lower Tapi Basin compared to other two methods [18, 19].

References

1. Pielke RA, Downton MW, Miller JB (2002) Flood damage in the United States, 1926–2000: a reanalysis of national weather service estimates. University Corporation for Atmospheric Research, Boulder, CO
2. Doocy S, Daniels A, Murray S, Kirsch TD (2013) The human impact of floods: a historical review of events 1980–2009 and systematic literature review. PLoS Curr 5
3. Bhat GK, Karanth A, Dashora L, Rajasekar U (2013) Addressing flooding in the city of Surat beyond its boundaries. Environ Urban 25(2):429–441
4. Al-Mashidani G, Lal PB, Mujda MF (1978) A simple version of Gumbel's method for flood estimation/version simplified de la method de Gumbel pour estimation des cures. Hydrol Sci J 23(3):373–380
5. Bhagat N (2017) Flood frequency analysis using Gumbel's distribution method: a case study of Lower Mahi Basin, India. J Water Resour Ocean Sci 6(4):51–54
6. Tumbare MJ (2000) Mitigating floods in Southern Africa. Paper presented at the 1st WARSFA/WaterNet symposium: sustainable use of water resources, Maputo, 1–2 Nov
7. Bhat MS, Alam A, Ahmad B, Kotlia BS, Farooq H, Taloor AK, Ahmad S (2019) Flood frequency analysis of river Jhelum in Kashmir basin. Quatern Int 507:288–294
8. Parikh K, Parikh J, Kumar M (2017) Vulnerability of Surat, Gujarat to flooding from Tapi River: a climate change impact assessment. Vayu Mandal 43(2):120–129

9. Cunnane C (1989) Statistical distributions for flood frequency analysis. Operational hydrology report (WMO)
10. Raghunath HM (2006) Hydrology: principles, analysis and design. New Age International
11. Hosking JRM, Wallis JR (1997) Regional frequency analysis. Cambridge CB2 1RP
12. Molini A, La Barbera P, Lanza LG, Stagi L (2001) Rainfall intermittency and the sampling error of tipping-bucket rain gauges. Phys Chem Earth Part C 26(10–12):737–742
13. Mangukiya NK, Mehta DJ, Jariwala R (2022) Flood frequency analysis and inundation mapping for lower Narmada basin, India. Water Pract Technol 17(2):612–622. https://doi.org/10.2166/wpt.2022.009
14. Saghafian B, Golian S, Ghasemi A (2014) Flood frequency analysis based on simulated peak discharges. Nat Hazards 71(1):403–417
15. Önöz B, Bayazit M (1995) Best-fit distributions of largest available flood samples. J Hydrol 167(1–4):195–208
16. Mishra DK (2001) Living with floods: people's perspective. Econ Polit Wkly 2756–2761
17. Patel DP, Srivastava PK (2013) Flood hazards mitigation analysis using remote sensing and GIS: correspondence with town planning scheme. Water Resour Manage 27(7):2353–2368
18. Timbadiya, PV, Patel PL, Porey PD (2015) A 1D–2D coupled hydrodynamic model for river flood prediction in a coastal urban floodplain. J Hydrol Eng 20(2):05014017
19. Kumar V, Cheng SYC, Singh AK (2016) Impact of flood on rural population and strategies for mitigation: a case study of Darbhanga district, Bihar state, India. Contemp Rural Soc Work J 8(1):5

Frequency Analysis Incorporating a Decision Support System Over Mahanadi Catchment in India

Neha Gupta and Sagar Rohidas Chavan

Abstract Different statistical criteria used for selecting the best fit for distributions are usually "biased" against the tail (large extreme events) as they give more weightage to the central tendency of the distribution. The extreme events are generally designated as the improbable events or outliers having less frequency of occurrence, resulting in the erroneous estimation of their magnitude and frequency. The present study evaluates the usefulness of the decision support system (DSS) to find a suitable class of probability distribution functions depending upon the tail heaviness. DSS analyzes the tail behavior of the sample data based on various graphical methods, viz., mean excess function plot, hill plot, log–log plot, max-sum ratio plot, and concentration profile. Once the distribution class is identified, the best fit distribution from various distributions in the class can be explored. The utility of the DSS is demonstrated through an application to the extreme precipitation data over the Mahanadi River basin. We have considered the gridded precipitation data obtained from the Indian Meteorological Department (IMD)-Pune having a resolution of 0.25°. Results show that almost all the graphical techniques combined to form a decision support system allow us to discriminate the exponential tail with a heavy tail, and one should rely on more than one graphical method for rational conclusions.

Keywords Heavy tails · Light tails · Decision support system (DSS) · Classes of distribution · Graphical method

Disclaimer: The presentation of material and details in maps used in this chapter does not imply the expression of any opinion whatsoever on the part of the Publisher or Author concerning the legal status of any country, area or territory or of its authorities, or concerning the delimitation of its borders. The depiction and use of boundaries, geographic names and related data shown on maps and included in lists, tables, documents, and databases in this chapter are not warranted to be error free nor do they necessarily imply official endorsement or acceptance by the Publisher or Author.

N. Gupta (✉) · S. R. Chavan
Department of Civil Engineering, Indian Institute of Technology Ropar, Ropar 140001, India
e-mail: 2017cez0006@iitrpr.ac.in

S. R. Chavan
e-mail: sagar@iitrpr.ac.in

P. V. Timbadiya et al. (eds.), *Flood Forecasting and Hydraulic Structures*, Lecture Notes in Civil Engineering 340, https://doi.org/10.1007/978-981-99-1890-4_22

1 Introduction

The interaction of various hydrological and climatic variables in space and time results in different natural processes. Considerable uncertainty is associated with the quantification of the natural process using any physical, analytical, or statistical tools as their behavior is not entirely known to us. Precipitation being a climatic phenomenon, is highly variable in space and time. It is a random variable bounded at zero with a monotonically decreasing Probability Density Function (PDF) tail [1]. The basic knowledge of the variability and the driving forces behind the dynamics of a natural process like precipitation is needed to be understood. Various applications in water resources like agriculture, irrigation, hydropower, water supplies, and aquatic systems are directly influenced by precipitation. According to a report by IPCC [2], changing climate has severe repercussions on human lives as it causes extreme events such as extreme precipitation, drought, forest fires, and coastal flooding in the latter half of the twenty-first century causing loss of life, economy, and ecosystems, worldwide.

Frequency analysis is the most frequently used probabilistic tool that helps understand the behavior and variability of natural processes in the likely future. Frequency analysis involves two primary steps (i) selection of the appropriate probability distribution model and (ii) estimation of the parameter based on the sample data. Estimated parameters from the conventional distribution fitting methods describe the data from the largest portion of a distribution, leaving the extreme events present in the tail as improbable events. Inaccurate estimation of magnitude, frequency, and probability of occurrence of extreme by the conventional fitting method can result in a severe threat to human beings [3]. Tail-fitting of probability distributions by considering observations above a particular threshold for parameter estimation [3–5] or using some empirical method like the obesity Index [6] can resolve the problem of estimating the probability of occurrence of an erratic precipitation event.

Previous studies like that of El Adlouni et al. [7], Ehsanzadeh et al. [8], Nerantzaki and Papalexiou [5], and Gupta and Chavan [6] have highlighted the importance of identifying the class of distribution with respect to their right tail before the selection of a particular model. El Adlouni et al. [7] showed the practical use of different graphical criteria that can classify the commonly used distribution into different classes suitable to represent the studied sample. Ehsanzadeh et al. [8] proposed and investigated the usefulness of an approach named as decision support system (DSS). This approach includes the practical procedure helpful in selecting the class of distributions before model selection, providing the best fit to the data set with respect to their right tail behavior. Several earlier studies related to grouping of the probability distributions based on the general properties and limiting behavior of the tails leading to their classification into different classes can also be found [9, 10]. The distributions commonly used in hydrology were classified in nested classes such as $A \subset B \subset C \subset D \subset E$ (where E is the lightest and A is the heaviest distribution class), as stated by the aforementioned studies. Five nested classes of distributions include

α-stable distributions in class A, Pareto-type tails in class B, Regularly varying distribution in class C, subexponential distributions in class D, and exponential distribution in class E. The class E distributions are characterized by non-existent exponential moments (given by $E(e^X) = \infty$). All distributions with a tail decreasing more slowly than any exponential tail are included in class D. The tail of distributions in class C decreases asymptotically according to the power function. The distributions in class C have tails similar to that of a Pareto distribution. Class B contains the distribution having the exact Pareto tail (and not asymptotically equivalent). This study does not focus on the distributions of Class A (stable distribution), which refers to the distribution with Pareto tails having $\alpha < 0$; hence, no further details are provided for this class. Among the remaining classes, distributions of class D have a heavier tail than class E distributions; class C distributions have a heavier tail than class D distributions, while the Pareto distributions belonging to class B have the heaviest tail of distributions among all classes. Lognormal is a limiting case having a tail between two classes, namely class D and class C [11, 12]. Lognormal distribution has similar generating mechanisms as that of power-law type distributions [7].

Several studies in the past have introduced various statistical graphical tools such as Mean Excess Function (MEF), Hill ratio plot, log–log, and Max-sum ratio plot [7, 13–19], which are helpful for exploratory analysis and tail discrimination. Recently, Fontanari et al. [20] introduced concentration profile (CP) plots, which were used for the identification of the parametric families of the loss distribution. All these graphical methods are robust in assessing the tail behavior of distributions; however, each method requires visual interpretation by the users. El Adlouni et al. [7] proposed using a set of graphical criteria for selecting the class of distributions that can adequately represent the annual peak flows of the Potomac River from 1895 to 2000. Ehsanzadeh et al. [8] identified the class of distributions of the datasets of three large hydroclimatic databases, viz., Reference Hydrometric Basin Network (RHBN), annual cumulative precipitation, and UNESCO annual maximum discharges, before the selection of the appropriate probability model with respect to the tail behavior using a DSS. The findings of the study revealed that distributions belonging to class C were found suitable for representing the majority of RHBN flood data, which in turn represents the extreme event with heavy tails. However, most UNESCO discharge and precipitation sample data belonged to class D, representing the relatively lighter-tailed processes. This study shows the need to discriminate among the different classes before the model selection, especially when sample data represent extremes. Nerantzaki and Papalexiou [5] recently advanced a graphical tool, namely MEF, into an algorithmic procedure and applied that to 21,348 daily precipitation records available globally to discriminate between exponential (or thinner) (class E) and heavier tails (like subexponential distribution of class D).

Authors in the present study have modified the approach of distribution classification given by El Adlouni et al. [7] and Ehsanzadeh et al. [8] by incorporating some advanced tools developed over time. The use of these graphical criteria (forming the DSS) helps in identifying the best class of distributions for the annual maximum precipitation series over the Mahanadi river basin, giving a precise estimation of extreme precipitation. Figure 1 illustrates the procedure incorporated in the DSS to

identify the appropriated distribution class for the sample data. Details of each tool used in the DSS are as follows: (i) Given a dataset first step is to apply a log–log plot. Log–log plot allows the identification of the distributions of class C by discriminating them with distributions of other classes like subexponential (i.e., class D) or exponential (class E). However, if the sample data is categorized as class C, three graphical statistical tools, namely, the max-sum ratio plot, Hill ratio plot, and CP, are used as part of the confirmatory analysis to confirm the conclusions drawn by the previous tool. (ii) When the given dataset is not categorized as class C, another graphical tool known as MEF is used. It helps in tail identification and discrimination of the distribution belonging to class D (subexponential) from that of class E (exponential). Hill ratio plot and CP are the two statistics used as the confirmatory analysis of the conclusions drawn by the earlier tool.

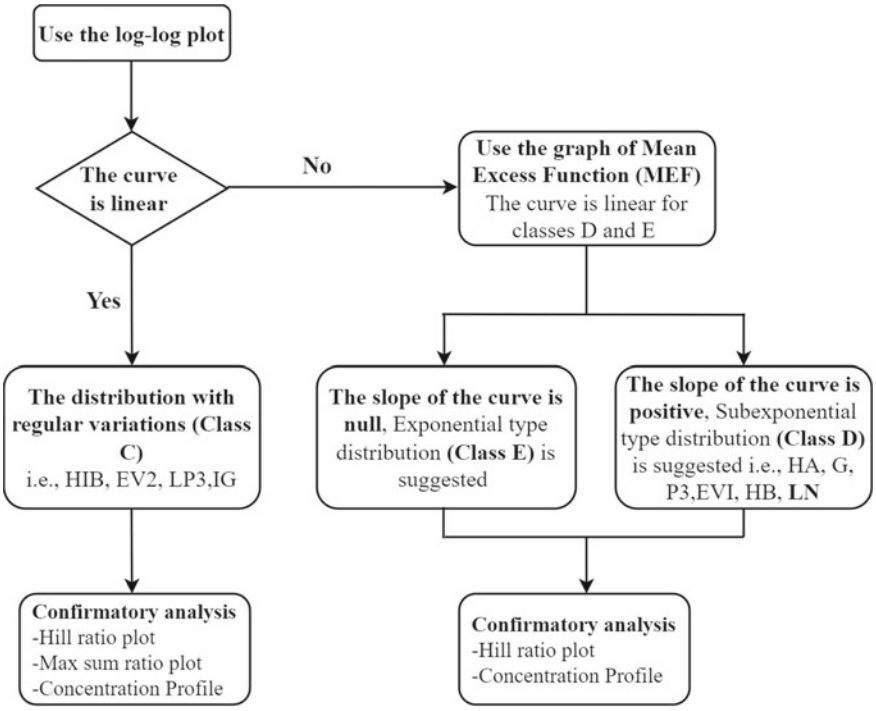

Fig. 1 Flow diagram showing the step-by-step procedure used for class discrimination in the DSS

2 Materials and Methods

2.1 Description of the Tail Discrimination Tools

This section provides a brief description of different graphical tools used in DSS. Embrechts et al. [21], Beirlant et al. [22], El Adlouni et al. [7], and Fontanari et al. [20] can be referred to for more comprehensive details of these methods. However, few important properties of each method used in DSS are presented in the following sections, which help us understand their role in selecting the appropriate class of distributions for any sample data.

2.2 Log–Log Plot

The log–log plot is a plot between the log of the empirical survival function and the log of the ordered values (u). This plot suggests that the tail probability for power-law type distribution (i.e., class C distributions) is represented by linearly decreasing behavior of the plot; however, such behavior is not observed for other classes like class D or class E (i.e., subexponential or exponential type distribution). To improve the interpretability of these plots, a linear fit is proposed, and an assessment based on the associated correlation coefficient is recommended. This plot helps us distinguish the distributions belonging to class C from classes like Classes D and E. However, it cannot discriminate between subexponential and exponential classes.

2.3 Mean Excess Function Plot (MEF)

The plot of the MEF (Embrechts et al. [21]) is based on the behavior of the function $e(u)$ given as:

$$e(u) = E[X - u | X > u] = \frac{\int_u^{\infty} (t-u) \mathrm{d}F(t)}{\mathrm{d}F(t)}, \quad 0 < u < x_F \tag{1}$$

where X is a random variable with distribution function F and right endpoint x_F such that $x_F = \sup\{x \in R\colon F(x) < 1\}$. The function $e(u)$ is called the mean excess function of X. For the Exponential distribution (light-tailed), the graphical representation of MEF is linear and constant. While, for the subexponential distribution (heavy-tailed), the tail function has a slope greater than zero (positive slope). This plot distinguishes the distributions of class D from class E\D (i.e., the distribution that belongs to class E but not class D) and hence, forms the basis for characterizing the distribution belonging to class D.

2.4 The Max-Sum Ratio Plot

The "max-sum" ratio plot is simply based on the consequence of the law of large numbers [23]. It suggests that for a sequence $X_1, X_2, \ldots, X_n$ of nonnegative i.i.d random variables, if for $p = 1, 2, 3 \ldots, n,\ E[X^p] < \infty$, then $R_n = M_n^p / S_n^p \to 0$ as $n \to \infty$, where $M_n^p = \max(X_1^p, \ldots, X_n^p)$ is the partial maximum of order p and $S_n^p = \sum_{i=1}^n X_i^p$ is the partial sum of order p. For visualization, the max-sum ratio R_n is plotted against n for several values of p. If the $R_n(p)$ jumps up and does not converge to zero for any p exceeding p_0, the presence of power-law type tail is indicated with tail index $\alpha = p_0$. For example, if for $p = 1, 2, 3, 4$, the $R_n(p)$ does not converge to 0, it shows the absence of existence of any finite moment for the variable. It is deemed that in such cases, we are dealing with such a fat-tailed phenomenon that that not even the first theoretical moment is finite, propounding that the inferences from the sample average and standard deviation are meaningless. The convergence of all the curves to zero suggests that the distribution does not belong to class C of regularly varying distributions. Hence in this study these plots are used to discriminate and characterize the distributions of class C only that do not belong to class D.

2.5 Generalized Hill Ratio Plot

Hill estimator is a classic non-parametric tail index estimator used especially for Pareto type distribution ($\xi > 0$) having an exact power-law type tail. This method suggests that a_n given in Eq. (2) is a consistent estimator of the tail index α if the tail is of regularly varying type (i.e., Class C) [13]. Let

$$a_n(x_n) = \frac{\sum_{i=1}^n I(X_i > x_n)}{\sum_{i=1}^n \log(X_i/x_n) I(X_i > x_n)} \tag{2}$$

where, I is an indicator function given as $I(X_i > x_n) = \left\{ \begin{array}{l} 1 \text{ if } X_i > x_n \\ 0 \text{ if } X_i < x_n \end{array} \right\}$.

For the understanding and visual assessment, $a_n(x_n)$ is plotted as a function of x_n and the plot is searched for some stable region. The region where $a_n(x_n)$ is stable tells us about an estimate of α. This plot is helpful in characterizing the distributions of class C by discriminating them from the distribution of class D\C. The Hill ratio plot converges to some non-zero constant value for the distribution of class C while it converges to zero for the subexponential distributions that do not have a power-law type tail (i.e., class D\C) [8].

2.6 Method Based on Concentration Profile

This plot is a tool based on the concept of using the concentration (or inequality) measure to analyze the risk dispersed in the tail. Concentration profile (CP) denoted by $G(\lambda)$ is a sequence of truncated Gini indices that can be used to discriminate and characterize different probability distribution tails. To form a concentration profile, all the observations in a sample are sorted in increasing order, and the Gini index [24] is computed recursively for the sample, excluding some points on the left-hand side. A sufficient number of observations denoted by k are required in the right tail while using this method. Generally, k varies between 1–5% of the originally ordered data points. A collection of exceedance distributions is obtained at every single observation, from left to right, by truncating the distribution. For different distributions Gini index is computed at different truncation levels λ, which indeed results in a truncated Gini index compared to the original distribution. Details of the theoretical CPs for some important distributions used in hydrology are given in Table 1. CP is an effective tool for characterizing distributions of class B (having a Pareto-type tail). Consequently, it discriminates the distribution of class C (for which tail decline asymptotically as power function) with that of class D, which does not have a power-law type tail. Also, this method can easily identify distribution from class E and the limiting distribution like lognormal.

The CP of some distributions eases their identification due to some peculiar characteristics, for example, the CP of the Pareto distribution is a constant slope horizontal line, where the height of the line varies according to the shape parameter of the distribution. Similarly, the CP of Exponential distribution always has an initial value of 0.5, for $\lambda = 0$. With the increase in the truncation level, it tends to decrease towards zero, first convexly and then concavely. The CP of Weibull distribution is also related to exponential CP. CP for a Weibull distribution with shape parameter $\alpha > 1$ (i.e., light-tailed distribution) particularly lies below the exponential CP, while Weibull with $\alpha < 1$ (i.e., heavy-tailed distribution) has a CP which lies uniquely above the exponential CP; in both cases, they do not intersect the exponential CP. For the lognormal CP, the case when shape parameter $\sigma < 1$, the starting point of the lognormal CP is below 0.5, i.e., $G(0) < 0.5$; while the case when $\sigma > 1$ the lognormal CP usually starts with $G(0)$ lying above 0.5. Compared to the CP of the Weibull distribution, the CP for a lognormal distribution is flatter, indicating that its tail decreases more slowly than the latter. For the light-tailed domain, CP exhibits a quick decreasing behavior (quick variability) with $G(0) < 0.5$.

Table 1 Theoretical CPs for some distributions used in this study

Distribution	Concentration profile $G(\lambda)$
Lognormal	$G(\lambda) = \frac{\int_{\lambda}^{1} (-1+2x-\lambda) e^{-\sqrt{2}\sigma erfc^{-1}(2x)} \mathrm{d}x}{(1-\lambda)\int_{\alpha}^{1} e^{-\sqrt{2}\sigma erfc^{-1}(2x)} \mathrm{d}x}$
Exponential	$G(\lambda) = \frac{1}{2-2\log(1-\lambda)}$
Pareto	$G(\lambda) = \frac{1}{2p-1} \; for \; p \in (1, +\infty)$

3 Study Area and Data Source

3.1 Mahanadi River Basin

The study area is an inter-state river basin known as the Mahanadi River basin (area $\approx$ 141,589 km^2) located in eastern India. The total catchment area of the basin spreads mainly over five States, namely Chhattisgarh, Orissa, Madhya Pradesh, Jharkhand, and Maharashtra. More than 99% of the Mahanadi catchment extends over Chhattisgarh and Orissa. Mahanadi basin experiences climate-induced hydrological extremes, which affect the availability of irrigation and drinking water supplies. Rainfall in the basin ranges between 1200–1400 mm, with an annual average of about 1291.92 mm. Hirakud reservoir, situated on the bank of the river Mahanadi, receives its inflow from the upper and middle parts of the sub-basins. It is one of India's biggest storage reservoirs and an essential infrastructure that ensures water security in the basin. The study is carried out for the entire basin.

3.2 Data Collection

The daily gridded data on rainfall were made available by IMD, Pune, for the entire basin ranging over 119 years (1901–2019) at 0.25° resolution. The precipitation data were collected from 6955 rain gauge stations installed across India [25], and the gridded data was developed using Inverse Distance Weighting (IDW) method. This latest data of 0.25° $\times$ 0.25° until 2019 is superior in representing the large-scale climatological features of rainfall over India.

The Mahanadi River basin and the 195 rainfall grids in the basin considered for the study are shown in Fig. 2. For this study, the annual maximum rainfall series is prepared from daily data for each grid lying in the catchment for the period 1901–2019 to investigate the suitability of the DSS methodology.

4 Results and Discussions

The data classification approach was utilized and checked for the validity of its application to the annual maximum precipitation series in the Mahanadi River basin for the time period 1901–2019. For demonstration purposes, different graphical tools used to assess the best-suited class for the sample data (i.e., the annual maximum precipitation database) at two IMD grid points numbered 62 (latitude 22.25°N and longitude 82.5°E), and 76 (latitude 20.75°N and longitude 83°E) are described as case studies. Figures 3 and 4 shows the result of the different graphical criteria (or tools) assessed for selecting the best-suited distribution class (heavy or light) for the dataset available at both the grids, respectively. As per the algorithm, we start

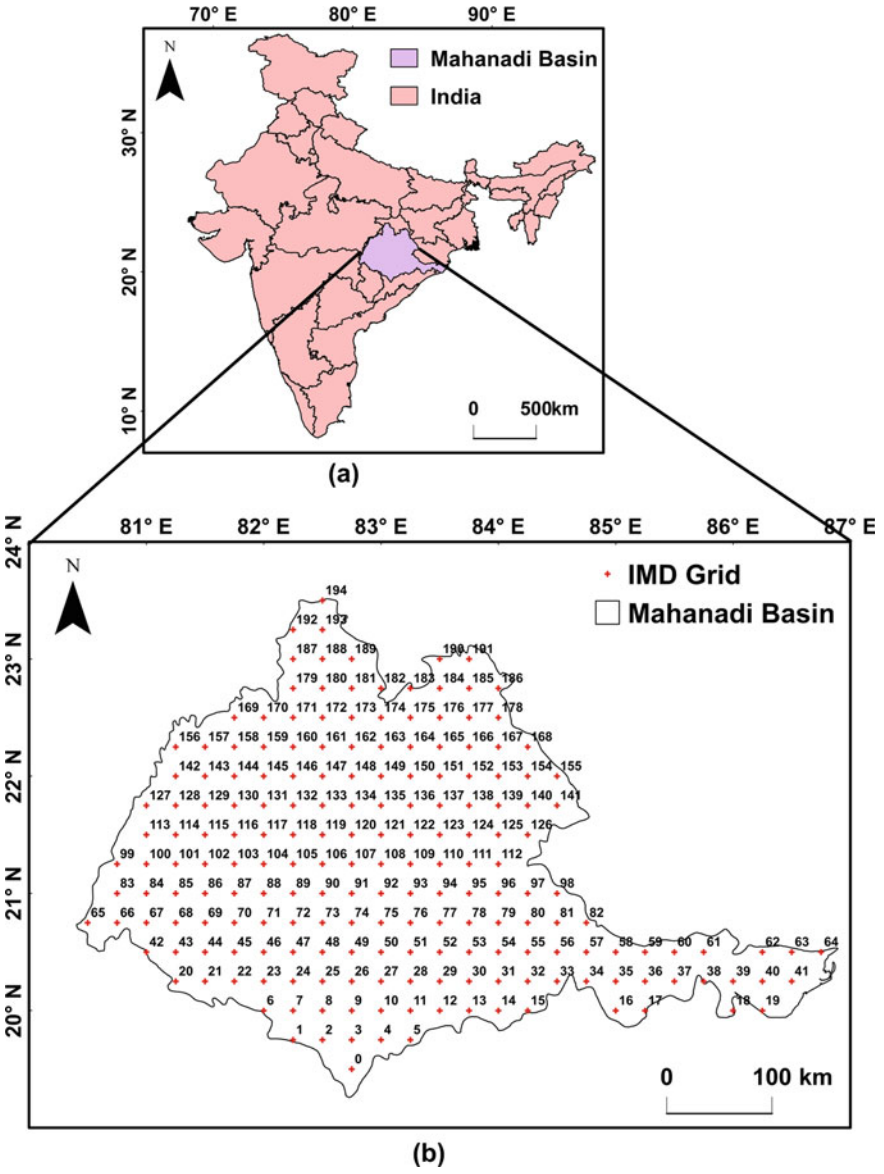

Fig. 2 Study area map along with the numbered IMD grids lying within the study area

with the log–log plot; tail probability in the case of power-law type distribution (i.e., class C) is represented by a linearly decreasing straight line but not for other classes (i.e., class D or E), respectively. If the slope of the log–log plot is not linear, another test, namely the MEF plot, is needed to be used. Figures 3a and 4a illustrate the log–log plot at IMD grids 162 and 76, respectively. The images reveals that

the observations for grid 162 follow a straight line more closely than those at grid 76. Hence, class C distributions (for example, Fréchet, Inverse gamma, log Pearson type 3), also known as regularly varying distributions, are suggested for this grid. In the case of grid point 76, the observations do not seem to appear as a straight line, suggesting that the sample is not from class C. We then use the MEF plot as per our DSS algorithm (see Fig. 1) for further characterization of the classes. The use of the MEF plot indicates that the sample data at grid point 76 might belong to either the subexponential (or exponential) class but not to the regularly varying class. As per the MEF plot, a linear plot with a slope equal to zero suggests an exponential type distribution, while a positively sloped linear MEF plot suggests a subexponential type distribution. Figure 4b reveals that the MEF plot for the dataset at grid 76 has a linear slope greater than zero, which helps us to assess that the class D distributions (i.e., Halphen A, Gumbel, Gamma, or Pearson Type 3) are best-suited for this grid point. Other tools like Hill ratio plot, Max-sum ratio, and CP were plotted for each grid as per their use mentioned above in the algorithm. These tools were also used by El Adlouni et al. [7], Ehsanzadeh et al. [8], and Fontanari et al. [20] to confirm the suggested choice given by the first two diagrams.

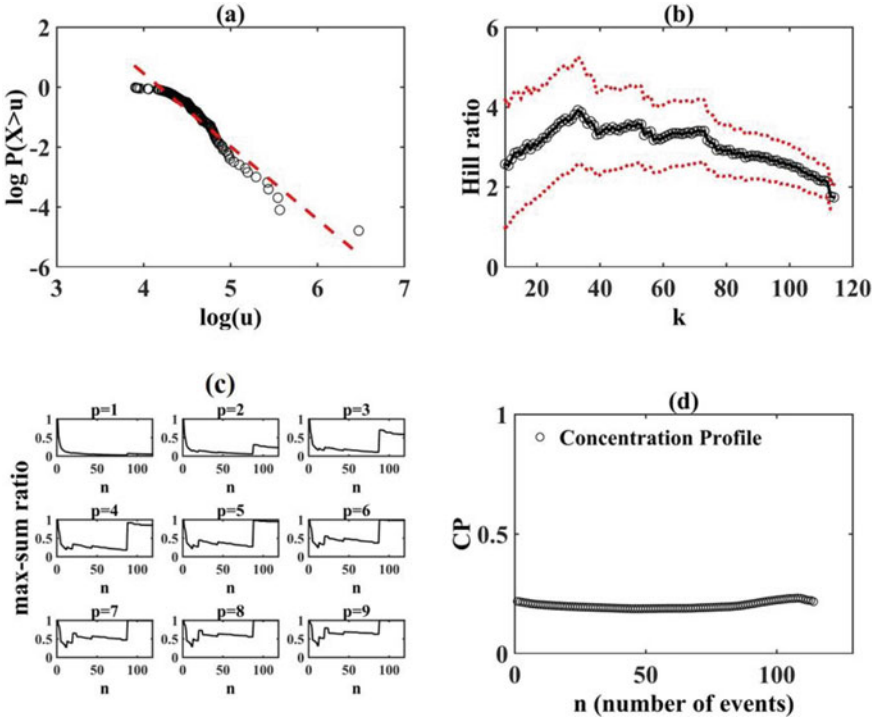

Fig. 3 Graphical criteria like log–log plot, hill ratio plot, max-sum ratio plot, and concentration profile for IMD grid point 162 (latitude 22.25°N and longitude 82.5°E)

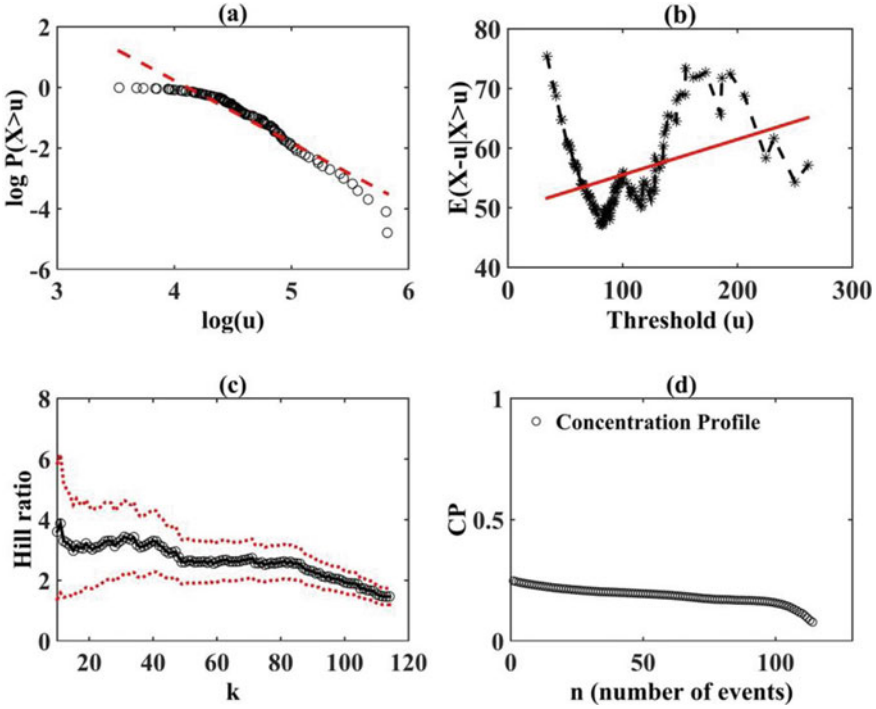

Fig. 4 Graphical criteria like log–log plot, Mean Excess plot, hill ratio plot, and concentration profile for IMD grid point 76 (latitude 20.75°N and longitude 83°E)

Figure 3b–d shows the Hill ratio plot, Max-sum ratio, and CP plot for grid point 162, while, Fig. 4c, d shows the Hill ratio plot and CP for grid point 76. The convergence of Hill's ratio plot towards a value different from zero at grid 162 (see Fig. 3b) confirms that the sample data can be adequately modeled by distributions of class C. Nevertheless, the convergence in the Hill ratio plot towards zero suggests that the underline distribution can be of subexponential or exponential type (i.e., class D or E), which is the case for grid point 76 (see Fig. 4c). The findings of the Hill plot confirm the one obtained previously from the log–log plot for both the grid point, respectively. Further, the max–sum ratio plot for grid point 162 (see Fig. 3c) illustrates that the max-sum ratio shows no convergence towards zero for values of p greater or equal to 3, thus confirming the characterization of the sample data as regularly varying type (i.e., Class C). Also, for grid point 162, CP exhibits nearly horizontal behavior (the last part of the plot is to be ignored for the limited amount of points considered), which can be seen as a signal of Paretian tails, signifying that the underlying distribution is of power-law type (i.e., having tail asymptotically similar to class B). Above mentioned criteria confirm that the probability distribution model at grid 162 belongs to class C. The CP of grid point 76 starts with $G(0) < 0.5$ and is decreasing and flatter in nature, suggesting a lognormal distribution which is included

in the subexponential class D. This observation is consistent with the decision made by log–log plot, mean excess function plot and Hill ratio plot in categorizing this station to classes D or E but not in class C. Lognormal distribution (LN2) is considered to have an asymptotic tail behavior such that it lies at the frontier of class C and D. The tail of the lognormal distribution is lighter than the tail of distributions in class C and heavier than those in class D. Cases where the true distribution of the sample data is of regularly varying type (class C), the use of LN2 distribution may results in estimated quantile lower than the actual value for a fixed return period, resulting in underestimation of the risk. However, for cases where the true distribution of the sample data belongs to Class D, the use of the LN2 distribution may overestimate quantiles. For this study, LN2 was considered as a member of Class D, keeping in mind the conservative outlook for the quantile estimation study (i.e., overestimation and consequently lower risk but higher costs).

Following the procedure outlined in the algorithm, IMD annual maximum precipitation database was classified into three classes of distribution (C–E). It was found that the application of DSS resulted in categorizing 49 (25.12%) grids in class C, 93 (47.69%) grids in class D, and 53 (27.17%) grids in class E out of 195 grids for which sample data was available. The characterization of the majority of the distribution in heavy-tailed classes (i.e., class C and D) suggests that the frequency and magnitude of extreme in the Mahanadi basin is high. CP was helpful enough to identify and categorize sample data in Class E; we see no need for any other statistical analysis for such a case.

5 Conclusions

Following conclusions are derived from this study:

- Different graphical techniques can be used with ease to classify different classes of distribution, especially Class C (regularly varying distributions), Class D (subexponential distributions), and Class E (exponential distribution). The decision support system is an effective and easy-to-use tool for discriminating distribution tails.
- All five methods considered in the study, namely the log–log plot, mean excess function plot, max–sum ratio plot, Hill ratio plot, and concentration profile lead to an accurate conclusion about the class of distribution at the different grid points.
- All methods except the empirical mean excess function can discriminate among class C and class D. The empirical mean excess method and concentration profile can detect exponential type tails.
- Findings of the study illustrate the potential of graphical tools in selecting an adequate class of distributions for representing the sample extremes.

- The use of concentration profile eases identifying the samples with Lognormal distribution, which have tail similarity with regularly varying distributions. From the point of view of conservative analysis regarding quantile estimation, lognormal distribution was included in Class D.
- Choice of the candidate distributions within any class can be made for any variable of interest by comparing different possible models within the class using criteria such as the Anderson darling test, Akaike Information Criterion, Bayesian Information Criterion, or New model selection test (NMST).

Acknowledgements The authors are grateful to the Indian Institute of Technology (IIT) Ropar for providing funding to procure data and facilitate this research. The authors are also thankful to India Meteorological Department (IMD) for providing precipitation data for this research.

References

1. Gupta N, Chavan SR (2021) Assessment of temporal change in the tails of probability distribution of daily precipitation over India due to climatic shift in the 1970s. J Water Clim Change 12(6):1492–1517. https://doi.org/10.2166/wcc.2021.008
2. IPCC (2018) Summary for Policymakers. In: Global warming of 1.5 °C. An IPCC special report on the impacts of global warming of 1.5 °C above pre-industrial levels and related global greenhouse gas emission pathways, in the context of strengthening the global response to the threat of climate change, sustainable development, and efforts to eradicate poverty. World Meteorological Organization, Geneva, Switzerland, p 32
3. Papalexiou SM, Koutsoyiannis D, Makropoulos C (2013) How extreme is extreme? An assessment of daily rainfall distribution tails. Hydrol Earth Syst Sci 17(2):851–862. https://doi.org/10.5194/hess-17-851-2013
4. Papalexiou SM, AghaKouchak A, Foufoula-Georgiou E (2018) A diagnostic framework for understanding climatology of tails of hourly precipitation extremes in the United States. Water Resour Res 54(9):6725–6738. https://doi.org/10.1029/2018WR022732
5. Nerantzaki S, Papalexiou SM (2019) Tails of extremes: advancing a graphical method and harnessing big data to assess precipitation extremes. Adv Water Resour 134:103448. https://doi.org/10.1016/j.advwatres.2019.103448
6. Gupta N, Chavan SR (2021) Characterizing the tail behaviour of daily precipitation probability distributions over India using the obesity index. Int J Climatol 42(4):2543–2565. https://doi.org/10.1002/joc.7380
7. El Adlouni S, Bobée B, Ouarda TBMJ (2008) On the tails of extreme event distributions in hydrology. J Hydrol 355(1–4):16–33. https://doi.org/10.1016/j.jhydrol.2008.02.011
8. Ehsanzadeh E, El Adlouni S, Bobée B (2010) Frequency analysis incorporating a decision support system for hydroclimatic variables. J Hydrol Eng 15(11):869–881. https://doi.org/10.1061/(ASCE)HE.1943-5584.0000261
9. Ouarda TBMJ, Ashkar F, Bensaid E, Hourani I (1994) Statistical distributions used in hydrology. Transformations and asymptotic properties. Scientific Report 31, Department of Mathematics, Univ. of Moncton, New Brunswick
10. Werner T, Upper C (2004) Time variation in the tail behavior of Bund future returns. J Futur Mark 24(4):387–398
11. Champernowne D (1953) A model of income distribution. J Econ 63:318–351
12. Martel B, El Adlouni S, Bernanrd B (2013) Comparison of the power of lognormality tests with different right-tail alternative distributions. J Hydrol Eng 18(1):1–9. https://doi.org/10.1061/(ASCE)HE.1943-5584.0000595

13. Hill BM (1975) A simple general approach to inference about the tail of a distribution. Ann Stat 1163–1174
14. Ghosh S, Resnick S (2010) A discussion on mean excess plots. Stochast Process Appl 120(8):1492–1517
15. Nieboer D (2011) Heuristics of heavy-tailed distributions and the obesity index. Dissertation, Delft University of Technology
16. Cooke RM, Nieboer D, Misiewicz J (2014) Fat-tailed distributions: data, diagnostics and dependence. Wiley, Hoboken, NJ
17. Roth M, Jongbloed G, Buishand TA (2016) Threshold selection for regional peaks-over threshold data. J Appl Stat 43(7):1291–1309. https://doi.org/10.1080/02664763.2015.1100589
18. Das B, Ghosh S (2016) Detecting tail behavior: mean excess plots with confidence bounds. Extremes 19(2):325–349. https://doi.org/10.1007/s10687-015-0238-9
19. Bonetti M, Cirillo P, Musile TP, Trinchero E (2016) An analysis of the number of medical malpractice claims and their amounts. PLoS ONE 11(4):e0153362. https://doi.org/10.1371/journal.pone.0153362
20. Fontanari A, Cirillo P, Oosterlee CW (2018) From concentration profiles to concentration maps. New tools for the study of loss distributions. Insur Math Econ 78:13–29. https://doi.org/10.1016/j.insmatheco.2017.11.003
21. Embrechts P, Klüppelberg C, Mikosch T (2003) Modelling extremal events for insurance and finance applications of mathematics. Springer, Berlin, Germany, p 648
22. Beirlant J, Goegebeur Y, Segers J, Teugels JL (2006) Statistics of extremes: theory and applications. Wiley
23. Cirillo P, Taleb NN (2020) Tail risk of contagious diseases. Nat Phys 16(6):606–613
24. Gini C (1912) Variabilità E Mutabilità. Reprinted in: Variabilità e Mutabilità, E Pizetti and T Salvemini, Memorie di Metodologica Statistica, Libreria Eredi Virgilio Veschi, Rome
25. Pai D, Sridhar L, Rajeevan M, Sreejith OP, Satbhai NS, Mukhopadhyay B (2014) Development of a new high spatial resolution (0.25° × 0.25°) long period (1901–2010) daily gridded rainfall data set over India and its comparison with existing data sets over the region. Mausam 65(1):1–18. https://doi.org/10.54302/mausam.v65i1.851

Application of Three Parameter Muskingum Method on Karun River

Nisanta Bhatta, Armandev Puhan, and K. K. Khatua

Abstract An efficient modification of the Muskingum method of flood routing has been verified, which yields the coefficients of Muskingum flood routing equation directly without the use of the graphical procedure. A simple conceptual model of lateral inflow has also been incorporated to account for any lateral inflow or outflow that occurs in the given reach. The incorporation of lateral inflow has been considered through a lateral inflow parameter along with the standard storage and weighing parameters, K and x. It also presents a much effective and direct approach for estimating the routing coefficients for the Muskingum model. Application of this extended Muskingum method has been verified on Karun river of Iran and the respective 6-h hydrograph has been plotted. It showed that the usual curb on the routing coefficients to sum to unity is not applicable in case of lateral inflow. The estimated outputs showed close correlation with the observed outflow.

Keywords Flood routing · Hydrologic model · Muskingum method · Lateral inflow

1 Introduction

Flood routing is the technique which is used to determine the hydrograph of a river section by employing the data of the upstream section. Routing allows us to solve various problems including flood by flood forecasting and reservoir and spillway design. Muskingum method is a hydrological flood routing model which describes the evolution of discharge waves in a river. There has been ample full of research that has been conducted which are related to the prediction and estimation of the two parameters K and x [1].

In the basic procedure, there is no inference to the lateral inflow along the reach through which a flood is being routed. Due to the presence of the tributaries of a river,

N. Bhatta · A. Puhan · K. K. Khatua (✉)
Department of Civil Engineering, National Institute of Technology Rourkela, Rourkela 769008, India
e-mail: kkkhatua@nitrkl.ac.in

P. V. Timbadiya et al. (eds.), *Flood Forecasting and Hydraulic Structures*, Lecture Notes in Civil Engineering 340, https://doi.org/10.1007/978-981-99-1890-4_23

the consideration of a lateral inflow is of paramount importance. The present study attempts to verify a three parameter model along with a direct way of estimating the Muskingum routing coefficient proposed by O'Donnell [2].

2 Materials and Methods

2.1 Basic Muskingum Method

In the basic Muskingum model, the terms relating to input to the reach, output from the reach, and storage in the reach can be related through a continuity equation:

$$I = O + \frac{\mathrm{d}S}{\mathrm{d}t}. \tag{1}$$

And by an empirical storage equation:

$$S = K\left[xI^m + (1-x)Q^m\right].$$

Taking $m = 1$, the equation simplifies to

$$S = K[xI + (1-x)O]. \tag{2}$$

In these equations, I is the rate of inflow, O is the rate of outflow, S is the storage, K is storage coefficient, and x is a weighing factor. It can be noted from the preceding equations that there is no reference to the lateral inflow. If we incorporate nonlinear Muskingum model, the value of m will not be equal to unity and the value of coefficients will change accordingly.

When we express (1) and (2) in a finite difference form for an interval of time, ΔT it leads to an equation:

$$O_{j+1} = c_1 I_j + c_2 I_{j+1} + c_3 O_j. \tag{3}$$

This equation allows the estimation of the outflow from the reach at the end of the time interval. The coefficient of Eq. (3) can be defined as.

$$C_1 = \frac{\Delta T + 2Kx}{\Delta T + 2K(1-x)}; C_2 = \frac{\Delta T - 2Kx}{\Delta T + 2K(1-x)}$$
$$C_3 = \frac{-\Delta T + 2K(1-x)}{\Delta T + 2K(1-x)} = 1 - C_1 - C_2. \tag{4}$$

The value of the parameters K and x can be found out by a trial and error graphical technique [3, 4]. Plot between S and $[xI + (1-x)O]$ is made with approximate value

of x considering the slope of the reach. The plot which is almost a straight line is chosen, and the corresponding value of x is adopted. The slope of the graph is taken as K.

2.2 Extended Muskingum Method

When we assume that there is no lateral inflow, then

$$\int I \mathrm{d}t = \int O \mathrm{d}t. \tag{5}$$

From here we can say that the change in storage is zero. The integration can be replaced with summation

$$\sum I = \sum O. \tag{6}$$

Considering there are n time intervals in the total time duration of the summation given in Eq. (6) which will yield n equations in the form given in (3) which can be written as

$$\begin{aligned}
O_2 &= c_1 I_1 + c_2 I_2 + c_3 O_1 \\
O_3 &= c_1 I_2 + c_2 I_3 + c_3 O_2 \\
&\vdots \\
O_{j+1} &= c_1 I_j + c_2 I_{j+1} + c_3 O_j \\
&\vdots \\
O_{n+1} &= c_1 I_n + c_2 I_{n+1} + c_3 O_n.
\end{aligned} \tag{7}$$

Adding all the sets of (7) and expressing it in the form of an equation

$$\sum_{2}^{n+1} O = c_1 \sum_{1}^{n} I + c_2 \sum_{2}^{n+1} I + c_3 \sum_{1}^{n} O. \tag{8}$$

We know that the summation of coefficients of basic Muskingum equation is always unity

$$1 = c_1 + c_2 + c_3.$$

When we incorporate lateral inflow, we know that apart from the water coming as an input from the main source there also be some amount of water that will be coming as a lateral inflow. We can say that there is a gain in the total input. Hence,

we multiply a gain factor r with the input

$$\sum I = r \sum O. \tag{9}$$

By neglecting the end ordinate effects, we may use (8) and (9) to yield

$$r = c_1 + c_2 + rc_3. \tag{10}$$

Now coming back to the second drawback, that is, approximation of coefficients by the use of graphical method which is time taking and prone to user error. We can use the n equations formed involving three unknown coefficients: d_1, d_2, and d_3. The equations are over-determined and can be solved efficiently to give the values of coefficients directly by using a matrix procedure [5].

Matrix formulation of (7)

$$\left|O_{j+1}\right| = \left|I_j \quad I_{j+1} \quad O_j\right|.|d_i|. \tag{11}$$

Let $|P| = \left|I_j \quad I_{j+1} \quad O_j\right|$ we will here get a matrix of n rows and 3 columns.

Multiplying both the sides by $|P|^{\mathrm{T}}$. We get

$$|P|^{\mathrm{T}}.\left|O_{j+1}\right| = |P|^{\mathrm{T}}|P|.|d_i|. \tag{12}$$

Again let us take $|Q| = |P|^{\mathrm{T}}.\left|O_{j+1}\right|$. It will yield a vector having 3 elements and $|R| = |P|^{\mathrm{T}}|P|$, which will give a 3×3 matrix which is inverted to get the values of the coefficients

$$|d_i| = |R|^{-1}.|Q|. \tag{13}$$

It is very interesting to note that without losing any information of the equations it has been condensed into a 3×3 matrix and values of the coefficients and be derived from them.

2.3 *Lateral Inflow Model*

The simplest assumption that can be made is the rate of lateral inflow is proportional to rate of inflow to the reach and the proportionality factor is taken as α. Such an assumption can be seen in the UK Flood Studies Report [Gain factor r is equal to $(1 + \alpha)$].

The continuity and empirical storage equations can be rewritten as

$$I(1 + \alpha) = O + \frac{\mathrm{d}S}{\mathrm{d}t} \tag{14}$$

$$S = K[x(1+\alpha)I + (1-x)O]. \tag{15}$$

After changing the coefficients of conventional Muskingum method to the extended Muskingum method (3) can be rewritten as

$$O_{j+1} = d_1 I_j + d_2 I_{j+1} + d_3 O_j. \tag{16}$$

The values of the coefficients of d_i can now be used to estimate the values of parameter K, x and α with the help of following formulae

$$K = \Delta T \frac{d_1 + d_2 d_3}{(1-d_3)(d_1+d_2)}; \quad x = \frac{1}{2}\left\{1 - \frac{d_2 + d_1 d_3}{d_1 + d_2 d_3}\right\}$$
$$\alpha = \frac{d_1 + d_2 + d_3 - 1}{1 - d_3}. \tag{17}$$

Though the values of d_i are it are itself enough to plot the reconstructed outflow but the other parameters can be used to compare the method with other methods.

We can also deduce

$$d_1 = (1+\alpha)\frac{\Delta T + 2Kx}{\Delta T + 2K(1-x)} = (1+\alpha)c_1$$
$$d_2 = (1+\alpha)\frac{\Delta T - 2Kx}{\Delta T + 2K(1-x)} = (1+\alpha)c_2$$
$$d_3 = \frac{-\Delta T + 2K(1-x)}{\Delta T + 2K(1-x)} = c_3. \tag{18}$$

As we would expect the conventional Muskingum method will become a special case of this method when value of lateral inflow parameter (α) will be equal to zero. We can also include a condition where instead of lateral inflow, lateral outflow occurs, and in this very case, the lateral inflow parameter (α) will return a negative value implying outflow.

2.4 Study Area and Data Source

2.4.1 Karun River Basin

The study area is Karun river basin (area $\approx$ 65,230 km^2) which originates in the Zard Kuh mountains in Zagros Range of western Iran at latitude of 30°26′ N and longitude of 48°10′ E in the Bakhtiari district of Iran. The index map of the Karun River basin is shown in Fig. 1.

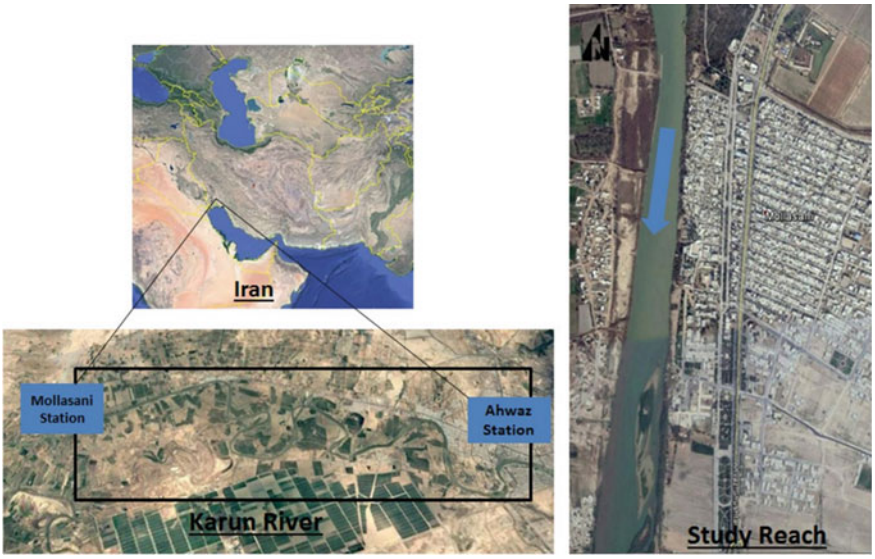

Fig. 1 Index map of study area [6]

2.4.2 Data Collection

The inflow and outflow data for Karun River used in this study has been obtained from two hydrometric stations of Mollasani and Ahwaz located on the U/S and D/S, respectively, of the Karun River reach, Iran, by the research department of Iran Water Resources Management Co. The data was collected from a previous research paper "Investigation the effect of using variable values for the parameters of the Linear Muskingum method using the particle swarm algorithm (PSO)" by Bazargan and Norouzi [6].

2.5 Selection of Input Parameters

The input parameters were selected based on the storage and morphology of the River. For the present study, K, x, α, and Δt are used as input parameters for estimating the outflow hydrograph. Here, K is the storage coefficient, x is the weighing factor, α is the lateral inflow coefficient, and Δt is the time interval. The data recorded from 30/11/2008 to 03/12/2008 was used to estimate the parameters of the extended Muskingum method.

3 Results and Discussions

The detailed application of the extended Muskingum model has been carried out for the data collected on the Karun River after incorporating the factor for lateral inflow. The values of d_1, d_2, and d_3 are calculated by matrix inversion analysis method using MATLAB programming. K, x, and α values are the calculated from equations given in (17). The reconstructed outflow data for $\Delta t = 6$ h can be seen in Table 1. It is observed that the reconstructed outflow values show quite resemblance with the recorded outflow data. The plot of recorded and reconstructed outflow hydrographs can be seen in Fig. 2.

For further analysis, the outflow data has also been reconstructed for $\Delta t = 1$ h, 2 h, 3 h, and 4 h, and it can be seen in Table 2. The only flaw that is observed is that initially the storage formula in (2) corresponds to the linear Muskingum model

Table 1 Recorded and reconstructed outflow for $\Delta t = 6$ h

Time (h)	Inflow (M^3s^{-1})	Outflow (m^3s^{-1})	Reconstructed outflow (m^3s^{-1})
0	105	108	108
6	110	110	102
12	117	112	104
18	201	113	112
24	446	131	176
30	788	236	363
36	1059	800	645
42	1154	922	903
48	1033	958	1034
54	920	925	992
60	775	860	903
66	650	770	780
72	527	677	660
78	424	588	543
84	340	509	441
90	277	436	355
96	233	373	288
		$\boldsymbol{d_1}$	**0.6343**
		$\boldsymbol{d_2}$	**0.036**
		$\boldsymbol{d_3}$	**0.2937**
		$\boldsymbol{K}$	**8.17273**
		$\boldsymbol{x}$	**0.327645**
		$\boldsymbol{\alpha}$	**− 0.05097**

Indicates the computed parameters.

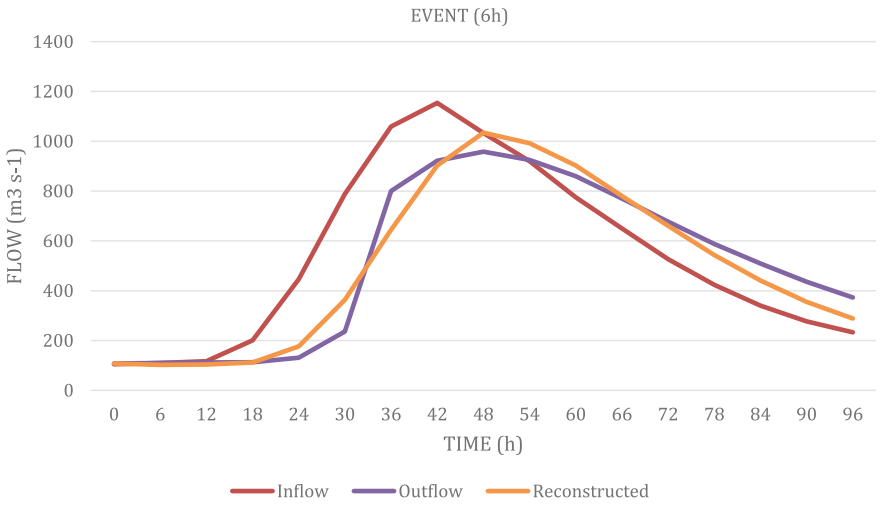

Fig. 2 Plot of recorded and reconstructed outflow for Karun River at $\Delta t = 6$ h

which is simplistic in nature and can be considered as a special case of nonlinear Muskingum model.

4 Conclusions

The following conclusions were obtained in the present study:

(i) The routing coefficient values found efficiently by the matrix inversion analysis of the recorded inflow and outflow data. In the least square sense, these coefficients are the best possible estimates.
(ii) It can also be inferred that the usual curb on the routing coefficients to sum to unity is not applicable in case of lateral inflow.
(iii) Further, this constraint doesn't affect the matrix technique, and the lateral inflow or lateral outflow is clearly indicated by the estimated routing coefficients.
(iv) The initial storage formula in Eq. (2) corresponds to the linear Muskingum model which is simplistic in nature and can be considered as a special case of nonlinear Muskingum model. Hence, an additional parameter can be incorporated to the storage equation and further modification of the coefficients of Eq. (3) can be done to increase the spectrum of the model [7].

Table 2 Recorded and reconstructed outflow for $\Delta t = 1$ h, 2 h, 3 h, and 4 h

Time (h)	Recorded event		Reconstructed outflow (m^3s^{-1})			
	I (m^3s^{-1})	O (m^3s^{-1})	$\Delta t = 1$ h	$\Delta t = 2$ h	$\Delta t = 3$ h	$\Delta t = 4$ h
0	105	108	108	108	108	108
1	106	108	107			
2	107	109	106	106		
3	107	109	106		105	
4	108	109	105	105		104
5	109	109	105			
6	110	110	105	105	104	
7	110	110	105			
8	111	110	105	105		103
9	111	110	105		104	
10	111	110	105	105		
11	114	111	105			
12	117	112	105	105	104	104
13	120	112	106			
14	122	112	107	106		
15	141	112	105		105	
16	160	112	106	105		105
17	177	113	110			
18	201	113	114	112	111	
19	227	114	120			
20	258	116	128	126		123
21	295	119	137		134	
22	340	122	149	147		
23	392	125	163			
24	448	131	182	179	176	172
25	505	137	204			
26	566	147	230	228		
27	627	158	260		254	
28	679	173	294	293		283
29	734	199	330			
30	788	236	369	368	368	
31	842	282	409			
32	895	357	450	451		449
33	943	428	493		496	
34	985	485	538	540		

(continued)

Table 2 (continued)

Time (h)	Recorded event		Reconstructed outflow (m^3s^{-1})			
	I (m^3s^{-1})	O (m^3s^{-1})	$\Delta t = 1$ h	$\Delta t = 2$ h	$\Delta t = 3$ h	$\Delta t = 4$ h
35	1024	542	582			
36	1059	800	626	631	635	637
37	1088	855	670			
38	1113	887	712	718		
39	1133	894	753		766	
40	1141	905	793	800		814
41	1150	915	828			
42	1154	922	862	870	880	
43	1138	928	894			
44	1124	928	920	930		948
45	1101	934	943		965	
46	1079	939	960	970		
47	1059	949	972			
48	1033	958	981	991	1002	1012
49	1018	944	985			
50	999	947	987	994		
51	981	946	986		1000	
52	962	934	984	989		1002
53	941	932	979			
54	920	925	973	977	982	
55	898	911	966			
56	876	909	956	959		964
57	855	898	945		949	
58	830	885	934	935		
59	806	872	921			
60	775	860	907	907	907	905
61	761	844	890			
62	737	831	874	871		
63	716	813	857		851	
64	693	801	839	836		827
65	671	784	821			
66	650	770	803	798	795	
67	620	754	786			
68	606	732	765	761		750

(continued)

Table 2 (continued)

Time (h)	Recorded event		Reconstructed outflow (m^3s^{-1})			
	I (m^3s^{-1})	O (m^3s^{-1})	$\Delta t = 1$ h	$\Delta t = 2$ h	$\Delta t = 3$ h	$\Delta t = 4$ h
69	586	725	745		737	
70	566	706	726	721		
71	546	691	707			
72	527	677	687	682	677	669
73	509	653	668			
74	491	639	649	643		
75	473	627	630		618	
76	456	612	611	605		591
77	440	600	592			
78	424	588	574	567	561	
79	408	577	556			
80	393	562	538	532		517
81	380	549	521		508	
82	366	535	504	497		
83	352	522	487			
84	340	509	471	464	458	450
85	328	497	455			
86	319	484	439	433		
87	308	472	425		412	
88	292	461	411	405		391
89	287	449	396			
90	277	436	383	376	372	
91	269	425	370			
92	259	415	358	351		337
93	252	404	346		335	
94	247	393	334	327		
95	241	383	323			
96	233	373	313	307	302	294
		$\boldsymbol{d_1}$	**0.2525**	**0.3344**	**0.4228**	**0.5239**
		$\boldsymbol{d_2}$	**− 0.1359**	**− 0.1022**	**− 0.0753**	**− 0.0573**
		$\boldsymbol{d_3}$	**0.8788**	**0.7578**	**0.6363**	**0.5093**
		$\boldsymbol{K}$	**9.416348**	**9.137914**	**8.898628**	**8.642833**
		$\boldsymbol{x}$	**0.176876**	**0.205766**	**0.241618**	**0.28824**
		$\boldsymbol{\alpha}$	**− 0.03795**	**0.04129**	**0.04454**	**0.04911**

Indicates the computed parameters.

Acknowledgements The authors acknowledge the research support and laboratory facilities received from Department of Civil Engineering, National Institute of Technology Rourkela, India.

References

1. Singh VP, McCann RC (1980) Some notes on Muskingum method of flood routing. J Hydrol 41:343–361
2. O'Donnell T (1985) A direct three-parameter Muskingum procedure incorporating lateral inflow. Hydrol Sci J 30(4):479–496
3. Linsley RK, Kohler MA, Paulhus JLH (1975) Hydrology for engineers. McGraw-Hill, London
4. Wilson EM (1983) Engineering hydrology. Macmillan, London
5. O'Donnell T (1966) Methods of computation in hydrograph analysis and synthesis. Recent trends in hydrograph synthesis, TNO Proc. No 13, TNO, The Hague
6. Bazargan J, Norouzi H (2018) Investigation the effect of using variable values for the parameters of the linear Muskingum method using the particle Swarm algorithm (PSO). Water Resour Manage 32:4763–4777
7. Stephenson D (1979) Direct optimisation of Muskingum routing coefficients. J Hydrol 41:161–165

Ensemble Flood Forecasting in India: Current and Future Prospects

Rashmi Yadav and Sanjaykumar M. Yadav

Abstract Flood forecasting plays a key role in the reduction of economic as well as life losses and is considered a challenging task in hydrology. Controlling the occurrence of extreme flood events is not in our hands, but deteriorating the losses is still conceivable. In India, the flood forecasting for most of the basins is based on the deterministic approach which needs to be strengthened for the early warnings and relief measure strategies. Over the world, the focus of the hydrologists and researchers is shifting in the direction of the implementation of ensembles of numerical weather predictions (NWP) for operational flood forecasting. India has made great achievements in building an ensemble prediction system for weather forecasting. Precipitation forecast is available at several spatial and temporal resolutions, but still, it needs improvement in the case of urban and smaller catchments. The paper discusses the need for the development of an integrated approach to hydrologic ensemble prediction system using meteorological forecasts, hydrological and hydraulic modeling, and post-processing for reliable early flood warning systems in India.

Keywords Ensemble · Numerical weather predictions · Operational flood forecasting · Flood warning systems

1 Introduction

Flood forecasting plays a critical role in the reduction of economic as well as life losses and is considered a challenging task in hydrology [1]. Analyzing the type and trends of high spatial and temporal variability of floods is crucial. In India, during the recent decades, many cities have faced extreme flooding, a few of them listed as

R. Yadav (✉) · S. M. Yadav
Department of Civil Engineering, Sardar Vallabhbhai National Institute of Technology, Surat, Gujarat 395007, India
e-mail: rashmiy276@gmail.com

S. M. Yadav
e-mail: smy@ced.svnit.ac.in

P. V. Timbadiya et al. (eds.), *Flood Forecasting and Hydraulic Structures*, Lecture Notes in Civil Engineering 340, https://doi.org/10.1007/978-981-99-1890-4_24

Hyderabad 2020, 2016, and 2000; Jaipur 2020; Surat 2006; Chennai 2015; Kerala 2020, 2019, and 2018; Kolkata 2020 and 2007 [2, 3]. Considering the time interval 1978–2006, a minimum of 44,992 fatalities happened as a consequence of 2444 flood events in India [4]. These are expected to increase over time due to the increasing population, land use and land cover changes, urbanization, unplanned settlement in the coastal or floodplain areas, climate change, and urban heat islands leading to more lives being vulnerable to flood disasters [5].

Presently, the methods which are adopted in India for the forecasting of floods are (i) Statistical correlations using the gauge to gauge, (ii) gauge-discharge data, (iii) multiple coaxial correlations by means of utilizing gauge, rainfall, and antecedent precipitation index (API) data. Intending flood forecasting, the Central Water Commission employs the models like HEC-HMS [6] and MIKE-11 [7–9] for hydrologic and hydrodynamic modeling. At present, CWC issues the flood warnings with a 72-h lead time.

2 Major Limitations of Flood Forecasting

(i) To manage flash floods, and spatial and temporal resolutions, in addition to the lead time, it must be improved in smaller watersheds and urban regions. CWC's current deterministic forecasting lead time in India is relatively short, up to three days. The accuracy and reliability of the predictions carried out for lead time greater than three days fall drastically and do not provide satisfactory results with the present deterministic approach.
(ii) Current models are incapable of reliably forecasting flash floods in urban areas and smaller catchments [10].
(iii) Deterministic flood forecasting systems do not incorporate meteorological and hydrological models.
(iv) Hydrologic forecasting in the ungauged basins [11–13].
(v) Computation of the uncertainties in the forecasts and incorporating them as a crucial component of warnings [14, 15]. The errors are not quantifiable in the observations (input), model structure, model parameters, or initial conditions.
(vi) Implementation of the flood forecasting warning systems [16]. (Communication systems and educational campaigns).

Around the world, the research and functioning of the flood forecasting systems are considerably giving more attention to the integration of meteorological and hydrodynamic modeling skills for higher reliability and accuracy [17]. An emerging technique of a reliable medium-range flood forecast can be the implementation of the ensembles of numerical weather prediction (NWP). A probabilistic forecast is presented in the form of a probability, such as one calculated by counting the number of ensemble members anticipating a certain occurrence [18].

Predicting the exact state of the atmosphere is not possible as the Earth's atmosphere is a complex and nonlinear system. Weather forecasts remain limited because

of the complexity in the numerical illustration of physical processes and sensitivity in outcomes of the pattern of initial conditions [19]. Two key qualities should be present in ensembles: accuracy and dependability, and the quality of their work should be assessed taking both into consideration [20]. Ensemble prediction system forecasts a high-rate product output with higher potential to extend the lead time and superior predictability. Ensemble methods allow the user to incorporate a set of predictions instead of using a single prediction [21]. The two approaches for that can be (i) combining various models to advance a single model, preferably can be called a multi-model ensemble, and (ii) using a single model but perturbing the starting point to give multiple inputs and produce multiple results.

3 Ensemble Techniques

The two methods for employing an ensemble can be (i) multi-model ensemble which can be explained as the combination of several models to advance a single model [22], and (ii) employing a single model but perturbing the initial conditions or parameters sceneries to give multiple inputs for producing multiple results.

For the advancement of the forecasting, ensemble techniques are proved as an efficient method [21]. The ensemble techniques are widely used in numerical weather prediction resulting in improved model accuracy and model uncertainty. Whatever the approach, whether multi-model or the perturbed initial conditions, the outcomes of these forecasting sets can subsequently be utilized in a variety of ways [23]. A basic scenario for probabilistic predictions is depicted in Fig. 1. Here, multiple forecast probabilities from diverse approaches are linearly united for the combination to generate the best ensemble forecast probability. Ensemble forecasting systems have the capacity to characterize the uncertainty that is essential in any forecast, which is a significant advantage.

The methods for creating ensemble prediction forecasts are rather simple. Numerous functioning ensemble prediction systems are centered on the Monte Carlo basis of numerical weather predictions as a result of a central investigation's discovery (the forecast of the control member) and others, which are created by altering the original circumstances (ensemble members or perturbed forecast) [24]. Figure 2 depicts the plot of discharge projected for individual ensemble forecast (solid line pointed as members), discharge that was noticed (pointed with the dashed black line), and four dashed horizontal lines presenting discharge warning lines (low warning level, medium waning level, high warning level, and extreme warning level).

Durai and Bhardwaj [25] used a multi-model ensemble technique for forecasting the quantitative precipitation over India. Authors considered a set of global NWP models, specifically ECMWF, JMA, GFS, and UKMO which are available globally, India's Meteorological Department in New Delhi used the data concurrently to achieve a multi-model ensemble (MME) approach with appropriate weights. In addition, a basic ensemble mean forecast is created and evaluated. The study's main goal was to assess the MME rainfall forecast skill development across India in a

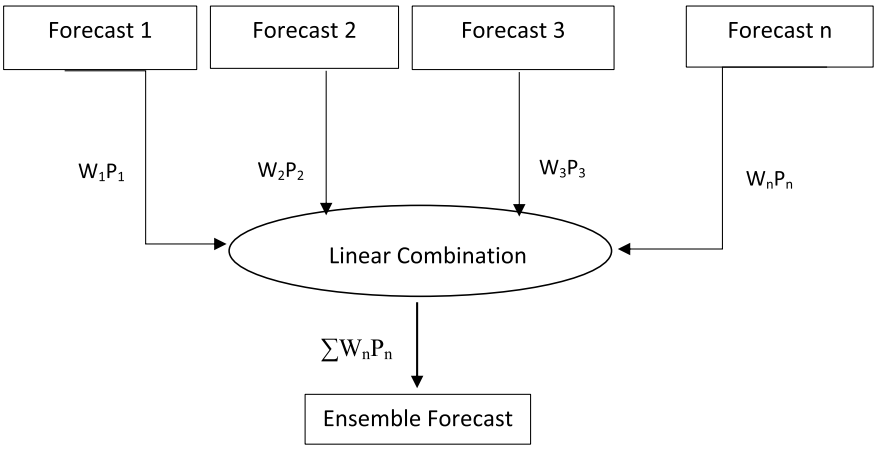

Fig. 1 Framework of a simple example for probabilistic predictions, where W_n represents weights for all individual P_n, the forecast possibilities, in a linear function

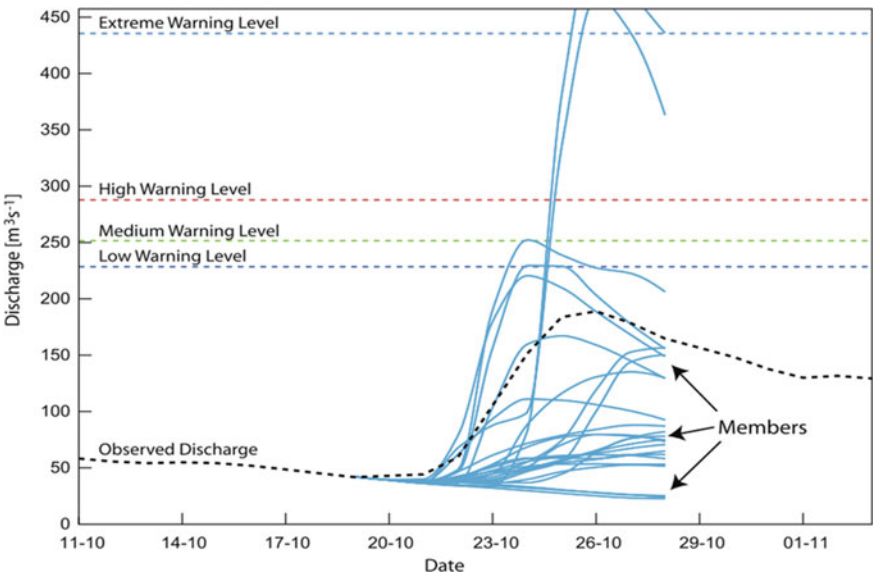

Fig. 2 Illustration of the representation of ensemble hydrograph for a flood event (for details refer to source Cloke and Pappenberger [24])

short- to medium-term timescale during the monsoon period of 2011. The methodology is carried out in three steps (i) estimation of the biases of the individual model, (ii) applying individual model bias correction, and creating bias-corrected ensemble mean forecast (considering equal weight for each model member), and (iii) computation of the model-dependent weights as the different model has different accuracy and

reliability, thus producing the rainfall forecast of weighted ensemble multi-model. MME forecast is inferior then individual model forecast, as seen by the spatial contour of RMSE and ACC.

4 Ensemble Flood Forecasting

Despite a slew of scientific and institutional roadblocks, moving to practical ensemble forecasting for flood control has become a reality [26], and numerous recent analysts have claimed that "ensemble forecasts are superior to deterministic forecasts" [1, 24, 27, 28]. In 2005, as part of the THORPEX project, the THORPEX Interactive Grand Global Ensemble (TIGGE) was launched [29, 30]. Users may obtain ensemble weather forecasts from ten different meteorological centers across the world using the TIGGE database. For the Chennai floods, Ghosh et al. [31] created India's first comprehensive expert urban flood forecasting system. The rainfall data were attained from NCMRWF for 2007–17 to generate the regional framework. The hindcast data were created using an ensemble model simulation with 22 ensembles for 2007–13 and 11 ensembles for 2014–15 (data accessible via TIGGE https://apps.ecmwf.int/datasets/data/tigge/). The combination of post-processed ensemble weather forecasts and multiple rainfall-runoff models serves as an effective method for ensemble streamflow predictions [32]. Multiple hydrological models were utilized to examine the uncertainty of ESPs associated to the selection of the rainfall-runoff model. For the enhancement in the precision of multi-category, Brier Skill Score statistical technique and ranking probability skill score may be used to make probability forecasts [29, 33]. Fan et al. [34] worked on streamflow forecasting system based on hydrologic modeling and quantitative precipitation forecasts (QPFs) for the Tocantins River watershed, situated in North of Brazil. To study the forecasting routine of flood discharges and streamflow components, a HEPS comprised of VIC and ECMWF medium-range precipitation forecasts was constructed and used for YZR watershed [12] (Table 1).

5 Uncertainties in HEPS Ensemble Flood Forecasting

Hydrologic ensemble prediction system (HEPS) for flood forecasting comprises of three components, namely ensemble precipitation forecast (EPF), hydrologic ensemble prediction (HEP), and dissemination of flood warnings. The uncertainty introduced in the forecasting system due to ensemble precipitation forecast can be because of the control model's starting conditions, model parameter errors, the errors in data assimilation, and errors induced during the observations. Downscaling and bias correction [42] of the assimilated ensemble data, terrain representation, errors in data assimilation, and the errors induced due model parameter selection of the hydrologic model in the prediction system are the uncertainties introduced in the

Table 1 Literature review of ensemble flood forecasting and ensemble datasets used

Author	Study area	Remarks	Datasets
Ghosh et al. [31]	Chennai, India	India's first comprehensive expert urban flood forecasting system was developed	NCMRWF, TIGGE datasets
Han and Coulibaly [35]	Humber River watershed	The performance of different weather forecast datasets was studied, including raw GEPS, bias-corrected GEPS, and their ensemble mean	GEPS
Liu et al. [36]	Yarlung Zangbo River basin, China	Assessed the HEPS' suitability for forecasting flood volume and elements in a cold and mountainous environment, as well as the model simulation and forecasting efficacy of an ensemble of selected pareto-optimal solutions against a single parameter set	ECMWF
Ran et al. [37]	Linxian Basin and Jiuzhaigou Basin, China	Evaluation and comparison of three NWP datasets' deterministic precipitation forecasting abilities	ECMWF, UKMO, CMA
Candogan Yossef et al. [38]	Major basins selected globally	Authors worked with objective of finding the capability of GEFS in prediction of the ensemble streamflow	ECMWF
Liu et al. [39]	Lanjiang Basin, China	Inevitably, a calibrated VIC is used in conjunction with a genetic algorithm that is run in parallel to generate ensemble flood predictions	TIGGE ECMWF
Fan et al. [34]	Tocantins River, Brazil	Model use for two flood occurrences, as well as future potential for using the ensemble forecasting system to predict floods	TRMM satellite rainfall, GEFS NCEP-NOAA
Durai and Bhardwaj [25]	India	The MME framework system is used to forecast rainfall across India utilizing an ensemble from a global NWP model that is operational	ECMWF, JMA, GFS, and UKMO
Tao et al. [29]	Huai River basin, China	Evaluation of how post-processing can improve raw rainfall forecasts produced by various NWPs models archived in TIGGE database. Overall performance was evaluated of different dataset outcomes	CMA, ECMWF, JMA, NCEP, UKMO

(continued)

Table 1 (continued)

Author	Study area	Remarks	Datasets
Yu et al. [40]	Shingu River basin, Japan	On the basis of most recent ensemble NWP, an assessment of the efficacy of ensemble flood forecasting for hydrological applications	JMA
Marty et al. [41]	Cevennes-Vivarais region (Southern France)	Analysis of the performance of a HEPS developed for small scale basin. Hydrometeorological ensemble predictions were given as inputs in hydrological models, to develop an integrated HEPS	NCEP, ECMWF
Nester et al. [42]	43 watersheds of Germany and Austria	Authors dealt with the uncertainty associated, such as flood forecast error (simulation and precipitation forecast error)	ECMWF, ALADIN
Hopson and Webster [43]	Ganges and Brahmaputra basins, Bangladesh	The Brahmaputra and Ganges Rivers were subjected to a fully automated technique that provided calibrated 1–10-day ensemble river flow predictions and severe flooding estimates	ECMWF
Olsson and Lindstrom [44]	Sweden	A probabilistic analysis of the first 18 months of daily predictions was conducted	ECMWF
Pietroniro et al.	St. Lawrence River basin, Montreal and Ottawa River basin	Discussion of utilizing MESH to enhance water resource management through provincial hydrometeorological modeling and ensemble forecasting	NCEP-NOAA
Gouweleeuw et al. [45]	Meuse River and Odra River basin	The European Centre for Medium-Range Weather Forecasts (ECMWF) integrated the global NWP model's deterministic and EPS hindcasts with the large-scale hydrological model LISFLOOD for severe flood occurrences	ECMWF
Addor et al. [46]	Sihl River, Zurich, Switzerland	Authors studied suitability of HEPS using the probabilistic approach for small watershed	GEFS, ECMWF

hydrologic ensemble prediction. Precariousness during the dissemination of flood warning can be due to the errors in the understanding and interpretation of the forecasts generated. There is a possibility of model parameter error and error due to wrong observations.

6 Challenges in the Ensemble Flood Forecasting

(i) The NWPs [47] that now compose the ensemble prediction system contributions to ensemble flood forecasting systems are not good enough; they must, for instance, be of better resolution, have higher ensemble members, and address the current bias and under dispersivity issues. Forecasters should strategize to enhance the number of ensemble members in the EPS and the resolution of their forecasts, in the long run, to adequately capture predictor covariance and distribution extremes [48]. (India produces 12 km resolution now which is the same as US NAEFS, still, Europe ECMWRF provides for 9 km resolution).

(ii) We do not grasp the whole variety and interface of uncertainties in forecast systems because we do not understand the total uncertainty in the system. Full uncertainty analysis is computationally intensive, and current EPS-based [49, 50] predictions do not produce actual flood probabilities because uncertainties are not fully addressed and some of the techniques' assumptions are violated. Two of the scientific difficulties mentioned include detecting the source of the prediction system's uncertainty and formulating the system interpretation for the consequences of uncertainty.

(iii) In flood ensemble prediction systems, current data assimilation approaches incorporate soil moisture, snow cover, or discharge, as well as some influence on hydrological skills [51]. The assimilation of hydrological data requires far more consideration than it now receives, particularly since it has been shown that the initial hydrological state has a substantial impact on the predicted lead time.

(iv) Due to the difficulty of evaluating probabilistic forecasts, we will have to rely on case studies of exceptional floods. We basically lack in availability of enough data (may never have enough) to undertake a statistical study of the value of flood forecasts based on EPS [52].

(v) The challenges of presenting imprecise probabilistic flood projections, as well as the assumptions that go into their construction. In most circumstances, the contribution of all of the system's numerous components to forecast error/uncertainty is not quantified or even subjectively evaluated [53]. More focused group studies are required to address the issue.

7 Summary and Conclusions

The paper presents an overview of ensemble flood forecasting research initiatives and challenges ongoing around the world.

(i) The potential to issue flood warnings is improved by using meteorological ensembles to generate ranges of hydrological predictions.

(ii) Hydrological ensemble forecasts are more accurate than deterministic projections [52].

(iii) The use of EPS in hydrological forecasting has shown to be a substantial advantage for a flood early warning system, since EPS-based predictions had a greater level of accuracy than deterministic-based forecasts. A collection of case studies and long-term evaluations demonstrating the benefits of EPS [24, 54].

(iv) More theoretical development of flood forecasting systems, as well as a compelling all-encompassing approach for coping with the cascading of uncertainty in an operational framework, is unquestionably necessary.

References

1. Jain SK, Mani P, Jain SK, Prakash P, Singh VP, Tullos D, Kumar S, Agarwal SP, Dimri AP (2018) A Brief review of flood forecasting techniques and their applications. Int J River Basin Manag 16:329–344. https://doi.org/10.1080/15715124.2017.1411920
2. Rangari VA, Sridhar V, Umamahesh NV, Patel AK (2019) Floodplain mapping and management of urban catchment using HEC-RAS: a case study of Hyderabad City. J Inst Eng Ser A 100:49–63. https://doi.org/10.1007/s40030-018-0345-0
3. Zope PE, Eldho TI, Jothiprakash V (2015) Impacts of urbanization on flooding of a coastal urban catchment: a case study of Mumbai City, India. Nat Hazards 75:887–908. https://doi.org/10.1007/s11069-014-1356-4
4. Singh O, Kumar M (2013) Flood events, fatalities and damages in India from 1978 to 2006. Nat Hazards 69:1815–1834. https://doi.org/10.1007/s11069-013-0781-0
5. Silva F V, Bonumá NB, Uda PK (2014) Flood mapping in urban area using HEC-RAS model supported by GIS. Int Conf Flood Manag 1–9
6. Martin O, Rugumayo A, Ovcharovichova J (2012) Application of HEC HMS/RAS and GIS tools in flood modeling: a case study for River Sironko—Uganda. 1:19–31
7. Khodashenas SR, Tajbakhsh M (2016) Management of urban drainage system using integrated MIKE SWMM and GIS. J Water Resour Hydraul Eng 5:36–45. https://doi.org/10.5963/jwrhe0501004
8. Ranaee E, Mahmoodian M, Quchani SR (2009) The combination of HEC-Geo-HMS, HEC-HMS and MIKE11 software utilize in a two branches river flood routing modeling. 2nd Int Conf Environ Comput Sci ICECS 2009 317–321. https://doi.org/10.1109/ICECS.2009.62
9. Timbadiya PV, Patel PL, Porey PD (2015) A 1D–2D coupled hydrodynamic model for river flood prediction in a coastal urban floodplain. J Hydrol Eng 20:1–18. https://doi.org/10.1061/(ASCE)HE.1943-5584.0001029
10. Molinari D, Ballio F, Menoni S (2013) Modelling the benefits of flood emergency management measures in reducing damages: a case study on Sondrio, Italy. Nat Hazards Earth Syst Sci 13:1913–1927. https://doi.org/10.5194/nhess-13-1913-2013
11. Hopson TM, Webster PJ (2010) A 1–10-day ensemble forecasting scheme for the major river basins of Bangladesh: forecasting severe floods of 2003–07. J Hydrometeorol 11:618–641. https://doi.org/10.1175/2009JHM1006.1
12. Liu L, Xu YP, Pan SL, Bai ZX (2019) Potential application of hydrological ensemble prediction in forecasting floods and its components over the Yarlung Zangbo River basin, China. Hydrol Earth Syst Sci 23:3335–3352
13. Ngongondo CS, Xu CY, Tallaksen LM, Alemaw B, Chirwa T (2011) Regional frequency analysis of rainfall extremes in Southern Malawi using the index rainfall and L-moments approaches. Stoch Environ Res Risk Assess 25:939–955. https://doi.org/10.1007/s00477-011-0480-x

14. Adams T, Ostrowski J (2010) Short lead-time hydrologic ensemble forecasts from numerical weather prediction model ensembles. World Environ Water Resour Congr 2010 Challenges Chang—Proc World Environ Water Resour Congr 2010 2294–2304. https://doi.org/10.1061/41114(371)237
15. Xuan Y, Cluckie ID, Wang Y (2006) Uncertainty analysis of hydrological ensemble forecasts in a distributed model utilising short-range rainfall prediction. Hydrol Earth Syst Sci Discuss 3:3211–3237. https://doi.org/10.5194/hessd-3-3211-2006
16. Perera D, Agnihotri J, Seidou O, Djalante R (2020) Identifying societal challenges in flood early warning systems. Int J Disaster Risk Reduct 51:101794. https://doi.org/10.1016/j.ijdrr.2020.101794
17. Demeritt D, Nobert Ś, Cloke H, Pappenberg F (2010) Challenges in communicating and using ensembles in operational flood forecasting. Meteorol Appl 17:209–222. https://doi.org/10.1002/met.194
18. Bellier J, Zin I, Siblot S, Bontron G (2016) Probabilistic flood forecasting on the Rhone River: evaluation with ensemble and analogue-based precipitation forecasts. E3S Web Conf 7. https://doi.org/10.1051/e3sconf/20160718011
19. Cloke HL, Schaake JC (2018) Handbook of hydrometeorological ensemble forecasting
20. Buizza R (2018) Ensemble forecasting and the need for calibration. Elsevier Inc.
21. Murray SA (2018) The importance of ensemble techniques for operational space weather forecasting. Sp Weather 16:777–783. https://doi.org/10.1029/2018SW001861
22. Goswami M, O'Connor KM (2007) Real-time flow forecasting in the absence of quantitative precipitation forecasts: a multi-model approach. J Hydrol 334:125–140. https://doi.org/10.1016/j.jhydrol.2006.10.002
23. Werner M, Reggiani P, De Roo A, Bates P, Sprokkereef E (2005) Flood forecasting and warning at the river basin and at the European scale. Nat Hazards 36:25–42. https://doi.org/10.1007/s11069-004-4537-8
24. Cloke HL, Pappenberger F (2009) Ensemble flood forecasting: a review. J Hydrol 375:613–626. https://doi.org/10.1016/j.jhydrol.2009.06.005
25. Durai VR, Bhardwaj R (2014) Forecasting quantitative rainfall over India using multi-model ensemble technique. Meteorol Atmos Phys 126:31–48. https://doi.org/10.1007/s00703-014-0334-4
26. Emerton R, Zsoter E, Arnal L, Cloke HL, Muraro D, Stephens EM, Salamon P, Pappenberger F (2018) Developing a global operational seasonal hydro-meteorological forecasting system : GloFAS v2. 2 Seasonal v1. 0. Geosci Model Dev Model Dev
27. Nanditha JS, Mishra V (2021) On the need of ensemble flood forecast in India. Water Secur 12:100086. https://doi.org/10.1016/j.wasec.2021.100086
28. Gomez M, Sharma S, Reed S, Mejia A (2019) Skill of ensemble flood inundation forecasts at short- to medium-range timescales. J Hydrol 568:207–220. https://doi.org/10.1016/j.jhydrol.2018.10.063
29. Tao Y, Duan Q, Ye A, Gong W, Di Z, Xiao M, Hsu K (2014) An evaluation of post-processed TIGGE multimodel ensemble precipitation forecast in the Huai river basin. J Hydrol 519:2890–2905. https://doi.org/10.1016/j.jhydrol.2014.04.040
30. Duan M, Ma J, Wang P (2012) Preliminary comparison of the CMA, ECMWF, NCEP, and JMA ensemble prediction systems. Acta Meteorol Sin 26:26–40. https://doi.org/10.1007/s13351-012-0103-6
31. Ghosh S, Karmakar S, Saha A, Mohanty MP, Ali S, Raju SK, Krishnakumar V, Sebastian M, Behera MR, Ashrit R, Murty PLN, Srinivas K, Narasimhan B, Usha T, Ramana Murthy M V., Thiruvengadam P, Indu J, Thirumalaivasan D, George JP, Gedam S, Inamdar AB, Murty BS, Mujumdar PP, Mohapatra M, Bhardwaj A, Basu S, Nayak S (2019) Development of India's first integrated expert urban flood forecasting system for Chennai. Curr Sci 117:741–745. https://doi.org/10.18520/cs/v117/i5/741-745
32. Zhang J, Chen J, Li X, Chen H, Xie P, Li W (2020) Combining postprocessed ensemble weather forecasts and multiple hydrological models for ensemble streamflow predictions. J Hydrol Eng 25:04019060. https://doi.org/10.1061/(asce)he.1943-5584.0001871

33. Wei W, Watkins DW (2011) Probabilistic streamflow forecasts based on hydrologic persistence and large-scale climate signals in central Texas. J Hydroinformatics 13:760–774. https://doi.org/10.2166/hydro.2010.133
34. Fan FM, Collischonn W, Quiroz KJ, Sorribas MV, Buarque DC, Siqueira VA (2016) Flood forecasting on the Tocantins River using ensemble rainfall forecasts and real-time satellite rainfall estimates. J Flood Risk Manag 9:278–288. https://doi.org/10.1111/jfr3.12177
35. Han S, Coulibaly P (2019) Probabilistic flood forecasting using hydrologic uncertainty processor with ensemble weather forecasts. J Hydrometeorol 20:1379–1398. https://doi.org/10.1175/JHM-D-18-0251.1
36. Liu L, Ping XuY, Li Pan S, Xu Bai Z (2019) Potential application of hydrological ensemble prediction in forecasting floods and its components over the Yarlung Zangbo River basin, China. Hydrol Earth Syst Sci 23:3335–3352. https://doi.org/10.5194/hess-23-3335-2019
37. Ran Q, Fu W, Liu Y, Li T, Shi K, Sivakumar B (2018) Evaluation of quantitative precipitation predictions by ECMWF, CMA, and UKMO for flood forecasting: application to two Basins in China. Nat Hazards Rev 19:05018003. https://doi.org/10.1061/(asce)nh.1527-6996.0000282
38. Candogan Yossef N, Van Beek R, Weerts A, Winsemius H, Bierkens MFP (2017) Skill of a global forecasting system in seasonal ensemble streamflow prediction. Hydrol Earth Syst Sci 21:4103–4114. https://doi.org/10.5194/hess-21-4103-2017
39. Liu L, Gao C, Xuan W, Xu YP (2017) Evaluation of medium-range ensemble flood forecasting based on calibration strategies and ensemble methods in Lanjiang Basin, Southeast China. J Hydrol 554:233–250. https://doi.org/10.1016/j.jhydrol.2017.08.032
40. Yu W, Nakakita E, Yamaguchi K (2013) Assessment of probabilistic flood forecasting using ensemble NWP rainfall with 30hr forecast time during typhoon events. Adv River Eng 19:235–240
41. Marty R, Zin I, Obled C (2013) Sensitivity of hydrological ensemble forecasts to different sources and temporal resolutions of probabilistic quantitative precipitation forecasts: flash flood case studies in the Cévennes-Vivarais region (Southern France). Hydrol Process 27:33–44. https://doi.org/10.1002/hyp.9543
42. Nester T, Komma J, Viglione A, Blöschl G (2012) Flood forecast errors and ensemble spread—a case study. Water Resour Res 48:1–19. https://doi.org/10.1029/2011WR011649
43. Hopson TM, Webster PJ (2010) A 1–10-day ensemble forecasting scheme for the major river basins of Bangladesh: forecasting severe floods of 2003–07. J Hydrometeorology 11(3):618–641
44. Olsson J, Lindström G (2008) Evaluation and calibration of operational hydrological ensemble forecasts in Sweden. J Hydrol 350:14–24. https://doi.org/10.1016/j.jhydrol.2007.11.010
45. Gouweleeuw BT, Thielen J, Franchello G, De RAPJ, Buizza R (2005) Flood forecasting using medium-range probabilistic weather prediction. Hydrol Earth Syst Sci 9:365–380
46. Addor N, Jaun S, Fundel F, Zappa M (2011) An operational hydrological ensemble prediction system for the city of Zurich (Switzerland): skill, case studies and scenarios. Hydrol Earth Syst Sci 15:2327–2347.https://doi.org/10.5194/hess-15-2327-2011
47. Awol FS, Coulibaly P, Tsanis I (2021) Identification of combined hydrological models and numerical weather predictions for enhanced flood forecasting in a Semiurban Watershed. J Hydrol Eng 26:04020057. https://doi.org/10.1061/(asce)he.1943-5584.0002018
48. Bisht DS, Chatterjee C, Kalakoti S, Upadhyay P, Sahoo M, Panda A (2016) Modeling urban floods and drainage using SWMM and MIKE URBAN: a case study. Nat Hazards 84:749–776. https://doi.org/10.1007/s11069-016-2455-1
49. Chakraborty P, Sarkar A, Bhatla R, Singh R (2021) Assessing the skill of NCMRWF global ensemble prediction system in predicting Indian summer monsoon during 2018. Atmos Res 248:105255. https://doi.org/10.1016/j.atmosres.2020.105255
50. Leutbecher M, Palmer TN (2008) Ensemble forecasting. J Comput Phys 227:3515–3539. https://doi.org/10.1016/j.jcp.2007.02.014
51. Komma J, Reszler C, Blöschl G, Haiden T (2007) Ensemble prediction of floods—catchment non-linearity and forecast probabilities. Nat Hazards Earth Syst Sci 7:431–444. https://doi.org/10.5194/nhess-7-431-2007

52. Roulin E, Vannitsem S (2005) Skill of medium-range hydrological ensemble predictions. J Hydrometeorol 6:729–744. https://doi.org/10.1175/JHM436.1
53. Xuan Y, Cluckie ID, Wang Y (2009) Uncertainty analysis of hydrological ensemble forecasts in a distributed model utilising short-range rainfall prediction. Hydrol Earth Syst Sci 13:293–303
54. Pappenberger F, Bartholmes J, Thielen J, Cloke HL, Buizza R, de Roo A (2008) New dimensions in early flood warning across the globe using grand-ensemble weather predictions. Geophys Res Lett 35:1–7. https://doi.org/10.1029/2008GL033837

Flood Estimation Studies for Lower Tapi—A Case Study

Annapurna Patra, Ujjal Chowdhury, and C. Srishailam

Abstract Flood is the most common and widespread natural severe weather event. A flood occurs when water levels rise over the top of river banks. In recent times, several Indian coastal cities such as Surat, Mumbai and Chennai have witnessed unprecedented flooding due to various causes such as heavy downpour, releases from the upstream dams, poor urban planning. In the urban flood-prone areas, it is essential to estimate the peak flood, time of peak, flood response of contributing catchments for planning, riverfront development (RFD) works, etc. The extreme rainfall depth and the catchment physiographic characteristics are required for the estimation of peak flood. Surat is one of the cities of Gujarat, situated in Lower Tapi Basin (LTB). The LTB is a flood-prone area and also witnessed at least ten major floods in the past century out of which the worst one was 2006. In view of the above, Surat Municipal Corporation (SMC) has a proposal of RFD for Tapi with in Surat City to minimize the devastation due to flooding as well as improve the aesthetic view. On request of SMC, CWPRS carried out flood estimation study for RFD works of Tapi. The present paper is a case study related to flood estimation at location of interests on Tapi, i.e. Kathore Bridge, Singanpur Weir and ONGC Bridge. For this study, delineation of LTB sub-catchments (i.e. downstream of Ukai Dam) and extraction of the physiographic parameters and also extreme value analysis IMD rainfall data were carried out. Estimation peak flood of contributing catchments of LTB for 25-yr, 50-yr and 100-yr return periods were carried out by adopting the CWC flood report (sub-zone-3B). Further, the peak flood of LTB catchments and Ukai Dam discharges were considered for the estimation of peak flood at location of interests.

A. Patra (✉) · U. Chowdhury · C. Srishailam
Central Water and Power Research Station, Pune 411024, India
e-mail: annapurna.patra@gmail.com

P. V. Timbadiya et al. (eds.), *Flood Forecasting and Hydraulic Structures*, Lecture Notes in Civil Engineering 340, https://doi.org/10.1007/978-981-99-1890-4_25

Keywords Lower Tapi · Surat · EVA · Flood estimation · Rainfall-runoff

1 Introduction

In recent times, several Indian cities such as Surat, Mumbai, Chennai, Kolkata, Bengaluru to name a few have witnessed unprecedented incidences of urban flooding due to various causes [1]. In all such events extreme rainfall with excess releases from the upstream dams, poor urban planning and failure of drainage system are considered as main reasons behind flooding. On the other hand, due to unplanned developments in these cities and utter negligence on the river regimes passing through the urban habitat have made these rivers as sinks for waste disposal and unapproachable for public purposes. However, in the recent past some cities have adopted the riverfront development activities (Sabarmati, Yamuna, Gomti, etc.) to make the rivers aesthetical good, useful for public recreation and also develop a sense of responsibility of the urban citizen to preserve the river ecosystems.

Taking the lead from the Sabarmati riverfront development in Ahmadabad and others, Surat Municipal Corporation (SMC) has a proposal of riverfront development (RFD) for Tapi which flows through the Surat City. SMC requested CWPRS to undertake the studies on estimation of flood for Tapi as regards the RFD work. The present study focuses on flood estimation of different free catchment in the RFD area, i.e. below Ukai Dam to ONGC Bridge. The objective of the study is to estimate the flood for different return period for RFD work for Tapi in Surat City.

2 Study Area

The stretch of Tapi River between Ukai Dam to the Arabian Sea is considered as Lower Tapi Basin (LTB) mainly occupying the Surat and Hazira twin cities along with tens of small towns and village by the river (Fig. 1). The study area in the present flood estimation study lies between the stretches of Tapi River from Kathore Bridge to ONGC Bridge. Ukai Dam is located on Tapi River at 105 km distance from Surat City and drains an area of 62225 km^2. Kakarapar weir is situated downstream of Ukai Dam with a catchment area of 62826 km^2. Three tributaries, namely Anjana, Ver khad and Dharampur join Tapi on the right bank below Ukai Dam, can bring sizeable floods to Tapi. Anjana River drains an area of 151.9 km^2 before it meets Tapi 12 km downstream of Ukai Dam. Ver River joins Tapi 31 km downstream of Kakrapar weir. The catchment area of Vera upto Tapi confluence is 463.2 km^2 while Dharampur tributary joins lower Tapi about 80 km downstream of Ukai and drains an area of 105 km^2 [2].

The flood contributions from Ukai Dam and Anjana Rivers result at Kakrapar weir, to which the catchment contributions from Vera tributary and the catchment

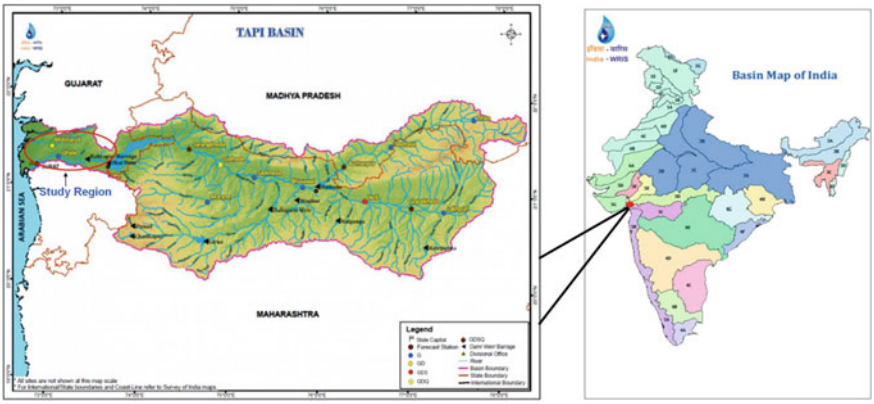

Fig. 1 Location map of Lower Tapi Basin

in between Kakrapar weir and ONGC Bridge needs to be considered for flood estimation. Thus the flood estimation is required for Tapi at Kathore Bridge, Singanpur Weir and at ONGC Bridge for flood routing studies that aid the riverfront development activities and also in arriving at the tailrace of barrage to safely convey floods to downstream.

3 Tapi Floods and Surat City

Flood in Surat is a common phenomenon. City climatic records of Surat states that from 1849 itself the city is experiencing yearly flood situations. The floods in Tapi River during years 1998 and 2006 have created havoc on Surat City lives and property and still fresh in the memory of people [3]. Therefore, it is of prime importance to estimate floods scientifically to minimize the property damage, save the souls and reduce infrastructure disturbances by identifying zones for floodproofing and also for developing flood forecasting/warning systems [4]. In such eventualities, it is imperative on the part of hydrologist to estimate flood with due concerns to the catchment characteristics and the climatic factors that prevailed in the catchment.

4 Flood Estimation for Lower Tapi

The flood estimation for a river basin assumes central role in all water resources-related studies and RFD is no exception to it. The steps involved to arrive at design flood are, delineation of catchment area of lower Tapi at desired points and compute the catchment characteristics (length, slope, area, etc.), processing of rainfall data, estimate flood hydrograph adopting suitable R-R model for catchments below the

Ukai Dam at Kathore, Singanpur and ONGC Bridges and its tributaries, viz. Anjana, Vera and Dharampur River to project their peak discharge components in this study, perform the extreme value analysis (EVA) of Ukai Dam releases.

5 Processing of Data

Processing of data includes collection, compilation, scrutiny and subsequently applying the requisite verification tools to prepare the data in a format that is accepted by the model being used. Basically, three types of data were used, viz. terrain data (catchment details), rainfall and flow data. The terrain data comprises of topographic elevation details of a catchment, the soil types and land use/land cover aspects and flow data include dream releases. The rainfall data from IMD and Ukai Dam releases from the SMC were collected for the study.

6 Catchment Delineation Using DEM

For the present study, 30 m DEM from the USGS (SRTM30) has been downloaded and used. The DEM is imported into the GIS environment (ArcGIS), processed. In the processing of DEM, the steps adopted were (i) filling the DEM, (ii) deriving the flow direction network, (iii) flow accumulation computations at each DEM grid, (iv) delineating the designated sub-catchments of lower Tapi and its tributaries.

The catchments delineated for river lower Tapi are (i) Ukai Dam to Kakrapar, (ii) Ukai Dam to Kathore Bridge, (iii) Ukai Dam to Singanpur Weir, (iv) Ukai Dam to ONGC Bridge, and also for the medium-sized catchments of tributaries to Tapi that could produce sizeable floods were, (a) Dharampur catchment, (b) Vera River catchment and (c) Anjana River catchment. The delineated catchments are presented in Fig. 2.

The catchment factors such as area, stream length, average slope and time of concentration were estimated and presented in Table 1.

7 Estimation of Mean Catchment Precipitation

The observed rainfall from Ukai, Kakrapara, Kamrej, Surat rain gauge stations was used to compute mean catchment precipitation adopting Theissen polygon method. The locations of the rain gauges with respect to the river catchment were projected in the GIS environment and Theissen polygons for the rain gauges for each of the catchments (Tapi at Kathore Bridge, Singanpur and ONGC Bridge and its tributaries, viz. Dharampur, Vera and Anjana) were developed. By adopting the weights of rain

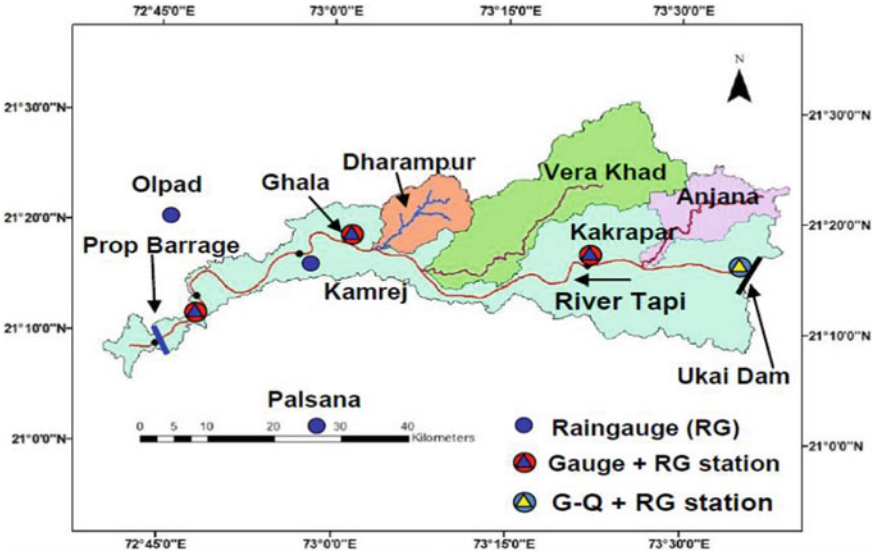

Fig. 2 LTB catchments from Ukai Dam to ONGC Bridge (Surat) with major tributaries

Table 1 Estimated catchment factors for lower Tapi and its tributaries

Catchment	Area (km^2)	Stream length (km)	Slope (m/km)	Time of concentration (h)
Ukai to Kathore Bridge	1599.0	82.80	4.99	12
Ukai to Singanpur Weir	1638.6	107.67	3.88	14
Ukai to ONGC Bridge	1678.0	119.96	3.48	15
Anjana	159.4	31.47	11.73	3
Vera	461.7	59.01	5.03	8
Dharampur	125.9	18.01	7.16	5

gauges, the weighted 1-day maximum rainfall for different return periods, i.e. 25-yr, 50-yr and 100-yr, were estimated and presented in Table 2.

8 Flood Estimation by Extreme Value Analysis Method

Design flood estimation may be performed by a frequency analysis of observed flows where these are available and adequate both in length and quality. From the observed data annual maximum series (AMS) of flood is prepared and used in EVA, which

Table 2 Weighted 1-day maximum rainfall for different return periods

River catchment	Estimated weighted 1-day maximum rainfall (mm)		
	25-yr	50-yr	100-yr
Ukai to Kathore Bridge	318.50	359.33	399.86
Ukai to Singanpur Weir	319.70	360.68	401.36
Ukai to ONGC Bridge	317.00	358.43	398.76
Anjana	299.80	338.58	377.06
Vera	313.21	352.82	392.14
Dharampur	358.06	404.63	450.86

is widely known as flood frequency analysis (FFA). In applying FFA to AMS, the estimation assumes that the series is random, without outliers and homogeneous. The procedures for EVA of observed peak discharge involve selecting and fitting an appropriate theoretical probability distribution to the data. In India, the widely used probability distribution for rainfall and flood discharge data is Extreme Value Type I (EV-I) widely known as Gumbel distribution [5]. The mathematical form of cumulative distribution function of EV-I is given as below:

$$F(X) = \exp\{-\exp[-(x-\alpha)/m]\}, -\infty < x < \infty, -\infty < \alpha < \infty,\ m > 0 \tag{1}$$

where *a* and m are the location and scale parameters of the distribution. The parameters (*a* and *m*) of EV-I are determined by maximum likelihood method (MLM) that requires an iterative method that can be implemented by using computer-oriented procedures. The estimators (*a** and m^*) of EV-I are given by:

$$m^* = \sum_i (x_i/n) - \left[\sum_i X_i \exp(-x_i/m^*) \Big/ \sum_i \exp(-x_i/m^*)\right] \tag{2}$$

$$\alpha^* = -m^* \log\left[\sum_i \exp(-x_i/m^*) \Big/ n\right] \tag{3}$$

The estimators are used to estimate the extreme event (XT) for different return periods by using Eq. (4), which is given as below:

$$XT = \alpha^* + YT\, m^* \ \text{ where } YT = -\text{Ln}(-\text{Ln}(1-(1/T))) \tag{4}$$

where n is the size of the sample, T is return period (year), x_i is the variable, i.e. AMS flood, and XT is the estimate of extreme value. The results of EVA of Ukai Dam discharges are presented in Table 3.

Table 3 Extreme daily maximum flood (m^3/s) adopting EV-I; Ukai Dam

T (return period)	Estimated daily discharge	95% confidence limit	
		Lower	Upper
25-yr	20,652.8	14,164.6	27,141.0
50-yr	23,896.2	16,277.8	31,514.6
100-yr	27,115.6	18,360.2	35,870.9

9 Flood Estimation by Synthetic Unit Hydrograph (SUH) Method

The unit hydrograph approach is based on the assumption that the shape of the hydrograph resulting from a rainfall event of a specified duration and large enough to exceed the infiltration capacity of the catchment will always be the same. As such the flood hydrographs resulting from rainfall events of varying intensities can be derived by scaling of the unit hydrograph. However, the unit hydrograph has to be defined for each catchment separately, where possible from the recorded rainfall and runoff observations. In Indian sub-continent, UH method developed for catchments by CWC by segmenting country into seven zones. This method is in general adopted for developing UH for river basins and further to estimating flood hydrographs. Tapi River catchment falls in CWC sub-zone 3B [6]. The SUH developed by CWC follows Snyder's method for this sub-zone with parameters such as, t_p, Q_p, T_B, T_m, W_{50}, W_{75}, W_{R50} and W_{R75} which are pictorially described in Fig. 3. The SUH parameters are estimated for Lower Tapi Basin by adopting equations given in Fig. 3.

$$q_p = 0.583\left(L/\sqrt{S}\right)^{-0.302}$$

$$t_p = 1.91\left(q_p\right)^{-0.763}$$

$$W_{50} = 1.1849\left(q_p\right)^{-0.976}$$

$$W_{75} = 0.955\left(q_p\right)^{-0.792}$$

$$W_{R50} = 0.738\left(q_p\right)^{-0.781}$$

$$W_{R75} = 0.438\left(q_p\right)^{-0.641}$$

$$T_B = 7.042\left(t_p\right)^{0.559}$$

$$Q_p = q_p * A$$

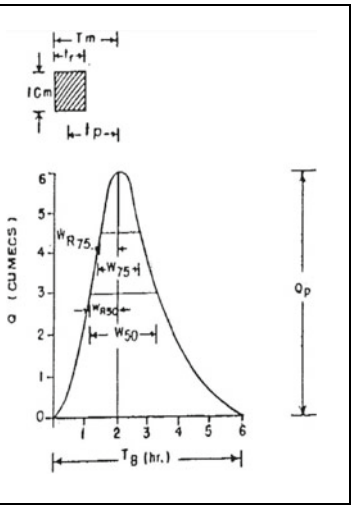

Fig. 3 Synthetic unit hydrograph and its parameters

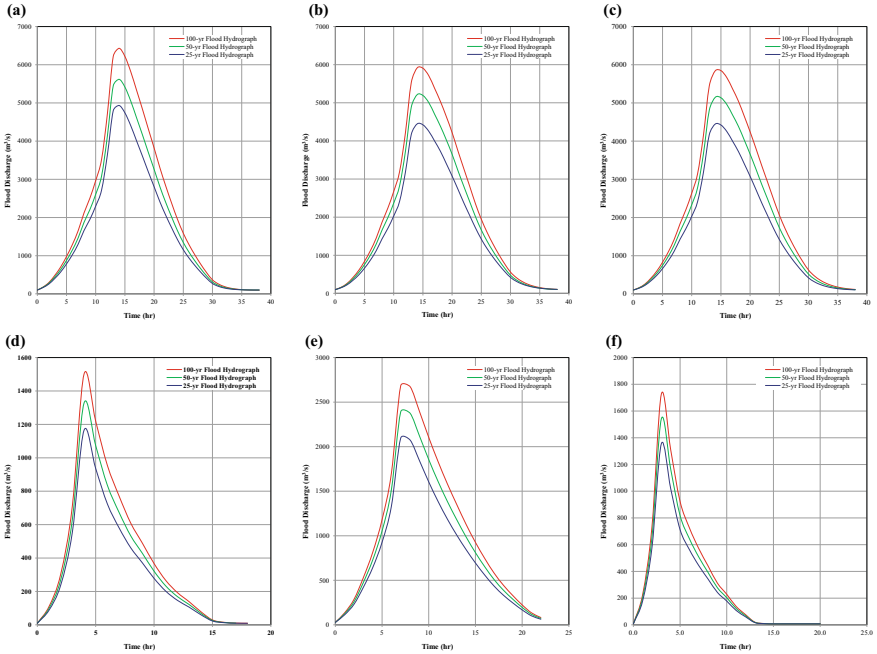

Fig. 4 **a** Flood hydrograph for different return periods of Tapi at Kathore Bridge. **b** Flood hydrograph for different return periods of Tapi at Singanpur Weir. **c** Flood hydrograph for different return periods of Tapi at ONGC Bridge. **d** Flood hydrograph for different return periods of Anjana River. **e** Flood hydrograph for different return periods of Vera River. **f** Flood hydrograph for different return periods of Dharampur River

For the study region of LTB, SUH is developed for main Tapi (1) Tapi from Ukai Dam to Kathore Bridge, (2) Tapi from Ukai Dam to Singanpur weir, (3) Tapi from Ukai Dam to ONGC Bridge and its tributaries, viz. (4) Anjana, (5) Vera and (6) Dharampur rivers. The UH thus developed for the LTB and tributaries to LTB are used for estimating the flood hydrograph for the selected design storms. The flood hydrographs for 25-yr, 50-yr and 100-yr return periods were developed for the above-mentioned river catchments which are presented in Fig. 4a–f. The estimated peak flood corresponding to catchments for respective return periods is presented in Table 4.

10 Estimation of Peak Flood at Location of Interest

The peak flood discharges at location of interest, viz. Tapi at Kathore Bridge, Singanpur Weir and ONGC Bridge for 25-yr, 50-yr and 100-yr return periods, were estimated by addition of moderated design discharge at Ukai Dam and respective

Table 4 Peak flood discharges of free catchment of Tapi below Ukai Dam

Catchments	Peak flood discharge (m^3/s)		
	25-yr	50-yr	100-yr
Tapi at Kathore Bridge	4933.7	5618.8	6431.1
Tapi at Singanpur Weir	4504.6	5210.9	5912.0
Tapi at ONGC Bridge	4443.7	5142.2	5846.7
Anjana River	1164.9	1327.6	1500.9
Vera River	2096.6	2391.5	2674.5
Dharampur River	1355.7	1542.1	1727.1

Table 5 Estimation of peak flood discharge at location of interest

Catchments	Peak flood discharge (m^3/s) for		
	25-yr	50-yr	100-yr
Tapi at Kathore Bridge	25,586.5	29,515.0	33,546.7
Tapi at Singanpur Weir	25,157.4	29,107.1	33,027.6
Tapi at ONGC Bridge	25,096.5	29,038.4	32,962.3

estimated peak flood discharge of Tapi free catchment for Tapi RFD works. The results are compiled in Table 5.

11 Conclusions

The paper presents a study on estimation of peak flood discharge of Tapi River free catchment below Ukai Dam to ONGC Bridge. For this purpose, the sub-catchments were delineated. By adopting the weights of rain gauges, the weighted 1-day maximum rainfall for different return periods, i.e. 25-yr, 50-yr and 100-yr, was estimated. The design discharge from Ukai Dam is derived by EVA. The flood hydrographs for 25-yr, 50-yr and 100-yr return periods were developed as per CWC flood estimation report sub-zone-3b. The estimated peak discharges for Kathore bridge are 25,586.5 m^3/s, 29,515.0 m^3/s and 33,546.7 m^3/s for 25-yr, 50-yr and 100-yr return periods, respectively. Similarly, the peak flood discharge at Singanpur Weir is estimated as 25,157.4 m^3/s, 29,107.1 m^3/s, 33,027.6 m^3/s for 25-yr, 50-yr and 100-yr return periods, respectively, whereas 25,096.5 m^3/s, 29,038.4 m^3/s and 32,962.3 m^3/s are for ONGC Bridge.

Acknowledgements The authors are grateful to Shri A. K. Agrawal, Ex-Director, CWPRS and Dr. R. G. Patil, Scientist-E, CWPRS, Pune, for encouragement and guidance during conduct of the studies and also accordingly permission to publish this paper.

References

1. Dhiman R, Renjith VR, Eldho TI, Inamdar A (2019) Flood risk and adaptation in Indian coastal cities: recent scenarios. Appl Water Sci 9(5):1–16
2. CWPRS (2018) Hydrometrological studies for estimation of flood and eveporation for riverfront development for Tapi river in Surat City for SMC, Gujrat. Technical report No. 5650, Central Water and Power Research Station, Pune
3. CWPRS (2009) Mathematical Model Studies for Prediction of flow in Tapi river reach from Ukai to Hazira for design of Flood Embankments. Technical report No. 4666, Central Water and Power Research Station, Pune
4. Joshi GI, Saha SD (2014) Tapi river flood risk map for Surat by using GIS. Indian J Appl Res 4(8):174–177
5. Ramesh C, Vivekanandan N, Surwade KB, Bapat AD, Mathew FT, Govindan S (2008) Extreme value analysis of rainfall in Mumbai region to aid estimation of severe flood. ISH J Hydraul Eng 14(3):102–117
6. CWC (2005) Flood estimation report for lower Narmada and; Tapi Subzone-3(B) (Revised) design office report no. LNT/3(b)/R-7/47/2004, Central Water Commission, New Delhi

Interlinking of Rivers (Godavari–Krishna–Pennar–Cauvery)

Rohitha, Sudheera, Renuka, Manisha, and Kamalini Devi

Abstract The present study examines the purpose of interlinking of rivers, which benefits mankind. It primarily focuses on interlinking the rivers by creating a system of manually developed canals where the river water is not attainable. The proposal is based on diverting the surplus water from the rivers receiving the high floods to the deficit rivers by connecting the manually developed canals. So, it will assist in diverting surplus water to the deficit rivers in case of necessity. The idea is to design canals that connect the rivers Godavari, Krishna, Pennar, and Cauvery to control floods and use surplus water for irrigation and other purposes. Manning's method is used for the design of canals. Flood frequency analysis has been shown for these four rivers. This analysis played a major role in executing the plan. According to the flood data, the rivers Pennar and Cauvery have had very low floods over the years, whereas the rivers Godavari and Krishna experience the high number of floods. So, the flood water is set to be diverted to the rivers Pennar and Cauvery. These auspicious results have enlarged the potential of success in planning. The main objectives are to draw water from the Godavari River to the Krishna River (Detailed notes on "Krishna River" by Wikipedia), from the Krishna River to the Pennar River, and from Pennar River to the Cauvery River. This can be ended by linking the reservoirs situated across these rivers by the link canals.

Keywords River basin · Tributaries · Diversions · Reservoirs · Canals · Flood frequency analysis · Design

Rohitha · Sudheera · Renuka · Manisha (✉) · K. Devi
Department of Civil Engineering, Vidya Jyothi Institute of Technology (A), Hyderabad, Telangana 500075, India
e-mail: korapalamanisha@gmail.com

K. Devi
e-mail: kamalinidevi1@gmail.com; kamalinidevi_civil@cbit.ac.in

Present Address:
K. Devi
Department of Civil Engineering, Chaitanya Bharathi Institute of Technology (A), Hyderabad, Telangana 500075, India

P. V. Timbadiya et al. (eds.), *Flood Forecasting and Hydraulic Structures*, Lecture Notes in Civil Engineering 340, https://doi.org/10.1007/978-981-99-1890-4_26

1 Introduction

Water is the most crucial natural resource following air, which is necessary for nourishing life on the earth. It is essential for drinking and industrial practices, for irrigation to encounter the growing food and fiber needs, for power generation, navigation and recreation. The precipitation in the country is typically limited to the monsoon season and is disproportionately distributed with reverence to both space and time. As outcome, some portions of the country are affected by recurrent droughts while other portions are affected by floods. Almost one-third of the country is drought prone [1]. In upcoming years, water will turn out to be a scanty resource due to growing thrust of the population and growing demand for several practices. Some researchers have predicted that by 2025 more than half of the world's population will face water-based calamity and recommended that by 2030, in some evolving regions of the world, water demand will beat supply by 50%. Therefore, it is not essential to highlight that water should be bound in the most methodical and well-organized manner. This is where the idea of the interlinking of rivers arises. By interlinking the rivers, we can harness the water that is going to waste into the ocean. So this will play a crucial role in the development of the country by enhancement, usage, and conservation of surplus water [2]. For example, every year, approximately 1500 to 2000 TMC of Godavari water ends up in the ocean. This can be harnessed by linking the rivers [3]. So, in this project, we are going to prepare a plan and design of canals to link the rivers Godavari, Krishna, Pennar, and Cauvery.

2 Flood Frequency Analysis

Flood frequency analysis [4, 5] is a procedure used by hydrologists to forecast flow values equivalent to specific return periods or the probabilities along a river. The flood frequency analysis is needed to know the occurrence of the floods in Godavari and Krishna rivers. The linking of these two rivers is to divert the surplus water to Krishna River. By these analyses, a canal of required capacity can be designed.

2.1 Godavari River

Godavari River is the second lengthiest river in the India after Ganga. It has an overall length of 1465 km from its origin (near Trimbak in Nashik district) to the end (flows into Bay of Bengal at Narasapuram in West Godavari district). In Telangana, four stations are present where the flow rate of Godavari River [6] can be measured. Dummagudem, Bhadrachalam, Kaleshwaram, and Eturunagaram are the four station points where the flow data are measured. Figures 1, 2, 3, and 4 show the flood data at those stations. The blue line shows the max. water level at the period. As per

the records, the highest flood in Godavari River [6] was recorded in 1986 with a magnitude of 3.6 million cusecs which caused devastating effects. But the floods after that were failed to have that magnitude till now. Even though the chances of occurring flood are high and there is a good flow.

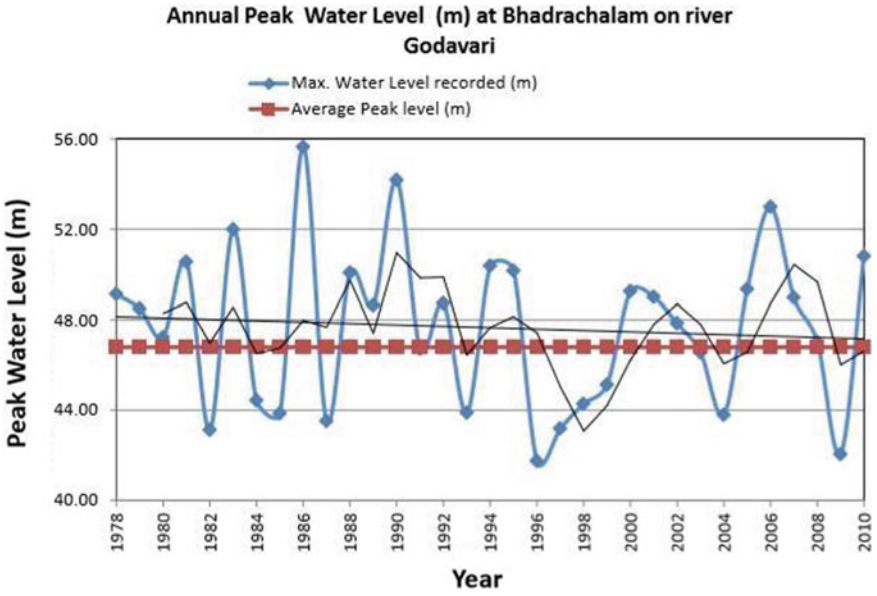

Fig. 1 Annual peak level (m) at Dummugudem

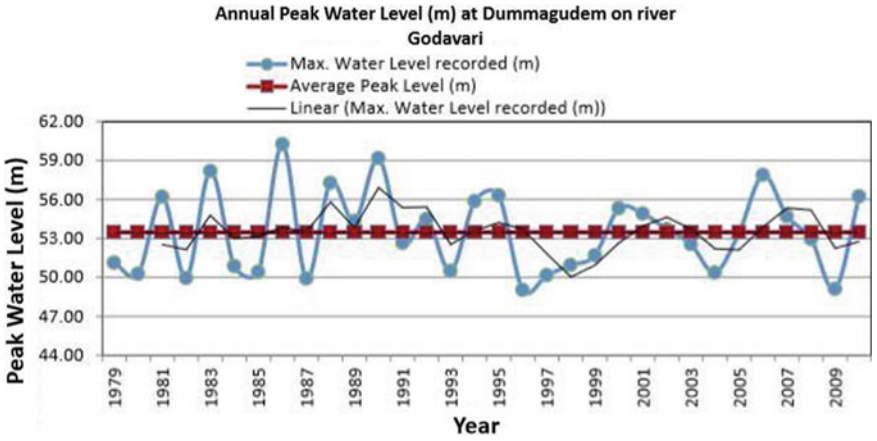

Fig. 2 Annual peak level (m) at Bhadrachalam

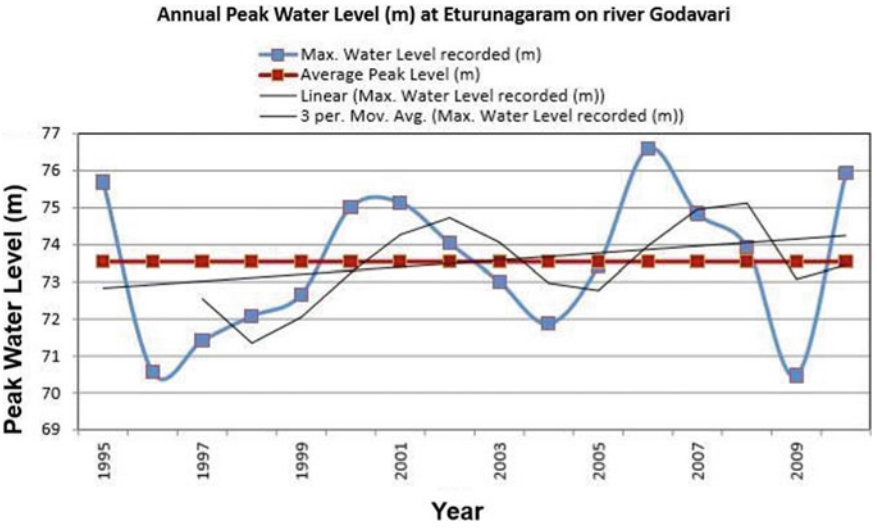

Fig. 3 Annual peak water level (m) at Kaleshwaram

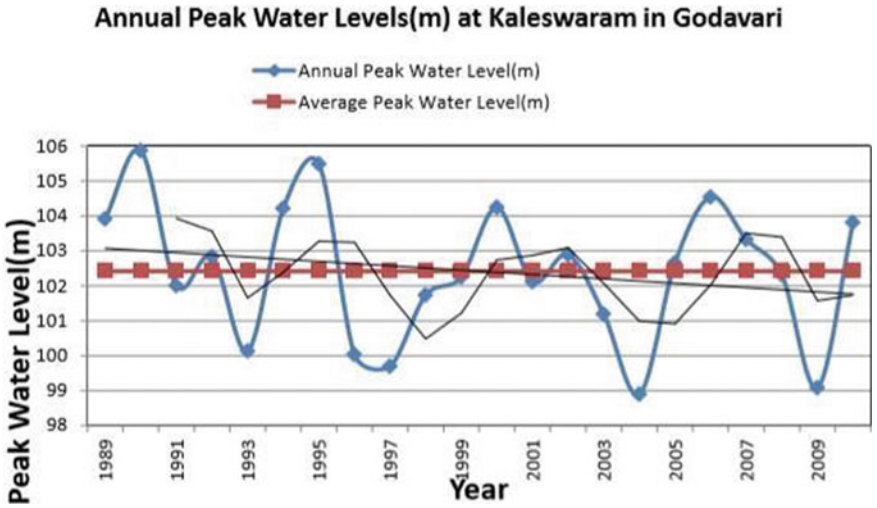

Fig. 4 Annual peak water level (m) at Eturunagaram

2.2 Krishna River

Krishna River is the fourth lengthiest river in India. It has a total length of 1400 km from its origin (Mahabaleshwar near Jor village in Satara district, Maharashtra) to its end (Bay of Bengal at Hamasaladeevi near Koduru in A.P. In Twin-Telugu states, Krishna River has larger flow length compared to TS.

Table 1 Krishna River flood data

Occurrence (Year)	Quantity (Lakh Cusecs)
Oct 7, 1903	10.60
Aug 11, 1914	9.48
Nov 2, 1917	9.55
Sep 24, 1949	9.24
Oct 2, 1964	9.87
Oct 17, 1998	9.32
Sep 21, 2005	7.40
Oct 5, 2009	10.94
Oct 26, 2013	4.67
Oct 24, 2016	1.39
Aug 17, 2019	8.21
Aug 23, 2020	6.00

Krishna River maintains a good flow even though there are fluctuations in flood levels. So, the river water can be easily diverted to Pennar and Cauvery (Table 1).

2.3 Pennar River

The Pennar River [7–9] is one of the major east flowing rivers in southern India. The total length of the river from origin (Chenna Kasava hill of the Nandidurg range in Karnataka) to its outfall in the Bay of Bengal (Nellore district of Andhra Pradesh) is 597 km.

If we look at the flood data, the highest flood in Pennar occurred in 2009 with a magnitude of 8.3 Lakh Cusecs. Prior to and following the flood in the previous year, the water level in the Pennar River was not recorded at such a high level. Furthermore, it is important to note that the Pennar River experiences seasonal flow. So, the excess water of Krishna can be diverted toward Pennar River, and the districts depended on this Pennar River can use of the diverted water from Krishna River (Table 2).

2.4 Cauvery River

The Cauvery is the third largest river in South India, and it is flowing over the states of Karnataka and Tamil Nadu. The total length of the river from origin (Talakaveri Kodagu district of the state of Karnataka) to its end point in the Bay of Bengal (Poompuhar in Mayiladuthurai district) is 800 km.

It receives less floods when compared to other three rivers. So, the water that is diverted to Pennar from Godavari and Krishna rivers will be used by Cauvery.

Table 2 Penna river flood data

Occurrence (Year)	Quantity (Lakh Cusecs)
1946	1.8
1995	4
2001	1.8
2009	8.3
Nov 22, 2010	1.35
Nov 19, 2015	2
Aug 23, 2019	3.45
Oct 20, 2019	0.1
Nov 29, 2020	2.9

2.5 Project Plan

To connect the rivers, a canal route plan is required. The possibilities to connect the rivers Godavari, Krishna, Pennar, and Cauvery [10] are listed below.

1. Polavaram to Srisailam (Godavari to Krishna link)
2. Srisailam to Pennar River (Krishna to Pennar link)
3. Nagarjuna Sagar Dam to Somasila reservoir (Krishna to Pennar link)
4. Somasila reservoir to Grand Anicut (Pennar to Cauvery link).

2.6 Polavaram to Srisailam Link

The Polavaram project is located at Polavaram, West Godavari district, A.P. It is a Concrete spillway, non-overflow masonry dam and earth dam. Polavaram is going to be the largest project in terms of discharge pushing back Three Gorges Dam to second place. Polavaram has a gross capacity of 194 TMC at an FRL of 150 ft from MSL and can discharge about 84 TMC for 110 days from its right canal. The Polavaram to Srisailam link is divided into seven links. Through these seven links, Godavari waters can be successfully diverted to Krishna River all the way to Srisailam (Fig. 5).

Link 1—Polavaram to Ibrahimpatnam: The link from Polavaram right canal to Ibrahimpatnam comes under link 1. It starts from Polavaram right canal to Pavitra Sangamamat Ibrahimpatnam as shown in Fig. 6. At present, the temporary project at Pattiseema can lift water from Godavari. So, this canal is needed to be linked from Pattiseema. But once the right canal construction is finished, the water can directly be drawn from it, though gravity flow to Ibrashimpatnam.

The link has a canal of length of 174 km from Polavaram and joins the cooling canal of length about 16 km. This cooling canal is used for drawing water from the Krishna River about 11,000 cusecs by pumping, as the part of the alternate cooling system for thermal station at Ibrahimpatnam.

Fig. 5 Polavaram to Srisailam canal route

Fig. 6 Emergency escape channel to Pennar River

Link 2—Ibrahimpatnam to Pulichintala Dam: The second link is from Ibrahimpatnam to Pulichintala dam as shown in Fig. 6. The water from Ibrahimpatnam should be lifted upto Pulichintala at it is at upstream. Normally, this lifting should be done from Prakasham barrage. But Vijayawada which is one of the major cities of A.P. is positioned on left abutment of the barrage. If water is drained to the barrage, there is a high chance of the Vijayawada city submerge. So, a new barrage 7.81 km has been proposed prior to Prakasham barrage with a capacity of 6 TMC. This link needs a canal length of 73.9 km, a tunnel length of 789 m, and pump house at Guntupalli barrage.

Link 3—Pulichintala Dam to Nagarjuna Sagar Tail Pond: Pulichintala dam is situated at Pulichinta village, Bellamkonda mandal, Guntur district, A.P. Pulichintala dam has a gross capacity of 45.77 TMC at FRL. It is a project which serves irrigation requirements, hydropower generation and flood control. Water is lifted from Pulichintala dam to Nagarjuna Sagar tail pond. This link has canal of length 73.9 km and a pump house to lift water to N.S.T.P.

Link 4—Nagarjuna Sagar Tail Pond to Nagarjuna Sagar: Nagarjuna Sagar tail pond is a multipurpose reservoir and it is situated 21 km downstream from the Nagarjuna Sagar Dam [11] across the Krishna River [12] with a gross storage of 6 TMC. It has a pump house that pumps water back to Nagarjuna Sagar and the power generation. So, this pump house can be used to lift the water that it has received from Pulichintala dam to Nagarjuna Sagar.

Link 5—Nagarjuna Sagar to Bugga Reservoir: The link 5 connects Nagarjuna Sagar to Bugga reservoir as shown in Fig. 6. Nagarjuna Sagar Dam in Fig. 7 [11] is a masonry dam constructed across the Krishna River, which mounts the border between Guntur district in A.P. and Nalgonda district in T.S. Already Nagarjuna Sagar main canal is linked to Bugga reservoir which will act as the link 5 with a length of 28.8 km as shown in the Fig. 8. However, the capacity of the Bugga reservoir should be increased from 3 to 10TMC.

Link 6—Bugga Reservoir to Marrivemula Reservoir: As the part of this link, it has been proposed for a construction of new balancing reservoir at Marrivemula of 120 TMC as shown in Fig. 8. Normally, it would have been to connect the Nagarjuna Sagar directly to Srisailam by skipping both link 5 and link 6. A canal cannot be dug through Nallamala forest as it is a restricted area for any type of construction. So, it has to take a detour by link 5 and link 6. This link needs a canal length of 19.6 km, a tunnel length of 5 km, and a pump house at Marrivemula.

Link 7—Marrivemula Reservoir to Srisailam: This link connects the Marrivemula reservoir to Saisailam reservoir which is at a distance of 85.7 km Srisailam dam across the Krishna River. The right main canal of the Srisailam project takes-off from this reservoir. The canal of length 145.36 km takes-off from Marrivemula reservoir and connects both reservoirs. It goes through two long tunnels.

2.7 Srisailam to Pennar River (Krishna to Pennar Link)

The purpose Krishna to Pennar link is to carry a part of the surplus water available at Srisailam by limited exchange of the excess water of the Godavari River planned to be carried to the Krishna River. The deviation of the water is proposed by making use of the existing Srisailam reservoir and Srisailam Right Main canal [2] (SRMC). The Pothireddipadu head regulator will draw water into SRMC, and the existing Banakacherla cross regulator and escape channel will discharge it into the Nippulavagu stream. Afterward, the water will flow through the natural streams of Nippulavagu, Galeru, and Kunderu and will reach the Pennar River. The link canal length is about 204 km, of which 180 km is through natural streams.

The proposed link diverts 2310 Mm^3 of water, from Srisailam Right Main canal [2] will be discharged into the Nippulavagu stream via the central cross regulator at Banakacherla and escape channel. The discharged water will be carried through the natural streams, namely Nippulavagu, Galeru, and Kunderu, and lastly reach the Pennar River near Elur village. These natural streams flow exclusively through Kurnool and Cuddapah districts. Santajutur anicut on Galeru river and the Rajoli anicut on Kunderu river are the two controlling structures located on natural streams.

2.8 *Nagarjuna Sagar Dam to Somasila Reservoir*

Nagarjuna Sagar reservoir is constructed across Krishna River [12] between Guntur district in Andhra Pradesh and Nalgonda district in Telangana. It has a storage capacity of 408.24 TMC. It is situated at 150 m from above Mean Sea level.

From Nagarjuna Sagar to Somasila link, we are proposing to divert 12,146 Mm^3 of surplus water. In order to divert the water through this link, we have two possibilities.

1. Extending the existing NSRBC upto Somasila reservoir.
2. Constructing the independent canal from Nagarjuna Sagar to Somasila reservoir which will be running simultaneously to the existing NSRBC.

From the above two possibilities, we are choosing the second possibility, because the distance between Nagarjuna Sagar reservoir to Somasila reservoir is 393.03 km. But the existing NSRBC length is only 202.75 km with the bed width of 73.5 km with the design discharge of 238.33 cumecs, and it has water carrying capacity of 3979 Mm^3, but the proposal water diversion is 3 times more than the existing canal water carrying capacity, and moreover, remodeling of existing NSRBC is not preferred as systems of irrigation suppliers will be get distributed during the remodeling.

So, the only possibility is constructing the new link canal of length 393.02 km from NS to SR, and the link canal will run parallel and adjacent to the existing NSRBC on its right side upto the length of 202.75 km; from this point, NSRBC will merge into the link canal; from there, canal link runs as a single canal upto Somasila reservoir.

Fig. 7 Nagarjuna Sagar Dam to Somasila reservoir link

Actually, from Nagarjuna Sagar, we are proposing to divert 10,521 Mm^3 of water; from that, 8167 Mm^3 of water will be carried by the link canal and remaining 2356 Mm^3 will be carried by existing NSRBC. The water carried by NSRBC (i.e., 2356 Mm^3) will be discharged at tail point (i.e., 202.75 km) so the discharged water will be used to irrigate as usually the 4.75 lakh hectares of land in Guntur and Prakasam districts, and additional 1623 Mm^3 of water will be added at the tail point of NSRBC from Pulichintala Right bank canal. So, from the point of amalgamate of link canal and NSRBC, 9790 Mm^3 of water will be carried through the link canal upto Somasila reservoir.

Somasila reservoir is constructed across Penna River, and it is having the storage capacity of 77.9 TMC and situated at 100 m from MSL. As height of Somasila reservoir (i.e., 100 m) from MSL is less than the height of Nagarjuna Sagar reservoir (i.e., 150 m), the proposed link canal is gravity canal having discharge of 488 cumecs (Fig. 7).

2.9 Somasila Reservoir to Grand Anicut (Pennar to Cauvery Link)

Somasila reservoir is built across the river Pennar near Somasila, in the Nellore district of A.P. The storage capacity of the reservoir is 77.9 TMC. The length of the dam is 352 m, and the top width of the dam is 18 m. The Somasila dam is planned

Fig. 8 Somasila reservoir to Grand Anicut link

to make use of the diverse water from the Pennar River to the Cauvery [13–15]. Water through gravity will reach to Somasila reservoir from the reservoirs Srisailam and Nagarjuna Sagar, which are located in the Krishna basin. It is the major storage reservoir in the Pennar River basin.

The link canal suggests to joining the existing Somasila reservoir and Grand Anicut across the Cauvery River in Tamil Nadu. There will be no submergence of land or adverse environmental impact.

We are proposing to divert a quantity of 8565 Mm^3 from Somasila reservoir through the link canal. As the proposed link canal carries 8565 Mm^3 quantity of water, of which 4221 Mm^3 of water is transferred to the Cauvery River basin, the length of the proposed canal is 529 km and has a designed capacity of 603.33 cumecs.

Table 3 Requirements

S.No.	Requirement name	Requirement No.
1	New canals	7
2	New tunnels	4
3	New pump houses	4
4	New barrages	1
5	New reservoirs	1

The discharged water can be used for irrigation of about 4.912 lakh ha of land. We are proposing to provide these areas falling in the Nellore and Chittor districts of Andhra Pradesh; Tiruvallur, Kancheepuram, Vellore, Tiruvannamalai, Villupuram, and Cuddalore districts of Tamil Nadu; and Pondicherry (U.T.) with irrigation from the water diverted through the link canal.

The Grand Anicut is built across the Cauvery River in Tiruchirappalli district. The Grand Anicut serves as a regulating structure across the Cauvery, without any storage. It serves to supply the requirements of the Grand Anicut canal for irrigation.

As the height of Grand Anicut (i.e., 60 m) from MSL is less than the height of Somasila reservoir (i.e., 100 m), the proposed link canal is a Gravity canal having a discharge of 603.33 cumecs (Fig. 8).

The total number of new canals, new tunnels, new pump houses, new barrages, and new reservoirs are given in Table 3.

3 Design of Canals

The design of canals [16] is done by using Manning's equation recommended by IS 10430-2000. Figure 9 shows the design sketch of the canal.

The Manning's equation [17] is given below,

$$V = (1/n)R^{2/3}S^{1/2},$$

where V = velocity of water, n = rugosity coefficient, S = bed slope, A = area of deep cut portion, P = wetted perimeter of the section, b = bed width, d = depth of water, θ = angle of side slope.

"n" the rugosity coefficient is suggested in the IS 10430-2000 for different kind of lining, and side slope is also referred basing on the type of soil considered.

The design parameters of the canal are discharge, bed width, water depth in the canal, side slope, bed slope, free board, and berm. These parameters are needed to be calculated for designing the canals. If discharge is known, water will be sent through each canal depending upon the requirement. Next the water depth is assumed for each canal relating to soil parameter through which it passes. Bed slop is also assumed based on the topography. The berm, side slope, and free bored are fixed as

Fig. 9 Overview of link canals

recommended in IS 10430-2000. Then by using the Manning's equation, bed width is calculated.

4 Results and Discussions

All the eight link canals interlink Godavari to Cauvery from Polavaram to Grand Anicut. For this linking, we need eight new canals, four new tunnels, four new pump houses, one new barrage, and one new reservoir. The eight new canals design results are given in Table 4.

5 Water Distribution

Based on the existing storage capacity of the reservoirs, we distributed the amount of water. The A.P. Government has taken up the Polavaram project in hoping to at least use 1100 TMC of Godavari water that is going waste. But, while it is under the construction, its potential is limited. So, only 252 TMC of water can be released from Polavaram right canal, from which 96 TMC will be used along the way to Ibrahimpatnam. The remaining water will used by the projects on Krishna River.

Table 4 Canal design results

Godavari River to Krishna River	
Link 1—Canal	**Polavaram to Ibrahimpatnam**
Discharge	327.73 cusecs (i.e., 11,574 cumecs)
Bed width	52.74 m
Water depth	5 m
Side slope	1.5:1
Bed slope	1 in 20,000
Free board	0.75 m
Berm	5 m
Link 2—Canal	**Ibrahimpatnam to Pulichintala**
Discharge	655.45 cusecs (i.e., 23,148 cumecs)
Bed width	92.61 m
Water depth	4.5 m
Side slope	1.5:1
Bed slope	1 in 10,000
Free board	0.75
Berm	5 m
Link 3—Canal	**Pulichintala to N.S.T. P.**
Discharge	655.45 cusecs (i.e., 23148 cumecs)
Bed width	92.61 m
Water depth	4.5 m
Side slope	1.5:1
Bed slope	1 in 10,000
Free board	0.75
Berm	5 m
Link 6—Canal	**Bugga Reservoir to Marrivemula Reservoir**
Discharge	655.45 cusecs (i.e., 23148 cumecs)
Bed width	101.58 m
Water depth	4 m
Side slope	1.5:1
Bed slope	1 in 8000
Free board	0.75 m
Berm	5 m
Link 7—Canal	**Marrivemula Reservoir to Srisailam Reservoir**
Discharge	655.45 cusecs (i.e., 23148 cumecs)
Bed width	26.45 m
Water depth	9.5 m

(continued)

Table 4 (continued)

Side slope	0.5:1
Bed slope	1 in 15,000
Free board	0.75 m
Berm	5 m
Krishna River to Pennar River	
Link Canal	**Nagarjuna Sagar to Somasila Reservoir**
Discharge	488 cumecs (i.e., 17,233.5 cusecs)
Bed width	25.26 m
Water depth	7 m
Side slope	0.25:1
Bed slope	1 in 8000
Free board	0.75 m
Berm	5 m
Pennar River to Cauvery River	
Link Canal	**Somasila Reservoir to Grand Anicut**
Discharge	603.33 cumecs (i.e., 21,306.3 cusecs)
Bed width	61.93 m
Water depth	6 m
Side slope	1.5:1
Bed slope	1 in 15,000
Free board	0.75 m
Berm	5 m

As the diverted water from Godavari River reaches the Krishna River, along with that some amount of surplus water of Krishna River will be diverted toward Pennar. So, from Krishna, we are diverting the water from two points, i.e., 82 TMC of water from Srisailam reservoir and 331 TMC of water from Nagarjuna Sagar Dam will be diverted toward Pennar River.

Due to this project, the benefited districts are Krishna, Vijayawada, Guntur, Nalgonda, Kurnool, Kadapa, Anantapur, Prakasham, Nellore, Mahbubnagar, Chittoor, Tiruvallur, Vellore, Kancheepuram, Tiruvannamalai, Villupuram, Cuddalore, and Pondicherry.

6 Conclusions

The long-term strategy of water deficit problem lies in making the interlinking of rivers challenges by building a network of dams, reservoirs, barrages, and canals throughout the geographical regions of the country.

Link canals from river Godavari to river Cauvery have the potential to draw the surplus water from Godavari and Krishna even at the time of high floods. Main objective of this linking is to take a full advantage of the floods in Godavari and Krishna River. These link canals connect various major projects on Godavari, Krishna, Penna, and Cauvery which forming a long chain. These projects are beneficial to all the districts in Andhra Pradesh, Telangana, and Tamil Nadu that fall under their command area.

We conclude in hopping for many new river interlinking projects like this to come in future, so that we can have a long network of river inter-linkings in the country that have the potential to carry water to the various parts of the country where the droughts are ruling.

Acknowledgements Foremost, we would like to express our gratitude to our advisor Associate Professor Dr. Kamalini Devi and Vidya Jyothi Institute of Technology for continuous support in this research. Our sincere thanks to the prior researchers for their experimental data and researchers in the references.

References

1. Kale et al (2016) Interlinking of rivers and its advantage
2. A report on "Srisailam Right Main Canal" by Irrigation Department. https://irrigationap.cgg.gov.in/wrd/static/approjects/Srisailam_right_bank_canal.html
3. Ameer S, Rafi A, Ahmad A (2016) Interlinking of rivers: concerns and benefits. J Civil Eng Environ Techno 3(6):544–548
4. Subramanya K, Engineering Hydrology. The McGrawn Hill Company
5. Dr. Punmia BC, Dr. Lal PBB, Er. Jain AK, Dr. Jain AK, Irrigation and water power engineering, 16th edn.
6. Detailed notes on "Godavari River" by Wikipedia. https://en.wikipedia.org/wiki/Godavari_River
7. https://en.m.wikipedia.org/wiki/Penna_River
8. https://dashamlav.com/kb/india/rivers/penna/
9. https://indiawris.gov.in/wiki/doku.php?id=pennar
10. Verma A, Kumar N (2015) Interlinking of rivers in India: proposed Sharda-Yamuna link. IOSR J Environ Sci Toxicol Food Technol (IOSR-JESTFT) 9(2, Ver. II):28–35
11. A report on "Nagarjuna Dam" by Irrigation Department. https://irrigationap.cgg.gov.in/wrd/static/approjects/Nagarjuna.html
12. Detailed notes on "Krishna River" by Wikipedia. https://en.wikipedia.org/wiki/Krishna_River#Krishna_Basin
13. https://en.m.wikipedia.org/wiki/Kaveri
14. https://indiawris.gov.in/wiki/doku.php?id=cauvery
15. https://www.britannica.com/place/Kaveri-River
16. Bansal DR (2010) Fluid mechanics and hydraulic machines (revised ninth edition). Laxmi Publications, New Delhi, India
17. IS 10430-2000 (First Edition), Criteria for Design of lined canals and guidance for selection of type of lining. New Delhi, India

Optimization of Hydraulic Design of Spillways and Its Appurtenant Structures—Role of Physical Model Studies

Prajakta Gadge, M. R. Bhajantri, and Kunal Kapur

Abstract Optimization in the design of spillway and energy dissipator is one of the crucial parts of the safety of the dams. Most of the hydropower projects are planned/under construction/commissioned in the north and north-east region due to high hydropower potential. Due to the steep slopes and fragile geology, the soil erosion rate is high during snowmelt and monsoon causing severe sedimentation problems. Considering topography, geology, and other site constraints, the design of a spillway is a challenging task for the design engineers. The design of the spillway for each project is unique and site specific. Physical model studies are an indispensable tool for analyzing the flow and optimizing the design of various components of spillway before execution at the site. The present paper emphasizes the role of the physical model to optimize the design of spillway and its appurtenant structures for the Arun 3 dam spillway, Nepal, which is under construction at the site. The sluice spillway is designed for passing the flood and flushing of sediments from the reservoir. Considering the dual purpose of the spillway, extensive studies were carried out for various ranges of discharges up to design discharge of 15,710 m^3/s for gated and ungated operation of spillway at CWPRS, Pune. Parametric studies were carried out especially for optimizing the design of ski-jump bucket considering the various upstream reservoir water levels and downstream tail water levels to achieve the satisfactory performance of energy dissipation. The findings obtained from the studies for the said project are discussed in detail in the paper. The physical model studies became useful to design the structure economically and hydraulically efficient.

Keywords Spillway · Energy dissipator · Physical model

P. Gadge (✉) · M. R. Bhajantri · K. Kapur
Central Water and Power Research Station, Pune 411024, India
e-mail: prajaktagadge@gmail.com

M. R. Bhajantri
e-mail: bhajan_mr@rediffmail.com

P. V. Timbadiya et al. (eds.), *Flood Forecasting and Hydraulic Structures*, Lecture Notes in Civil Engineering 340, https://doi.org/10.1007/978-981-99-1890-4_27

1 Introduction

Due to steep gradient and mountainous topography, Nepal is blessed with the abundant hydro-resources. However, the construction of hydropower projects in such regions is a very challenging and difficult task due to fragile geology, hydrologic variability, geotechnical constraints, difficult terrain, sparse hydro-meteorological network, etc. Most of the hydropower plants in the Himalayan Rivers are affected by excessive rate of sedimentation which primarily decreases the capacity (life) of the reservoir and fundamentally causes erosion causing the reduction in efficiency and life of the turbine [1]. Also, the formation of new glacial lakes and the potential for glacial lake outburst floods (GLOFs) are recent challenges in the Himalayan region. As such, any change impacting these processes may have serious consequences on hydropower projects or cause severe damage to these projects across the country, whether they are in the planning phase, under construction, or completed.

Arun 3 H. E. Project has been contemplated as a run-of-river scheme, located on Arun River, a principal tributary of Kosi River in Eastern Nepal. The dam site is near Num Village, and the power house site is near the Siding Village of Sankhuwashabha District in Nepal. The diversion dam is envisaged to be a concrete gravity dam of about 70 m in height with its top level at El. 849 m, FRL at El. 845 m, and MDDL at El. 835 m. The spillway is designed to pass the design discharge of 15,710 m^3/s (PMF of 8880 m^3/s plus GLOF of 6830 m^3/s) through five orifice openings of size 9 m wide $\times$ 14.85 m high with crest level at El. 795 m. An underground powerhouse has been provided on the left bank of the river with an installed capacity of 900 MW (4×225). A ski-jump bucket has been provided for energy dissipation. Figures 1 and 2 show the plan and cross section of the spillway.

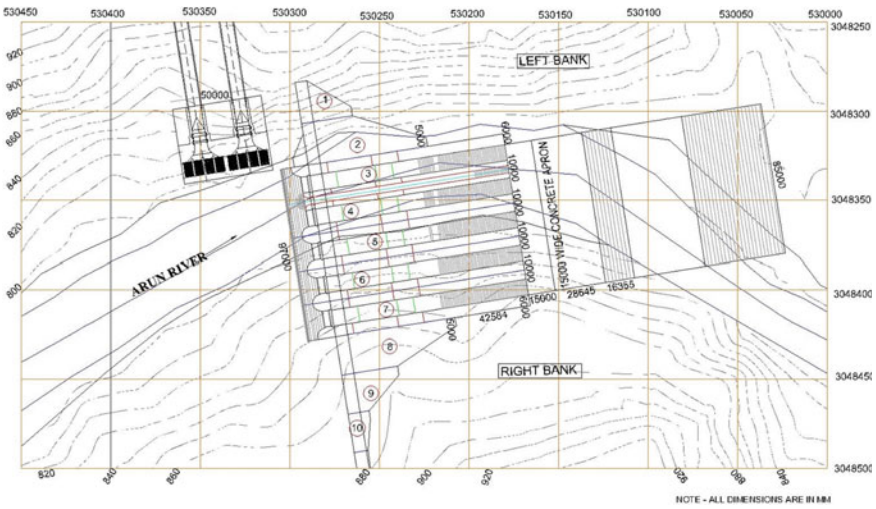

Fig. 1 Plan of the spillway

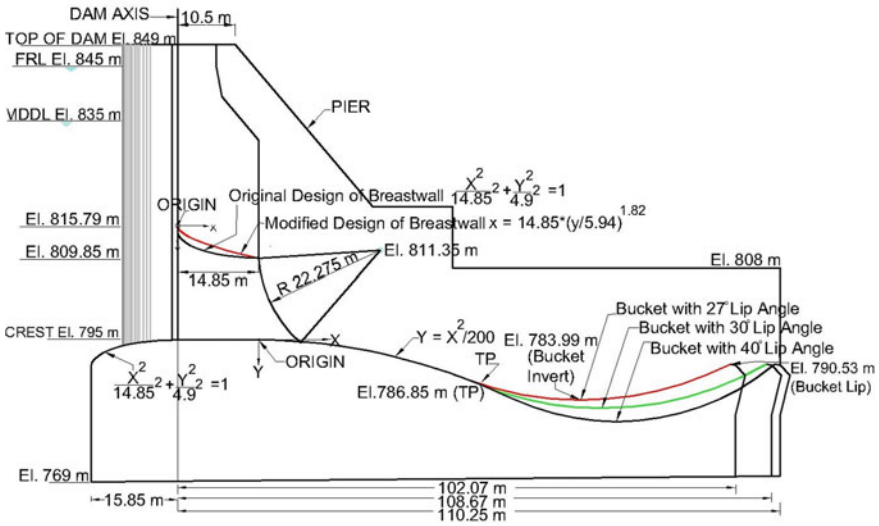

Fig. 2 Cross section of the spillway

Physical modeling is widely used to investigate the design and operational issues in hydraulic engineering. Based on extensive studies carried out on the physical model at CWPRS, the design of spillway profiles and energy dissipator was optimized to achieve the satisfactory performance of the Arun 3 dam spillway. The physical model setup and results obtained from the studies are discussed in the following subsections.

2 Physical Model Setup

Care should be taken in selection of scale of model in such a way that Reynolds number should be sufficiently large to be in the fully turbulent flow regime [2, 3] Gravity is the predominant force in free surface flows such as flow over spillways, weirs, sluices, and channels. Based on Froude number criteria, a model was constructed to a geometrically similar scale of 1:50 with Perspex/PVC sheets. The model was reproduced in a flume with transparent Perspex on the right side so as to visualize the flow conditions upstream and downstream of the spillway including the performance of the energy dissipator. One full span with ski-jump bucket was reproduced. The left side wall of the model was reproduced in PVC foam sheet. The entire model was painted with PU paint so as to have a smooth surface. Figure 3 shows a side view of the physical model. Piezometers were provided along the center of the span for hydrostatic pressure measurement. Necessary arrangements were made for the measurement of discharge, pressures, and water levels. The tail water levels were

maintained downstream of dam axis at chainage 350 m as per the tail water rating curve supplied by project authorities.

Based on Froude number criteria, the values of discharge and velocity observed on the model were converted to prototype dimensions by multiplying scale ratio $(Lr)^{2.5}$ and $(Lr)^{0.5}$, respectively, where Lr is the scale used in the study. Similarly, the values of pressures and water surface profiles were converted by multiplying scale ratio $(Lr)^{1}$. Studies were carried out for the entire range of discharges up to the design discharge of 15,710 m^3/s for the gated and ungated operation of the spillway. Table 1 presents the list of experiments conducted on the model.

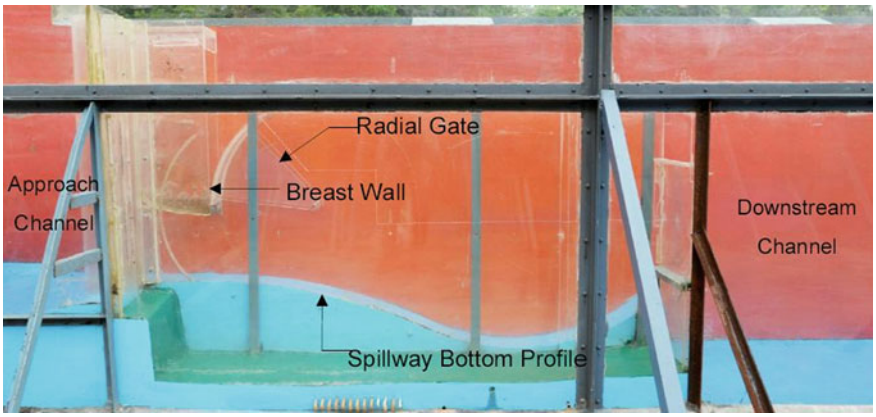

Fig. 3 Side view of the physical model

Table 1 List of experiments conducted on physical model

Sr. no.	Discharge (m^3/s)	RWL El (m)	Gate operation	TWL at 350 m downstream of dam axis (m)
1	3928	809.4	Ungated	796.45
2	(25%)	845	Gated	
3	7855	816.96	Ungated	800.68
4	(50%)	845	Gated	
5	11,783	826.03	Ungated	803.57
6	(75%)	845	Gated	
7	15,710	841.07	Ungated	805.88
8	(100%)	845	Gated	

3 Results for Preliminary Design of Spillway

Hydraulic model studies were conducted for assessing the performance of the original design of spillway with bucket lip angle 40° (refer to Fig. 2) in respect of estimating the discharging capacity, pressures over spillway surface, and performance of energy dissipator for the conditions mentioned in Table 1. The results obtained from the studies are discussed in detail in the following subsections.

3.1 Discharging Capacity of Spillway

The design of the spillway with a ski-jump bucket with a radius of 45 m, lip angle 40°, and invert at El. 780 m was tested on the model [4]. The studies indicated that the design discharge of 15,710 m^3/s could be passed at RWL El. 841.07 m as against MWL El. 849 m through all five spans. The discharge of 17,315 m^3/s could be passed at MWL with all five spans in operating conditions. In one gate inoperative condition, the discharge of 13,850 m^3/s could be passed at MWL El. 849 m which was more than PMF of 8880 m^3/s. Hence, the discharging capacity of the sluice spillway is considered to be adequate. The upper nappe of the jet was not following the breast wall bottom profile at FRL El. 845 m for ungated operation of the spillway. Unstable flow conditions with an intermittent detachment of flow were observed below the breast wall bottom profile as shown in Fig. 4. Therefore, it was suggested to modify the profile in order to avoid flow separation, stabilize the flow conditions and further improve the discharging capacity of the spillway.

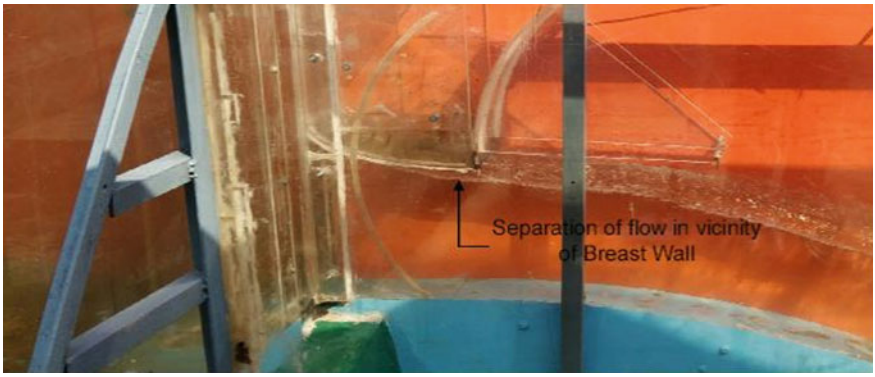

Fig. 4 Flow condition in the vicinity of breast wall bottom profile

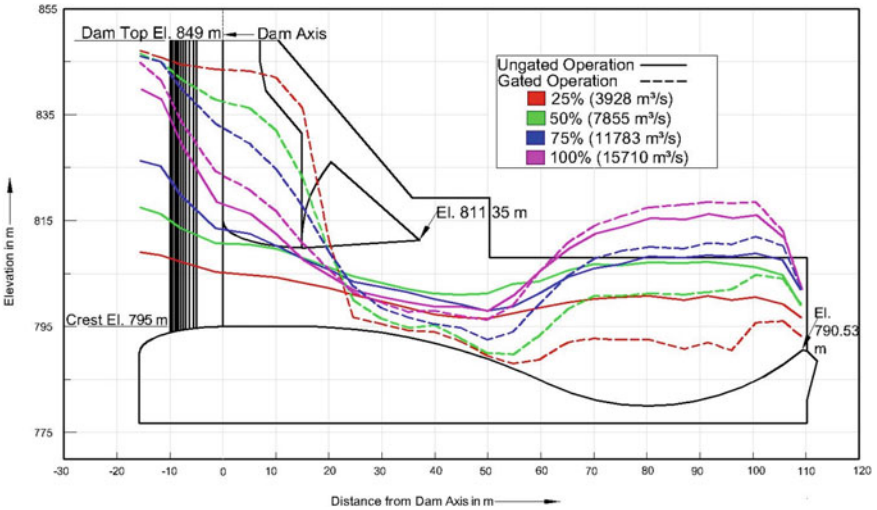

Fig. 5 Pressure distribution along spillway surface with bucket lip angle 40°

3.2 Pressure Distribution Over Spillway Surface

To optimize and measure the susceptibility of the spillway surfaces, piezometric pressures were measured on the bottom profile of the spillway at various locations along the center line of the spillway for various conditions mentioned in Table 1. The pressures were found to be positive throughout the length of the spillway. The cavitation indices were found to be greater than the critical cavitation index of 0.2 for the entire range of discharges. The pressures on the spillway surface were found to be acceptable for gated as well as ungated operation of the spillway as shown in Fig. 5.

3.3 Performance of Energy Dissipator

The performance of the ski-jump bucket was observed for the entire range of discharges for the ungated and gated operation of the spillway. For gated operation, submerged ski action was observed for the entire range of discharges. However, a high-velocity jet was able to push the high tail water preventing the submergence of the bucket. Clear ski action was not observed for any of the reservoir water levels up to FRL for the ungated operation of the spillway. The hydraulic jump was seen forming in the bucket while passing 50% of the design discharge and below with ungated operation of the spillway. Surface rollers of hydraulic jump riding over the sluggish jet below were seen forming in the bucket region due to high tail water levels resulting in cascading flow over the bucket lip. As the spillway is designed

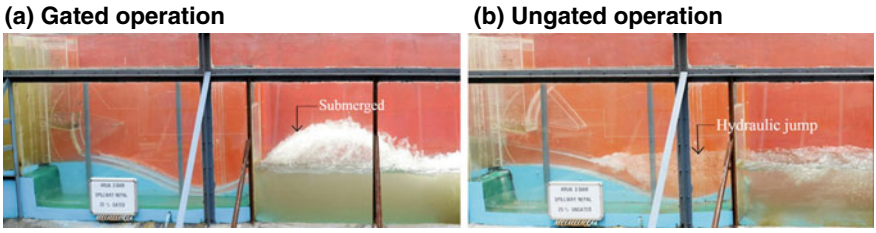

Fig. 6 Performance of energy dissipator for gated and ungated operation of spillway for discharge of 3928 m^3/s (25% of design discharge)

for flushing of sediment deposited in the reservoir, the roller action of the hydraulic jump with sediment-laden water may cause abrasion damage to the spillway surface and bucket. In view of this, it was suggested to modify the energy dissipator by reducing the lip angle of the bucket from 40 to 30° and 27° (as shown in Fig. 2) to achieve satisfactory energy dissipation for the ungated operation of the spillway. Figure 6a and b shows the flow conditions over the spillway and the performance of the ski-jump bucket for the gated and ungated operation of the spillway respectively.

The spillway design with bucket lip angle 40° was found to be suitable in terms of discharging capacity and pressure distribution on the spillway surface. However, the performance of the ski-jump bucket was not found satisfactory especially for passing 50% design discharge and below for ungated conditions of the spillway. Further studies were carried out for modified design with lip angles 30° and 27° to optimize the design of spillway and energy dissipator considering entire ranges of discharges. The results obtained from the studies are discussed in the following sections.

4 Results for Modified Design of Spillway

Parametric studies were carried out to assess the performance of the modified design of the spillway with reduced lip angles of 30° and 27° of the ski-jump bucket. The designs of both the alternatives were incorporated into the model and studies were carried out sequentially after completing the previous studies. Experiments were conducted for the entire range of discharges and reservoir water levels for gated as well as ungated operation of the spillway [5].

The studies indicated that the upper nappe of the jet follows the modified breast wall bottom profile for the entire width of the orifice flow regime thus making the complete height of the orifice fully effective for modified spillway profiles. Discharging capacity was found to be the same as that obtained for the original design of spillway. However, stable flow conditions were observed under breast wall bottom profile at FRL El. 845 m. Hence, it was recommended to adopt the modified design for further studies (refer to Fig. 2). Hydraulic model studies were also

conducted to assess the discharging capacity of the sluice spillway with the partial and equal opening of all the five radial gates for various water levels up to MWL El. 849 m. The gate openings ranged from 1 to 14 m for various reservoir water levels up to MWL El. 849 m. The partial gate opening in these studies was taken as the vertical distance of the gate lip above crest El. 795 m. The discharging capacity curves for the spillway with all the five spans operating and for various gate openings are shown in Fig. 7. These results would be useful in planning the operation of spillway [6].

Piezometric pressures were measured for various conditions mentioned in Table 1, at locations on the bottom profile of the spillway for ungated as well as gated operation as shown in Figs. 8 and 9, respectively. Acceptable pressure distribution with cavitation index values more than the critical cavitation index of 0.2 was observed over the spillway surface for alternative designs of the ski-jump bucket.

The spillway design with bucket lip angle 30° was found to be suitable in terms of discharging capacity and pressure distribution on the spillway surface. However, the performance of the ski-jump bucket was not found satisfactory, especially for passing 25% design discharge with ungated conditions of the spillway. Submerged ski action was observed for the entire range of discharges for gated operation. A high-velocity jet emerging from the bucket was able to push the high tail water preventing the submergence of the bucket. For ungated operation, there was marginal improvement

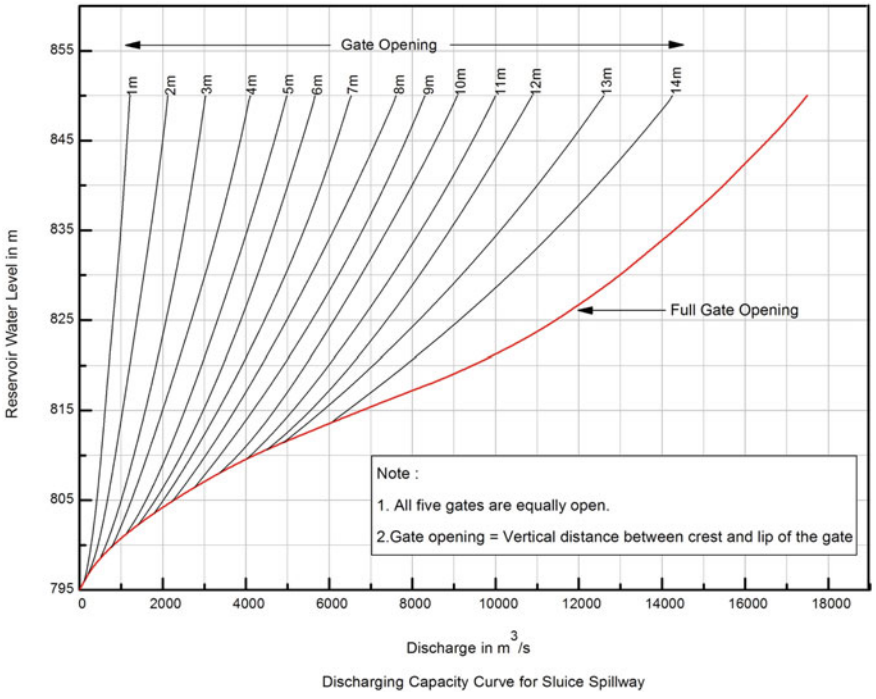

Fig. 7 Discharging capacity curve for full and partial operation of gates

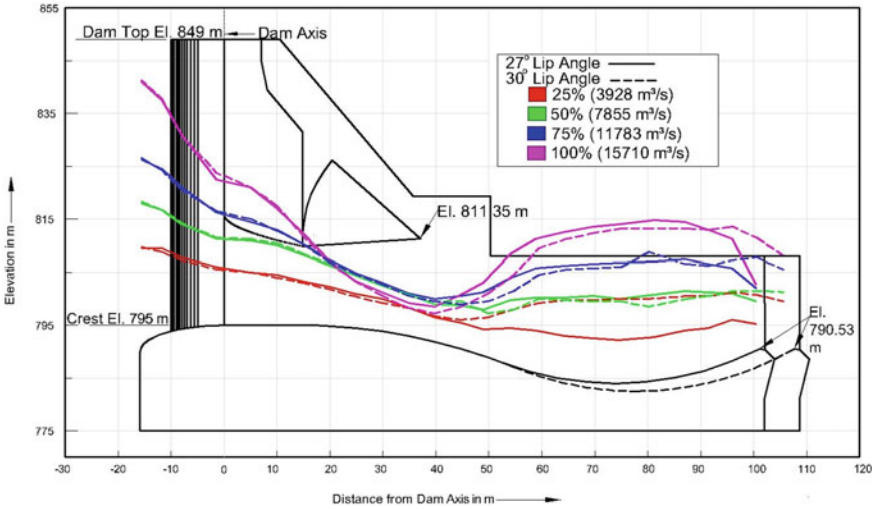

Fig. 8 Pressure distribution over spillway surface for ungated operation

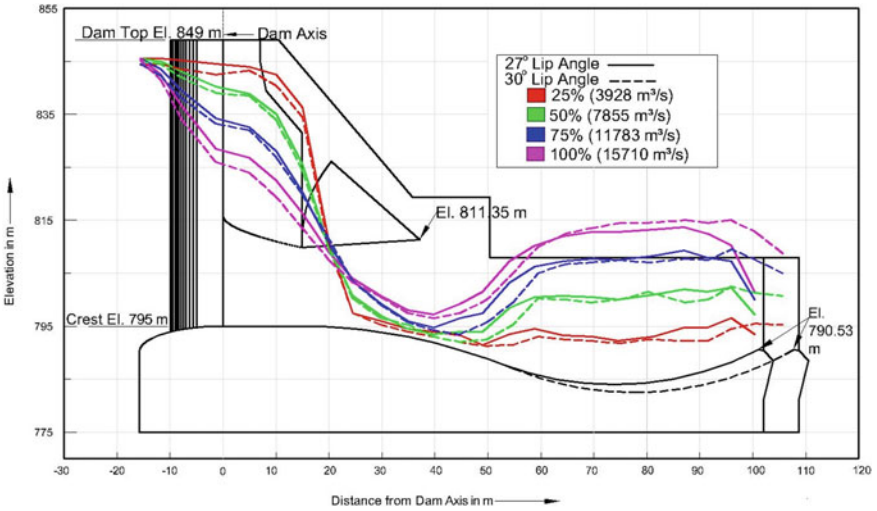

Fig. 9 Pressure distribution over spillway surface for gated operation

in the performance of the ski-jump bucket for the modified design. Hydraulic jump forming in the bucket for the original design vanished for the modified design, and submerged ski action was observed while passing 50% design discharge through the sluice spillway. For 25% design discharge, the formation of the hydraulic jump was still persisting in the bucket for ungated operation.

Modification of the ski-jump bucket with a reduced lip angle of 27° raised the bucket invert by about 4 m to improve the performance of the energy dissipator. The studies indicated that the submergence of the bucket was reduced resulting in the formation of ski action for 25 and 50% of design discharges for ungated conditions as shown in Fig. 10. However, tail water levels corresponding to these discharges are found to be very sensitive as a slight increase in level by about 0.2–0.5 m affected the flow conditions in the bucket. The submerged ski action turns into hydraulic jump formation for a slight increase in tail water level. As the spillway will be used for reservoir flushing, care must be taken to remove the sediments deposited in the bucket periodically. There was no further scope to raise the invert of the bucket as the difference between spillway crest and bucket lip was less, i.e., 4.5 m, and the crest of the spillway was fixed considering the sill level of power intake structure and requirement for effective flushing of sediments. However, the jet was able to push the high tail water preventing the submergence of the bucket for discharges higher than 50% design discharge. For gated operation, submerged ski action was observed for the entire range of discharges. Figure 11 shows the performance of the energy dissipator for the gated operation of the spillway.

A concrete apron properly anchored to the fresh rock and keyed at the downstream end was suggested to provide for protection of spillway toe from undermining as the flow will cascade over the lip of the bucket for low discharges.

Fig. 10 Performance of energy dissipator for ungated operation of spillway

Fig. 11 Performance of energy dissipator for gated operation of spillway

5 Conclusion

Nepal is gifted with huge hydropower potential. Arun-3 H. E. Project has been contemplated as a run-of-river scheme, located on the Arun River in Eastern Nepal. The sluice spillway for Arun 3 dam was designed for the dual purpose of passing the flood and flushing of sediments of the reservoir. Taking into consideration the dual purpose of the structure, optimization of the design of the spillway was a challenging task. Systematic studies carried out on a physical model with 1:50 scale 2D sectional model helped in finalizing the design of the spillway. Parametric studies were carried out especially for optimizing the design of ski-jump bucket with lip angles 40°, 30°, and 27° considering the various upstream reservoir water levels and downstream tail water levels for gated and ungated operating conditions to achieve the satisfactory performance of energy dissipation. Based on extensive studies, the design of the spillway with bucket lip angle 27° was finalized. The findings obtained from the final design are discussed in detail below:

- Design discharge of 15,710 m^3/s could be passed at RWL El. 841.07 m as against MWL El. 849 m through all five spans. In one gate inoperative condition, the discharge of 13,850 m^3/s could be passed at MWL El. 849 m which was more than PMF of 8880 m^3/s. Hence, the discharging capacity of the sluice spillway was considered to be adequate.
- The discharges were measured with the equal opening of all five gates ranging from 1 to 14 m for various reservoir levels up to MWL El. 849. These results would be useful in planning the operation of the spillway.
- Acceptable pressure distribution was observed over the spillway surface, thus minimizing the possibility of cavitation damage along the surface.
- The performance of the energy dissipator with bucket lip angle 27° was found to be satisfactory for all ranges of discharges for the gated and ungated operation of the spillway. However, tail water levels were found to be very sensitive as a slight increase in level by about 0.2–0.5 m affected the flow conditions in the bucket for lower discharges. The ski action turns into a hydraulic jump formation.
- As the spillway will be used for reservoir flushing operation, care must be taken to remove the sediments deposited in the bucket periodically. For gated operation, submerged ski action was observed for the entire range of discharges. A high-velocity jet was able to push the high tail water preventing the submergence of the bucket.

Acknowledgements The authors are thankful to Shri. A. K. Agrawal, Director, and Shri Y. N. Srivastava, Scientist 'E', CW&PRS for their constant encouragement and valuable guidance in preparation of this paper. The authors are thankful to the SJVN and Arun-3 Power Development Company (P) Ltd. (SAPDC), for constant interaction during the course of studies. The contribution of Dr. (Mrs.) V. V. Bhosekar, Former Director, CWPRS, is gratefully acknowledged for the studies.

References

1. Bhosekar VV, Gadge PP (2017) Guidelines for hydraulic design of Orifice spillway. Technical Memorandum, CWPRS, Pune
2. Pfister M, Chanson H (2014) Two-phase air-water flows: scale effects in physical modelling. J Hydrodyn 26(2):291–298
3. USBR (1980) Hydraulic laboratory techniques. A Water Resources Technical Publication, U. S. Bureau of Reclamation, Denver, Colorado
4. CWPRS Technical Report No. 5746 (2019) Hydraulic model studies for spillway of Arun 3 H. E. Project, Nepal, 1:50 Scale 2-D sectional model
5. CWPRS Technical Report No.5774 (2020) Hydraulic model studies for modified design of spillway of Arun 3 H. E. Project, Nepal, 1:50 Scale 2-D sectional model
6. CWPRS Technical Report No.5919 (2021) Hydraulic model studies for discharging capacity for full and partial gate operation of Arun 3 Dam Spillway, Nepal, 1:50 scale 2-D sectional model

Recent Trends in the Design of Auxiliary/ Additional Spillways for Flood Management—Some Hydraulic Considerations

B. S. Sundarlal, R. R. Bhate, and M. R. Bhajantri

Abstract Auxiliary spillways are generally provided to supplement the main or service spillways for augmenting the discharging capacity and will be operated when floods in excess of the capacity of the service spillway are to be encountered. Though they serve as secondary spillways, the functions of auxiliary spillways extend to flushing of floating debris, floating ice formations from the reservoir, especially in Himalayan regions where ice formation is expected due to climatic conditions. The energy dissipators for these spillways are different from that of the main spillways and are governed by site specific conditions. Overtopping has been the most common cause of failure of embankment dams due to inadequate spillway capacity in most of the cases. Failure of dams thus becomes a major concern in providing safety assurance and rehabilitation. It is of utmost important to estimate the design outflow flood/ PMF accurately with the latest available methods/techniques to design the spillways for flood management. Providing additional spillway/auxiliary spillway with proper design along with the service spillway at the conceptual stage of the project itself perhaps will avoid the problem of reassessing the spillway capacity of existing dams and providing alternative solutions to manage the exceptional flood events as is being done in recent times for existing projects. Provision of additional spillway/ auxiliary spillway needs hydraulic model testing for adopting the most efficient and techno-economically feasible design. This paper describes the hydraulic model studies conducted at CWPRS, Pune, for few hydro power projects wherein various hydraulic aspects considered for evolving safe and efficient design of auxiliary/ additional spillways that forms part of the main spillways and efficacy of the energy dissipators of these spillways for managing the flood.

Keywords Auxiliary/Additional spillway · Discharging capacity · Design flood · Hydraulic model studies

B. S. Sundarlal (✉) · R. R. Bhate · M. R. Bhajantri
Central Water and Power Research Station, Pune 411024, India
e-mail: srinivasaslal@gmail.com

P. V. Timbadiya et al. (eds.), *Flood Forecasting and Hydraulic Structures*, Lecture Notes in Civil Engineering 340, https://doi.org/10.1007/978-981-99-1890-4_28

1 Introduction

Spillways have been classified according to their function as service spillways, auxiliary spillways and emergency spillways. Additional/auxiliary spillway includes any spillway that may be utilized infrequently for operation of the reservoir. The overall advantages and disadvantages of service, additional and emergency spillways should be considered in the planning and design of a reservoir project. When the spillway has to cater for huge incoming floods, its size also has to be enormously large. If the topography of the dam site enables provision of two spillways, viz. one located in the main river portion which would cater for the floods of frequent incidents, called as service spillway and an auxiliary spillways on one of the flanks of the of the river, may have to be provided invariably to manage the huge floods, which would be activated when floods in excess of the capacity of the service spillway are to be encountered. Though they serve as secondary spillways, the functions of auxiliary spillways extend to flushing of floating debris, floating ice formations from the reservoir, especially in Himalayan regions where ice formation is expected due to climatic conditions. The energy dissipators for these spillways are different from that of the main spillways and are governed by site specific conditions.

Overtopping has been the most common cause of failure of embankment dams due to inadequate spillway capacity in most of the cases. Approximately, one-third of dam failures can be attributed to inadequate spillway capacity. Failure of dams thus becomes a major concern in providing safety assurance and rehabilitation. Hydrological planning based on local information/data is coming of age. This has led to a need of reassessing spillway capacity for existing dams. It has become more concerned in working out alternatives for managing exceptional flood events when the reservoir is maintained at its maximum holding capacity. In order to release the excess of the flood/revised PMF safely to the downstream, the most feasible alternative of providing an additional spillway for the existing dams has become a recent development in flood management. On existing dams, such measures may not be practical or may involve high investment costs, particularly because such additional capacity may be needed only for the floods of very low probability. Provision of additional spillway/auxiliary spillway meets the requirement of surplussing total spillway flood discharge/PMF (as the case may be) safely to the downstream which when properly designed along with the service spillway at the conceptual stage of the project itself perhaps will avoid the problem of reassessing the spillway capacity of existing dams and providing alternative solutions to manage the exceptional flood events as is being done in recent times for existing projects.

Provision of auxiliary/additional spillway needs hydraulic model testing for adopting the most efficient and techno-economically feasible design. This paper describes the hydraulic model studies conducted at CWPRS, Pune, for evolving safe and efficient design of auxiliary/additional spillways that forms part of the main spillways and efficacy of the energy dissipators of these spillways for managing the flood discharge. Various modifications were recommended that were adopted for the most safe and efficient design of additional/auxiliary spillways for different projects.

2 Case Studies

Case studies are often the best way to describe the hydraulic aspects that are studied on a physical model for a particular project to arrive at safe and efficient designs of spillways. Case studies of model studies for auxiliary/additional spillways conducted along with service spillways for various hydraulic aspects of a Western Himalayan project, Chamera Stage-III Hydroelectric Project, Himachal Pradesh and Sardar Sarovar Project, Gujarat, are presented in this paper, and from the results of these studies, general conclusions are drawn which are very much useful for practising design engineers in the field of dam engineering.

3 Western Himalayan Project

3.1 Technical Details of Project

A Hydroelectric project situated in Western Himalayan region for generation of 330 MW of power comprising a 37 m high and 160 m long concrete faced rockfill dam (CFRD) where in an auxiliary spillway was provided along with the main spillway was studied for assessing its performance with the help of model studies. The initial design and the modified design was studied on the 1:40 scale 3D comprehensive model which was adopted in the prototype after assessing its performance to be satisfactory. Photos 1 and 2 show the upstream and downstream view of dry model of the main and auxiliary spillways. The main spillway was provided with three orifice openings of size 7.0 m wide $\times$ 9.5 m high with crest level at El. 2370 m. The FRL and MWL have been fixed at El. 2390 m and El. 2393 m, respectively. The main spillway is required to have the maximum capacity of 2000 m^3/s at FRL with any two gates open. A ski-jump bucket was provided for energy dissipation. An approach channel with bottom at El. 2368 m upstream of spillway and a 45 m long concrete apron at El. 2363 m downstream of ski-jump bucket have been provided. A high level ice channel spillway has been provided on the left bank as an auxiliary spillway designed to pass ice blocks from intake area to the river downstream. The original design of auxiliary spillway with its crest at El. 2389 m was a stepped spillway consisting of a spilling channel of width 12.5 m, with two spans separated by a pier. Three numbers of steps with different widths with lateral slope towards the main spillway were provided. Figures 1, 2 and 3 show the plan of spillway, section along centre line of the spillway and section of the auxiliary spillway, respectively, for the original design.

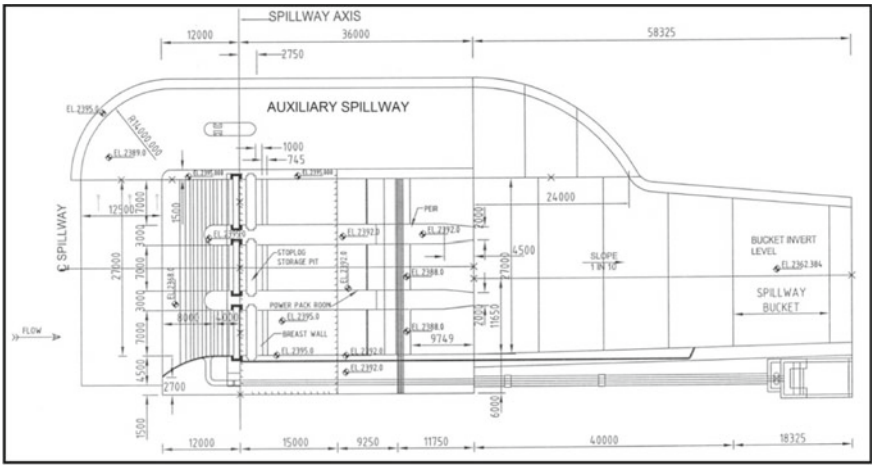

Fig. 1 Plan of main and auxiliary spillways (original design)

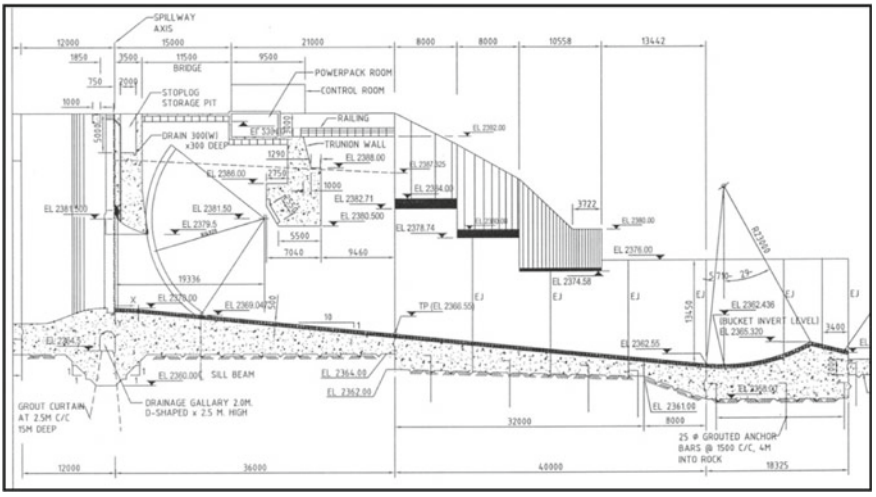

Fig. 2 Section along centre line of spillway (original design)

3.2 Studies with Original Design of Auxiliary Spillway

Performance of auxiliary spillways designed for flushing of ice was observed for different operating conditions. The auxiliary spillway was seen operating along with main spillway. It was observed that the flow was cascading over the large steps and falling as a jet on the main spillway chute, thereby disturbing the main spillway flow. It was also seen that ice cubes could not be flushed and carried downstream over the main spillway chute. Hence, it was necessary to modify the design of auxiliary

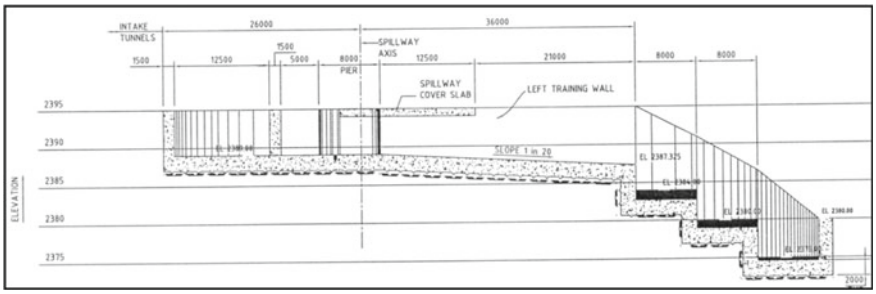

Fig. 3 Section of auxiliary spillway (original design)

Photo 1 Upstream view of the spillway along with auxiliary spillway

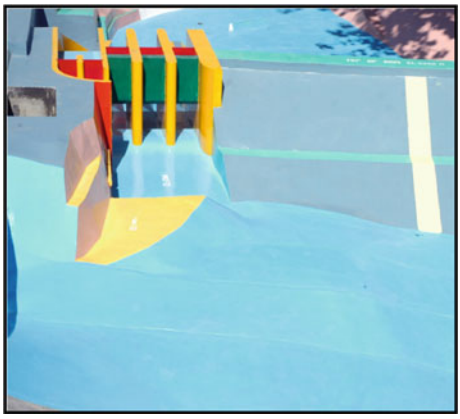

Photo 2 Downstream view of the spillway along with auxiliary spillway

spillway. Photo 3 shows the flow conditions over the main and auxiliary spillways for the original design (Figs. 4, 5 and 6).

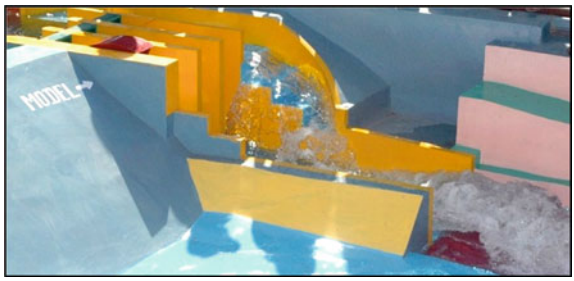

Photo 3 Flow conditions over the main spillway and auxiliary spillway

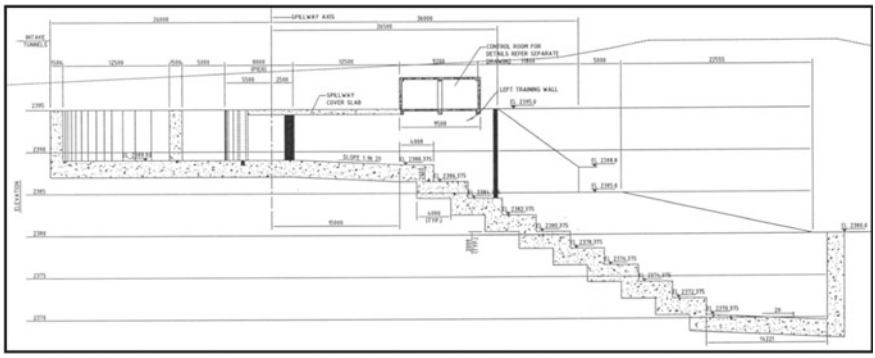

Fig. 4 Plan of main and auxiliary spillways (modified design)

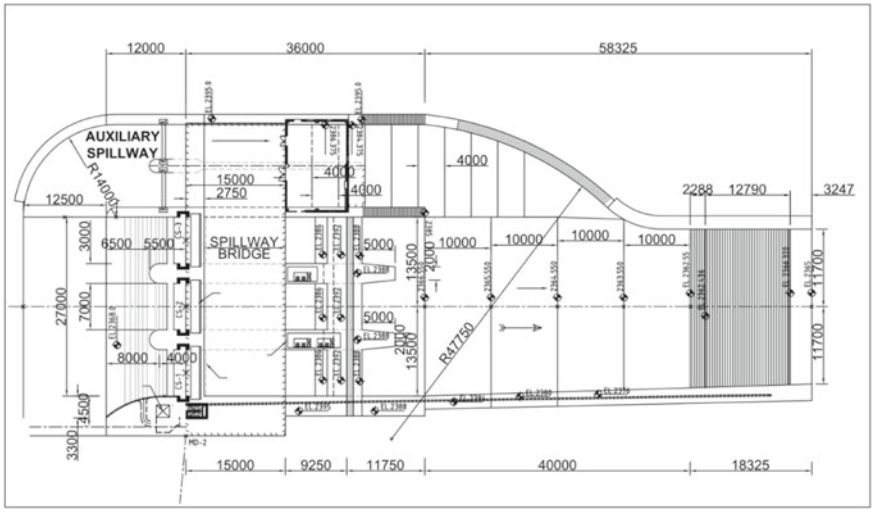

Fig. 5 Section of main and auxiliary spillways (modified design)

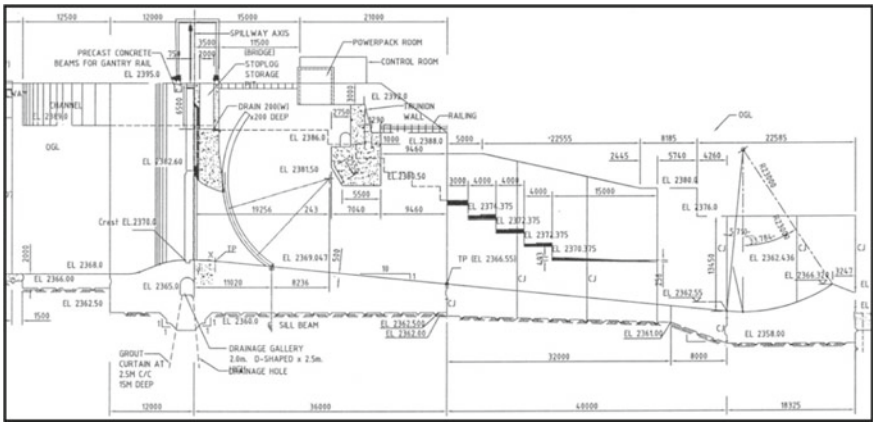

Fig. 6 Section of auxiliary spillway (modified design)

3.2.1 Flow Conditions Upstream and Downstream of Auxiliary Spillway

Auxiliary spillway was seen operating along with main spillway while passing discharges of 500 m^3/s and 1000 m^3/s and maintaining RWL at FRL El. 2390 m. The flow was cascading as a nappe flow with mild impact over steps and falling across the left training wall of the main spillway. The impact of the falling jet over the main spillway flow was reduced to a minimum for the modified design of the auxiliary spillway. Flow conditions upstream and downstream of the auxiliary spillway were also observed by passing various sizes of wooden pieces modelled in lieu of ice blocks through the auxiliary spillway maintaining FRL El 290 m. The sizes (proto) and shapes of wooden blocks used for flushing were square shaped blocks of sides 1 m × 1 m with 0.24 m thickness, 2 m × 2 m with 0.24 m thickness, triangular shaped blocks of sides 2.4 m × 2.4 m × 2.4 m with 0.48 m thickness, 1.4 m × 1.4 m × 1.4 m with 0.24 m thickness, circular-shaped blocks of 2 m diameter with 0.48 m thickness and 1.2 m diameter with 0.24 m thickness. It was observed that all the wooden blocks have been flushed through the auxiliary spillway. Thus, the flow conditions over the auxiliary spillway were satisfactory, and hence, the performance of the auxiliary spillway was found to be acceptable. Photos 4 and 5 show the flow conditions upstream and downstream of the auxiliary spillway while flushing the wooden blocks (ice blocks in proto) in the model.

While passing a discharge of 500 m^3/s through both main and auxiliary spillways maintaining FRL, by passing various sizes of wooden blocks, it was observed that the wooden blocks had the tendency to deposit in front of the main spillway spans. In view of this, it was suggested to install a log-boom in front of the spillway spans and to make some arrangements to divert the ice blocks that will be deposited in front of the log-boom towards the auxiliary spillway so that they can be flushed to the downstream. The log-booms may be designed to withstand the drag forces caused

Photo. 4 Upstream flow conditions in the vicinity of the main spillway and auxiliary spillway with various sizes and shapes of ice blocks with $Q = 500$ m^3/s through main and auxiliary spillway at FRL

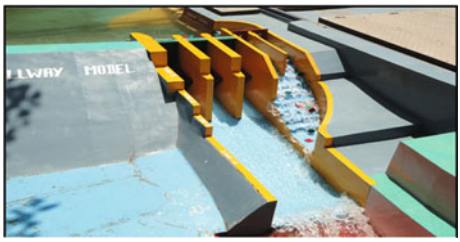

Photo 5 Downstream flow conditions over the auxiliary spillway and main spillway with various sizes and shapes of ice blocks for $Q =$ 500 m^3/s through main and auxiliary spillway at FRL

by the surface velocities in the reservoir in front of the spillway spans and resulting tension in the cable while anchoring at both the ends.

4 Chamera Stage-III Hydroelectric Project

4.1 Details of Project

Chamera H.E. Project, Stage-III is located in Chamba District of Himachal Pradesh. It is a run-of-the-river scheme to generate 231 MW of power utilizing a gross head of the order of 230 m. The project comprises a 68 m high and 78 m long concrete gravity dam. The main spillway is 55.5 m long and equipped with breast walls. The spillway has been designed for passing the PMF of 11,400 m^3/s at FRL EL.1397 m. The energy dissipation arrangement was in the form of a 50 m long stilling basin. The original design of the surface spillway consisted of three bays of 12.5 m width separated by 5 m thick central piers and 4 m thick end piers with crest El 1360 m. The spillway has three radial gates each 12.5 m (wide) $\times$ 16.5 m (high) in size with breast wall arrangement. In order to comply with the requirement of one extra gate during PMF, an additional tunnel spillway was provided on the right bank with crest at El. 1382 m. having 11 m diameter tunnel with ski-jump bucket as energy dissipator, in the original design. Figures 7 and 8 show the plan and section of the surface spillway. Figure 9 shows plan and section of the tunnel spillway. Photos 6 and 7 show the upstream view and downstream view of the model.

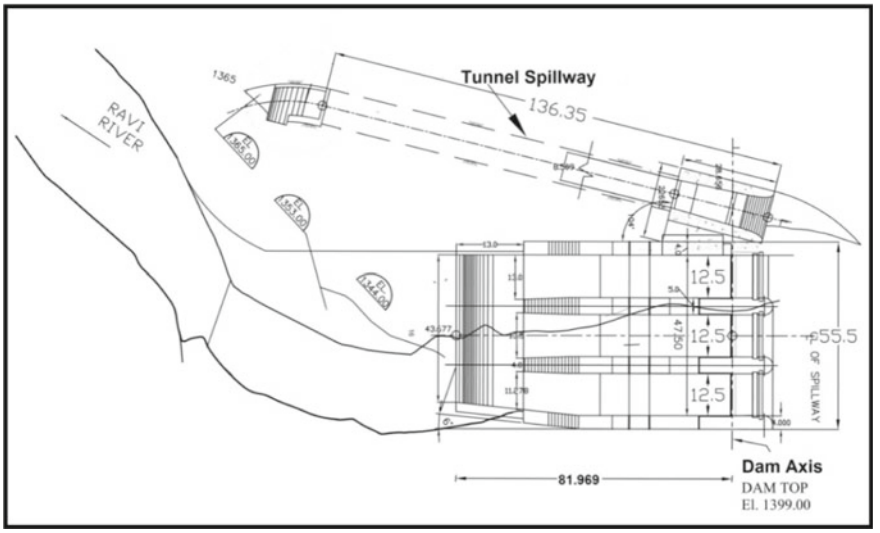

Fig. 7 Plan of surface and tunnel spillways

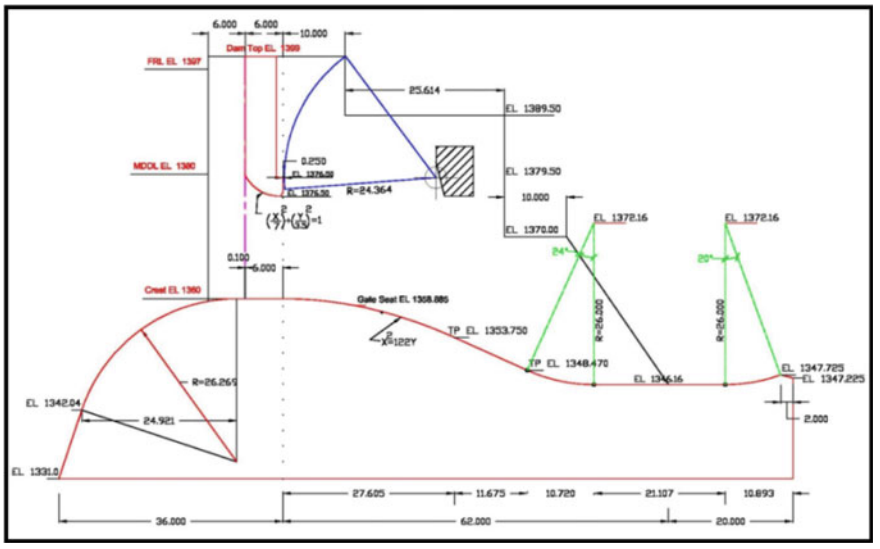

Fig. 8 Section of surface spillway

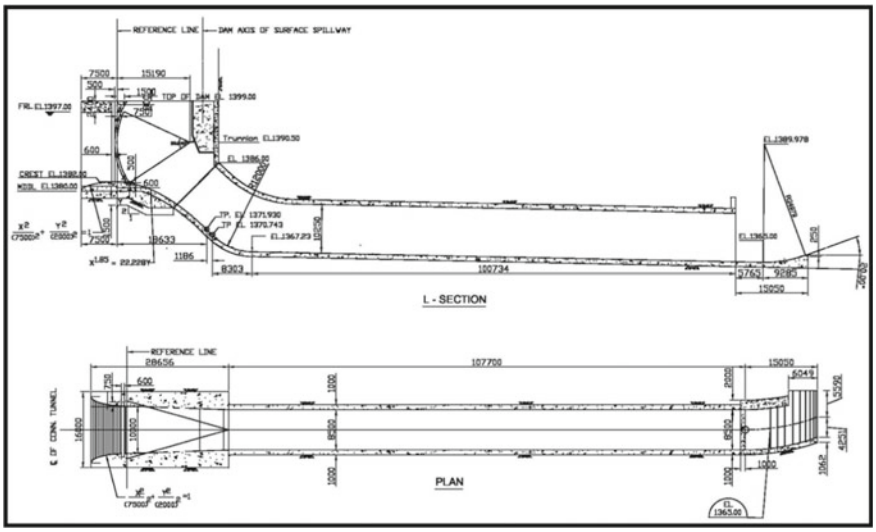

Fig. 9 Plan and section of tunnel spillway

Photo 6 Upstream view of model

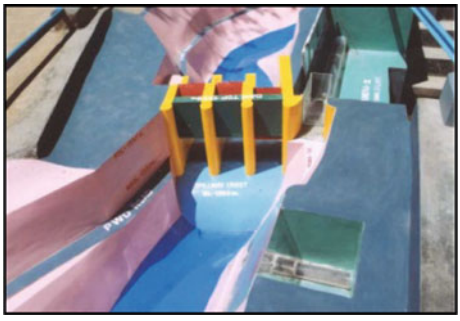

Photo 7 Downstream View of model

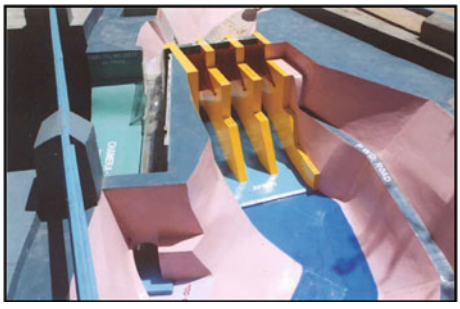

4.2 Studies for the Original Design

Hydraulic model studies were conducted on a 1:60 scale 3D comprehensive model for the following aspects for entire range of discharge and reservoir water levels:

- Discharging capacity of the orifice and tunnel spillways
- Performance of spillway and energy dissipator for tunnel spillway with original and modified design.

4.2.1 Performance of Tunnel Spillway with Original and Modified Design

Studies with original design have shown that the discharging capacity of the spillway was adequate. The performance of the tunnel spillway was observed for entire range of water levels from MDDL El. 1380 m to FRL El. 1397 m. The approach flow conditions upstream of the tunnel spillway were uniform without any circulation or return flows for the entire range of water levels. No vortex formation was seen for the maximum discharge of 11,400 m^3/s. The water surface profile over the crest of the tunnel spillway was touching the sides of the semicircular portion of the roof at the inlet portal. Therefore, it was suggested that the roof of the tunnel at the entrance may be raised by at least 2 m for a length of 20 m. The performance of tunnel spillway was not satisfactory for the discharges of 5700 m^3/s and above when passed through both surface and tunnel spillways because there was a backing of flow at the outlet end of the tunnel due to high tail water levels resulting in cessation of ski-action and formation of hydraulic jump in the tunnel. Photo 8 shows the performance of the energy dissipator of the tunnel spillway while passing a discharge of 1000 m^3/s through tunnel spillway and 12,560 m^3/s from the main spillway at FRL. Therefore, it was recommended that the horizontal portion of the tunnel may be raised by about 3 m. The ski-jump bucket at the downstream end of the tunnel was not performing satisfactorily. Therefore, it was suggested that the flow could be allowed to cascade over the adequately protected downstream rock portion instead of a regular energy dissipation arrangement.

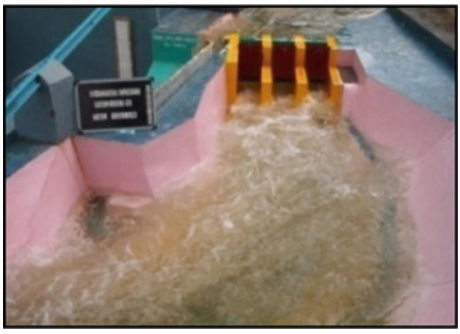

Photo 8 Performance of energy dissipator for $Q =$ 1000 m^3/s from Tunnel spillway and $=$ 12,560 m^3/s from main spillway at FRL

Studies were carried out with the revised design of tunnel spillway. As the ski-jump bucket at the downstream end of the tunnel spillway was not performing satisfactorily, no energy dissipator was proposed downstream, and the flow was allowed to cascade over the downstream rock portion. Due to insufficient rock cover and very steep right bank, it was difficult to locate inlet and outlet portals for tunnel spillway. In view of this, tunnel spillway as additional spillway has been removed, and the design of the spillway had been revised consisting of an open channel chute spillway with a ski-jump bucket adjacent to the main spillway due to site constraints.

4.3 Performance of Chute Spillway (Revised Design)

The revised design of additional spillway consists of a chute whose width tapers from 10 m at the dam axis to 7 m at the lip of the ski-jump bucket. Ski-jump bucket with a 20° exit angle has been provided as the energy dissipator. Figures 10 and 11 show the plan and section of spillways for the revised design.

The revised design of chute spillway was incorporated in the existing 1:60 scale comprehensive model, and studies were carried out to check adequacy of chute spillway in respect of discharging capacity, water profiles and pressures over the chute spillway and to assess the performance of ski-jump bucket of chute spillway. Photo 9 shows the performance of energy dissipator for a discharge of 4010 m^3/s (2850 m^3 through service spillway + 1160 m^3/s through chute spillway) at FRL El. 1397 m.

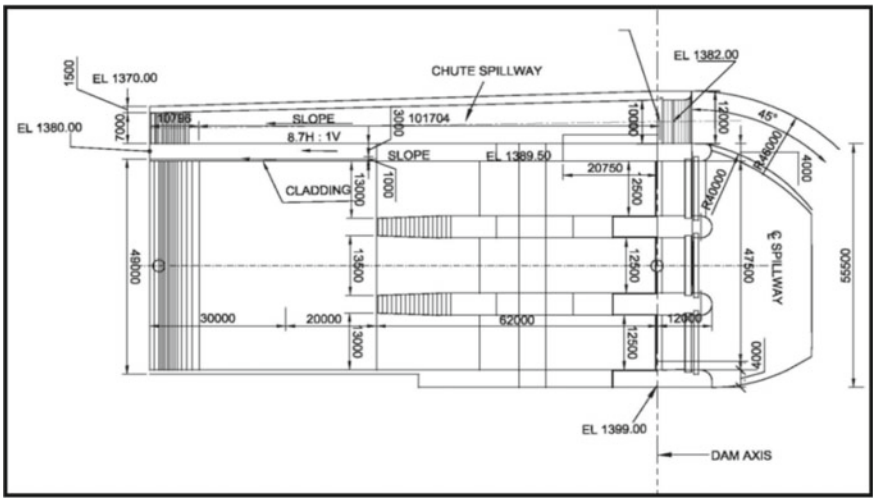

Fig. 10 Plan of surface and chute spillway (revised design)

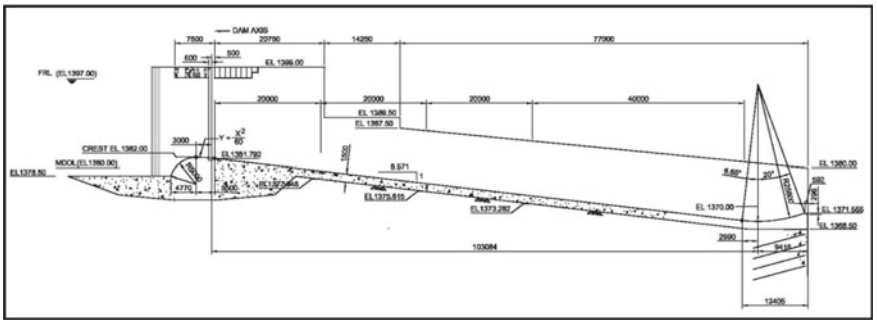

Fig. 11 Section of chute spillway

Photo 9 Performance of Energy dissipator of the chute spillway for $Q = 4010$ $(2850 + 1160)$ m^3/s at FRL El 1397 m

4.3.1 Results for the Revised Design

- A discharge of 1160 m^3/s could be passed through the chute spillway at FRL El.1397 m. A discharge of 12,560 m^3/s could be passed through both main and chute spillways operating simultaneously with reservoir water level at EL 1397 m as against the design maximum discharge of 11,400 m^3/s. Thus, the combined discharging capacity of the spillway was found to be adequate.
- The water surface profiles in the chute spillway were contained within the training walls for all the conditions and the ski-jump jet impinges at the centre of the river for discharges higher than 500 m^3/s. The pressures observed along the centre line of the chute and sides of the training walls were positive for the entire range of discharges.
- The performance of the ski-jump bucket was satisfactory for the combined discharge of 8550 m^3/s and below through main and chute spillways. For the maximum discharge of 12,560 m^3/s through the main and chute spillway, there was partial submergence of the lip of the ski-jump bucket of the chute spillway due to high tail water level.

Cascading flow was observed over the bucket lip up to RWL El. 1383.2 m. Hence, adequate protection measures were required to be provided to protect the excavated rock downstream and along left and right hill slopes. Overall performance of the chute spillway was found to be satisfactory.

5 Sardar Sarovar Project, Gujarat

5.1 Details of Project

Sardar Sarovar Project is located on river Narmada in the state of Gujarat. The concrete gravity dam is 165 m high and 1200 m long. It is provided with a 30 span spillway of width 18.3 m separated by 4.7 m thick piers and equipped with radial gates 18.3 m × 14.7 m. The probable maximum flood (PMF) was worked out to be 170,000 m^3/s, and the corresponding design maximum outflow discharge was 141,484 m^3/s. FRL is at El.138.68 m, and MWL is at El 140.1 m. The spillway layout was studied for the PMF outflow conditions. The service spillway of 23 spans has a sloping-cum-horizontal stilling basin as energy dissipator, and the seven spans auxiliary spillway has two spillway chutes terminating in ski-jump buckets. The seven span auxiliary spillway has been divided into four spans having ski-jump bucket with invert at El.40.177 m and three spans with ski-jump invert at El. 59.85 m. Figures 12, 13 and 14 show the general layout plan of the spillways, section of the main spillway and section of the auxiliary spillway.

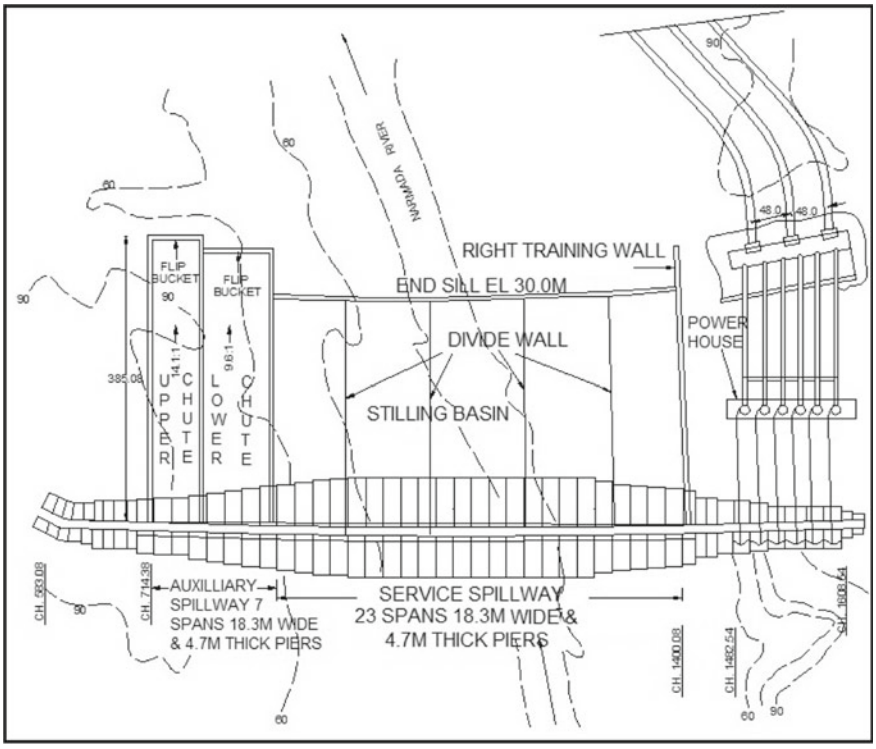

Fig. 12 General layout plan of spillway

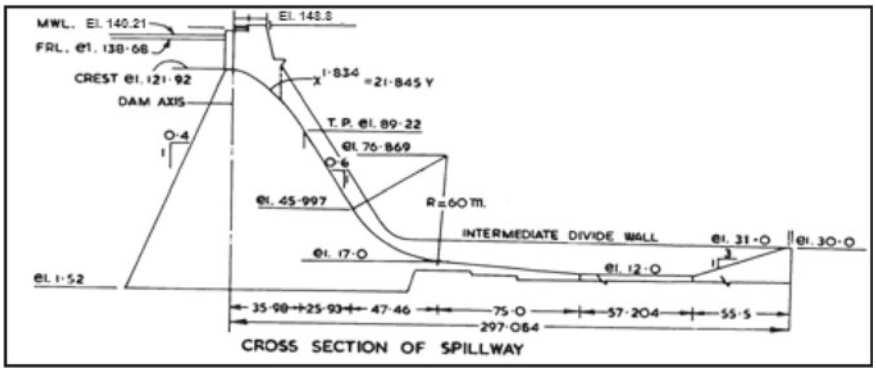

Fig. 13 Section of service spillway

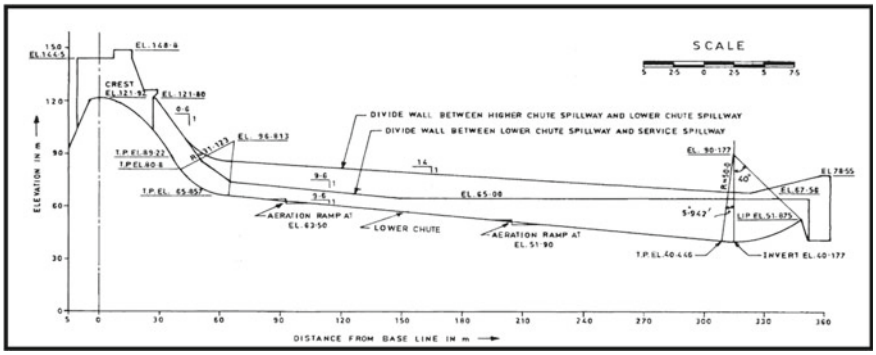

Fig. 14 Section of auxiliary spillway

Hydraulic model studies were conducted at CWPRS for assessing the discharging capacity for full and partial gate operation on a 1:150 scale comprehensive spillway model. Studies relevant to auxiliary spillway only are described as follows:

- Layout of the main and auxiliary spillway
- Discharging capacity of the spillway (service and auxiliary spillway)
- Flow conditions and operation of auxiliary spillway.

5.2 Layout of the Main and Auxiliary Spillway

Model studies for the various alternative layouts of the spillway along with the energy dissipator were conducted, and the layout as shown in Fig. 12 was finalized.

Table 1 Discharges for significant reservoir water levels (with gates fully open)

Sr. No	RWL in m	Discharge in m^3/s	No. of spans
1	138.68	65,000	23
2	140.21	74,720	23
3	140.21	96,600	30
4	142.21	113,640	30
5	147.65	170,000	30

5.3 Discharging Capacity of the Service and Auxiliary Spillways

The Project Authorities indicated that the 23 span service spillway would be operated up to FRL El 138.68 m and for higher reservoir water levels all the 30 spans of the spillway including seven spans of auxiliary spillway would be operated. The studies for discharging capacity of spillway with radial gates fully open with 23 and 30 spans operating were conducted for the entire range of discharges up to the design maximum discharge of 170,000 m^3/s. Various discharges for the significant reservoir water levels while operating 23 and 30 spans respectively are given in Table 1.

5.4 Operation of Auxiliary Spillways

As the discharge increases above 65,000 m^3/s, the auxiliary spillways are to be operated uniformly till their full opening. With the reservoir level rising to El. 140.21 m, the lower chute comprising four spans will be operated first followed by the upper chute with three spans. The lower and higher chutes would cascade initially before the clear ski-action sets in. Studies indicated that the lower and upper chute spillways required about 6.5 and 5.5 m gate openings respectively with reservoir water level at MWL El. 140.21 m for a clear ski-action. In such circumstances, the cross flow from the higher chute to lower chute may not cause any unfavourable flow conditions or damage to the lower chute spillway, as the same would already be operating. Extensive protection works for strengthening downstream of auxiliary spillways to take care of erosion due to cascades were suggested by CWPRS, which had been implemented at site. The performance of the auxiliary spillways was found to be satisfactory. Photo 10 shows the flow conditions downstream of the spillway and energy dissipator for both the main and auxiliary spillway on a 1:150 scale comprehensive model.

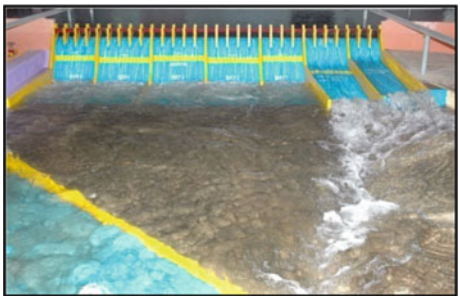

Photo 10 Flow conditions for $Q = 96{,}600\ m^3/s$, with service and auxiliary spillways operating

5.5 Schedule of Gate Operation

Hydraulic model studies were conducted for passing the discharge through the spillway for various combinations of gate openings and spillway spans.

A schedule of gate operation for the service and auxiliary spillways was evolved as follows:

- Operate the service spillway up to the discharge of all 23 spans which is about $65{,}000\ m^3/s$
- Operate the auxiliary spillway, i.e. remaining seven spans only if the outflow exceeds $65{,}000\ m^3/s$.

6 Results and Discussion

In all the three case studies, the performance of the original and revised designs of auxiliary/additional spillways have been assessed based on the flow conditions observed on the models for various operating conditions and other hydraulic parameters. The performance of the revised designs had been assessed by comparing the flow conditions which were improved or better with respect to the original design. The main hydraulic parameter such as discharging capacity of the spillway with auxiliary/additional spillway under operation was assessed and its adequacy was ensured to pass the design flood.

From the case study of a Western Himalayan project, an efficient design of auxiliary spillway along with the energy dissipator in the form of a stepped spillway was arrived at by conducting hydraulic model studies to flush the ice cubes in the vicinity of the power intake. Studies carried out for additional tunnel spillway provided along with the service spillway for Chamera-III, H. E. Project with two alternative designs on the model. As tunnel spillway was not performing satisfactorily, it was replaced with a chute spillway, the performance of which was found to be satisfactory in respect of discharging capacity, flow conditions over the spillway and energy dissipator. This facilitates the requirement of one extra gate to cater for Probable Maximum Flood.

In the case of the Sardar Sarovar project, performance of the two auxiliary spillways provided in the form of chutes followed by ski-jump buckets was found to be satisfactory in respect of discharging capacity. The recommendations made for operating the auxiliary spillways and the gate operation schedule proposed were of very much useful to the project authorities in the operation of main and auxiliary spillways which will ensure safe spillway operation to pass the design flood downstream safely. Thus, from the results of the model studies, it was shown that provision of auxiliary/additional spillways with proper design and operation would ensure effective flood management which is of utmost importance for any dam project.

7 Conclusions

General conclusions drawn from the results of the model studies are as follows. Hydraulic model studies played a vital role in evolving safe and efficient design of Auxiliary/additional spillways provided along with service/main spillways for different projects with different types of energy dissipators. Provision of additional spillway/auxiliary spillway along with the service spillway meets the requirement of surplussing flood discharge/PMF (as the case may be) safely to the downstream, which when properly designed at the conceptual stage of the project itself perhaps will avoid the problem of reassessing the spillway capacity of existing dams and providing alternative solutions to manage the exceptional flood events as is being done in recent times for existing projects. Provision of auxiliary/additional spillways with proper design and operation would ensure effective flood management which is of utmost importance for any dam project. The service spillways along with auxiliary/additional spillways constructed based on the recommendations from the hydraulic model studies conducted at CWPRS, for the project of a Western Himalayan river, Chamera Stage-III H.E. project, H.P, and Sardar Sarovar Project, Gujarat, are operating satisfactorily.

Acknowledgements The authors are grateful to Shri. A. K. Agrawal, Director, CWPRS, for encouragement and permission to publish this paper. The authors are also thankful to the project and design engineers from NHPC and Sardar Sarovar Project authorities for constant interaction during the course of studies. The help of all the staff in conducting the studies and compiling the data is gratefully acknowledged.

Estimation of Pressure in a Plunge Pool with Rectangular Plunging Jet

Sushma Vyas and Y. N. Srivastava

Abstract The ski jump spillways with ski jump buckets are used commonly to deflect the jet far away in downstream spillways when it is not possible to provide a hydraulic jump type dissipator. The bucket deflects the high velocity jet into the air and discharges into a plunge pool at a considerable distance away from the toe of the dam. To safeguard the dam structure, it is very important to predict the pressure on the plunge pool bed. The characteristics of a jet influences the energy dissipation and pressure on the bed of the plunge pool. In the present study, parameters related to the characteristics of a jet were measured, and pressures on the bed of the plunge pool were estimated with different empirical formulae or plots given by various researchers obtained through experiments or scale models.

Keywords Spillway · Orifice · Plunge pool · Scour · Pressure · Rectangular jet

1 Introduction

Orifice spillway with low level sluices and ski jump bucket type energy dissipator is commonly used in the upper Himalayan Rivers which have very steep bed gradients. The energy dissipation from ski jump is accomplished by throwing a jet away at a large distance away from the dam body so that the main dam is not endangered by the scour caused by the jet of water. The jet is subjected to air resistance, air entrainment, and impingement at the river bed. During its fall, the jet absorbs air, and its thickness or core changes as a result of gravity. Plunging ski jump jets frequently fall from a considerable height, traverse some distance in the air before striking the water surface and break down due to turbulence. The behavior of the jet in the ski jump buckets is more similar to a three-dimensional jet, but its resemblance is more to a two-dimensional jet. The jets issuing from ski jump spillways are either square or rectangular in cross sections and are often inclined while striking the water surface.

S. Vyas (✉) · Y. N. Srivastava
Central Water and Power Research Station, Pune 411024, India
e-mail: vyassush13@gmail.com

P. V. Timbadiya et al. (eds.), *Flood Forecasting and Hydraulic Structures*, Lecture Notes in Civil Engineering 340, https://doi.org/10.1007/978-981-99-1890-4_29

It is a common practice to provide the pre-excavated plunge pool with water cushions to receive the impact of falling jets. The diffusion of jets in a plunge pool dissipates the energy of the falling jet and reduces the pressure fluctuations at the base of the plunge pool. The water cushion in the plunge pool, pressure on the pool floor is influenced by the characteristics of the jet. The volume of air present in the pool also influences the pressure.

In the present study, measurements of parameters related to plunging jet striking into the plunge pool and the pressures on the plunge pool floor were discussed. Pressures were measured on the plunge pool floor and compared with the experimental data. Parameters such as jet drop length, jet breakup length, lateral spread of jet, and jet impingement point were measured and compared with the results of few researchers.

2 Literature Review

Researchers have studied various parameters and characteristics of jets such as jet breakup length, jet lateral spread, jet penetration depth, and diffusion in the mass of water and energy and pressures imparted on the pool bottom. The striking jet in the plunge pool causes huge turbulence surface fluctuations, and the jet breaks down into individual clusters stated by [1–3]. The combined effects of jet spreading and air entrainment decrease the mean and fluctuating dynamic pressures on the pool floor.

Jet breakup length is defined as the distance between the origin of the jet and the point where the jet clusters begin to form. The jet is completely developed, and it is a continuous mass up to the jet breakup point. The characteristics of a plunging circular jet (top view) given by [2] shown in Fig. 1 while a schematic view of a falling rectangular jet into a plunging pool from an arch dam is shown in Fig. 2, respectively.

2.1 Jet Break Up Length

To calculate the jet breakup length, many researchers proposed different formulae.

Ervine et al. [2] proposed the following expression for estimation of break up length:

$$\frac{L_b}{D_o {F^2}_o} = \frac{1.05}{C^{0.82}} \tag{1a}$$

where L_b is jet breakup length, D_o is the equivalent Jet diameter at the origin, F_o is the Froude number, and C is the turbulence parameter. Turbulence parameter (C) can be expressed in terms of Froude number and Turbulence intensity (T_u).

$$C = 1.14 T_u F_o^2 \tag{1b}$$

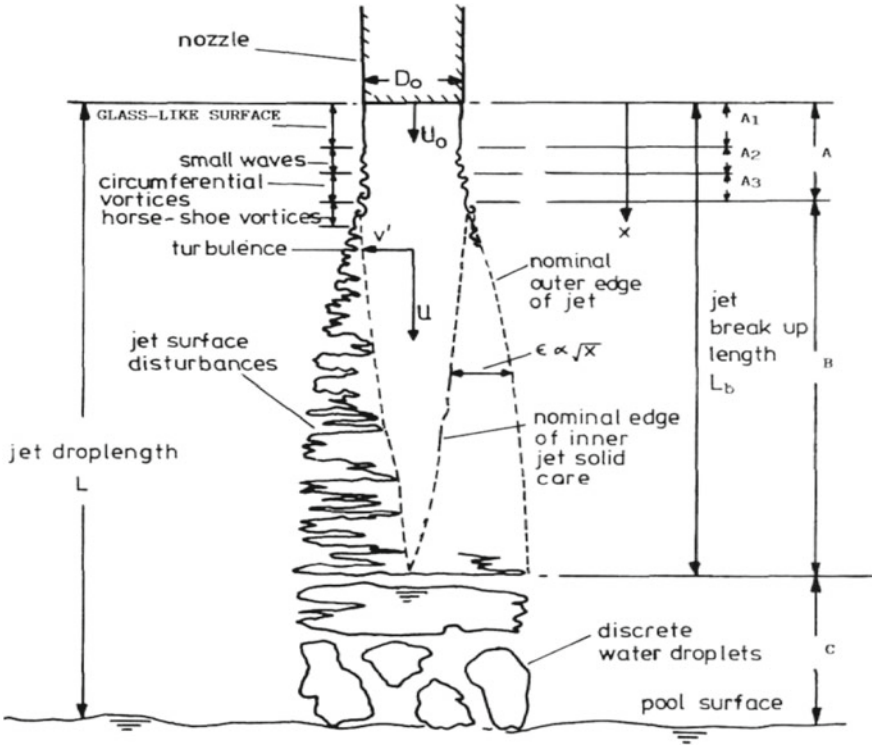

Fig. 1 Characteristics of plunging circular jet (top view)

Elsawy et al. [4] proposed equations for calculating jet breakup length based on discharge and turbulence intensity range (T_u).

$$\text{For } T_u \text{ at } \%\ L_b = 60 * Q^{0.39} \tag{2a}$$

$$\text{For } T_u \text{ at } 3\%\ L_b = 17.4 * Q^{0.31} \tag{2b}$$

$$\text{For } T_u \text{ at } 8\%\ L_b = 4.1 * Q^{0.2} \tag{2c}$$

where Q is discharge passing through the spillway span. The equation for the break up length based on specific discharge (q) proposed by [5] is

$$L_b = 6 * q^{0.32} \tag{3}$$

Elsawy et al. [4] suggested turbulence intensity T_u of the jet from 0 to 8%, while $T_u = 0$–5% suggested by [6].

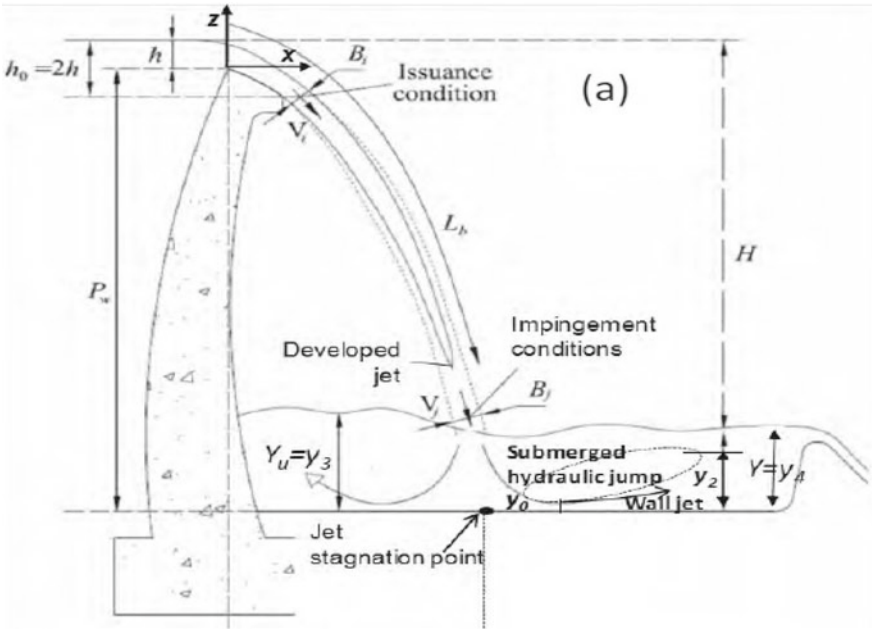

Fig. 2 Schematic view of falling rectangular jet into a plunging pool from an arch dam (side view)

2.2 Lateral Spread of Jet

The spreading of the jet affects the pressure coefficient. Lateral spread of the jet is calculated using Eq. (4) proposed by [2].

$$\varepsilon = \frac{1.14 T_u U^2}{g} \left[\sqrt{\frac{2L_u}{D_o F^2{}_0} + 1} - 1 \right] \tag{4}$$

where L_u is the length of fall from the origin of the jet and U is the jet velocity at distance (L_u) measured from the origin.

2.3 Jet Penetration Depth

Penetration depth of a jet is defined as the maximum depth to which jet bubbles would penetrate. This is an important factor to enhance energy dissipation and to promote air entrainment. As quoted by Guyot et al. [7], there are two procedures to predict penetration depth (a) by using semi empirical equations based on either continuity or momentum equations (b) by using empirical formulae (see Table 1).

Table 1 Formulae to penetration depth

Author name	Empirical formulae
McKeogh and Ervine [8]	$H_p = 2.6(U_j D_j)^{0.32}$
Nakasone [9]	$H_p = \frac{2}{3} H$
Falvey and Ervine [10]	$\frac{U_j}{U_t} = 3.12\left[\frac{D_j}{H_p} + 4\tan \propto \left(4\frac{H_p}{D_j}\right)\tan^2 \propto\right]$
Clanet and Lasheras [11]	$\frac{H_p}{D_j} = \frac{U_j}{(2\tan\propto)U_t}$

Where H_p is penetration depth of jet, U_j and D_j is a velocity and diameter of jet at entry of plunge pool, U_t is bubble terminal velocity $\approx$ 0.22–0.25 m/s [10, 11], H is the fall height of jet from reservoir level to tail water level, and α is jet open angle under free surface

2.4 *Classification of Jet Based on Jet Parameters and Water Cushion in the Plunge Pool*

Various researchers [3, 12–14] have given another type of classification of jet based on plunge pool depth or water cushion in the plunge pool (Y), fall height H, jet breakup length L_b, and Jet thickness (B_j). Figure 3 shows classification of jet and pressure fluctuations as per H/L_b and Y/B_j ratio.

For undeveloped jets, pressure peaks substantially decrease as depth of water in the plunge pool increases, and these pressure peaks have similar constant pressure patterns above and below the mean pressure. While for developed jet cases, much more fluctuations are observed, and this is due to the presence of a turbulent shear-layer impacting on the plunge pool bottom, due to this there is a larger pressure distribution region than undeveloped jets. This effect increases with the fall height and the water cushion.

2.5 *Pressure Coefficients at Plunge Pool Floor*

Ervine et al. [2] derived the relation between the pressure coefficients and ratio of pool depth to diameter of the jet. Figure 4 shows variation of pressure coefficient with respect to the ratio of Y/D_j.

Martins and Viseu [15] had given expressions to calculate turbulent pressures acting at the bottom of the plunge pool acting more at the point of impact of the jet.

The mean dynamic pressure is given by Eq. (5)

$$P_d = 20\frac{q^{1.73} H^{0.395}}{g^{0.865} Y^{1.99}} \tag{5}$$

The maximum observed value of the pressure fluctuation expressed as

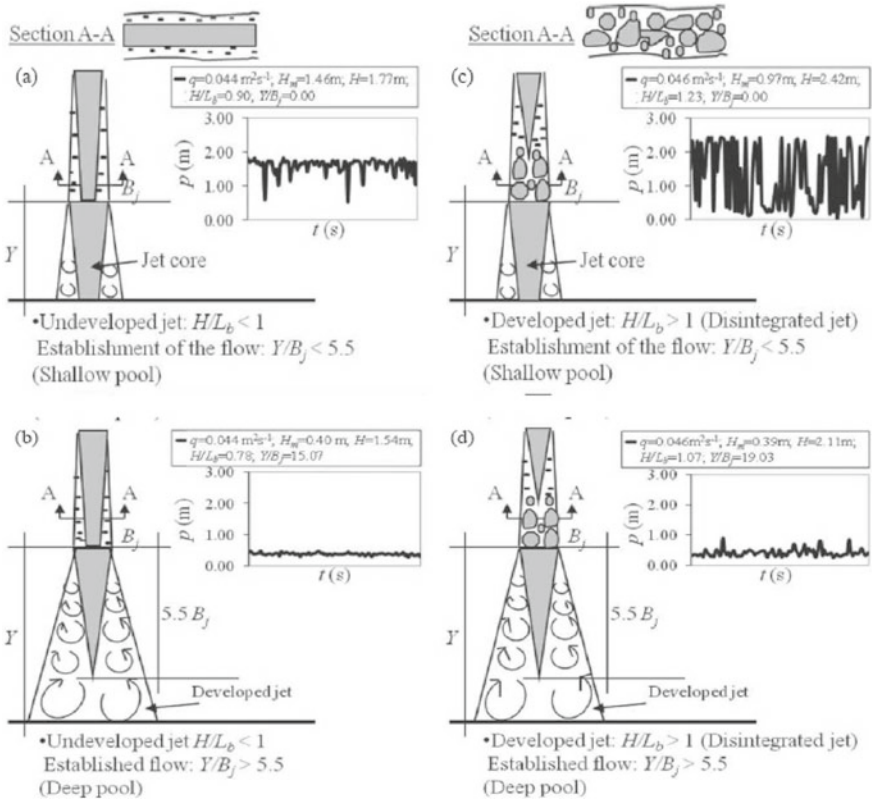

Fig. 3 Classification of jet and pressure fluctuations according to H/L_b and Y/B_j ratio given by Castillo et al. [3, 12, 13]

$$P\prime_{\max} = \frac{H}{2} 0.73^{(Y/y_c)} \tag{6}$$

The maximum dynamic pressure can be computed as sum of mean dynamic pressure and maximum pressure fluctuations and it is expressed as

$$P^{'}{}_{\max} = \overline{P_d} + P^{'}{}_{\max} \tag{7}$$

$$P^{'}{}_{\max} = H \text{x } 0.68^{(Y/y_c - 1.5)} \tag{8}$$

where q is a specific discharge, y_c is a critical depth of water, P_d is Mean dynamic pressure, $P'_{\max}$ is the maximum value of pressure fluctuation, and $P_{\max}$ is the maximum dynamic pressure.

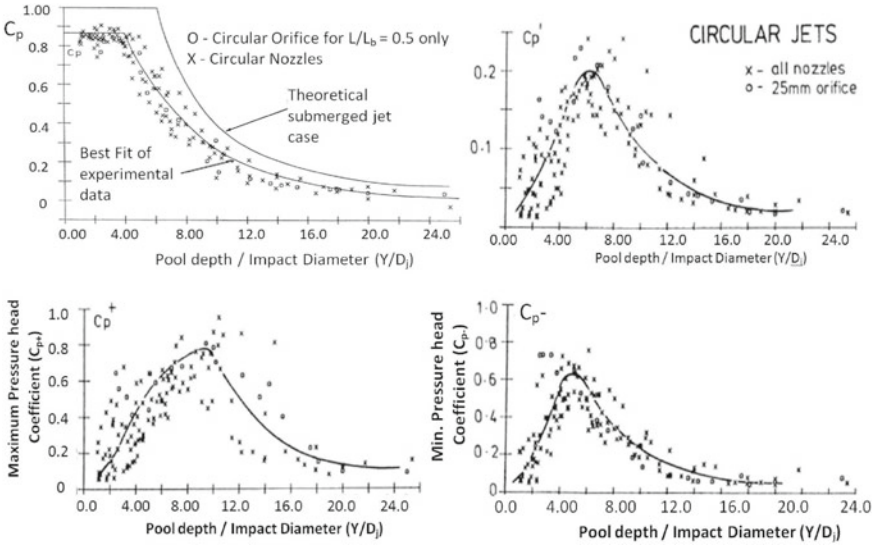

Fig. 4 Variation of coefficient of mean dynamic pressure (C_p), coefficient of RMS pressure fluctuations (C'_p), and pressure extremes coefficients (C_{p+} and C_{p-}) with plunge pool depth

3 Project Details

The studies were conducted on a 1:50 scale physical model of a spillway in the Union Territory of Jammu and Kashmir. The project envisages construction of four orifice spillways and two overflow crest spillways. The orifice spillway consists of 4 spans of 9.0 m width and 12.50 m height with an elliptical bottom profile of breast walls. The energy dissipator is provided in the form of a ski jump bucket with a preformed plunge pool.

4 Experimental Facility

A two-dimensional physical model was constructed to a geometrically similar scale of 1:50 in a flume. The model includes a part of the upstream river, orifice spillway, breast walls and ski jump bucket profile and downstream plunge pool. The model was fabricated using transparent acrylic and PVC foam sheets. Photo 1 shows the side and downstream view of the model. Figure 5 shows the sketch of the sectional view of the model.

Photo 1 Side view of the dry model of spillway and plunge pool

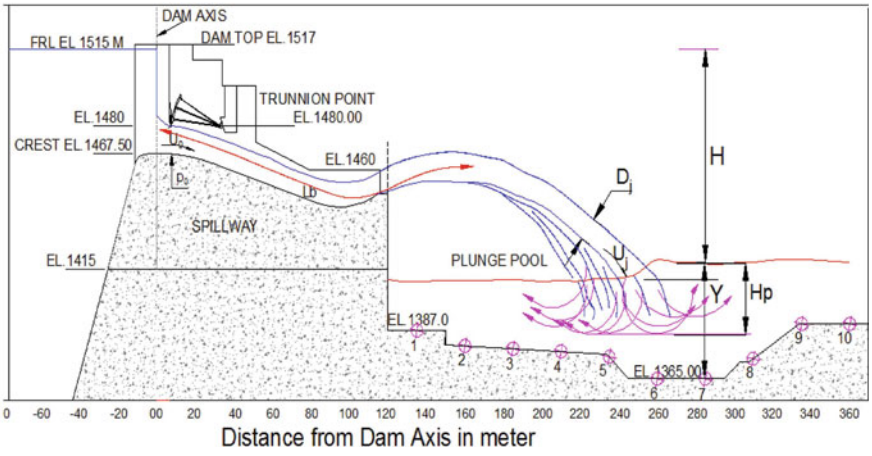

Fig. 5 Sketch of sectional view of model

5 Experimental Methodology

The experiments were carried out for four different percentages of discharges through orifice spillway and ski jump profile and respective tail water levels. Table 2 gives the operating conditions and the range of jet tests carried out in the model. The flow area of opening, velocity of the jet leaving orifice, and velocity of jet at impingement point were measured on the model.

Table 2 Operating conditions and the range of jet test

Operating condition (%)	Discharge passing	Size of orifice opening	Area of orifice opening	Equivalent diameter of opening (D_o)	Equivalent diameter of orifice opening (D_o) in model scale	Initial velocity U_o in model scale = Q/A	Froude number (F_o)
	m^3/s	m	m^2	m	m	m/s	
100	10,815.88	9 × 12.5	112.5	11.968	0.239	3.399	2.218
75	8111.91	9 × 10.45	94.05	10.943	0.219	3.049	2.081
50	5407.94	9 × 7.25	65.25	9.115	0.182	2.930	2.191
25	2703.97	9 × 3.4	30.6	6.242	0.125	3.124	2.823

5.1 Jet Parameters

The ratio of height measured between upstream and downstream water level and break up length (H/L_b) is calculated, and it is found that (H/L_b) ratio was less than one (1) for all operating conditions. Therefore, the jet is undeveloped (see Fig. 3). Similarly, the ratio of plunge pool depth to diameter of jet (Y/D_j) is calculated, and it ranges between 3.79 and 5.75; hence, water cushion depth is insufficient for 100, 75, and 50% operating conditions which will result in more pressure peaks at the bottom of the plunge pool.

5.2 Jet Breakup Length

With very large turbulence fluctuations in the model, the turbulence intensity was not possible to measure with available devices because of very small jet thickness and therefore, turbulence intensity was assumed as per suggestions of Elsawy et al. [4].

The lateral spread of the jet is calculated using Eqs. (1a, b, 2a, b, and c and 3), and results obtained are compared with actual measurements. The comparison of calculated and measured jet breakup length is given in Table 3.

5.3 Lateral Spread of Jet

In order to calculate the spreading of the jet as it moves toward the plunge pool, the velocity of the jet at the entry of the pool surface is measured on a physical model for all operating conditions. Then by using available data, the jet spread is calculated

Table 3 Comparison of calculated and measured jet break up length

Operating condition (%)	Assume turbulence intensity (T_u)	Jet breakup length (L_b) calculated from Eq. (1a, b) [2]	Jet breakup length (L_b) calculated from Eq. (2a, b and c) [4]	Jet breakup length (L_b) calculated from Eq. (3) [5]	Jet breakup length (L_b) Measured in model
Unit	%	m	m	m	m
100	5.9	3.02	5.72	3.29	3.05
75	4.9	3.22	5.28	3	3.21
50	4	3.23	4.72	2.64	3.21
25	2.7	3.34	3.89	2.11	3.35

Table 4 Comparison of calculated and measured jet spread

Operating condition (%)	Measured velocity of jet at the entry of pool surface (U) in m/s	Lateral spread of jet (ε) calculated from Eq. (4) by [2] in m	Lateral spread of jet (ε) Measured in model in m
100	3.5	0.60	0.62
75	3.5	0.50	0.45
50	3.4	0.41	0.35
25	2.7	0.27	0.25

by using Eq. (4) and compared with the measured jet spread on the model. The comparison of calculated and measured jet spread is given in Table 4.

5.4 Jet Penetration Depth

For different operating conditions, jet penetration depth is measured physically on the model, and then it is compared with calculated penetration depth using equations proposed by various researchers [8–11]. The comparison of calculated and measured jet penetration depth is given in Table 5.

Table 5 Calculated and measured penetration depth (H_p)

Operating condition (%)	Plunge pool depth in model in m (Y)	H_p [10]	H_p [8]	H_p [9]	H_p [11]	H_p measured in model
100	0.9	0.512	2.264	1.400	6.84	0.90
75	0.8792	0.449	2.060	1.414	5.98	0.87
50	0.8456	0.355	1.760	1.436	4.77	0.74
25	0.78	0.2	1.270	1.480	2.99	0.52

Table 6 Calculated pressure coefficients with respect to ratio of (Y/D_j)

Operating condition (%)	Ratio of Plunge pool depth to diameter of jet	Mean Dynamic Pr. coefficient by [2]	RMS Fluctuation Pr. coefficient by [2]	Max Pr. head coefficient by [2]	Min. Pr. head coefficient [2]
	Y/D_j	C_p	C'_p	C_{p+}	C_{p-}
100	3.79	0.875	0.12	0.4	0.49
75	4.32	0.815	0.14	0.48	0.62
50	4.97	0.71	0.18	0.55	0.64
25	5.75	0.625	0.195	0.62	0.6

Table 7 Calculated mean dynamic pressure coefficients

Operating condition (%)	Ratio of height and break up length	Ratio of Plunge pool depth to diameter of jet	Mean dynamic Pr. coefficient by [3] for $H/L_b > 0.5$	Mean dynamic Pr. coefficient by [16] for $H/L_b < 1$	Mean dynamic Pr. coefficient by [16] for $Y/B_j > 5.5$	Mean Dynamic Pr. coefficient by [2]
	(H/L_b)	(Y/D_j)	C_p	C_p	C_p	C_p
100	0.69	3.79	0.50	0.93	1.1707	0.875
75	0.66	4.32	0.49	0.94	1.0545	0.815
50	0.67	4.97	0.47	0.93	0.9244	0.71
25	0.66	5.75	0.44	0.94	0.7909	0.625

5.5 *Pressure Coefficients*

The pressure coefficients were calculated using method proposed by [2, 3, 16], and results are given in Tables 6 and 7. Figures 6 and 7 show the plot of pressure coefficients with respect to ratio of the dimensionless pool depth or water cushion (Y/D_j).

5.6 *Turbulent Pressure Acting on Plunge Pool Floor*

Pressures were computed with another method given by Martins and Visue [15] (Eqs. 5, 6, 7, and 8). The comparison of calculated and measured piezometric pressures in the model is given in Table 8.

Turbulent pressure acting on the plunge pool floor is also calculated using coefficients obtained from curves given by [2, 6, 17]. The calculated turbulent pressure

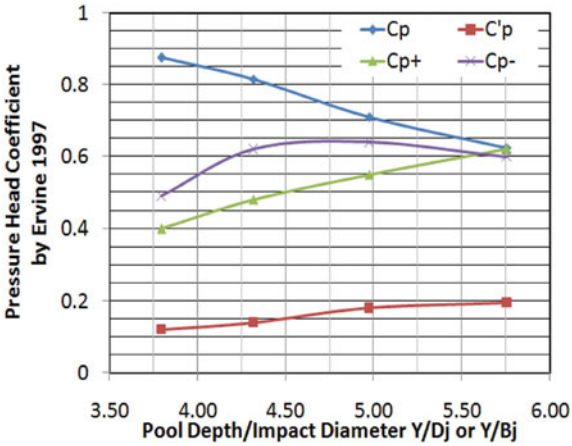

Fig. 6 Pressure coefficient variation with respect to ratio of (Y/D_j)

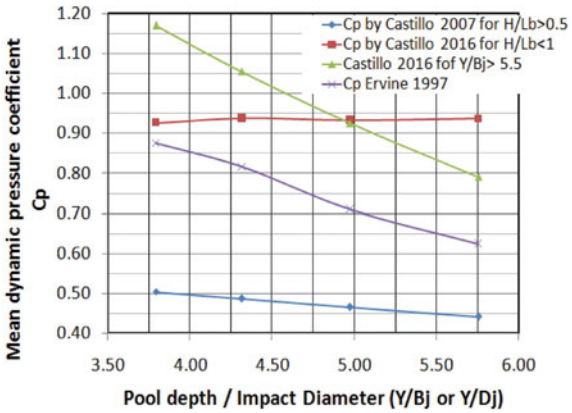

Fig. 7 Mean dynamic pressure coefficients by researchers [2, 3, 16]

Table 8 Calculated pressures proposed by Martins and Visue [15] and measured pressures on plunge pool floor (proto scale)

Operating condition (%)	Mean Dynamic Pressure by Eq. (5)	Maximum value of Pr. fluctuation by Eq. (6) [15]	Maximum dynamic Pr. by Eq. (7) [15]	Maximum dynamic Pr. by Eq. (8) [15]	Measured maximum piezometric Pr. in model	Measured minimum piezometric Pr. in model
	P_d	P'_{max}	P_{max}	P_{max}	P_{max}	P_{min}
100	147.46	17.81	165.27	54.53	49.5	31.27
75	93.38	15.5	108.88	46.17	46.25	30
50	49.6	12.31	61.91	34.99	42	29.02
25	17.5	7.65	25.14	19.55	39.25	24.75

Table 9 Comparison of calculated pressures from pressure coefficients proposed by Ervine et al. [2] and measured pressures on plunge pool floor (proto scale)

Operating condition (%)	Y/D_j	Mean Dynamic Pr. from C_p by [2]	RMS Fluctuation Pr. from C'_p by [2]	Max Pr. head from C_{p+} by [2]	Min. Pr. head from C_{p-} by [2]	Measured maximum piezometric pressure	Measured minimum piezometric pressure
	Y/D_j	P_{mean}	P_{rms}	P_{max}	P_{min}	P_{max}	P_{min}
100	3.79	71.70	48.66	57.20	59.95	49.5	31.27
75	4.32	69.69	48.38	59.12	63.54	46.25	30
50	4.97	62.83	47.49	58.20	60.80	42	29.02
25	5.75	50.19	42.49	50.10	49.74	39.25	24.75

acting on the plunge pool floor compared with measured pressures is given in Tables 9 and 10.

6 Discussion

Jet parameters and plunge pool parameters were used to calculate pressure coefficients and pressure on the plunge pool floor. The plunge pool water cushion depth parameter (Y/D_j) ratio in the model was between 3.79 and 5.75, where Y is water cushion depth and D_j is equivalent jet diameter. This ratio implied that plunge pool had shallow depth, and energy dissipation is insufficient in the plunge pool. From the classification of jet [16], all jets were undeveloped because (H/L_b) ratio was less than 1. In such cases where ($H/L_b < 1$), researchers have mentioned that pressure peaks at the bottom of the plunge pool have a similar constant pressure pattern above and below the mean pressure [16]; however, this pattern of pressure variation was not found in the present physical model.

From Table 3, it can be seen that the measured jet breakup length calculated by the method given by [2, 5] is nearly matched with measured values in the model. Table 4 shows that the measured lateral spread of the jet is nearly matched with calculated values obtained with the equations given by Ervine et al. [2].

Penetration depths calculated by various researchers [8–11] could not match with the observed values in the model presumably due to undeveloped jets in the model (see Table 5). Tables 6 and 7 show the computation of pressure coefficients by [2, 3, 16]. Computed values for pressure coefficients given by [2, 16] for $H/L_b < 1$ are matched with marginal variation of 10%.

The maximum dynamic pressure measured in the model and given in Table 9 are consistent with the experimental results of Martins and Viseu [15]. However, mean and maximum fluctuating dynamic pressures computed by various authors for model parameters are differing significantly as given in Table 10. It is also observed that the

Table 10 Comparison of calculated maximum dynamic pressures proposed by various authors (proto scale)

Operating condition (%)	Ratio of (Y/D_j)	Maximum dynamic Pr. by [17]	Maximum dynamic Pr. by [6]	Maximum dynamic Pr. by [15]	Maximum dynamic Pr. by Eq. (8) proposed by [15]	Maximum dynamic Pr. by [2] from C_{p+}	Measured maximum piezometric pressure	Measured minimum piezometric pressure
	(Y/D_j)	P_{max}	P_{max}	P_{max}	P_{max}	P_{max}	P_{max}	P_{min}
100	3.79	134.11	172.90	165.27	54.53	57.20	49.5	31.27
75	4.32	137.28	115.85	108.88	46.17	59.12	46.25	30
50	4.97	142.74	67.85	61.91	34.99	58.20	42	29.02
25	5.75	154.74	28.93	25.14	19.55	50.10	39.25	24.75

computed maximum dynamic pressures are in the range of 1.5–3.0 times the mean piezometric pressure measured in the model.

7 Conclusion

A rectangular jet in the ski jump spillway provided with a plunge pool of the north-western Himalayan region was studied in a 1:50 scale model. The plunge pool cushion depth parameter (Y/D_j) is in the range of 3.79–5.75, and jet parameter (H/L_b) is less than 1. The parameters related to jet such as jet penetration depth, jet breakup length, and lateral spread of the jet were measured and computed from literatures. Computed and measured values were broadly matching. Similarly, mean dynamic pressure coefficients and turbulent pressures were computed from the guidelines given by various investigators. Mean maximum pressure measured in the model matched with few conditions, but differences for other cases were not significant. Maximum dynamic pressures computed by various authors differ significantly, but maximum values are in the range of 1.5–3.0 times mean piezometric pressure measured in the model.

Acknowledgements The authors (1 and 2) are grateful to Shri. A. K. Agrawal, Director, CWPRS for his constant encouragement, suggestions, and kind permission to publish the paper. The authors are also grateful to Project Engineers for constant interaction and valuable inputs during the course of studies.

References

1. Mason PJ (1983) Energy dissipating crest splitters for concrete dams. International Water Power and Dam Construction 35(11):37–40
2. Ervine DA, Falvey HT, Wither W (1997) Pressure fluctuations on plunge pool floors. IAHR Journal of Hydraulic Research 35(2)
3. Castillo LG (2007) Pressures characterization of undeveloped and developed jets in shallow and deep pool. IAHR World congress, Venise
4. Elsawy E, Mckeogh E, Ervine D (1980) Effert of turbulence intensity on the rate of air entrainment by plunging water jets. ICE Proceedings 69:425–445
5. Horeni P (1956) Disintegration of a free jet of water in air. Byzkumny ustav vodohospodarsky prace a studie, Sesit 93, Praha, Pokbaba (in Czech)
6. Khatsuria RM (2005) Hydraulics of spillways and energy dissipators. Marcel Dekker Publication
7. Guyot G, Rodriguez M, Pfister M, Matas J, Cartellier A (2016) Experimental study of large scale plunging jets. In: Crookston B, Tullis B (eds) Hydraulic structures and water system management. 6th IAHR international symposium on hydraulic structures, Portland, OR, 27–30 June, pp 195–208
8. McKeogh EJ, Ervine DA (1981) Air entrainment rate and diffusion pattern of plunging liquid jets. Chem Eng Sci 36:1161–1172
9. Nakasone H (1987) Study of aeration at weirs and cascades. J Environ Eng 113:64–81
10. Falvey H, Ervine D (1987) Behavior of turbulent water jets in the atmosphere and in plunge pools. Proceedings of the Institution of Civil Engg, Part 2 83:295–314

11. Clanet C, Lasheras JC (1997) Depth of penetration of bubbles entrained by a plunging water jet. Phys Fluids 9:1864
12. Castillo-E LG (1989) Metodología experimental y numérica para la caracterización del campo de presiones en los disipadores de energía hidráulica. Aplicación al vertido en presas bóveda. PhD Thesis. Technical University of Cataluña. Barcelona, Spain
13. Castillo LG, Carrillo JM, Sordo-Ward A (2014) Simulation of overflow nappe impingement jets. J Hydro Informatics 16(4):922–940
14. Puertas J, Dolz J (2005) Plunge pool pressures due to a falling rectangular jet. Journal of Hydraulic Engineering 131(5):404–407. Accessed 110317. https://doi.org/10.1061/(ASCE)0733-9429(2005)131:5(404)
15. Martins R, Viseu T (1994) Plunge pool slab design taking into account turbulent pressures. In: 9th APD-IAHR Congress
16. Castillo LG, Carrillo JM (2016) Pressure and velocity distribution in plunge pools. In: 2nd international seminar on dam protection against overtopping Ft. Collins, Colorado, USA, 7–9 Sept 2016. ISBN: 978-1-1889143-27-9
17. Castillo-E LG (2006) Aerated jets and pressure fluctuation in plunge pools. In: 7th international conference on hydro science and Engineering (ICHE-2006). 10–13 Sept, Philadelphia, USA

Hydraulic Design of Spillway Approach Channel of Polavaram Irrigation Project, Andhra Pradesh

Vankayalapati S. Ramarao and Yogendra Nath Srivastava

Abstract The approach channel is meant for diversion of flood towards the spillway. Proper alignment of approach channel minimizes oblique flows in the approach channel and in front of spillway and also improves the discharging capacity of spillway because of favourable approach flow conditions and also, avoid endanger of spillway abutments. An upstream guide bund contributes to this by smoothly guiding the flow towards spillway thereby improving the flow conditions infront of spillway. CWPRS, Pune carried out hydraulic model studies on a geometrically similar 1:140 scale Froudian model of spillway of Polavaram dam to optimize the layout of approach channel and guide bund. Various alternatives of approach channel and guide bund have been incorporated and model studied on the model of spillway to assess the flow pattern in approach channel and performance of upstream guide bund for different flood conditions. The layout comprising of about 2000 m long approach channel with width varied from 1000 m to 450 wide (at narrow section) with 500 m long straight guide bund was recommended. The model studies showed that, with this layout, there was reduction in the velocities near left abutment of spillway when compared with other layouts. Frequent and periodic formation of swirling flows in front of spillway; vortexes shedding along the guide bund, sharp rise of water surface on the outer boundary of vortices were eliminated. Water surface profiles were contained in front of spillway piers and overtopping was eliminated. On the upstream of spillway, maximum velocities of the order of 1.6–7.7 m/s were observed along Ch. 100 m. The layout has been adopted by the project authorities and construction of project is in progress. In this paper, the authors explained the results of hydraulic model studies conducted on various layouts approach channel and guide bund of Polavaram irrigation project, Andhra Pradesh.

Keywords Approach channel · Guide bund · Hydraulic design · Spillway · Spill channel

V. S. Ramarao (✉) · Y. N. Srivastava
Central Water and Power Research Station, Khadakwasla, Pune 41102, India
e-mail: ramaraovs2@gmail.com

P. V. Timbadiya et al. (eds.), *Flood Forecasting and Hydraulic Structures*, Lecture Notes in Civil Engineering 340, https://doi.org/10.1007/978-981-99-1890-4_30

1 Introduction

Spillway is a structure incorporated to pass out design flood safely to its downstream through energy dissipator along with spill channel. To enable the spillway to optimize its function, an approach channel is excavated to divert the flood towards spillway. Also, guide bund is provided in front of spillway to guide the flow smoothly towards the spillway and also minimizes the oblique flows infront of spillway and while doing so, protects the spillway flanks from subjecting to high velocity swirls. Polavaram Irrigation Project is on Godavari River, in West Godavari district, Andhra Pradesh, and is designed to meet the demands of irrigation, drinking water and power generation. The project provides irrigation benefits to 4 lakh acres under left main canal and to 3.2 lakh acres under right main canal. Moreover, hydroelectric power with installed capacity of 960 MW and water supply for industries in Visakhapatnam are also envisaged under the project. Project design flood is estimated at 101,941 m^3/s and probable maximum flood (PMF) is estimated at 141,583 m^3/s, which is required to be passed through spillway comprising of 48 spans of size 16 m (W) $\times$ 20 m (H). The full reservoir level (FRL) is at El. 45.72 m and gross storage capacity at FRL is 194 TMC with a live storage capacity of 75.20 TMC. The other components of project include spill channel, approach channel, pilot channel, ECRF dam with plastic concrete diaphragm wall, concrete dam, guide bund between ECRF and spillway. Approach channel is excavated to channelize Godavari River water through the spillway that is located on right bank. Figure 1 shows the plan of project along with the approach channel, spillway, spill channel, power intake structure and tailrace channel.

2 Hydraulic Model Studies on Various Layouts of Approach Channel

To optimize the hydraulic design of approach channel along with upstream guide bund, hydraulic model studies were carried out on a geometrically similar scale model of spillway and power intake, of 1:140, that was constructed in CWPRS, Pune. Entire river topography was plastered after consolidating moorum beneath, by incorporating river cross sections up to 4800 m upstream and 3700 m downstream of the dam axis. Original layout of project comprising of approach channel of width 660 m and length 2310 m with bed elevation at El. 17 m, spill channel of width 1000 m and length 2780 m with bed elevation varies from El. 8.8 m to 8.26 m, pilot channel of width 450 m and length 660 m with bed elevation at El. 8.26 m were reproduced with cement plaster. Fabricated spillway with divide walls extended to pier Nos. 16, 23, 32 and 40 and power intake structures with 12 head race tunnels (HRT) made of PVC/acrylic were incorporated in the model. Stilling basin of spillway with invert at El. 7.25 m and solid end sill with top El. 12 m was casted in cement mortar. The training walls with top at El. 35.5 m were extended up to the end of stilling basin. A

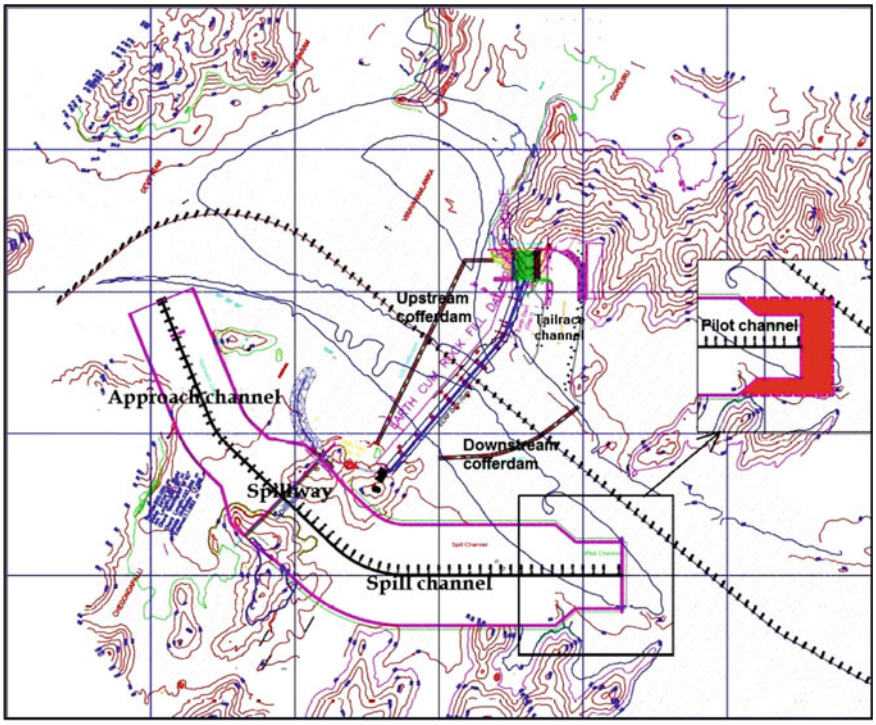

Fig. 1 Plan of Polavaram irrigation project, A.P.

15 m long concrete apron with top at El. 8.80 m was joined with spill channel bed downstream of spillway. Figure 2 shows aerial view of model of original layout of approach channel with a curved guide bund. The accepted relationship of hydraulic similitude, based on Froudian criteria was used to express the mathematical relation between the dimension and hydraulic quantities of the model and the prototype. The general relations expressed in terms of model scale are given in Table 1.

Table 1 Froudian model scale relation for various dimensions

Dimension	Scale relation
Length (m)	1:140
Area (m^2)	1:19,600
Velocity (m/s)	1:11.832
Discharge (cumecs)	1:231,910.32
Time (s)	1:11.832
Manning's '*n*'	1: 2.2787

2.1 Original Layout of Approach Channel 660 m Wide with 760 m Long Curved Guide Bund [1]

Original layout of approach channel was of length 2310 m with bed elevation at El. 17 m. The width was 660 m at the entrance and expands to 1000 m at Ch. 200 m upstream of dam axis. A guide bund of 760 m long was provided along the left flank in transverse to the spillway, as shown in Figs. 1 and 2.

2.1.1 Approach Flow Conditions along Spillway Upstream

Approach flow conditions along the upstream of spillway for various discharges up to design flood indicated that the flow enters the spillway in multiple directions viz., from right side of approach channel, entrance of approach channel and through the passage between Paidipaka hill and upstream guide bund. This caused oblique flow conditions in approach channel as the flow is predominantly moving towards the left and centre of spillway. At Ch. 100 m upstream, the velocities of the order of 2.4, 5.8 and 3 m/s were observed along left, centre and right of spillway for PMF and 2, 3.6 and 1.7 m/s for 50% of PMF. At Ch. 200 m upstream, the velocities of the order of 4, 7.8 and 2 m/s were observed along left, centre and right of spillway for PMF and 2, 4.6 and 1.4 m/s for 50% of PMF. For discharges higher than 25% of PMF, flow was seen accelerating along the guide bund and rapids were seen forming. Velocities of the order of 4–12 m/s were observed along the guide bund for discharges from 25 to 100% of PMF. Figure 3 shows flow conditions in approach channel and near

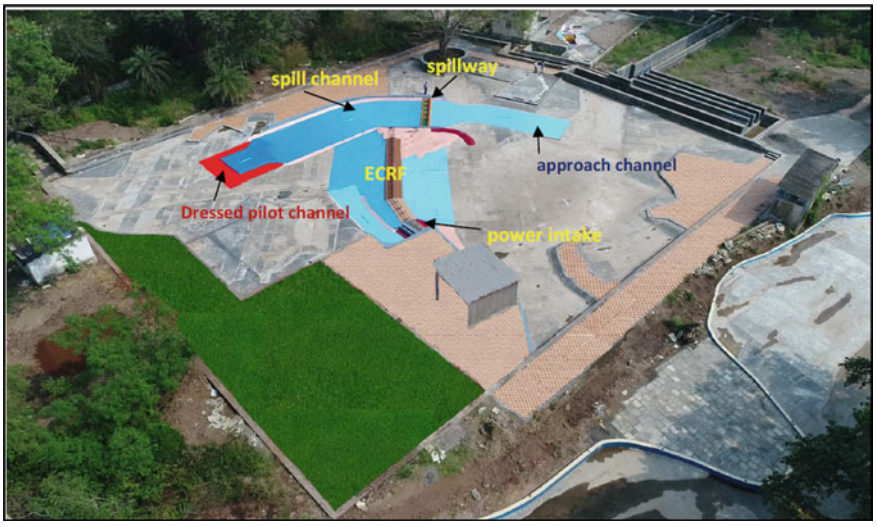

Fig. 2 Aerial view of 1:140 scale model of various components of Polavaram Irrigation project

Fig. 3 Flow conditions in the approach channel and near the guide bund

guide bund while passing of design flood of 141,583 m^3/s (PMF) for all gates in open condition.

2.2 Approach Channel 200 m Wide, Without Guide Bund [2]

11th Dam Design Review Panel (DDRP) meeting held on 6th January 2019 at Polavaram suggested conducting model studies with modified layout of approach channel 200 m wide and without left guide bund. Figure 4 shows the layout of project with modified approach channel and without guide bund. Existing 1:140 geometrically similar scale 3-D model of spillway has been used for carrying out the studies. Existing approach channel of length about 2110 m (barring Ch. 200 m upstream of spillway) was filled with brickbats and cement plaster and upstream river portion was reproduced with cement plaster. Modified approach channel at a slope of 1 in 10,000 was reproduced in cement plaster and joined to the existing river bed. Existing upstream curved guide bund was removed as per the suggestion of DDRP. Figure 5 shows the aerial view of modified approach channel without left guide bund.

2.2.1 Approach Flow Conditions Along Upstream of Spillway

For the modified layout of approach channel, flow conditions along upstream of spillway indicated that similar to the original design of approach channel, that the flow enters the spillway with a multi-directional approach and was causing oblique flow conditions in approach channel, even with the removal of guide bund. However, upstream velocities are increased due to reduced section of approach

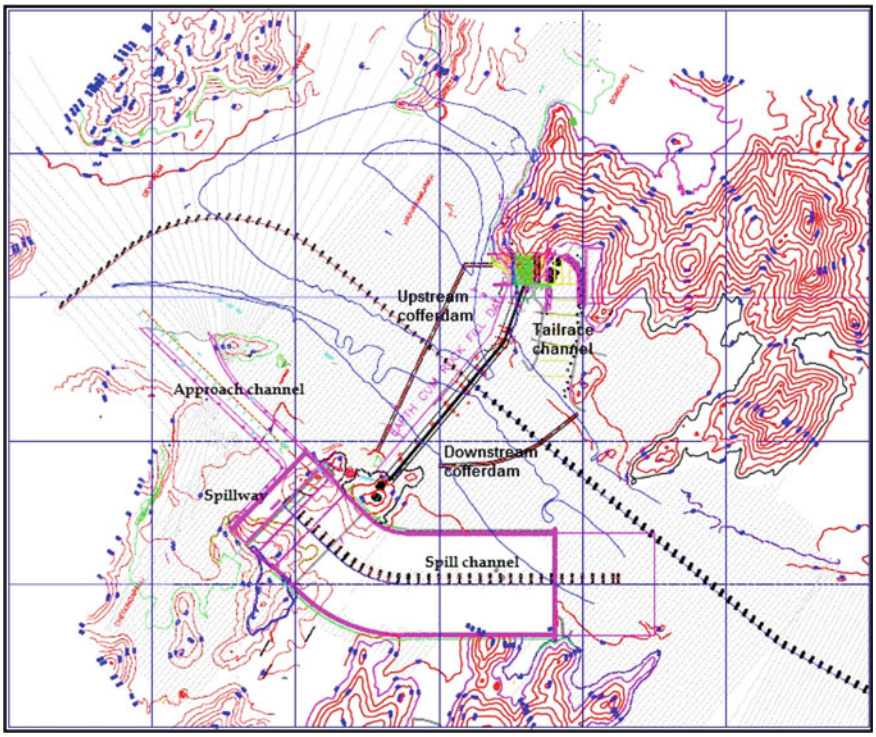

Fig. 4 Layout of the project with modified approach channel 200 m wide

channel. Figure 6 shows flow conditions in modified approach channel while passing discharge 141,583 m^3/s (PMF) for ungated operation of spillway. For ungated operation of spillway, at Ch. 100 m upstream, the velocities of the order of 13.6, 9.2 and 2.5 m/s were observed along left, centre and right of spillway for PMF and 9, 5 and 1.3 m/s for 50% of PMF. At Ch. 200 m upstream, the velocities of the order of 11.6, 9 and 2.9 m/s were observed along left, centre and right of spillway for PMF and 8.3, 3.9 and 1 m/s for 50% of PMF. Violent flow conditions were observed along left abutment for removal of curved guide bund since the flow is impinging into the channel. Figure 7 shows flow conditions near left abutment for passing discharge 141,583 m^3/s (PMF) for ungated operation of spillway.

2.3 Approach Channel 450 m Wide at Narrow Section with a Straight Guide Bund of 500 m Long [3]

During the 16th meeting of the Dam Design Review Panel (DDRP) held on 19–20th February 2021 at Rajahmundry, the panel opined that to optimize the layout

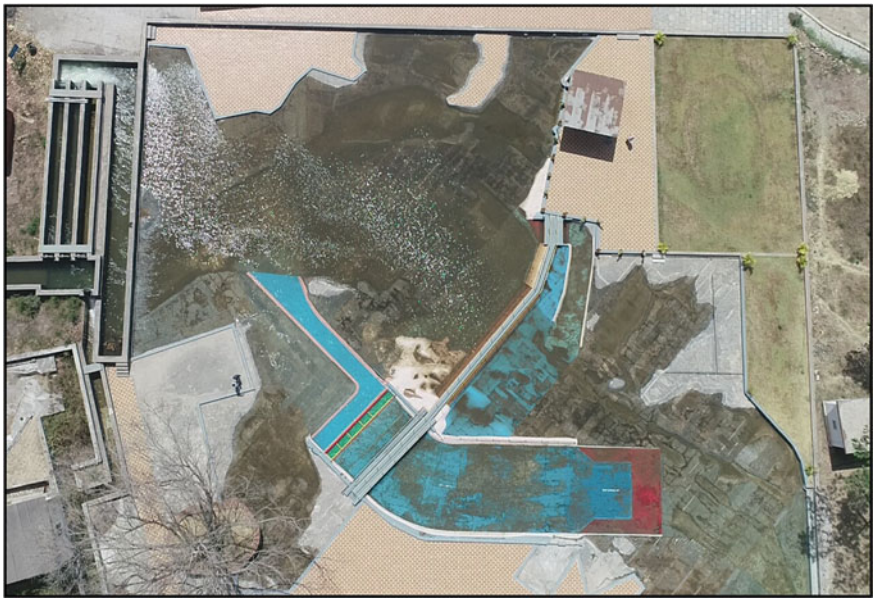

Fig. 5 Aerial view of modified approach channel

Fig. 6 Flow conditions in approach channel ($Q = 141{,}583\ m^3/s$, ungated operation of spillway)

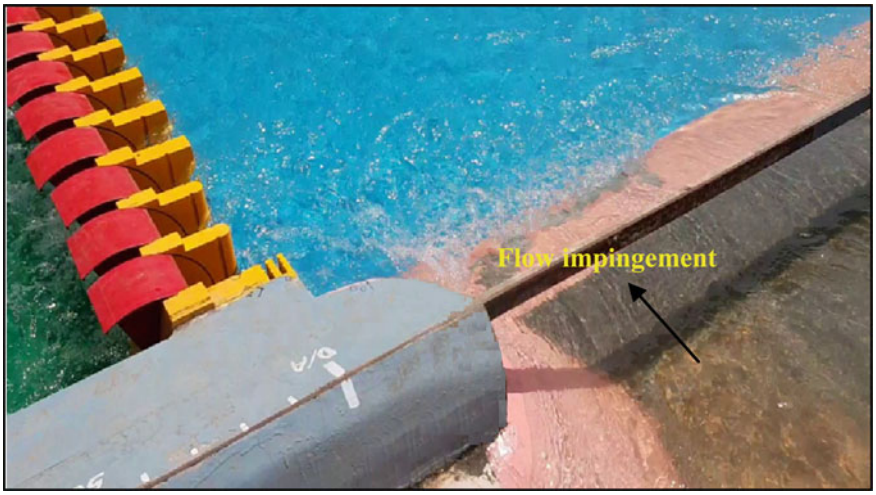

Fig. 7 Flow conditions near the left abutment

of approach channel and guide bund, the model study shall be conducted by incorporating 450 m long straight upstream guide bund and dumped hill-cut materials stacked over a length of about 1500 m to the left of the approach channel. The dumped hill consisted of overburden rock fragments and soil excavated in nearby areas. In the existing 1:140 scale model of spillway, guide bund and dumped hill were reproduced to ascertain flow conditions along approach channel, in front of spillway, in the vicinity of guide bund and downstream of spillway. The top elevation of the dumped material was dressed to EL. 50 m. The dumped hill materials were fully impervious in the model. The approach channel was further widened by eliminating the curvature and made straight on the right side. However, the width of the channel at the narrowest section is 450 m. This gradually becomes 1000 m at about 300 m upstream of the spillway. Figure 8 shows the plan of layout comprising approach channel, spillway, guide bund and dumped hill-cut materials and Fig. 9 shows the upstream view of modified approach channel, guide bund and dumped hill-cut materials. Hydraulic model studies were conducted on the model for 60% of PMF and PMF (141,583 m^3/s) conditions for ungated operation.

2.3.1 Spillway Discharging Capacity for Ungated Operation

Studies indicated that the discharging capacity of spillway improved as probable maximum flood (PMF), 141,583 m^3/s can be passed at reservoir water level (RWL) El. 44.95 m when compared with El. 45.35 m, for original design (Technical Report No. 5576 of March 2018). 75% of PMF (106,187 m^3/s) can be passed at RWL El. 41.8 m, 60% of PMF (84,950 m^3/s) at El. 39.8 m, 50% of PMF (70,792 m^3/s) at El. 38.28 m and 25% of PMF (35,396 m^3/s) at El. 34.38 m. This layout was showing

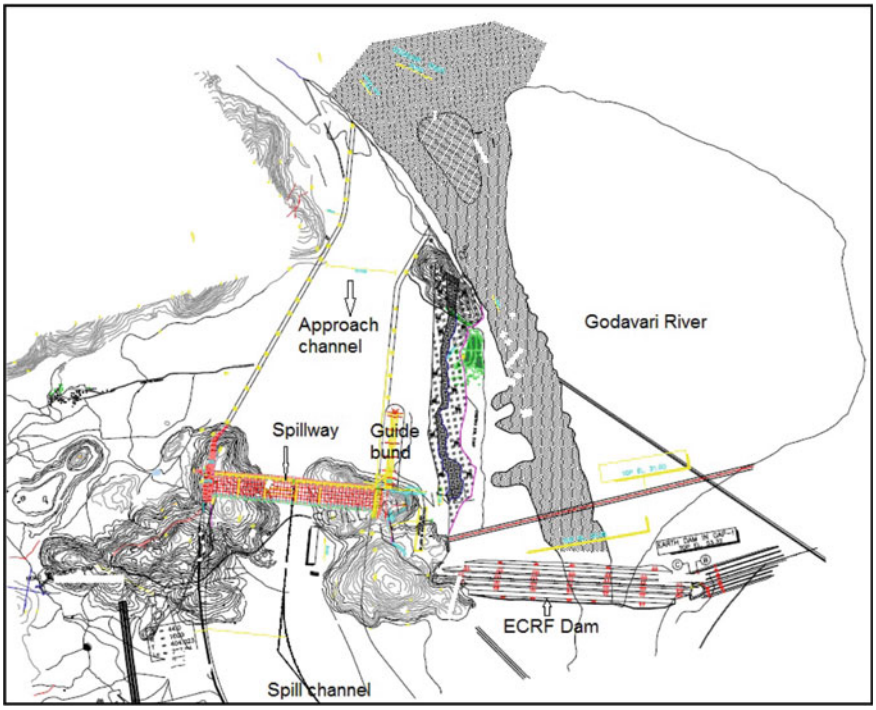

Fig. 8 Plan of layout of the project comprising modified approach channel, guide bund and dump hill

improvement in flood releasing capacity of spillway for wider approach channel with nearly uniformly distributed approach flow in front of spillway.

2.3.2 Flow Conditions Along Approach Channel, in the Vicinity of Guide Bund and in Front of Spillway

Along the approach channel, the flow conditions were seen nearly uniformly distributed. But the narrow section at the upstream end of the approach channel created non-uniform flow fields. It was recommended that the narrow section of approach channel may be widened as per feasible site condition, to further improve the flow pattern in the approach channel.

Incorporation of 500 m long straight guide bund reduced the velocities near left abutment of spillway. Frequent and periodic formation of swirling flows in front of spillway was eliminated. Vortex shedding along the guide bund was also eliminated. The sharp rise of water surface on the outer boundary of vortices was eliminated. Water surface profiles were contained in front of spillway piers and overtopping was not observed.

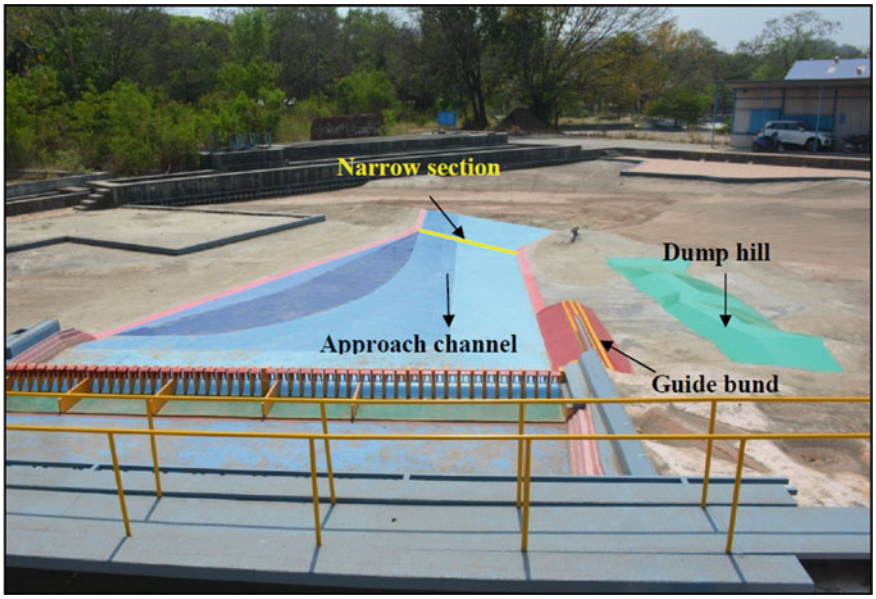

Fig. 9 Upstream view of layout with modified channel and guide bund approach channel, guide bund and dump hill

Stacked dumped hill materials were seen acting as a barrier preventing lateral entry of flow from ECRF reservoir. However, there was a narrow gap lying between dump hill of rock cut materials and G-Hill (hill connecting upstream coffer dam), which needs to be plugged to prevent lateral high velocity flow hitting the guide bund. The gap between Paidipaka hill and dump hill of rock cut materials also needs to be plugged to prevent high velocity flows entering the approach channel.

An artificial pool is being created between the dumped hill materials and guide bund stabilizing flow and reducing the velocities along the left flank of the spillway. Along the spillway axis, the maximum velocities were 4 m/s, 5.5 m/s and 4 m/s along the left, centre and right side of the spillway, respectively, for PMF condition; for 60% of PMF, the maximum velocities were 1 m/s, 4 m/s and 3.1 m/s along the left, centre and right side of the spillway, respectively. At Ch. 100 m upstream of the spillway, the maximum velocities were 1.3 m/s, 7.7 m/s and 1.6 m/s along the left, centre and right side of the spillway, respectively, for PMF condition. For 60% of PMF, the maximum velocities were 0.7 m/s, 5.5 m/s and 1.3 m/s on to the left, centre and right side of the spillway, respectively. No return currents could be measured along the left flank of the spillway. At Ch. 200 m upstream of the spillway, the maximum velocities were 1.7 m/s, 8.6 m/s and 1.1 m/s on the left, centre and right side of the spillway, respectively, for PMF condition. Return currents of the order of 1.6 m/s were observed on left flank. For 60% of PMF, the maximum velocities were 1.2 m/s, 6.2 m/s and 1 m/s on the left, centre and right side of the spillway, respectively. However, the approach velocities were observed maximum along the centerline of

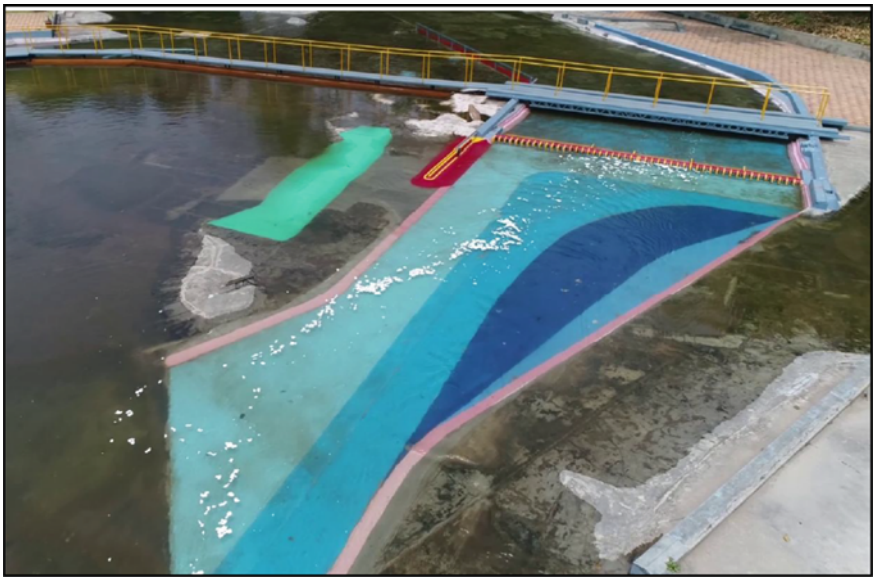

Fig. 10 Flow conditions along the approach channel for PMF condition

the approach channel. Maximum velocities of the order of 10 m/s were observed at the Ch. 500 m upstream of the spillway, along the centre of approach channel for PMF and 7.8 m/s for 60% of PMF. Maximum velocities of the order of 1.4–1.8 m/s and 3–6.5 m/s were observed to the left of guide bund due to intrusion of flow from ECRF side towards guide bund for 60% of PMF and PMF, respectively. Figures 10 and 11 show flow conditions along the approach channel, in the vicinity of the guide bund and in front of the spillway for PMF condition. It was recommended to plug the gap between dumped hill and hill that connects upstream coffer dam. Along the nose of the guide bund maximum velocity observed was 1.8 m/s and 6.5 m/s for 60% of PMF and PMF, respectively.

3 Comparison of Three Layouts of Approach Channel

The velocities observed along the approach channel for various layouts of approach channel of widths varying from 200 to 660 m for various operating conditions up to PMF indicated that the flow conditions were improved substantially along the left and right flanks of spillway for layout with 450 m wide at narrow section. The velocities in the approach channel along left flank and in the vicinity of guide bund were reduced substantially.

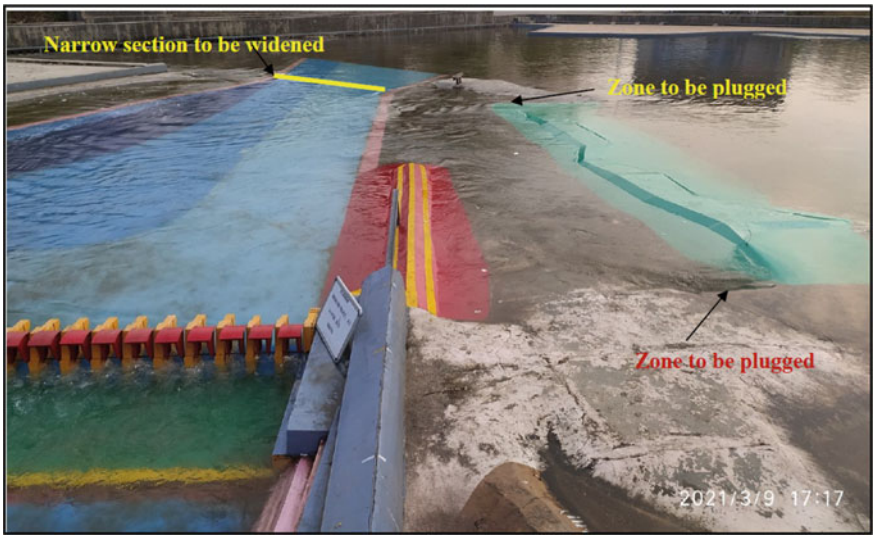

Fig. 11 Flow conditions in the vicinity of the guide bund for PMF condition

4 Conclusions and Recommendations

Spillways are important structures concerning dam safety and approach channel is instrumental in diverting the flows into the spillway without creating oblique approach flow conditions in front of spillway. Upstream guide bund is also vital in guiding the flows towards spillway without destabilizing the spillway abutments. Hydraulic design of spillway and its components economizes original/ modified design of spillways and its components for their satisfactory performance. For Polavaram irrigation project, Andhra Pradesh, modifications were required for approach channel and guide bund to improve their performance in smoothly guiding the flows towards the spillway. The layout with 450 m wide approach channel at narrow section with 500 m long straight guide bund provided satisfactory results than other layouts and the same was recommended. The PMF could be disposed of through the spillway at RWL El. 44.95 m against RWL El. 45.35 m for original layout, showing marginal improvement in discharging capacities due to modified approach channel with predominant straight forward approach flow conditions. Layout of 500 m long straight guide bund does not create severe swirling flows along the left flank of the spillway and velocities along left flank reduced. Dump hill was acting as a barrier preventing lateral flows entry into approach channel from ECRF reservoir. An artificial pool was seen created between dump hill and guide bund stabilizing flow conditions and reducing the velocities along the left flank of spillway. The gap between dump hill and G-hill needs to be plugged to prevent high transverse velocity and velocity along the guide bund for stability of guide bund pitching. The gap between Paidipaka hill and dump hill needs to be plugged to prevent high

transverse velocity flows entering the approach channel. The dump hill comprises overburden material and may be thoroughly strengthened to prevent erosion due to seepage and piping. If the dump hill gets eroded, heavy flows may enter approach channel which may destabilize the stability of guide bund and spillway upstream area. So, it was recommended to take precautions to prevent leakage through the dump hill.

The recommendations of CWPRS based on hydraulic model studies conducted on 1:140 scale geometrically similar scale model is being implemented and the project is under construction.

Acknowledgements The authors are thankful to the Director, CWPRS for the encouragement in publishing technical papers. Authors are also grateful to project authorities of Andhra Pradesh Water Resources Department (APWRD) for providing technical data for conducting studies.

References

1. CWPRS Technical Report No. 5576 (2018) Hydraulic model studies for spillway and power intake of Polavaram Irrigation Project, Andhra Pradesh, 1:140 scale 3-D comprehensive model
2. CWPRS Technical Report No. 5707 (2019) Hydraulic model studies modified approach channel of spillway of Polavaram Irrigation Project, Andhra Pradesh, 1:140 scale 3-D comprehensive model
3. CWPRS Technical Report No. 5949 (2021) Additional hydraulic model studies for modified approach channel with upstream guide bund and modified spill channel of Polavaram Irrigation Project, Andhra Pradesh, 1:140 scale 3-D comprehensive model

Performance of Geometry of Gate Lip Angle—A Case Study

Kanhu Charan Sahu, Koppalakonda Rajesh, and Akhilesh Kumar Agrawal

Abstract Gate lip angle is defined as the angle which is given by the ratio of vertical distance as measured between the skin plate bottom edge and the bottom edge of gate, to thickness of gate as measured from the upstream face of gate bottom edge to the upstream edge of skin plate bottom edge. Gate lip angle has a profound influence on gate vibrations, cavitations and down pull of the gate. Hence lip angle of the gate plays an important role in the design of gate structure. It is unfortunate that in spite of many hydraulic model studies over the years by eminent researchers on a variety of practical and impractical gate bottom lips, no guidance is available to the practical gate designer to determine gate lip geometry. So the model study on gate lip has its own importance so far the gate design is concerned. This paper provides case studies guidelines to know the performance of lip angles from the model study. The results of model studies on geometry of lip angle are presented in this paper. The information from the model studies might be useful to the designers and could be taken as reference for similar type of geometry of lip angle study in future.

Keywords Gates · Lip angle · Skin plate · Cavitation · Down pull

1 Introduction

Gate designers are aware that the geometry of gate lip plays a vital role in determining the satisfactory gate performance. The gate lip has profound influence with regard to the cavitations damage to the gate, gate vibrations, down pull/uplift on gate. Hydraulic model studies have been conducted on various projects to study the performance of geometry of gate lip angle at CWPRS. Majority of such studies were intended for observing the performance of the gate lip angle in gate study to develop an optimum

K. C. Sahu (✉) · K. Rajesh · A. K. Agrawal
CW&PRS, Pune 411024, India

A. K. Agrawal
e-mail: agrawal_ak@cwprs.gov.in

P. V. Timbadiya et al. (eds.), *Flood Forecasting and Hydraulic Structures*, Lecture Notes in Civil Engineering 340, https://doi.org/10.1007/978-981-99-1890-4_31

geometry of the gate lip. The objective of the study is to eliminate cavitations damage, eliminate vibrations, minimize down pull and avoid uplift.

A large number of model studies and publications referred from Naudascher [1], Sagar [2], US Bureau of Reclamation [3], Dhillion [4] were predominantly pre occupied with down pull. Such studies, therefore, invariably resulted in adopting conservative lip angles in new gate designs. Thus, Davis' "Handbook of Applied Hydraulics" showed an example lip angle of 35° for gate with upstream skin plate and upstream seal. Some designers adopt larger conservative lip angles for upstream skin plate gates with upstream seals without substantial justification. To illustrate this point, hydraulic model studies are important.

The aim of this paper is to focus on geometry of the lip angle influence on the hydraulic aspects considered individually so as to provide guidelines to the designer in selecting geometry of the lip angle.

2 Lip Angle

The gate bottom geometry is usually defined by the lip angle θ which is determined as.

d = the vertical distance between the gate bottom edge and the bottom edge of the bottom of the gate.

t = the thickness of gate measured from the upstream edge of gate to bottom edge of skin plate.

$\tan \theta = d/t$.

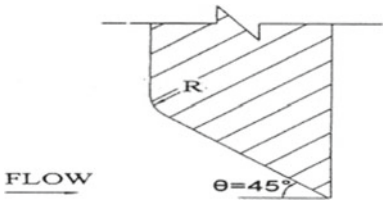

3 Influencing Factors on the Gate Lip

Submerged or free flow downstream of gate, aeration downstream of gate, upstream or downstream skin plate are the main factors which have significant influence on the gate lip hydraulics. Thus, the gate bottom geometry should be carefully studied for

free flow or submerged flow conditions, immediately downstream of the gate. Aeration is an important factor which also has a significant impact on the performance of the gate lip. As high velocity flows beneath the gate have a tendency to carry away the air with them, thus creating low pressure zones often with fluctuating air pressures in these zones. The availability of air and demand for aeration to such zones, thus become a very significant factor impacting the successful hydraulic performance of gate lip geometry. The other factors that have influence on the hydraulics of gate bottom geometry are head on the gate during operation, shape of the bell mouth entrance, gate slot geometry, bottom seal shape, downstream conduit slope and conduit geometry downstream and upstream [1].

4 Need for Hydraulic Model Studies and Modelling Criteria

The design of a gate structure needs assessment of lip angle that would be provided on the gate structure. The pressure forces acting on the lip of gate is the most important in the gate installations. The pressure forces of the gate and its magnitude are evaluated at various gate openings with respect to predefined gate lip angle. Generally, the model gates are integral parts of models of outlet conduits or tunnel in which they are installed. The scale of hydraulic model should be chosen in such a way that the minute details of the gates such as gate lip angle, gate girders and tunnel including gate slots, gate well, etc. are reproduced in the model precisely. Scaling, designing and operating the gate models are complex due to hydrodynamic/structural interactions. The design of a hydraulic model for a gate structure with gate lip angle needs assessment of likely pressure forces that would act on the lip of the gate structure [3, 4]. Therefore, a physical model would be best suited for the same to get suitable gate bottom geometry.

5 Experimental Analyses

5.1 Silt Flushing Tunnel and Gate Model

Tala H.E. Project is situated in western Bhutan near Honka, 3.0 km downstream of existing Chukka Tail Race. A 91 m high concrete dam is being constructed across river Wangchu for diversion of 171 cumec of discharge for generation of 1020 MW of electricity at 820 m head through a 2.2 km long head race tunnel (HRT). The concentration of suspended sediments in Wangchu River is likely to be high during floods, however, the desilting basin has been designed to cater up to 2000 ppm. Three

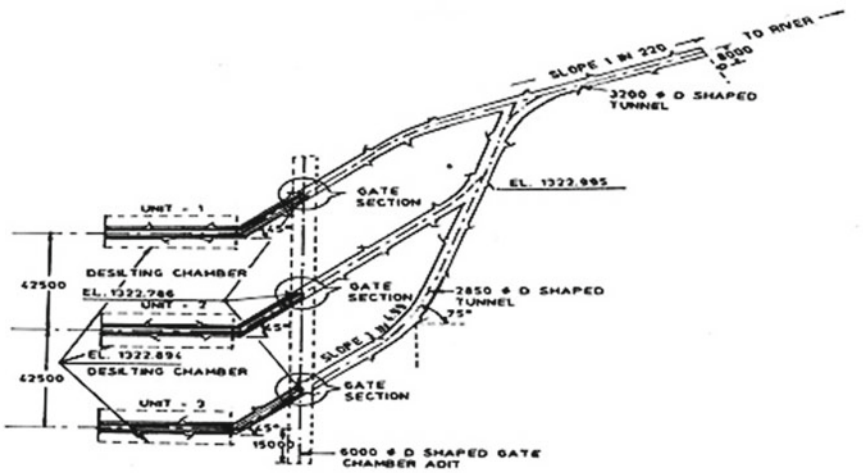

Fig. 1 Sectional plan of silt flushing tunnel system

units of desilting basin have been provided for the removal of sediments coarser than 0.2 mm from the HRT. Each unit is of 250 m long, 18.5 m high and 13.92 m wide. Three numbers of flushing conduits of size 0.75 m (W) × 1.2 m (H) below each desilting unit will discharge into a separate D-shaped branch tunnel, downstream of desilting unit with control gates. Figure 1 shows, the sectional plan of silt flushing tunnel system. The studies were conducted on a 1:12 scale, geometrically similar sectional model of the silt flushing tunnel and gate. Studies were conducted to check the geometry of gate lip, flow visualization in the tunnel, discharging capacity of the tunnel and air demand downstream of gate.

The down pull is influenced considerably by the variation in several factors such as flow characteristics, fluid properties, geometry of gate, etc. High velocity flow below the partial open gate may cause considerable reduction in hydrodynamic pressure on the bottom surface of the gate. These pressures can be as low as vapour pressure of water and may lead to structural damage to the gate grooves and the portion on the downstream of the groove due to cavitation. High head gates may experience vibration during its operation [2]. The principal cause of vibration are vortex trail formed downstream of the gate, pressure fluctuations at the gate bottom and leakage through seals.

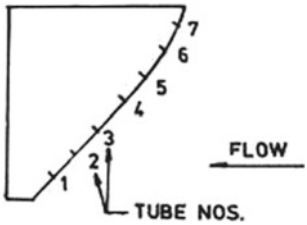

Fig. 2 Positions of piezometers

5.2 Geometry of the Gate Lip

Studies were conducted to observe the pressure distribution on the 45° gate lip for different water levels in the cunnette at different positions of the service gate. Seven piezometers were provided on the gate lip as shown in Fig. 2 and the hydrostatic pressures were measured by connecting the piezometers to water manometer. It was observed that the hydrostatic pressures on the lip for different gate openings and water levels between El.1345 m and El.1363 m were positive throughout. Piezometric pressures in terms of water head on different piezometers are shown in Fig. 3 and the hydraulic performance of the gate with 45° lip angle was satisfactory as positive pressures were observed for entire range of gate openings and water levels.

5.3 Air Demand Downstream of Gate

Flow condition was observed in the tunnel downstream of the gate section during partial gate operation of gate. It was observed in the model that for gate opening varying from 10 to 30%, the flow does not touch the roof of the D-shaped tunnel on downstream of the gate resulting in sufficient aeration of the tunnel portion in the downstream vicinity of the gate (refer photographs). As such provision of air vent is not necessary. However, the horizontal roof portion between the gate and D-shaped tunnel may be flared upwards in the downstream direction from EL.1324.884 m to EL. 1326.734 m in a length of 2.1 m, up to the roof of the tunnel. This modification will help in providing adequate aeration to the tunnel portion in the vicinity of the gate.

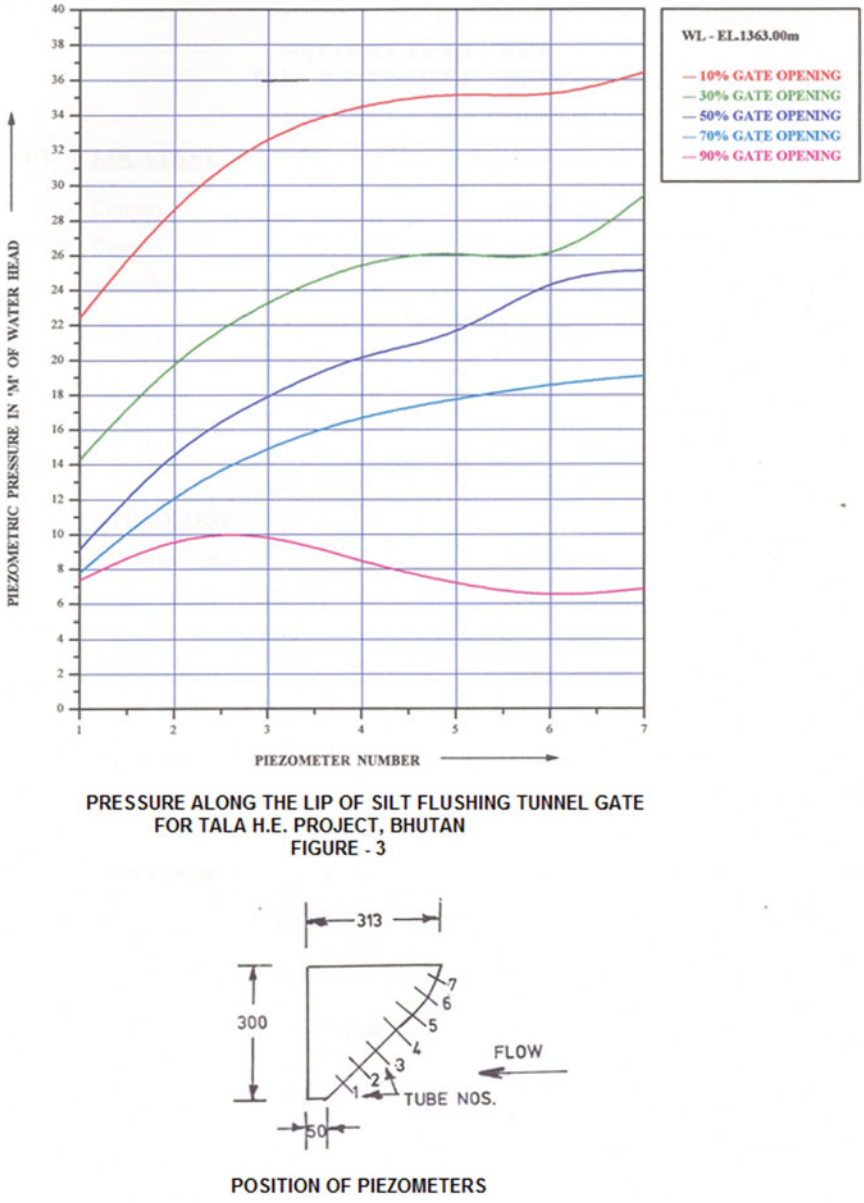

Fig. 3 Pressure along the lip of silt flushing tunnel gate for Tala H.E. Project, Bhutan

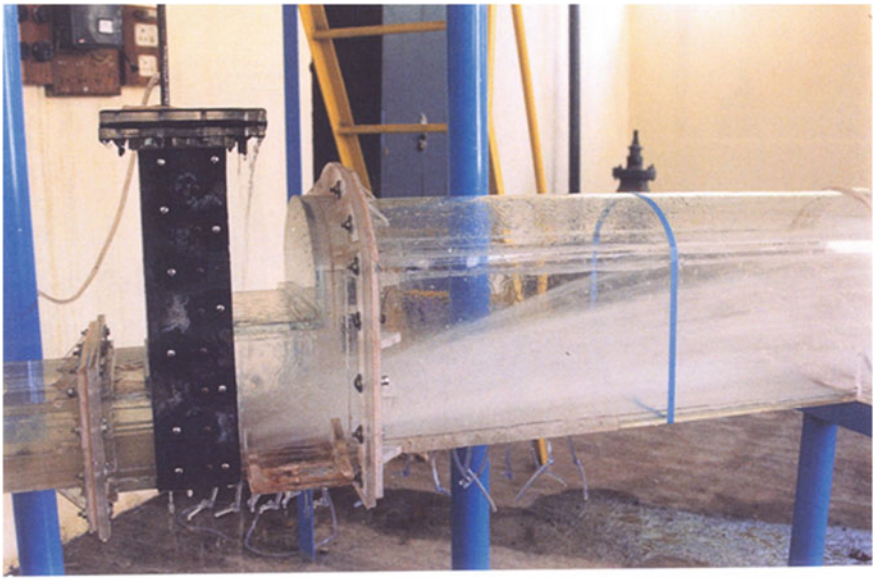

PHOTOGRAPH - 1
FLOW CONDITION IN THE TUNNEL AT 10% GATE OPENING
FOR WATER LEVEL EL.1363m

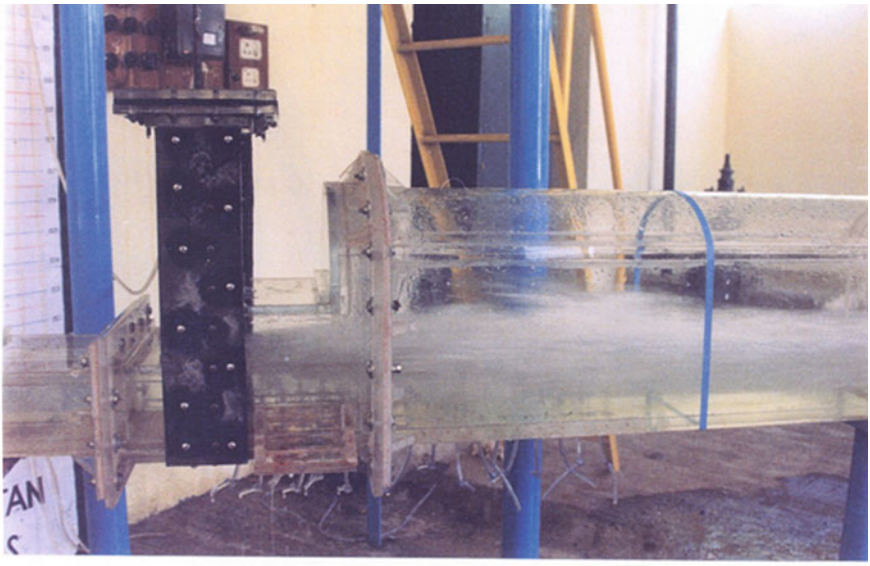

PHOTOGRAPH - 2
FLOW CONDITION IN THE TUNNEL AT 100% GATE OPENING
FOR WATER LEVEL EL.1363m

5.4 Irrigation By-Pass Tunnel, Sardar Sarovar Project, Gujarat

The Sardar Sarovar Project is located at 5.63 km, upstream of Navagam village in Bharuch District of Gujarat. The project comprises a concrete gravity dam 1210 m long and 155 m high across the river Narmada. The project generates 1200 MW of power. Two irrigation by-pass tunnels, each of 5.50 m diameters bifurcate into two limbs of 2.6 m × 3.90 m size at its exit. The total length of tunnel including bifurcation is 241.23 m. Each irrigation tunnel is designed to discharge 316 m^3/s. Two vertical slide type service gates of size 2.6 m (W) × 3.9 m (H) are provided at the exit of each tunnel bifurcation to control the discharge passing through tunnels. The studies were conducted on a 1:25 scale geometrically similar sectional model of IBPT. Figure 4 shows, sectional plan of irrigation by-pass tunnel system.

High velocity flow below the partial open gate may cause considerable reduction in hydrodynamic pressure on the bottom surface of the gate. These pressures can be as low as vapour pressure of water and may lead to structural damage to the gate grooves and the portion on the downstream of the groove due to cavitation. High head gates may experience vibration during its operation. The principal cause of vibration are vortex trail formed downstream of the gate, pressure fluctuations at the gate bottom and leakage through seals.

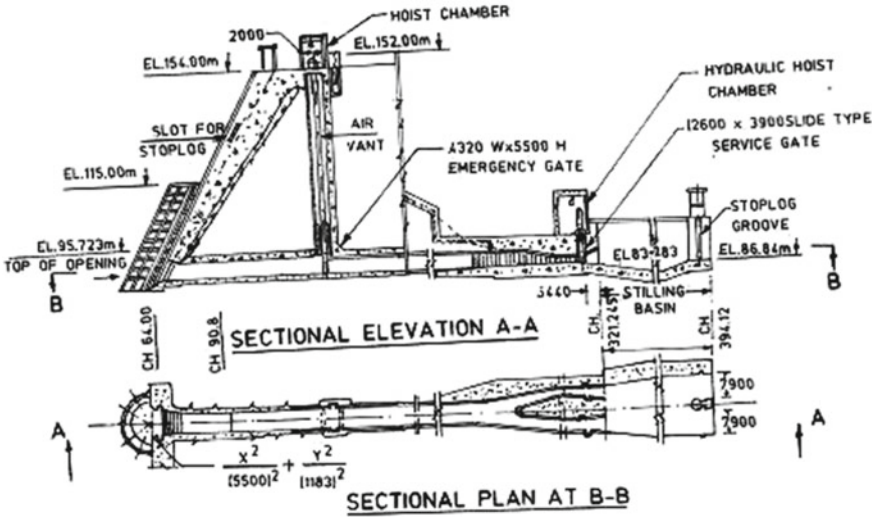

Fig. 4 Sectional plan of irrigation by-pass tunnel system

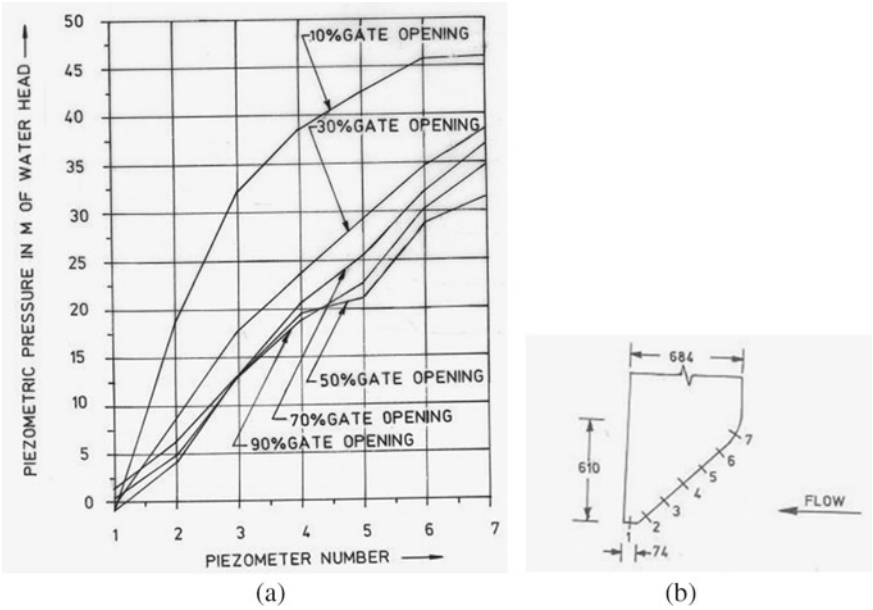

Fig. 5 **a** Pressure along the lip of the gate. **b** Position of piezometers on the lip

5.5 Geometry of the Gate Lip

Studies were also conducted to observe the pressure distribution on the 45° gate lip for different water levels at different positions of the service gate. Figure 5a shows, pressures on the gate lip for various gate openings. Piezometers were fixed on the gate lip as shown in Fig. 5b and the hydrostatic pressures were measured by connecting the piezometers to water manometer. It was observed that the hydrostatic pressures on the lip for different gate openings and water levels between MDDL to FRL were positive throughout. Therefore, the gate lip with 45° lip angle was found to be hydraulically satisfactory.

5.6 Air Demand

When high head conduit gate is partially opened, a high velocity flow occurs on the downstream of the gate resulting in sub-atmospheric pressure. These pressures can be as low as vapour pressure of water and may lead to structural damage due to cavitation and vibration. In order to avoid cavitation and to minimize the vibration, adequate supply of air from the atmosphere is of vital importance. To supply air, the conduit is connected to the atmosphere through an air vent located just downstream of the gate. The size and location of the air vents are decided by conducting the

hydraulic model studies. The velocity of air is measured with the help of a pitot tube attached with a manometer board. Studies indicated that supply of air in the downstream vicinity of the service gate under such flow conditions was not adequate through 600 mm dia air vent which was provided by project authority. In view of above, it was necessary to increase size of air vent to 1000 mm dia for proper aeration.

6 Conclusion

This paper briefly discusses the influence of the gate lip geometry on the hydraulic aspects of cavitations, vibration down pull and uplift individually. The references taken for the above case studies are as mentioned in the references. The case study described above for the projects amply demonstrates the necessity of gate lip profile and air demand for normal operation of the gate for various water levels. Without model studies, it could have been very difficult to assess these parameters. Moreover, the lip angle of 45° observed on the model was to be satisfactory as positive pressures were observed for entire range of water levels.

The aeration required downstream of the gate was also considered during the studies. It was concluded that for SFT model, the air vent downstream of gate is not necessary as sufficient air was available from downstream of the tunnel. Studies indicated for IBPT that supply of air in the downstream vicinity of the service gate under such flow conditions is not adequate through 600 mm dia air vent. In view of above, it would be necessary to increase size of air vent to 1000 mm dia for proper aeration. The findings from the model studies could serve as guidelines to design of similar gate structures for accelerated development of hydropower.

Acknowledgements The authors wish to thank Shri A. K. Agrawal, Director, CWPRS for the encouragement and permission for publishing this paper.

References

1. Naudascher E (1991) Hydrodynamic forces. IAHR structures design manual, International Association of Hydro Research, Stockholm, Sweden
2. Sagar BTA (1977) Downpull in highhead gate installations, Parts 1, 2 and 3. Water Power and Dam Construction (3–5)
3. US Bureau of Reclamation (1957) Model studies of hydraulic downpull forces that act on palisades type regulating slide gate and on the glendo fixed wheel gate. Hydraulic Laboratory Report M, Hyderabad
4. Dhillion GS (1978) Modern trends in design and research of highhead gates with reference to downpull. All India Seminar on Hydraulic Gates, Hyderabad

Hydraulic Design of Plunge Pool Downstream of Ski-Jump Bucket of Orifice Spillways

A. Kulhare, R. R. Bhate, and M. R. Bhajantri

Abstract The Himalayan region is blessed with perennial rivers and heads required for hydropower generation. This blessing comes with challenges like flash floods, cloudbursts, high sediment load, etc. Low-level spillways, in the form of orifice spillways, are an oblivious choice in this region considering their capacity to flush the sediments during floods. Special considerations for the design of energy dissipators are required for orifice spillways. As an energy dissipator, ski-jump buckets are used in most spillways where tailwater depths are shallow for hydraulic jumps to form downstream of spillways. Most commonly, scour holes occur downstream from the point of impingement of the ski-jump jet. These retrograding scour holes may become a threat to the spillway structure itself and hence need to be assessed carefully. To prevent an uncontrolled erosion of riverbanks and the river bed, a preformed plunge pool is provided. Taking into consideration the geological features at the site and the water jet impact location, the size, location, bed level and the slopes on both flanks of the plunge pool are decided. The physical model studies have traditionally been used to predict equilibrium scour depth and its location and extent. Despite the qualitative nature of these studies, past experiences suggest that the ultimate scour is realized in the prototype after a long period of operation when the rock fragments and behaves as non-cohesive material. Dimensions of the plunge pool including location, width, length, depth and upstream and downstream slopes can be worked out using the model observations. Two such case studies are discussed in this paper where the effect of hydraulically optimized plunge pool in substantial dissipation of kinetic energy of incoming flow jet and reduction in water level fluctuations in the powerhouse tail pool located just downstream of the spillway was observed.

Keywords Hydraulic model · Ski-jump bucket · Scour depth · Plunge pool · Tail pool

A. Kulhare (✉) · R. R. Bhate · M. R. Bhajantri
Spillways and Energy Dissipators Division, Central Water and Power Research Station, Pune 411024, India
e-mail: akulhare@live.com

P. V. Timbadiya et al. (eds.), *Flood Forecasting and Hydraulic Structures*, Lecture Notes in Civil Engineering 340, https://doi.org/10.1007/978-981-99-1890-4_32

1 Introduction

There is typically no sufficient tailwater available in hilly areas, which makes ski-jump bucket energy dissipators ideal. The possibility of scouring downstream of the spillway is a major consideration in the design of ski-jump buckets; installation of such spillways is restricted to river beds with generally sound rock. The ski-jump jet directs the water jet into the air, and then into the plunge pool formed when it hits the tailwater, causing a change in the river bed level. As a result, changes in the riverbed can alter its geometry. The stability of spillway structures may be endangered if the depth of the scour holes becomes significant and reaches the structure foundations. The jet impact causes the scour to develop both upstream and downstream of the point of impingement. Scour develops gradually until a depth of equilibrium is reached, and a sufficient depth of water is available to dissipate the energy of the ski-jump jet. Mason and Arumugm [1] concluded from his prototype experiences on several projects that unacceptable scour is by no means restricted to soft rocks and has in many cases occurred alongside hard igneous rocks also. In the Himalayan region, rocks are fragile, and this could lead to uncontrolled scour and landslides upon impact from the ski-jump jet. To avoid these hazards, preformed plunge pools are needed. Plunge pool design plays a significant role in the dissipation of energy, which involves determining the size and location of plunge pools. The extent of maximum scour must be determined to determine the depth of the plunge pool.

The depth of scour is governed by several hydraulic, morphologic and geotechnical factors like (refer to Fig. 1) discharge intensity q, the height of fall H_1, bucket radius R, bucket lip angle, tailwater depth d_w, type of rock, size of rock d_{50}, degree of rock homogeneity, and time and mode of operation of spillway [2]. In order to determine the safety of the dam and the adjoining structures, it is necessary to estimate the depth of the scour hole formed.

Various researchers have developed different empirical and semi-empirical formulae for scour depth estimation as reported by Veronese [3], Damle et al. [4], Wu [5] and Lopardo et al. [6]. However, the scour prediction has remained undetermined; the main reason being the complexity of the phenomenon. The Bureau of

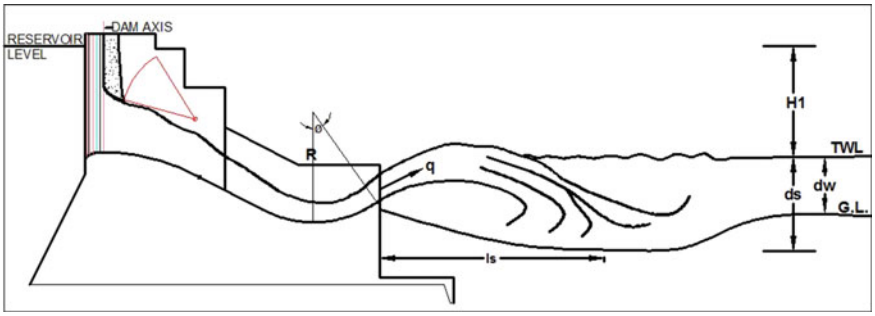

Fig. 1 Scour downstream of the ski-jump bucket spillway

Indian Standards 1985 suggests the use of the Veronese formula [3] given below for the estimation of the ultimate depth of scour below tailwater level.

$$ds = 1.9\, q^{0.54} H_1^{0.225} \tag{1}$$

Wu's formula [5]

$$ds/H_1 = 2.11\left\{q/\sqrt{\left(q H_1^3\right)}\right\}^{0.51} \tag{2}$$

Martin's formula [7]

$$ds = 1.5\, q^{0.6} H_1^{0.1} \tag{3}$$

Another set of formulae was derived from prototype observations or model studies in the form of $ds = K\, q^a \times H^b$, where the two coefficients were determined through regression analysis. Among all Damle equations [4], only the exponents of the product (qh) conformed to the concept of stream power.

The empirical formulas rely on idealization, approximation and an average of widely varying prototype conditions. There are large differences between the depths calculated by these formulae. In addition, the rock properties at the site are not taken into account in these formulae. As a result, they may predict scour depths that may be considered unrealistic. Prediction of equilibrium scour depth and its location for designing of preformed plunge pool is done traditionally through physical model studies at CWPRS, Pune [9–11].

2 Model Studies for Designing of Plunge Pool

There are no empirical formulae that indicate the likely scouring pattern at the site. Physical model scour studies are required to determine the extent and likely pattern of scouring expected downstream of the ski-jump bucket for designing the plunge pool. Modelling the process of scouring rocky beds due to the impact of high-velocity jets is nearly impossible; therefore, a practical simulation approach is used in the model depending on the objective of the study. Beds are reproduced by disintegrated fragments which can be carried downstream by the flow. A sand-gravel mix is usually selected for the bed without regard for the size that would result from rock disintegration. There is a layer of sand placed at the potential scour location, below the level of the river bed and above the likely ultimate scour. A scour profile is observed after allowing water to flow over it for a specified period. Despite the qualitative nature of the studies, past experiences have shown that scour manifests itself in the prototype after many years of operation as rocks fragment and behave as non-cohesive materials.

As a result of comparing all discharge and reservoir water levels observed on the model, a comprehensive understanding of ski-jump jet and scour profiles can be determined. The location and size of the plunge pool are determined by these studies. The scour pit usually forms downstream of the point of impact of the ski-jump jet. Figure 2a, b shows the scour envelope for ungated and gated flows, respectively.

Depending on the site conditions, the plunge pool can be unlined, lined or preformed. The construction of lined plunge pools is impractical; however, it may be necessary if the geology is extremely fragile. Depending on the geological conditions of the site, transverse slopes on both flanks of the plunge pool can be decided. Additionally, the ski-jump jet is likely to spread laterally in downstream directions and would also wear on the side slopes. Therefore, it is imperative to implement adequate banking protection measures to ensure the protection of excavated banks.

The present paper describes the role of physical model studies conducted at CWPRS, [12] for real-world cases for designing the preformed plunge pools. Two projects have been taken for discussing the results of physical model studies for designing a plunge pool.

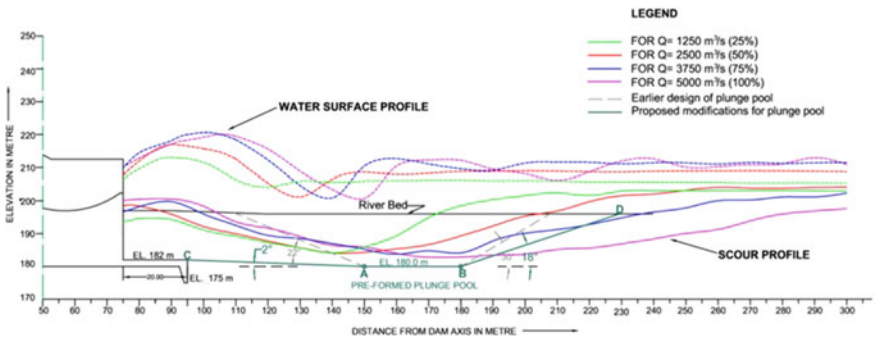

(a) Gated operation of spillway

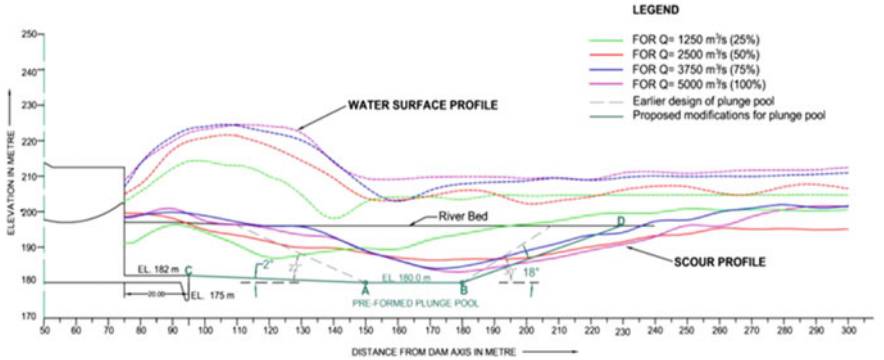

(b) Ungated operation of spillway

Fig. 2 A typical configuration of plunge pool based on scour envelopes

3 Case Study—I

The Pare H.E. Project has been planned as a run-of-river scheme on the Dikrong/Pare river downstream of the powerhouse of the first stage of the Ranganadi H.E. Project in the Papumpare district of Arunachal Pradesh. The project envisages the construction of a 78-m-high concrete gravity diversion dam, about 3-km-long water conductor system and a surface powerhouse with an installed capacity of 110 MW. Figure 3 shows the layout of the project. The breast wall spillway has been provided to pass the flood as well as to flush the sediment deposited in the reservoir into the river downstream. The spillway is designed to pass the maximum design outflow flood of 5000 m^3/s through three orifice openings of size 10.4 m wide × 14 m high with crest level at El. 216 m. The FRL and MWL have been fixed at El. 245.15 m and 246.215 m, respectively. Radial gates have been provided at the downstream face of the breast wall for controlling the outflow discharge. A ski-jump bucket of 18 m radius and 40° lip angle with a preformed plunge pool is provided for energy dissipation. Figure 4 shows the section of the spillway.

The river portion downstream of spillway up to chainage 355 m downstream of dam axis was reproduced with cohesionless erodible material (sand) of mean size (d_{50}) of about 1 mm, and the river banks beyond El. 230 m were reproduced rigidly in the existing 1:60 scale geometrically similar 3-D comprehensive model for assessing the maximum depth and pattern of scour for various discharges. Figure 5 shows the spillway and downstream riverbed with erodible material up to chainage 355 m. River banks beyond El. 230 m were reproduced rigidly in the model which is not the actual site condition. In view of this, the scour pattern observed near the banks is not realistic and hence is ignored. However, the scour profiles in the river portion are indicative of the depth of scour and location of the deepest scour hole. The scour

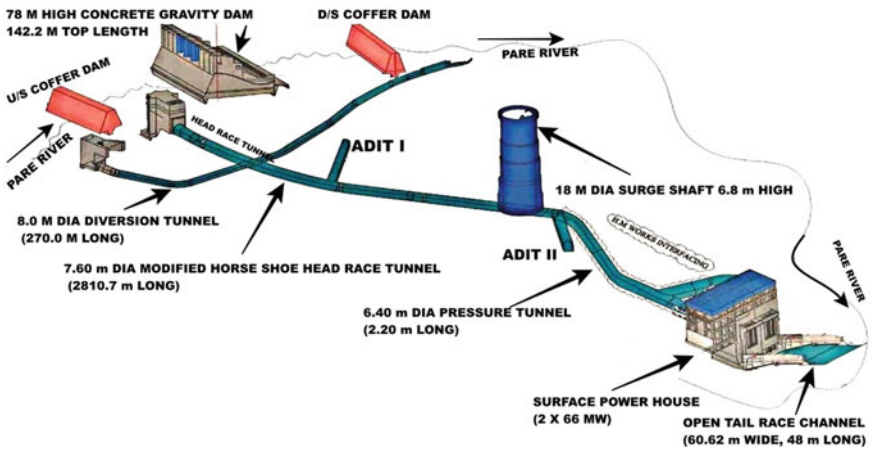

Fig. 3 Layout plan of the project

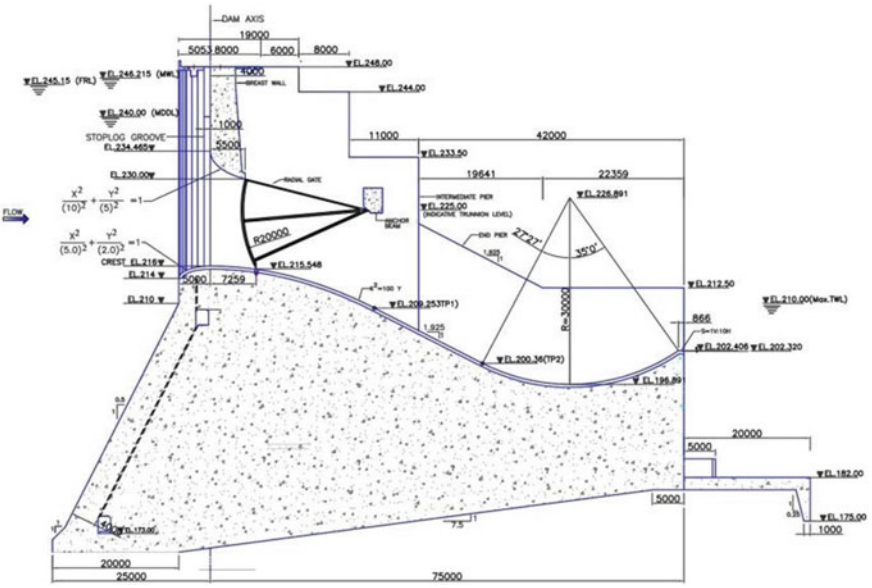

Fig. 4 Cross section of the spillway

studies were conducted for discharges of 5000, 3750, 2500 and 1250 m^3/s passed for gated as well as ungated operations of the spillway as mentioned in Table 1.

Fig. 5 Downstream view of the model showing reproduction of river portion with erodible material

Table 1 List of experiments conducted for scour studies

Sr. No	Discharge (m^3/s)	RWL (m)	Spillway operation	Figure No.
1	1250 (25%)	245.15	Gated	Figure 8
2	2500 (50%)	245.15		
3	3250 (75%)	245.15		
4	5000 (100%)	245.15		
5	1250 (25%)	224.28	Ungated	Figure 9
6	2500 (50%)	228.83		
7	3250 (75%)	232.56		
8	5000 (100%)	235.65		

Necessary arrangements were made for measurement of discharge, reservoir water levels, tailwater levels and scour profiles. The accepted equations for similitude, based on Froudian criteria, were used to express the mathematical relationship between the dimensions and hydraulic parameters of the model and the prototype.

Hydraulic model studies indicated that the deepest scour reached up to El. 182.8 m at chainage 170 m downstream of dam axis for design discharge 5000 m^3/s for the ungated operation of the spillway. Observed deepest scour elevation found very close agreement with the minimum scour depth as per Damle's empirical equation [4]. For the gated operation of the spillway, the scour reached up to El. 183.10 m at chainage 180 m downstream of the dam axis.

The ski-jump jet is also likely to spread laterally in the downstream directions and would also abrade along the side slopes causing saturation of hill slopes. It was suggested to pass low discharges up to 1600 m^3/s through the central span of the spillway. Operation of the central span would be beneficial in safeguarding the river banks against erosion and landslides due to the saturation of hill slopes. Suitable protection, if necessary, may be provided to the excavated banks after considering the stability of the rock from the geological consideration and spray generated due to the ski-jump jet. It was also recommended that an apron of length 20 m be laid and anchored to the rock. A key at the downstream end of the apron may be provided to protect the toe of the dam from undermining due to the flow cascading over the lip of the bucket for low discharges and reservoir water levels. Figures 6 and 7 show the flow conditions on the physical model and the development of the scour downstream of the spillway.

Longitudinal scour profiles along the centreline of the spillway for gated and ungated operations of the spillway are shown in Figs. 8 and 9, respectively. The location of the maximum depth of scour varies for various operating conditions of the spillway. The preformed plunge pool with bottom El. 180 m as proposed earlier is also shown in these figures.

It can be seen from the figures that scour profiles for most of the discharges would be contained in the proposed preformed plunge pool downstream of the spillway except for scour profiles near the downstream slope of the proposed preformed plunge

Fig. 6 Flow condition in the river downstream of the spillway, $Q = 5000\ m^3/s$ (100%), FRL El. 245.15 m

Fig. 7 Scoured river bed downstream of the spillway, $Q = 5000\ m^3/s$ (100%), FRL El. 245.15 m

pool. It was suggested to make the downstream slope flatter with an angle of 180 to prevent the progressive erosion of the downstream slope of the preformed plunge pool. The width of the ski-jump bucket at the lip is 49.2 m, and as such the same width may be provided for the plunge pool. Hence, the size of the plunge pool proposed was 49.2 m (W) × 30 m (L) with a bottom at EL. 180 m located between chainage 150 and 180 m downstream of the dam axis. It was suggested that an upstream longitudinal

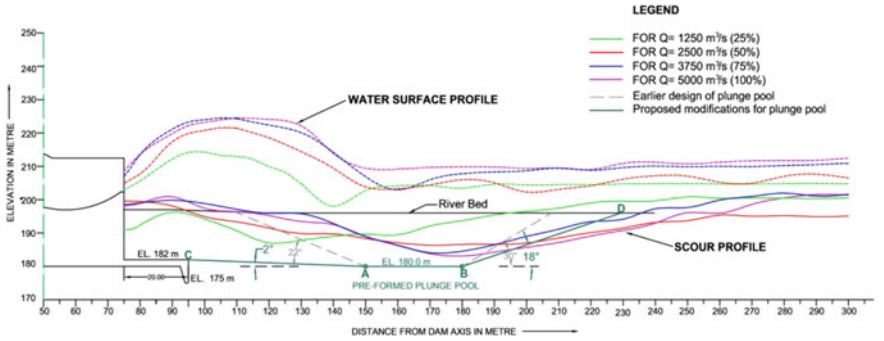

Fig. 8 Water surface and scour profile along the centre line of the spillway for gated operation of the spillway

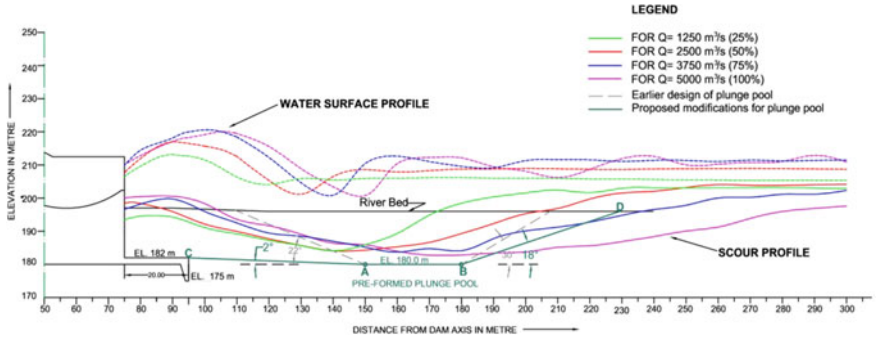

Fig. 9 Water surface and scour profile along the centre line of the spillway for ungated operation of the spillway

slope may be provided by excavating up to the downstream end of the 20 m long concrete apron at El. 182 m. Longitudinal slopes upstream and downstream of the plunge pool work out to be 20 and 180, respectively. It was also recommended that the transverse slopes on both the flanks of the plunge pool may be decided based on geological conditions prevailing at the site.

4 Case Study—II

The case study discussed below is one of the proposed mega hydropower projects located on the border of Assam–Arunachal Pradesh. The project envisages the construction of a 116-m-high and 271-m-long concrete gravity dam to generate 2000 MW (8 units of 250 MW each) of power using 91-m gross head. The spillway is designed for a maximum outflow flood of 35,000 m^3/s at MWL El. 208.25 m.

The spillway consists of 9 spans of 11.5 m (W) × 14.0 m (H) with breast walls and crest at El. 145 m. The energy dissipation arrangement envisaged is in the form of a ski-jump bucket. Considering geological constraints and to reduce bank excavations, the plunge pool proposed is in front of the middle six spans out of the total nine spans. The nine spans of the spillway are provided at three different levels resulting in different throw distances and angles of impact of the jet through different spans for the same discharge. This makes the hydraulic model studies more involved. Figure 10 shows the plan and cross section of the proposed spillway.

Hydraulic model studies for the assessment of scour were conducted on a 3-D comprehensive model with a geometrically similar scale of 1:90. The model included

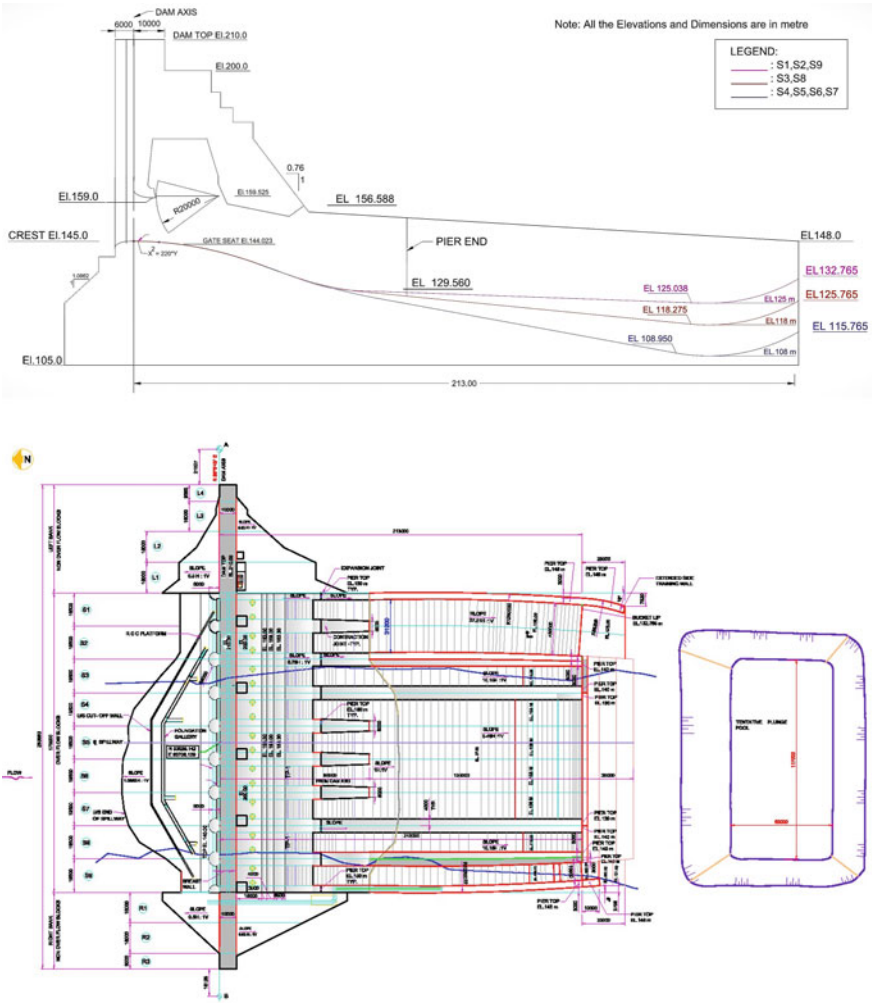

Fig. 10 Cross section and plan of the spillway

river reach up to 800 m upstream and 1000 m downstream of the dam axis, respectively, along with the powerhouse tail pool. The curved left deflector wall with the deflector angle of 160 was provided to deflect the flow towards the plunge pool proposed in front of the middle spans. For carrying out scour studies, the most common method of representing the geological features of the river bed and banks in the vicinity of the anticipated plunge pool scour region in the physical model is the use of cohesionless erodible material to reproduce the river topography. In order to quantify the maximum depth of scour and scour pattern for various discharges for the river portion downstream ski-jump bucket lip between chainage 243 m and chainage 510 m downstream of the dam axis, cohesionless erodible material (sand) of d_{50} about 2 mm in size was used. To achieve a near-realistic pattern of scour in the river, it was considered appropriate to reproduce the scour pit vertically with rigid sides to avoid collapsing of excess material from the side flanks. The river portion between contours El. 30 m and El. 100 m (between chainages 243 and 510 m) was reproduced erodible, and the riverbanks above these elevations were kept rigid. Figure 11 shows the view of the spillway scour pit with erodible bed material. Necessary arrangements were made for measurement of discharge, reservoir and tailwater levels, scour profiles and fluctuations in the tail pool.

The scour studies were conducted for various discharges with partial gate openings mentioned in Table 2. The tailwater levels at chainage 450 m downstream of the dam axis were maintained while conducting experiments. The deepest scour depths and their chainage observed for various experimental conditions are tabulated. Figures 12 and 13 show the flow conditions downstream of the spillway and the observed scour

Fig. 11 Spillway scour pit with erodible bed material

pattern for the design discharge of 50% of PMF with the gated operation of the spillway.

To avoid uncontrolled scour damage, pre-excavated plunge pools are normally provided downstream of the ski-jump bucket. This is particularly important for the spillways in the Himalayan region where the geology is fragile and gorges are narrow. The pre-excavated plunge pool geometry has to be based on the expected natural scour geometry. A complete geometry including ultimate scour depth, length, upstream and downstream slope has been suggested by Taraimovich (1978) [8]. The scour profiles obtained from the model studies were used to evolve the dimensions of the plunge

Table 2 Deepest scour depths observed for various experimental conditions

Discharge in m^3/s	Spans operating	Location and elevation of scour in m			
		FRL El. 205 m		RWL El. 190 m	
		Chainage (m)	Elevation (m)	Chainage (m)	Elevation
6000	S4-S7	380	71.25	380	72.40
6000	S3-S8	380	78.85	380	81.30
10,000	S1-S8	360	76.50	360	80.60
12,000	S1-S9	400	77.50	380	78.40
17,500 (50%)	S1-S9	400	67.10	380	68.00
26,250 (75%)	S1-S9	400	56.40	380	57.70

Fig. 12 Flow conditions downstream of the spillway

Fig. 13 Scour pattern for the design discharge of 50% of PMF with the gated operation of the spillway

pool for the present case study which matched well with the guidelines provided by Taraimovich [8].

In this case, the deepest scour observed for various discharges was found to be around chainage 380 m. There were constraints for providing a preformed plunge pool like downstream cofferdam at ch. 400 m and tail pool at ch. 465 m. To dissipate the kinetic energy of the jets, the preformed plunge pool with bottom El. 70 m from chainage 300–360 m with longitudinal upstream and downstream slopes was proposed as shown in Fig. 14. The longitudinal section of the plunge pool was acceptable for the pre-dam construction stage to facilitate the excavation work of the plunge pool at the site. The actual scour pattern will presumably follow the scour envelopes as obtained in the model studies. Once the spillway is operated for higher discharges, the downstream slope of the plunge pool would change as there won't be a cofferdam after the commissioning of the project. Hence, it was suggested to consider this aspect while finalizing the design of the plunge pool. The spillway toe also needs to be protected from damage caused by the flow cascading over the lip of the bucket by providing a concrete apron downstream of the bucket. The partially completed spillway blocks would cause the water to cascade over the bucket lip during construction. After the spillway has been completed, the cascading flow will occur at the operation's beginning and end. As a precaution against cascading flow undermining the toe of the bucket, concrete aprons must be provided between the lip of the bucket and the plunge pool.

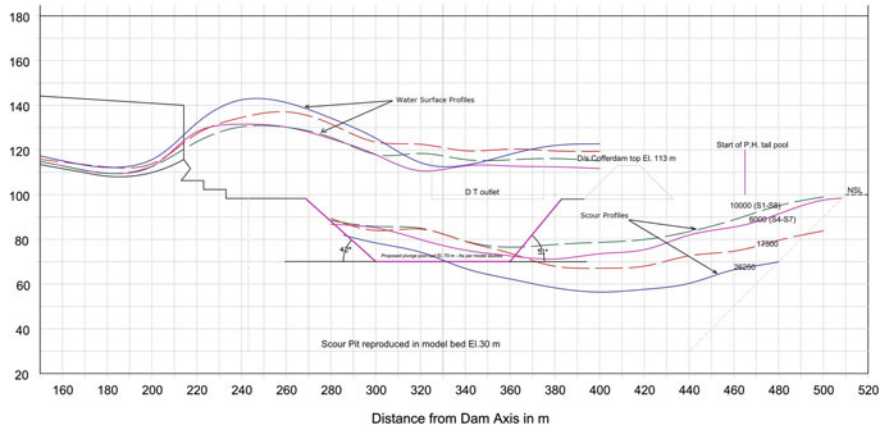

Fig. 14 Water surface and scour profile along the centre line of the spillway for the gated operation of the spillway

5 Conclusions

The assessment of scour depth and design of plunge pool is very complicated because the scour process is a time-dependent complex dynamic process and varies with many factors including hydraulic, morphologic and hydrologic conditions, as well as characteristics of the structure. The design of the plunge pool for its location, size and shape is decided based on scour studies on physical models and evaluating the site constraints. In the first case study, based on the location of the maximum depth of scour and pattern observed in the physical model, a preformed plunge pool with bottom El. 180 m proposed with the downstream slope flatter with an angle of 180 to prevent the progressive erosion and the upstream longitudinal slope by excavating up to the downstream end of the 20-m-long concrete apron at El. 182 m. It was suggested to provide the same width of 49.2 m for the plunge pool as the width of the ski-jump bucket at lip. Hence, the size of the plunge pool proposed was 49.2 m (W) × 30 m (L) with the bottom at EL. 180 m located with longitudinal slopes upstream and downstream of plunge pool work out to be 20 and 180, respectively. In the second case study, there were geological and structural restrictions to decide the size and extent of the plunge pool. To avoid excessive bank cutting, the width of the plunge pool was restricted to central six spans out of nine spans and the water jets were diverted using deflector walls. There was a coffer dam 180 m downstream of the lip, and the tail pool is just 260 m downstream of the lip. In view of this, the preformed plunge pool with bottom El. 70 m from chainage 300 m to 360 m with longitudinal upstream and downstream slopes of 440 and 510, respectively, were suggested. The plunge pool design suggested based on model studies for the above two case studies was accepted by project authorities. The plunge pool as evolved through model studies has been provided at Pare H.E. project, and it is under construction for the second H.E. project in the case study.

Acknowledgements The authors are thankful to Dr R.S. Kankara, Director, Shri A.K. Agarwal, Ex-Director and Shri Y.N. Srivastava, Additional Director, CWPRS, Pune, for encouragement and permission to publish this paper. The authors are grateful to the Project Engineers for financing the studies and for their active participation, discussions and valuable suggestions during the studies. The help of all the staff in conducting the studies is gratefully acknowledged.

References

1. Mason PJ, Arumugm K (1985) A review of 20 years of scour development at Kariba Dam. In: 2nd international conference on the hydraulics of floods and flood control, Cambridge, England, Sept
2. Azamathullah H, Ghani A, Zakaria NA, Lai SH, Chang CK, Leow CS (2008) Genetic programming to predict ski-jump bucket spillway scour. Science Direct 20(4):77–484
3. Veronese A (1937) Erosion of a bed downstream from an outlet. Colorado A&M College, Fort Collins, Colo
4. Damle PM, Venkataraman CP, Desai SC (1966) Evaluation of scour below ski-jump buckets of spillways, CWPRS Golden Jubilee Symposia, vol 1
5. Wu CM (1973) Scour at downstream end of dams in Taiwan. Sediment Transportation vol 1. In: Proceedings of the international association for hydraulic research symposium on river mechanics (4 vol) Bangkok, Thailand, 9–12 Jan 1973
6. Lopardo RA, Lopardo MC, Casado JM (2002) Local rock scour downstream from large dams. In: Proceedings of international workshop on rock scour due to high velocity jets, Lausanne, Switzerland, pp 55–58
7. Martins R, Viseu T (1994) Plunge pool slab design taking into account turbulent pressures. In: 9th APD-IAHR congress, Aug 1994
8. Taramovich II (1978) Deformation of channels below high head spillways on rock foundations. Hydrotechnical Constructions
9. Kulhare A, Bhajantri MR, Bhosekar VV (2017) Physical & numerical simulation of scour downstream of ski-jump bucket spillway—a case study. HYDRO-2017, Ahemdabad, Gujarat, 21–23 Dec 2017, pp 815–825
10. Bhajantri MR, Bhate RR, Bhosekar VV (2014) Design of energy dissipators in Himalayan region. INCOLD Journal 3:10–18
11. Khatsuria RM, State of Art on Computation (1992) Prediction and analysis of scour in rocky beds downstream of ski jump spillways. CWPRS platinum jubilee symposia
12. CWPRS Technical Report Nos. 4922, 5051 and 5449 (2012, 2013 and 2016)

Prediction of Discharge Coefficients for Trapezoidal Labyrinth Weir with Half-Round (HR) and Quarter-Round (QR) Crest

Mohammad Danish Mustafa, Talib Mansoor, and Mohammad Muzzammil

Abstract A labyrinth weir allows more flow for a given head and channel width relative to other linear weirs due to the additional crest length. Earlier research explored the correlation between discharge magnification ratio to head to weir height ratio for a different configuration. Discharge coefficient depends on head to weir height ratio, crest shape, crest thickness, apex configuration, and sidewall angle. Continued efforts have been made to develop an equation for discharge coefficient in terms of these parameters. Several equations relating discharge coefficient with head to weir height ratio using polynomial fit up to sixth order for each side wall angle are available in literature. Some investigators related the coefficients of polynomial with side wall angle resulting in a complex form of equation for the discharge coefficient. An attempt has been made to develop a relatively simple discharge coefficient equation involving lesser number of coefficients in terms of head to weir height ratio and sidewall angle. Some of the salient features of the study are described in the present paper.

Keywords Hydraulic structure · Hydraulic design · Coefficient of discharge · Trapezoidal labyrinth weir

Notations

N	Number of cycles
P	Weir height
g	Acceleration due to gravity
h	Head over weir
t	Sidewall thickness
A	Apex inside width (HRL and QRL)
α	Side wall angle

M. D. Mustafa (✉) · T. Mansoor · M. Muzzammil
Department of Civil Engineering, Aligarh Muslim University, Aligarh 202001, India
e-mail: mdmustafa@myamu.ac.in

P. V. Timbadiya et al. (eds.), *Flood Forecasting and Hydraulic Structures*, Lecture Notes in Civil Engineering 340, https://doi.org/10.1007/978-981-99-1890-4_33

L_1	Weir side leg length
D	Apex outside width
C_d	Coefficient of discharge
Q	Volumetric flow rate
$\eta = (H_T/P)$	Head to weir height
H_T	Total head
β	Angle of approach flow
θ	Cycle arc angle
L_c	Centreline length of sidewall
M_r	Magnification ratio

1 Introduction

A labyrinth weir is a linear weir symmetrically folded in a plan for providing a longer crest length. These types of weirs require less freeboard in the upstream reservoir than that in linear weir which facilitates flood routing and increases reservoir storage capacity. The typical layout of the labyrinth weir is shown in Fig. 1.

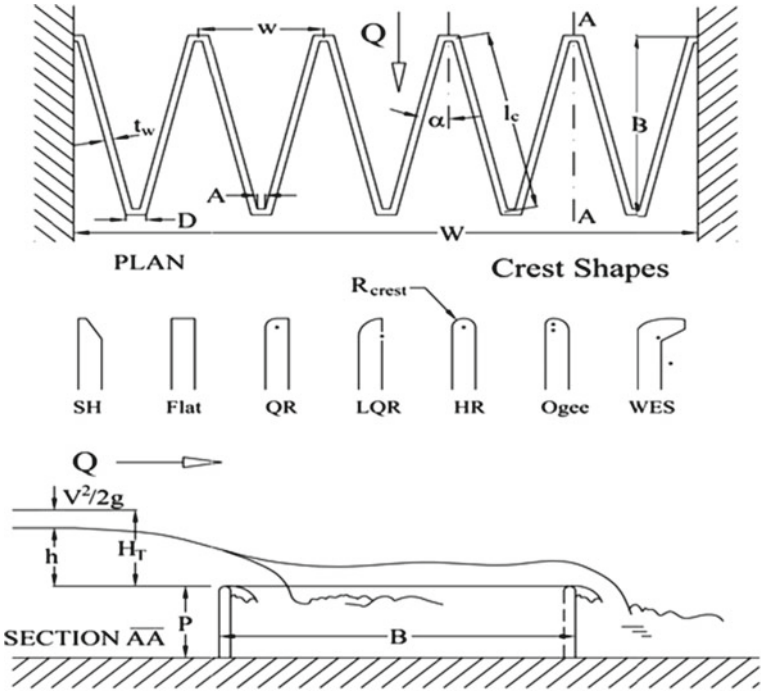

Fig. 1 Labyrinth weir geometric and hydraulic variables [5]

Discharge, Q over labyrinth weir is computed using linear weir equation [1].

$$Q = \frac{2}{3} C_d L \sqrt{2g} {H_T}^{3/2}, \tag{1}$$

where C_d is discharge coefficient, g is the acceleration due to gravity, L is effective weir crest length, and H_T is total head above weir crest including velocity head. The capability of the weir is affected by various factors like the angle of sidewalls (α), apex width, approach channel condition, head to weir height ratio ($\eta = H_T/P$), and vertical aspect ratio (W/P), where W is width of one cycle. Taylor et al. [2] conducted experiments on labyrinth weir with triangular, trapezoidal, and rectangular plan forms. They presented results in the form of graphs between magnification ratio ($m_r = Q_{\text{labyrinth}}/Q_{\text{linear}}$) and η. They concluded that m_r decreases with an increase in η. Darvas [3] used the data of model studies of Worona and Avon labyrinth weirs to develop a set of curves for designing labyrinth weirs. Houston [4] studied a scale model of the UTE dam's labyrinth weir.

Tullis et al. [1] performed experiments to investigate the effect of η and α on the performance of linear labyrinth weirs and concluded that the efficiency of a labyrinth weir decreases with an increase in the head to weir height ratio. Using regression analysis, they proposed equations for C_d with η employing fourth order polynomial fit for each side wall angle (6°–35°). Willmore [6] conducted an experimental study on quarter-round, half-round, and ogee crest-shaped trapezoidal labyrinth weirs and plotted a graph between C_d versus η for a different configuration. He further obtained best-fit C_d equations using a polynomial of third to sixth order. Using the design curve of Tullis et al. [1], Ghare et al. [7] plotted a graph between $C_{d\max}$ versus η for different α and proposed equation for maximum discharge coefficient for the design of labyrinth weir. Ghodsian [8] conducted experiments on two cycle triangular labyrinth weir having different crest shapes (half-round, quarter-round and, sharp, flat top). He proposed a discharge coefficient equation in terms of weir head to weir height ratio and weir side leg length to width ratio (L_1/W) of one cycle. Kumar et al. [9] also related C_d with H_T/P and α for one cycle of sharp crested triangular planform weir. Carollo et al. [10] investigated outflow over sharp crested two cycle triangular labyrinth weir with different side wall angles and proposed an equation for discharge magnification. Crookston et al. [11] investigated the labyrinth weir nappe interference that decrease discharge efficiency, including local submergence. They demonstrated parametric methods for determining the size of the nappe interference region as a function of weir geometry and flow parameters. Khode et al. [12] carried out experimental studies on trapezoidal labyrinth weirs for side wall angles 8°, 10°, 20°, and 30° covering a wider range of flow conditions. They defined discharge coefficient in two forms, i.e. C_{dl} = discharge coefficient per unit length of labyrinth weir and C_{dw} = discharge coefficient per unit width of labyrinth weir and obtain relationship between discharge coefficient and head to weir height ratio using fourth degree polynomial for each side wall angle. Seamons [13] performed experiments on eight models of labyrinth weir with different upstream apex widths to investigate the effect of nappe interference. Vatankhah [14] proposed a general equation incorporating α

in the following form.

$$C_d = \left(k_0 + k_1\eta^{k_2\eta^{k_3}+k_4}\right)\left[k_5 + k_6(\sin\alpha)^{k_7}\right] + \left(k_8 + k_9\eta^{k_{10}} + k_{11}\eta^{k_{12}}\right)^{k_{13}}\left[k_{14} + k_{15}(\sin\alpha)^{k_{16}}\right]^{k_{17}} \quad (2)$$

He developed two different regression equations for quarter-round and half-round trapezoidal labyrinth weir using the data collected by Tullis [1]. Based on the comparison of both the regression equations, he found that for small values of α from 6° to 20°, the curves of the discharge coefficient ratio $C_{d\mathrm{HR}}/C_{d\mathrm{QR}}$ show similar trends with reasonable similarity, while different behaviour was found for $\alpha = 35°$ with a lower discharge coefficient ratio. He suggested exploring the reason for this phenomenon using the supplementary data for α in the range of 20°–35°. This issue is considered important to improve the flow conditions for weirs and to use a more efficient crest shape for trapezoidal labyrinth weirs. The optimal value of η and α was also found to be $\eta = 0.101$ and $\alpha = 20.54$, which correspond to a maximum value of $C_{d\mathrm{HR}}/C_{d\mathrm{QR}} = 1.194$. Bilhan et al. [14] investigated the effect of nappe breakers in trapezoidal labyrinth weirs using a support vector regression (SVR) and extreme learning machine (ELM). Employing the data of the experimental study of Bilhan et al. [14], they proposed a fifth-degree polynomial fit equation for C_d. Some of the equations for discharge coefficient proposed by various researchers are summarized in Table 1.

Literature review on labyrinth weir indicates that magnification ratio is related to head to weir height ratio for a different configuration. Discharge coefficient is a function of η, α, and the crest shape, and it is expressed in the polynomial form for η (up to sixth degree) and coefficients of polynomial were related to α. It is worthwhile to note that using a polynomial of degree n for labyrinth weirs having m configurations (different side wall angles) requires $m*(n + 1)$ coefficients leading to a complex form of equation for estimation of discharge coefficient. In the present study, an attempt has, therefore, been made to develop a relatively simple discharge coefficient equation involving few coefficients in terms of head to weir height ratio and sidewall angle.

2 Generalized Discharge Coefficient Equation

Discharge over a labyrinth weir depends on various parameters like head, weir height, sidewall angle, the shape of a crest, number of cycles, etc.

Dimensional analysis carried out in earlier studies indicated that discharge coefficient is mainly a function of head to weir height ratio. Side wall angle α plays an important role in the interference of nappe which ultimately affects the discharge. Therefore, in the present study, an attempt has been made to correlate the discharge coefficient with η and α. For this purpose, experimental data of Willmore [6] and

Table 1 Discharge coefficient predictors reported by some investigators

Author	Proposed equation	Remarks	Weir type	Crest type
Tullis et al. [1]	$C_d = 0.49 \pm B\left(\frac{H_T}{P}\right) - C\left(\frac{H_T}{P}\right)^2 + D\left(\frac{H_T}{P}\right)^3 - E\left(\frac{H_T}{P}\right)^4$	$0.05 \leq H/P \leq 1$	Trapezoidal–4 cycles	SC-FT-QR-HR
Ghodsian [8]	$C_d = 1.06\alpha^{1.5}\left(\frac{H}{P}\right)^{-0.606}\left(\frac{L}{W}\right)^{-0.237}$	$0.3 \leq H/P \leq 0.7$	Triangular- 2 cycles	SC-QR-HR-FT
Kumar et al. [9]	$C_d = (-0.065\theta^3 + 0.318\theta^2 - 0.537\theta + 1.190) + (0.090\theta^3 - 0.570\theta^2 + 1.460\theta - 1.670(h/p)$	$0 < h/p < 0.7$	Triangular plan form	SC
Khode et al. [12]	$C_w = B_\circ + B_1\left(\frac{H_T}{P}\right) + B_2\left(\frac{H_T}{P}\right)^2 + B_3\left(\frac{H_T}{P}\right)^3 + B_4\left(\frac{H_T}{P}\right)^4$	$0.1 \leq H/P \leq 0.7$	Trapezoidal–2 cycle	FT
	$\frac{Q}{Q_n} = \left[1 + \frac{\left(\frac{\iota}{\sqsupseteq} - 1\right)}{5.988\left(\frac{H}{\sqsupseteq}\right)^{1.419} + 1}\right]$	$0 .1 < h/p < 0.7$	Trangular labyrinth weir	SC
Crookston and Tullis [15]	$C_{d(\alpha)} = \alpha\left(\frac{H_T}{P}\right)^{b\left(\frac{H_T}{P}\right)^C} + d$	$0.05 \leq H/P \leq 0.9$	Trapezoidal–2 and 4 cycles	HR-QR
	$C_d = A \times (\eta)^{B\times(\eta)^C} + D$	$0 .1 < h/p < 0.7$	Trapezoidal labyrinth weir	HR and QR
	$C_d = i + j(\eta) + k(\eta)^2 + \iota(\eta)^3 + m(\eta)^4 + n(\eta)^5$	$0 .1 < h/p < 0.7$	Trapezoidal labyrinth weir	

Seamons [15] have been utilized to develop a generalized discharge coefficient equation for trapezoidal labyrinth weir with half-round (HR) and quarter-round (QR) crest shapes with η ranging from 0.04 to 0.8 and α from 6° to 35°.

Considering the following form of discharge coefficient:

$$C_d = a_1 + a_2(\eta)^{b_1} + a_3(\alpha)^{b_2}, \tag{3}$$

where a_1, a_2, a_3, are coefficients and b_1 and b_2 are exponents. Using Minitab software, the values of coefficients and exponents were determined. The following best-fit equation was obtained:

$$C_d = -0.118 - 0.486(\eta)^{0.72} + 0.559(\alpha)^{0.169}. \tag{4}$$

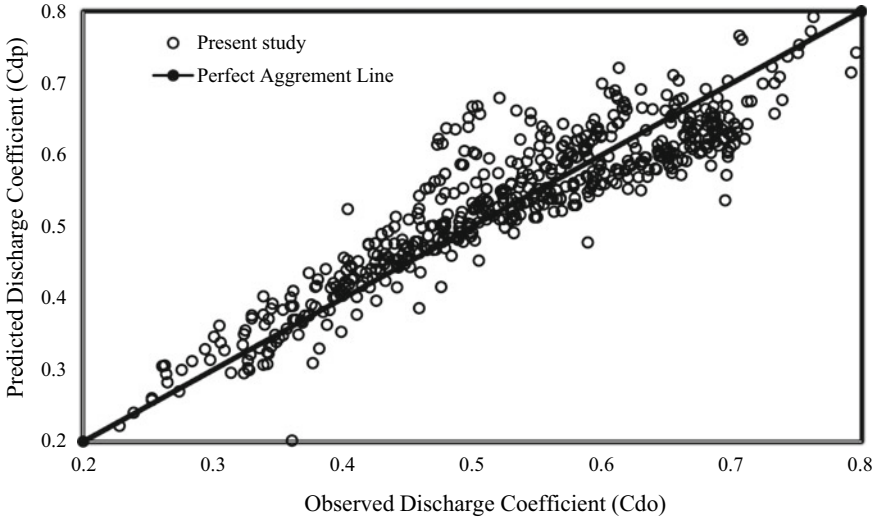

Fig. 2 Comparison of predicted and observed coefficient of discharge (C_d)

Using Eq. (4), discharge coefficient was calculated for known values of η and α from the data set of Willmore [6]; Seamons [15] and a graph is prepared between the predicted discharge coefficient C_{dp} and observed discharge coefficient C_{do} as shown in Fig. 2. A perusal of Fig. 2 indicates that the majority of data points lie on the perfect agreement line.

3 Validation of Proposed Equation

The data of seven prototype dams having labyrinth shape with sidewall angle $9.14° \leq \alpha \leq 23.6°$ have been selected for validation. Table 2 gives the data of the prototype dam with their discharge coefficients (C_{do}) along with the computed discharge coefficient (C_{dpp}) of the present study. The percentage error in estimation of C_d varies from − 11.06 to 9.27% with an average of − 0.20%. This table also includes the values of discharge coefficient provided by Khode et al. [16] having error variation of − 11.51–6.94% with an average of 0.69%. The quantile plot shown in (Fig. 3) indicates that the data points lie close to line of perfect agreement except one point corresponding to Carty USA dam.

Table 2 Comparison of coefficient of discharge of prototype dam with the coefficient of discharge predicted by empirical equations

Location	α	P	H_T	η	N	L	Q	C_{do}	C_{dpp}	C_{dpk}	Error (%)	
											Present study	Khode
Bartletts ferry, USA	14.5	3.43	2.44	0.644	20.5	1441	5920	0.365	0.405	0.407	− 11.06	− 11.51
Boardman, USA	19.44	3.53	1.80	0.500	2	109.2	387	0.497	0.510	0.491	− 2.61	1.20
Carty, USA	19.40	2.76	1.80	0.642	2	109.2	387	0.497	0.451	0.490	9.27	1.41
Dungo, Angola	15.20	4.30	2.40	0.560	4	115.5	576	0.454	0.447	0.434	1.67	4.45
Hyrum, USA	9.14	3.66	1.82	0.500	2	91.44	262	0.402	0.398	0.374	0.91	6.94
Navet, Trinidad	23.6	3.05	1.68	0.550	10	137	481	0.546	0.520	0.521	4.79	4.58
Ute dam, USA	12.15	9.14	5.8	0.630	14	1024	15,574	0.369	0.385	0.377	− 4.37	− 2.25
Average Percentage Error											− 0.20	0.69

Note A = Sidewall angle, P = Weir height, H_T = Total head, N = Number of cycle, L = Crest length, Q = Total flow, C_{do} = Coefficient of discharge observed, C_{dpp} = Coefficient of discharge of present study, C_{dpk} = Coefficient of discharge of Khode

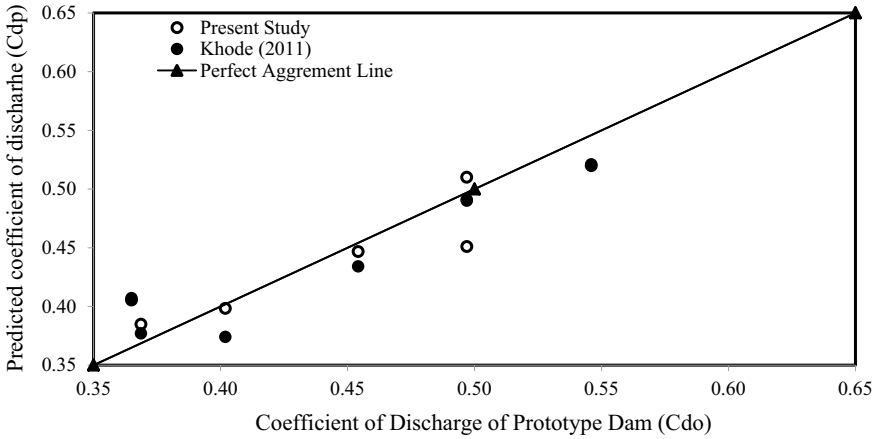

Fig. 3 Comparison of coefficient of discharge of prototype dam with the coefficient of discharge predicted by empirical equations

4 Conclusion

Labyrinth weirs in many cases are favourable design solutions to regulate upstream water elevation and increase flow capacity. Due to the complex design characteristic, the coefficient of discharge of labyrinth weir can be applied for the sidewall angle α in varying from 6° to 35°. A simple discharge coefficient equation in terms of η and α has been obtained using regression analysis in the present study. Discharge coefficients computed using proposed equation give an average error of − 0.20% for prototype dams and comparable with the value reported in literature by Khode et al. [16].

References

1. Tullis JP, Amanian N, Waldron D (1995) Design of labyrinth spillway. J Hydraul Eng 121(3):247–255
2. Hay G, Taylor N (1970) Performance and design of labyrinth weirs. J Hydraulic Eng 96(11):2337–2357
3. Darvas L (1971) Discussion of performance and design of labyrinth weirs. J Hydraulic Eng ASCE, 97, vol 80
4. Houston K (1982) Hydraulic model study of Ute dam labyrinth spillway. Report No. GR-82-7, U.S. Bureau of Reclamation, Denver
5. Crookston BM, Paxson GS, Savage BM (2012) Hydraulic performance of labyrinth weirs for high headwater ratios. In: 4th IAHR international symposium on hydraulic structures, pp 9–11
6. Willmore C (2004) Hydraulic characteristics of labyrinth weirs. M.S. Rep, Utah State University, Logan
7. Ghare AD, Mhaisalkar VA, Porey PD (2008) An Approach to Optimal Design of Trapezoidal Labyrinth Weirs. World Applied Sciences Journal 3(6):934–938

8. Ghodsian M (2009) Stage–discharge relationship for a triangular labyrinth spillway. In: Proceedings of the institution of civil engineers water management, vol 162, no. 3, pp 173–178. https://doi.org/10.1680/wama.2009.00033
9. Kumar S, Ahmad Z, Mansoor T (2011) A new approach to improve the discharging capacity of sharp-crested triangular plan form weirs. Flow Meas Instrum 22:175–180. https://doi.org/10.1016/j.flowmeasinst.2011.01.006
10. Carollo FG, Ferro V, Pampalone V (2012) Experimental investigation of the outflow process over a triangular labyrinth-weir. J Irrig Drain Eng 138(1):73–79. https://doi.org/10.1061/(ASCE)IR.1943-4774.0000366
11. Crookston BM, Tullis BP (2012) Labyrinth weirs Nappe interference and local submergence. J Irrig Drain Eng 138(8):757–765. https://doi.org/10.1061/(ASCE)IR.1943-4774.0000466
12. Khode BV, Tembhurkar AR, Porey PD, Ingle RN (2012) Experimental studies on flow over labyrinth weir. J Irrig Drain Eng 138(6):548–552. https://doi.org/10.1061/(ASCE)IR.1943-4774.0000336
13. Seamons TR (2014) Labyrinth weirs: a look into geometric variation and its effect on efficiency and design method predictions. USU thesis
14. Bilhan O, Emiroglu ME, Miller CJ, Ulas M (2018) The evaluation of the effect of nappe breakers on the discharge capacity of trapezoidal labyrinth weirs by ELM and SVR approaches. Flow Measurement and Instrumentation 64:71–82. https://doi.org/10.1016/j.flowmeasinst.2018.10.009
15. Seamons TR, Seamons TR, DigitalCommons (2014) USU labyrinth weirs: a look into geometric variation and its effect on efficiency and design method predictions
16. Khode BV, Tembhurkar AR, Porey PD, Ingle RN (2011) Determination of crest coefficient for flow over trapezoidal labyrinth weir. World Appl Sci J 12(3):324–329

Design of Dam Spillway Cum Downstream Wave Basin Physical Model for Kalpasar Project—A Case Study

P. A. Kashyape, R. R. Bhate, H. B. Jagadeesh, and Prabhat Chandra

Abstract Government of Gujarat has major proposal of development a multipurpose project, Kalpasar in the Gulf of Khambat. This project consists of constructing a 30 km long dam and concrete spillway of about 2.3 km length with 105 numbers of gates. After completion of this project, it is estimated that about 10,000 mm^3 of fresh water could be made available to the Saurashtra Peninsula; along with this other benefits were perceived related to use of the dam to support a transportation link between Surat and Bhavnagar districts, to fisheries development etc. Since year 1995 various feasibility and other studies had been carried out for the project by various research and academic institutes. Various studies are also under progress at CWPRS for the development of Kalpasar project; one of them is hydraulic physical model study to finalize the design of spillway by simulating discharge over spillway along with the effects of sea waves on the downstream of the dam. This dam spillway cum wave basin is a captive model housed in hanger of size 60 m × 40 m and developed to the scale of 1:55 G.S. (geometrically similar). In this model at one end spillway with about 90numbers of gates and on downstream of spillway at a distance of 31.79 m (about 1750 m in prototype), a unidirectional random sea wave generator having wave flap of length 33 m controlled by SCADA is proposed. On this model, it is proposed to test discharging capacity of spillway with full and partial operation of gates along with performance of energy dissipater for various tidal levels with superimposition of waves, water surface profiles for entire range of discharges, pressures over spillway surface under the influence of waves and tides for entire range of discharges. This paper presents the glimpses of the hydraulic design of dam spillway cum downstream wave basin physical model for Kalpasar.

Keywords Dam · Spillway · Discharging capacity · Wave basin · Wave generator

P. A. Kashyape (✉) · R. R. Bhate · H. B. Jagadeesh · P. Chandra
Central Water and Power Research Station, Pune 411024, India
e-mail: kashyapeparag@gmail.com

P. V. Timbadiya et al. (eds.), *Flood Forecasting and Hydraulic Structures*, Lecture Notes in Civil Engineering 340, https://doi.org/10.1007/978-981-99-1890-4_34

1 Introduction

Gujarat is a water scarce state with having only 2% of water resources of India [10]. As per 2011 census per capita availability of water in Gujarat is 1050 cubic meter annually which is far less than the national average per capita water availability (1567 m^3 per annum) of India. As per estimates total surface water availability in Gujarat is about 38,100 MCM and at present state is having water storage capacity of 20,480 MCM in its total 196 major and medium projects [10]. In order to overcome on the situation of water scarcity in the state, Government of Gujarat has proposed project of closure of Gulf of Khambat by constructing a 30 km long dam across it, which will result in storage of 10,000 MCM of surface water [8]. This project will be a multipurpose one which supports a transportation link between Surat and Bhavnagar districts; it will help to bring 10.54 lakh ha of land in Saurashtra region under irrigation [8] and also to fisheries development etc. This Kalpasar dam is proposed to have a spillway of length 2310 m and having 105 numbers of gates. Since early 1990s, various feasibility and other studies had been carried out for the project by various research and academic institutes. Various studies are also under progress at CWPRS for the development of Kalpasar project; one of them is hydraulic physical model study to finalize the design of spillway by simulating discharge over spillway along with the effects of sea waves on the downstream of the dam. The design of this physical model for Kalpasar project is challenging one since it comprises dam spillway at one end, random sea wave generation system at another to create wave basin on the downstream of spillway and water recirculation system. A designed layout of model is shown in Fig. 1.

2 Design and Discussion

2.1 Physical Model of Kalpasar

As shown in Fig. 1, this model is housed in hangar of size 60 m × 40 m. In this model at one end spillway with about 90 numbers of gates and on downstream of spillway at a distance of 31.79 m in model (about 1.75 km in prototype), a unidirectional random sea wave generator having wave flap of length 33 m and water recirculation system is proposed.

2.2 Selection of Scale

In order to achieve similitude in model and prototype depending upon requirement of problem a suitable model scale is selected. Scale for coastal engineering physical models of waves is varied from 1:100 to 1:150, while that of for spillway and energy

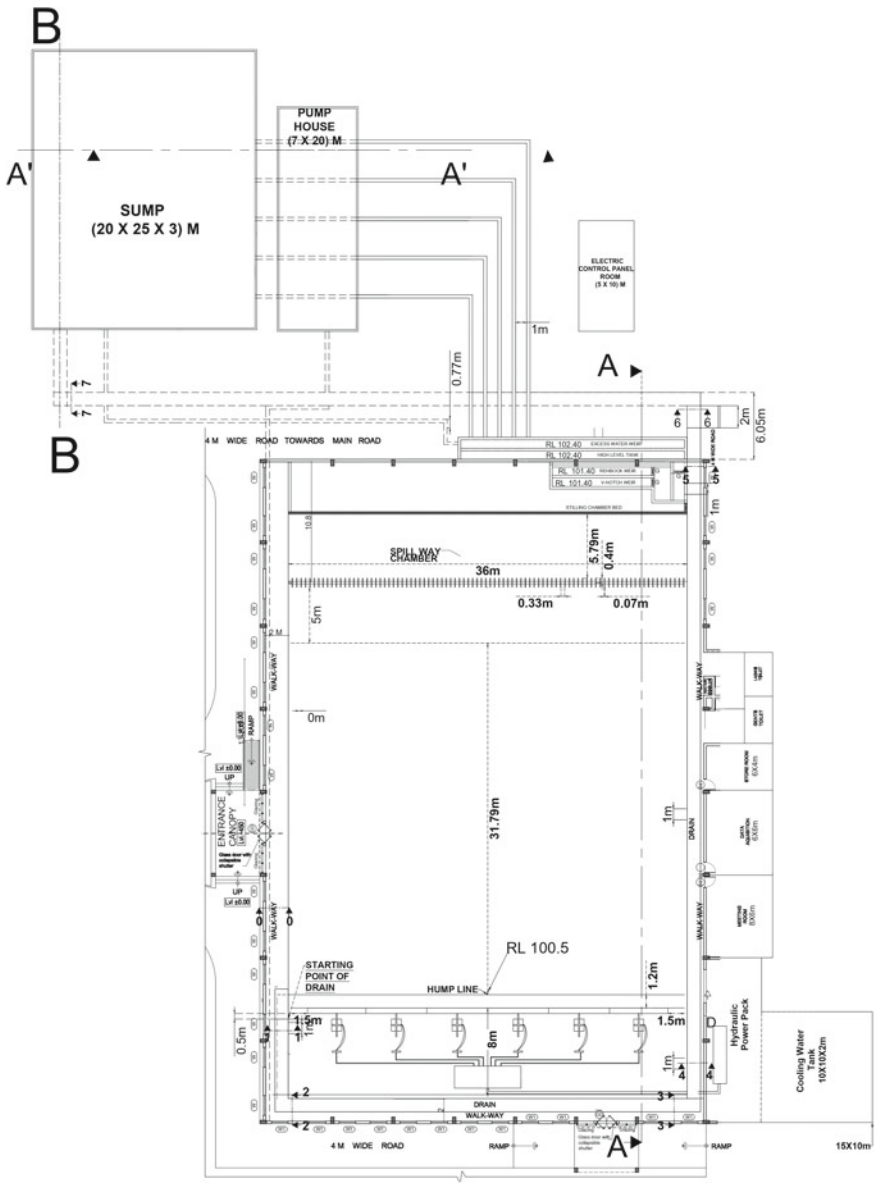

Fig. 1 Layout of Kalpasar model

dissipator is varied in range of 1:25–1:60. In case of spillway and energy dissipator, larger the section in model better will be interpretation of results. However if scale showing larger sections in model is selected for coastal engineering models, then it will lead to increase in the cost of Random Sea Wave Generation (RSWG) system and power requirement. Since, this Kalpasar model is a combination of both sea wave basin and dam spillway the scale for this model is selected as 1:55 geometrically similar.

2.3 Spillway and Energy Dissipator in Model

The proposed spillway is about 2.3 km long consisting of 105 spans of 18 m width each divided with 5 m thick piers. The spillway is designed [7] to pass the flood of the magnitude of 120,000 m^3/s [4]. Energy dissipator provided is in the form of 50 m long stilling basin with invert El of − 10 m. Figure 2 shows the plan and cross section of the proposed design of spillway. The 1:55 scale GS spillway model based on Froudian simulation criterion will be utilized to finalize the proposed design. In the available width of 36 m, about 90 spans of spillway would be reproduced. The spillway and stilling basin will be constructed in masonry and finished in smooth cement plaster painted with enamel paint. Piers, breast walls, and gates will be fabricated in FRP/perspex. The following aspects would be studied on this model:

1. Discharging capacity for the conditions of free overflow and submergence by the tide levels with superimposed waves.
2. Pressures on crest and appurtenant structures for various hydraulic conditions
3. Performance of energy dissipator for different operating conditions and under varying tide levels. The objective would be to optimize the design so as to make it workable for as many conditions as possible.
4. Measures for protection of spillway and appurtenant structures from the attack of waves and storm surge.

2.4 Random Sea Wave Generation in Model

The Gulf of Khambat is tide dominant region with maximum tidal range of about 11 m [5]. However, Sanil Kumar et al. [9] observed that the significant wave height (H_s) in the Gulf of Khambat is about 1.6 m during south-west monsoon and wave direction between 180° and 225°, while Kumar et al. [6] observed the same about 1.8 m. National Institute of Ocean Technology (NIOT), Chennai, in its survey report carried out for Gulf of Khambat Development Project observed that H_s in the region between 0.8 and 5.2 m with wave period between 8 and 12 s; and waves are from South-West and North-East direction [1, 2]. Also at CWPRS, a mathematical model study for wave tranquility at downstream side of spillway for Kalpasar is under

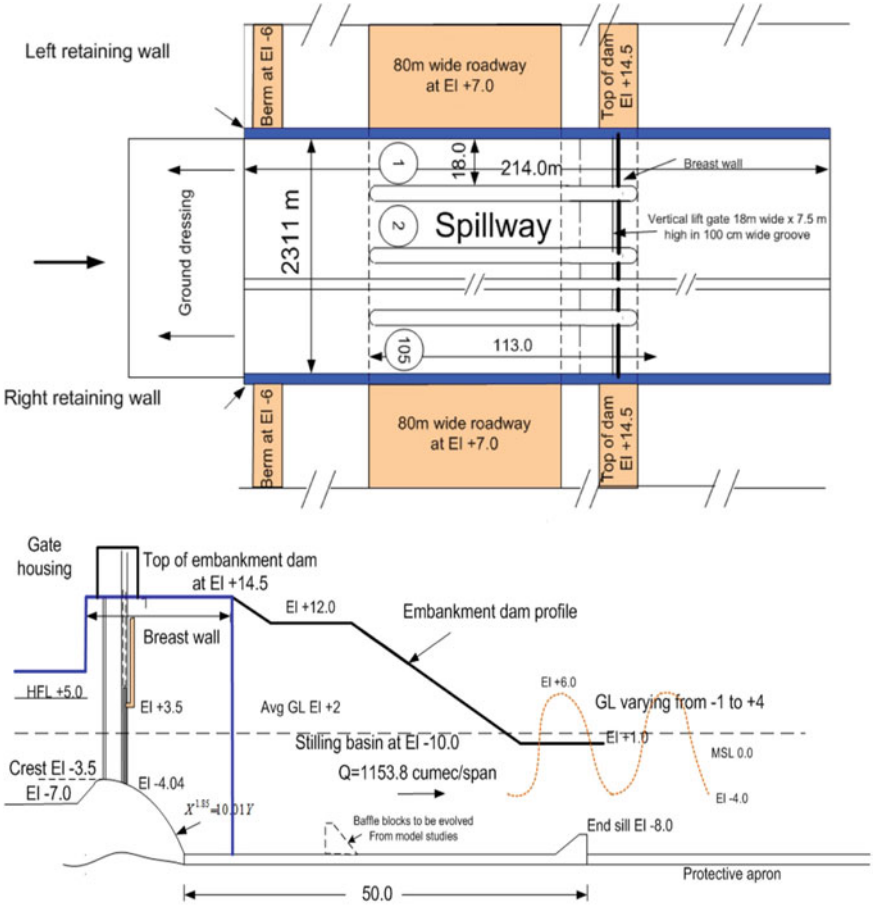

Fig. 2 Plan and cross section of proposed spillway

progress, and preliminary results of this study that shows the H_s in the region are within the range of 3.29–5.31 m. Considering all these in this model RSWG system is designed to generate unidirectional sea waves having significant wave height (H_s) up to 4 m and wave period (T_p) of 10 s, considered as superimposed over various tidal levels. Figure 3 shows the water levels considered for the design of RSWG in model with respect to corresponding levels in prototype.

RSWG system consist of Hydraulic Power Pack (HPP), SCADA controlled electro-hydraulic servo system, six numbers of wave boards each of 5.5 m length connected to separate servo valves (total six servo valves) synchronized to make wave board of 33 m long, data acquisition system. Schematic flowchart of this system is shown in Fig. 4. Waves will be generated by moving a piston operated wave boards by an electro-hydraulic servo system through servo actuators which is controlled by a signal generating unit [3].

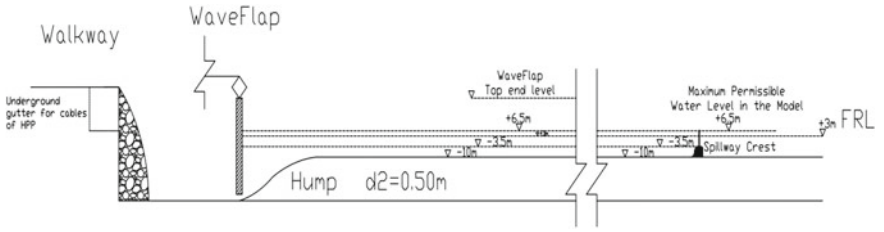

Fig. 3 Water levels considered for design of RSWG system

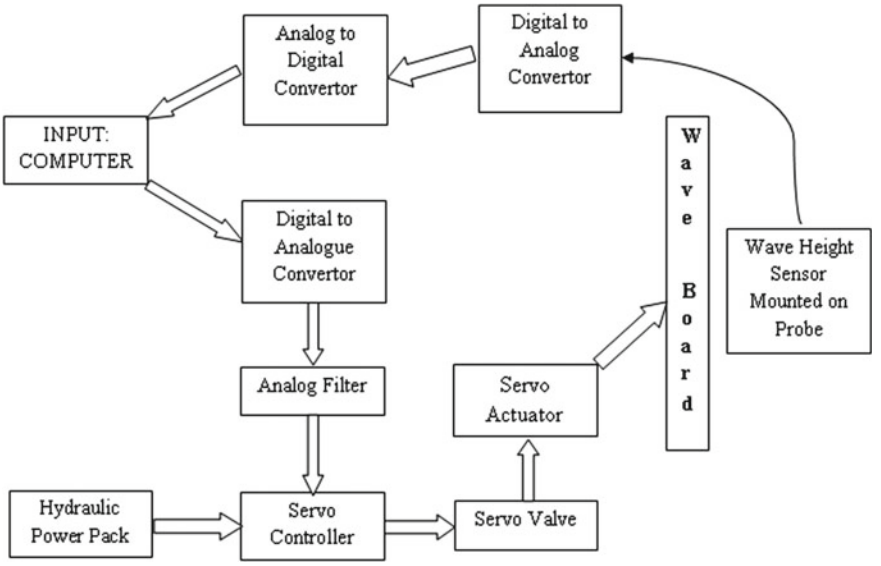

Fig. 4 Flowchart of sea wave generation system at CWPRS

2.5 Water Recirculation System

Water recirculation system of model consisting of a sump of capacity 1500 m^3 (25 $\times$ 20 $\times$ 3 m), high head water tank of size 20 $\times$ 2 $\times$ 1 m, overflow weir, Rehbock weir, V-notch weir, stilling basin chamber, wave basin, and returning channel. Water from sump will be pumped in to high head tank at a rate of 20 cusec then it enters in to Rehbock and V-notch weir after that it enters in to the stilling basin chamber then it enters in to the upstream reservoir of dam and flows over the spillway and enters in to stilling basin portion. On the downstream of spillway, a wave basin will be created in order to generate the wave of different wave heights (H_s up to 4 m with T_p of 10 s) for different conditions. Excess water from wave basin is allowed to enter in to retuning channel of rectangular cross section of size 1.2 $\times$ 0.6 m with slope of

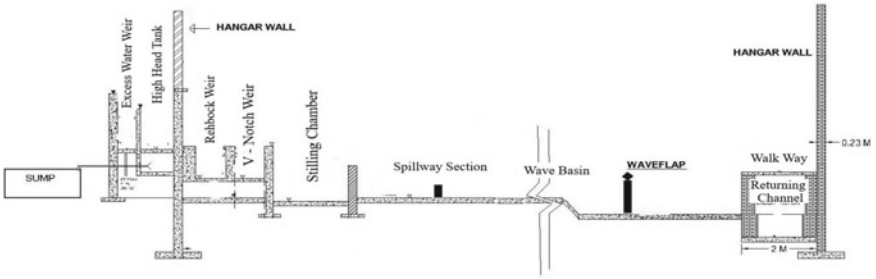

Fig. 5 Cross section showing water circulation system in model

1:400 and length 180 m. At end water again enters in to sump. A cross section of this system is shown in Fig. 5.

3 Conclusions

This model is unique one which consists of both spillway and random sea wave basin. Studies on this model will be helpful in

- Design of spillway of Kalpasar dam.
- Assessing the discharging capacity of spillway.
- Operation of spillway gates and performance of energy dissipator.
- The impact of downstream wave conditions on the spillway discharging capacity can be studied on this model, as well as downstream flow conditions due to interaction of sea waves and discharge over spillway.

Acknowledgements The authors are thankful to Shri. A. K. Agrawal, Director, CWPRS, for the encouragement and granting permission to publish the paper. Authors are also thankful to the Kalpasar Project Department, Government of Gujarat, for sponsoring the model studies.

References

1. Annexure C (Wave) of hydrodynamic & sediment model studies and related measurement for Gulf of Khambhat Development. Report by National Institute of Ocean Technology, Chennai, Sept 2017
2. Bathymetric survey in Gulf of Khambhat—Northern portion. Report by National Institute of Ocean Technology, Chennai, Aug 2017
3. Chary PV, Erande RS, Ranade SD, Kudale MD (2017) Design of hydraulic power pack system for servo-hydraulic random sea wave generators for design of port layouts. IJRMET 7(1):80–88
4. Estimation of PMF, design flood & spillway capacities for Gulf of Khambat Development Project (2017). Indian Institute of Technology Roorkee, Roorkee, India

5. Satheesh Kumar J, Balaji R (2017) Estimation of tidal current energy along the Gulf of Khambhat using three-dimensional numerical modeling. International Journal of Ocean & Climate Systems 8(I):10–18
6. Kumar VS, Anand NM (2004) Variations in wave directions estimated using first and second order Fourier coefficients. Ocean Eng 31:2105–2119
7. River Hydraulics, Springer Science & Business Media LLC (2022)
8. Specific Studies Report (1999) Kalpasar—Gulf of Khambat Development Project, vol 1
9. Sanil Kumar V, Ashok Kumar K (2010) Waves & currents in tide dominated location off Dahej, Gulf of Khambat, India. Mar Geod 33(2):218–231
10. WRD Data Bank of Gujarat. https://guj-nwrws.gujarat.gov.in/showpage.aspx?contentid=1463&lang=english. Accessed 4 Sept 2021

Hydraulic Design of Pipeline of Right Bank Canal of Lendi Inter-State Irrigation Project, Maharashtra

Vankayalapati S. Ramarao and Yogendra Nath Srivastava

Abstract The hydraulic design of the pipeline is generally evaluated for its hydraulic functioning, which involves the assessment of passing the design discharge through it. It depends upon the adequacy of gross head and pipe diameter; precautions need to be taken to avoid water hammer in the pipeline, avoidance of negative pressure, avoidance of air-entrainment. The application of the energy equation shows that parameters such as discharge, pipe diameter, head loss, gross driving head, surface roughness of pipe are interdependent. Design period of the project and aging of the pipeline affect surface roughness and friction losses in the pipeline. The verification of the adequacy of diameter (for pipe with given flow rates, length of pipeline and available gross driving head) involves determination of friction factor with necessary allowance for ageing and calculation of head loss due to friction and form losses. Friction loss refers to fraction of pressure lost by flowing fluids through a pipeline. Form loss is due to the obstructions present in the line of flow, it may be due to change in alignment, may be due to a bend or a control valve or anything which changes the course of motion of the flowing fluid. Desk studies were conducted in CWPRS, Pune to assess hydraulic suitability of MS Pipeline of right bank main canal (Telangana canal), which is intended to divert 6.527 m^3/s irrigation water to Telangana. From desk studies, it was found that, considering the roughness coefficient of epoxy enameled steel pipe line as 0.89 mm, the proposed diameter of pipe of 2 m and parallel pipes of 1.6 m each were found to be adequate to carry the design discharge with the available gross head of 16.25 m and the Project is under construction.

Keywords Lendi irrigation project · Pipeline · Hydraulic design · Water hammer · Air entrainment · Intake · Off take · Left bank main canal · Right bank canal

V. S. Ramarao (✉) · Y. N. Srivastava
Central Water and Power Research Station, Khadakwasla, Pune, Maharashtra 411024, India
e-mail: sramaraov@gmail.com

P. V. Timbadiya et al. (eds.), *Flood Forecasting and Hydraulic Structures*, Lecture Notes in Civil Engineering 340, https://doi.org/10.1007/978-981-99-1890-4_35

1 Introduction

Lendi is an inter-state project between the states of Telangana (then Andhra Pradesh) and Maharashtra. The project was designed 35 years ago in 1986 on River Lendi, a tributary of River Manjeera and proposed to construct a project at Gonegaon village of Mudkhed Taluka, in Nanded district of Maharashtra, with the capacity of 6.36 TMC of water. In this, Maharashtra utilises 3.93 of TMC to irrigate 27,000 acres. The Telangana State utilises 2.43 TMC water for irrigating 22,000 acres in Madnoor and Bichkunda mandals. Apart from irrigation, Lendi project provides drinking water to various villages in Nanded and Nizamabad districts (Fig. 1).

The left bank main canal up to Ch. 18.98 km. is common to Maharashtra and Telangana and is designed for 13.534 m^3/s discharge. The length of the left bank canal beyond the Ch. 18.98 km is 28.46 km and is in Maharashtra. At Ch. 18.98 km, off take point of the right bank main canal, pipeline canal (Telangana Canal) is provided. Through the right bank main canal, discharge of 6.527 m^3/s is proposed to be diverted for Telangana. But a segment of the right bank canal from the off take point to the Ch. 7.5 km lies in Maharashtra. The right bank canal (Telangana Canal) between the Ch. 7.5 km until end Ch. 34.57 km transit through Telangana. The component of the right bank canal laid in Maharashtra from the off-take point (Ch. 0.0 km.) to the Ch. 7.5 km is provided with MS pipeline. The ground profile for the canal upto 7.5 km i.e. up to Telangana border is very undulating and hilly in

Fig. 1 Index map of Lendi inter-state irrigation project, Maharashtra (http://www.irrigation.telangana.gov.in/img/projectspdf/lendi) [2]

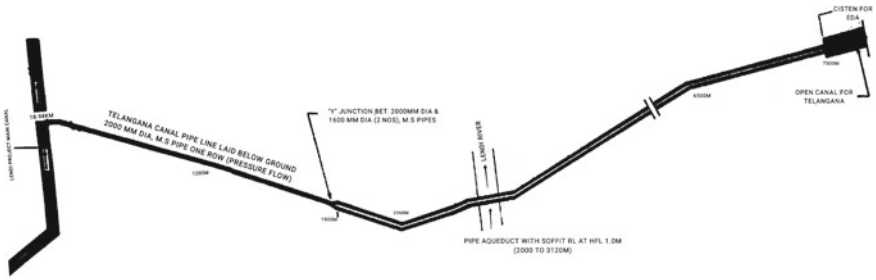

Fig. 2 Plan of Telangana canal of Lendi inter-state irrigation project, Maharashtra

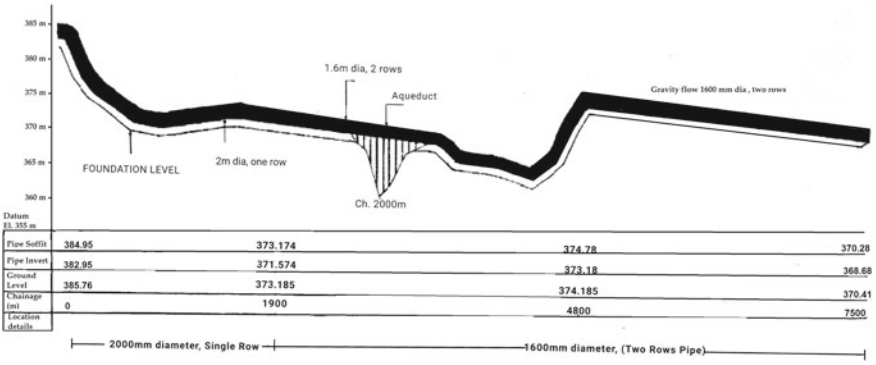

Fig. 3 Longitudinal section of Telangana canal of Lendi Inter-state irrigation project, Maharashtra

nature, open canal incurs distribution losses and earth work is costly, so to economize the construction cost and optimize the irrigation potential of the Project, MS pipe canal work was conceived. The dia of pipeline is 2 m for first 1.9 km and 2 Nos of 1.6 m from 1.9 to 4.8 and upto 7.5 km, considering that the 2 m dia pipe may not provide required discharge within available driving head. Figures 2 and 3 show plan and longitudinal section of Telangana canal of the Project. Since the ground is undulating, there are bends provided and thrust blocks are provided at bends to cope up with unbalanced forces.

2 Analysis of Design

The right bank canal (Telangana Canal) at Ch. 0.0 m (i.e. off-take point) to Ch. 7.5 km. is provided with MS pipeline. The design of the pipeline was evaluated for hydraulic functioning, which involves the verification of adequate gross head and pipe diameter, maintenance of positive pressure in the pipeline, avoidance of negative

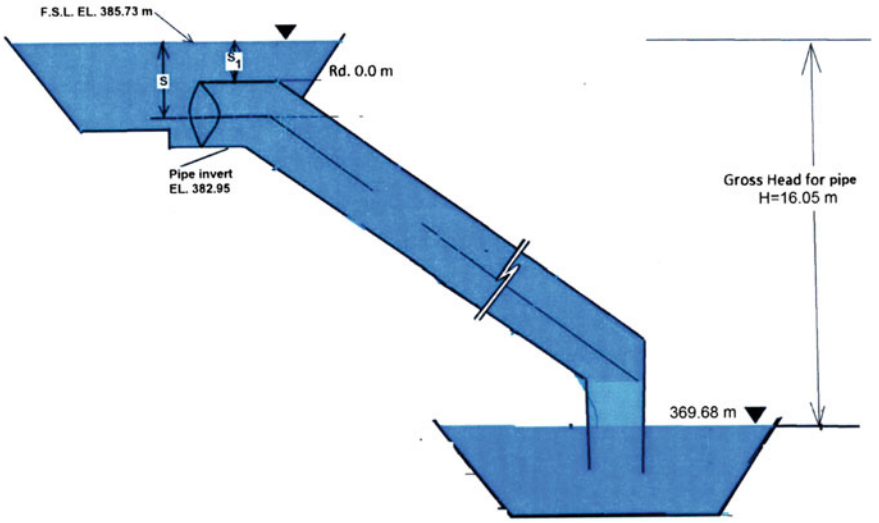

Fig. 4 Schematic definition of gross head available between Ch. 0.0 m and Ch. 7.5 km

pressure, avoidance of air-entrainment through intake structure and precautions to avoid water hammer in the pipe line.

2.1 Gross Available Head for MS Pipeline

The gross available head for the Telangana Canal for the maximum discharge of 6.527 m^3/s is driving head in a gravity system for a pipe discharging freely and is the elevation difference between the water level at entry point of pipe (El. 385.73 m at Ch. 0.0 km) and elevation of centre line of pipe at the exit of pipe (El. 369.48 m at Ch. 7.5 km), which is 16.25 m. If pipe is not discharging freely (i.e. exit of pipe is submerged in water pool), the gross driving head would be equal to water level elevation difference between the Full Supply Level (FSL) at RL 385.73 m and exit of pipe at Ch. 7.5 km. Figures 4 shows Schematic definition of gross head available between Ch. 0.0 m and Ch. 7.5 km.

2.2 Adequacy of Pipe Diameter

The application of the energy equation shows that parameters such as discharge, pipe diameter, head loss, Gross driving head, surface roughness of pipe are interdependent. Design period of the project and aging of pipeline affect surface roughness and friction losses in pipeline [1].

The verification of adequacy of diameter (for pipe with given flow rates, length of pipeline and available gross driving head) involves determination of friction factor (for Darcy-Weisbach formula) with necessary allowance for ageing and calculation of head loss due to friction and form losses. Friction loss refers to fraction of pressure lost by flowing fluids through a pipeline. Form loss is due to the obstructions present in the line of flow, it may be due to change in alignment, may be due to a bend or a control valve or anything which changes the course of motion of the flowing fluid.

1. If the calculated head loss is equal to the available head loss i.e. gross available/ driving head of 16.25 m, the diameter provided is exact.
2. If the calculated head loss is less than the available head loss i.e. gross driving head of 16.25 m, the actual discharge will be higher than the required discharge. The difference in calculated head loss and gross driving head can be made up by providing a control valve in order to provide required discharge. The valve will provide the necessary pressure drop. In this situation, another alternative is to reduce the diameter of pipeline.
3. If the calculated head loss is more than the available head loss i.e. grosses driving head (16.25 m), the attainable discharge may reduce. The actual discharge will be less than the required discharge. To increase the actual discharge, either the diameter of pipe selected to deliver required discharge (without throttle) is enhanced or gross driving head is increased. The enhanced diameter will reduce the calculated head loss.

Since determination of adequacy of pipe diameter is related to head loss computations, in the subsequent sections, head loss would be computed.

2.2.1 Head Loss Due to Friction by Darcy–Weisbach Equation

Due to limitations of the Hazen–Williams equation, Darcy–Weisbach equation has been considered for head loss computation.

The Hazen–Williams formula is an empirical formula and is applicable for fully developed flow. The application of the formula is accurate only if the operation of the pipe is located within the transition or smooth turbulent-flow regimes. The exponent of Hazen William's equation is dependent on the pipe diameter and energy grade line slope. The original Hazen-Williams formula is obtained for hydraulic radius (R) = 0.3 m and slope of energy line (S) = 1/1000 where $S = h_f/L$; h_f = frictional head loss and L = length of pipeline. But designers have used this formula over a wide range of diameters and friction slope. This may result in error as high as ± 30% in the evaluation of velocity. To overcome this problem, Modified Hazen-Williams (MHW) formula has been proposed by Jain (1978) (Refer Bhave and Gupta [1]). MHW formula is given by $V = 143.5 C_R R^{0.6575} S^{0.5525}$, where C_R = Coefficient of roughness, R = hydraulic radius and S = Slope of Energy line. The practice of using the same value of C_R for different diameters and discharges is not proper. Liou [8], Fabian and Marcelo [3], Swamee and Sharma [11] have mentioned in detail about the limitations of the Hazen–Williams formula.

The head loss (h_f) due to friction for flow of water in the pipeline was estimated using Darcy–Weisbach formula because it is a dimensionally homogeneous formula and it has a complete range of application whether operation of the pipe is located in the transition, smooth or turbulent-flow regimes.

$$h_f = f\frac{L}{D}\frac{V^2}{2g} = \frac{8fLQ^2}{\pi^2 g D^5}$$

where h_f = head loss or average shear stress or friction loss, f = Darcy friction factor, D = diameter of pipe, L = length, V = velocity and Q = discharge, $g = 9.81$ m/s^2. The explicit equation for friction factor (f) by Swamee and Jain [10] has been used.

Darcy friction factor (f) proposed by Jain (1976) (Refer Bhave and Gupta [1]),

$$\frac{1}{\sqrt{f}} = 1.14 - 2\log\left(\frac{K_s}{D} + \frac{21.25}{Re^{0.9}}\right)$$

This equation is almost equivalent to following equation

$$f = \frac{0.25}{\left[\log\left(\frac{K_s}{3.7D} + \frac{5.72}{Re^{0.9}}\right)\right]^2}$$

Darcy friction factor proposed by Swamee and Jain [10],

$$f = \frac{0.25}{\left[\log\left(\frac{K_s}{3.7D} + \frac{5.74}{Re^{0.9}}\right)\right]^2}$$

where K_s = surface roughness and Re = Reynolds number.

2.2.2 Surface Roughness for Commercial Pipes

The surface roughness parameter for steel/epoxy enameled steel affects frictional losses as well as total losses. The surface roughness of commercial pipes varies greatly in average roughness height, form and roughness pattern. It is impossible to describe surface roughness completely by a single dimension. The artificially roughened pipes by uniform sand grains have been used in hydraulic experiments. To overcome this problem, the concept of equivalent surface roughness of any commercial pipe has been introduced in the literature which would yield the same value of friction factor in the same diameter pipe as for the flow under similar conditions in an artificial roughened pipe. In the ensuing sections, for simplicity, the equivalent surface roughness of commercial steel pipes is termed as surface roughness.

The literature review suggests the wide range of value of surface roughness (K_s) for new commercial pipes varying from 0.005 to 0.6 mm. The surface roughness varies with time due to buildup of solid deposits, organic growth, ageing and manufacturing

tolerances and to avoid reduction of full design discharge, higher surface roughness up to 0.89 mm [1] and even further higher values for a service of 30–60 years of the pipeline has been mentioned in the literature. For example, for encrusted surfaces, surface roughness is 2 mm [6, 7].

In a prototype experimental study on 2.4 m diameter water supply pipeline with discharge of 3.5 m^3/s at BMC (Bombay Municipal Corporation) Network in Bhandup, Greater Mumbai has indicated tuberculation between 10 and 25 mm inside the pipeline. Thus surface roughness can go up to 25 mm [4].

2.2.3 Form Losses

These are minor losses which occurred due to change of form of the pipeline. These losses are caused due to change of section, valves, bends, joints, etc. For the Lendi pipeline, the form losses due to bends, entry and exit of the pipeline are assessed. Table 1 gives the details of form loss coefficients.

Table 1 Form loss coefficients due to bends/entry/exit

Form loss coefficients due to bends			
Number of bends	Loss coefficient	Total loss coefficient	Remarks
9	0.09	0.81	Between Ch 0.0 m–1900 m, there are 9 horizontal bends For $r/D = 3$(assumed), angle of bend = 35 degrees (max), loss coefficient is 0.09 [9], r is radius of bend at centerline
9	0.09	0.81	For $r/D = 3$, angle of bend = 35°, loss coefficient is 0.09 [9]
Head loss coefficients due to entry			
1	0.5	0.50	
Head loss coefficients due to exit			
1	1	1.00	
Head loss coefficient due to Y-junction			
1	1	1.5	
Total form loss Coefficients up to 1.9 km = 2.285 (0.975 + 0.5 + 0.81 = 2.285) and from 1.9 km to 7.5 km (1.5 + 0.81 + 1 = 3.31)			For portion up to 1.9 km; only 9 bends are considered for calculating head loss in addition trashrack losses and entry loss

Trash rack loss coefficient for 50% chocking condition, $K_t = 1.45 - 0.45$. $R - R^2 = 0.975$. R = Ratio of net area through trash rack bars to gross area of the racks and supports, Trash rack Loss = $K_t = V^2/2\,g$ (It is assumed that trashrack would be placed near Ch. 0.0 km.)

The surface roughness parameter for epoxy enameled steel pipe varying from 0.005 to 0.89 mm was considered for the desk studies. Since the surface roughness varies with time, higher surface roughness up to 0.89 mm and even further higher values of 2 mm for a service of 30–60 years of the pipeline is usually taken.

2.2.4 Total Head Loss and Suitability of Pipeline [2]

The total head loss is summation of both friction losses and form losses. For the Lendi pipeline, friction losses and form losses are calculated for the assessment of suitability of the pipeline to carry the design discharge through the pipeline. Tables 2, 3 and 4 give the details of total head losses, hydraulic gradient line (HGL) and pressure at the soffit of the pipeline for various chainages for the given length of 7500 m, diameter of 2 and 1.6 m (parallel pipes), discharge of 6.527 m^3/s. To calculate the HGL, the head loss through only one branch is needed to be taken into consideration. As a result, the pipe from Ch. 4.8 to 7.5 km becomes pressurized.

From Table 5, it may be observed that the total head loss for the pipe surface roughness of 0.89 mm, between Ch. 0.0 and 1.9 km is 3.94 m and between Ch. 1.9 and 7.5 km (for single branch of pipelines) is 8.593 m; thus adding together to 12.53 m. This total calculated head loss is lesser than the gross available head of 16.25 m. The maximum total head loss for the pipe surface roughness of 2 mm between Ch. 0.0 km. to 1.9 km is 4.626 m and between Ch. 1.9 and 7.5 km (for single branch of pipelines) is 10.257 m; thus adding up to 14.883 m. Therefore the existing pipe diameters are said to be adequate to deliver the design discharge. Table 5 shows actual discharge passing through the pipeline for given surface roughness of pipeline at the gross driving head of 16.25 m.

3 Provision of Air and Other Valves Recommended [5]

Air valves are normally required in the pressure pipe zone and are provided to release the entrapped air from the system. The diameter of the riser pipe should be a minimum of 10% of the diameter of the buried pipe and should extend a minimum of 60 cm above HGL. Air valves are recommended at all points where there is change in the direction of flow. They are provided at every 150 m on the straight length of pipeline, for field irrigation pipes. Vacuum Relief valves shall be provided at all summits in the pipeline. Drain valves are to be provided at the lowest soffit points of pipelines. If the velocity in the pipes is below 0.6 m/s, scour valves need to be provided as per the site conditions at deep river locations. Provision of control valve was also recommended to control the flow rate, since the discharge passing through the pipeline is higher than the design discharge as shown in Table 5.

Table 2 Total headloss, HGL and Pressure at Soffit of pipe between Ch. 0.0 m and Ch. 1.9 km

Discharge, Q (m^3/s)	Diameter of pipe, D (m)	Area of pipe, A (m^2)	Velocity, V (m/s)	Surface rough-ness, K_s (mm)	Friction factor, f	Head loss, h_f (m)	Total loss (m)	Pipe soffit level @ 0 m	Pipe soffit level @ 1900 m	Total energy line (TEL) @ 1900 m	Hydraulic gradient line (HGL) @ 0.0 m	HGL @ 1900 m	Pressure @ soffit @ 1900 m
6.527	2	3.143	2.077	0.89	0.016	3.437	3.94	384.95	373.174	381.680	385.620	381.461	8.287
6.527	2	3.143	2.077	2.00	0.019	4.124	4.626	384.95	373.174	380.994	385.620	380.774	7.600

Table 3 Total headloss, HGL and Pressure at Soffit of pipe between Ch. 1.9 and 4.8 km

Discharge, Q (m^3/s)	Diameter of pipe, D (m)	Area of pipe, A (m^2)	Velocity, V (m/s)	Surface rough-ness, K_s (mm)	Friction factor, f	Head loss, h_f (m)	Total loss	Pipe soffit level @ 1900 m	Pipe soffit level @ 4800 m	TEL @ 4800 m	HGL @ 1900 m	HGL @ 4800 m	Pressure @ soffit @ 4800 m
3.264	1.6	2.011	1.62	0.89	0.017	4.22	4.664	373.174	374.78	377.016	381.461	376.882	2.102
3.264	1.6	2.011	1.62	2.00	0.021	5.082	5.526	373.174	374.78	375.468	380.774	375.334	0.554

Table 4 Total headloss, HGL and Pressure at Soffit of pipe between Ch. 1.9 and 7.5 km

Discharge, Q (m^3/s)	Diameter of pipe, D (m)	Area of pipe, A (m^2)	Velocity. V (m/s)	Surface roughness, K_s (mm)	Friction factor, f	Head loss, h_f (m)	Total loss	pipe soffit level @ 1900 m	pipe soffit level @ 7500 m	TEL @ 7500 m	HGL @ 1900 m	HGL @ 7500 m	Pressure @ soffit 7500 m
3.264	1.6	2.011	1.62	0.89	0.017	8.149	8.593	373.174	370.28	373.087	381.461	372.953	2.673
3.264	1.6	2.011	1.62	2.00	0.021	9.813	10.257	373.174	370.28	370.737	380.774	370.603	0.323

Table 5 Actual discharge passing through the pipeline for given surface roughness of pipeline at the gross driving head of 16.25 m

S. No	Gross driving head	Surface rough-ness, K_s (mm)	Actual discharge passing, Q (m^3/s)
1	16.25	0.005	13.25
2	16.25	0.02	12.62
3	16.25	0.89	7.88
4	16.25	2	7.39

4 Conclusions

By considering the roughness coefficient of epoxy enameled steel pipe line as 0.89 mm, the proposed diameter of pipe of 2 m and parallel pipes of 1.6 m are considered to be adequate to carry the maximum design discharge 6.527 m^3/s with the available gross head loss of 14.20 m. When the surface roughness increases to 2 mm, designed discharge reduces marginally. Gravity flow takes place in the pipe Ch. between 4.8 and 7.5 km. When surface roughness is less than 0.89 mm, the calculated head losses are lower than the available head loss and thus a higher discharge will take place through the pipe canal. To overcome the higher discharge, the difference in the pressure drop can be made up by providing a control valve. Provision of air valves, vacuum relief valves, drain valves and scour valves are necessary for smooth hydraulic functioning of the pipeline. The project is under execution based on the recommendations of desk studies carried out in CWPRS.

Acknowledgements The authors are very much grateful to Dr. R. S. Kankara, the Director, CWPRS, Pune for his continued encouragement and support in writing technical papers. Authors are also grateful to project authorities of Lendi Irrigation Project for their support in providing required data during desk studies. Support of staff of SED Division is also acknowledged.

References

1. Bhave PR, Gupta R (2006) Analysis of water distribution networks. Narosa Publishing House Pvt. Ltd., New Delhi
2. CWPRS Technical Report No. 4989 (2012) Desk studies for mild steel pipeline for right bank canal (A.P. Canal), Lendi Major Irrigation Project, Nanded District, Maharashtra. http://www.irrigation.telangana.gov.in/img/projectspdf/lendi
3. Fabian AB, Marcelo HG (2003) Hydraulic design of large-diameter pipes. J Hydraul Eng 129(11):839–846
4. Furness RA (2006) Experimental and theoretical Studies in large diameter water supply lines. Web Portal Flow Meter Directory
5. Guidelines for planning and design of piped irrigation network, Part-1 (2017) Central water commission. Ministry of Water Resources, River Development & Ganga Rejuvenation, Government of India, July 2017

6. IS: 2951 (Part I) (1965) Recommendations for estimation of flow of liquids in closed conduits (head loss in straight pipes due to frictional resistance)
7. IS: 2951 (Part II) (1965) Recommendations for estimation of flow of liquids in closed conduits (head loss in valves and fittings)
8. Liou CP (1998) Limitations and proper use of the Hazen-Williams equation. J Hydraul Eng 124(9):951–954
9. Miller DS (1994) Discharge characteristics. IAHR hydraulic structures design manual 8, Balkema, Rotterdam
10. Swamee PK, Jain AK (1976) Explicit equations for pipe flow problems. J Hydraul Eng 102(5):657–664
11. Swamee PK, Sharma AK (2008) Design of water supply pipe networks. Wiley, New York

Study of Chute Blocks in Stilling Basins with Low Froude Number

S. H. Kulkarni and Y. N. Srivastava

Abstract Stilling basin with a low Froude number in the range of 2.5–4.5 is associated with appurtenances like chute block, end sill, etc. These auxiliary devices are provided as additional measures for improving the efficiency of the hydraulic jump in the basin. Experiments were conducted on the 2D sectional model of the Polavaram Irrigation Project at CWPRS, Pune, for testing the performance of spillway and energy dissipator. The effect of adding a chute block was compared with the performance of spillways without chute blocks. The objective of the study was to compare energy dissipation in the stilling basin of Polavaram Irrigation project, AP, for spillways provided with chute blocks and spillways without chute blocks.

Keywords Stilling basin · Low Froude number · Hydraulic jump · Chute block · Energy dissipation

1 Introduction

1.1 Polavaram Project

The Polavaram Irrigation Project is located on the Godavari River in West Godavari District, Andhra Pradesh. The project comprises two Earth dams and one Earth cum Rockfill (ECRF) dam on River Godavari. The spillway with an Ogee crest at El. 25.72 m is located on the right bank saddle provided with 48 numbers of radial gates of size 16 m × 20 m. The spillway structure is connected by an Approach channel from the reservoir, and then spillway discharge is conveyed through a Spill channel and a Pilot channel to the river downstream. The Full Reservoir Level (FRL) is at El. 45.72 m. The probable maximum flood (PMF) is 141,583 m^3/s, and the project design flood is 101,943 m^3/s. Due to close proximity of Sir Arthur Cotton (SAC)

S. H. Kulkarni (✉) · Y. N. Srivastava
CWPRS, Pune 411024, India
e-mail: kulkarni_sumedha@rediffmail.com

P. V. Timbadiya et al. (eds.), *Flood Forecasting and Hydraulic Structures*, Lecture Notes in Civil Engineering 340, https://doi.org/10.1007/978-981-99-1890-4_36

Fig. 1 General layout plan

Barrage at Dowlaiswaram, the maximum tailwater levels are substantially higher than the crest of spillway. The general layout plan is shown in Fig. 1.

1.2 Hydraulic Jump Type of Stilling Basin

The project is provided with the most common type of energy dissipator hydraulic jump type of stilling basin which converts the supercritical flow from the spillway into subcritical flow régime. Stilling basin is provided to form an efficient hydraulic jump, dissipation of excess energy, and protection of the surrounding area from erosion or undermining. The hydraulic jump generates significant eddies and reverses flow rollers to facilitate energy dissipation.

1.3 Low Froude Number Stilling Basin

The high unit discharges with low head in the spillways of the Polavaram project result in a low Froude number in the range of 2.5–4.5. In low Froude number, the efficiency of hydraulic jump in dissipating energy is less because the high-velocity jets with oscillating jumps enter the stilling basin, and dampening of such waves is difficult. Each oscillation generates a wave, which is difficult to dampen [1]. The approaching jet oscillates intermittently from bottom to surface. Energy dissipation for the entire range of discharges for the low Froude stilling basin is rather difficult. The chute blocks are one of the energy dissipating appurtenances provided on inclined

sections of spillways at the entrance to the stilling basin prior to the hydraulic jump to a shorter length of hydraulic jump. A chute block reduces the tendency of the jump to sweep off the apron at tailwater elevations below conjugate depths and improve the performance of basin. Large chute blocks direct a jet into the base of roller in order to strengthen and intensify the roller, thereby stabilizing the jump [2].

1.4 Chute Blocks and Dentated End Sill in the Stilling Basin-Original Design

In the original design, chute blocks of height 11.5 m and top width 5.75 m on the sloping glacis of each spillway were provided to serrate and lift up flow at the entrance of stilling basin and help stabilize the flow. Initially, it was expected that the deficiency in the tailwater due to raised basin level would be compensated with the inclusion of chute blocks. The floodwater is discharged from the spillway into a 110 m long and 1043.40 m wide stilling basin. The floor level of stilling basin is at El. 9.25 m and the crest level of the dentated end sill at El. 14.0 m. The height of the dentated end sill with respect to the floor of stilling basin is 4.75 m. The height (with respect to stilling basin floor), width, and height of dents in the dentated end sill are 1.75 m, 3.5 m, and 3.0 m, respectively [3]. The longitudinal section of the spillway and stilling basin along with details of chute block and end sill in the original design is shown in Fig. 2.

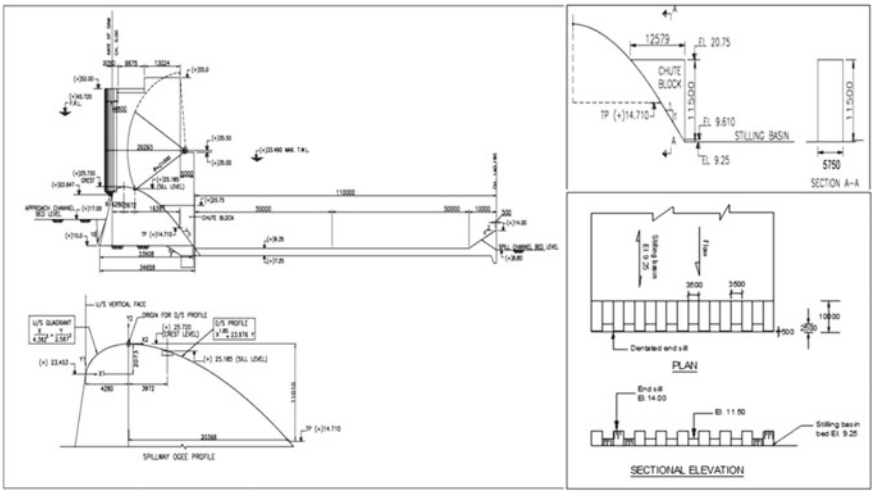

Fig. 2 Longitudinal section of the spillway (original design)

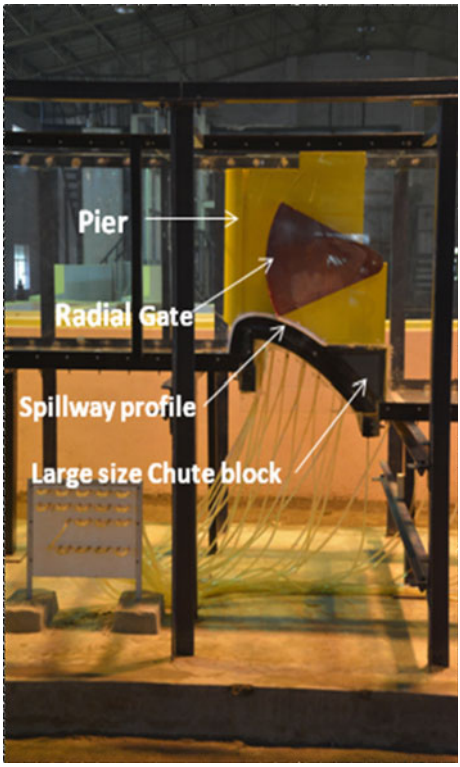

Photo 1 Side view of the model

2 Hydraulic Model and Studies

A 1:50 scale two-dimensional (2D) sectional model based on Froudian criteria, incorporating a part of the Approach channel, one full span and two half spans of spillways, piers, and gates, and stilling basin was constructed in a glass flume. Discharge was measured on a thin crested Rehbock weir. Photos 1 and 2 show the view of the spillway with chute blocks proposed in the original design [3]. Comparative performance of chute blocks for inclusion and without inclusion in the spillways was studied to determine the performance of basin and energy dissipation.

3 Original Design—Spillway with Large Chute Blocks

In the original design, the size of chute blocks was provided as per BIS code 4997–1968. The performance of stilling basin and chute blocks was observed for the entire range of discharges up to the maximum discharge of 141,583 m^3/s. The corresponding tailwater levels downstream of the dam axis were maintained. The hydraulic jump

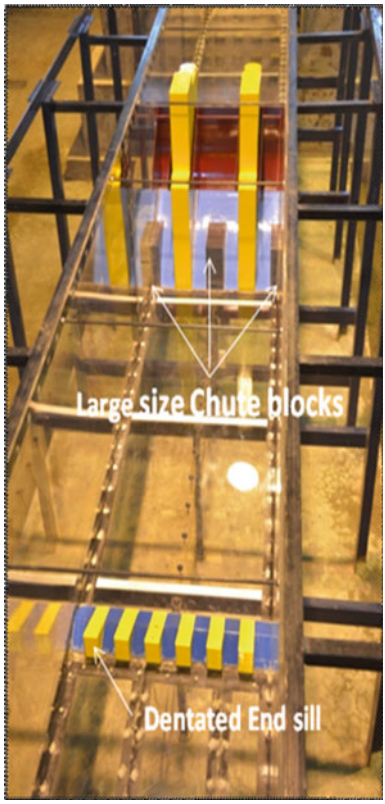

Photo 2 Model view from downstream

was highly sensitive to the slight change in tailwater level. The provided size of chute blocks was found to be excessively large and encroaching the spillway crest profile as the fall from spillway crest to the stilling basin floor level was only 16.47 m. Only a height of 5.47 m remained as a clear spillway profile. Thus, the chute blocks were totally disturbing the flow from the spillway.

Photo 3 shows the flow conditions in the stilling basin. Table 1 enumerates the performance of stilling basin for the discharges of 100, 75, 50, and 25% of maximum discharge.

3.1 Modified Design I—Spillway with Smaller Chute Blocks

See Fig. 3.

The performance was studied again on the 2D sectional model. Observations are given in Table 2.

In this modified design with small size chute block, flow condition is observed from Photo 4.

Photo 3 Flow condition on chute block and in stilling basin for design maximum discharge with gates fully open in original design

3.2 Modified Design II—Spillways Without Chute Blocks

In the second modified design, chute blocks are totally eliminated. An intense hydraulic jump is forming in the stilling basin. Flow condition is observed from Photo 5.

3.3 Velocity Distribution in Stilling Basin

Velocities were measured using current meter in original as well as in all modifications for the entire range of discharges across the stilling basin for different lengths. Comparison of velocity distribution is shown in Fig. 4 in the stilling basin for discharge (Q) = 70,791.5 m^3/s for fully open gates with large, small, and without chute blocks indicated that in the original design large chute blocks were causing reduction of bottom or bed velocities at 100 m distance from dam axis in stilling basin, which may cause reduction in erosion near the bed.

Average velocities were also measured along the stilling basin for the entire range of discharges for spillway gates full and partial operating conditions with large size

Table 1 Model observations—with large chute blocks

S. No	Discharge m^3/s	Gate operating condition	RWL in m	TWL in m at Ch. 140 m	Flow condition
1	141,583 (100%)	Ungated	45.72	32.96	Hydraulic jump is forming in the stilling basin. High-velocity flow is continued beyond the end sill. A high chute block is preventing the distribution of energy across the width or transverse direction in the stilling basin near the chute block
2	106,187.25 (75%)	Ungated	42.5	31.25	Similar flow conditions as for 100% discharge. However less turbulence conditions in the stilling basin
		Gated	45.72	31.25	Similar flow conditions as above but more separation near chute block
3	70,791.5 (50%)	Ungated	38.5	28.75	Hydraulic jump is forming in the stilling basin. More mixing at the entrance of stilling basin due to secondary circulations near chute block
		Gated	45.72	28.75	Same as above, flow is riding over chute block
4	35,395.75 (25%)	Ungated	34.2	25.93	Mild hydraulic jump. Flow is riding over chute block. Secondary circulations are forming near the chute block
		Gated	45.72	25.93	Similar as above

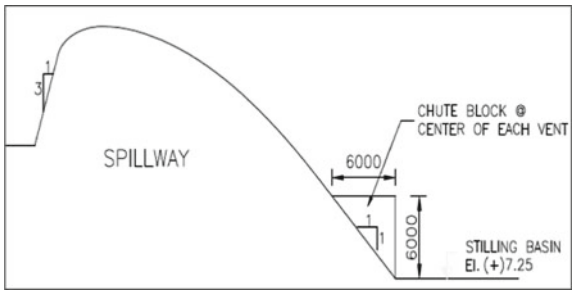

Fig. 3 Details of small size chute block

chute block, small size chute block, and without chute block designs. A comparison of average velocities is shown in Fig. 5.

From Fig. 5, it is observed that for all the discharges, large chute blocks cause low velocities in the stilling basin. When spillway discharge was reduced to 50% of maximum discharge (Q) = 70,791.5 m^3/s, velocities with smaller chute blocks and without chute blocks became of the same order.

Table 2 Model observations—with smaller chute blocks

S. No	Discharge m^3/s	Gate operating condition	RWL in m	TWL in m at Ch. 140 m	Flow condition
1	141,583 (100%)	Ungated	45.72	32.96	Hydraulic jump is forming in the stilling basin. High-velocity flow is continued beyond the end sill
2	106,187.25 (75%)	Ungated	42.5	31.25	Flow conditions are similar to 100% discharge. Introducing mild separated and cross flows at the entrance of stilling basin
		Gated	45.72	31.25	Similar flow conditions as above but more separation near chute block
3	70,791.5 (50%)	Ungated	38.5	28.75	A mild hydraulic jump is forming in the stilling basin. Nominal mixing at the entrance of stilling basin due to secondary circulations near chute block compare to earlier discharges
		Gated	45.72	28.75	Same as above, flow is riding over chute block
4	35,395.75 (25%)	Ungated	34.2	25.93	Mild hydraulic jump. Flow is riding over chute block. Secondary circulations are forming near chute block
		Gated	45.72	25.93	Similar as above

4 Discussions

The performance of stilling basin with large size chute blocks and dentated end sill at the end of stilling basin was investigated for the entire range of discharges up to the design maximum discharge. Large size chute blocks, smaller size chute blocks, and without chute blocks provided at the junction of the spillways stilling basin were studied.

As can be seen from Table 1 and Photos 1 and 2, a large chute block is preventing the distribution of energy across the width of stilling basin at the beginning only at higher discharges. Chute blocks were not contributing to the dispersion of flows in the stilling basin.

From Table 2, it can be seen that flow is riding over the smaller chute blocks, and it is introducing a lot of separated and cross flows at the entrance of stilling basin.

Chute blocks whether bigger or smaller were not contributing to the stabilization of hydraulic jump. Flow mixing as more intense and well-defined roller formation at the entrance of the stilling basin without chute blocks.

Photo 4 Flow condition on chute block and in stilling basin for design maximum discharge with gates fully open in modified design-I

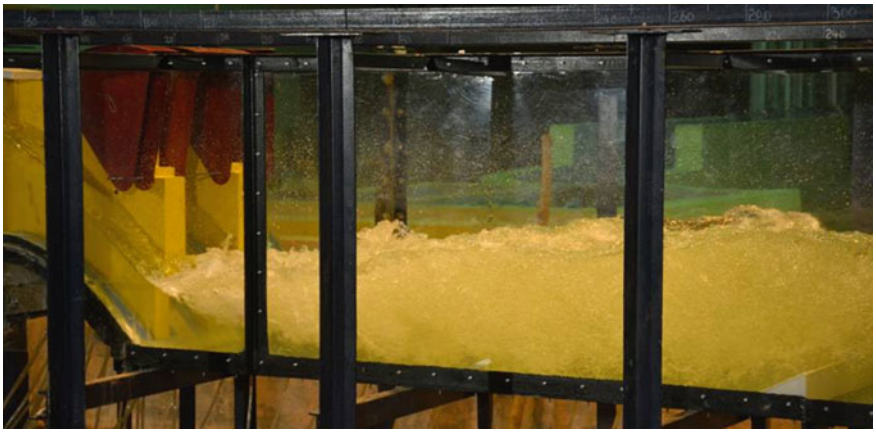

Photo 5 Flow condition without chute block in stilling basin for design maximum discharge with gates fully open in modified design-II

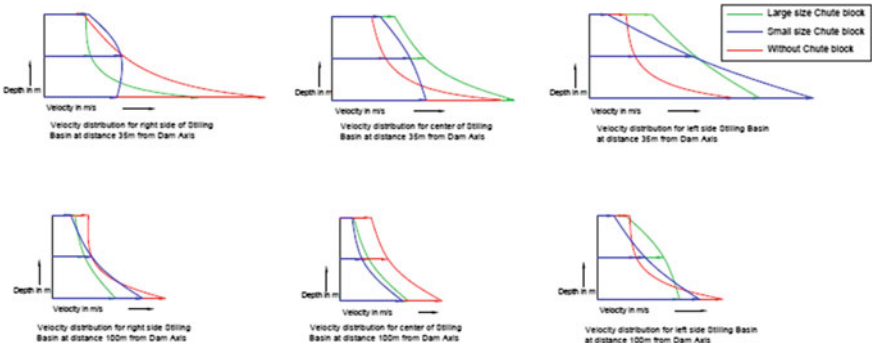

Fig. 4 Velocity distribution in stilling basin for discharge (Q) = 70,791.5 m^3/s for gates fully open condition in original and two modifications

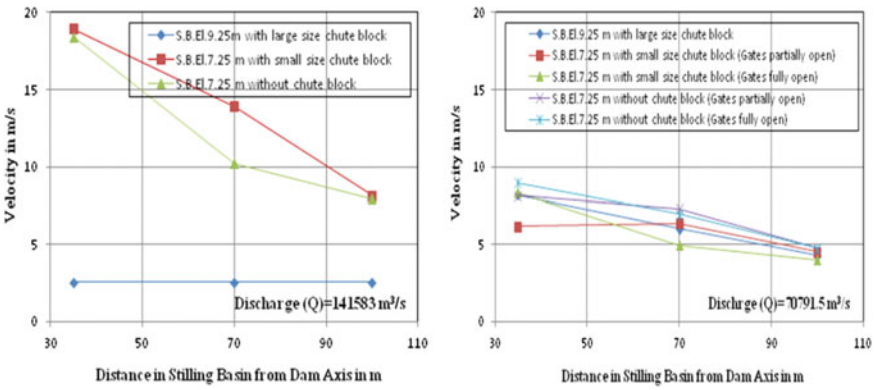

Fig. 5 Comparison of average velocities along the stilling basin for different discharges of the spillway with gates fully and partially open condition in original and two modifications

5 Conclusions

Chute blocks were preventing the distribution of energy across the width of stilling basin. Smaller chute blocks were introducing large flow separations and cross flows at the entrance of stilling basin. Size of chute block had no effect on the stabilization of hydraulic jump. Large chute blocks were causing reduction of bottom or bed velocities.

Acknowledgements The authors are grateful to Shri A.K. Agrawal, Director, Central Water and Power Research Station, Pune, for providing kind permission to publish the paper. Authors are grateful to APWRD, AP, for giving opportunity for model studies.

References

1. Khatsuria RM (2005) Hydraulics of spillways and energy dissipators. Marcel Dekker, New York
2. Peterka AJ (1983) Hydraulic design of stilling basins and energy dissipaters. Engineering Monograph no. 25, USBR
3. CWPRS (2017) Pune technical report no. 5483

Hydropower Potential in India: A Review

Varun Mishra, Ruchi Khare, and Rutuja Chavan

Abstract India being a developing nation, the requirements increase day by day which leads to the crisis of resources. Energy sources are mostly affected because of increase in the mechanisation and different development schemes. Specially if we talk about the energy sector, the increase in the demand is just an effect of urbanisation. As someone said very right, "Everything comes with a price", so the question is what price you willing to pay? Ample amount of production and distribution of energy becomes a major task today. The environmental aspect and continuous depletion of fossil fuels concern its availability in future and force it to look forward to alternative sources. Sources of energy which are considered to be renewable like hydro, wind and solar can become a boon for the future generation. Currently, in India, the energy contribution by hydropower by utilising water potential is around 12.4% (including small hydropower) of total energy generation, whereas renewable sources share up to 18%. So, there is a need for proper functioning and sustainable methods where the renewable sector can be uplifted. In India, hydroelectric energy capacity is roughly calculated as 148,700 MW having load factor of 60%. In India, the overall hydroelectric power for FY 2019–20 was 156 TWh (excluding SHP) having average CF as 38.71%. This paper reviews major literature on the generation capacity of hydropower. A review on different alternatives available to fulfil the energy demand and to investigate the different types of correlations developed by previous investigators. The study also focuses on small hydropower development its benefits and cause. In India, small hydropower plants contribute around 4671 MW of electricity, and around 526 MW is under construction. Using small hydropower can make a sustainable growth in the energy sector. Furthermore, the study also put forward the suggestions for development in the energy scenario along with policies offered by the government.

Keywords Energy · Hydropower · Renewable sources · Small hydropower plants

V. Mishra (✉) · R. Khare · R. Chavan
Department of Civil Engineering, Maulana Azad National Institute of Technology Bhopal, Bhopal 462003, India
e-mail: varunmishra919@gmail.com

R. Chavan
e-mail: rutujamchavan@manit.ac.in

P. V. Timbadiya et al. (eds.), *Flood Forecasting and Hydraulic Structures*, Lecture Notes in Civil Engineering 340, https://doi.org/10.1007/978-981-99-1890-4_37

1 Introduction

Electricity is amid the vital field of infrastructure, essential for economic advancement and well-being of country. The continual improvement of Indian economy requires development and expansion of infrastructure.

India's energy field is considered to be one of the most diversified in the world. Both conventional and non-conventional energy sources are responsible for power generation. The oil, coil, nuclear power, natural gas and hydro are some of major conventional sources while domestic waste, solar, wind and agriculture are feasible non-conventional sources.

In recent years, electricity consumption is increasing very rapidly and is expected to be further grow. So, to overcome the crisis and manage the proper distribution effectively in the country, massive addition to the installed generating capacity is obligatory [1].

In a survey of FY2018, India ranks fourth in overall power generation in Asia Pacific Region out of 25 countries. India secured 4th in wind power, 5th in solar power and 5th in renewable sources installed capacity until 2018. With these achievements and prudent steps to invest in the clean energy, India becomes the only country among G20 Nations that is on track to reach targets under Paris Agreement [1]. In FY2022 (until May 2021), the total installed capacity in India stands at 234.72 GW of Thermal Energy, renewable energy at 95.65 GW, 46.21 GW of Hydro energy and 6.78 GW of Nuclear energy. By the end of 2022, solar energy is expected to contribute 114 and 67 GW from wind power. Since government promoting renewable sources of energy, it is expected to boost up and achieve a target of 227 GW by 2022 [1].

According to World Water Assessment Programme (WWAP, 2014) and IEA 2011, India is at fifth position in world when it comes to production of electricity but still more than 288 million of India's population is living without electricity. There is a campaign called *power for all* initiated by the Indian government to make sure the accessibility of electricity in village areas by 2019. As per International Energy Agency (IEA) projections, country might put up more than 600 million new consumers of electricity by the end of 2040, due to which electricity demand may grow up to 5%.

India comprises many rivers which carry enormous amount of water potential and can be utilised to generate power. Using easily available native resources hydropower is capable of generating sustainable energy. This can solve chronic energy problem of the country [2]. With more than sufficient amount of water potential available, hydropower in India becoming the boon for Indian economy. As day-by-day population increases, power consumption and demand increase and to overcome that there is need of some alternatives which not only satisfy the demands but also comes as a supporting factor to boost and endorse the economy. Thermal source amid one of the high costs per kwh power generation comes with some limitations of polluting the environment but still maximum power generation in India is using coal as a fuel. This needs to be changed, when we have the alternatives and not only in sufficient

quantity but in massive, only what we need is proper engineering and steps to utilise that power. That alternative source is hydropower.

2 Power Sector in India

India is enriched with many rivers which have a huge water potential available and can be utilised to generate power fulfilling the increasing demand and stabilise the fluctuation in peak hours. Power sector in India is divided in three sectors, private sector, Central (Federal) sector and State sector and renewable energy sources (RES) contains Wind Energy, Solar Energy, Waste Power from industrial and urban areas, Biomass Power and Gasifier and Small Hydro Project.

India's overall collective installed energy generation potential from various sectors is 386,888 MW (July 2021). Figure 1 shows that 27% of the total installed capacity is contributed by private sector, whereas 48% is contributed by and 25% by Central government. Further, fuel consumption wise scenario shown in adjacent figure where thermal sector using coal is on top with 56% and hydro contribute 12.1% of total installed capacity. With rising trend of small hydro plants, hydropower is becoming a supporting factor in the power sector of India. As SHPs can be installed at lower kinetic head with less than 25 MW of capacity, it acts as supporting hand for the fluctuating demands in power supply, specially at the peak hours [4].

Figures 2 and 3 show the total generation in power in last decade and percentage growth in total generation yearly.

2.1 Renewable Energy Sector

In Paris Agreement for the Period 2021–2030, Nationally Determined Contribution (NDC) embraces some special conclusions those are

1. Reduction in the emission concentration by 33–35% of its GDP by 2030 from 2005 level.
2. To reach around 40% aggregate electricity installed capacity using renewable energy sources by 2030 using low-cost global finance and transmission of technology.

India has reached a collective installed renewable energy potential (excluding large hydro) of about 92.54 GW within which 5.47 GW was built-on in the period April 2020 till January 2021. In the course of April 2014–Jan 2021, the installed renewable potential of India has increased by 2.5 times, and the installed solar energy potential has increased fifteen times. Internationally, today India ranks 4th in renewable energy potential, 4th in Wind power, and 5th in Solar Energy Capacity [4].

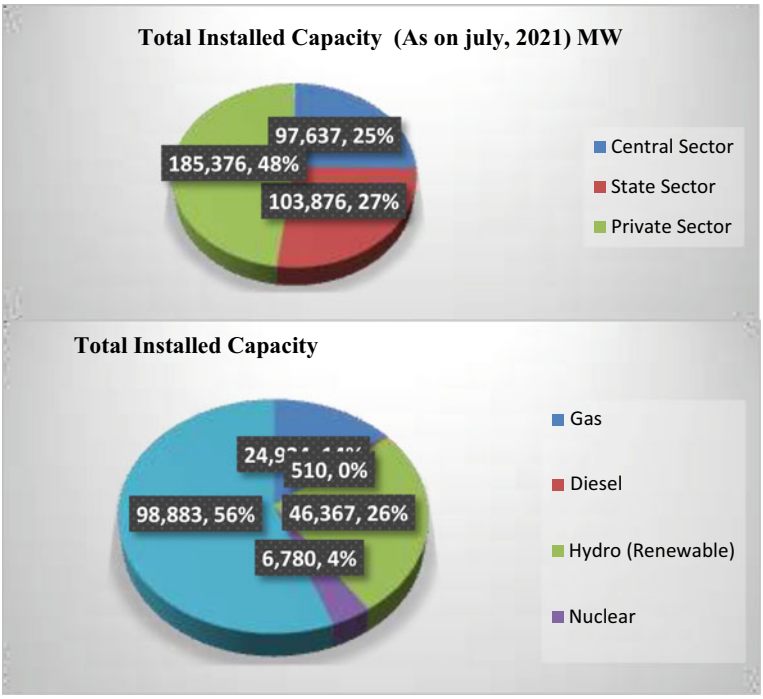

Fig. 1 Installed capacity of different energy sources [3]

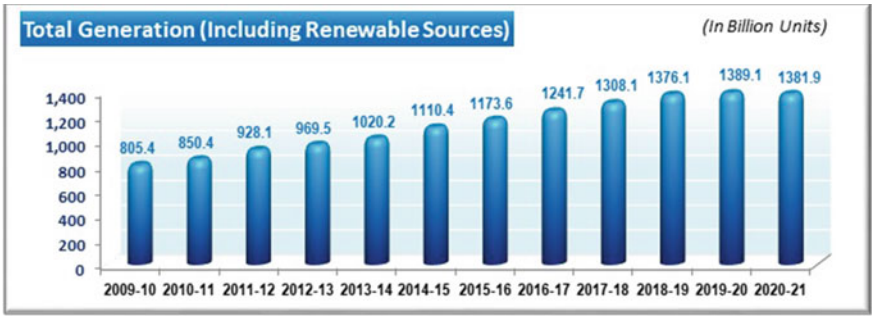

Fig. 2 Total power generation in last decade [1]

India is a country which has highest growth rate in terms of renewable energy sources. According to REI Report, around 64.2 billion US dollars is the estimated investment in renewable energy projects and programmes between 2014 and 2019 [3, 4] (Table 1).

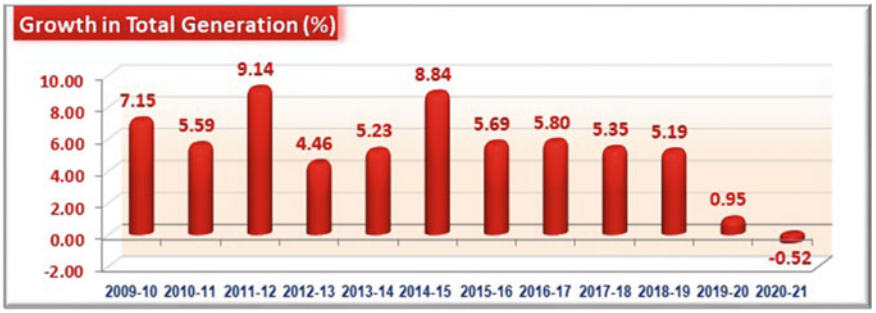

Fig. 3 Percentage growth in total power generation [1]

Table 1 India's RE sector at a glance [3]

Year	Installed RE capacity (in GW)	% share of RE in total installed capacity	Generation from renewable sources (in BU)	Total generation from all sources (in BU)	% share of RE in generation
2014–15	39.55	14.36	61.78	1110.18	5.56
2015–16	46.58	15.23	65.78	1172.98	5.60
2016–17	57.90	17.68	81.54	1241.38	6.56
2017–18	69.77	20.24	101.83	1303.37	7.81
2018–19	78.31	21.95	126.76	1375.96	9.21
2019–20	87.07	23.52	138.32	1390.93	9.95
2020–21	92.54	24.53	111.92	1017.81	11.00
	(Up to Jan	(Up to Jan	(Up to Dec	(Up to Dec	(Up to Dec
	2021)	2021)	2020)	2020)	2020)

2.2 Scenario of Hydropower in India

Concept of hydropower is developed by taking benefit of kinetic energy unconstrained falling water. Conversion of water's potential energy into mechanical and electrical energy using turbine rotation by water is the idea behind working of hydroelectric plant. Hydropower is a renewable, economic and non-polluting source of energy. Hydropower plants have essential adaptability of quick start, stop and load variations handout operational tractability and aid in enhancing reliability of power system. Hydropower sources are the best option for meeting the peak demand.

Hydropower is a clean and renewable source of energy which doesn't concern about the fuel economically as well as the availability is also not the factor of much deal. The efficiency of a hydropower is also high (90%) compared to thermal (35%) and gas of (50%). Hydropower projects are generally categorised in two segments, i.e. small and large hydro plants. In India, the main two highest energy contributors are large and small hydropower, which satisfy the demand under peak and

fluctuating load conditions. In Indian scenario, hydropower stations up to 25 MW installed capacity comes under SHP projects and comes under the Ministry of New and Renewable Energy (MNRE) [5].

Table 2 shows the state-wise installed Hydro projects as per consecutive year, starting from year 1981 when first plant (Baira Siul) has been installed in the country in Himanchal Pradesh with 180 MW capacity, three units of 60 MW each to Kishanganga project of J&K in 2018 with 330 MW capacity. Highest installed capacity is found to be in Madhya Pradesh since 2005 with 1000 MW of capacity [6] (Fig. 4).

In 2019–20 annual report, CEA gave some figures about the hydropower development according to the basins, in terms of installed capacity. In this report CEA mentioned, as on 31 March 2020, out of the installed capacity, venture in operation is only 28.15% or 40,913.6 MW, and those under working was 7.84% which is about 11,393.5 MW of the total capacity available. Thus, a lot of potential still needs to be developed [1, 6].

As per the annual report published by CEA in 2019–20, Fig. 5 shows the basin wise status of hydro potential which is assessed, developed and under developed. Brahmaputra basin has the highest potential assessed till date and some major projects are being developed. Central Indian River basins are among the lowest hydro potential development [1].

Government of India is also enforcing pumped storage schemes (PSS) for which 63 new sites has been assigned. The power estimated from this project is around 96,529.6 MW. Currently, 9 PS projects (> 25 MW) are constructed which has 4785.60 MW total installed capacity. 3 PSS (1580 MW) are under development [1].

Under an initiative of 50,000 MW in the year 2003–04, CEA involved in the project of planning of Preliminary Feasibility Reports (PFRs) for 162 hydroelectric projects which planned to be spread over 16 states. Out of 162 projects (47,930 MW), 37 projects (20,435 MW) have already been prepared.

In the FY2018-19 itself hydro potential of 140 MW additionally has been accomplished against the target of 840 MW in the year 2018–19. This shows the venture of new projects specially concerning hydroelectric plants. Similarly, for the FY 2019–20, 300 MW of capacity additionally potential gained against the target of 1190 MW in the year 2019–20. Table 3 shows the surplus energy gained during the year 2019–20. Against the estimated target of 136.93 BU, the actual potential generated in the year 2019–20 was 155.76 BU, found out 13.75% more than the target [1].

3 Development of SHP in India

There is no any proper explanation of small hydropower (SHP). In general, SHPs are defined by its power output. Different nations have their different criteria of categorisation, having 5–50 MW as upper limit. Ministry of New and Renewable Energy (MNRE) is responsible for SHP classification in India. SHP is those hydropower

Table 2 State-wise installed capacity in India [6]

Name of project	State/UT	No of units × unit capacity	Total capacity (MW)	Year of commission
Baira Siul	Himachal Pradesh	3 × 60	180	1981
Loktak	Manipur	3 × 35	105	1983
Salal	UT of Jammu & Kashmir	6 × 115	690	1987
Tanakpur	Uttarakhand	3 × 31.4	94.2	1992
Chamera-I	Himachal Pradesh	3 × 180	540	1994
Uri-I	UT of Jammu and Kashmir	4 × 120	480	1997
Rangit	Sikkim	3 × 20	60	2000
Chamera-II	Himachal Pradesh	3 × 100	300	2004
Indira Sagar	Madhya Pradesh	8 × 125	1000	2005
Dhauliganga	Uttarakhand	4 × 70	280	2005–06
Dulhasti	UT of Jammu and Kashmir	3 × 130	390	2006–07
Omkareshwar	Madhya Pradesh	8 × 65	520	2007
Teesta-V	Sikkim	3 × 170	510	2008
Sewa-II	UT of Jammu and Kashmir	3 × 40	120	2010
Chamera-III	Himachal Pradesh	3 × 77	231	2012
Teesta Low Dam-III	West Bengal	4 × 33	132	2013
Nimmo-Bazgo	UT of Ladakh	3 × 15	45	2013
Chutak	UT of Ladakh	4 × 11	44	2013
Uri-II	UT of Jammu and Kashmir	4 × 60	240	2014
Parbati-III	Himachal Pradesh	4 × 130	520	2014
Teesta Low Dam-IV	West Bengal	4 × 40	160	2016
Jaisalmer	Rajasthan	1 × 50	50	2016
Solar power	Tamil Nadu	1 × 50	50	2018
Kishanganga	UT of J&K	3 × 110	330	2018

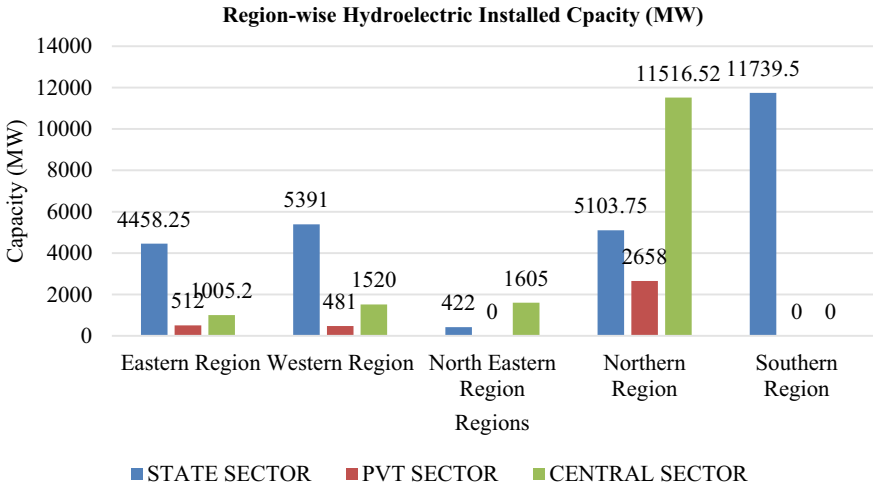

Fig. 4 Region-wise installed capacity [6]

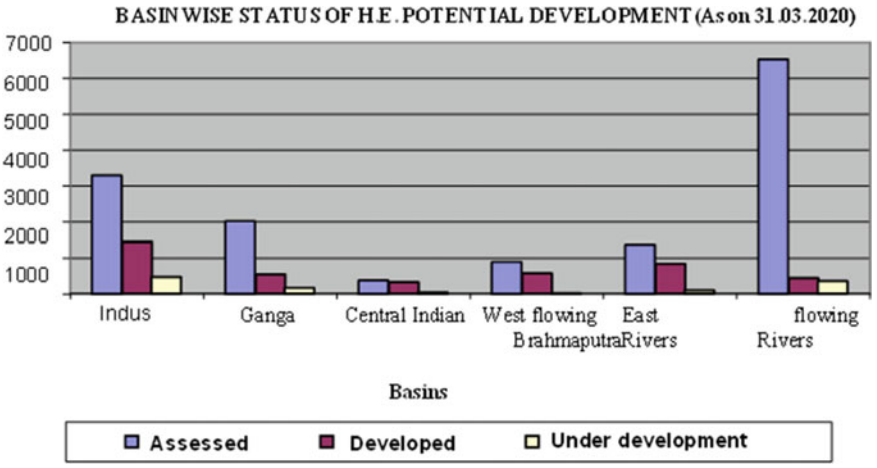

Fig. 5 Basin wise study of H.E. potential development [1, 6]

Table 3 Target versus actual energy generation in year 2019–20 [1]

Region	Generation (BU)		Deviation (±)
	Target	Actual	(%)
Northern	71.51	80.55	12.64
Western	12.20	17.81	45.98
Southern	27.12	31.75	17.07
Eastern	19.24	20.82	8.21
N-Eastern	6.85	4.82	− 29.63
All India	136.93	155.76	13.75

schemes which has capacity of up to 25 MW. In 1897, the first SHP was developed in Darjeeling Hills, West Bengal, having 130 kW capacity. Taking inspiration from this project in 1902 Karnataka also developed Sivasamudram plan (4.5 MW) in Mysore. This project was responsible for energy supply to kolar gold mines [5].

MNRE in India has been working in rising SHP projects. The SHP as renewable energy sources is very important because the technology used in it is indigenous. Also SHP is advisable because it does not fail in summer and provide maximum energy in peak cyclic demand. Such plants show potential of over 21,135 MW [7].

Alternate Hydro Energy Centre (AHEC) of IIT Roorkee has done a study in 2016 for estimating the overall potential from small/mini hydel projects and finds out 21,135.37 MW of power from 7135 sites generating enough potential to supply during fluctuating demands. The hilly States of country primarily Uttarakhand, Jammu and Kashmir, Arunachal Pradesh and Himachal Pradesh comprise about 50% of total potential. The probable States which are actively generating and contributing in power supply are Maharashtra, Chhattisgarh, Karnataka and Kerala.

MNRE as a governing body has taken the measures to encourage the development of SHPs in an organised way and expand reliability and quality of the projects. Commercial field and organisations have been attracted towards investing in SHP projects as by getting various physical and financial inducements. For remote village electrification, Ministry is endorsing new designs of water mills to make power generation more efficient. State government is also building up micro hydel projects up to 100 kW [8].

4 Govt Policies and Norms

For promoting small hydel projects, government has taken some initiatives to encourage the development of SHPs. As water being State subject, the actual implementation of SHP projects is governed by the State policies. Only state has the right to control and develop the projects. The Ministry (MNRE), being the nodal Ministry for the development and establishing of small hydro sector in the country provides wide structure by way of motivating the sector development through various measures [8].

Recently govt emphasis on a Small Hydropower Projects, the main objective of this scheme is to inspire the State Government entities and Independent Private Producers (IPPs) to setup new plans to realise the 21,000 MW potential in phased manner [9]. Some salient features of schemes are providing subsidy for the private sector, renovation and modernization of existing projects, support of water mills and setting up micro-projects (up to 100 KW capacity) [8, 10].

To satisfy the whole country's peak demand and power requirement at the end of 12th Plan, a potential addition of more than 90,000 MW has been appraised during 12th Plan (2012–2017), which consist of 40,000 MW of hydroelectric power. Central Electricity Authority (CEA) has provided many hydroelectric power generation related reports and manuals which are available on official site. A few of them are the best application in hydroelectric power generation, preliminary ranking study

of hydroelectric projects, strategies for agreement of concurrence of hydroelectric scheme, instructions for building of DPRs for hydroelectric projects, project tracking status reports, project clearance status reports and status of 50,000 MW hydroelectric initiative reports [11].

5 Problems in Hydropower Generation

Hydropower is one of the major used renewable energy sources and contributing a huge share in overall electricity generation in developing countries like India. A few decades ago, hydropower reservoirs were found to be a clean source of renewable energy, but after the pre-industrial era (1990s), these reservoirs become one of the sources for affecting environment.

5.1 Climatic Effect on Hydropower

Some models have been developed to understand the climatic effect on the hydropower generation, based on the reservoir configuration and utility energy need to study the influence of weather sequences on the performance. Performance analysed on the basis of fluctuation of water level below the reservoir capacity. Models track daily water level of reservoir, but mainly focus on the minimum water level throughout the year, by which it can be found that the maximum size of dam needed to assure continuous operation and generation of electricity [12].

Various studies have been conducted at many locations by considering the model and all of this analysis however focus attention on the importance of sequence and timing of precipitation events, where the impact of changed, climate could guide to large variations or be almost insignificant. The results of model analysis and studies of climate-induced changes compared to technological changes vary between 10 and 12%. These results proved that hydroelectric generating systems are highly sensitive towards climatic fluctuations. In some measures, small climate changes can escort to major changes in the draw-down of reservoir levels. The climatic effect, however, varies greatly form one region to another. Finally, it can be concluded that an extreme value analysis of annual minima would give useful info regarding reservoir system performance, including signs of condition where reservoir may become dry, in future [13].

6 Conclusion

With the increasing world energy demand and consumption, the requirements cannot be satisfied for so long with fossil fuels. There needs an alternative to give an edge to the probability of the climate collapse and outspread of wars for natural resources. The twenty-first century in Indian history will be strongly interpret by the way India faces and resolves the energy crisis. It is found that the resources and potential available in the country, which can be utilised in a precise and formulated manner to satisfy the energy demand along with stabilising the fluctuation specially in summer. India enriched with much water potential, so, if its energy can be utilised properly, hydropower sector can be one of the best and most economical power sources in India. Government has recently developed some schemes to promote development of hydroelectric power and thus giving special benefits to accelerate hydropower development in its power development plans, a tariff subsidy been given to keep up the development of hydroelectric power and an effort to fulfil the country's energy requirement. In this era of new technologies, SHP and pump storage-based projects could become best choice to overcome the fluctuations in demand, as these projects cost less and can be installed without any massive dam or reservoir. In India, SHP projects expansion can also be a significant means for regional economic development, mainly for various underdeveloped states, having extreme potential for evolving new SHP projects, which is limitless and evergreen source of energy. It can be concluded that

- India contributes around 4671 MW of electricity and around 526 MW is under construction in the form of small hydropower plants.
- Collectively total installed energy generation potential from various sectors is 386,888 MW (till July 2021). Specially private sector with renewable energy sources on top with around 50% of contribution to total installed capacity.
- Highest installed capacity is found to be in Madhya Pradesh since 2005 with 1000 MW capacity.
- Brahmaputra basin has the highest potential assessed till date and some major projects are under developed, whereas Central Indian River basins are among the lowest hydro potential development.

References

1. Central Electricity Authority, India. Available: https://cea.nic.in. Accessed on 28 Sept 2012
2. Singh R, Sood YR (2009) Transmission tariff for restructured Indian power sector with special consideration to promotion of renewable energy sources. In: TENCON (2009–2009) IEEE region 10 conference. IEEE, pp 1–7
3. Ministry of power. Available: www.powermin.nic.in. Accessed on 2 Sept 2021
4. Robinson PJ (1997) Climate change and hydropower generation. Int J Climatol J Roy Meteorol Soc 17(9):983–996

5. Sharma NK, Tiwari PK, Sood YR (2013) A comprehensive analysis of strategies, policies and development of hydropower in India: special emphasis on small hydro power. Renew Sustain Energy Rev 18:460–470
6. Khan R (2015) Small hydro power in India: is it a sustainable business? Appl Energy 152:207–216
7. Chaurasiya PK, Prasad V, Khare R (2013) Scenario and risk of hydro power projects in India. Int J ChemTech Res 5(2):1068–1075
8. Ministry of New and Renewable Energy Annual Report 2020–21. Available: https://mnre.gov.in/. Accessed on 5 Sept 2021
9. Nautiyal H, Singal SK, Sharma A (2011) Small hydropower for sustainable energy development in India. Renew Sustain Energy Rev 15(4):2021–2027
10. Saxena P, Kumar A (2010) Hydropower development in India. In: Proceedings of the international conference on hydraulic efficiency measurement, Roorkee, India
11. Kusre BC, Baruah DC, Bordoloi PK, Patra SC (2010) Assessment of hydropower potential using GIS and hydrological modeling technique in Kopili River basin in Assam (India). Appl Energy 87(1):298–309
12. Agarwal SS, Kansal ML (2020) Risk based initial cost assessment while planning a hydropower project. Energ Strat Rev 31:100517
13. Mishra S, Singal SK, Khatod DK (2011) Optimal installation of small hydropower plant—a review. Renew Sustain Energy Rev 15(8):3862–3869

Assessment of Seismic Potential for a Hydroelectric Project: A Case Study

Sachin N. Khupat, Chaman Singh, Suman Sinha, S. Selvan, Anamika Saha, and Rizwan Ali

Abstract A seismic network of microearthquake recorders around a proposed dam site is required to establish to assess the seismicity of the project area. Microearthquake studies are useful in delineating active seismic zones and to assess the seismic potential of the faults in the area which is utilized for selecting suitable location of the project. This paper is based on the study conducted for Sawalkote Hydroelectric Project, Jammu & Kashmir. Seismological network of six observatories at and around the dam axis within the radius of 50 km has been established by installing broadband seismographs for microearthquake measurement in the project area. The seismic activity has been recorded for a period of six months. A total of 387 earthquakes have been recorded within the radius of 200 km with varying magnitude from M_L 1 to M_L 4.9 from the project site. The 'a' and 'b' value obtained are 3.323 and 0.516, respectively.

Keywords Sawalkote hydroelectric project · Microearthquake · Seismological network · Seismic activity

1 Introduction

Many countries have made various procedures and protocols to assess seismic potential of the selected site before constructing any large civil structures such as hydroelectric projects, nuclear reactor, irrigation dams and barrages, etc. In India, National

S. N. Khupat (✉) · C. Singh · S. Sinha · S. Selvan · A. Saha · R. Ali
Engineering Seismology Division, Central Water and Power Research Station, Pune 411024, India
e-mail: sachinkhupat@cwprs.gov.in

C. Singh
e-mail: chaman@cwprs.gov.in

S. Sinha
e-mail: suman.sinha@cwprs.gov.in

R. Ali
e-mail: rizwan_Ali@cwprs.gov.in

P. V. Timbadiya et al. (eds.), *Flood Forecasting and Hydraulic Structures*, Lecture Notes in Civil Engineering 340, https://doi.org/10.1007/978-981-99-1890-4_38

Committee on Seismic Design Parameter (NCSDP) and INCOLD are such bodies which have laid down the procedures and protocols to follow before constructing any large dam of height more than 30 m. Generally, hydroelectric projects are constructed in high mountain ranges which comes in high seismic zones, in which it is intuitive to assess seismic potential of the region which enables project authority to build civil structures far from any potential active seismo tectonic feature. There are various techniques available to assess seismic potential or to delineate any seismo tectonic feature in the project region, such as seismic hazard analysis, microearthquake studies, borehole logging and seismic tomography, etc. in which, seismic hazard analysis is based on historical earthquake catalogue of higher magnitude events which generally helps to design the civil structures and sometimes completely fail to find any new seismo tectonic activity. Borehole logging and other techniques are very costly and difficult to deploy in high mountain ranges. Microearthquake studies is rugged, easy to deploy and one of the best non-invasive technique, which is generally based on earthquakes events of less than 3 magnitude which must be recorded by establishing a seismological network for a period of six months.

Recently, to delineate subsurface seismo tectonic activity, CWPRS has carried out the microeathquake studies for Sawalkote hydroelectric project. This paper is based on this study. Swalkot project envisages construction of a 192.5 m high roller compacted concrete (RCC) gravity dam across Chenab River near the village Sedhu in Ramban and Udhampur District, Jammu and Kashmir, at Lat. 33° 11′ N and Long. 75° 06′ E. The reservoir water will mainly be used for hydropower generation with installed capacity of 1856 MW using discharge of 1293 Cumecs at a net head of 154.40 m. The site is located in Himalayan region which is seismically very active region and lies in seismic zone IV of the seismic zoning map of India as per IS 1893:2016. The project site lies between thrust and main boundary thrust (MBT). Towards the northern part of the project site, main central thrust and Kishtwar fault are the dominant faults. The Chenab basin lies in the north-western Himalayan complex and is situated between latitude 32° to 34° 15′ N and longitude 74° to 78° E approximately.

In such a complex seismo tectonic framework of project area, it is necessary to delineate the subsurface tectonic activity around the project area. A seismic network comprising six stations at and around the dam site has been established to monitor seismic activity of the region. The six observatories, namely Tangar (Dam axis), Shalgadi, Shanderi, Kuriya Pul, Choki Chaura and Aithem have been constructed and Guralp 40 T digital microearthquake seismometers were installed in each observatory. The earthquake data has been recorded up to six months from these observatories.

2 Tectonic and Seismic Activity of the Area

The local geology in the project area constitute the rock formations of Murrees which comprises sandstone, clay stone and siltstone of lower Miocene age, Numulitics comprises olive colour shale and Numulitic limestone with coal seams at the base of Eocene age and Sirban limestone having siliceous dolomite, limestone with occasional shale bands of Neoproterozoic age.

Generally, the river Chenab flows from northeast to southwest direction. The Murrees of Sirban limestone and Numulitic limestone have in between contact of fault in nature. That fault is known as Sawalkote fault, while the Chakka fault is in between the Sirban limestone and Numulitic limestone. The Sirban limestone unit is present as an 'inlier' having the Murrees in the upstream side and Numulitic limestone in the downstream side.

The seismicity in an area is generally associated with seismo tectonic features like faults, folds, thrusts, shear zones, etc., which are termed as the tectonic features. Major tectonic features in the region of Sawalkote H.E. project along with location of the six seismological observatories superimposed on the tectonic features with historical earthquakes within 200 km radius from dam site are shown in Fig. 1. In the southern part several hot springs are located in the Pir Panjal range between MCT and MBT. Two of these lie almost on MBT, while the others are aligned sub-parallel to the Kishtwar fault. West of project site, there is regionally the most extensive major neotectonic fault, Jhelum fault. It is a N-S trending left lateral wrench fault which separates Peshawar basin from Kashmir basin. Its conjugate set is the Mangla fault, which is a right lateral wrench fault. Here, high-grade complex fold is overlain by low grade-cover sequence. The main structural feature of the sub-Himalaya is represented by the northly dipping thrust, i.e. Salt range thrust and Reasi thrust. Geological evidences, particularly from the eastern part of the salt range, indicate that uplift has mainly occurred in the last one million year, thus pointing towards the neotectonic activity along the thrust plane. Several other faults and lineaments are also present in the area. While in the latter, the movement is left lateral. Neotectonics activity is evident in both these faults.

3 Site Selection and Installation of Seismographs

The seismic noise surveys have been performed at various locations in the area of 50 km around the project site prior to select suitable site for seismological network. The Guralp CMG 40 T sensors have been used to record the continuous ground motion at these sites for half an hour period. It was observed that noise levels at these sites lie within new high noise model (NHNM) and new low noise model (NLNM) as suggested by Peterson [6]. The details of seismological observatories are given below in Table 1.

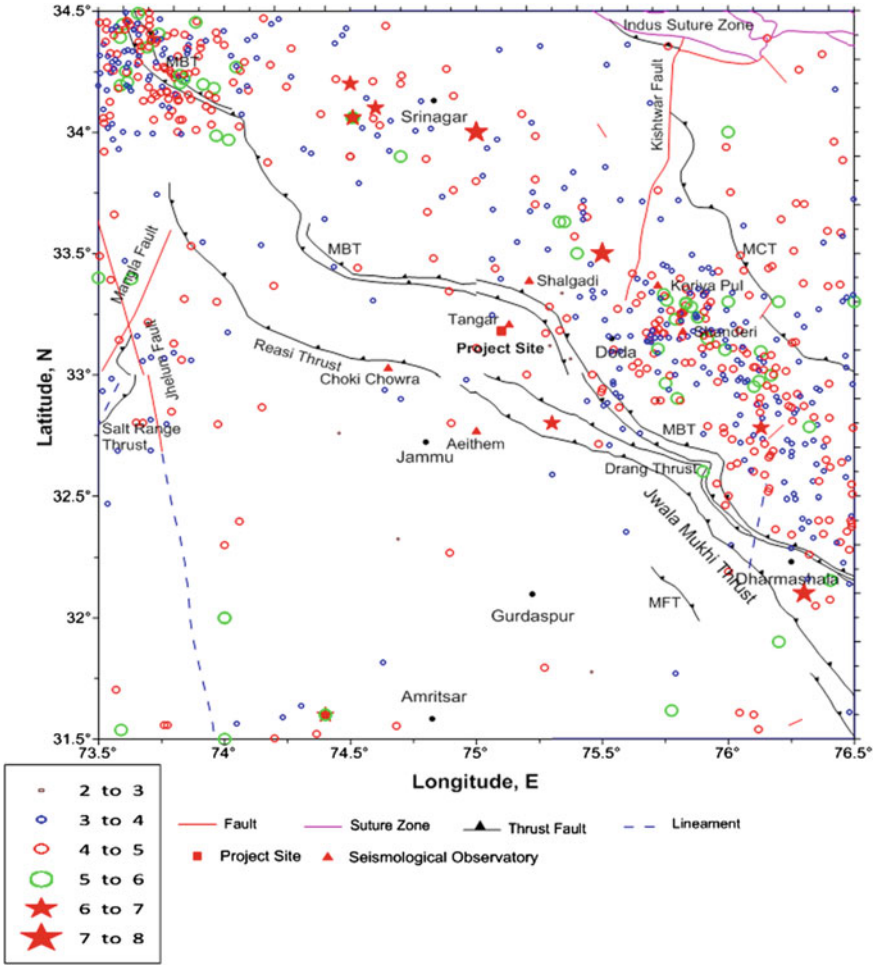

Fig. 1 Major tectonic features in the Sawalkote H.E. project region with historical earthquakes and established seismological network

Table 1 Location of seismological stations

S. No	Name of the station	Latitude (°N)	Longitude (°E)	Elevation (m)	Rock type
1	Tangar (near dam)	33° 12.44′ N	75° 07.57′ E	871	Sandstone
2	Shalgadi	33° 23.64′ N	75° 12.78′ E	1730	Slate
3	Shanderi	33° 11.10′ N	75° 49.23′ E	1274	Schist
4	Kuriya Pul	33° 22.27′ N	75° 43.22′ E	1149	Gneiss
5	Choki Chaura	33° 01.54′ N	74° 38.87′ E	660	Sandstone
6	Aithem	32° 46.47′ N	75° 00.00′ E	535	Sandstone

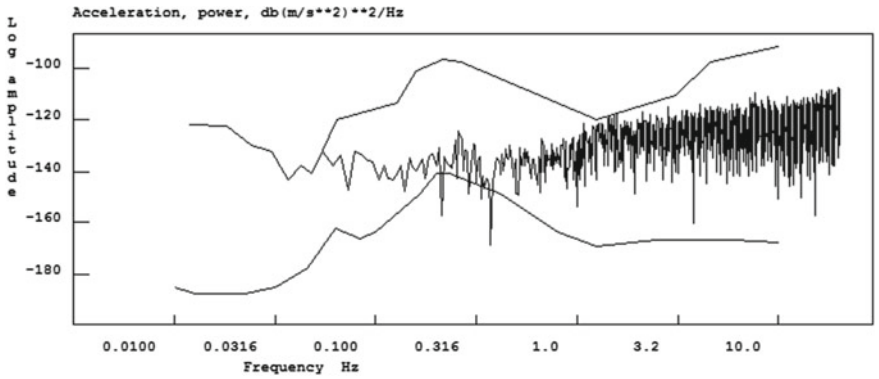

Fig. 2 Noise spectra of vertical component (Z) of Tangar station

Investigation for seismic noise on vertical and horizontal components has been estimated using the data obtained during the field visit. Based on detailed noise survey, it has been observed that the noise level of all the stations except Tangar, remains within the low and high level globally accepted Peterson noise curves for estimating the station's performance. At Tangar station, high noise level when compared with other sites has been observed in the frequency band 1–3 Hz, but lies within the upper and lower bounds of Peterson curves. Noise spectra of vertical and horizontal components of Tangar (Dam axis) are shown in Fig. 2.

To monitor the seismic status of the various tectonic features in the area of Sawalkote H.E. project in a comprehensive way, five CMG 40 T seismographs with data acquisition system (DAS) and one GeoSIG make accelerograph have been installed. The sensitivity of the sensor is 1600 V/m/s and the data acquisition system is of 24 bits. A concrete block of $2'' \times 2''$ with proper anchorage to the ground has been constructed for keeping the sensor and digitizer. To minimize the noise, power supply has been kept away from the sensor. For uninterrupted power supply, solar panel along with electricity supply has been provided to record data continuously for a period of six months. Time synchronization has been done with the help of global positioning system (GPS). The seismic waveform has been recorded continuously at the rate of 100 samples per second. The study has been performed for 1.5° around the project site.

4 Analysis and Interpretations of Data

Various model of crustal velocity have been reported for the computation of theoretical trave time for the Himalayan region. Velocity model used for the present study is given in Table 2. This velocity model consists of six uniform layers with interfaces at depths 0.0, 10.0, 15.0 18.0 and 46.0 having P-wave velocity 5.27, 5.55, 5.75, 6.24 and 8.20 km/s, respectively. The location parameter has been selected when the

Table 2 Velocity model

Depth (Km)	P-wave velocity (Km/s)
0	5.27
10	5.55
15	5.45
18	6.24
46	8.20

RMS values of residuals between observed and calculated travel times are very less. The error associated with latitude, longitude and depth is considered to be less than 10 km, however in some cases the estimated error associated with latitude, longitude and depth is more than 10 km and for those for which depths are not calculated, the default depth is 15 km.

In SEISAN, magnitudes are calculated using coda, amplitude and spectral level. Parameters are given in the station file using the RESET TEST variables. For magnitude based on amplitude, the amplitude must be given in nanometers in the input file. In this study, the local magnitude of earthquake has been calculated using maximum trace amplitude. The formula used to calculate local magnitude M_L is

$$M_L = a \log_{10}(\text{amp}) + b \log_{10}(\text{dist}) + c\text{dist} + d$$

where a, b, c, d are constants, $\log_{10}$ is logarithm to the base 10, amp is maximum ground amplitude (zero-peak) in nm and dist is hypocentral distance in km. Following formula is used to calculate the magnitude

$$M_L = \log_{10}(\text{amp}) + 1.11 \log_{10}(\text{dist}) + 0.00189\text{dist} - 2.09$$

The gain of the Wood-Anderson instrument has been assumed as 2080. Amplitude of 1 mm of the Wood-Anderson seismogram is then 106 nm/2080 and inserting this amplitude in above expression with a distance of 100 km gives magnitude 3 as originally defined by Richter. Based on analysis and interpretation of recorded data for six months duration, it has been observed that, total of 776 earthquakes has been recorded ranging M_L from 0.5 to 5.8. Out of 776 earthquakes, 387 earthquakes have occurred within epicentral distance of 200 km from the project site. The maximum earthquake magnitude recorded within epicentral distance of 200 km during the study period is M_L 4.9. Magnitude wise distribution of 387 earthquakes events is given in Table 3. Epicentral distribution of these located 387 earthquakes is shown in Fig. 3.

During the study period of six months, total 70 earthquakes have been recorded within 50 km radius from dam axis, ranging M_L from 0.5 to 4.4. The depth range for these earthquakes are from 5 to 87 km. Figure 4 shows the distribution of earthquakes with tectonic features of the region with respect to depth within 50 km radius from dam site. Figures 5 and 6 show the distribution of earthquakes within 50 km with respect to epicentral distance and magnitude, respectively. Figure 7 shows a typical microearthquake event recorded of magnitude 5.8.

Table 3 Magnitude distribution

Magnitude	Number of events
$0.5 < M_L \leq 1.5$	191
$1.5 < M_L \leq 2.5$	147
$2.5 < M_L \leq 3.5$	36
$3.5 < M_L \leq 4.5$	9
$4.5 < M_L \leq 5.0$	4

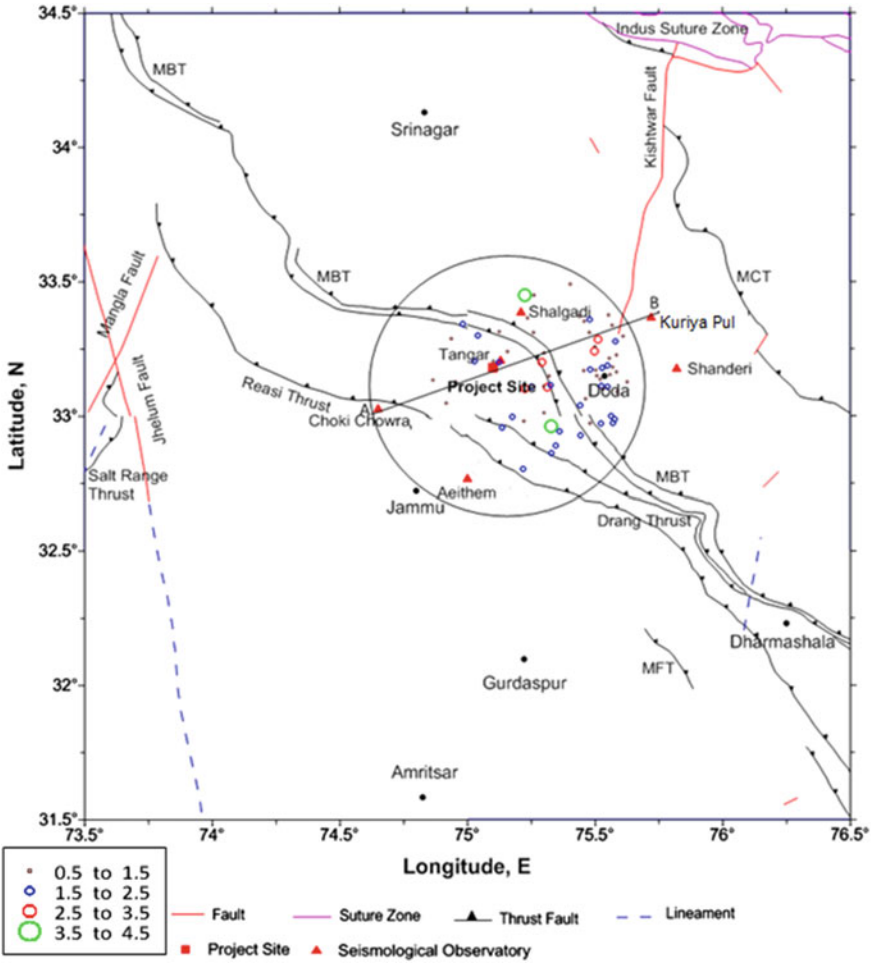

Fig. 3 Epicentral distribution of all located earthquakes within 50 km

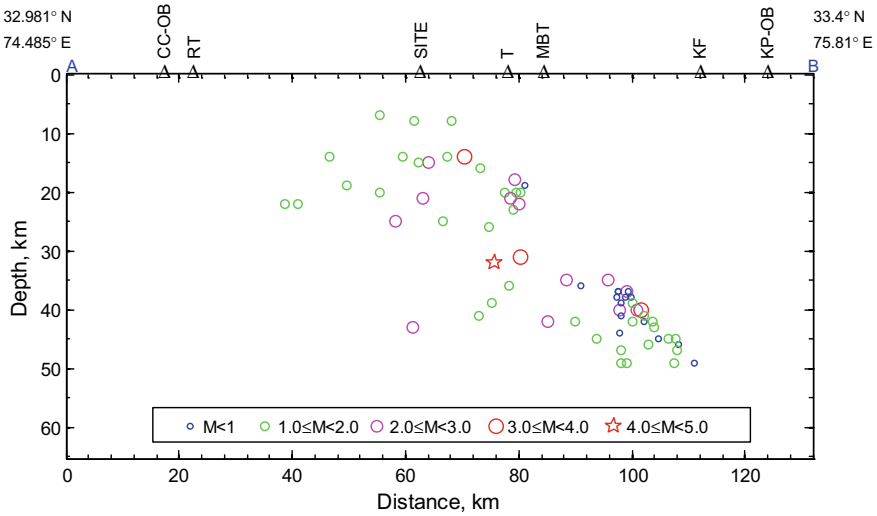

Fig. 4 Depth section of located earthquakes within 50 km radius from dam axis

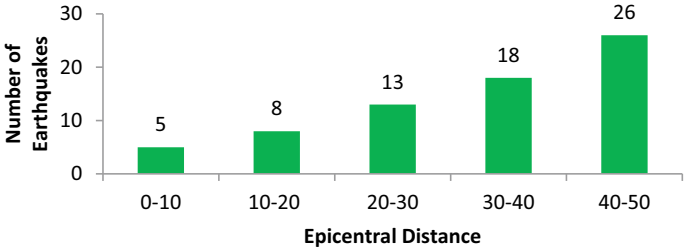

Fig. 5 Frequency distribution of earthquakes with epicentral distance within 50 km from dam

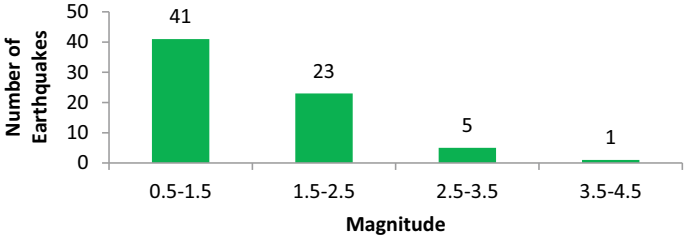

Fig. 6 Frequency distribution of earthquakes with magnitude within 50 km from dam site

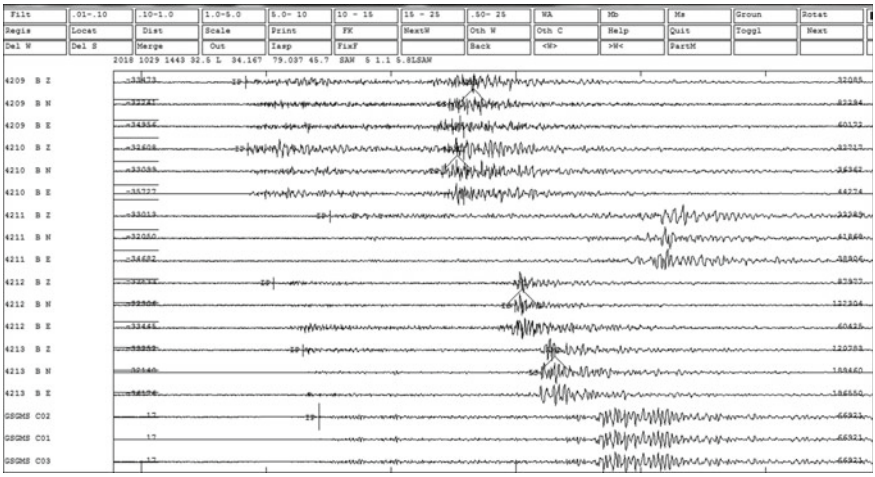

Fig. 7 Largest magnitude earthquake recorded by Sawalkote seismological network (ML 5.8)

The relationship between earthquakes magnitude of and their frequency of occurrence has been plotted empirically with power law relationship by Omori (1902). He plotted logarithmic plot of Tokyo earthquakes in terms of frequency distribution of maximum. The following relationship is explained in terms of Omori plot that was proposed by Ishimoto and Iida (1939):

$$n(A) = kA^{-m}$$

where $n(A)$ is the number of earthquakes of amplitude 'A' and magnitude m, and 'k' is a constant. Gutenberg and Richter [3] relationship between frequency and magnitudes is used to calculate seismicity parameters in probabilistic seismic hazard analysis. The classical equation of FMD can be described in terms of number of earthquakes occurring in a given region as a function of their magnitude 'M' as,

$$\log(N) = a - b * M$$

where 'N' is the cumulative number of earthquakes with magnitude equal to or more than M, and 'a' and 'b' are constant related to overall seismicity rate in a region and slope of the line obtained when magnitude is plotted against the logarithm of the number of events. An increase in applied stress or effective stress results in decreased b-value [7]. A smaller 'b' value probably means that the stress is high. Describing b-value is also related to the depth [5, 9] (Wyss et al. 1997, 2001). The b-value can be estimated either by linear least square regression or by maximum-likelihood method [2, 8].

In the present study, the six month data has been used starting from Oct 2018 to April 2019. A total of 387 events having magnitude range M_L 0.5 to M_L 4.9 within

Table 4 Magnitude frequency data analysis

M_L	N	Log(N)
1	387	2.587711
1.5	292	2.465383
2	190	2.278754
2.5	105	2.021189
3	49	1.690196
3.5	30	1.477121
4	13	1.113943
4.5	8	0.90309
5	4	0.60206

200 km from dam site has been considered for calculating '*a*' and '*b*' value. The '*a*' and '*b*' values obtained from Sawalkote seismological network are 3.323 and 0.516, respectively (Table 4).

5 Discussions of Results

A seismological network of six microearthquake observatories has been installed by around the project area to monitor the seismic potential of the project area for a period of six months. A total of 387 earthquakes has been recorded during the span of six months within 200 km having magnitude range M_L 0.5 to M_L 0.4.9. Only 70 earthquakes have been recorded within 50 km radius with depth up to 87 km. Only 5 events have been recorded within 10 km radius from dam axis. Total 387 events having magnitude range M_L 0.5 to M_L 4.9 within 200 km from dam site has been considered for calculating '*a*' and '*b*' value. The '*a*' and '*b*' values obtained from Sawalkote seismological network are 3.323 and 0.516, respectively.

6 Conclusions

In India, the hydroelectric projects are constructed in high mountain ranges which generally come in higher seismic zones. Seismic studies are necessary to assess seismic potential of the project site which comes under seismic zone IV and V. Microearthquake investigation is carried out in such areas to delineate the seismo tectonic features in and around the project site. This information is very vital in selection of location for important structures. Hence, before construction of major structures like dams microearthquake studies should be conducted.

References

1. Aki K (1965) Maximum likelihood estimate of b in the formula $\log N = a - b\,M$ and its confidence limits, Bull Earthquake Res Inst Tokyo Univ 43:237–239
2. Aki K (1995) Reviews of Geophysics 33:243–247. https://doi.org/10.1029/95RG00396
3. Gutenberg B, Richter CF (1944) Bulletin of the Seismological Society of America 34:185
4. Gutenberg B, Richter CF (1994) Frequency of earthquake in California. Bull Seism Soc Am 34(4):1985–1988
5. Mori J, Abercrombie RE (1997) J Geophys Research 102:15081–15090. https://doi.org/10.1029/97JB01356
6. Peterson J (1993) Observation and modeling of seismic background noise. U.S. Geological Survey open file Report
7. Urbancic TI, Trifu C-I, Long JM, Young RP (1992) Pure and Applied Geophysics 139:449
8. Ustu T (1965) A method for determining the value of b in a formula $\log N = a - bM$ showing the magnitude–frequency relation for earthquakes. Geophys Bull Hokkaido Univ 13:99–103
9. Wiemer S, Benoit JP (1996) Geophysical Research Letters 23:1557–1560. https://doi.org/10.1029/96GL01233
10. Wyss M (1973) Towards a physical understanding of earthquake-frequency distribution. Geophys J Roy Astron Soc 31:341–359
11. Wyss M (1973) Nature 242:255–256. https://doi.org/10.1038/242255a0

Risk and Uncertainty in Hydro-power Development in Uttarakhand Post Kedarnath and Chamoli Flood Disasters in Uttarakhand

S. K. Mazumder and Shivdayal Sharma

Abstract The state of Uttarakhand is situated in the upper reaches of the Indian sub-continent. It is also locally termed as—Dev Bhoomi as it houses many of the famous temples attracting millions of tourists and pilgrims from within and outside the country. This state is also blessed with rivers fed by natural glaciers as well as rains contributing to a huge hydro-power potential. (UJVNL) The main source of income for the state is through hydro-power development and tourism. The state having a hilly terrain does not support the establishment of large industries, and hence, migration is increasing year by year. Thus, promoting hydro-power production and promotion of tourism are some of the feasible options for economic development. If hydro-power development is scuttled, it will be difficult to arrest mass migrations from these states. Uttarakhand has a hydro-power potential of the order of 20,000 MW against which only about 3164 MW (16% approx.) has been harnessed so far (Agarwal and Kansal in Water Energy Int 59, 2017). The state is gifted by nature with rivers like Ganga, Yamuna, Kosi providing an ideal location for hydro-power development. Unfortunately, most of hydro-power projects under development were stayed by The Supreme Court of India (2013) after Kedarnath flood disasters that occurred in Uttarakhand in June-2013. Situation has worsened further after the current Chamoli flood in Feb-2021. In the present paper, authors have discussed about the above flood disasters and their impact on hydro-power development in the state.

Keywords Hydro-power · Glacier · Landslide · Flood · Sedimentation Uttarakhand

S. K. Mazumder
Civil Engineering, DCE(nowDTU), Delhi, India
URL: https://www.profskmazumder.com

S. Sharma (✉)
Expert—Hydrology and Hydraulics, M/S Growever Infra Pvt Ltd, Delhi, India
e-mail: shivdayal.sharma@gmail.com

P. V. Timbadiya et al. (eds.), *Flood Forecasting and Hydraulic Structures*, Lecture Notes in Civil Engineering 340, https://doi.org/10.1007/978-981-99-1890-4_39

1 Introduction

After independence, the necessity of constructing water-resource and hydro-power projects was felt, and many multi-purpose projects were conceived and executed. Uttarakhand was formed out of Uttar Pradesh after the bifurcation of the state in the year 2000. The status of an independent state, however, brought in pressures on the Govt. for development of infrastructures of Uttarakhand including its capital Dehradun. The growth process in Uttarakhand has been limited to the plain districts eluding the hilly areas, as most of the manufacturing units are located in the plain districts. There is an urgent need for meeting the productive employment demands of the poor population in the state. This can be achieved through an efficient and reliable access to energy for the rural population. The development, dependent on the conventional energy sources for the plains, might not prove much effective in the hills due to its difficult terrain.

2 Natural Resources of Uttarakhand

The state lies in the Himalayan range and has a highly diversified topography. The climate and vegetation vary greatly with elevation, from glaciers at the highest elevations to subtropical forests at the lower elevations. The highest elevations are covered with ice and bare rocks. Only three districts, namely Dehradun, Udham Singh Nagar, and Haridwar, lie mainly in the plains. The rest of the thirteen districts lie primarily in the hilly regions. The Yamuna and the Ganga—the two major rivers in the western Himalayan region—directly impact the lives of a large population living in the northern part of India, more so in Uttarakhand. The glacier-fed rivers of Uttarakhand are an important resource for the Ganga basin, with many rivers contributing to the irrigation potential of some of India's most densely populated states such as Uttar Pradesh, Bihar, Delhi, and Haryana. Despite the presence of glaciers and perennial rivers in the state, in addition to plenty of rainfall, the availability of water to local people is not up to expectations due to lack of storage.

3 Natural Disasters

Owing to the fragility of its mountain, economy of the state of Uttarakhand is vulnerable to natural disasters [5] due to a number of reasons, e.g. earthquake, wild fire/forest fire, landslides, floods, etc. During the last five years, the residents in Uttarkashi, Bageshwar, Rudraprayag, and Pauri Garhwal districts (Fig. 1) reported that the same in higher proportion and the loss of life/property/assets/livelihoods, etc., from floods was reported as far greater compared to earthquakes.

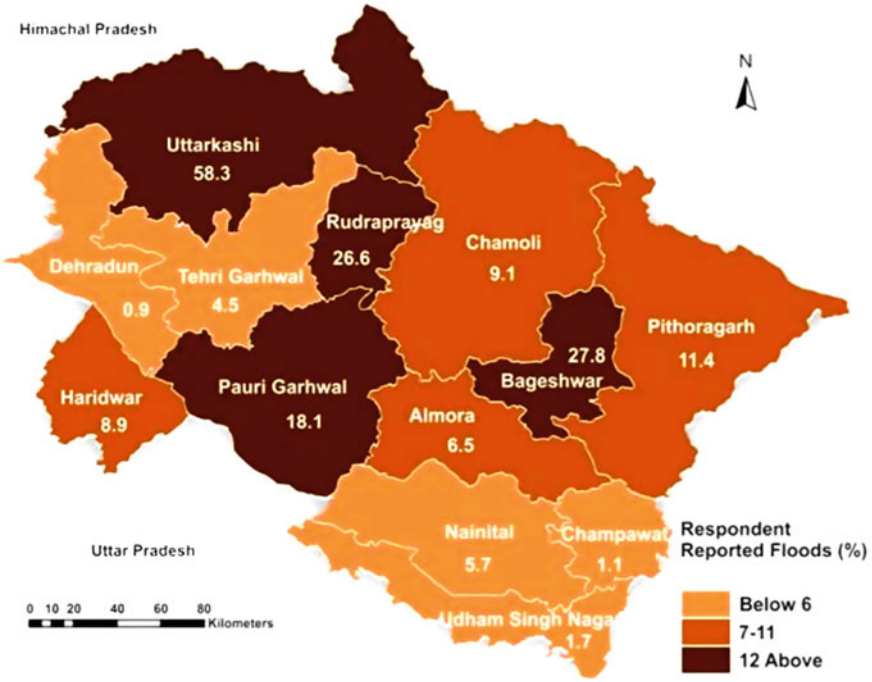

Fig. 1 Uttarakhand districts vulnerable to floods (%). *Source* Aggarawal [1]

4 Kedarnath Flood

In June 2013, a mid-day cloudburst centred the North Indian state of Uttarakhand caused devastating floods and landslides, becoming the country's worst natural disaster since the 2004 tsunami. Debris blocked the rivers, causing major overflow. More than 5700 people were "presumed dead by 16 July, 2013". Destruction of bridges and roads left about 300,000 pilgrims and tourists trapped in the valleys leading to three of the four Hindu Chota Char Dham pilgrimage sites. A joint study by the World Bank and the Asian Development Bank estimated that damage (Fig. 2a and b) to public infrastructure—roads, water transport, buildings—amounted to nearly $700 million [8].

5 Causes of the 2013 Flood Disaster

Large parts of the state experienced about 250–400 mm rainfall. The uppermost glacial region between Gangotri to the Nandadevi National Park received an estimated 350–400 mm in a period of about 48–72 h. Meteorological studies indicate that during the 1960s, the day and night temperature on mountains was the same. But

Fig. 2 **a** Destruction of buildings, **b** damage of roads [5]

in the last decade, the day temperature has increased considerably as compared to the night temperature building situation of cloud bursting and flash floods. Besides rainfall, rampant deforestation, slope cutting, blasting of rocks, haphazard disposal of debris, and riverbank constructions were also responsible for the huge destruction. The government also got pressurized and resorted to rapidly widen the roads and other infrastructure so as to accommodate the tourist inflow which is a major source of livelihood for a large number of people of the state. All these caused devastating floods and landslides in the Kedar valley and many other river valleys of Uttarakhand as shown in Fig. 3 [11, 12].

6 Chamoli Flood

The Chamoli flood disaster began on 7 February 2021 in the environs of the Nanda Devi National Park, a UNESCO World Heritage Site in Uttarakhand. It was caused by a large rock and ice avalanche consisting of material dislodged from Ronti peak. It caused flooding in the Chamoli district, most notably in the Rishiganga river, the Dhauliganga river, and in turn the Alaknanda—the major headstream of the Ganges. The disaster left over 200 killed or missing, most were workers at the Tapovan dam site [9].

7 Sequence of Events

- Chamoli floods occurred on 7–8 Feb. due to landslide triggered by detachment of massive rock from Nandadevi glacier from an elevation of 5600 to 3800 msl.

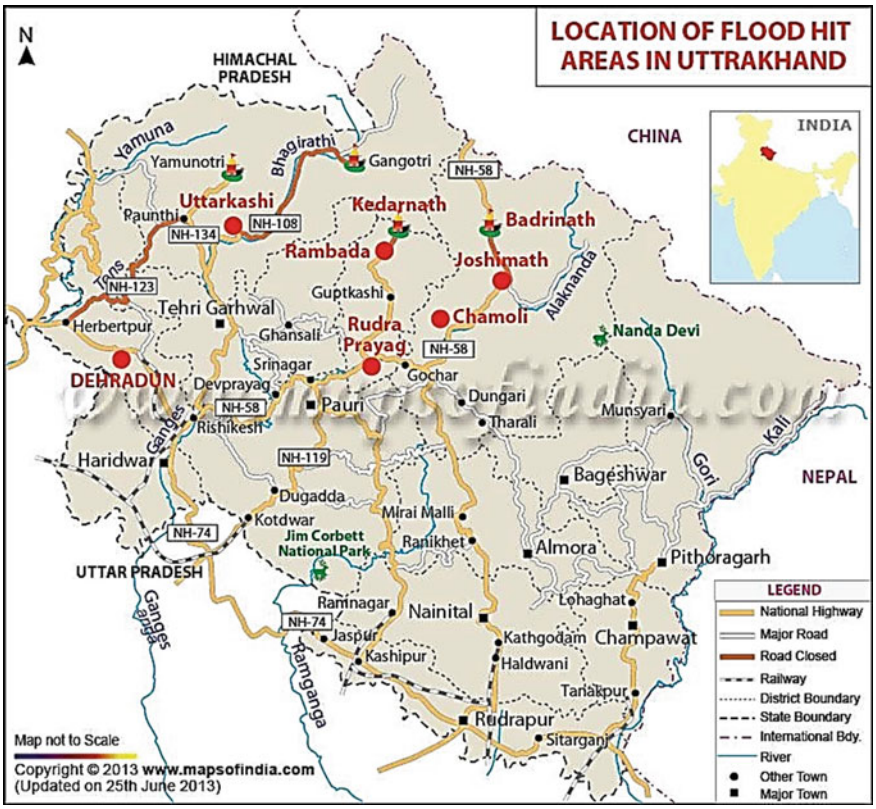

Fig. 3 Location of flood hit (June, 2013) areas in Uttarakhand

- Large amount of snow/mud/sediment/boulder/debris brought by the landslide caused aggradation of river bed and consequent rise in flood levels in the rivers Rishiganga and Dhauliganga and Alkananda—all tributaries of river Ganga.
- Due to steep slope of the terrain (S), heat generated in friction caused melting of snow and sudden increase in flow magnitude (Q), flow velocity (V), and stream power ($P = \gamma QS$) resulting in wash out of several bridges and barrages and damage to several hydel projects under operation/construction in the valley.

8 Causes of Chamoli Flood

Outer Garhwal Himalayas in Uttarakhand state, the average minimum temperature in the area falls below zero degree (Fig. 4a). There is a steady rise in maximum temperature in the area (Fig. 4b) over the years (1980–2019) due to global warming/climate change. Also, the area is subjected to high rainfall (Fig. 5) in February and July. It is believed these climatic factors caused landslide, avalanche, or a glacial lake outburst

flood (GLOF), resulting in flooding of Chamoli district, after a portion of the Nanda Devi glacier broke off. A large ice avalanche was previously released somewhere between 19 September and 9 October 2016 (Fig. 6), which caused deposition of ice ~ 1.5 * 10^7 m^3 and bedrock in the valley below. The resulting destabilization of the rock mass was due to the lack of ice cover, glacial de-buttressing, stress-release fracturing and increased exposure to solar radiation. An increased freeze–thaw cycle, in combination with a large snowfall event, preceding the event of 7 February 2021 and rapid melt water production, may have favoured the fracturing of rock. Fracture zones at the runout of the rockslide visible before the event suggest that such detachments have happened at the same location previously too. Permafrost thaw and frost cracking has been used to explain increased rockfall activity in the Alps [6, 7]. At roughly 5600 above msl, a crack had formed on the side of the mountain. Researchers monitored satellite images to investigate the cause of landslide; but it is difficult to conclude. Crack can be seen in Fig. 7a in a satellite image of the peak, which was captured on 2 February—five days before the disaster. The horizontal line of the crack is much more visible when the satellite is zoomed in, as shown in Fig. 7b. Using satellite imageries, it was possible to see that the crack had been developing for some time—with evidence of the first crack visible in the satellite image from 1 January 2020. Enormous block of rock and ice fell into the valley on 7 February. It is estimated that the block was over 2 million cubic metres in size and fell nearly 2 km, almost vertically, before impinging on the valley floor. As mentioned, the block fell 1800 m (from 5600 to 3800 masl) into the valley below. Dr Scott Watson, [3, 4], University of Leeds, believes that the mass of rock and ice ploughed through a deposit of rock and ice due to the lack of ice cover, glacial de-buttressing, stress-release fracturing, and previous avalanche in 2016 triggering landslide with a huge trail of dust as it travelled down the valley generating immense heat and melting of ice illustrated in Fig. 8a and b.

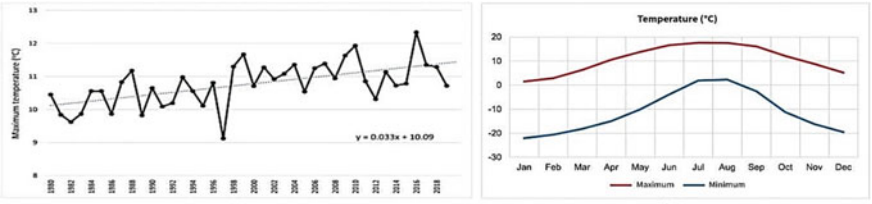

(a) (b)

Fig. 4 **a** Average monthly temperature. Maximum temperature trends in the Chamoli area. *Data source* ERA5 reanalysis data, 1980–2019

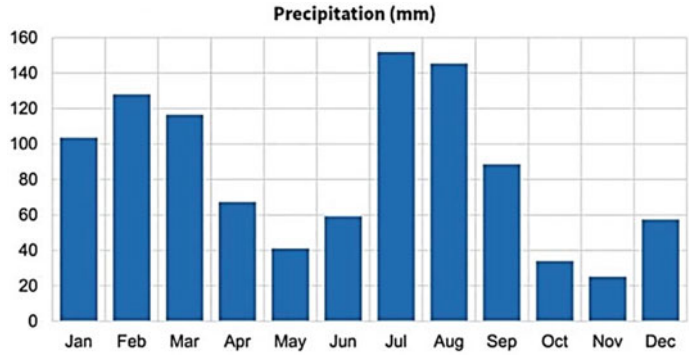

Fig. 5 Average monthly precipitation of the area (1980–2019)

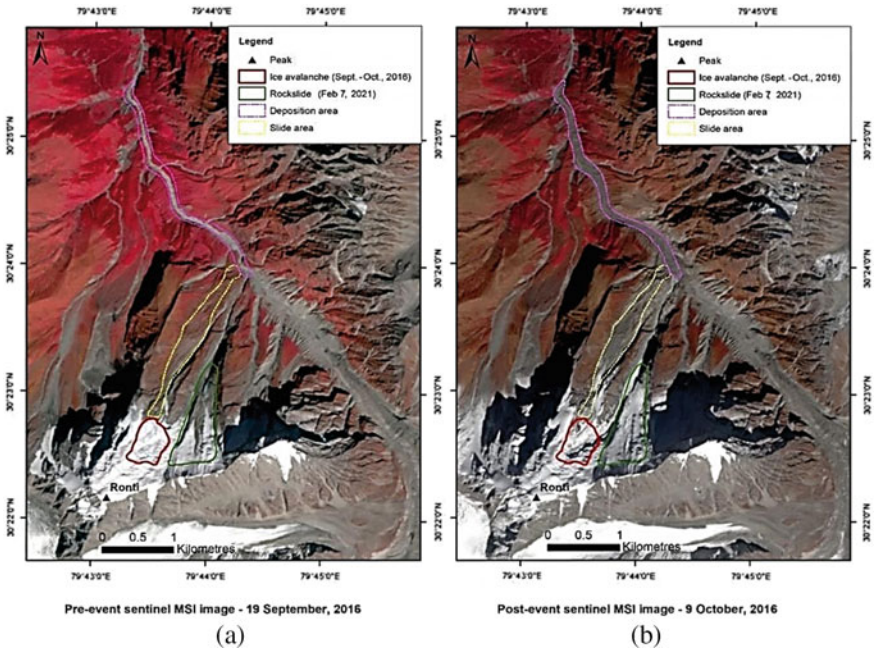

Fig. 6 **a** Pre event picture, **b** post event pictures showing avalanches

9 Risk and Uncertainty of Hydro-power Development in Uttarakhand

The flash floods have raised public anger over hydro-power projects that the government considers essential to decarbonize the nation's electricity generation. Experts say that the event, induced by the effect of global warming on melting glaciers, was

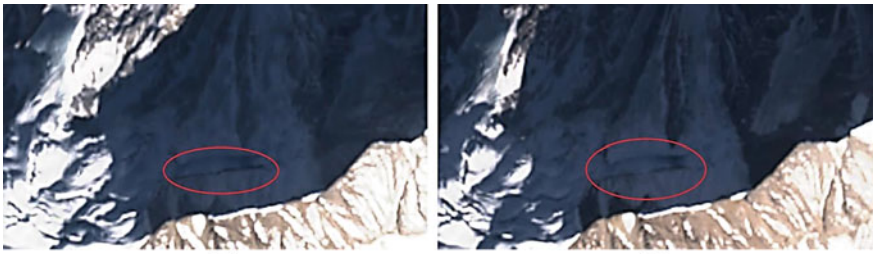

(a) (b)

Fig. 7 Close-up view of the crack propagating in the mountain. Pic: SentinelHub

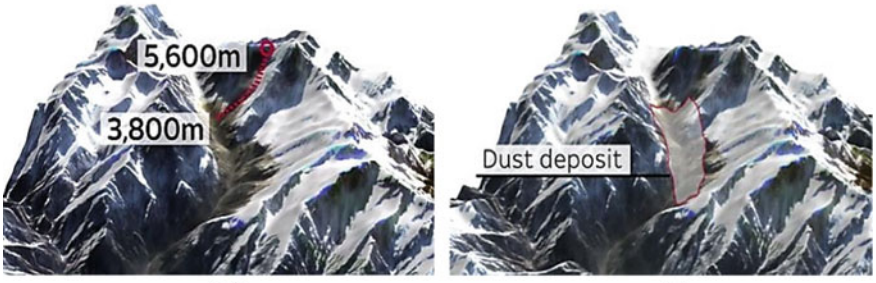

(a) (b)

Fig. 8 **a** Rock/Ice mass fall hilltop to valley. Huge trail of dust (red) in the valley. Satellite Image: Dr Scott Watson, COMET, University of Leeds

made worse by construction of infrastructures like roads and hydro-power plants. Large-scale blasting, tree felling and tunnelling, and loss of sensitive eco-system most certainly add to the risk and uncertainty of hydro-power projects planned by the Govt. of India for the development of the country in general and Uttarakhand in particular. As per Himanshu Thakkar, Anon [3] coordinator of the New Delhi-based South Asia Network on Dams, Rivers and People [4], which studies the social and environmental impact of water-related projects in India—they are a force multiplier in the destruction. Table 1 gives the details of damages due to Chamoli flood in 2021. The fate of NTPC's 520-MW Tapovan-Vishnugad hydel project hangs in balance as India's largest power company is estimated to have suffered a loss of Rs. 1500 crore due to damage to their construction caused by the flash flood. The event and related avalanche made of debris flow/flood caused damage to four hydro-power projects along the Rishi Ganga, Dhauliganga, and Alaknanda River path. The Rishi Ganga Hydro-power Project (13.2 MW) near Raini village, located 14 km downstream from the impact site, was the first to be hit by the debris after the rockslide. The unfinished Tapovan-Vishnugad Hydro-power Project (520 MW), 8 km downstream from Rishi Ganga Hydro-power Project, was the second hydro-power plant hit by the flood. The diversion dam of this run-of-the river type project faced massive damage from sedimentation and the dam was filled with debris, which can be seen

Table 1 Hydro-power projects damaged in Chamoli flood

S. No	Name	(Latitude/ longitude)	Capacity (status)
1	Rishi Ganga Hydro-power Project	30.478/ 79.699	13.2 MW (operational)
2	Tapovan-Vishnugad Hydro-power Project	30.493/ 79.628	520 MW (under construction)
3	Vishnuprayag Hydro-electric Project (Jaypee Group)	30.566/ 79.547	400 MW (operational)
4	Vishnugad Pipalkoti Hydro-electric Project	30.433/ 79.424	444 MW (under construction)

in the remote sensing images taken before and after the event. Two power projects NTPC's Tapovan-Vishnugad hydel project and the Rishi Ganga Hydel Project were extensively damaged with scores of labourers trapped in tunnels as the waters came rushing in. At least 32 people were dead and over 190 missing.

The risk and uncertainty in the development of hydro-power in the Himalayan areas in general and Uttarakhand in particular after the disasters of 2013 and 2021 floods have to be accepted. The only way to overcome such uncertainty and risk lies in more advanced research study [10] of the Himalayan area with high untapped potential for future development of hydro-power in the Himalayan region in general and Uttarakhand in particular.

10 Summary and Recommendations

Conservation of environment is a serious issue all over the world. It is more so in states like Uttarakhand—a land that witnessed the Chipko Movement. India is a developing country, and the country needs electric power for the development of its infrastructure and livelihood opportunities for the large and aspiring Indian population. In the light of this, we have to decide the suitability of hydro-electric projects in the Himalayan states like Uttarakhand where thermal and solar power generation are not popular due to non-availability of coal and its undulating terrain full of mountains.

The Himalayas are the source of a large number of perennial rivers. The slope of the mountains is very steep with largely uninhabited valleys at many places. Due to nature's gift of water and terrain head, run-off the river type hydro-electric development is ideal for power generation. However, the floods of 2013 and 2021 cast shadow on the Govt. proposal as it was found that dams like The Tehri actually acted like a flood-control measure. It should, however, not forgotten that risks and uncertainty are there in all walks of life. Attempt must be made to analyse and understand the risk with real-time data obtained from both physical survey and remotely sensed satellite imageries–areas where India has made phenomenal progress over the years.

Real-time and accurate data about meteorological conditions can help to better regulate the reservoir levels to accommodate and forecast the floods. More research in the area of climatology is the need of the hour to accurately predict rainfall and other extreme events like cloudburst, etc., so that the reservoirs can be emptied before the rains. The construction activities need to be regulated, and zoning norms need to be developed scientifically in areas near river banks and implemented strictly. Many studies have revealed that the debris left over near the river banks during construction of dam's flow back into the river increasing the sediment load of rivers during the floods. The government agencies should frame clear-cut rules for the disposal of left-over debris in dam construction sites. Safety measures also need to be implemented and developed during the construction stage. The construction activities should also be properly rescheduled keeping in mind the rainfall season.

It is necessary to undertake model studies of the structures across the rivers to develop a prior understanding of river behaviour after construction and particularly during massive floods. Disaster preparedness is also critical because all of the Himalayan states lie either in seismic Zone IV or V. These areas are the most vulnerable to strong earthquakes. The disaster management plans of HEPs need to be carefully reviewed and approved. The local communities must be involved in all stages of the project right from inception to monitoring to operation. Afforestation must be done in tracts that are denuded. The selection of trees should be made judiciously taking local conditions into account. There are some varieties of vegetation that arrest erosion and hold the soil. Such varieties should be planted in sites denuded by construction of dams. In the design of hydraulic structures planned in the slide prone areas like Uttarakhand, it is essential to consider the extraordinary rise in water level due to landslides and consequent aggradation and sudden rise in flood level (HFL) much higher than the normal design HFL corresponding to design HFL of a given return period.

References

1. Aggarwal V (2021) Climate change impact on Water Power Project in Himalayan Region—acase study for Chamoli district of Uttarakhand. M. Tech. thesis submitted to Dehi Technology University, Delhi
2. Agarwal S, Kansal M (2017). Issues of hydropower development in Uttarakhand region of Indian Himalaya. Water Energy Int 59
3. Anon n.d. (2021a) Himanshu Thakkar—SANDRP. Retrieved 22 May 2021a. https://sandrp.in/tag/himanshu-thakkar/
4. Anon n.d. (2021b) The catastrophic landslide and flood in Chamoli in Uttarakhand: the sequence of events—the landslide blog—AGU blogosphere. Retrieved 22 May 2021b. https://blogs.agu.org/landslideblog/2021/02/08/chamoli-2/
5. CBIP (2013) Natural disaters with special reference to Uttarakhand. Souvenir Publication by CBIP
6. Deline P, Gruber S, Delaloye R, Fischer L, Geertsema M, Giardino M, Hasler A, Kirkbride M, Krautblatter M, Magnin F, McColl S, Ravanel L, Schoeneich P (2014) Ice loss and slope stability in high-mountain regions. In: Snow and ice-related hazards, risks, and disasters. Elsevier Inc., pp 521–561

7. Gruberber S, Haeberli W (2007) Permafrost in steep bedrock slopes and its temperatures-related destabilization following climate change. J Geophys Res Earth Surf 112(2):2–18. https://doi.org/10.1029/2006JF000547
8. Madan MM (2013) Hydro-power-a key to disaster management. Paper publication in the souvenir of natural disasters with special reference to Uttarakhand—org. CBIP, New Delhi
9. Mazumder SK (2021) Future of hydro-power development in Himalayas post Chamoli Flood Disaster. J 'Viewpoint'. CEAI, June
10. Mazumder SK (2017) Hydro power development—some problems and remedial measures. Invited paper published in the ISH News bulletin by Indian Society for Hydraulics, Vol 26, No 1 and 2, March–July
11. Mazumder SK (2014) Flood damages in Kedarnath and its impact on hydro-power development. ISH News Lett 23(1)
12. Misra RN, Aggarwal SC, Sharma A (2013) Disaster in Uttarakhand—its causes, impact on infrastructure development and mitigation measures. Paper published in the Souvenir of natural disasters with special reference to Uttarakhand—org. CBIP, New Delhi, Dec 2
13. Supreme Court of India (2013) Report of expert body constituted on the directions issued by the Hon'ble Supreme Court of India—vide judgment dated 13.08.2013 in the case of Alaknanda Hydro Power Co. Ltd. versus Anuj Joshi & others arising out of Civil Appeal no. 6736 of2013 (SLP (C) no. 362) of 2012), with appeal no. 6746–6747 of 2013 arising out of SLP (C) no. 5849–5850 of 2012 and TC (C) no. 55–57 of 2013. assessment of environmental degradation and impact of hydroelectric projects during the June 2013 Disaster in Uttarakhand
14. UJVNL Hydropower projects in Uttarakhand. https://www.ujvnl.com/hydro-power-projects-in-Uttarakhand

Logging and Tracer Study—An Integral Part of NDT for Seepage Through Hydraulic Structures

Rolland Andrade, Amol Chunade, and B. Suresh Kumar

Abstract Effective and efficient practices towards structural management are necessary in order to get appropriate solution to problems pertaining to the maintenance, rehabilitation and safety of hydraulic structures. Majority of the present hydraulic structures in India are withering due to age and hence pose structural deterioration and distress. Suitable planning, assessment and diagnosis are necessary in order to decipher the cause, so as to implement suitable remedial measures to repair and ensure their safety. Distresses in the body of the dam and canals, viz. fissures, volume expansion, deformation, etc., may lead to structural failure, which can be catastrophic both in terms of property and life. The risk of structural failures can be reduced by regular inspections and monitoring, identifying the deficiencies or flaws and accordingly implementation of a comprehensive rehabilitation measure. In the recent past, the awareness towards dam safety has encouraged the development of numerous techniques, which are capable of identifying the location of seepage through body or foundation of hydraulic structures, hence preventing them from disaster. Here the authors have highlighted the effectiveness of an integrated approach towards deciphering of seepage, through well logging and tracer study in hydraulic structures; and the remedial measures with relevant case studies. Borehole logging and tracer study forms an integral part of non-destructive technique (NDT); hence, they can be extended for delineating the path of seepage through any hydraulic structure(s).

Keywords Borehole logging · Tracer · Seepage · Hydraulic structures

R. Andrade (✉) · A. Chunade
Isotope Hydrology Division, Central Water and Power Research Station, Pune 411024, India
e-mail: andrade.rolland@gmail.com

B. Suresh Kumar
Hydraulic Analysis and Prototype Testing Division, Central Water and Power Research Station, Pune 411024, India

P. V. Timbadiya et al. (eds.), *Flood Forecasting and Hydraulic Structures*, Lecture Notes in Civil Engineering 340, https://doi.org/10.1007/978-981-99-1890-4_40

1 Introduction

Safety of hydraulic structures, especially dams, canals, hydropower plants, etc., is of utmost importance for safeguarding these national assets and the benefits derived from them. Even though utmost care is taken in planning, designing and execution stages, there are incidences of distress in these hydraulic structures. Dam failures in the past have been further aggravated by the fact that majority of the dams does not have proper supervision and maintenance which is needed for assuring their structural safety and operational integrity. Hence, it is necessary that the dams should be reassessed for their safety through modern approaches and standards. Health evaluation of a dam is a vital parameter from the dam safety management point of view. Almost every dam experiences certain amount of seepage as the impounded water seeks the path of least resistance through the structure. Generally, seepage is noticed through the body of the dam, the structure–foundation interface or through the geological inhomogeneities present in the nearest vicinity of the structure. Location of source of seepage and timely remediation can avert a catastrophe [1]. In order to determine the safety aspects of any hydraulic structure, it is very essential to identify the areas of water loss and seepage entry points through the structures as precisely as possible. This information is extremely crucial for adapting the remedial measures necessary to decrease or avert seepage and thus may provide a cost effective solution.

In the recent past, many investigation techniques/methods have been developed through state-of-the-art technology towards detecting and mapping seepage through hydraulic structures. Water balance, flow velocity, tracers, temperature, infrared ray sensing, acoustic emission and geophysical methods are few such methods. Among these, 'borehole logging' and 'tracer technique' are non-destructive (NDT) and are also cost-effective tools adopted in assessing the safety of hydraulic structures. Moreover, it aids in evaluating the efficacy of remedial measures. In this paper, the authors have highlighted the effective use of borehole logging and tracer technique in deciphering the source of seepage and also to delineate the seepage path through dams and canals. A conceptual model portraying the application of these two methods in dam site (see Fig. 1), to reduce the seepage from the dam.

2 Causes of Distress in Hydraulic Structures

There are several reasons identified towards seepage through dams and canals, mostly on the basis of types of hydraulics structures.

- Earthen dams: Seepage mainly occurs through the embankment, foundation and through abutments, probably due to absence of filter protection or improper filter design, washing out of particles or blockage of drains, poor compaction, open seams, cracks caused by earth movement, etc.

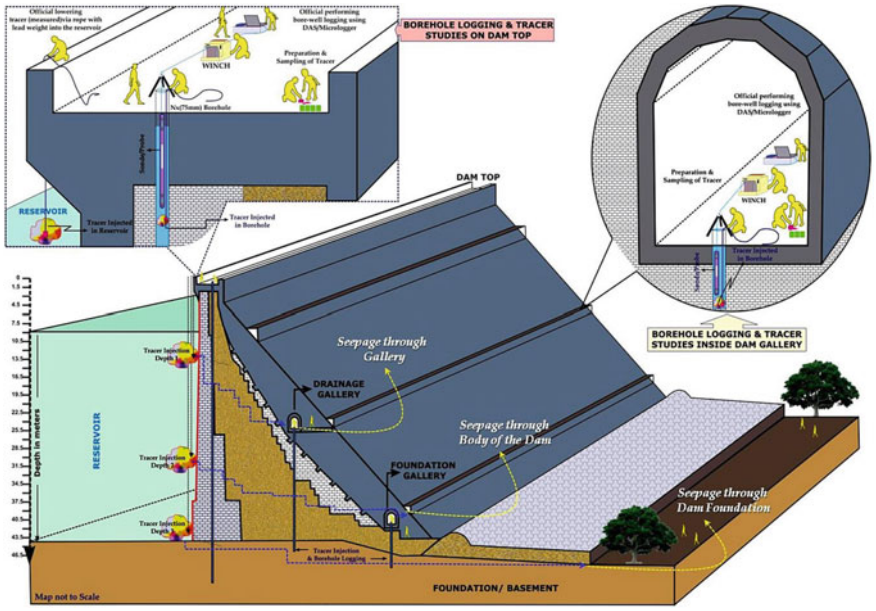

Fig. 1 Conceptual model showing well logging and tracer studies carried over a dam body

- Masonry dams: Seepage path is mainly through the body caused by absorption of moisture by the weak zone, temperature effects, leaching, extreme uplift pressure, deficiencies in the construction, etc. as shown in Fig. 2.
- Concrete dams: Deficiencies during construction, disintegration and scaling, erosion, efflorescence, cracks, etc. are the major causes for seepage.

Inappropriate site investigation towards geological foundations can also be a key factor towards dam seepage resulting in their failures. The transition between the masonry (or) concrete dam and earthen dam demands special care and detailing during its designing and construction phase, as it comprises discontinuity in the material property; hence, the same may cause reservoir water to move from upstream portion to downstream portion, through the contact surface of masonry/concrete and in earthen dam at their junction. Hence, it is necessary to attend such problems in order to avert possible structural failure.

3 Techniques: Seepage Detection

Seepage through hydraulic structure is an intricate problem in the field of geotechnical engineering; as the hydraulic structures are heterogeneous, nonlinear and anisotropic in nature. Hence, seepage studies pertaining to any hydraulic structure should involve

Fig. 2 Schematic representations of different types of distresses in hydraulic structures

regular physical inspection, detailed information of the site geology and hydrogeological information of the affected area. A single investigation technique will not be sufficient to detect or identify seepage; hence, a combination of technique(s) may result in successful leakage detection. There are several methods of which the non-destructive testing (NDT) is widely adopted to ascertain the exact path and source of seepage. Tracer and well logging studies are aptly integrated to decipher the source and extent of seepage and also to decipher mechanical properties towards strengthening of the structures. Integration of these two investigation methods can depict the in-situ engineering properties, potential seepage pathways, lithological variations, solution activity and interconnectivity of seepage path. Consequently, a most suitable remedial measure(s) can be adopted to rehabilitate the same.

3.1 Borehole Logging Techniques

Borehole logging technique is used in seepage investigations for identifying cracks/voids and permeable zones, in and around any hydraulic structure. The techniques are also applied for detecting engineering parameters of dam like bulk density, sonic velocities and mechanical properties of the rock. Basically, the study involves lowering of a sensing device (probes/sonde) in a borehole (preferably Nx size) and to

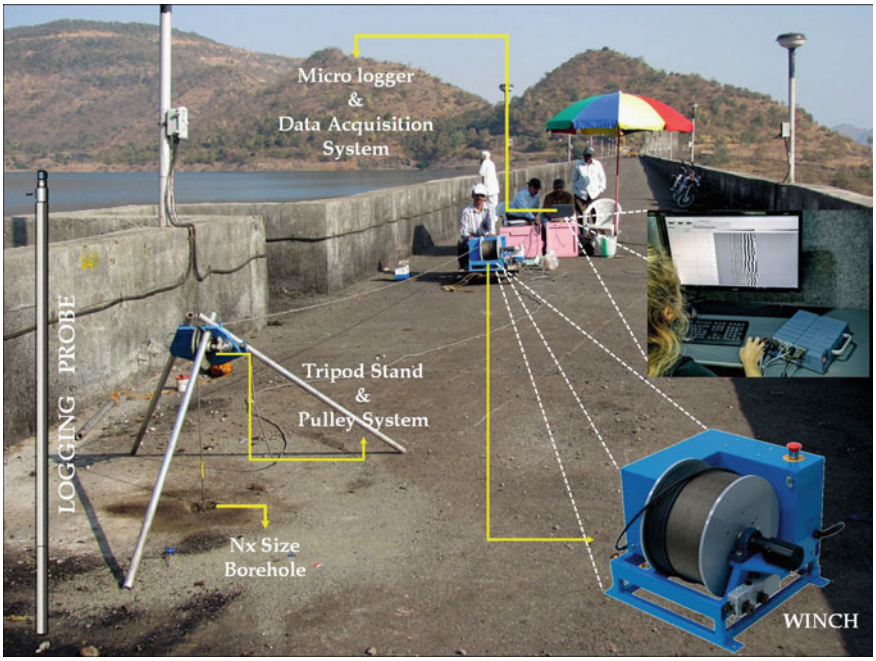

Fig. 3 Schematic representation of borehole logging carried out at dam top

obtain a continuous record of depth measurement (vs.) variation in certain physical properties of rocks/lithology in the bore hole (see Fig. 3). The subsurface geological conditions and physical properties can be determined directly or indirectly from the properties measured by these techniques. Borehole logs are analysed and interpreted to decipher the subsurface lithological variations, formation geometry, resistivity, porosity, compressional and shear wave velocities (V_p and V_s), moisture content, water bearing strata and movement of water.

3.2 Gamma-Gamma (Density) Logging

It is basically the record of the intensity of gamma radiation emitted from a gamma source present with the probe after it is back scattered, and the same is attenuated within the borehole and surrounding rocks. Gamma log is used mainly towards the measurement of bulk density and porosity of rocks. A radioactive source of a thallium-activated sodium iodide crystal, and a photo-multiplier tube contained in this logging probe emits medium energy gamma rays into the formations. Later, these gamma rays collide with the electrons in the formation. During each collision, the gamma ray loses a certain amount of its energy to the electron and further continues with diminished energy. This type of interaction is called Compton scattering. Density

probe is so designed that the tool response is predominantly due to this phenomenon. Attenuation of gamma radiation is proportional to the bulk density of material it passes through [2]. Sonde used for density logging contains a concentrated source of mono-energetic gamma rays, 10 mCi (milli curie), Caesium—137 gamma source or Cobalt-60 (^{60}Co), the detector usually a scintillation counter. Since the tool is short, adjacent beds or bed thickness have little distorting effect. The instrument must be calibrated for different formation densities and hole diameter. The errors in bulk density obtained by this method are of the order of ± 5%. Porosity can be derived from bulk density by the relation

$$\text{Porosity} = \frac{\text{Grain density} - \text{Bulk density}}{\text{Grain density} - \text{Fluid density}}$$

Grain density can be derived from laboratory analyses of cores samples. Fluid density in most water wells may be assumed to be 1 gm/cm^3. Errors in porosity calculated from density log depend on the accuracy of grain and fluid densities used.

3.3 Calliper Logging

It is a continuous record of change in the borehole diameter measured by a probe equipped with tensioned mechanical arms or an acoustic transducer. This log is essential in interpreting other logs that are affected by changes in borehole diameter [2]. Calliper log is recommended to be carried out in all boreholes. It also provides indirect information on the subsurface lithology and rock quality. Borehole diameter usually varies with the hardness of the strata, presence of fracture and also cementation of subsurface material. It can identify the porous zones in a borehole by deciphering the depth of each zone, which shows the presence of excessive mud filter cake that gets built up on the walls of the borehole.

Calliper probes are basically electromagnetic device having one or more number of arm (i.e. two, three, four or six) probe designs. The electrical signals are transmitted to the surface through an armoured cable. Some calliper systems average the movement of all the arms and record only the change in average diameter with depth.

3.4 Acoustic/Sonic Logging

This system uses medium- to high-frequency acoustic (sonic) energy transmitted from a sonde in order to acquire seismic velocities of the geologic or in-situ material in the borehole. The frequency spectrum of the wave depends on the source frequency spectrum and is usually in the 5–30 kHz range [3]. It is basically a record of transit time of an acoustic pulse between a transmitter and receiver embedded in a probe. Sonic logging is generally used for porosity measurement and identification

of fractures. Basically, all acoustic logging devices contain one or two transmitters that convert electrical energy to acoustic energy, which is transmitted through the environment as an acoustic wave. The receivers then convert the acoustic energy back into electrical energy for transmission up the cable. The transmission velocity of the seismic waves can be calculated by travel times and distance travelled from transmitter to receiver. There are generally two basic types of acoustic waves received after transmissions through the rocks, i.e. compressional or *P* waves, shear or *S* waves, and surface waves. Compressional waves travel faster and hence arrive first, followed by the shear waves and the surface waves. The radius of investigation of the sonic tool varies with frequency and wavelength of the elastic wave as well as with the sonic velocity. It is reported to be 3 times the wavelength [4].

3.5 Tracer Techniques

Tracer technique is basically injecting a predetermined quantity of tracer into a borehole located near to the suspected seepage zone of the hydraulic structure and observing either the dilution of the tracer in the injection bore holes itself or by detecting its arrival in the observation bore holes located near the injection boreholes in the probable direction of seepage [5]. Tracers are generally non-hazardous and non-toxic chemical compounds, salts or dyes behaving exactly similar to the materials to be traced but differ from them by a particular property, which may be either physical or chemical including radiochemical [6]. Classification of tracers are categorized into two groups: (i) Conventional tracers and (ii) isotope tracers including stable isotopes, viz. ^{13}C, ^{2}H, ^{18}O, environmental isotopes, viz. tritium, heat, etc. and unstable isotopes like ^{3}H, ^{51}Cr, ^{60}Co, etc. [7].

3.6 Laboratory Fluorometer

A fluorometer is a device, wherein the light from a lamp is allowed to pass through an excitation filter that transmits light of wavelength range similar to that of the sample compound to be measured. The light then passes through the sample, which emits light proportional to the intensity of the exciting light. The emitted light is then allowed to pass through an emission filter that selects the appropriate wavelength range, which is then detected by a photo-multiplier tube, where a readout device indicates the relative intensity of light reaching it. Thus with different light sources and filter combinations, the fluorometer can discriminate between different fluorescent materials.

4 Case Studies

Several studies pertaining to deciphering of weak zones through hydraulic structures, viz. dams and canals, have been carried out using non-destructive testing (NDT) comprising borehole logging and tracer studies. Based on investigation results, appropriate remedial measures towards repair material and methodology of repairs are generally recommended.

4.1 Determining Weak Zones Through Bhama Askhed, Maharashtra, India

Bhama Askhed irrigation dam was constructed on Bhama River, Maharashtra, India. The tail channel of the dam is located over the chloroacetic porphyritic basaltic flows, which are closely jointed at various angles causing the rock to split into blocks. These rocks are underlain by volcanic breccias with red tachylitic basaltic matrix [1]. During the monsoon of 2005, it was observed that 13 RCC panels were lifted up and displaced in the Energy Dissipater Assembly (EDA) which was under construction. The spillway portions along with damaged and dislocated panels are shown in Fig. 4. In order to decipher the cause of damage and dislocation of the RCC panels, nuclear borehole logging and tracer studies were carried out. Based on nuclear density logging, bulk density of the formation was determined and also calliper logging carried out to determine extent of joints and fractures in the borehole. Tracer studies were also carried out to ascertain whether leakage observed was directly responsible for dislocation of RCC panels.

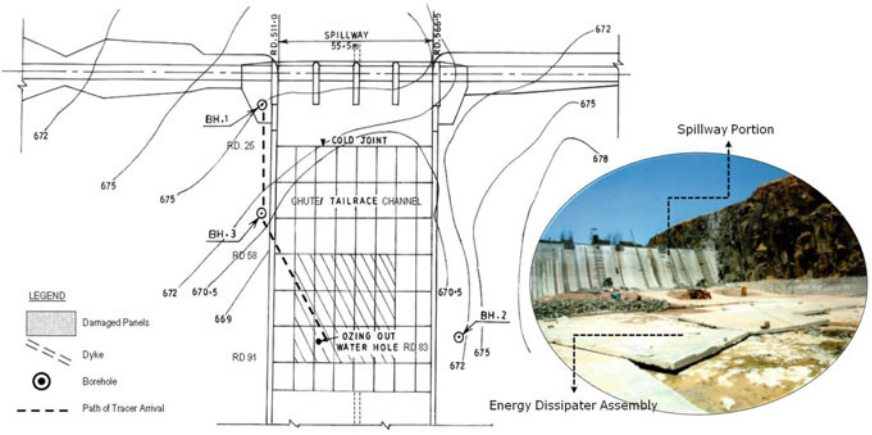

Fig. 4 Schematic representation of the dam spillway and EDA section wherein borehole logging and tracer studies

The results of density logging indicated weak and permeable zones at depth 34 m in the boreholes corresponding to the red breccia zone. Tracer studies were conducted by injecting sodium fluorescein dye in a borehole drilled in the foundation at 34 m, and samples were collected in the adjacent borehole and also in the tail channel where oozing of water was observed. The analysis of tracer sample indicated the presence of tracer in the sampling locations. These studies revealed that oozing of the water in the EDA might be due to leakage through the permeable zone formed by weak red breccia in the foundation [1].

4.2 Detection of Seepage in Indira Sagar Dam, Madhya Pradesh, India

The Indira Sagar dam is a concrete gravity dam constructed on river Narmada Madhya Pradesh, India. In addition to irrigation, the project has a powerhouse with an installed capacity of 1000 MW consisting of 8 units of 125 MW each. The foundation of the dam comprised of upper Vindhyan group with thickly bedded quartzite and ferruginous sand stones with occasional lenses of silt/clay stone. The dam instrumentation data revealed that the piezometers installed in dam body in Block No. 25 indicated high values of the uplift pressure [8]. In order to decipher the weak and permeable zones, borehole logging was undertaken at selected site in the body of dam, abutment and intake gallery. Further, to delineate the path of seepage in the abutment, drainage gallery and downstream face of dam tracer studies were undertaken at both maximum and minimum, reservoir levels [9].

The nuclear logging revealed the presence of weak- and low-density zones, indicating the presence of cracks. In order to delineate the path of seepage observed in the drainage gallery, tracer studies were planned and the same were conducted systematically. Based on logging results, the low-density and weak zones at different depths were selected for injecting the tracer in the boreholes. The tracer was also injected in the reservoir at different depths for confirming or ruling out the occurrence of seepage from these depths [8]. The results of tracer studies showed that borehole and porous holes in Block 25 are interconnected with reservoir through open joints. Arrival of tracer in the borehole at Block No. 28 and in the drift when tracer was injected in the reservoir indicated that the likely path of seepage could be from the hillock in the abutment. Tracer injected in borehole at Block No. 28 and its arrival in borehole at Block No. 25 confirmed that the path of seepage was from hillock. The tracer injected in the Head Race Channel near the abutment and its arrival at the seepage points in the adit/intake gallery, indicated that the path of seepage could be probably through the abutment (or) hillock as shown in Fig. 5. The studies revealed that the probable path of seepage might be through the hillock [8].

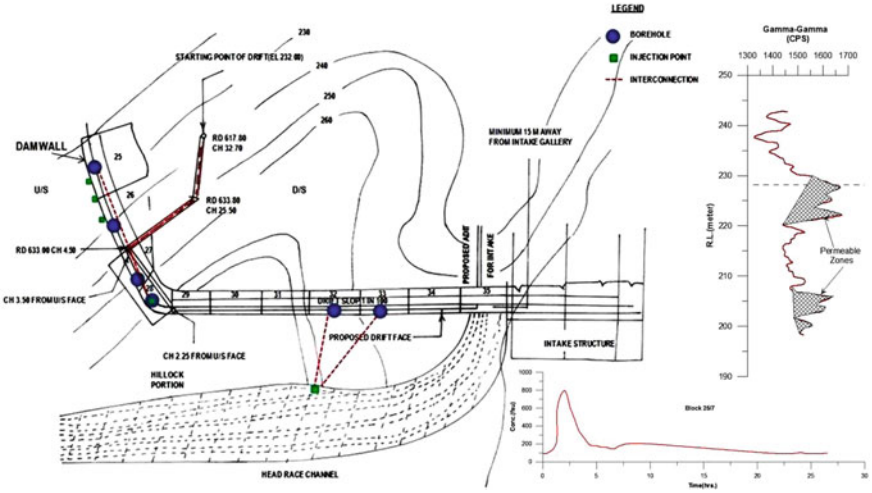

Fig. 5 Schematic representation of logging and tracer carried out in dam top, gallery and head race channel of the dam

4.3 Evaluation of Seepage Losses in Indira Gandhi Main Canal, Rajasthan, India

Indira Gandhi Main Canal (I.G.M.C), Rajasthan, India, is the biggest desert area irrigation project, which has a command area of 15.4 lac hectares in the north-western part of Rajasthan, India. A revised plan of construction of main canal was approved in 1970, in which it was decided to line the entire canal with concrete tiles. I.G.M.C is lined 195-km-long comprising of nine branches; three of which are lift irrigation schemes and 21 distributaries. The area under I.G.M.C is an undulating topography with arid region along the northern region of Rajasthan. Interdunal flats and shifting dunes with characteristically stratified soil comprising gypsiferous, calcareous soil with aeolian sand overburden [10].

Excessive seepage was observed by the I.G.M.C, project authorities between Reference Datum (RD) 0 and 100 which is about 30 km in stretch on both the banks of the canal, lined with clay tiles in two layers. Factors like seepage losses from channels, excessive use of canal systems, relatively low groundwater levels and absence of natural drainage might have been the major cause for water logging at both banks of the canal. Suspecting such probable causes, tracer technique was take up to measure the filtration velocity, seepage losses and permeability of the entire zone, without interrupting the normal activity of the main canal [10].

Ten boreholes (150 mm dia. and up to a certain depth to meet 2–3 m water within borehole), namely B1 to B4 and B6 to B9 on the left bank and B5 & B10 on the right bank of I.G.M.C as shown in Fig. 6 was used for point dilution method. All these boreholes were drilled at regular interval of nearly 5 m from the edge of the canal in order to measure subsurface seepage losses and filtration velocity through the

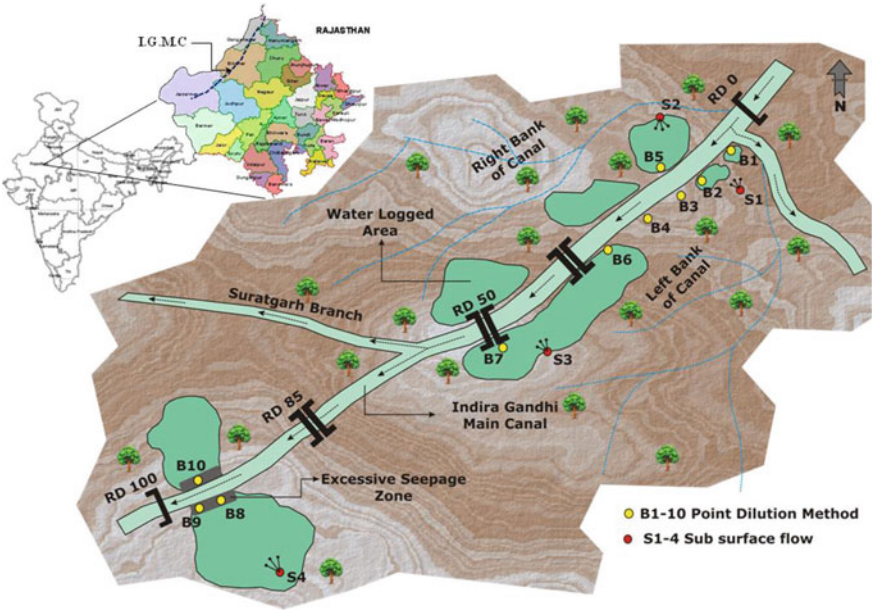

Fig. 6 Schematic view of I.G.M.C, Rajasthan, India

formation, using sodium fluorescein dye as a tracer. At each borehole location, three piezometers, 10 m apart, were used towards the measurement of depth of water table. Four sets (one injection borehole and three piezometers in each set) of boreholes, namely S-1, S-3 and S-4 on left bank and S-2 on right bank (Fig. 6), were used for the measurement of filtration velocity and permeability from subsurface seepage at the same water logged area. Based on dilution rate of tracer (sodium fluorescein dye), filtration velocity and seepage loss were estimated and permeability was calculated using subsurface seepage [10].

The low, moderate to high and excessively high seepage zones were well complemented by the filtration velocity of corresponding boreholes. The RD 100.00 indicated an excessive seepage zone, and the same was well supported by both high filtration velocity (3.27×10^{-7} m/sec) and permeability (0.32×10^{-4} m/sec) at site S-4 (Fig. 7) might be due to damaged canal lining [10].

5 Conclusions

Systematic understanding and proper diagnosis are the key factors for a successful and cost-effective restoration or strengthening of hydraulic structures. There might be various reasons, viz. improper location for foundation, defects in construction or from unusual events like reduction in stability, etc., which might demand the necessity

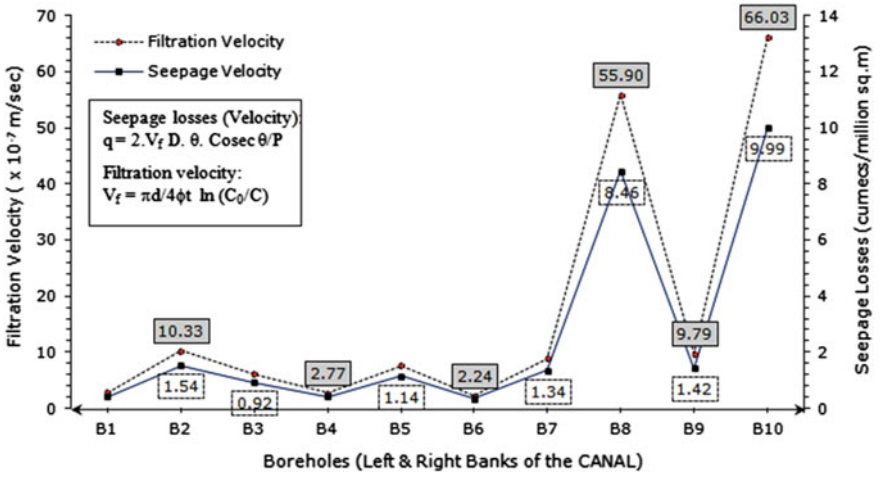

Fig. 7 Representation of filtration velocity and seepage losses at water logged area between RD 0 to 100, I.G.M.C, Rajasthan

for strengthening of hydraulic structure. Under all circumstances, in order to ensure safety, the first step is to temporarily lower the reservoir level and then visually inspect the structure to identify probable causes of deterioration. In this paper, the application of NDT techniques is explained, which enables in the assessment towards the health of hydraulic structures, before implementing remedial measures. From the case studies discussed, it is very evident that NDT investigations can pinpoint the area of seepage and thus provide cost-effective remedial measures. These techniques can also be used to check the efficacy of the remedial measures adopted.

Acknowledgements The authors bestow their sincere thanks to Shri A.K.Agrawal, Director CW & PRS, for promoting this publication and giving an opportunity to present the same in HYDRO-2021 International Conference.

References

1. Kamble RK, Panvalkar GA, Chunade AD (2011) Mapping seepage in the tailrace channel Bhama-Askhed dam: a case study. Bull Eng Geol Environ 70(4):643–649
2. Keys WS (1990) Borehole geophysics applied to groundwater investigations, USGS, Denver, USA
3. Crain ER (Ross) (2004) Crain's petrophysical handbook. Rocky Mountain House, Alberta, Canada
4. Pirson SJ (1963) Hand book of well log analysis. Prentice Hall Inc., p 326
5. Todd DK (1980) Ground water hydrology. Wiley, New York
6. Moser (1995) Groundwater tracing, tracer technologies for hydrological systems. In: Proceedings of a boulder symposium. IAHS, Publ.no. 229, 119
7. Gaspar E, Onescu M (1972) Radioactive tracers in hydrology. Elsevier Publications, Bucuresti

8. Panvalkar GA, Chunade AD (2017) Tracing dam seepage using nuclear logging and tracer techniques—a case study. ISH J Hydraul Eng 311–316.https://doi.org/10.1080/09715010.2017.1376293
9. Kamble RK, Muralidhar B, Hanumanthappa MS, Patil AV, Edlabadkar JS (2013) Multiple approaches to analyse and control seepage in hydraulic structures. ISH J Hydraul Eng 7–13.https://doi.org/10.1080/09715010.2013.821787
10. Andrade R, Bhowmick S, Pund A (2017) Tracer an effective tool in detecting canal seepage: case studies from Northern India. Sustain Water Resour Manage 25–31.https://doi.org/10.1007/s40899-017-0083-x

Tracer Techniques—a Diagnostic Tool in Seepage Detection of Hydropower Projects

A. D. Chunade, G. A. Panvalkar, and B. Suresh Kumar

Abstract Hydropower, an important and widely used renewable source of energy, has the ability to generate electricity without emitting greenhouse gases thereby providing pollution-free electricity to the human being. As a majority of hydroelectric projects are constructed on dams, it is often necessary to assess the health of the structure and take steps towards attaining its safety. Although a large number of causes may lead to failures of dams and hydroelectric plants, weather events like storms and hurricanes that result in natural flooding and landslides are a major concern. In addition to widespread loss of life and property, the consequences of these natural events often result in seepage problems, either during the pre or post construction stages. Hence, locating the source and path of seepage and incorporating suitable remedial measures plays a significant role in assessing the risk and uncertainty in hydropower development and management. During the construction of Ghatghar Hydroelectric Project, Maharashtra, heavy monsoon caused a natural landslide ensuing heavy seepage at many locations in the approach tunnel of the powerhouse. As this could affect in loss of electricity generation, it was important to establish the source of leakage and delineate the path. Accordingly, tracer studies were undertaken to for identifying sources of seepage by establishing interconnection, if any, between the seepage points in the approach tunnel and the intake of reservoir. This paper signifies the utility of "Tracer Techniques" as a diagnostic tool for seepage mapping and suggesting suitable remedial measures to mitigate it.

Keywords Hydropower · Tracer · Seepage · Approach tunnel

A. D. Chunade (✉) · G. A. Panvalkar · B. Suresh Kumar
Central Water and Power Research Station, Pune 411024, India
e-mail: amolchunade00@gmail.com

G. A. Panvalkar
e-mail: ga.panvalkar@cwprs.gov.in

P. V. Timbadiya et al. (eds.), *Flood Forecasting and Hydraulic Structures*, Lecture Notes in Civil Engineering 340, https://doi.org/10.1007/978-981-99-1890-4_41

1 Introduction

Hydropower is one of the vital options for providing power supply, the world over for many reasons. First and foremost, it is a renewable energy resource for sustainable development by producing cheap power locally. Secondly, hydropower reliance on imported fuels that depend on price volatility, supply uncertainty and foreign currency requirements is greatly reduced. Thirdly, it provides multiple benefits like water storage for drinking and irrigation, drought-preparedness, flood control protection, aquaculture and recreational opportunities. About 16% of global electricity share is accounted for by hydropower, and this is expected to grow in future. In developing countries, an enormous potential exists as hydro's technical potential is five times the current utilization rate. However, developing a hydro project is challenging as there are considerable uncertainties associated with hydrology (impacting power generation and its revenues) and geology (leading to substantial increase in construction costs). The other significant factors affecting the construction of hydropower projects include inaccessible sites at remote locations, difficulties in obtaining site licences and permits due to involvement of many stakeholders with conflicting rights and responsibilities.

The generation of hydroelectric power is a complex process, which involves construction of dam's, formation of reservoirs and a penstock that allows water to flow from the reservoir to a turbine's propeller. Moving water can generate electricity. Moving water has kinetic energy which when falls on turbine blade generates mechanical energy. Turbine turns the generator rotor which creates electricity. This electricity is generated due to water as primary source; hence, it is called as hydroelectric power. The power house houses the turbines and generator along with penstocks feed. Power houses are generally constructed in dams for producing hydropower.

The purpose of constructing a "Pumped storage hydroelectric scheme" is to reduce or even out the load on generators. Such plants have two reservoirs—an upper and a lower reservoir. These power plants are usually used for generating energy for peak load demand, and during off-peak hours, the same water pumped back from lower level reservoir to high head reservoir for further use. Thus, these pumped storage plants assist in increasing the load factor of other existing power plants and also generate additional capacity to satisfy the peak load demands. The unique feature of such power plants is that very small quantity of water is required for its entire operation, once the head water and tail-water reservoirs are completely filled with water. The same unit is thus capable of working as generating unit when water flows from high level to tail-water reservoir and as pumping unit when the water is pumped from the lower tail-water reservoir to the reservoir at higher level.

As these hydropower plants are an important source of power for mankind, they must have the ability to function properly for a long time. It is therefore crucial to adapt effective management practices so that that these power plants are well maintained. Efficient management practices include regular monitoring, maintenance and repairs. Timely detection, mapping and economic repairs to mitigate the seepage are often necessary to prevent failure of these structures. Seepage detection is often

a complex geotechnical engineering problem having a degree of uncertainty as the hydraulic structures are heterogeneous, nonlinear and have anisotropic material [1]. The investigation of this problem requires the integrated use of different techniques. Along with other hydrological and geophysical studies, "Tracer Techniques" have been effectively used to detect seepage and then study the efficacy of the applied remedies.

This paper discusses the application of tracer technique to identifying source and path of seepage caused by a landslide at Ghatghar Hydropower Project, Maharashtra, India.

2 Design and Geology of the Ghatghar Pumped Storage Scheme

Ghatghar Pumped Storage Scheme is situated in Thane and Ahmadnagar districts, Maharashtra state. It envisages the construction of two reservoirs. The upper reservoir is situated on Pravara River, a tributary of River Godavari near village Ghatghar, Taluka Akole, District Ahmadnagar, and lower reservoir is located on Shahi Nala, a tributary of Ulhas River near village Chonde, Taluka Shahapur, District Thane. This dam is the first Roller Compacted Concrete (RCC) constructed large dams in India. Ghatghar Hydroelectric Project generates 250 MW power [2].

Geologically, the project area is situated on massive (compact) basaltic formation (Deccan Basalt) having a few fracture zones intersecting the approach tunnel and a thin soil cover.

The water conductor system with underground power house is located near lower dam site. The water conductor system consists of upper intake structure in the upper reservoir, a steel lined pressure shaft of 696 m in length and 4.25–3.5 m diameter at 58° to vertical; Tail Race Tunnel (TRT) 590 m in length, and lower intake structure at the end of Tail Race Tunnel. A tail surge well of 11 m diameter and 137 m depth is provided on TRT. Emergency gates are provided at upper as well as lower intake structure. The surge tank or well is a necessary engineering arrangement for the smooth functioning of the power plant. It serves the dual purpose of storing excess water when not required by the turbine (in case of sudden rejection of load) and also supply additional water when required by turbine (in case of sudden opening of valve).

The powerhouse complex comprises two caverns to accommodate two Francis-type reversible turbines, generator units and two three-phase transformers, respectively. The dimensions of machine hall are 123.40 m (length) × 23.4 m (width) × 47 m high housing the two 125 MW turbine—generator units, i.e. reversible turbines. The transformer hall cavern is 81.35 m long, 20 m wide and 30 m high having two 220 KVA transformers. Both the caverns are parallel to each other and separated by a 40-m-wide rock pillar. The system involves recycling of water between the upper and lower reservoirs with a head of 400 m. It is operated on a weekly basis with

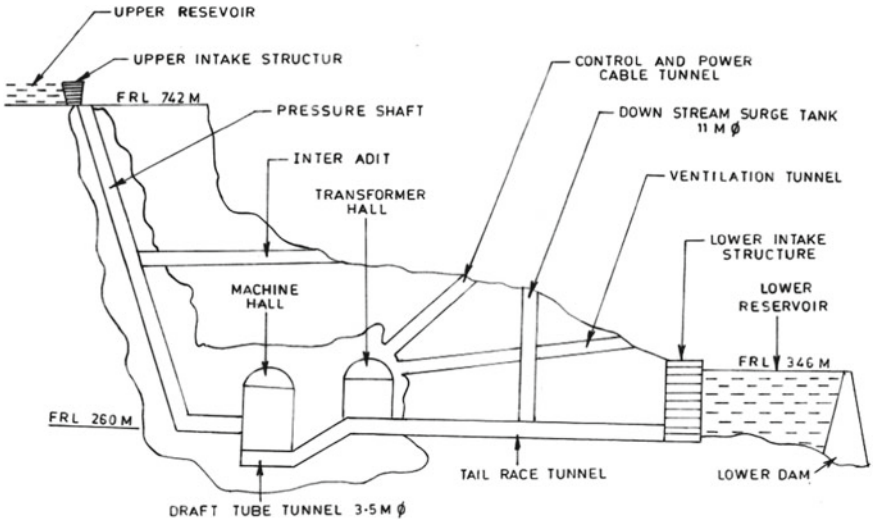

Fig. 1 Schematic diagram of Ghatghar Pumped Storage Scheme

generation for six hours daily during peak hours of demand and pumping for seven hours during off-peak hours [2]. Figure 1 shows schematic diagram of Ghatghar Pumped Storage Scheme.

In the monsoon during the construction, installation stage was in progress, a natural landslide resulted in floodwater and debris entering in the underground powerhouse of Ghatghar Project. All erected equipment were under water in the powerhouse. After the removal of debris from the powerhouse especially from sump pit, the work could be resumed only after a year.

During the subsequent monsoon, while construction of the lower reservoir was in progress, heavy leakages were observed at a few places in the Approach Tunnel (AT). As the storage reached the designed FRL, heavy seepage of about 300 l/min (maximum) was noticed at one location inside the Approach Tunnel and profuse leakage was noticed in nearly 70% of length along the AT. Hence, with an apprehension that the leakage waters could originate from the lower reservoir and this in turn would subsequently lead to head loss for the generation of electricity, it was required to find out the cause of seepage and delineate the path using tracer techniques.

3 Previous Work

A study conducted by Bhabha Atomic Research Centre (BARC) using environmental isotopes revealed that isotopic concentration of seepage water and reservoir water was same. This result has ruled out the phenomenon of contribution of ground water towards seepage.

4 Methodology

4.1 Tracer Techniques

In tracer techniques, a predetermined quantity of tracer is injected into the borehole or suspected entry points in the upstream face of the dam, and its arrival is monitored in leakage points towards the downstream side of the dam. Tracers are nonhazardous and nontoxic chemical compounds, salts and dyes, having unique passive-type nature, which behave exactly similar to the materials to be traced but differ from them by a particular property, which may be physical or chemical including radiochemical [3]. The major objectives of using tracers techniques in geotechnical studies are to determine (1) seepage in dams and irrigation canals, (2) location of seepage entry zones, delineating seepage path, assessing the efficiency of remedial measures, examination of soundness of bedrock, etc. (3) hydraulic parameters of subsurface flow and (4) interconnection between solution cavities, etc.

The choice of tracer is important as its must behave like the material to be traced but should be distinguishable from it for purposes of detection [4]. Tracer test has been successfully used to investigate the seepage in dams and to evaluate the effectiveness of remedial measures in seepage areas.

Although a wide variety of tracers are available, dyes remain, among the most prominent subsurface water tracers. Fluorescent dye tracers are popular because of their relatively easy handling, the seemingly simple analysis, the high sensitivity of the analysis, the low detection and toxicity limit and consequently, the small quantity of tracer needed in field experiments [5].

Uranine (sodium fluorescein) dye commonly used in dam seepage studies is a reddish-brown powder that turns vivid yellow-green in water. This tracer has no smell and has proven to be nonhazardous for human beings and animals specifically in concentrations which are employed in tracing tests [6]. Seepage measuring technology by tracer method has been playing an irreplaceable role in quantitatively explaining some difficult problems in major projects [7]. Hien and Khoi [8] describe the use of isotope tracer techniques for assessing seepage through the earthen dam at a hydropower dam in Vietnam. Central Water and Power Research Station has successfully employed nuclear density logging and tracer techniques to delineate the path of the seepage in hydraulic structures [9].

5 Instrumentation

A laboratory fluorometer, (TD-700), manufactured by M/s Turner Design, USA, was used for the tracer studies. The fluorometer works on the principle of optics where the light from an ultraviolet lamp is passed through an excitation filter, which in turn transmits light of a specific wavelength to the sample compound being measured. The light passes through the sample, which emits light proportional to the intensity

of the exciting light. The emitted light is then passed through and emission filter of appropriate wavelength which can be detected by a photo-multiplier tube which indicates then the relative intensity of light reaching it. Thus, with different light sources and filter combinations, the fluorometer can be used to discriminate the different fluorescent materials.

6 Field Study and Discussion

Identification of seepage path by tracer techniques in a complex structure requires proper planning and implementation of sequential steps in the study. The seepage path has to be traced systematically in a stepwise manner. Accordingly, it was proposed to carry out the studies in a phased manner to confirm or eliminate the possible source and seepage path from particular location of the structure. Tracer studies were planned to establish interconnection, if any, between (i) Tail Race Tunnel (TRT) and seepage in the Approach Tunnel (AT), (ii) reservoir through fracture at 700 RD and seepage in the AT, (iii) reservoir at RD 300 and seepage in the AT. The general layout of Ghatghar Pumped Storage Scheme and injection and sampling points of tracer studies are shown in Fig. 2. The tracer studies involved injecting the sodium fluorescein dye at a particular location and monitoring its arrival, if any, at the seepage locations along the length of the AT. The tracer studies were conducted during different seasons when the water in the reservoir and TRT were at different levels to confirm or rule out the possibility of seepage from different locations and depths.

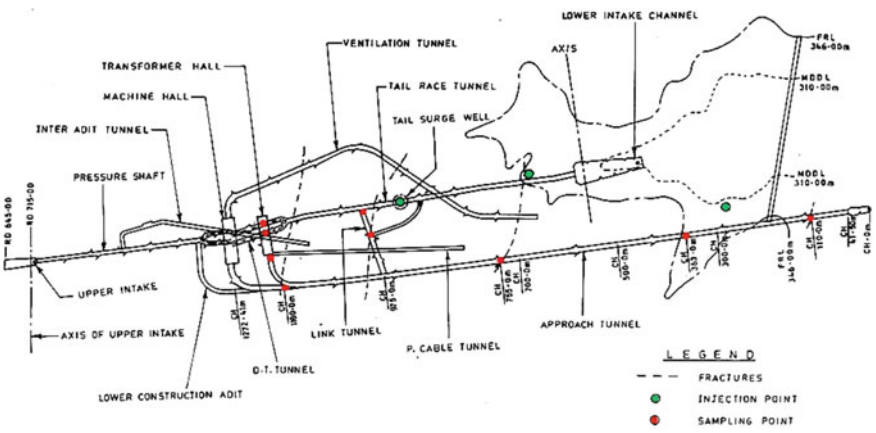

Fig. 2 Layout of Ghatghar pump storage scheme showing details of tracer studies

6.1 I Injection

The sodium fluorescein dye was first injected in the surge well/shaft at a depth of 120 m from the top. During this period, reservoir was depleted and as such it was not connected with TRT. Thus, it was presumed that the water was present only in the TRT. After injection, round-the-clock sampling was undertaken in the approach tunnel at different locations like CH.1180, link tunnels, machine room and butterfly valves at hourly intervals. The samples were collected and stored in plastic containers of 50 ml capacity. The samples collected at the respective sampling locations were analysed fluorometer for ascertaining the arrival or nonarrival of the tracers at the respective sampling locations. Arrival of tracer was indicated as the peak value as read from the fluorometric analysis.

6.2 II Injection

The dye (sodium fluorescein) was injected in the reservoir near the extended fracture zone (at 700 RD, Ch1700 of TRT), which crosses the tailrace tunnel. Sampling was undertaken in Approach Tunnel at ten different locations where seepage was observed. Sampling was conducted at every four-hour interval, round the clock, and samples were analysed on fluorometer. Sampling was carried out for 10 days.

6.3 III Injection

The dye (sodium fluorescein) was injected in the reservoir around Ch. 300 towards AT and sampling carried out at two locations—CH. 110 and Ch. 363, at four-hour interval, round the clock, and samples analysed on fluorometer and results were plotted as concentration versus time. Locations where the concentration of tracer has not shown values above the concentration of the background samples were considered as nonarrival of the tracer.

The injection of tracer at different locations and its arrival in seepage points are shown in Table 1.

The data obtained from the fluorometer was used for plotting the tracer breakthrough curves of time versus concentration in full scale units. The time of first appearance of the tracer in the fluorometer was marked by the increase of tracer concentration above an almost constant background values recorded before the start of test. The study of the tracer breakthrough curves for the tracer injected in the surge shaft at 120 m depth from top and analysis of samples from link tunnel and seepage from Ch. 1180 had shown the presence of sodium fluorescence dye. This indicated that tracer has arrived at these locations from Surge Tank of TRT. This revealed that

Table 1 Results

Injection No	Points of tracer injection	Sampling points	Points of tracer arrival	Observations
I	Surge shaft at 120 m depth from top	Approach Tunnel (AT)—Ch. 1180, link tunnel 2 (LT2), butterfly valves (BF1 and BF2)	1. LT-2 after 19 h 2. Ch. 1180 after 45 h	Interconnection exists between TRT and seepage at Ch. 1180
II	Reservoir near fracture at Ch. 1700 of TRT	AT—Ch. 110, Ch. 363, Ch. 755, Ch. 1180, LT2&LT3 junction, LT2 plug, LT 3 plug, Cable Tunnel (CT) outlet, Ventilation Tunnel (VT) outlet, butterfly valve BF1 pit	No arrival	Interconnection between reservoir and seepages in the Approach Tunnel could not be established
III	Reservoir around Ch. 300 of AT	AT Ch. 110, Ch. 363	No arrival	Interconnection between reservoir and seepages in the Approach Tunnel could not be established

an interconnection could exist between TRT and seepage at Ch. 1180. The plot of the breakthrough curve is shown in Fig. 3

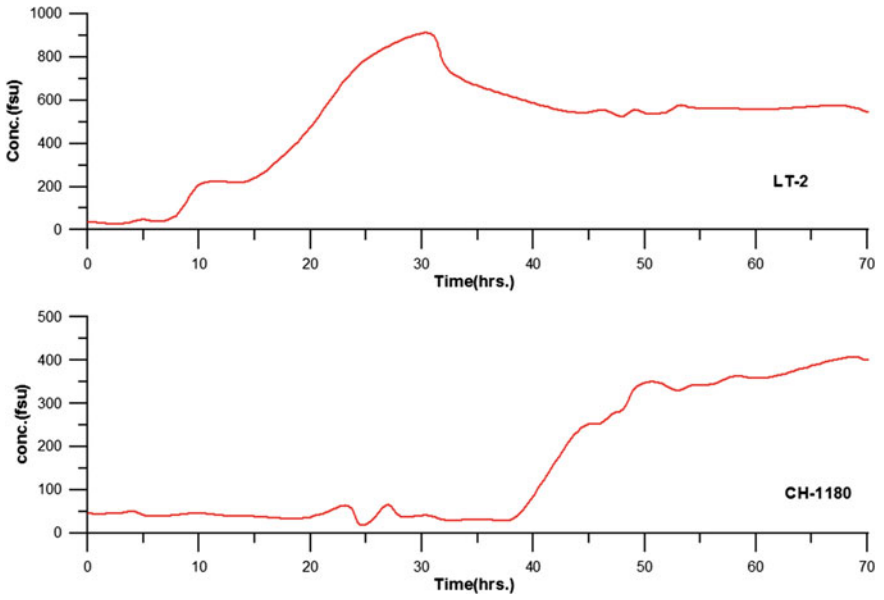

Fig. 3 Typical tracer arrival curves for injection in surge well at Ghatghar project, Maharashtra

Similar analysis was carried out for the tracer injected at other locations. Tracer injected in reservoir when it was depleted and not connected with TRT did not arrive in the seepage points in the approach tunnel. This has indicated that reservoir water may not be emerging through the fault extending between reservoir and power house. Thus, the possibility of interconnection between reservoir and seepage points in the approach tunnel could be ruled out. This indicates that reservoir water may not be emerging through the geological fault existing between reservoir and powerhouse.

For the tracers injected in the reservoir near fractures at Ch. 1700 (TRT), the analysis of water samples from seepage locations for nine consecutive days did not show the presence of tracer at any of the sampling locations, thereby ruling out the possibility of an interconnection between reservoir and seepages in the approach tunnel.

Similarly, for the tracers were injected in the reservoir near fractures at Ch. 300 (AT), and the analysis of water samples from seepage for eleven consecutive days failed to detect arrival of tracer which further confirmed any interconnection between reservoir and seepages in the approach tunnel.

7 Conclusions

In this study, the application of tracer techniques highlights the significance of delineating the potential seepage path and identifying the seepage prone zones. The qualitative analysis of the fluorescent dye tracer studies established the fact that for tracer injected in surge shaft of TRT (when TRT was not connected with reservoir), dye appeared in the seepage at Ch. 1180 and Link Tunnel. It can be concluded that interconnection between TRT water and seepage at Ch. 1180 was established. This has also revealed that source of seepage was reservoir and path of seepage might be from TRT. It was suggested that the leakage flow at that point must be diverted away from the power house. It was also recommended to undertake suitable repairs of TRT during the lean period of power generation.

Acknowledgements The authors are grateful to Director, CWPRS, Pune, for his encouragement and permission to publish this paper. The authors are indebted to the retired scientists of the institute who had contributed in the cited case studies. The authors are also thankful for the co-operation provided by the Project Authority.

References

1. Panvalkar GA, Chunade AD (2017) Tracing dam seepage using nuclear borehole logging and tracer techniques, a case study. ISH J Hydraul Eng 311–316
2. CWPRS Technical Report No 4748, Tracer studies for leakage in approach tunnel of underground power house at Ghatghar pumped storage hydroelectric project, Maharashtra

3. Moser H (1995) “Groundwater tracing”, tracer technologies for hydrological systems. In: Proceedings of a boulder symposium. IAHS, publ. no. 229, 119
4. Gaspar E, Onescu M (1972) Radioactive tracers in hydrology. Elsevier Publications
5. Leibundgut C, Maloszewski P, Kulls C (2009) Tracers in hydrology. Wiley, UK, pp 415
6. Benischke R (2001) Fluorescent tracers in hydrology: principals, instrumentation, physico-chemical properties, analytics Institute for Geothermic and Hydrogeology, Joanneum Research, Graz-Austria
7. Zhao M, Wang H, Sun X, Zhang Y (2011) Comparison between the isotope tracking method and resistivity tomography of earth rock-fill dam seepage detection. Engineering 3:389–399
8. Hien PD, Khoi (1996) Application of isotope tracer techniques for assessing the seepage of the hydropower dam at Tri An, South Vietnam. J Radio Anal Nucl Chem
9. Kamble R, Panvalkar GA, Chunade AD (2011) Mapping seepage in tailrace channel, Bhama Askhed Dam, a case study. Bull Eng Geol Environ 70:643–649

Fluorescent Dye Tracer Tests for Seepage Detection in Earthen Dams

G. A. Panvalkar, Archana K. Pund, B. Suresh Kumar, and A. K. Agrawal

Abstract Seepage and its control measures are important aspects during the design and construction stages of earthen dams. Despite the fact that all dams are designed to lose some water through seepage, it is always a matter of concern when water finds its way out through a weak area in the dam or works its way through the foundation or abutment, as it can pose a threat to dam safety. This seepage problem will lead to instability of embankments causing sloughing of slopes due to the rising pore water pressure and internal erosion which may further cause piping of embankments. Generally, the seepage analysis is carried out in earthen dams to analyse the phreatic line, the pore pressure within the dam or its foundation, the exit gradient at the downstream face of the dam and the amount of seepage flow that may pass through the dam's cross sections. Excessive seepage in earthen dams could ultimately lead to its failure. Dam seepage detection often requires integrated use of different techniques. Among these, dye tracer techniques are often always necessary as they are an economic and proven tool providing a detailed perspective into dam seepage investigations. These non-destructive tracer tests facilitate in identifying seepage zone and probable path both qualitatively and quantitatively. The main objective of this paper is to highlight the significance of dye tracer techniques for identifying the seepage in earthen dams along with some important case studies carried out by CWPRS in Kota Barrage, Rajasthan; Rockfill Dam at Sardar Sarovar project, Gujarat; and Salaulim Dam, Goa. The application of these tracer techniques was useful in pinpointing the seepage prone zones, and suitable cost-effective remedial measures were recommended to mitigate the seepage.

Keywords Earthen dam · Fluorescent dye · Piping · Seepage · Tracer techniques

G. A. Panvalkar (✉) · A. K. Pund · B. Suresh Kumar · A. K. Agrawal
Central Water and Power Research Station, Pune 41102, India
e-mail: govindpanvalkar@gmail.com

P. V. Timbadiya et al. (eds.), *Flood Forecasting and Hydraulic Structures*, Lecture Notes in Civil Engineering 340, https://doi.org/10.1007/978-981-99-1890-4_42

1 Introduction

Generally, any dam constructed around the world is unique. The construction of a dam includes an integration of many disciplines like structural, hydraulics, hydrology, geology, etc. Although the key purpose of a dam is storage and safe retention of water, it must be structurally stable to withstand the superimposed loads with minimal seepage losses. Dams can then be classified broadly based on the type of construction material used, viz. embankment/earthen dams constructed from earth and rockfill materials and concrete dams constructed from mass concrete.

Earthen dams have been in existence since ancient times as they were constructed using the readily available earth and rock materials in the vicinity. In many ancient dams, lack of sufficient knowledge often resulted in seepage leading to their failure. In the early twentieth century, the application of science and mathematics played an important role during the design and construction of dams. Further incorporating seepage control measures during construction stage enhanced the safety of these structures.

The design and construction of earth and rockfill dams is complex because of the nature of the varying foundation conditions and wide range of properties of materials available for use in the dam [1]. The topographic and foundation conditions at dam site play an important role in construction of earth and rockfill dam. Embankments are of two main types: (i) earthen embankments where the selected soil is compacted uniformly and intensively into different layers that make bulk of the dam volume; (ii) rockfill embankments have an impervious core of compacted earth-fill material. The bulk of volume is made of coarse gravels, crushed rocks and boulders. The stability of outer shell of a rockfill embankment depends on the frictional forces acting in between each rock gravel piece that ensures its safety against failure by sliding during earth quakes.

2 Design Criteria of Earthen Dam

Earthen dams are advantageous as they can be sited on a wide range of foundation conditions, use naturally available materials and are relatively less costly. Based on the construction design, the different types of earthen dams include homogenous, zoned or diaphragm.

2.1 Homogenous Embankments

A purely homogeneous embankment dam is composed of a single type of must be sufficiently impervious to provide an adequate water barrier. As purely homogenous embankments are unsafe, a modified homogenous embankment is designed with

a small amount of suitably placed pervious material to control seepage action. In addition, an internal drainage system in the form of filters, toe drains, etc. further enhances the safety of the structure.

2.2 Zoned Embankments

A zoned earth-fill embankment has a central impervious core surrounded by upstream transition zones, downstream filters and drains. The outer zones composed of earth, gravel or rock fill, which are considerably stronger than the core. They are normally constructed in areas where several materials such as clays, silts, sands, gravels and rock are available. Zoned embankments have an added advantage that different materials are so positioned in various zones such that their best properties are used beneficially and poor properties reduced. As such, zoned earthen embankments are generally superior having better stability and low seepage.

2.3 Diaphragm Embankments

The bulk of the embankment is constructed from pervious material like sand, gravel or rock. A thin diaphragm of impermeable material acts as a water barrier. The position of this impervious diaphragm may vary from the upstream face to a centrally located diaphragm. The diaphragm or membrane may consist of asphaltic concrete, reinforced concrete, metal, compacted earth-fill or geomembrane. If compacted earth-fill is used as a embankments, the diaphragm is called a thin core.

3 Seepage and Control Measures

All earth and rockfill dams are subject to seepage, as the impounded water follows paths of least resistance through the embankment, foundation and abutments. Seepage may range from a wet patch to a flowing spring. Lush dark green vegetation in the downstream area is a prominent seepage marker. Uncontrolled seepage may cause excessive uplift pressures, instability of the downstream slope, piping through the embankment and/or foundation, and erosion of material by its migration into open joints in the foundation and abutments. These conditions are critical earthen dam safety issues. Modern dam designs incorporate seepage control measures during the construction phase by using cut-offs, filters and providing adequate drainage. These systems must stop migration of soil particles but should allow seepage to drain freely. An earthen dam must therefore be safe and stable during the phases of construction as well as its operation.

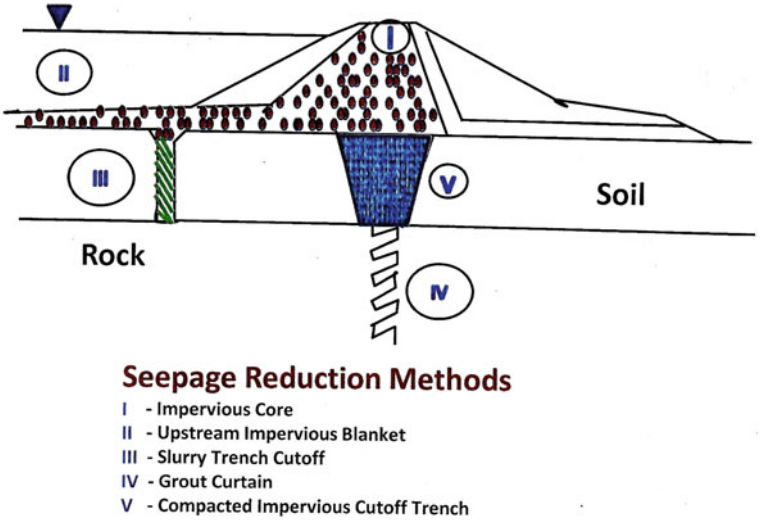

Fig. 1 Schematic diagram of seepage reduction methods in earthen dams

The presence of pervious zones in the foundation requires the use of cutoff trenches and an impervious zone within the embankment to control the seepage. Additionally, filters and other drainage features are also constructed to control seepage or leakage that may find its way through impervious zones and to protect against internal erosion. Toe drains are added to provide seepage control.

In pervious foundations, relief wells are sometimes used to control seepage or reduce pore pressures at greater depths in the foundation (Fig. 1).

3.1 Seepage Control Through Earthen Foundations

Dams constructed on earthen foundation are subjected to under-seepage which may cause excessive uplift pressure or piping below the foundation. Techniques to control under-seepage from earthen foundations include providing of horizontal drains, cutoffs that include compacted back filled trenches, cement-bentonite slurry walls and concrete cutoff walls. Moreover, upstream impervious blankets, downstream seepage berms, relief wells and trench drains are also provided.

3.2 Seepage Control Through Rock Foundations

In the dams constructed on rock foundations, seepage is normally controlled by curtain grouting of the foundation, cutoff trenches which are normally back filled with

compacted impervious material, bentonite slurry or cement and upstream impervious blanket. These cutoff trenches and upstream impervious blankets are also further extended into the abutments as a seepage control measure.

3.3 Postconstruction Seepage and Its Control Measures

Generally, leakage in dams occurs when seepage concentrates through a weak area in the dam in three different ways, viz. (i) through the body of the dam, (ii) through the interface between the structure and the foundation and (iii) through geological inhomogeneities occurring in the vicinity of the structure. The economic consequences of the loss of water from such areas lead to structural instability. It is, therefore, essential to identify the areas of water loss and seepage entry points in the dams for adapting the remedial measures.

Regular monitoring is essential to detect seepage and prevent dam failure. This includes the review and evaluation of existing project data. It is essential to study the history of the dam to determine whether the seepage condition is in a steady state or varying state. It is also important to maintain written records of seepage exit points, quantity and content of seepage flow, size of wet area, type of vegetation, etc. Instruments are also used to monitor seepage. Discharge measuring apparatus like V-notch is used to measure flow rates and piezometers installed within the embankment provide information about the saturation level or phreatic surface through the dam. In addition, the rate and content of flow from outlet of toe drains, relief wells and weep holes must be monitored and documented regularly. Normal maintenance consisting of removing obstructions like debris, gravel, sediment, mineral deposits and rodent nests must be periodically carried out to allow free drainage of water. Postconstruction, seepage can be controlled at exit points by installation of toe drains and relief wells.

The need for reducing the water loss through seepage and prevent dam failure has often led to costly remedial measures without a thorough understanding of the problem. A lack of proper understanding often results in inappropriate leakage investigations resulting in repairs that are unsuccessful in controlling seepage. In addition to engineering aspects, the repair methodology should also focus on hydrogeological aspects of the dam site.

4 Dam Seepage Detection Techniques

Analysis and detection of seepage in earthen dams require a multidisciplinary approach. It involves stability analysis of dams, seepage investigations for hydraulic structures, hydrogeological investigations for groundwater-related problems, assessment of behavioural aspects of rock mass for hydraulic structures, determination of properties of concrete and assessing suitability of epoxy compounds, etc. [2]. The

assessment of seepage is based on the measurement of several parameters such as seepage rates, seepage losses, hydraulic conductivity (k), permeability, mapping of seepage variability within a section, etc. It is essential to know whether the seepage condition is in steady state or changing with time and the scale (in order of few tens of kilometres to hundreds of kilometres), as well, before the selection of suitable method(s) to be applied [3]. Techniques such as water balance, flow velocity, tracers, temperature, infrared ray sensing and geophysical techniques have been widely used by many researchers. Panthulu et al. [4] have used the geophysical self-potential method to identify seepage-prone zones in an earthen embankment in a dam in Rajasthan, India. Over the years, "tracer techniques" have been successfully used to understand the water flow in the dam and offer economic solutions to mitigate seepage risks. The non-destructive "tracer technique" is discussed in this manuscript citing some successful studies.

4.1 Tracer Techniques

Tracer tests are one of the most reliable and efficient means of gathering subsurface information. In general, tracer is a substance added to a material in a chemical, biological or physical system to mark that material for study and to observe its progress through the system or to determine its final distribution.

The properties of the tracers are stable and sensitive in nature, easily soluble in cold water, easily detectable at low concentrations, water-like movement and without degradation during the time frame of interest. The major objectives of using tracer techniques are to determine (1) seepage in dams, (2) location of seepage entry zones, delineating seepage path, assessing the efficacy of remedial measures, (3) hydraulic parameters of subsurface flow or seepage through hydraulic structures, (4) interconnection between solution cavities and (5) seepage losses through irrigation canals etc.

Generally, tracer tests are performed by introducing a natural or artificial in a water flowing system at a known position and time (injection point), which usually consists of a well, a piezometer or a sinkhole. The appearance and concentration of the tracer are then monitored at target points, such as wells, piezometers or springs. Velocity of water flow is calculated from the time difference between injection and first detection, while other information, such as the type of flow, can be obtained from the analysis of concentration variation with time. By tracer test, leakage can be detected accurately, quickly and timely, which is of great significance in underground leakage monitoring [5].

Although a wide variety of tracers are available, dyes are the most prominent subsurface water tracers. Fluorescent dye tracers are popular because of their relatively ease in handling, the apparently simple analysis, the high sensitivity of the analysis, the low detection and toxicity limit and consequently, the small quantity of tracer needed in field experiments. Fluorescent tracers are also attractive because of

the linearity of the calibration curve in the measuring scale and their very low toxicity levels as compared to other tracer substances [6]. Panvalkar and Chunade [7] have successfully applied fluorescent dye tracer technique to detect seepage through the dam body and hillock in the abutment at Indrasagar Dam, MP, India. Nasseh et al. [8] used two different types of tracers to investigate seepage in Bidvaz dam and confirmed seepage in the left abutment through limestone.

4.2 Principle of Fluorescence and Instrumentation

Fluorescence is a physical property of certain atoms and molecules. It is a molecule ability to absorb light energy at one wavelength, and then instantaneously re-emit light energy at another, usually longer wavelength. Each fluorescent dye has a characteristic excitation wavelength (wavelength of light that it absorbs) and a characteristic emission wavelength (wavelength of light that it emits when molecules relax and return to their ground state). A fluorometer is used for detection and measurement of fluorescence dyes.

Two techniques for conducting tracer studies are generally used:

4.3 Single-Well Technique (Point Dilution Technique)

The method involves direct measurement of filtration velocity by measuring the rate of dilution of tracer injected in a borehole having a laminar flow of water under natural or induced hydraulic gradient. A known quantity of tracer is injected, and its rate of dilution is monitored in the same hole. The concentration of a tracer decreases as a result of horizontal flow of water. Thus filtration velocity and permeability can be determined. Single-well technique is usually necessary for the localization and evolution of groundwater movement through geological formations. This method is widely used to measure the filtration velocity of the lithology, seepage losses as well as permeability [9] using the following equations:

$$V_{\mathrm{f}} = \pi d/4\phi t \ \ln\left(C_0/C\right) \tag{1}$$

where

V_{f} filtration velocity,
d borehole diameter,
ϕ hydrodynamic distortion coefficient,
t time taken for tracer concentration to fall from C_0 to C.

The permeability of the formation is computed using the filtration velocity (V_{f}) and the hydraulic gradient (i):

$$k = V_f / i \tag{2}$$

4.4 Multi-well Technique

The method is utilized to determine direction of flow and seepage velocity through porous medium. Thus, hydraulic interconnection between two water bodies, if any, can be established. The method involves injecting a predetermined quantity of tracer in one of the boreholes and monitoring its appearance in a number of boreholes located at the downstream, in the anticipated direction of flow. The injected quantity of tracer lasts long enough to detect the tracer in the monitoring boreholes. From the transit time, or the peak concentration, the seepage velocity can be estimated [10].

5 Case Studies

The application of these tracer techniques to detect seepage in earthen embankment and rock-filled dams is explained with various case studies.

5.1 Kota Barrage, Rajasthan

Kota Barrage is a composite structure comprising partly earthen dam and the rest a masonry spillway (total length 551.6 m). The right flank earthen dam abutting against an old palace complex and the spillway portion are founded on completely different foundations. The spillway portion is founded on hard sandstone rock strata, while most of the portion in the earthen dam has pervious base comprising sand, gravel and boulders. This necessitated different types of treatments to be incorporated during the construction. Accordingly, a masonry positive cutoff wall and a grout curtain were provided where the bedrock was fairly deep. In addition, upstream clay blanket, downstream filter drains, inverted filter and relief wells were also provided in the deepest part of the embankment to control foundations seepage, if any and prevent soil erosion. Even after completion of the barrage in 1960, seepage in the right bank earthen dam was observed. Due to the perpetual seepage on the right flank in the palace portion, visible cracks in the various buildings of palace started appearing and continued developing with time. Grouting was undertaken to arrest the seepage but failed to be effective in earthen portion as grout material got washed off.

Geologically, the bed rock comprises hard massive sandstone with open bedding joints. A few transverse vertical joints intersect the bedrock. The right flank earthen dam is abutting against the thick talus deposits comprising silty soil mixed with

pieces of stone, ash, earthen patches, bricks, etc. (deposited during the construction activities in the palace area) overlying the horizontally bedded reddish brown sandstone bedrock.

As the seepage continued to grow alarmingly, it was necessary to decipher the origin of seepage by establishing the exact interconnection between the source (seepage entry point) and the exit point at the location of severe discharge by tracer techniques. As such, five boreholes, viz. BH-1, BH-2, BH-3, BH-4, BH-5 and grout holes (18, 19, 20), were selected for conducting the studies (Fig. 2) using the multi-well technique. The tracer solution was prepared by dissolving 100 gm rhodamine in 200 L of water and was then injected in the BH-5. Its arrival was monitored in boreholes BH-1 to BH-4, grout holes 18, 19 and 20 and at the seepage discharge location in the downstream. The analysis of the samples indicated that the maximum tracer concentration was observed at the discharge location and also in BH 4.

It was clear from the analysis that the BH 5, the discharge location and BH 4 were connected hydraulically. Quantitative analysis of the data indicated a seepage velocity of 2.17 m/min for the water flowing from BH 5 to discharge location and velocity of 1.62 m/min for the water flowing from BH-5 to BH-4. A filtration velocity of 4.01×10^{-2} m/day in BH 5 was deciphered using point dilution method. These high velocity values may be indicative of large crevices in the subsurface sandstone in the palace complex [11].

5.2 Sardar Sarovar Project, Gujarat

Sardar Sarovar (Narmada) Dam is a multipurpose project, among other structures, consists of four earth core rockfill dams, constructed to negotiate the rugged topography in the initial head reach of the main canal, creating four balancing reservoirs (Fig. 3). Of these, at rockfill dams No. 4 seepage was observed. As such, after partial impounding, hydrogeological and tracer studies were conducted. Geologically, area of both the rockfill dams (No. 3 and No. 4) comprises Deccan trap lava flows with intermittent agglomerate, tuff, volcanic breccia and red bole layers. The Deccan trap basalts are of cretaceous to Eocene period. The cretaceous sedimentary rocks like limestone and sandstone were also exposed in the foundation excavation. As this area is in the vicinity of Narmada—Sone lineament, many geological faults were encountered during excavation. As such, the weak features like shear zones, joints faults which were encountered during construction were suitably treated. Curtain grouting was carried out to a depth of 10 m below the cutoff trench foundation level [12].

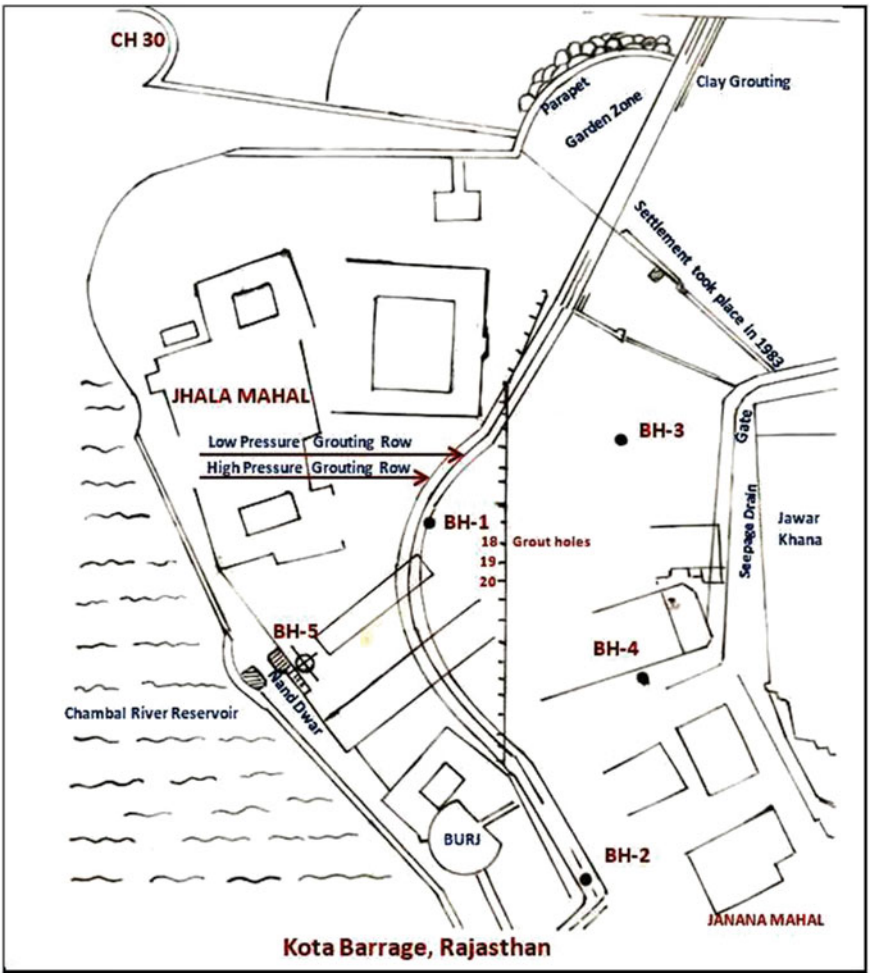

Fig. 2 Layout of Kota Barrage, Rajasthan, showing the details of tracer studies

5.3 Rockfill Dam No. 4 (RFD 4)

The construction of the 505-m-long and 36.7 m high rockfill dam was completed in the year 1982. Subsequently, after partial impounding, seepage was observed at the outlet of the toe drain and was measured regularly using the '*V*' notch. It was apprehended that with the pond attaining full reservoir level after completion of construction of the main dam, the discharge would increase. In order to delineate the cause of this seepage and to study the seepage flow mechanism, tracer studies were conducted along with geophysical and hydrochemical studies using an integrated approach. Figure 4 shows the typical cross section of RockFill Dam,

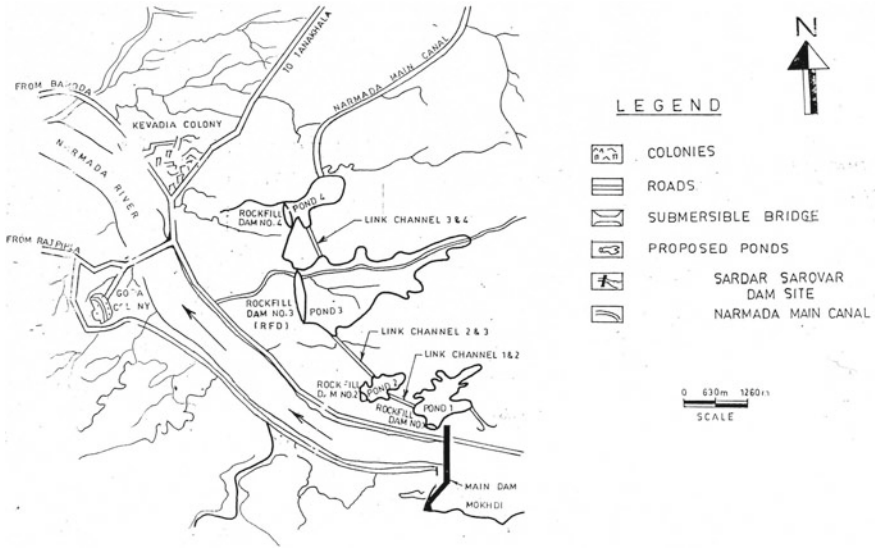

Fig. 3 Index map showing rockfill dams, Sardar Sarovar project, Gujarat

Sardar Sarovar project, Gujarat. Tracer studies were carried out to determine the flow velocity through impervious core as well as to find the interconnection if any between the reservoir water and seepage. The drilling of boreholes for tracer studies was not possible due to presence of rip-rap. Hence, to conduct these studies, three salt bags each containing 50 kg of sodium chloride (common salt) were hung at Ch. 170, Ch. 205 and Ch. 245 located 61.0 m upstream of the central line. The arrival of tracer (salt) was monitored by collecting water samples from the '*V*' notch located about 9.0 m downstream from the centre line. The results indicated that the maximum concentration of salt was recorded after about 16 days. Based on these studies, the determined flow velocity of about 1.25 m/day through the impervious core was considered high compared to the design value of core permeability, i.e. 0.32 m/day. However, tracer studies qualitatively confirmed the interconnectivity between reservoir water and discharge through '*V*' notch. It was inferred that the source of seepage was partly through the foundation and partly through the structure of the dam. Based on these studies, it was recommended that additional grouting would be required in case discharge increased with increase in the reservoir level [13].

5.4 Salaulim Dam, Goa

The Salaulim Dam in Goa is a composite structure of earth-cum-masonry type with central masonry/concrete duckbill spillway and an 847-m-long earthen portion on

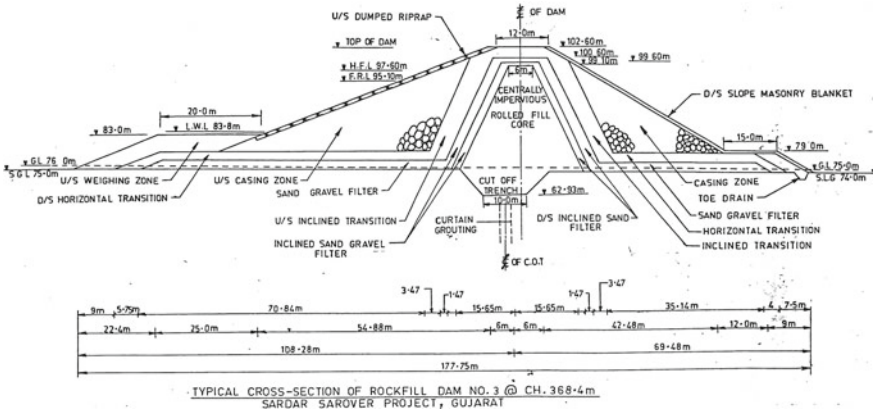

Fig. 4 Cross section of rockfill dam, Sardar Sarovar project, Gujarat

right and left banks. The height of dam is 42.70 m above the deepest foundation level. Excessive seepage was noticed on the downstream toe of the earthen portion and through the laterites in the vulnerable zones in the left flank of the dam. Figure 5 shows the plan of Salaulim Dam with excessive seepage zones.

Based on recommendations of the Dam Safety Panel Committee, tracer studies were conducted in the earthen portions of left and right banks to detect the cause of seepage and determine the seepage parameters. For this purpose, boreholes were drilled and perforated pipes of 19 m length were installed in both the injection and observation boreholes. The studies were conducted using different dyes like sodium chloride, potassium permanganate, Rhodamine-B and sodium fluorescein at different locations. Both the single-well point dilution technique and multi-well methods were

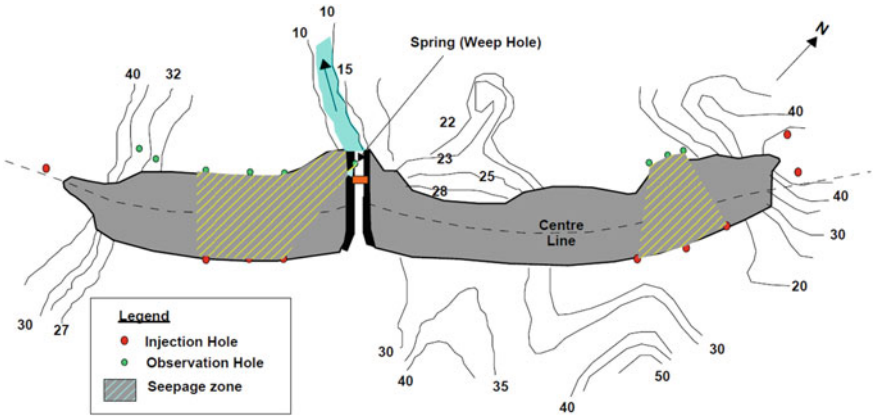

Fig. 5 Plan of Salaulim Dam showing excessive seepage zones

employed to determine the filtration velocity, permeability and other seepage parameters. In the left bank portion, tracers were injected in the injection boreholes drilled at Ch. 200, Ch. 250 and Ch. 300 and samples collected in the observation boreholes situated in the downstream portion at distances varying between 90 and 150 m.

The average time of tracer arrival ranged from 10 to 66 days based on the distance between the injection and observation boreholes and the strata in the earthen dam portion. Similar results were also obtained on the right bank portion. The tracer studies also revealed interconnection between the injection points and the respective sampling locations. In the left bank portion, the permeability values as obtained from tracer studies ranged between 2.6×10^{-4} cm/sec and 5.5×10^{-4} cm/sec. These values corroborated with the permeability values determined by conventional methods. This indicated that the tracer travelled through the highly permeable layer through the COT section and had travelled a distance of about 125 m in the downstream side. It was apprehended that a local layer of high permeability resulted in high seepage velocity. The output of these studies was beneficial in the design and construction of diaphragm wall that would enable the reduction of excessive seepage [14].

6 Conclusions

Tracer techniques have proved to be a valuable tool to find out seepage in the field of water resource management. Tracers both conventional and environmental have been successfully used to investigate a number of hydrological as well as geotechnical problems. Although seepage control measures are incorporated in the design of earthen dams during construction, safety of the structure and uncontrolled seepage is often an important issue in the postconstruction stage. The major pitfalls causing failure in earthen dams often include irregular monitoring and maintenance, use of improper construction material and often ageing of the structures. It is here where CWPRS has successfully applied tracer techniques in detecting seepage and recommending suitable remedial measures to mitigate the seepage and attain the safety of the structure. In Kota Barrage, the tracer studies confirmed the interconnectivity between the seepage entry point in the upstream portion and the discharge locations in the downstream of the barrage. Tracer studies qualitatively confirmed the interconnectivity between reservoir water and discharge through '*V*' notch in the Rockfill Dam No. 4 of Sardar Sarovar project, Gujarat. In Salauli Dam, Goa, the tracer travelled through the highly permeable layer through the COT section and had travelled a distance of about 125 m in the downstream side. Tracer techniques are useful in pinpointing the seepage prone zones thereby providing cost-effective remedial treatment and preventing dam failures. A number of critical and complex dam seepage investigations problems related to seepage through the dam body, foundation, abutments and unsuitable geological settings can be successfully solved economically using these non-destructive tracer techniques.

Acknowledgements The authors are grateful to Director, CWPRS, Pune, for the encouragement and permission to publish this paper. The authors are indebted to the retired scientists of the institute who had contributed in the cited case studies. Facilities and cooperation provided by the project authorities are acknowledged with thanks.

References

1. U S Army Corps of Engineering (2004) General design and construction consideration for earth and rockfill dam-manual
2. Gaspar E, Onescu M (1972) Radioactive tracers in hydrology. Elsevier Publications
3. Alam M, Butha M (2004) Comparative evaluation of canal seepage investigation techniques. J Agric Water Manag 66:65–76
4. Panthulu TV, Krishnaiah C, Shirke JM (2001) Detection of seepage paths in earth dams using self potential and electrical resistivity methods. Eng Geol 59(3–4):281–295
5. Hung Y-C, Chen T-T, Tsai T-F, Chen H-X (2021) A comprehensive investigation on abnormal impoundment of reservoirs—a case study of Qionglin reservoir in Kinmen Island. Water 13:1463
6. Leibundgut C, Maloszewski P, Kulls C (2009) Tracers in hydrology. Wiley, UK
7. Panvalkar GA, Chunade AD (2017) Tracing dam seepage using nuclear borehole logging and tracer techniques, a case study. ISH J Hydraul Eng 311–316
8. Nasseh S, Ghafoori M, Hafezi Moghaddas N, Lashkaripour GR (2013) Investigation of seepage paths in left abutment of Bidvaz dam using tracing technique. Int J Emerg Technol Adv Eng 3(4):719–724
9. Pitrak M, Mares S, Kobr M (2007) A simple borehole dilution technique in measuring horizontal ground water flow. Ground Water 45(1):89–92
10. Huseby O, Valestrand R, Nævdal G, Sagen J (2009) Natural and conventional tracers for improving reservoir models using the ENKF approach. In: EUROPEC/EAGE conference and exhibition. Society of Petroleum Engineers, Amsterdam
11. CWPRS Technical Report No. 2776, Tracer studies at the Kota Barrage, Kota, Rajasthan
12. Shirke JM, Panthulu TV, Panvalkar GA (1996) Hydrogeological studies for delineation of seepage zones at rockfill dams, Sardar Sarovar (Narmada) project, Gujarat. National conference of hydraulics, IIT Kanpur (HYDRO 1996), pp 371–376
13. CWPRS Technical Report No. 3080, Tracer and hydrogeological investigations for seepage at rockfill dam No. 4, Sardar Sarovar (Narmada) Project, Gujarat
14. CWPRS Technical Report No. 2410, Report on the tracer studies at Salauli Dam, Goa

Discharge Coefficient Estimation of Arched Labyrinth Weir Using Gene Expression Programming

Faisal Ahmad, Ajmal Hussain, and Mujib Ahmad Ansari

Abstract A weir is an overflow structure that is constructed across or parallel a river or open channel flow to measure or control the discharge. Weirs may be classified based upon their shape, nature of discharge, width of crest, and nature of crest. The crest length of an arched labyrinth weir is extended by the arch and the provision of notches. In this work, gene expression programming (GEP), a substitute for the traditional regression technique, is persented to estimate the coefficient of discharge (C_d). The experimental data collected from literature has been used for training and validation of the GEP model. Utilising a set of statistical metrics, the proposed GEP models outputs for both the training and validation stages are assessed. Performance of the GEP model is compared with traditional equations-based regression model.

Keywords Arched labyrinth weir · Gene expression programming · Upstream froude number · Coefficient of discharge

1 Introduction

With respect to a specific channel width and upstream depth, a labyrinth weir is a control structure whose crest length is increased by folding it in plan, thus improving discharge capacity in relation to linear overflow control mechanisms. In an arched labyrinth weir, the length of the crest is lengthened by the arch and the provision of notches, which is primarily used as a spillway for dams where the spillway measurement is limited. Many studies in current years have looked at the labyrinth weirs hydraulic efficiency, mostly it relates to geometrical traits. Labyrinth weir research has been going on for decades, with contributions from [1–5], etc.

F. Ahmad · A. Hussain · M. A. Ansari (✉)
Department of Civil Engineering, Zakir Husain College of Engineering and Technology, AMU, Aligarh 202002, India
e-mail: mujibansari68@gmail.com

F. Ahmad
e-mail: faisal.ahmad@zhcet.ac.in

P. V. Timbadiya et al. (eds.), *Flood Forecasting and Hydraulic Structures*, Lecture Notes in Civil Engineering 340, https://doi.org/10.1007/978-981-99-1890-4_43

For the resolution of various issues in water resources engineering, a variety of artificial intelligence techniques, including artificial neural networks (ANNs), adaptive neuro-fuzzy inference systems (ANFISs), gene expression programming (GEP), support vector machines (SVM), and group method of data handling (GMDH), are widely used [6–13]. These new techniques frequently have a high degree of accuracy when predicting future values of relevant variables. They are sturdy and able to adjust to fluctuations and data noise.

Recently, GEP proved to be very useful in water resources engineering application. Ghani and Azamathulla [14] used GEP to investigate sediment transport in a sewer system. Fernando et al. [15] used the GEP technique to create a rainfall-runoff model, whereas Eldrandaly and Negm [16] used GEP to predict water resource data.

In the present study, data collected by Ansari et al. [9] through laboratory experiments in free-flow situation over sharp-crested labyrinth weir were used. The flume chosen for the experiment was 12.8 m long, 0.5 m wide, and 0.39 m deep. A weir of an arched labyrinth design was placed 8.5 m from the flume's intake. The discharge through the arched labyrinth weir was measured using a rectangular weir that was installed at the end of the flume. The collected data were used to establish the correlation for estimation of C_d by GEP technique.

Dimensional analysis was performed by Ansari et al. [9] to estimate the functional relationship for the coefficient of discharge for arched labyrinth weir. It is possible to describe the coefficient of discharge of an arched labyrinth weir as a function of velocity in the cross-section of the basin (V), head above the weir crest (H_T), gravitational acceleration (g), crest span (L), the primary channel's breadth (B), height of crest (P), dynamic viscosity (μ), and density of water (ρ).

The functional relationship for the arched labyrinth weir may be expressed as

$$C_d = f\left(L_P/B, H_T/P, 1/F^2, \mu/\rho V B, N\right) \tag{1}$$

f denotes the inflow Froude number. Impact of the Reynolds number, $R_e = \rho V B/\mu$ is comparatively unimportant in open strait flows and, therefore, may be removed from Eq. (1). The concluding relationship for C_d, may be represented as

$$C_d = f\left(L_P/B, H_T/P, F_r, N\right) \tag{2}$$

Since the N is constant, therefore Eq. (2) changes to

$$C_d = f\left(L_P/B, H_T/P, F_r\right) \tag{3}$$

In the current work, GEP has been employed to examine the impact of various geometric and flow factors on C_d and to establish the link between the dependent and independent variables of Eq. (3).

Table 1 Range of data [9]

Parameter	Unit	Range of data	
		Min	Max
Q	l/s	7.1	24.62
B	m	0.5	0.5
y	m	0.187	0.285
L_P/B	m	1.237	2.113
H_T/P	m	0.045	0.416
F_r	–	0.005	0.122

2 Material and Methods

2.1 Data Collection

Ansari et al. [9] conducted the experiments for arched labyrinth weir under subcritical flow condition. For detailed experimental works, one may refer to the works of Ansari et al. [9]. The range of data collected is presented in Table 1.

2.2 Gene Expression Programming (GEP) Model

Gene expression programming (GEP) is a method of generating a computer programme to model a phenomenon that mimics biological evolution [17, 18]. It is an expression encoding system that enables the rapid use of a comprehensive range of mutation and cross-breeding methods [19]. Each generation becomes healthier and fitter as a result of this selection method. Every generation absolutely reproduces and passes on unaltered fittest individual.

By effectively training the data set, gene expression programming uses genes to convey genetic information to create a variety of very different things, from basic mathematical models to complicated decision trees and neural networks. In order to achieve a target variable with a high R value, GEP additionally creates a strong interrelationship amongst the variables acquired by dimensional analysis by training the data set for an adequate number of generations up to generations without improvement are achieved by concurrently optimising the other parameters of the GEP model. One or more genes connected by a linking function make up a chromosome. It usually works effectively with one to ten genes per chromosome. Extra genes are needed for more intricate tasks. To identify the preeminent grouping of the model building parameter of GEP and determining the most favourable value of population size, gene

Table 2 Optimised value of GEP model

Parameter	Optimised value
Population dimension	34
Quantity of genes per chromosome	3
Gene head size	8
Maximum generations	8000
Generation without improvement	1000
Linking function	Addition
Fitness function	RRSE
Expression function set	+, −, *, /
Mutation rate	0.044
Inversion rate	0.1

head length, gene per chromosome, maximum generation, and generations without improvement (GWI) were found by minimising the variation between the estimated values and the desired output of GEP model. Table 2 shows the optimised parameters used in developing the present GEP model for estimation of C_d for arched labyrinth weir.

The explicit formulation of GEP model for estimation of C_d for arched labyrinth weir has been optimised as follows:

$$C_d = \left[F_r - \left(\left(\frac{F_r}{F_r - \frac{H_T}{P}}\right)\right) + \frac{H_T}{P}\right] + \left[F_r * \left(\left(\left(\frac{6.191}{\frac{L_P}{B}}\right) * (3.171 * F_r)\right) - \frac{L_P}{B}\right)\right] + \left[0.689/\left(\frac{L_P}{B}\right) + 0.315\right] \quad (4)$$

It can be seen from Eq. (4); there are 3 sub-expressions (I, II, and III) associated to individual gene as shown in Fig. 1. The values of a, b, c, and d are 6.191, 3.171, 0.689, and 0.315, respectively.

The discharge coefficient of an arched labyrinth weir in open channels has been calculated using present GEP model and actual values shown against each for training, validation, and all data sets in Fig. 2a–c.

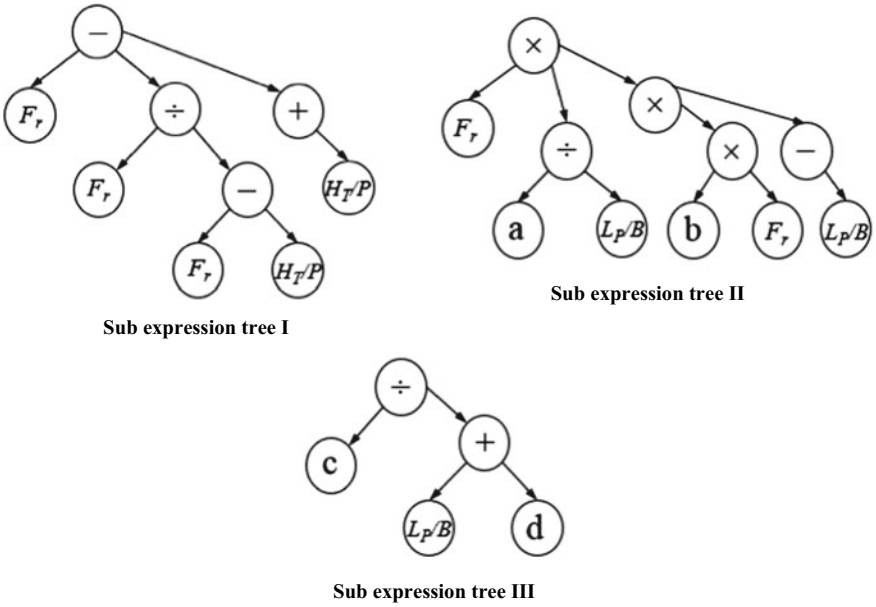

Fig. 1 Sub-expression trees (I, II, and III) associated to gene for the Eq. (4)

3 Evaluation of Existing and Proposed Models

To choose the best effective model for C_d of arched labyrinth weir, an assessment has been made between existing (Ansari et al. [9], Eq. (5)) and established models by means of the identical data. Based on the error estimation metrics R (coefficient of correlation), root mean square error (RMSE), average absolute deviation (AAD), and mean absolute percentage error (MAPE), which are shown in Table 3, the model accuracy is evaluated. Table 3 analysis reveals that the GEP model is superior than the current regression model for estimating the Cd. For training data, the GEP model has the best R value (0.920) and the lowest RMSE value (0.065) compared to the regression model ($R = 0.890$ and RMSE $= 0.060$). All of these models for the validation data sets show a pattern that is quite similar. On the basis of Fig. 2 and Table 2, it is noticed that predicted values of the GEP model are more accurate as compared to the existing regression model. Therefore; the GEP model may be used in order to calculate the discharge coefficient of the arched labyrinth weir.

$$C_d = \left[\left(\left(L_P/B\right)^{-0.67}\left(H_T/P\right)^{-0.8}\left(\frac{F_r}{0.05 + F_r}\right)\right)\right] \tag{5}$$

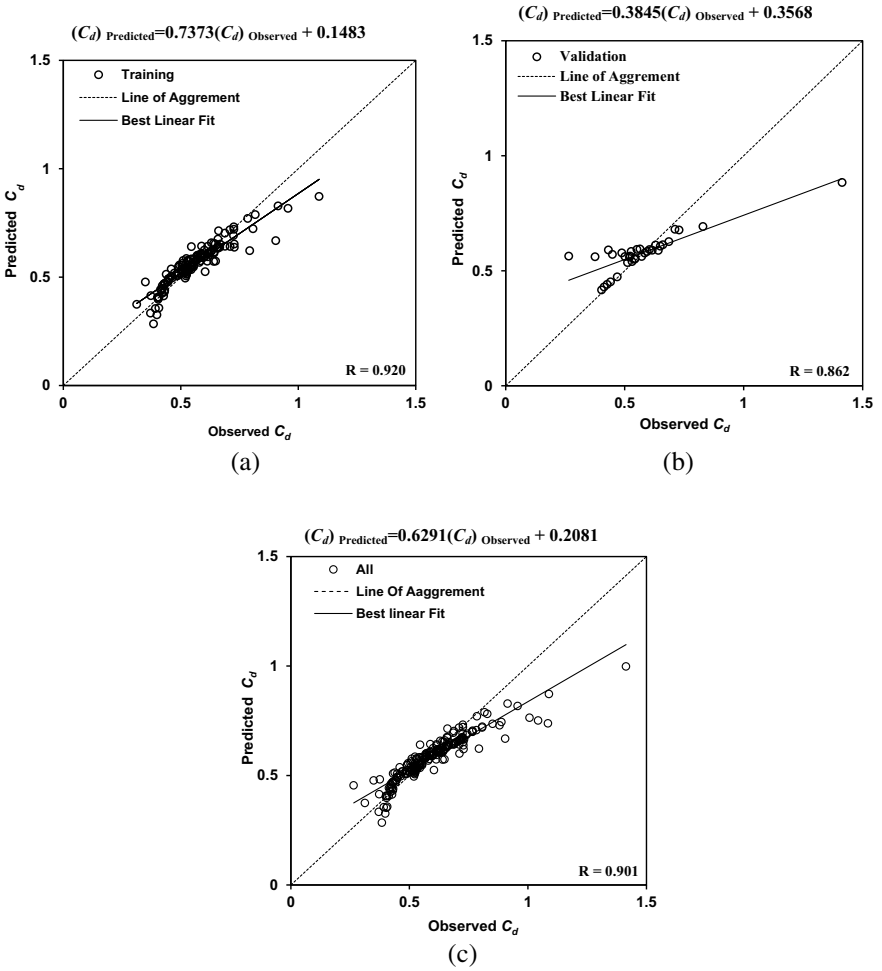

Fig. 2 **a** Experimental and calculated values of C_d (training data sets). **b** Experimental and calculated values of C_d (validation data set). **c** Experimental and calculated values of C_d (all data sets)

Table 3 Performance metrics of existing and developed relationships

S. No	Source	Relationships		Performance parameter				
				R	RMSE	AAD	MAPE	Data set
1	Ansari et al. [9]	Equation (5)		0.895	0.050	7.599	7.603	All
				0.890	0.060	7.758	7.437	Training
				0.893	0.052	7.616	7.520	Validation
2	Present GEP model	Equation (4)	Random per cent	0.901	0.069	7.139	6.892	All
				0.920	0.065	6.937	6.579	Training
				0.862	0.123	11.874	12.897	Validation

4 Conclusion

The results of the current investigation lead to the following conclusions:

(i) A general model for calculating the discharge coefficient for arched labyrinth weir using GEP has been created.
(ii) Due to the GEP models low error and high correlation coefficient, its predictions were typically more accurate than those provided by ordinary regression equations. The network configuration of the GEP model is recommended for overall use to predict the discharge coefficient for arched labyrinth weir.

Acknowledgements The authors are thankful to the Chairman Department of Civil Engineering, ZHCET, AMU, Aligarh for providing necessary laboratory facilities. The authors gratefully acknowledge the financial support for this research provided by the **Council of Scientific and Industrial Research (CSIR)**, Government of India, New Delhi, India.

References

1. Taylor G (1968) The performance of labyrinth weirs. PhD thesis, University of Nottingham, Nottingham, UK
2. Crookston B (2010) Labyrinth weirs. PhD dissertation. Utah State University Library, Logan, Utah, pp 44-66, 95-122
3. Darvas L (1971) Discussion of performance and design of labyrinth weirs, by Hay and Taylor. J Hydraul Eng ASCE 97(80):1246–1251
4. Hay N, Taylor G (1970) Performance and design of labyrinth weirs. J Hydraul Div 96(11):2337–2357
5. Houston K (1982) Hydraulic model study of ute dam labyrinth spillway. US Bureau of Reclamations, Denver, Colo., # GR 82–13, 41p
6. Ansari MA, Athar M (2013) Artificial neural networks approach for estimation of sediment removal efficiency of vortex settling basins. ISH J Hydraul Eng 19(1):38–48
7. Ansari MA (2014) Sediment removal efficiency computation in vortex settling chamber using Artificial Nueral Networks. Water Energy Int Res Dig 71(1):54–67
8. Ansari MA, Hussain A, Ahmad F (2019) Prediction of coefficient of discharge of arched labyrinth weir using ANN technique. In: "Hydro 2019", 24th international conference on hydraulics, water resources and coastal engineering, 18–20 Dec 2019, organized by Osmania University, Hyderabad, India
9. Ansari MF, Hussain A, Ansari MA (2020) Experimental studies and model development of flow over arched labyrinth weirs using GMDH methods. J Appl Water Eng Res. https://doi.org/10.1080/234249676.2020.1799443
10. Ahmad F, Ansari MA, Hussain A, Jahangeer J (2021) Model development for estimation of sediment removal efficiency of settling basins using group methods of data handling. J Irrig Drain Eng 147(2):04020043. https://doi.org/10.1061/(ASCE)IR.1943-4774.0001532
11. Ahmad F, Ansari MA, Hussain A, Jahangeer J (2021) Closure to "model development for estimation of sediment removal efficiency of settling basins using group methods of data handling. J Irrig Drainage Eng. 147(12):04020043. https://doi.org/10.1061/(ASCE)IR.1943-4774.0001532

12. Himanshu SK, Pandey A, Shrestha P (2017) Application of SWAT in an Indian river basin for modeling runoff, sediment and water balance. Environ Earth Sci 76(1):3. https://doi.org/10.1007/s12665-016-6316-8
13. Hussain A, Ansari MA, Ahmed MN, Ahmad F, Jahangeer J (2022) Model development for energy dissipation over gabion stepped weirs using GEP and GMDH techniques. Can J Civ Eng 49(6):969–979. https://doi.org/10.1139/cjce-2021-0197
14. Ghani AA, Azamathulla HM (2010) Gene-expression programming for sediment transport in sewer pipe systems. J Pipeline Syst Eng Pract, ASCE 2(3):102–106
15. Fernando AK, Shamseldin AY, Abrahart RJ (2012) Use of gene expression programming for multimodel combination of rainfall-runoff model. J Hydrol Eng ASCE 17(9):975–985
16. Eldrandaly K, Negm AA (2008) Performance evaluation of gene expression programming for hydraulic data mining. Int Arab J Inf Technol 5(2):126–131
17. Azamathulla HM, Ghani AA, Leo CS, Chang CK, Zakaria NA (2011) Gene-expression programming for the development of a stage-discharge curve of the pahang river. Water Res Manage 25:2901–2916
18. Azamathulla HM (2012) Gene expression programming for prediction of scour depth downstream of sills. J Hydrol 460:156–159
19. Ferreira C (2006) Gene expression programming; Mathematical modelling by an artificial intelligence, 2nd edn. Springer, Heidelberg

Application of ANN in Estimating IRED of Stepped Gabion Weir

M. Danish, M. A. Ansari, and A. Hussain

Abstract A rectangular basket assembled from a hexagonal mesh of heavily galvanised steel wire, filled with rock stacked atop one another to form a weir structure, is known as a Gabion weir. They are porous structures that can sometimes be vegetated and are considered an aesthetic structural solution with minimal habitat. Recently, the stepped gabion weirs have become a popular structure replacing stepped spillways that can check floods. The performance of an artificial neural network, one of the robust machine learning techniques, is investigated in predicting the inverse relative energy dissipation of the stepped gabion weir. The proposed ANN model in the present study is then compared with different machine learning techniques available in the literature. Based on performance parameters, it is observed that the proposed ANN model has the highest accuracy compared to the GMDH and GEP models in predicting the relative energy dissipation of the stepped gabion weir.

Keywords Inverse relative energy dissipation (IRED) · Artificial neural network · Stepped gabion weir · Gabion number

1 Introduction

Gabion weir is a broad crested weir made up of netted (wire mesh) box filled with stone aggregates. The wire mesh is often hexagonal, though it can also be square, rectangular, or circular. Depending on the size of the stone aggregates, its size may

M. Danish (✉)
Civil Engineering Section, University Polytechnic, Aligarh Muslim University, Aligarh 202001, India
e-mail: mohddanish.bp@amu.ac.in

M. A. Ansari · A. Hussain
Department of Civil Engineering, Zakir Husain College of Engineering and Technology, Aligarh Muslim University, Aligarh 202001, India
e-mail: maansari@zhcet.ac.in

A. Hussain
e-mail: ajmal.hussain@zhcet.ac.in

P. V. Timbadiya et al. (eds.), *Flood Forecasting and Hydraulic Structures*, Lecture Notes in Civil Engineering 340, https://doi.org/10.1007/978-981-99-1890-4_44

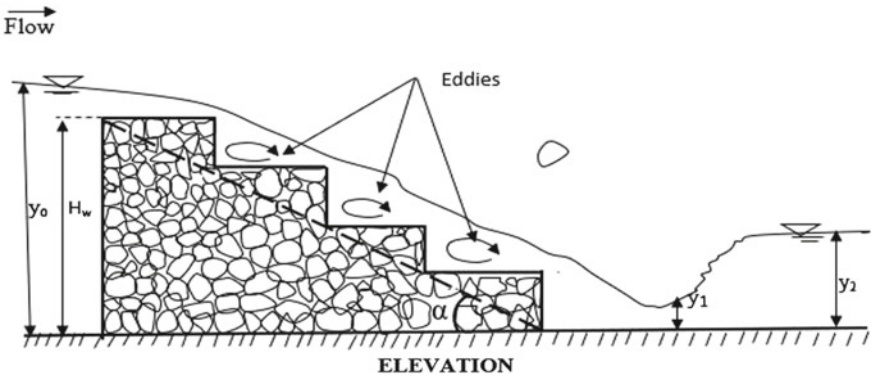

Fig. 1 Stepped gabion weir [15]

change. The shape of stone aggregates may be flaky, round, well-graded, uniformly graded, gap graded, or vary according to availability. The size of stone aggregates may vary according to availability at the source site. The porosity of the gabion aids in water transmission and lowers the water load behind the structure. Gabion weirs enable the simple movement of aquatic life and materials that can be moved by flowing water. The inhibiting bacteria between the granular surfaces of the gabion weir decompose organic matter. Due to this biochemical reaction, the river or canal water flowing through the pores of the gabion weir gets purified. Hence, they provide an economical alternative in areas where abundant stones are available [1–3]. The study of flow hydraulics over gabion weir is still under investigation, as it depends on the complexity of the structure and various hydraulic effects due to flow through porous media. Figure 1 shows the sketch of flowing water upstream to downstream through a stepped gabion weir and the hydraulic jump formation downstream.

Additionally, a stepped gabion weir is an inexpensive way to disperse energy from upstream to downstream. Energy is lost through jet impingement and friction losses through the rock fill as a result of the mixing of flow through the rock with flow over the crest. Vortex flow and high turbulences are produced as a result of the gabion weir's increased roughness and momentum transfer, which helps to dissipate energy. As a result, the stilling basin's size decreases [4, 5]. Stephenson [6, 7] developed calculations for energy loss and chute drop for permeable gabion-stepped spillways. During skimming, flow regime stepped spillways frequently operate at high discharges. Form losses cause large energy and momentum transfer from the mainline to the recirculation zones for a coherent stream formed by step edges, creating a pseudo-bottom (i.e. a bottom that is not solid) [8–10]. Whilst Kells [11–13] explored the interactions between seepage and free-surface flows gabion weirs, Peyras et al. [14] studied the flow patterns and energy dissipation of stepped gabion weirs.

Numerous scholars have investigated energy dissipation across the stepped gabion weir [11, 16, 17]. As artificial intelligence (AI) techniques for tackling difficulties in

hydraulic engineering, artificial neural networks (ANNs), gene expression programming (GEP), and group method of data handling (GMDH) have lately grown in prominence [18–27]. The energy dissipation equation has previously been produced by researchers using dimensional analysis and nonlinear regression analysis, although this method is less accurate and requires time-consuming calculations. As a result, this practice has lost favour in the modern, advanced world. To forecast inverse relative energy dissipation (IRED) in stepped gabion weirs, Hussain et al. [15] introduced the GMDH and GEP model.

The literature assessment indicates that there has not been a comprehensive computational examination of IRED based on AI techniques in general and particularly ANN, and that work in this area is urgently needed. In the present study, an artificial neural network is used to calculate the inverse relative energy dissipation (IRED) in a stepped gabion weir.

2 Materials and Method

2.1 Data Collection

In this study, 108 experimental datasets about the energy dissipation of flow over the stepped gabion weir under skimming flow conditions were obtained from the literature and used to build an artificial neural network model [5, 28, 29]. The results have been compared with the GMDH and GEP models proposed by Hussain et al. [15]. Table 1 includes a list of the range of these data. The correlation between IRED and the other parameters can be expressed as [15]:

$$\text{IRED} = f(m, e, \eta, \text{Fr}, y_1/H_w)$$

where $m = \tan(\alpha)$ is the slope of the weir, e is the porosity of gabion material, η is the gabion number defined as q^2/gH_w^3, q is discharge per unit width, g is the acceleration due to gravity, Fr is Froude number just before the jump, y_1 is tailwater depth before the jump, and H_w is the height of the gabion weir.

Table 1 Non-dimensional factors gathered from the literature and employed in the current study

Parameters	Details	
	Minimum value	Maximum value
IRED	1.1730	7.2990
η	0.0000722	0.0670
m	0.5000	1.7320
e (%)	11.3718	72.6637
Fr	2.1146	6.4731
y_1/H_w	0.0120	0.1900

2.2 ANN Model

An alternative computational method known as artificial neural networks (ANNs) is based on the extensive network of biological systems and parallel processing architecture. The goal of ANN research is to simulate the brain as a computational device that is equivalent to the brain for a variety of computational tasks that are challenging for ordinary serial computers. ANNs are set up with several parallel, interconnected processing devices (called nodes) following conventional topologies. The collective behaviour of ANN exhibits the capacity to learn from training patterns or data, retain such patterns, and generalise them [30–34].

In this study, the artificial neural network (ANN) model was trained using the observed IRED data as the output variable whilst defining the m, e, η, Fr, and y_1/H_w as the input variables in MATLAB. Eighty per cent and twenty per cent of the 108 data points were split between the training and validation datasets, respectively. The Levenberg–Marquardt backpropagation technique was initially used to train the network. As an activation function, the sigmoid function was employed. As illustrated in Fig. 2, the network was originally configured with a hidden layer of five neurons, five input layers, and one output layer.

3 Results and Discussion

Random numbers were used as the initial settings for all weights and bias values. The hidden nodes were put through trials even though the input and output node counts were fixed. According to the correlation coefficient, the one generating the most accurate findings was chosen. When the network performance at 24 epochs reached 0.0735, the neural network training was terminated. The validation of the model was stopped when the error computed between the observed IRED and predicted IRED had the maximum number of instances near the zero-error line, as shown in Fig. 3. The learning curve of the present ANN model is shown in Fig. 4. The plot of observed versus predicted values of IRED for training and all datasets are shown in Figs. 5 and 6, respectively. The correlation coefficient for training and all datasets is found to be 0.982 and 0.978, respectively. It can be observed from these figures that all the

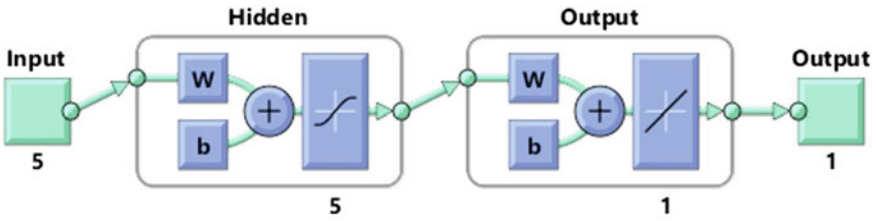

Fig. 2 Artificial neural network developed in the present study

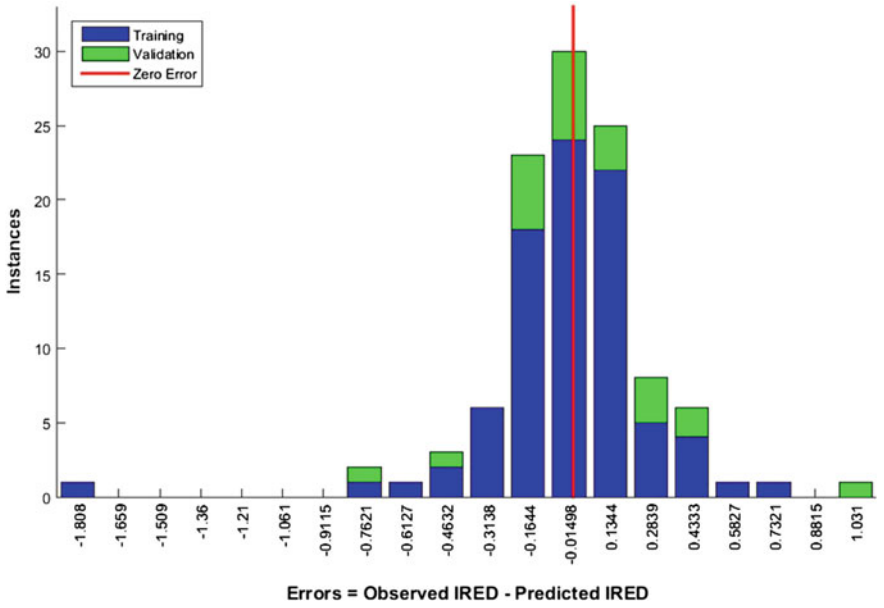

Fig. 3 Error histogram for training and validation data

data points fall on the line of perfect agreement, which is almost coincidental to the best linear fit line.

3.1 A Comparison of GMDH, GEP, and ANN Models

Using the same dataset, comparisons between the ANN model and the GMDH and GEP models proposed in the literature [15] were made to assess the suggested ANN model's accuracy in estimating the IRED of the stepped gabion weir. The various performance parameters for different datasets are listed in Table 2 for comparison. The GMDH and GEP models have correlation coefficients (R) of 0.973 and 0.963, respectively, whereas the ANN model has R equal to 0.978 and performs better in terms of prediction accuracy. The root mean squared error (RMSE) of 0.324 for the ANN model is the least compared to the RMSE of 0.355 and 0.415 for GMDH and GEP models. Further observation reveals that the accuracy of the ANN model's training ($R = 0.982$ and RMSE $= 0.312$) is higher than that of the GMDH ($R = 0.979$ and RMSE $= 0.313$) and GEP models ($R = 0.969$ and RMSE $= 0.376$).

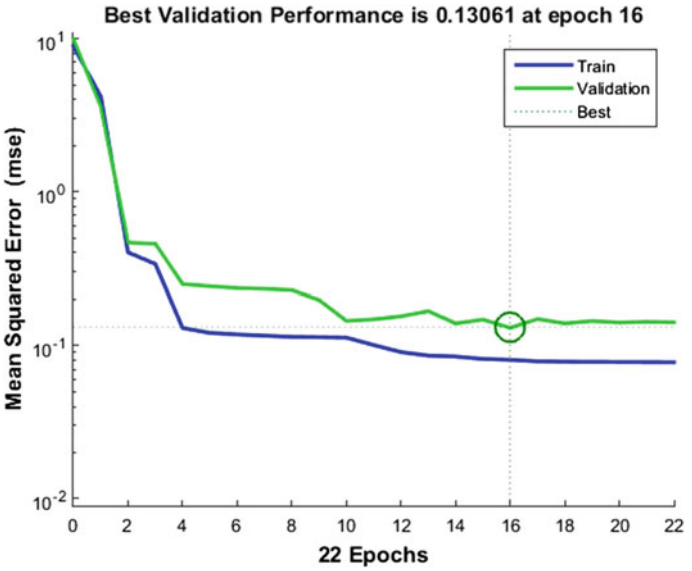

Fig. 4 Learning curve of ANN model proposed in this study

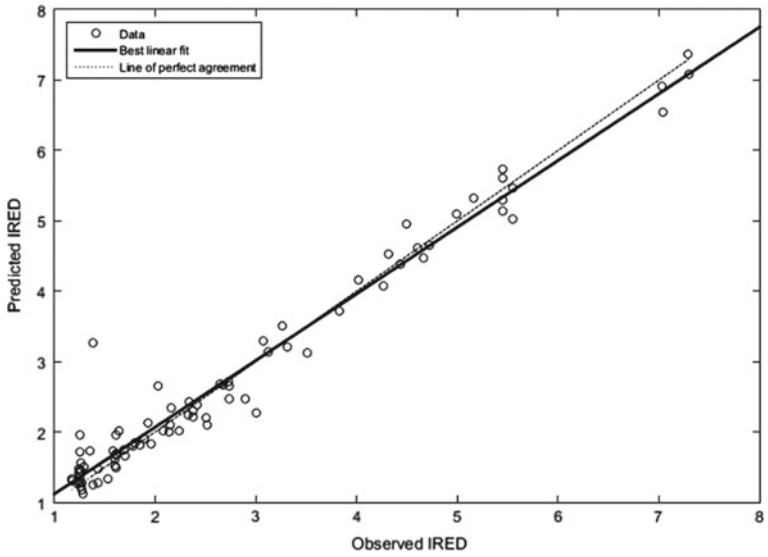

Fig. 5 Observed IRED versus predicted IRED for training data

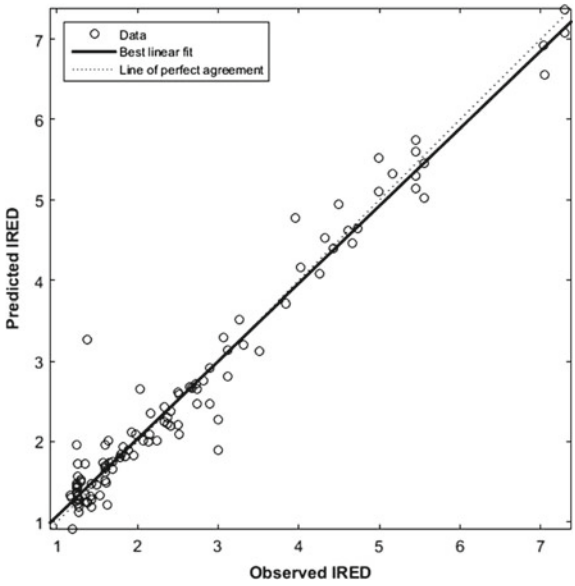

Fig. 6 Observed IRED versus predicted IRED for all data

Table 2 Performance comparison of GMDH, GEP, and ANN models

Models	Performance parameters	Training data	Validation data	All data
GMDH model [15]	*R*	0.979	0.964	0.973
	RMSE	0.313	0.445	0.355
GEP model [15]	*R*	0.969	0.959	0.963
	RMSE	0.376	0.493	0.415
ANN model (present study)	*R*	0.982	0.950	0.978
	RMSE	0.312	0.365	0.324

4 Conclusions

Gabion weirs allow the easy passage of materials that exist with flowing water and the movement of aquatic life. Hence, for flood control purposes, they provide an economical alternative in areas where stones are abundantly available. Various researches have been conducted on the energy dissipation of stepped gabion weirs, and various regression models have been proposed. Estimating the inverse relative energy dissipation of stepped gabion weirs has recently been proposed using a group method of data handling and gene expression programming. In this paper, the artificial neural network was applied to predict the inverse relative energy dissipation of the stepped gabion weir. It was discovered that this model performed more effectively than gene expression programming, regression, and the group method of data handling. The correlation coefficient (R) and root mean squared error (RMSE) were used to compare

the models. Compared to the GMDH ($R = 0.973$ and RMSE $= 0.355$) and GEP ($R = 0.963$ and RMSE $= 0.415$) models, the ANN model constructed in this work shows improved prediction performance with $R = 0.978$ and RMSE $= 0.324$.

References

1. Mohammed HI (2010) Flow over gabion weir. J Irrig Drain Eng. https://doi.org/10.1061/(ASCE)IR.1943-4774.0000215
2. Zhang G, Chanson H (2014) Two-phase flow on a gabion stepped spillway: cavity and seepage air-water motion. In: Proceedings of 19th Australasian fluid mechanics conference, Melbourne, Australia
3. Zhang G, Chanson H (2016) Gabion stepped spillway: interactions between free-surface, cavity and seepage flows. J Hydraul Eng. https://doi.org/10.1061/(ASCE)HY.1943-7900.0001120
4. Hager WH, Vischer DL (1995) Energy dissipators. In: IAHR Hydraulic structures design manual series. CRC Press, p 9
5. Chinnarasri C, Donjadee S, Israngkura U (2008) Hydraulic characteristics of gabion-stepped weirs. J Hydra Engg, ASCE 134(8):1147–1152
6. Stephenson D (1979) Gabion energy dissipators. In: Proceedings of the 13th ICOLD congress, Q. 50, R. 3, New Delhi, India, pp 33–43
7. Stephenson D (1988) Stepped energy dissipators. In: Proceedings of the international symposium on hydraulics for high dams, IAHR, Beijing, pp 1228–1235
8. Rajaratnam N (1990) Skimming flow in stepped spillway. J Hydra Engg 116(5):587–591
9. Chamani MR, Rajaratnam N (1999) Characteristics of skimming flow over stepped spillways. J Hydra Engg 125(4):361–368
10. Chanson H, Toombes L (2004) Hydraulics of stepped chutes: the transition flow. J Hyd Res 42(1):43–54
11. Kells JA (1993) Spatially varied flow over rockfill embankments. Can J Civil Eng 20(5):820–827
12. Kells JA (1994) Energy dissipation at a gabion weir with through flow and overflow. In: Annual conference Canadian society for civil engineering, Winnipeg, Canada, pp 26–35
13. Kells JA (1995) Comparison of energy dissipation between nappe and skimming flow regimes on stepped chutes–discussion. J Hyd Res 33(1):128–133
14. Peyras L, Royet P, Degoutte G (1992) Flow and energy dissipation over stepped gabion weirs. J Hydra Engg 118(5):707–717
15. Hussain A, Ansari MA, Ahmed N et al (2021) Model development for energy dissipation over gabion stepped weirs using GEP and GMDH techniques. Can J Civ Eng. https://doi.org/10.1139/cjce-2021-0197
16. Shariq A, Hussain A, Ahmad Z (2020) Discharge equation for the gabion weir under through flow condition. Flow Meas Instrum. https://doi.org/10.1016/j.flowmeasinst.2020.101769
17. Al-Fawzy AM, Al-Mohammed FM, Alwan H (2020) Energy dissipation in gabion weirs. IOP Conf Ser Mater Sci Eng. https://doi.org/10.1088/1757-899X/671/1/012068
18. Ansari MA (2014) ANN model for prediction of length of hydraulic jump on rough beds. Int J Civ Eng Technol 5(3):23–31
19. Danish M (2014) Prediction of scour depth at bridge abutments in cohesive bed using gene expression programming. Int J Civ Eng Technol (IJCIET) 5(11):25–32
20. Danish M, Alam J, Muzzammil M (2016) Scour depth prediction at bridge abutments in cohesive bed using group method of data handling. In: Proceedings of the international conference on hydraulics water research and coastal engineering (Hydro 2016), CWPRS Pune, India
21. Ansari MF, Hussain A, Ansari MA (2020) Experimental studies and model development of flow over arched labyrinth weirs using GMDH methods. J Appl Water Eng Res. https://doi.org/10.1080/234249676.2020.1799443

22. Ahmad F, Ansari MA, Husain A, Jahangeer J (2021) Model development for estimation of sediment removal efficiency of settling basins using group method of data handling. J Irrig Drain Eng 147(2):04020043
23. Hussain A, Shariq A, Danish M, Ansari MA (2021) Discharge coefficient estimation for rectangular side weir using GEP and GMDH methods. Adv Comput Des 2(6):135–151. https://doi.org/10.12989/acd.2021.6.2.135
24. Alam J, Muzzammil M, Danish M (2015) Flood frequency analysis using gene expression programming. In: Symposium on hydrology, Indian Association of Hydrologists (IAH), New Delhi, India
25. Danish M, Alam J, Muzzammil M (2017) A soft computing approach to flood frequency analysis of river Ganga. In: Proceedings of the 22nd international conference on hydraulics, water resources and coastal engineering (Hydro 2017), Ahmedabad, India
26. Muzzammil M, Alam J, Danish M (2015) Scour prediction at bridge piers in cohesive bed using gene expression programming. Aquatic Procedia 4:789–796. https://doi.org/10.1016/j.aqpro.2015.02.098
27. Muzzammil M, Alam J, Danish M (2015) The GMDH model for prediction of scour at bridge pier in cohesive bed. In: 20th international conference on hydraulics, water resources and river engineering, Hydro 2015 international, IIT Roorkee, India
28. Salmasi F, Chamani MR, Zadeh DF (2012) Experimental study of energy dissipation over stepped gabion spillways with low heights. IJST Trans Civ Eng 36(C2):253–264
29. Khatibi R, Salmasi F, Ghorbani MA, Asadi H (2014) Modelling energy dissipation over stepped-gabion weirs by artificial intelligence. Water Resour Manage 28(7):1807–1821
30. Kumar V, Yadav SM (2021) Real-Time flood analysis using artificial neural network. In: Recent trends in civil engineering. Springer, Singapore, pp 973–986
31. Muzzammil M, Alam J, Danish M (2015) Application of gene expression programming in flood frequency analysis. J Indian Water Resour Soc 35(2):1–6
32. Balkhair KS (2002) Aquifer parameters determination for large diameter wells using neural network approach. J Hydrol 265:118–128
33. Ansari MA, Ansari SA, Alam S (2018) Computation of scour depth below pipelines using artificial neural networks. Water Energy Int 61(6):55–62
34. Ansari MA, Athar M (2013) Artificial neural networks approach for estimation of sediment removal efficiency of vortex settling basins. ISH J Hydraul Eng 19(1):38–48. https://doi.org/10.1080/09715010.2012.758415

Hydraulics of Morning Glory Spillway—An Overview

Prajakta Gadge and M. R. Bhajantri

Abstract Morning glory spillway is one of the water conveyance structures from the reservoir to downstream and is named due to its horny shape. In this type of spillway, water passes through a vertical shaft, horizontal or nearly horizontal tunnel, and joins the downstream river channel. They are used advantageously at dam sites in narrow canyons with steep abutments. The cost of construction of the morning glory spillway is low due to the use of a diversion tunnel constructed at the time of dam construction as a horizontal tunnel. This paper gives an overview of the morning glory spillway in respect of its hydraulic design considerations and different hydraulic aspects that need to be studied in evolving the efficient design of the spillway. The paper presents the desk study of the tunnel spillway of Lakya Tailing Dam, Kudremukh, Karnataka, studied at CWPRS, Pune, along with the discussion of the behavior of the spillway at the project site. This dam plays a vital role in running the Kudremukh Iron Ore Plant. At the project site, vibrations were experienced while passing the discharge over the morning glory spillway inlet. CWPRS carried out the detailed desk studies considering theoretical design considerations and recommended to provide aeration pipe on the spillway crest and suggested strengthening of morning glory inlet shaft. The study is discussed in detail in the present paper.

Keywords Morning glory spillway · Vertical shaft · Diversion tunnel · Energy dissipator

1 Introduction

The morning glory spillway is attractive which can often be constructed at less cost than other types and it is readily adapted to dams in narrow, steep canyons. The vertical shaft spillway of large capacity generally has a morning glory crest, so the spillway is called a morning glory spillway. Figure 1 shows the view of morning glory intake. The crest profile of a morning glory intake conforms to the lower surface of a

P. Gadge (✉) · M. R. Bhajantri
Central Water and Power Research Station, Pune 411024, India
e-mail: prajaktagadge@gmail.com

P. V. Timbadiya et al. (eds.), *Flood Forecasting and Hydraulic Structures*, Lecture Notes in Civil Engineering 340, https://doi.org/10.1007/978-981-99-1890-4_45

nappe flowing over an aerated sharp-crested circular weir for various combinations of P/Rs and Hs/Rs as shown in Fig. 2.

In contrast to the crest profiles of straight spillways, where the profiles become flatter with increasing heads, the crest profiles for circular weirs become steeper as the head increases. USBR [3] has defined the crest profile in terms of upstream and downstream quadrants for selected conditions of P/Rs = 0.15, 0.30 and 2.0, and Hs/Rs = 0.2 to 2, similar to the crest profiles for straight ogee spillways.

Structures with vertical shafts are designed to operate either with free flow, submerged flow, or both. Generally, a free weir flow prevails over the crest for Ho/Rs up to about 0.45, partly submerged weir flow for Ho/Rs values between 0.45 and 1.0, and above this value, the weir is completely submerged and the coefficient of discharge sharply falls. However, morning glory spillways are typically designed to only operate in the crest control range (free flow) as larger discharges could result in adverse flow conditions in the downstream conduit or tunnel (slug and/or pressure flow). The circular crest should converge to the shaft; the diameter of the shaft would

Fig. 1 Typical view of morning glory intake

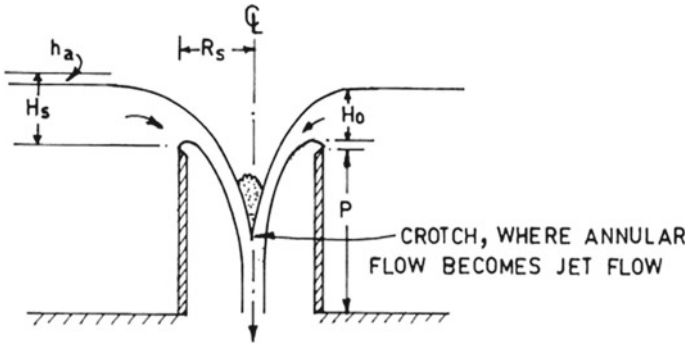

Fig. 2 Crest profile for morning glory spillway intake

generally be the same as the diameter of the downstream leg or tunnel. Generally, the tunnel section is selected, so that it will not flow more than 75–80% full at the downstream end for the maximum discharge.

Aeration and de-aeration are very important features of this type of spillway as the entrapped air may become explosive leading to the catastrophic condition. The air entrainment mechanism is closely related to the type of flow conditions in the shaft and has been schematically illustrated in Fig. 3. Khatsuria [2] has reported the general consideration for the morning glory spillway. At the beginning of overflow with low water levels, the discharge characteristics are similar to a weir control and the flow in the shaft clings to the walls as a relatively thin sheet. The volume flow rate of air is determined by the shear action of the air–water interface and by entrainment into the mass of water. This type of flow has been designated as Region I. The quantity of air entrained increases with discharge, and with the increase in discharge, a point is reached when the sheet of water is sufficiently thick to completely seal the air passage at the lower end of the shaft. This water discharge separates Region I from Region II. This type of flow is characterized by an annular hydraulic jump. Further increase in the discharge merely causes the location of the jump to move upward in the vertical shaft. The quantity of air entrained then decreases with discharge. When the jump reaches a point near the top of the shaft, the flow is said to become submerged.

The paper presents the desk study of tunnel spillway of Lakya Tailing Dam, Kudremukh, Karnataka studied at CWPRS [1].

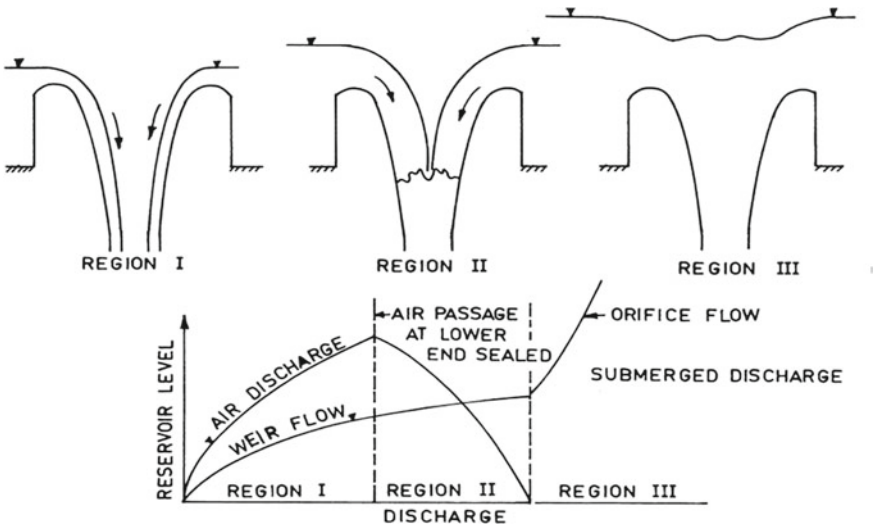

Fig. 3 Flow conditions in the shaft

2 Case Study

2.1 The Project

The Lakya Dam is located at Kudremukh in Chickmaglur District of Karnataka state about 110 km from the coastal city of Mangalore. Figure 4 shows the index map of the project. The iron ore taken from the mines contains 38% useful material, and the remaining 62% contains residual iron content of 22% is tailing which is required to be stored. For storage of tailings, a 100 m high earth dam is constructed on Lakya holey, a tributary of Bhadra River. Construction of the tailing dam took place in two stages. The construction of the 65 m high Lakya Dam was completed in 1980 in the first stage, and in the second stage in 1994, the dam was raised from 65 to 100 m. The Lakya Dam with the top at El. 890 m and a total capacity of 245 million cum was designed for a PMF discharge of 854 m^3/s inflow. Flood routing studies were carried out, and maximum water level El. 874.4 m and routed discharge of 33 m^3/s were worked out corresponding to a morning glory spillway inlet crest at El. 875 m. The Lakya holey stream is at an elevation of El. 1427 m and travels 7.9 km before meeting Bhadra River near Kudremukh. It drains an area of 18.7 km^2 up to Lakya Dam site. The catchment area of Lakya holey is moderately wide fan shaped and receives an annual rainfall of about 7000 mm. The purpose of the reservoir is to store tailings and meet the plant process water requirement. Figure 5 shows the view of the tailing deposits from the intake tunnel leading to the KIOCL plant.

There were no regulatory devices provided for spillage of flood except tunnel spillway. In the first stage, a 17.5 m wide and 160 m long chute spillway was provided on the right bank to take care of the design flood of 611 m^3/s at FRL El. 850 m. While

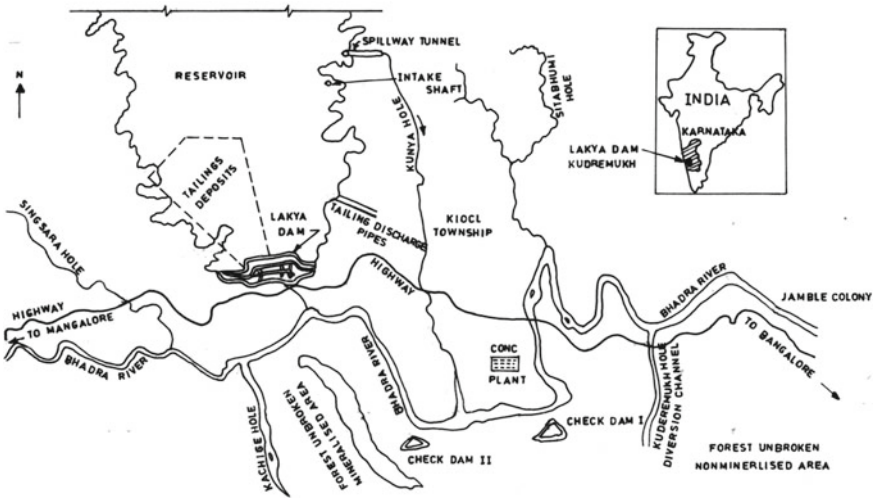

Fig. 4 Index map of the project

Fig. 5 View of tailing deposit from intake tunnel leading to plant

raising the dam, the chute spillway provided on the right bank of the earth dam got buried in the body of the dam and a 3.75 m(H) × 4 m (W) D-shaped tunnel spillway with control structures at different elevations was provided as a flood surplussing arrangement. Two inlets at El. 875 m and El. 885 m were provided for surplussing the water. Both the morning glory inlet at El. 875 m and the overflow inlet at El. 885 m which are connected to the same tunnel spillway are located at about 200 m from the Lakya Dam along the left flank of the reservoir. The inner diameter of the shaft at the morning glory crest is 3.5 m which reduces gradually to 2.1 m at El. 872.293 m. From El. 866 m, a 900 bend begins which joins the existing D-shaped tunnel. An overflow spillway inlet in the form of an inclined shaft with the crest at El. 885 m connecting to the tunnel spillway was constructed to surplus the flood at a later stage when the use of the morning glory spillway inlet will be stopped by plugging the upstream face of the intersection of an inclined shaft with a horizontal tunnel. Figure 6 shows the cross section of the tunnel spillway. Figure 7 shows the details of the morning glory intake. Figure 8 shows a view of the morning glory intake.

At the tunnel spillway exit, a stilling basin was provided for energy dissipation. The downstream channel was protected by providing gabions along the banks. A secondary weir was constructed at about 100 m downstream to boost up the tail water levels to ensure jump formation in the stilling basin. The tunnel spillway discharges in Kunya holey stream which joins river Bhadra after traversing about a kilometer.

A morning glory inlet at El. 875 m connected with the tunnel spillway is in use since 2001. At the project site, vibrations were experienced while passing the discharge of the order of 16–27 m^3/s over the morning glory spillway inlet and the

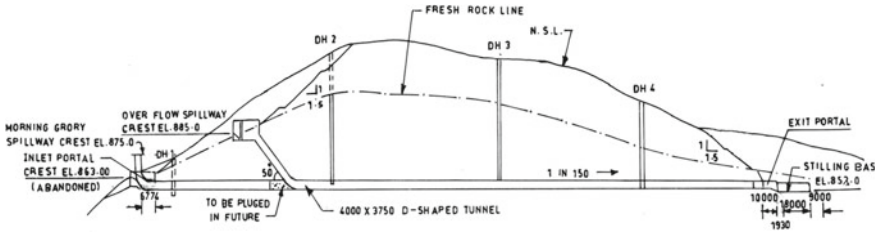

Fig. 6 Cross section of tunnel spillway

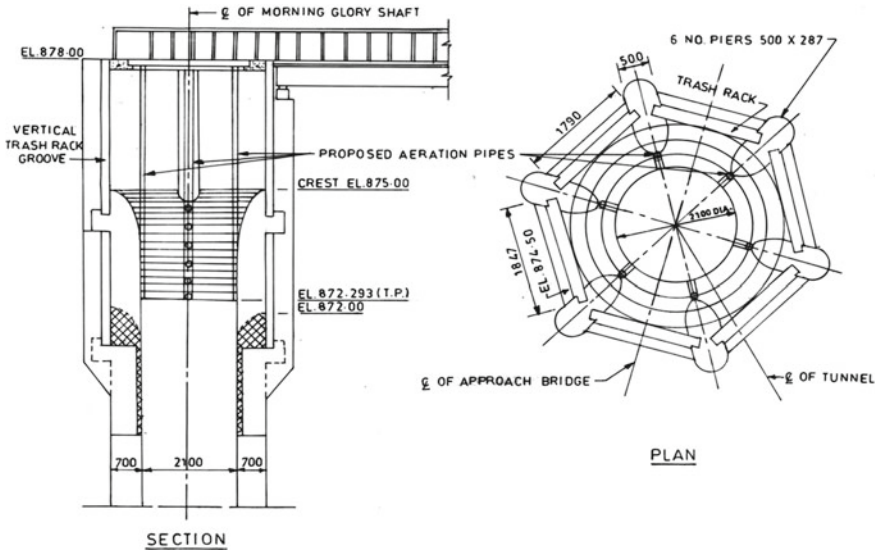

Fig. 7 Details of morning glory spillway intake

noise was heard during the operation of the spillway. Therefore, the desk studies were referred to CWPRS for assessing the hydraulic adequacy of the tunnel spillway to pass the design discharge and performance of the spillway.

2.2 Desk Study

The design for the morning glory spillway was worked out based on the procedure given in "Design of Small Dams—USBR Publication" and found to be in order. The discharging capacity curve based on the above calculations is depicted in Fig. 9. The design maximum outflow of 33 m^3/s could be passed with a maximum reservoir water level of 877.32 m as against the top of pier El. 878 m. Therefore, the discharging capacity of the morning glory spillway inlet was found to be adequate.

Fig. 8 View of morning glory intake

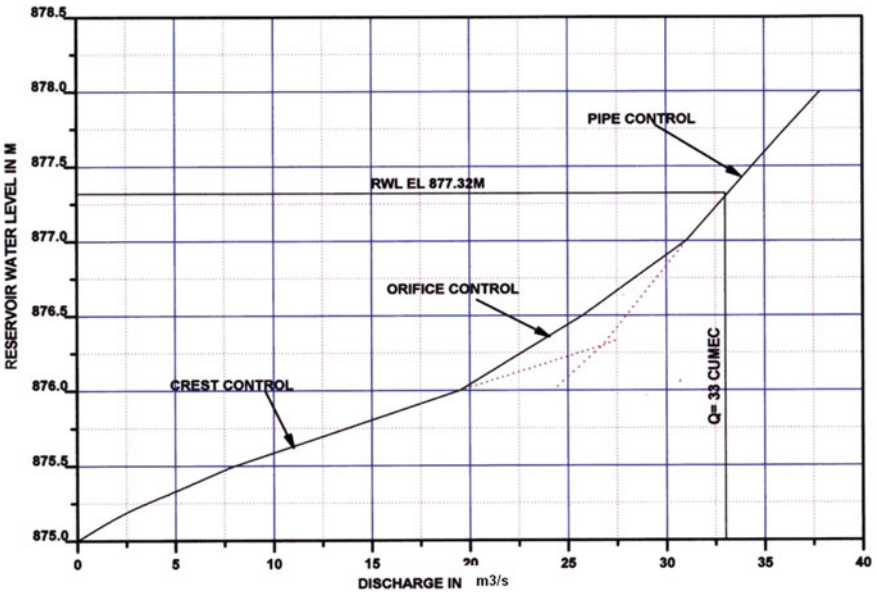

Fig. 9 Discharging capacity curve of morning glory spillway inlet

At the project site, vibrations were experienced while passing the discharge of the order of 16–27 m^3/s over the morning glory spillway inlet. The flow approaching the spillway was calm and quiet without any formation of vortices. The crotch in the morning glory was moving up and down approximately by 2 m. The noise was heard during the operation of the spillway. Accordingly, vibrations were measured using a vibration meter at the site. Table 1 gives the reservoir levels, discharge passed, and maximum vibrations recorded in microns quiet.

It was observed that the head over the crest was in the range of 0.86–1.6 m. The intensity of vibrations increased as the depth of overflow increased. This phenomenon was correlated with the discharging capacity curve with respect to head over crest (h). The region between $h = 0$ to 1 m was in the crest control zone; $h = 1$–2 m was the orifice control zone which is between the crest and pipe control zone; $h =$ 2 to 3 m was in the zone of pipe control. The vibrations were experienced when the discharge of the order of 16–27 m^3/s was passed over the morning glory spillway inlet. This range of discharges falls in the transition zone.

For the circular weir, the water profiles for the higher heads fall inside those for the lower heads closer to the spillway profiles. Therefore, if the morning glory inlet is designed for the maximum water head, sub-atmospheric pressures along the lower part of the nappe will occur for water heads less than maximum. In such case, aeration is required to ventilate the nappe from downstream of the crest, so as to introduce air in between the vertical face and lower water surface profile to avoid make and break action and consequent vibrations of the shaft. Therefore, it was suggested to provide aeration pipes along the periphery of the morning glory crest. Initially, two pipes of 5 cm (2 inch) diameter each were installed inside the crest in two opposite spans with the view to release the air trapped in the flow. However, it was observed that air was being sucked through the pipe and the intensity of vibrations was reduced. Subsequently, these pipes were replaced by three bigger size pipes of 10 cm (4 inch) diameter. Figure 10 shows the view of these pipes.

It was observed at the site that vibrations were again experienced where the reservoir was at El. 876.44 m and the morning glory spillway inlet was passing a discharge of approximately 25 m^3/s. During the site visit, it was observed that the pipes were not along the periphery of the crest and the cross bracings to keep the pipe in position were obstructing the flow. Hence, it was recommended to install a 10 cm (4 inch) diameter pipe each along the inner side of the pier to improve the

Table 1 Vibrations measured in the morning glory inlet structure by using vibration meter

Date	Rainfall (mm)	Reservoir level m	Discharge m^3/s	Maximum vibrations in microns
10–7–2001	86.00	876.60	27.16	400
11–7–2001	32.00	876.42	25.053	150
12–7–2001	5.00	876.20	22.78	60
13–7–2001	24.00	876.00	19.49	25
14–7–2001	10.00	875.86	16.07	11

Fig. 10 Aeration pipes in morning glory spillway inlet

aeration of flow and reduce the vibrations as shown in Fig. 7. It was also suggested to strengthen the morning glory inlet shaft to reduce/withstand vibrations.

3 Conclusion

Morning glory spillways are commonly used in large dam projects due to their lower construction costs by using an existing diversion tunnel as a horizontal tunnel. This paper highlighted the desk study for Lakya Dam at Kudremukh, Karnataka, carried out at CWPRS, Pune. This dam plays a vital role in running the Kudremukh Iron Ore Plant. At the project site, vibrations were experienced while passing the discharge over the morning glory spillway inlet. Based on the desk studies, recommendations were provided to install aeration pipes to improve the aeration of flow and to strengthen the morning glory inlet shaft to reduce/withstand vibrations. Accordingly, the aeration pipes were installed at the site which resulted in reducing the intensity of vibrations.

Acknowledgements The authors are thankful to Shri. A. K. Agrawal, Director, and Shri Y. N. Srivastava, Additional Director, CWPRS for their constant encouragement and valuable guidance in the preparation of this paper. The authors are thankful to the Indian Council of Forestry Research and Education (ICFRE) and Kudremukh Iron Ore Company Ltd. (KIOCL) for constant interaction during the course of studies. The contribution of Dr. (Mrs.) V.V. Bhosekar, Former Director, Shri P.

B. Deolalikar, Former Joint Director, and Mrs. M.I. Sridevi, Former Research Officer, are gratefully acknowledged for the studies.

References

1. CWPRS Technical Report No.4144 (2004) Desk studies for assessing the hydraulics of tunnel spillway of Lakya dam at Kudremukh, Karnataka
2. Khatsuria RM (2004) Hydraulics of spillway and energy dissipators. Marcel Dekker publication, New York, NY
3. USBR (1987) Design of small dams. United States Bureau of Reclamation 3rd edition, US Govt. printing office, Washington D. C.

Review of Non-destructive Testing Methods Used for Structural Safety Assessment of Civil Structures

Prakash Kumar Palei, Vijay K. Ghodake, S. S. Kumar, and R. Ali

Abstract Non-destructive testing (NDT) method plays a significant role in the qualitative assessment of civil engineering structures. NDT is defined as the method of inspecting, monitoring and evaluating the strength properties of various types of civil engineering structures without damaging the structure. It is a very safe, fast, cost-effective, and efficient method for assessment of properties of a material. NDT methods are based on the assumption that certain physical and chemical properties of a material can be linked to structural strength and durability. There is a phenomenal rise in construction activities in the field of civil engineering in the recent few years. Testing and quality control are essential at various points throughout the life of construction to ensure its safety. Most significant structures, such as buildings, bridges, and dams, are subjected to extreme stress conditions all the time, and their performance is likely to alter over time. As a result, NDT methods must be used to examine the structural safety of these structures. In the present paper, the most commonly used NDT methods such as rebound hammer, ultrasonic pulse transmission, impact echo, and resonance frequency test methods used for assessment of quality of various types of civil structures have been discussed and illustrated. The fundamental principles of these methods are also explored in regard to their potential.

Keywords Non-destructive testing · Assessment · Monitoring · Structural

1 Introduction

Non-destructive testing (NDT) methods have been attracting more and more attention due to their consistency and effectiveness in assessing the overall quality of a material. NDT methods are considered as powerful tools for estimating the in-situ quality of

P. K. Palei (✉) · V. K. Ghodake · S. S. Kumar · R. Ali
Central Water and Power Research Station, 411 024, Pune, India
e-mail: prakash.palei@cwprs.gov.in

R. Ali
e-mail: rizwan_ali@cwprs.gov.in

P. V. Timbadiya et al. (eds.), *Flood Forecasting and Hydraulic Structures*, Lecture Notes in Civil Engineering 340, https://doi.org/10.1007/978-981-99-1890-4_46

existing concrete structures with regard to their strength and durability. In-situ testing of concrete is becoming more and more important in comparison with a traditional random sampling of concrete for material analysis [1, 2]. Mostly NDT methods such as rebound hammer, ultrasonic pulse transmission technique, sonic wave transmission technique, impact echo test method, and resonance frequency test method have been used for detection of anomalies and qualitative assessment of structural safety of various types of civil structures such as dams, powerhouses, aqueducts, turbo generation foundations, bridges, barrages, and historical monuments [1]. The application of these methods for evaluating strength parameters of structures has been around for more than three decades; now in the present century, NDT methods have become more refined, as it has evolved from a simple hammer to highly developed ground penetrating radar [3]. Practically, all structures exposed to nature deteriorate with time due to a number of factors such as fire, earthquake, alkali aggregate reaction, flood, manmade disasters, and aging. Inspection personnel faces lots of difficulty in determining the in-situ quality of concrete/masonry part of the structure that has experienced decay in absence of direct sampling of material from the structure. The major disadvantage of material sampling is that it requires the inspector to remove core sample from a portion of the structure. Removing cores from a concrete structure is an invasive process that might weaken the structure and provide long-term stability risk, particularly in RCC structures. Therefore, such invasive methods are not advisable to carry out on the structures. Moreover, testing of cores may give information for a limited zone of the structure which may not represent the health status of the whole structure. In such scenario, completely non-invasive NDT methods have been playing an important role for assessing the overall quality of the structure. The main objective of non-destructive testing (NDT) is to obtain in-situ material properties of structure without damaging it. It gives several information about the integrity of the structure such as homogeneity, Young's modulus of elasticity, modulus of rigidity, Poisson's ratio, and location of defects. NDT methods can be used to test the quality of a newly manufactured part, or to test the service conditions of a part already in use, and also to decide the remedial measures to be undertaken to improve the structural integrity of distressed structures. Therefore, it is a tool which has been successfully used not only in quality control, but in failure prediction and analysis also. NDT can be of immense help by reducing the risk involved and consequently can build confidence in the structural engineer. In the present paper, the major NDT methods applied for testing civil structures for assessment of quality of various types of structures are discussed and illustrated.

2 Non-destructive Testing Methods

2.1 Ultrasonic Pulse Transmission Method

Ultrasonic testing is an NDT technique that measures the time taken by the stress waves to travel through a solid medium to determine its properties. The time of travel of stress waves can then be used to determine the acoustic velocity of a given material. The acoustic velocity of the material enables the inspector to make a judgment about the quality of a structure.

The method is based on the principle that the propagation velocity of elastic (mechanical) waves through a material depends on several material parameters such as density, porosity, and degree of saturation and is independent of the shape and size of the structure [4]. Thus, the propagation velocity of elastic waves gives an indication of the quality and homogeneity of the material in the direction of wave transmission through the structure. Higher wave velocities correspond to better quality of the material, and the distribution of wave velocities along different paths of wave transmission through a structure provides a safe method for quick assessment about the quality of the material [4–6]. Portable ultrasonic non-destructive digital indicating tester (PUNDIT) equipment used for ultrasonic pulse velocity measurement and different types of possible arrangement of transducers are shown in Fig. 1.

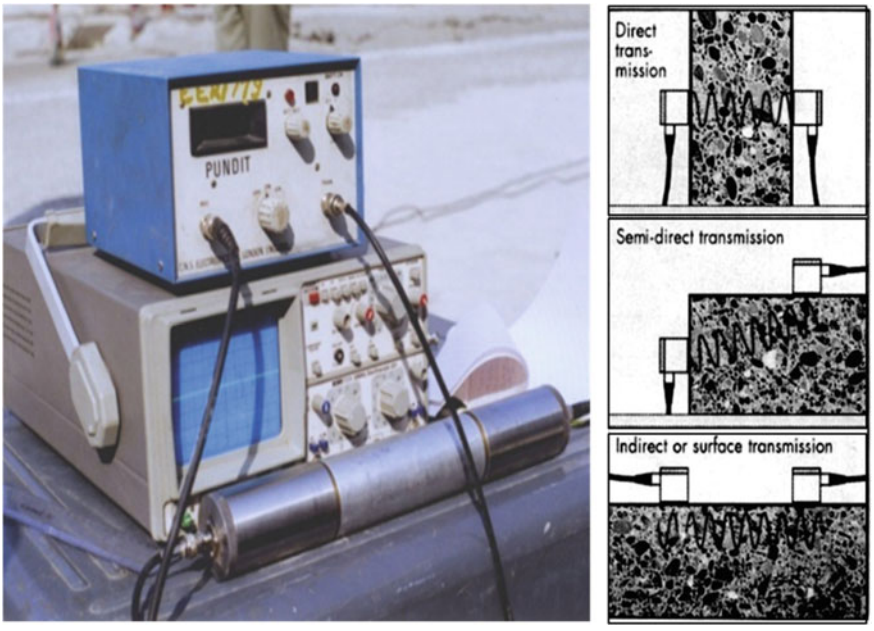

Fig. 1 Equipment used for ultrasonic pulse velocity measurement and different types of arrangement of transducers

Table 1 Compressional wave velocity criteria as per IS-13311 (Part 1): 1992

Sl. No.	Velocity, km/s	Quality of concrete
1	Above 4.5	Excellent
2	3.5–4.5	Good
3	3.0–3.5	Medium
4	Less than 3.0	Doubtful

Velocity of propagation of compressional waves (V_c), density (ρ), and the Poisson's ratio for an infinite, homogeneous, isotropic, and linearly elastic medium are interrelated with modulus of elasticity by the following relationship:

$$E_d = V_c^2 \rho \frac{(1+\mu_d)(1-2\mu_d)}{(1-\mu_d)} \tag{1}$$

Since ρ and μ_d vary insignificantly for a particular type of concrete, value of E_d, which is considered as a measure of the quality of concrete, depends mainly on the elastic compressional wave velocity. From the above equation, it is evident that higher the velocity of compressional wave for a given concrete mass, better the quality of concrete. Thus, estimation gives an assessment of the in-situ quality of a given concrete mass. The quality of concrete in terms of uniformity, absence of internal defects, cracks and segregation, etc., indicative of the level of workmanship employed, can thus be assessed using IS-13311 (Part 1): 1992 guidelines given in Table 1, which have been evolved for characterizing the quality of concrete in structures in terms of the ultrasonic pulse velocity [4].

2.2 Example Study: Ultrasonic Testing of T.A. Foundation of Unit No. 6 of Rourkela Steel Plant, Odisha

The Captive Power Plant No.1 (CPP-I) of Rourkela Steel Plant (RSP), Odisha, has five sets of 25 MW steam turbine-alternators (T.A.). Steel Authority of India Limited (SAIL), Rourkela Steel Plant, Odisha, requested CWPRS, to conduct the in-situ studies toward non-destructive testing (NDT) for assessment of quality of in-situ concrete for turbine-alternator (T.A.) of Unit No. 6 for Captive Power Plant No.1 (CPP-I). Accordingly, the study has been carried out to find the in-situ quality of concrete. In-situ ultrasonic testing in progress at site is shown in Fig. 2. In-situ non-destructive testing (NDT) by UPV has been carried out on six columns, five deck beams, and four pedestals. For UPV test, the procedure has been adopted as per BIS guidelines (IS: 13,311 (Part 1): 1992. In order to carry out the UPV test, first, the concrete surfaces of the beam, pedestal, and columns have been made plain, smooth, and dust free. Concrete surfaces of the beam and columns, especially those on the turbine side, have been found to have been smeared by oil mixed with coal dust.

Fig. 2 In-situ ultrasonic test in progress

All possible efforts have been made to have concrete surfaces at the observational grid point, plain, smooth, and dust free by removing dust, thin film of paint, loose plaster, etc. Both horizontal and vertical lines at an interval of 250 mm have been marked on a pair of opposite faces or adjacent faces of the columns or beams along their height or length, respectively. Grid points formed by intersections of these vertical and horizontal lines have been marked and numbered identically on the opposite/adjacent faces of the columns/beams for easy identification as well as for placing transducers. In order to cover maximum portion of the T.A. foundation and to arrive at reasonable conclusion regarding the quality of in-situ concrete as well as to locate any region of poor quality of concrete, a system of grid depending upon the requirement of each structural member has been adopted. Grease has been applied at each grid point to secure a good acoustic coupling between the transducers and the concrete faces. The results of the ultrasonic test for columns 1 and 1A are presented in the form of contours in Fig. 3. The quality of the concrete has been found to be of good to very good. These results enabled the project authority to assess the structural safety of the T.A. foundation for smooth operation of the generation unit.

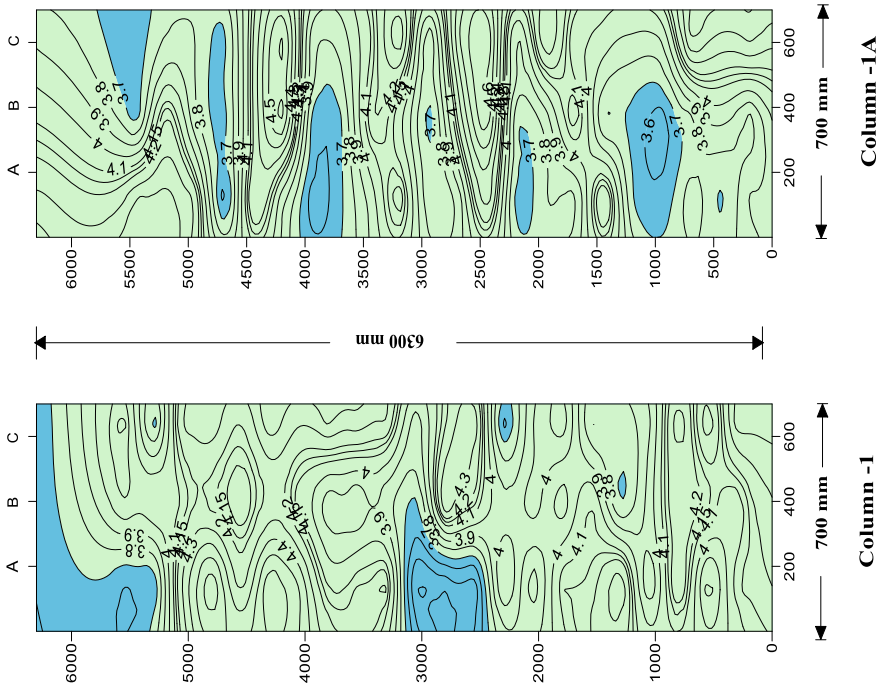

Fig. 3 Velocity contours depicting the quality of the in-situ concrete of columns 1 and 1A

3 Rebound Hammer Method

Non-destructive surface hardness method is a non-invasive testing method for determining the strength characteristics of a material. The standard rebound hammer test was developed in 1948 by Swiss engineer Ernst Schmidt [7].

The working principle of this method is that the rebound of an elastic mass depends on the hardness of the surface against which the mass impinges. Figure 4 shows the rebound hammer instrument used for non-destructive testing of concrete.

It is a very handy instrument which is easy to operate and can produce fairly accurate results from the estimated average of a number of tests conducted on the

Fig. 4 Schmidt rebound hammer

same location of the surface [9]. It consists of a spring-controlled mass that slides on a plunger inside a tubular housing. When the plunger of the rebound hammer is pressed against the concrete surface, the spring-controlled mass rebounds and the level of such rebound depends upon the surface hardness. Therefore, surface hardness and rebound numbers are considered to be related to compressive strength of concrete. The working procedure of the rebound hammer test is schematically shown in Fig. 5. The columns and beams of the T.A. foundation were tested also by rebound hammer method as per the procedure mentioned in IS 13311 (Part 2): 1992 [10]. Empirical correlations have been provided by the manufacturer to estimate the value of compressive strength from the rebound number values; however, the testing conditions of the manufacturer might be different from the conditions in which the measurement has been carried out. Therefore, it is recommended to carry out a test-specific correlation procedure where a number of concrete cubes with varying strength are prepared and tested by both standard rebound hammer and compression-testing machine. The results of the two tests are then used to develop an empirical correlation which will be used for the prediction of compressive strength from the rebound number value.

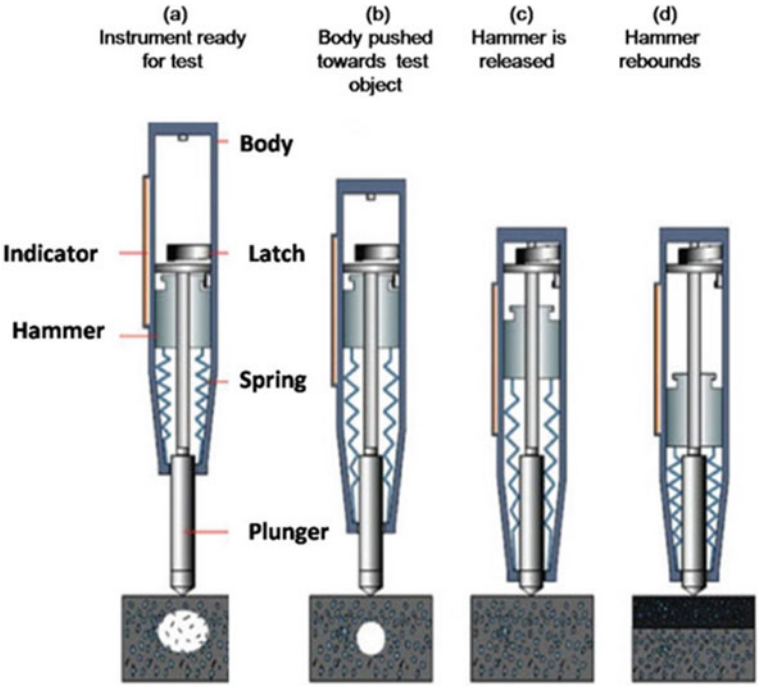

Fig. 5 Rebound hammer test procedure [8]

4 Example Study: Rebound Hammer Testing of T.A. Foundation of Unit No. 6 Rourkela Steel Plant, Odisha

Rebound hammer test has been carried out for assessing the surface hardness and likely compressive strength of concrete of the T.A. foundation of Unit No.6 of RSP, Odisha. The test has been conducted on each grid point where UPV has been carried out. The standard rebound hammer provides a simple, easy, and reasonable method to estimate concrete strength properties. However, the results of the test on concrete depend on several factors such as smoothness of the surface, geometric properties of the test specimen, age of the test specimen, surface and internal moisture conditions of the concrete, type of coarse aggregate, type of cement, type of mold, and carbonation of the concrete surface [8]. In-situ rebound hammer testing in progress at Rourkela Steel Plant (RSP), Odisha, is shown in Fig. 6. Schmidt rebound hammer test for all the columns and beams for RSP, Odisha, has been carried out based on the procedure mentioned in IS 13311 (Part II): 1992, and the rebound number criteria adopted for grading of the quality of concrete is presented in Table 2.

Fig. 6 In-situ rebound hammer test for cone column is in progress at site

Table 2 Rebound hammer test criteria

Qualitative interpretation of rebound hammer test		
Sr. No.	Average rebound number	Quality of concrete
1	> 40	Very good hard layer
2	30–40	Good layer
3	20–30	Fair
4	< 20	Poor concrete

Rebound hammer test results for columns and beams are provided in Table 3. In this context, it is to note that, as per IS guidelines, rebound indices are only indicative of compressive strength of concrete up to a limited depth from the surface. Thus, if the concrete in a particular member contains internal micro-cracking, flaws, heterogeneity, etc., rebound hammer indices will not indicate the same. The probable accuracy of the prediction of the strength parameters of concrete by this method in a structure is about 15% [11].

It is therefore recommended that the standard rebound hammer test may be used as a method of testing inconsistency of strength properties between concrete samples rather than as a substitute for standard compression testing [12]. The rebound hammer test has indicated the presence of good to very good quality of concrete in T.A. Unit 6.

Table 3 Results of the rebound hammer test of concrete of T.A. Unit-6

Test part	No. of obs.	Min. rebound number	Max. rebound number	Avg. rebound number	Remarks
Col.1	22	37	54	46	Good to very good
Col.2	22	40	65	51	Good to very good
Col.3	20	41	70	51	Very good
Col.1A	22	32	57	47	Good to very good
Col.2A	21	44	68	55	Very good
Col.3A	35	37	70	51	Good to very good
LB1-2	25	33	71	52	Good to very good
LB 1A-2A	28	38	59	49	Good to very good
LB 2A-3A	10	37	54	46	Good to very good
TB1-1A	10	36	55	49	Good to very good

5 Resonance Frequency Test Method

Fundamental resonant frequencies obtained from resonant frequency test can be used to evaluate dynamic elastic and shear modulus of concrete, masonry, and foundation rock core samples. This method has been used successfully for estimation of dynamic properties such as modulus of elasticity, shear modulus, and Poisson's ratio of materials. Test is generally carried out by following guidelines of ASTM C 215- 02 [13]. In this method, the specimens are subjected to longitudinal, transverse, and torsional mode of vibrations at different frequencies to determine the resonant frequency. The fundamental resonant frequencies are determined by exciting the specimen either by impact or by forced resonance method. A lightweight pickup unit in contact with the specimen monitors the response of the specimen. The value of the frequency triggering maximum response is the resonant frequency of the specimen. The equipment used for testing consists of an electronic unit with a sine wave oscillator, a power amplifier, pickup units for measuring response of the test specimen, and a test bench for mounting of specimens. An oscilloscope connected with the main unit ensures the occurrence of resonance by display of Lissajous patterns on the oscilloscope.

6 Example Study: Estimation of Dynamic Properties of Rock Core Samples

Rock core samples obtained from various project sites have been tested in the laboratory for finding the dynamic properties like dynamic Young's modulus of elasticity, modulus of rigidity, and Poisson's ratio. The tests have been carried out by exciting the sample under longitudinal as well as torsional mode of vibration.

7 Sample Details

For geological sub-surface investigations, nine rock core samples have been collected from project site located at Tamil Nadu for resonance frequency tests. Photographs of the samples are shown in Figs. 7, 8, and 9. Length-to-diameter (L/D) ratio of the samples have been found to be varying between 2.5 and 4.8.

Fig.7 Rock samples from BH-01

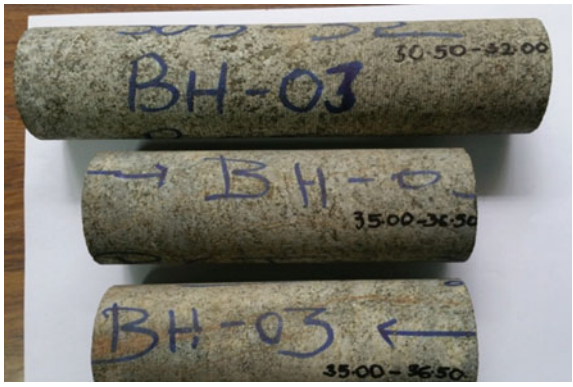

Fig. 8 Rock samples from BH-03

Fig. 9 Rock core samples from BH-07

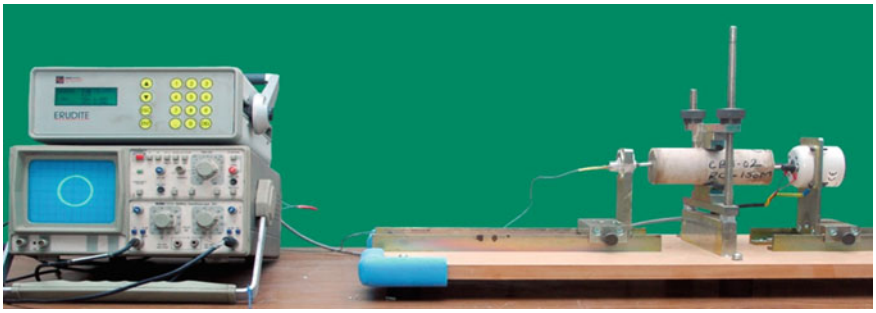

Fig. 10 Resonance frequency test setup in longitudinal mode of vibration

8 Test Under Longitudinal Mode of Vibration

The specimens are tested for finding the resonant frequency in longitudinal mode to determine dynamic Young's modulus of elasticity (E_d). Figure 10 shows the photograph of the test setup used for measurement of resonant frequency of test specimen.

The specimen is supported at the center on the test bench, vibrations have been imparted to the specimen at one end of the specimen by the vibrator through a physical contact, and the response has been picked up at the other end with an accelerometer. The support has been provided at the center of the specimen in a way so that sample may vibrate freely in a longitudinal mode. The frequency of vibration was varied through auto-mode or manual mode till resonant frequency (n') in fundamental mode of vibrations was detected by the instrument. An oscilloscope attached with the main unit displays the Lissajous patterns on occurrence of resonance. The fundamental frequency in longitudinal mode (n') is further used to estimate the dynamic Young's modulus of elasticity.

9 Test Under Torsional Mode of Vibration

The specimens have also been tested for resonant frequency in torsional mode to determine dynamic modulus of rigidity (G_d). Figure 11 shows the photograph of the test setup. In this mode, vibrator has been placed laterally at the side of one end of the specimen. The pickup has been also placed laterally at the side of the other end of the specimen. The frequency of vibration has been varied through auto-mode or manual mode till resonant frequency (n″) in fundamental mode of vibrations is detected by the instrument. The occurrence of resonance is also displayed by the Lissajous patterns on the oscilloscope. The fundamental frequency in torsional mode (n'') is further used to estimate the dynamic modulus of rigidity.

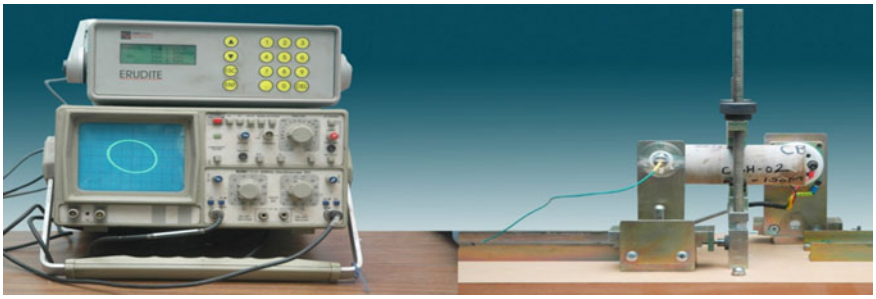

Fig. 11 Resonance frequency test setup in torsional mode of vibration

It has been observed that the dynamic Young's modulus of elasticity, dynamic shear modulus of rigidity, and dynamic Poisson's ratio are found to vary between 35.50 GPa to 50.35 GPa, 20.67 GPa to 34.13 GPa, and 0.18 to 0.27, respectively.

10 Conclusions

In the present paper, different NDT techniques applied for qualitative assessment of civil structures have been reviewed with the help case studies conducted for assessment of in-situ quality of T.A. foundation of RSP, Rourkela, Odisha, and estimation of dynamic properties of foundation rock materials resonance frequency test method. It has been observed that combination of ultrasonic pulse velocity test and rebound hammer test method has been really useful for assessing the in-situ quality of the concrete in T.A. foundation of RSP, Odisha. Rebound hammer and ultrasonic pulse velocity test has the potential to determine in-situ strength of concrete materials. However, to estimate compressive strength from the results of these non-destructive tests, experiments have to be performed in the laboratory in order to develop a statistical correlation. Presently, enough study has not been carried out to correlate ultrasonic wave velocity with concrete mix design. Most of the research that has been applied to the non-destructive testing of concrete has concentrated on the abilities and refinement of the method itself. Therefore, further studies need to be carried out to develop statistical relationship between rebound number values and ultrasonic pulse velocity in different grades of concrete. Apart from the techniques discussed in this paper, there are many other NDT techniques such as ground penetrating radar, impact echo, and seismic refraction which can be used for assessment of in-situ quality of concrete structure.

Acknowledgements Authors are thankful to Director, Central Water and Power Research Station (CWPRS), Pune, for the encouragement and support to publish the paper.

References

1. McCann DM, Forde MC (2001) Review of NDT methods in the assessment of concrete and masonry structures. NDT E Int 34(2):71–84
2. Shaw P, Xu A (1998) Assessment of the deterioration of concrete in NPP—causes, effects and investigation methods. NDT.Net 3:2
3. Lim MK, Cao H (2013) Combining multiple NDT methods to improve testing effectiveness. Constr Build Mater 38:1310–1315
4. IS 13311 (Part-I) 1992 Indian standard non-destructive testing of concrete-methods of test, Part-I Ultrasonic pulse velocity
5. Agarwal SP, Krishna N, Wedpathak AV, Guha SK (1972) Non-destructive testing of concrete and masonry structures. In: Proceedings of 42nd research session of CBIP, vol 3, Madras, T.N., pp 1–12
6. Wedpathak AV, Marwadi SC, Bhandwalkar PK, Gosavi PD, Guha SK (1980) Application of non-destructive test techniques for assessment of in-situ quality of conrete in large concrete structures. In: Proceedings of 48th research session of CBIP Hyderabad, A.P., pp 111–124
7. Kolek J (1969) Non-destructive testing of concrete by hardness methods. Institute of Civil Engineers, London
8. Malhotra VM, Carino NJ (2004) CRC handbook on nondestructive testing of concrete. CRC Press Inc.
9. Greene GW (1954) Test hammer provides new method of evaluating hardened concrete. J Am Concrete Inst 26(3):249–256
10. IS 13311 (Part II) 1992, Indian standard non-destructive testing of concrete-methods of test, Part-II Rebound Hammer Test
11. Gehlot T, Sankhla SS, Gupta A (2016) Study of concrete quality assessment of structural elements using rebound hammer test. Am J Eng Res (AJER) 5(8):192–198
12. Kumavat HR, Chandak NR, Patil IT (2021) Factors influencing the performance of rebound hammer used for non-destructive testing of concrete members: a review. Case Stud Constr Mater 14:e00491
13. ASTM: C 215–02, Standard test method for fundamental transverse, longitudinal, and torsional resonant frequencies of concrete specimens

Safety of Hydraulic Structures Against Vibrations Generated Due to Operation of Turbine Unit—A Case Study

Vijay Ghodake, Prakash K Palei, S. Santhosh Kumar, and Rizwan Ali

Abstract Hydraulic structures such as dam, powerhouse, aqueduct, and barrages or any other structures are designed to withstand certain level of vibration. These structures produce particular signature of vibrations. A change in the signature of vibrations in these structures or its parts indicates the presence of abnormality. Powerhouse operation is one of the main reasons of vibrations in the dam structure and powerhouse civil structure; thus, periodical vibration monitoring due to operation of generation unit will enhance the performance of the generation unit by minimizing the chances of sudden failure. The effects of vibration sometimes can be very severe. Excess level of vibration can cause reduction in efficiency of generator machinery and may damage the unit. Vibrating machinery can create noise, cause safety problems, and lead to degradation in plant working conditions. Hence, monitoring of vibration gives important information about the structural safety of these structures which helps to take remedial measures for reducing vibrations. The present paper is based on the details of the vibration measurement studies carried out for safety of dam and powerhouse structure during the operation of Unit No. 3 of Kadana Hydroelectric Project, Gujarat, in generation as well as in pump mode condition. Vibrations measured at preselected locations, viz. dam top, near penstock gate, inspection gallery, penstock gallery, generator floor, turbine floor, and turbine pit and at draft tube gate during the operation of Unit No. 3 both in generation mode as well as in pump mode under different operating conditions. Various available international standards have been reviewed to recommend the safe vibration level

V. Ghodake (✉) · P. K. Palei · S. S. Kumar · R. Ali
Central Water and Power Research Station, Pune 411024, India
e-mail: vkghodake@yahoo.co.in

P. K. Palei
e-mail: prakash.palei@cwprs.gov.in

S. S. Kumar
e-mail: santhosh.sk@cwprs.gov.in

R. Ali
e-mail: rizwan_ali@cwprs.gov.in

P. V. Timbadiya et al. (eds.), *Flood Forecasting and Hydraulic Structures*, Lecture Notes in Civil Engineering 340, https://doi.org/10.1007/978-981-99-1890-4_47

for the safety of dam, powerhouse structure, and the generation unit. Based on analysis of the vibration results, it has been found that the observed vibration levels are well below the adopted safe vibration levels of the respective structures.

Keywords Vibration · Turbine · Peak particle velocity · Safe vibration level · Powerhouse

1 Introduction

Vibration monitoring of hydropower station (HPS) is very important because it states the present condition and the performance of the machineries/equipments used in the powerhouse [1]. Periodical vibration monitoring is necessary for hydropower station which enables to take remedial measures if excessive vibrations levels observed which in turn helps to avoid damages to civil structures and equipments installed [2]. At the time of power generation in HPS, unwanted vibrations create problems such as damages of equipments and power failure. Vibration monitoring system measures the vibrations and states the status of abnormal vibrations for the particular part. In the structural or equipment health monitoring, vibration studies plays vital role. In the vibration studies, selection of measurement locations, viz. ground or at various elevation, importance of the structures, viz. nuclear powerhouse, hydroelectric power station, thermal power station, dam, aqueduct, weir, historical monuments, type of structures, viz. concrete, masonry, earthen, or composite, are the governing factors. Considering various safety criteria for vibration levels acceptable to the structures, remedial measures will be suggested if vibrations exceed the safety level.

2 Methodology Adopted and Instrumentation

Generally vibrations have been measured by engineering seismographs. The important parts of an engineering seismograph are tri-axial seismometer, amplifying system, and recording mechanism. The tri-axial seismometer is used to record the vibrations, and it converts the mechanical motion into electrical signal. The amplifying system assists to magnify these electrical signals suitable for recording, and the recording mechanism finally preserves the vibration records. The instrument has facilities to record three components of vibration, i.e., peak particle velocity (PPV), in three mutually perpendicular directions of motion, viz., longitudinal (L), vertical (V), and transverse (T) directions. The instrument can be operated in manual mode or single shot trigger mode or continuous trigger mode to measure peak particle velocity or displacement or accelerations of the vibratory motions. Vibration acceptance levels can be expressed in peak values or RMS values. Peak values, or "Zero-Peak" values, are a direct measure of the amplitude of an oscillating signal mostly expressed the vibration observed near the civil structures such as dams and buildings. RMS or "root

mean square" is a statistical measure of a moving set of values. The vibration level observed in the non-rotating parts of machines like turbine bearings, pump bearings, etc., is generally expressed in "root mean square" (RMS) values. In contrast to the peak velocity amplitude, the root-mean-square velocity amplitude of a vibrating machine tells us about the vibration energy in the machine. The higher the vibration energy, the higher is the RMS velocity amplitude.

Seismographs of model "MiniMate (DS-077)" manufactured by M/s Instantel Inc., Canada, and seismographs of brand "Mini Supergraph" manufactured by M/s NOMIS Seismographs, USA, are one of the vibration monitoring system for measuring vibration levels on the ground and civil structures. The instruments, i.e., MiniMate, DS-077, and NOMIS Mini Supergraph are shown vide Fig. 1a, b, respectively. These instruments have facilities to record three components of ground vibration. DS-077 can record ground vibration up to a peak particle velocity of 127 mm/s and with a flat frequency response of 2–250 Hz. The minimum vibration trigger level for this model is 0.254 mm/s. NOMIS Mini Supergraph records ground vibration up to a peak particle velocity of 254 mm/s with a flat frequency response of 2–400 Hz. The details of vibration recorded can be viewed readily on a LCD display immediately. The instruments can also be connected to a PC for retrieval of the vibration data for further processing.

Vibration study involves measurements of vibrations at different conditions and locations. The vibrations are measured in three directions: vertical, longitudinal, and transverse by using tri-axial accelerometers, signal conditioners, ADC module, and a P.C. Based on vibration measurement studies due to the generation of power, safety of the civil structures and generation unit can be ensured after comparison with the standard guidelines.

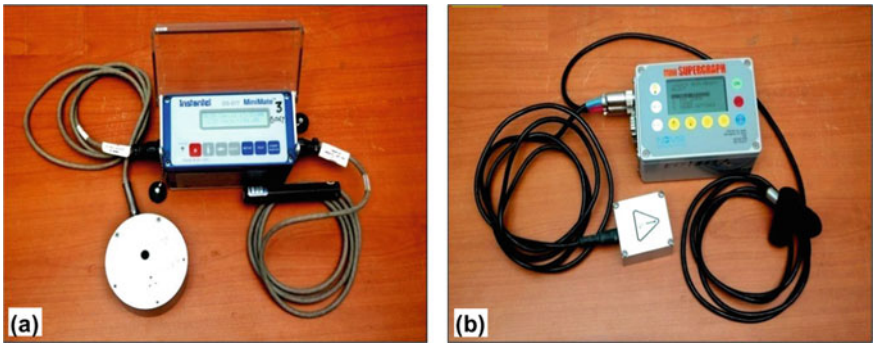

Fig. 1 **a** MiniMate, DS-077 from M/s Instantel Inc., Canada and **b** Mini Supergraph, from M/s NOMIS Seismograph, USA

3 Safety Criteria for Effect of Vibration on Civil Structures

Buildings and civil structures are fairly resilient to vibration. However, excessive vibration levels can induce different levels of structural damages such as initiation of new cracks and widening of existing cracks. The risks of vibration-induced damages are commonly evaluated by taking into account of the magnitude and frequency of recorded vibration together with consideration of the type of structure. For ensuring the safety of various structures against ground vibrations, safety standards are commonly suggested in terms of the peak particle velocity (PPV) and associated predominant frequencies in order to ensure a minimal risk of vibration-induced damage. However, very few standards are available to ensure safety of structures against machine vibrations. Traditionally, industrial/powerhouse structures, subjected to dynamic loads due to machine vibrations, are designed in such a way that the major natural frequencies of the structure do not coincide with the frequency of machine vibrations and in addition, the design of the structure with adequate factor of safety has been made so that it can withstand higher levels of vibrations. A review of few safety criteria available worldwide for various types of civil structures against transient and continuous vibrations are as follows:

- The British Standards (BS 7385: Part 2: 1993) [3] recommend peak velocity level of 50 mm/s at 4 Hz and above for ensuring safety of reinforced or framed structures, industrial and heavy commercial buildings against transient vibrations. For continuous vibrations, this value needs to be reduced by 50%.
- The German Standard (DIN 4150: Part 3: 1999) [4] provides guidelines in terms of peak particle velocity (PPV) for assessing continuous vibrations on different types of structures. The code recommends a PPV level of 10 mm/s, 5 mm/s, and 2.5 mm/s for all frequency ranges for the safety of the industrial buildings, dwellings, and sensitive structures from continuous ground vibrations as presented in Table 1.

Though several criteria as mentioned above are there, in order to safeguard different type of civil structures, subjected to continuous vibrations, in the present case, after reviewing recommendations from different standards as well as experience gathered by CWPRS from various case studies, vibration levels of 3 mm/s and 10 mm/s

Table 1 Vibration standards for evaluating long-term vibration on structures, DIN 4150–3:1999

Group	Type of structure	Peak particle velocity (mm/s)
1	Buildings used for commercial purposes, industrial buildings, and buildings of similar design	10
2	Dwellings and buildings of similar design and/or use	5
3	Structures that because of their particular sensitivity to vibration, do not correspond to those listed in lines 1 or 2 and have intrinsic value (e.g., buildings that are under a preservation order)	2.5

have been adopted as the safe vibration level for the dam and powerhouse structure, respectively.

Most of the criteria recommend vibration levels in terms of peak velocity, which are the maximum peak values of the three components of vibrations. However, damage to a structure can occur if peak velocity in any of the components exceeds the safe limit. Ground vibration, being a vector quantity, is described completely by all the three components (vertical, longitudinal, and transverse) of motion taken together. Therefore, the resultant of all the three components of motion is used in the present study rather than any single component of motion. The resultant of three components of vibration is estimated as follows:

$$V_R = \sqrt{V_T^2 + V_V^2 + V_L^2} \tag{1}$$

where V_T, V_V, and V_L correspond to maximum vibration level observed in transverse, vertical, and longitudinal directions, respectively. Use of resultant vibration estimated as above (pseudo vector sum) over maximum peak velocity introduces some additional safety margins [5].

In this paper, a case study pertaining to vibration measurement in Kadana Hydroelectric Project, Gujarat, carried out during the generation of power at different load generation conditions and at pumping mode condition has been discussed in detail.

4 Case Study: Vibration Measurement Study on Dam and Powerhouse Structure of Kadana HEP Under Different Operating Conditions

Kadana Dam is an earthen and masonry type composite dam with a height of 66 m and a length of 1.551 km. The dam is situated across river Mahi near village Kadana in Kadana Taluka of Mahisagar District of Gujarat State (Fig. 2) under Gujarat State Electricity Corporation Limited (GSECL), an undertaking of the Government of Gujarat. Main purpose of the dam is irrigation, hydropower generation, and flood protection. The dam was constructed during the period 1968–1979 after an agreement in the year 1966 between the Gujarat and Rajasthan states for development and utilization of water from Mahi River. Panoramic view of Kadana Dam with part of the reservoir is shown in Fig. 3.

The dam is having a total power generation capacity of 240 MW having four generating units of 60 MW each. View of the powerhouse from dam top, with four transformer units, is shown in Fig. 4.

The field study involved measurement of vibration during generation mode at various locations, viz. dam top near penstock gate of Unit No. 3, penstock gallery, generator floor upstream and downstream, turbine floor and turbine pit, inspection gallery, and draft tube gate. Measurement of vibration has been carried out during pump mode at 30%, 90%, and 100% speed and at 50 MW load at various locations

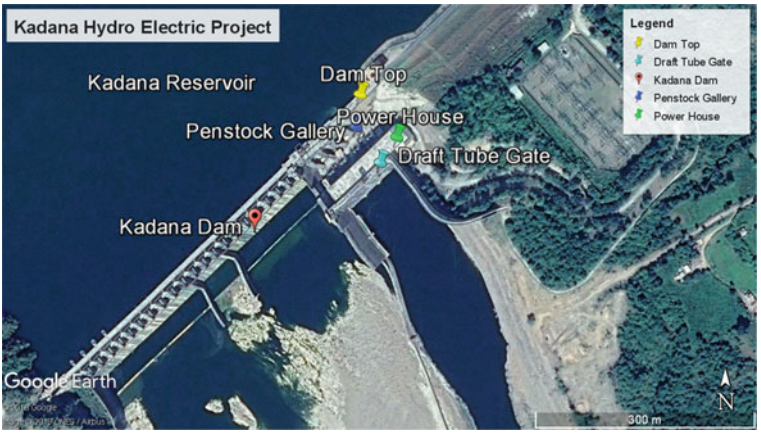

Fig. 2 Google Earth view of Kadana Dam spillway, powerhouse, and surrounding areas

Fig. 3 Downstream view of Kadana Dam, Gujarat

of Unit No. 3 at the same locations. In-situ vibration measurement studies during generation mode as well as pump mode operation of Unit No. 3 of powerhouse have been carried out by conducting two field visits during October and December 2018, respectively.

For conducting the study, seven seismograph units, out of which five nos. of "MiniMate (DS-077)" seismographs and two nos. of Mini Supergraphs, have been installed at several preselected locations for the measurement of vibration in the present study. The three component engineering seismograph has been positioned at

Fig.4 Inside view of powerhouse with 4 × 60 MW units

different preselected locations during testing which are shown in Figs. 5, 6, 7, 8, and 9 with a 2–3 kg loose sand bag above it.

Fig. 5 Near penstock

Fig. 6 Inspection gallery

Fig. 7 Turbine guide bearing

Fig. 8 Turbine pit

5 Discussion on Results

Ambient vibration measurement has been carried out at all the preselected locations, with the units not in operation. Subsequently, vibration measurements have been performed during the operation of Unit No. 3 in generation mode under different loading conditions.

The vibration measurements have also been performed in pumping mode at different speeds under no load condition as well as at full load condition. In generation mode, vibrations have been recorded at two different loads, i.e., at 35 MW and 55 MW. Vibration measurements during pumping mode at different speeds such as 30, 90, 100% under load, and no load condition of Unit No. 3 have been undertaken. Results of vibration measurements at preselected locations in dam structure and powerhouse of Unit No. 3 for pumping mode operation is presented in Table 2. It has been found that the vibration levels are observed in the range of 0.11–3.95 mm/s which are well within the recommended safe vibration levels. Through vibration measurement, structural safety of the powerhouse at different power generation and sudden rejection loads has been assessed successfully.

Fig. 9 Draft tube gate

Table 2 Vibrations in dam structure and powerhouse of Unit No. 3

Sl. No.	Test location	Generation mode at 35 MW	Generation mode at 55 MW	Pump mode at 100% Speed; load: Nil	Pump mode at 100% speed; load: 50 MW
		Resultant PPV (mm/s)			
1	Dam top	0.11	0.41	0.41	1.02
2	Dam structure penstock	0.21	0.47	NT	1.51
3	Draft tube gate	0.82	0.78	0.11	2.47
4	Generator floor	1.79	1.38	0.85	3.95
5	Turbine pit structure	1.20	0.98	0.56	1.53
6	Inspection gallery	0.11	0.19	0.41	0.41

6 Conclusions

- Vibration measurement is very important and effective tool for assessing structural safety of the important structures such as powerhouses, dams, bridges, barrages, and monumental structures.
- The safe limits of vibrations are required to be considered carefully depending upon the nature of the structure and conditions of the vibration. Higher values allowed by few countries may be applicable in that country due to high quality of construction on account of frequent earthquakes. In Indian scenario, lower value of vibrations required to be considered due to omission or under estimation of earthquake loads during construction of very old hydraulic structures. Hence, after reviewing recommendations from different safety standards as well as CWPRS experience gathered from various case studies, vibration levels of 3 mm/s and 10 mm/s are being adopted as the safe vibration level for the dam and powerhouse structure, respectively.

Acknowledgements Authors are grateful to Director, CWPRS, Pune, for encouragement and support to publish the paper.

References

1. Mohanta RK, Chelliah TR, Allamsetty S, Akula A, Ghosh R (2017) Sources of vibration and their treatment in hydro power stations—a review. Eng Sci Technol Int J 20:637–648
2. Wei X, Zhen YM (2016) Study of the vibration transmission and path recognition of an underground powerhouse using energy finite element method, shock and vibration 2016:5039578
3. BS 7385-2: 1993, ISO 4866:1990, Evaluation and measurement for vibration in buildings—Part 1: guide for measurement of vibrations and evaluation of their effects on buildings
4. DIN 4150-3:1999-02, Structural vibration—Part 3: effects vibration on structures German Institute of standards, Deutsch Norm
5. Dowding CH (1985) Blast vibration monitoring and control. Prentice-Hall, Inc., Englewood Cliffs, NJ 07632, 297

Studies to Determine In-Situ Strength Parameters of Stone Masonry of Massanjore Dam, Jharkhand

Sanjay A. Burele, G. C. Singarkar, Pravuram Panda, K. A. M. Bagwan, and Rizwan Ali

Abstract In India most of the dams have become aged. Due to ageing, various distresses have been observed in these dams which has raised apprehensions about structural safety of these dams. For assessing structural safety of the dam's in-situ material properties are required as input parameters. This paper is based on such a study to determine in-situ strength parameters of stone masonry of Massanjore Dam, Jharkhand. Field studies by flat jack tests were carried out by CWPRS, Pune to compute in-situ stresses, static modulus of deformation and Poisson's ratio. Evaluated compressive strength of masonry for applied pressure was compared with design strength. The evaluated modulus of deformation, Poisson's ratio and compressive strength are used for carrying out stability analysis of dam. Six flat jack tests (5-horizontal and 1-vertical) each were conducted on downstream (D/S) face as well as on upstream face (U/S) in random rubble stone masonry. Average E_m values by flat jack test for random rubble stone masonry was 12.95 and 15.90 GPa for downstream and upstream faces, respectively. Average Poisson's ratio values by flat jack test for random rubble masonry was 0.215. The range of evaluated compressive strength of masonry for applied pressure was ranging from 50.09 to 92.28 kg/cm^2.

Keywords Flat jack · Induced in-situ stresses · Modulus of deformation · Poisson's ratio · Evaluated compressive strength

1 Introduction

Most of the masonry dams in India are showing distresses in the form of seepage, cracking, leaching of material, large deflections, etc. Moreover these dams were constructed long back without consideration of any earthquake forces or very small

S. A. Burele (✉) · G. C. Singarkar · P. Panda · K. A. M. Bagwan · R. Ali
Central Water and Research Station, Pune 411024, India
e-mail: burelesanjay@rediffmail.com

R. Ali
e-mail: rizwanali@cwprs.gov.in

P. V. Timbadiya et al. (eds.), *Flood Forecasting and Hydraulic Structures*, Lecture Notes in Civil Engineering 340, https://doi.org/10.1007/978-981-99-1890-4_48

earthquake forces have been considered. These distressed has raised concerns about structural safety of these dams as per present day analysis practices. Recently, CWPRS has conducted one field study towards assessment of in-situ material properties of dam body. This paper has highlighted the findings of the study and relevance towards estimation of in-situ properties for assessing stability of Massanjore dam. Massanjore Dam, popularly known as the Canada Dam, is constructed across the Mayurakshi River and is surrounded by forests and hills. This 47.25 m high and 661.58 m long dam was constructed in 1955. It is a gravity structure constructed in coarse rubble masonry. The reservoir has an area of 67.4 km^2 (16,650 acres), when full and has a storage capacity of 620,000,000m^3 (500,000 acre·ft). The length of the overflow portion is 225.60 m and is controlled by 21 gates, of 9.144 m width. The design discharge is 4443 m^3/s. The full reservoir level is 121.34 m and the flood level is 122.56 m. The Google imagery of Massanjore dam is shown in Imageries 1 and the downstream and upstream views of Massanjore dam are shown in Photo 1.

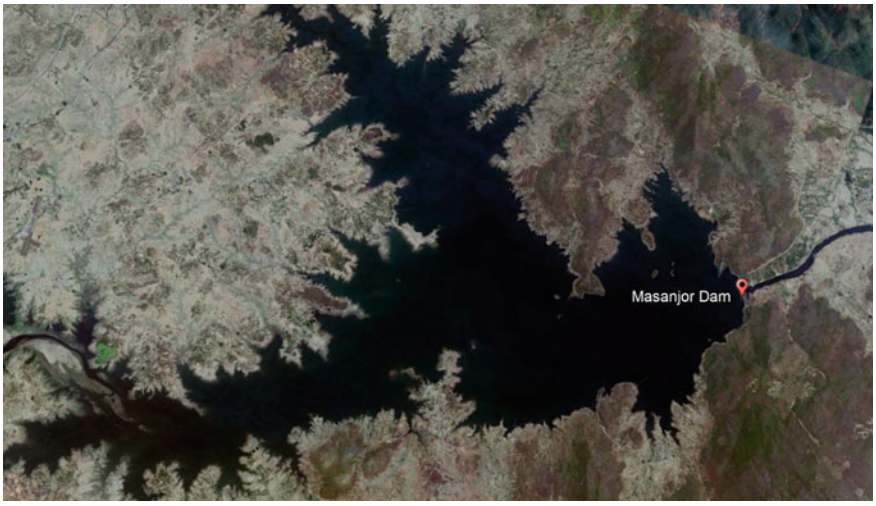

Imageries 1 View of the entire Massanjore Dam

Photo 1 Downstream and upstream view of Massanjore Dam

For estimation of the material properties on the upstream and downstream surfaces of the dam, flat jack tests have been conducted. The flat jack method is unique as it provides a direct measure of masonry strength and modulus parameters. The equipments used for carrying out flat jack tests are very simple and cost effective. The study consists of an overview of measurement of strength parameters by in-situ stress test, in-situ deformability test and Poisson's ratio test carried out by flat jacks, at the Massanjore dam.

1.1 Non-destructive Stresses Evaluating Methods

Out of the several methods devised for measuring in-situ stresses, three methods, i.e. over coring, hydraulic fracturing and flat jack methods have been widely used in rock masses. These are described in detail in, ISRM [4]. All these methods are based on the assumption that the rock mass is linearly elastic, homogeneous and isotropic in the zone influencing the measurement. From a practical point of view, a simpler technique which would enable a number of measurements to be made easily and cheaply will be useful for determination of representative stress in a masonry dam. The flat jack method is one of such techniques. Moreover, for determining stresses and material deformability in the rock structure of tunnels and mines, flat jack techniques are well established [1]. Thereafter, the technology of the flat jack test was modified and is widely used for evaluation of brick and stone masonry structures in Italy by Rossi [5, 6, 7] for measuring deformation in old/new structures, Rossi developed initial specifications for the optimum size and placement of flat jack's techniques. In China, Wang and Wang [9] developed a thick flat jack, which has a feature to record with large displacement capabilities in very soft masonry materials. Sachhi-Landriani and Taliercio [8] conducted a study on extensive nonlinear finite element analyses of both the single and double flat jack tests in masonry. The results showed that the numerical models to be generally in support of experimental evidence, and offered some insight concerning the effect of certain assumptions on the accuracy of the results. They have also recommended that if the two flat jacks test is carried out up to the failure strength, the failure stress should be reduced by 20% to yield the unrestrained compressive strength.

1.2 Test Locations

Deformation modulus, evaluated strength and Poisson's ratio were determined in random rubble stone masonry of the Massanjore dam. Six flat jack tests (5-horizontal and 1-vertical) were conducted on the downstream (D/S) face of the dam. On the upstream side (U/S), six flat jack tests (5-horizontal and 1-vertical) were conducted as shown in Fig. 1.

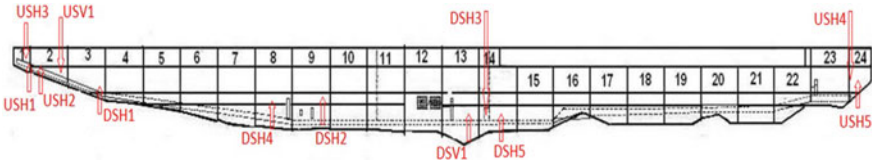

Fig. 1 Upstream view of Massanjore Dam showing U/S and D/S flat jack test locations

2 Methodology and Evaluation of Properties

2.1 Flat Jack Test

Flat jack test is based on the principle of partial stress release that involves the local elimination of stresses, followed by controlled stress compensation. The Indian Standard [2, 3, 4] on flat jack describes the method and the test procedure. A thin flat jack (Photo 2) of thickness 10 mm of size 30 × 30 cm is introduced by making a slot into the surface of the structures and hydraulic pressure is applied through oil pump to the masonry (Photo 3).

This causes a partial restoration of the initial displacement field, which at some point reach (approximately) the previously measured values. The necessary pressure is called cancellation pressure and can be related to the compressive stress in the direction normal to the slot. By pressuring the jack using oil pump, deformation takes place against the axial load of the structure and is measured using dial gauge. The factors like size and shape of flat jack and slot placed an important role while calculating the in-situ parameters.

The flat jack test is based on various assumptions viz., stress in place of the test is compressive, state of stresses in the place of the measurement is uniform, stress

Photo 2 Set of flat jack, dial gauge and pins

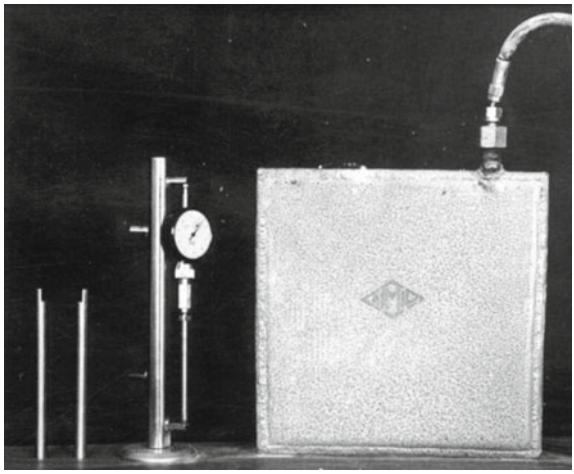

Photo 3 Placing of dial gauge after fixing flat jack between the two pins

applied to masonry by the flat jack is uniform, value of stresses (compared with compressive strength) allows the masonry to work in an elastic regime, masonry surrounding the slot is homogenous and masonry deforms symmetrically around the slot.

2.2 Evaluation of Induced Stresses

In actual tests, the length of the slot may be bigger than the jack and the slot may not have uniform width. Further, the stress acting in the plane parallel to the major axis affects the contraction of the slot. This cancellation of pressure is then corrected for the influence of slot size, reference point position and the stress acting parallel to the major axis of the slot, to obtain corrected stress acting perpendicular to the slot (Fig. 2). The stress acting perpendicular to the horizontal slot is considered as Q and perpendicular to the vertical slot is considered as Q. S and Q are the stresses induced in the slot after the slot has been made. Values of induced stress, S in the vertical direction and Q in the horizontal direction are determined by solving two equations simultaneously using cancellation pressure values of vertical and horizontal slots.

$$CP * K_1 = S * K_2 + Q * K_3 \tag{1}$$

where

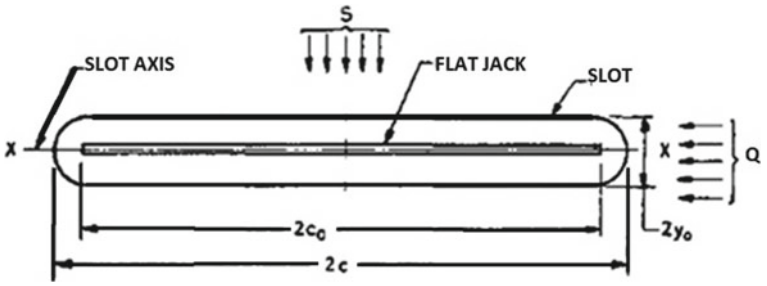

Fig. 2 Stress field around slot

$$K_1 = C_o\left[(1-\upsilon)\left(a_o - \frac{Y}{C_o}\right) + \frac{1+\upsilon}{a_o}\right]$$

$$K_2 = \left(\frac{1+\upsilon}{a}\right)(C + Y_o) + \left(a - \frac{Y}{C}\right)[C(1-\upsilon) - 2\upsilon Y_o]$$

$$K_3 = Y_o\left[2\upsilon\left(a - \frac{1+\upsilon}{a}\right)\right]$$

Using this $\boldsymbol{S}$, $\boldsymbol{Q}$, and $\boldsymbol{K}_1$ value normal stresses, angle of shear, shear stresses, maximum shear stresses and estimated compressive strength of masonry for applied pressure are evaluated.

2.3 Evaluation of Static Modulus of Deformation, E_m

The elastic properties of the masonry are determined from stress displacement envelope by applying hydraulic loading and unloading in the embedded flat jack with the help of hydraulic pumps. The stresses existing in the structure can also be determined by flat jack method as per IS–13,946, Part 4 (1994), which comes in the category of non-destructive test. Flat jack tests are carried out, by fixing two reference pins on the masonry surface at about 25.4 cm apart. The distance between the pins are recorded with reference to a fixed distance on an invar rod by means of a deformeter with dial gauge of accuracy 0.001 mm. A thin slot is cut in the masonry surface by drilling a series of overlapping drill holes by 20 mm dia hollow bit drill machine. The process relieves masonry surface of the stresses that originally existed.

In flat jack test the stress displacement envelope obtained during stressing/destressing of the slot for measuring cancellation pressure is used to evaluate deformation modulus, $\boldsymbol{E_m}$. The $\boldsymbol{E_m}$ is calculated using the relation (2);

$$\boldsymbol{E}_m = \frac{(2 * \boldsymbol{K} * \boldsymbol{P})}{\boldsymbol{w}} \tag{2}$$

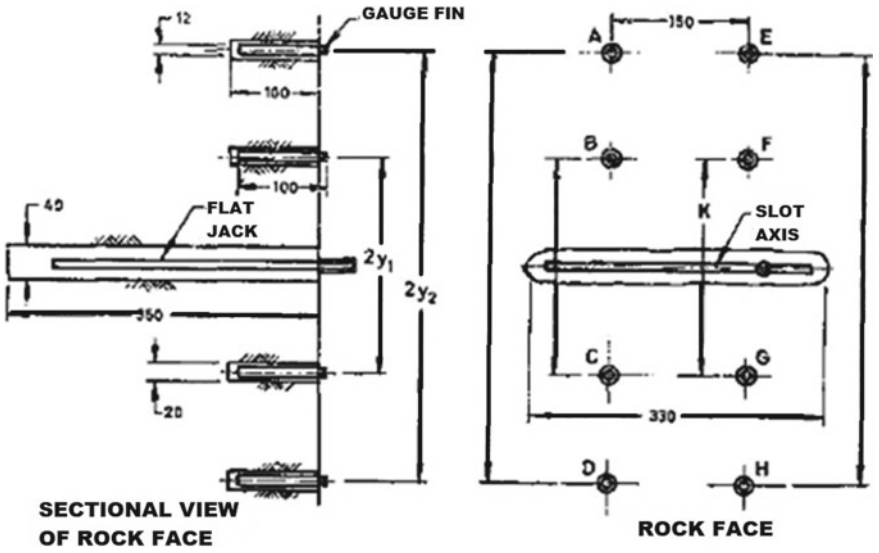

Fig. 3 Details of slot and gauge points

where $\boldsymbol{P}$ is the stress and $\boldsymbol{w}$ is the corresponding displacement between the reference pins located on either side of the slot. Co-efficient $\boldsymbol{K}$ accounts for the position of pins, size of slot, size of flat jack and the influence of Poisson's ratio. The $\boldsymbol{E_m}$ is determined using Eq. (3);

$$E_m = \frac{2PC_o}{w}\left[(1-\upsilon)\left(a_o - \frac{Y}{C_o}\right) + \frac{1+\upsilon}{a_o}\right] \tag{3}$$

$$\boldsymbol{a_o} = \sqrt{1 + \frac{\boldsymbol{Y}^2}{\boldsymbol{C_o}}}$$

where, $\boldsymbol{P}$ = Stress applied, $\boldsymbol{w}$ = the amount of convergence between two points spaced at equal distance $\boldsymbol{Y}$, $2\boldsymbol{C_o}$ = the length of flat jack, υ = Poisson's ratio (Fig. 3).

2.4 Evaluation of In-Situ Poisson's Ratio *(ϒ)*

While determining E_m value, K is determined by adopting the assumed value of υ. When Poisson's ratio is to be determined then convergence of the slot is to be measured between four reference pins (Photo 4), i.e. two pins on either side of the slot, fixed at a known distance prior to cutting of the slot. The consecutive stress displacement envelope is obtained for outside pins fixed at a distance of about 34.5 cm and the inside pins fixed at a distance of about 25.4 cm while hydraulic stressing of

Photo 4 Fixing of four pins for determining in-situ Poisson's ratio

the flat jack. K is determined for inside and outside pins using assumed value of υ. Two equations for K & E_m for inside and outside pins in terms of υ are generated. The unknown value of υ is calculated by solving these two simultaneous equations.

3 Discussions on Results

Twelve flat jack tests were conducted, six each on the upstream and downstream face of the dam. The tests were conducted in random rubble stone masonry. The values of static modulus of deformation on the downstream and upstream faces of the dam in random rubble masonry are computed and are presented in Table 1.

DSH-2S and DSH-2D, USH-1S and USH-1D—double pin fixed for calculation of Poisson's ratio.10 kg/cm^2 = 1 MPa, 1000 MPa = 1GPa.

Some of the stress/deformation cycles for flat jack tests on downstream and upstream side of dam are shown in Figs. 4 and 5.

Table 1 Flat jack test result at different locations of Massanjore Dam

SI. No.	Flat jack No.	Block	RL in m	Deformation modulus, E_m GPa	Poisson's ratio, υ	Estimated compressive strength of masonry for applied pressure, Kg/cm^2
01	DSH- 1	03	106.99	12.93	–	85.32
02	DSH-2S	09	98.19	10.19	–	50.09
	DSH-2D	09	98.19	13.47	0.21	80.39
03	DSH-3	14	91.39	9.09	–	52.19
04	DSH-4	08	98.39	*6.68*	–	62.22
05	DSH-5	14	90.79	15.93	–	92.28
06	DSV-1	13	90.99	16.09	–	–
07	USH-1S	01–02	116.09	15.01	–	53.69
	USH-1D	01–02	116.09	19.91	0.22	83.74
08	USH-2	02	114.39	17.73	–	53.56
09	USH-3	01	117.79	10.52	–	54.02
10	USH-4	23–24	113.39	16.57	–	62.13
11	USH-5	24	113.69	12.27	–	62.21
12	USV-1	02	114.69	19.32	–	–

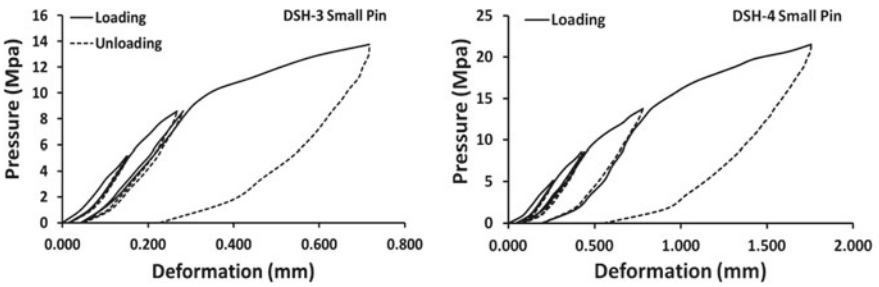

Fig. 4 Pressure versus deformation cycles for flat jack tests on downstream of Massanjore Dam

The average E_m values computed for upstream and downstream face are 15.90 GPa and 12.95 GPa, respectively. Upstream face E_m value is observed to be on higher side, probably due to grouting treatment done on the upstream face by using galvanized mesh with grouting. The value of E_m computed for the location DSH-4 is observed to be too low and has not been considered while finding average value. Hence, this value is not to be considered for further analysis. The Poisson's ratio value determined for the DSH-2D (small pin and long pin) and USH-1D (small pin and long pin) locations are 0.21 and 0.22, respectively. Average Poisson's ratio values by flat jack test for

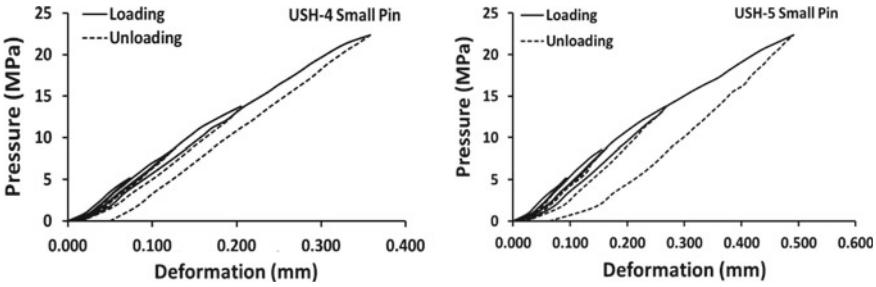

Fig. 5 Pressure versus deformation cycles for flat jack tests on upstream of Massanjore Dam

random rubble masonry is 0.215. The range of evaluated compressive strength of random rubble masonry for applied pressure is between 50.09 and 92.28 kg/cm^2.

4 Conclusions

The paper presented the flat jack test is very useful and easy to use with no damage to the existing/new structure for estimation of in-situ material properties particularly in masonry dams. The study showed that flat jack tests are cheaper than extraction of large size cores and laboratory testing. The study also indicated the flat jack once embedded in the structure is required not to be extracted, so it becomes part of the structure and causes no damage in the structure. Flat jacks can be fixed at any location on the structure so that the strength parameters can be determined for multiple locations on the surface of the structure. Flat jack test gives fairly reasonable values of the material properties and is being used as an alternative to extracted core testing.

Acknowledgements The authors are thankful to Shri A.K. Agrawal, Director, CW&PRS, Pune for the encouragement and giving permission to publish this paper.

References

1. Binda Maier L, Rossi PP, Sacchi-Landriani G (1983) Diagnostic analysis of masonry buildings. In: Proceedings of international association for bridge and structural engineering (IABSE) symposium on strengthening of building structures-diagnosis and therapy, Venice, Italy, pp 43–79
2. IS 13946 Part IV (1994) Code of practice for in-situ determination of rock properties by flat jack. Indian Standard Institution, New Delhi
3. IS 7746 (1975) Code of practice for in-situ shear test on rock. Indian Standard Institution, New Delhi

4. ISRM (1987) Suggested methods for rock stress determination. Int J Rock Mech Min Sci 24:53–74
5. Rossi PP (1982) Analysis of mechanical characteristics of brick masonry tested by means of nondestructive in-situ tests. ISMES Publication No. 167, Bergamo, Italy
6. Rossi PP (1985) Flat-jack test for the analysis of mechanical behaviour of brick masonry structures. In: Proceedings of the 7th international brick masonry conference, vol 1, Melbourne, Australia, pp 112–119
7. Rossi PP (1987) Recent developments of the flat-jack test on masonry structures. In: Proceedings of the workshop Italy-USA, evaluation and retrofit of masonry structures, USA, pp 257–285
8. Sachhi-Landriani G, Taliercio A (1986) Numerical analysis of the flat jack test on masonry walls. J de MecaniqueTheorique 5(3):313–339
9. Wang Q, Wang X (1988) Evaluation of compressive strength of brick masonry in-situ. In: Proceedings of the 8th international brick/block masonry conference, Dublin, Ireland, pp 145–176

Non-invasive Diagnostic Methods for Structural Health Monitoring of Concrete Gravity Dams—Case Study of Umiam Dam

Suragani Santhosh Kumar, Vijay K. Ghodake, Prakash K. Palei, and Rizwan Ali

Abstract Dams are an integral part of a nation's assets that provide various benefits in the form of irrigation sources, drinking water supply, flood moderation, power generation, recreation, maintaining flow in the river, industrial use, etc. In addition, there are instances that the dam tops also serve as roads for public transportation thereby causing additional vibration load on the dam body, which is random, periodic or dynamic in nature. Though these forces are minute in nature, yet capable of causing distress in the dam body over the service period of the dam. Anticipated damages on account of failure of dams can be in terms of loss of life, loss of property, natural environment, etc. apart from hampering economic development. Ageing dams need extra care due to distress and long-term stability issues. This paper highlights the potential of vibration engineering technique to monitor the operational safety of the structure over periodic intervals and nondestructive assessment of the quality of concrete. One such hydraulic structure that serves as road for public transportation is the Umiam Dam, forming a part of National Highway-40, linking states in the north-eastern region. Owing to transportation use of the dam top since decades, vibration measurements and in-situ quality assessment has been conducted, to verify the operational safety of the structure. With ever-increasing traffic, owing to economic developments, it is anticipated that distress in the structure may increase abnormally

S. Santhosh Kumar (✉) · V. K. Ghodake · P. K. Palei · R. Ali
Vibration Technology Division, Central Water and Power Research Station, Pune 411024, India
e-mail: santhosh.sk@cwprs.gov.in

V. K. Ghodake
e-mail: ghodake_vk@cwprs.gov.in

R. Ali
e-mail: rizwan_ali@cwprs.gov.in

P. V. Timbadiya et al. (eds.), *Flood Forecasting and Hydraulic Structures*, Lecture Notes in Civil Engineering 340, https://doi.org/10.1007/978-981-99-1890-4_49

that warrants for prior remedial measure such as diversion of bulk carrier through an alternate by-pass road to safeguard the dam.

Keywords Vibration level · Dam safety · Traffic-induced vibrations · Peak particle velocity (PPV)

1 Introduction

Post-Independence, India has witnessed a host of economic developments in terms of advancement of science and technology, healthcare, automobiles, employment, agriculture, thermal/hydel/nuclear/atomic power generation, roads and buildings, for all which civil infrastructure stands as an essential segment without which it is impossible to think of roadmap to development. In the recent times, owing to enhanced carbon print on the planet, tremendous stress is being laid on power generation by renewable energy methods such as hydroelectric power plants, atomic and nuclear power to cater to the growing power needs. In view of this, it is imperative that periodic monitoring of such hydraulic structures employed in renewable energy is of utmost importance. Besides power generation, some hydraulic structures are also in use for general purposes like transportation, recreation/pilgrimage spots, etc. While most of general-purpose applications of hydraulic structures are harmless, except a few like mass-drills, heavy duty cargo transportation associated with repetitive loads could induce vibrations in the structure and initiate faults or promote any pre-existing cracks/voids. As such, it becomes very essential to keep a watch on the structural safety of such massive civil constructions. Moreover, most of the dams in India have become aged above 40 years. Several distresses in the form of cracking, excessive deformation, swelling, etc., are being observed in these old dams due to ageing, earthquakes, alkali aggregate reactions, adverse reservoir and climatic conditions, seepage, etc. To improve/restore the structural integrity of these dams, emphasis is being laid on rehabilitation under the auspicious Dam Rehabilitation and Improvement Project (DRIP), through World Bank assistance in multiple phases.

There have been numerous studies that focused on the effects of vibration from highway/metropolitan traffic on civil structures such as adjacent residential buildings, heritage structures [1–3]. However, limited studies have been reported on effects of vibration from traffic on hydraulic structures such as concrete gravity dams. This paper is based on a case study carried out at CWPRS towards assessment of structural safety under traffic movement over the dam in north-east region of India against the induced vibrations.

The Umiam Stage-I, Hydro Electric Project in Meghalaya, India; commissioned in the year 1965, is one such hydraulic structure that also serves as road for public transportation apart from power generation. The dam top is a part of National Highway-40; between Guwahati and Shillong, that links the states in the north-eastern region. As a consequence of vehicular traffic, the dam is subjected to periodic loading that may cause distresses in the structure. Vibration monitoring studies conducted in the past

during 2011 indicated that the vibrations due to traffic over the dam were within safe limits [4]. As a consequence of increased developmental activities in the north-eastern region, there has been significant increase in vehicular traffic, inclusive of bulk cargo carriers. As a part of dam health monitoring, it is envisaged to conduct vibration measurements to ascertain the soundness of the structure, with respect to traffic-induced vibrations [5]. The study includes measurement of vibration at various locations on the dam due to the heavy vehicular traffic. The vibration measurements have been carried out at different monoliths of the dam and road bridge at different locations, viz. footpath, adjoining road, road railings, downstream face, spillway piers and drainage gallery for different traffic conditions. Based on vibration measurement studies due to the heavy vehicular traffic over the dam, the adverse vibration levels have been identified which has been very helpful for assessing structural safety of the dam and finalize necessary remedial measures to safeguard the dam.

2 Monitoring of Traffic-Induced Vibrations on Umiam Concrete Dam

2.1 Umiam Concrete Gravity Dam

The study area is Umiam concrete gravity dam, measuring 1950.72 m in length, 72.54 m in height and 101.22 m in width; at latitude of 25° 39' N and longitude of 91° 54' E. The dam is located across Umiam River in the East Khasi Hills District of Meghalaya at a distance of about 87 km from Guwahati and 16 km from Shillong in Meghalaya, India. The dam consists of 11 blocks with two overflow spillway bays (12.2 m × 12.2 m each), two radial gates, a 2.05 km HRT, two penstock lines of 1.98 m diameter and 530 m length each with a Power House capable of generating 36 MW electricity from four generating units of 9 MW capacity each. The index map of the Umiam Dam is shown in Fig. 1a followed by the downstream view in Fig. 1b. Figure 2 shows the two-lane road on the top of the dam, the footpath on upstream side of the dam and the side railings on both the sides. The road is a part of the National Highway (NH-40) and is the main link road to the states of Mizoram, Tripura and Assam besides the whole of Meghalaya. Since the road on the top of the dam that is more than 50 years old, forms a part of national highway, heavy traffic is passing over it, in view of which the safety of the dam due to traffic-induced vibrations is of serious concern. In view of the above, vibration measurement studies were envisaged to assess the impact of traffic.

The vibration measurements have been conducted at several locations of the dam and on the road passing over the dam with traffic on the dam road. Vibrations in terms of peak particle velocity (PPV) in longitudinal, vertical and transverse directions were measured. To assess the safety of the dam against the vibrations due to heavy traffic on the dam, the measured vibration levels have been compared with the

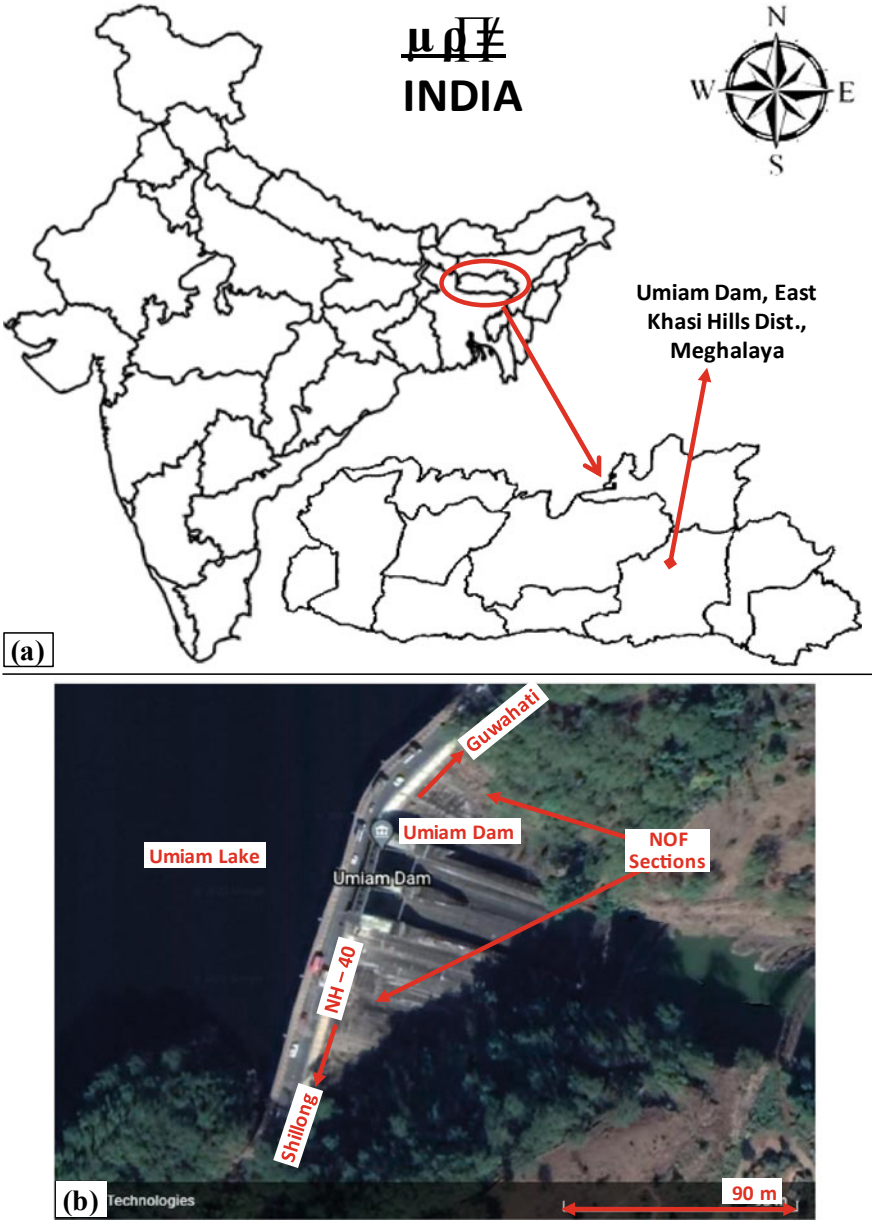

Fig. 1 **a** Location map of Umiam Dam in East Khasi Hills Dist., Meghalaya. **b** Downstream view of the dam showing two spillways through three piers and non-overflow sections on either side

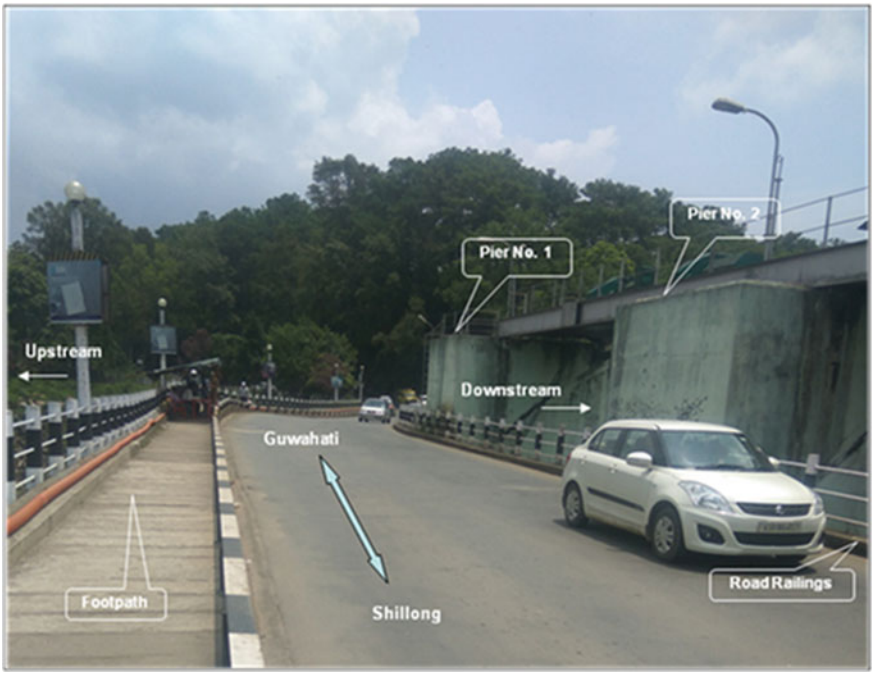

Fig. 2 Spillway piers along with the footpath and the road railings and road on top of dam

currently available various safety criteria for traffic vibrations. Before commencement of vibration measurements, detailed site inspection has been conducted to figure out suitable locations for vibration monitoring at different locations of the dam and road bridge.

Figure 3 shows the upstream elevation of Umiam Dam with the location of overflow and non-overflow blocks along with vibration monitoring locations selected on the downstream side, marked as red dots (●). At the top of the dam, 7.32 m (24') wide two-lane road with a six-feet-wide footpath on upstream side has been provided with railings on both the sides. Figure 4 shows schematic diagram indicating vibration monitoring points at different locations on top of Umiam Dam, Meghalaya.

The traffic consisted of light vehicles, medium vehicles and heavy vehicles. The traffic vibrations in terms of peak particle velocity in longitudinal, vertical and transverse directions have been measured using Digital Engineering Seismograph, Model Mini-Mate, at total 98 locations. Vibration measurements have been carried out for entire length of the dam, viz. footpath, adjoining road, road railings, downstream face, spillway piers and drainage gallery of block no. 7 as indicated in Fig. 5a–e, respectively.

(a) *Locations on the footpath and adjoining road*: For each of the block, on upstream side at two end points (a) and (c) and a middle point (b) on the middle of the

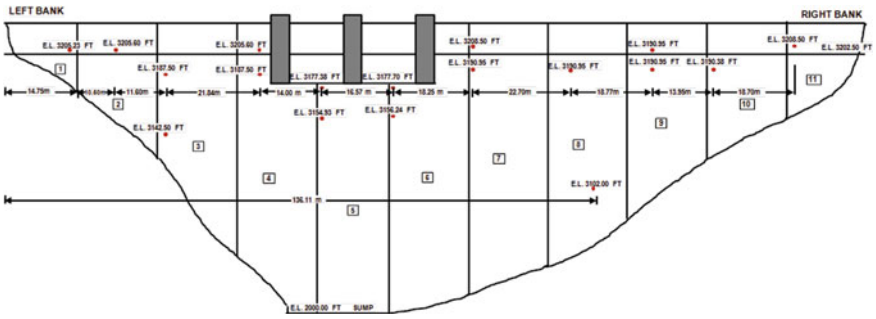

Fig. 3 Vibration monitoring locations on downstream face of Umiam Dam, Meghalaya

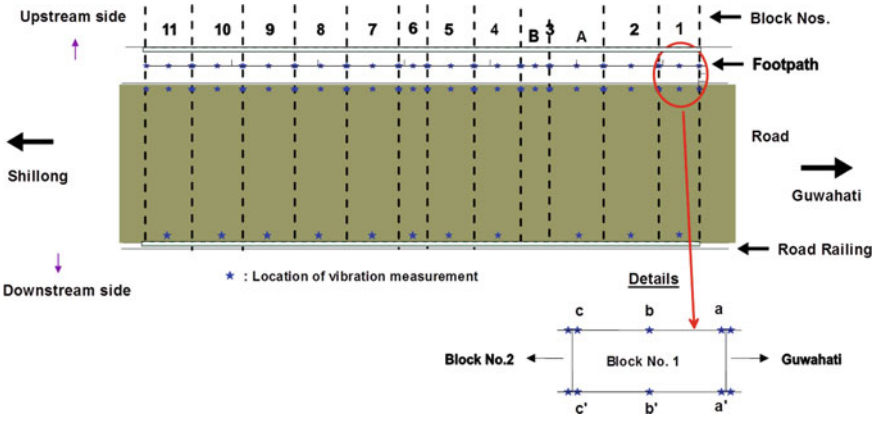

Fig. 4 Schematic showing vibration monitoring points atop the Umiam Dam, Meghalaya

footpath and at similar locations (a′), (b′), (c′) on the road at same chainage. Test locations—66 Nos. (6 pts on each block × 11 blocks) (Figs. 5a and 4).

(b) *Location near the road railings*: At the base of side railings on the downstream side of the road on all eleven blocks. Test locations—11 Nos. (Figs. 5b and 4).

(c) *Location on spillway pier*: At the centre of each of the three spillway pier on block nos. 4, 5 and 6. Test locations—3 nos. (Fig. 5c).

(d) *Locations on downstream face of the dam*: At various levels on the downstream face of all blocks. Test locations—17 Nos. (Figs. 5d and 3).

(e) *Locations in the Drainage Gallery*: In the drainage gallery of block no. 7 at level 3102' Test locations—1 no. (Fig. 5e).

Digital Engineering Seismograph (Mini-Mate, M/s Instantel Inc., Canada) shown in Fig. 6a has been used for recording vibrations generated from the vehicular traffic on the Umiam Dam. The unit is capable to record peak particle velocity (PPV), in longitudinal (L), vertical (V) and transverse (T) directions either in manual mode, single-shot trigger mode or continuous trigger mode. Displacement/Velocity/

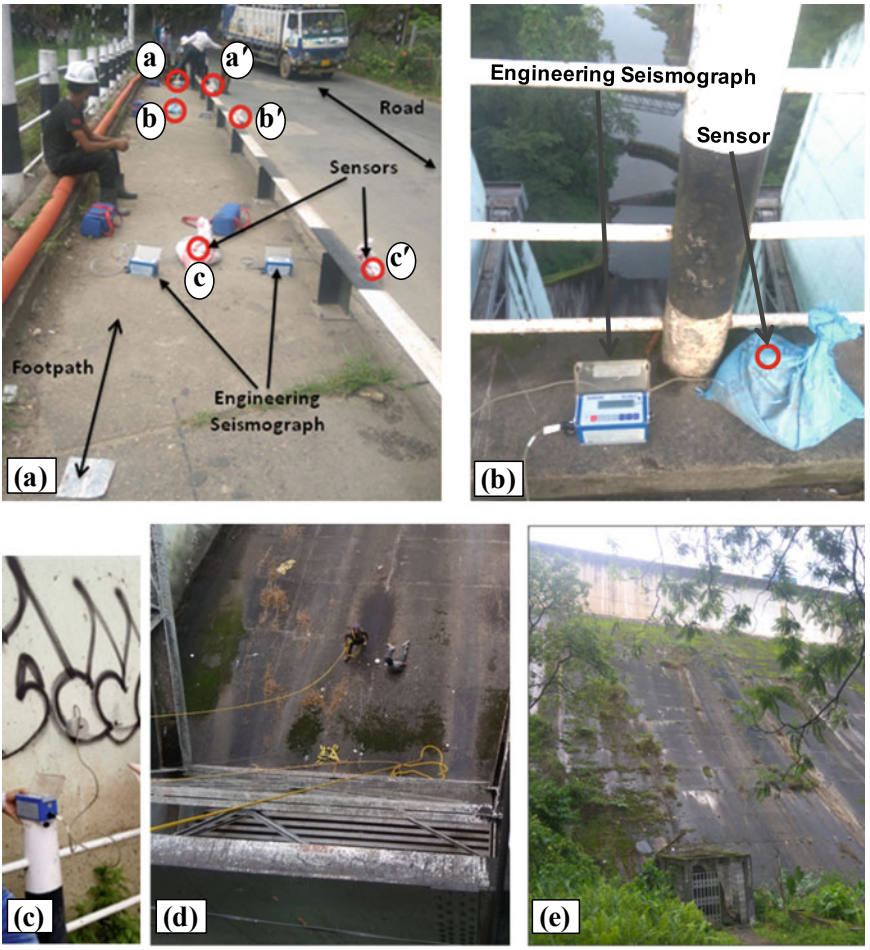

Fig. 5 Vibration measurements for entire length of the dam, viz. **a** over the footpath and adjoining road, **b** road railings, **c** piers, **d** spillway and **e** drainage gallery

Acceleration time histories of vibrations exceeding a pre-set trigger level can be recorded. As the trial measurements of vibration levels were below the minimum trigger level of the instrument, all tests were conducted in manual mode with recording time of 10 s. The sensor of the seismograph was fixed on the downstream face as well as on spillway piers of the dam by using a 'Hammer and Expand-Type Threaded Stud' as in Fig. 6b. The velocity–time histories acquired at a fixed sampling rate of 1024 samples/second, when analysed generate Event Records mainly consists of PPV readings and time series for vibrations in L, V and T components, zero crossing frequency (Hz), peak acceleration (g), peak displacement (mm), peak vector sum, etc. apart from recording details.

Fig. 6 A digital engineering seismograph (mini-mate, M/s Instantel Inc., Canada)

2.2 Safety Criterion Adopted

Vibrations from highway traffic, trains and most construction operations with the exception of blasting and pile driving are considered to be continuous vibrations. The safe levels for continuous vibrations are not well defined, and mostly, they are for safety of human beings, residential structures (buildings) or historical monuments rather than for hydraulic structures like dam, bridges or road passing over the dam. The safety criteria for various structures against induced vibrations are mainly in terms of the peak particle velocity response (PPV) and the associated frequency. Few criteria related to the traffic vibrations are presented here.

2.3 Transport and Road Research Laboratory (TRRL) Criterion

The TRRL's Whiffen and Leonard [6] in UK have conducted research on continuous vibrations and proposed the summary of continuous vibration levels in terms of peak particle velocity (PPV) limit and the reaction of people and effects on the buildings as in Table 1:

Table 1 Vibration level safety criteria as per Whiffen and Leonard [6]

PPV, mm/s	Human reaction	Effects on buildings
0.15–0.50	Threshold of perception	Unlikely to cause damage of any type
2.00	Readily perceptible	Virtually no risk of architectural damage
2.50	Threshold of annoyance	Upper level for ruins and ancient monuments
5.00	Annoying to people in buildings	Threshold risk of architectural damage to normal dwellings (plastered walls, etc.)
10–15	Considered unpleasant	Architectural damage/possible minor damage

Table 2 Vibration-level safety criteria based on Swiss Traffic Standard [7]

Building class	Vibration source (continuous)	Frequency range (Hz)	Safe PPV (mm/s)	Frequency range (Hz)	Safe PPV (mm/s)
I	Machines, traffic	10–30	12	30–60	12–18
II	Machines, traffic	10–30	8	30–60	8–12
III	Machines, traffic	10–30	5	30–60	5–8
IV	Machines, traffic	10–30	3	30–60	3–5

Class I: Buildings of steel or reinforced concrete, such as factories, retaining walls, bridges, steel towers, open channels; underground chambers and tunnels with/without concrete lining
Class II: Foundation walls and floors in concrete, walls in concrete or masonry; stone masonry retaining walls; underground chambers and tunnels with masonry linings; conduits in loose material
Class III: Building of steel/reinforced concrete with wooden ceilings and walls in masonry
Class IV: Construction very sensitive to vibration: objects of historical interest

Swiss Traffic Standard (SN 640 312:1978, Swiss Association for Standardization).

The Swiss developed a standard for both transient and continuous vibrations. This standard takes into account the type of construction and includes a category for historic items. This standard is very conservative, and safe limit is considered for two frequency ranges, i.e. 10–30 Hz and 30–60 Hz. Table 2 shows the safe limits for machine/traffic vibrations based on the class of structures to be safeguarded.

2.4 Frequency-Dependent Safety Criterion Due to Siskind et al. [8]

The safety criteria in terms of peak velocity response and associated frequency are mainly available for blast-induced vibrations of the residential structures. The popular frequency-dependent safety criterion after Siskind et al. [8] is shown in Fig. 7.

This was developed using damage data of United States Bureau of Mines (USBM) for several test structures subjected to ground vibrations due to mining blasts. According to this criterion, for frequencies between 3.8 and 15 Hz, a peak velocity response of 19.0 mm/s is safe for residential structures. For frequencies above 40 Hz, a constant peak velocity response of 50 mm/s is safe for houses. Safe levels for frequencies below 3.8 Hz and between 15 and 40 Hz are suggested as constant displacements of 0.76 mm and 0.2 mm, respectively.

In the absence of separate guidelines for the non-residential structures like road bridges over dam, the criterion due to Siskind et. al. [8] has been adopted in the present study to assess the safety of the Umiam Dam.

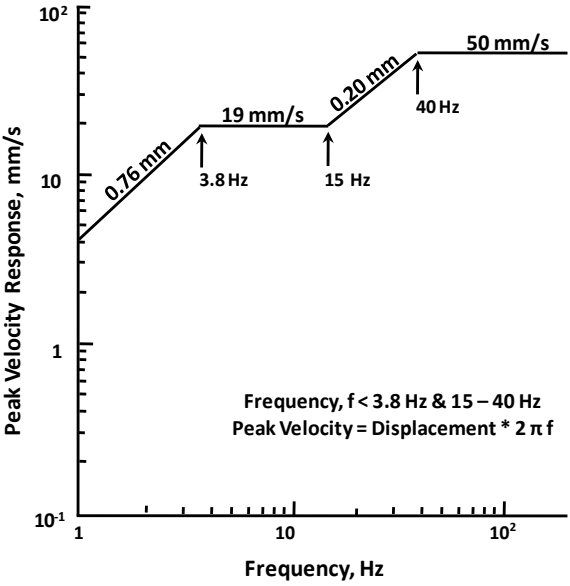

Fig. 7 Frequency-dependent safety criterion in terms of the peak velocity response of residential structures subjected to blast vibrations [8]

3 Discussion on Results

To monitor the vibrations generated due to traffic on the top of Umiam Dam, peak particle velocity has been measured at 98 different locations (Fig. 6), viz. on footpath, on road, near road railing, on three piers, on downstream face of the dam and inside the drainage gallery. The time histories of the traffic vibrations in terms of PPV for all three components have been acquired and event reports have been generated. From the event reports, the traffic vibration frequencies were evaluated, and for majority of the events, the frequencies were found to be in the range of 10–30 Hz. As discussed in Sect. 2.3, from the three criteria the safe vibration level due to traffic on bridges/dams is mentioned to be in the range of 5–12 mm/s for frequency range of 10–30 Hz. From the analysis of the vibration results, it is observed that though heavy traffic is passing over the dam bridge, the vibration levels at all the locations on the downstream face, footpath, road, near railings and in the dam body were very low. The vibration levels recorded on downstream face of dam are shown in Table 3. While the maximum vibration levels recorded on footpath—road, road railings of all blocks are shown in Table 4, and those on spillway piers are shown in Table 5.

The vibration levels observed at downstream face shown in Table 3 indicate that PPV values recorded are very insignificant, i.e. $\approx$ 0.064 mm/s. Very low level of vibration has been observed at some of the locations on the downstream face and hence could not be recorded by the instrument. Similar vibration level is recorded inside drainage gallery, i.e. 0.064 mm/s.

Table 4 gives the observed PPV levels at different locations of the foot path and adjoining road in the upstream side and road railings on the downstream side, for all

Table 3 Observed maximum peak particle velocity response (PPV) in mm/s at the downstream face on block nos. 1 to 11 (Figs. 1b and 3)

Test site	PPV, mm/s										
	Block No.										
	1	2	3	4	5	6	7	8	9	10	11
A	–	–	0.064	0.064	0.064	0.064	0.064	0.064	0.064	0.064	–
B	–	–	0.064	–	0.064	0.064	0.064	–	–	–	–
C	0.064	0.064	–	0.064	–	–	–	–	0.064	–	0.064

Table 4 Observed maximum peak particle velocity response on the footpath, road (Ref. Fig. 6a) and road railings (Ref. Fig. 5b) for block nos. 1–11

Block No.	PPV, mm/s at test location						
	Footpath–road						Road railings
	(a)	(a′)	(b)	(b′)	(c)	(c′)	
1	0.064	0.064	0.064	0.064	0.064	0.064	No trigger
2	0.064	0.064	0.064	0.064	0.064	0.064	0.064
3	0.064	0.064	0.064	0.064	0.064	0.064	0.064
4	0.064	0.127	0.064	0.064	0.254	0.254	0.064
5	**0.445**	**1.080**	**0.254**	**0.445**	**1.334**	**1.334**	**2.858**
6	**0.508**	**0.381**	**2.730**	**1.334**	**0.381**	**0.381**	**1.207**
7	0.064	0.064	0.064	0.064	0.064	0.064	0.064
8	0.064	0.064	0.064	0.064	0.064	0.064	0.064
9	0.064	0.064	0.064	0.064	0.064	0.064	0.254
10	0.064	0.064	0.064	0.064	0.064	0.064	0.064
11	0.064	0.064	0.064	0.064	0.064	0.064	0.064

Bold numbers to be noted from Fig. 3 that blocks 4, 5 and 6 serve as foundation for Piers 1, 2 and 3, that support radial gates for spillways. Observations indicate that notable levels of vibration have been restricted to this section of the dam body

Table 5 Observed maximum peak particle velocity response (PPV) in mm/s in three piers guiding spillways of Umiam Dam (Ref. Fig. 5c)

Sl. No.	Test location	PPV (mm/s)
1	Pier No. 1 (block no.4)	0.127
2	Pier No. 2 (block no.5)	0.127
3	Pier No. 3 (block no.6)	0.064

the blocks of Umiam Dam. The observed maximum PPV values for these locations lie between 0.064 and 2.730 mm/s for foot path and adjoining road, whereas the maximum PPV for road railings on the downstream side lies between 0.064 and 2.858 mm/s.

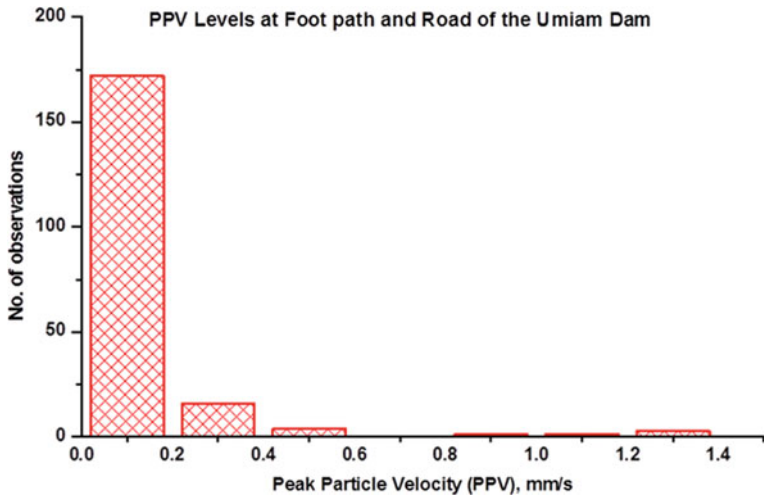

Fig. 8 Distribution of vibration levels observed at footpath and on the road for all the blocks of Umiam Dam

Table 5 gives the values of PPV at the centre of three spillway piers for all three components, and it is found that the observed PPV values lies between 0.064 and 0.127 mm/s. A distribution of vibration levels observed at different locations on Foot path and on the road for all the blocks of Umiam Dam is shown in Fig. 8. The distribution indicates that maximum number of observations of vibration levels fall in the range of 0.0–0.2 mm/s. While, only a few observations are in the range of 0.4–1.4 mm/s which are within the acceptable level of vibration level.

Table 6 gives the maximum PPV values recorded on different blocks of the dam and are found to be in the range of 0.064–2.858 mm/s. From the above observations, it can be noted that the vibration levels induced by traffic on the top Umiam Dam are very low and are well within the recommended safe vibration levels. Though the vibration levels are found to be low and within the safe limits, it is not advisable to have continuous vibrations due to heavy traffic on such important structure like a dam. Moreover, considering the importance of the Umiam Dam, it is justified to conduct long-term vibration monitoring by installing vibration monitoring system at the dam site.

4 Conclusions

Vibration measurements become essential on important structures whenever heavy mechanical activities take place in the vicinity of these structures, for assessing structural safety of the same. Whenever continuous vibration activities are taking place, continuous vibration monitoring system should be installed on such structures.

Table 6 Maximum PPV for each of the block of Umiam Dam

Sl. No.	Block No.	Maximum PPV, mm/s	Max. Acceleration 'g'
1	1	0.064	0.007
2	2	0.064	0.007
3	3	0.064	0.007
4	4	0.254	0.027
5	5	**2.858**	**0.033**
6	6	**2.730**	**0.027**
7	7	0.064	0.007
8	8	0.064	0.007
9	9	0.254	0.007
10	10	0.064	0.007
11	11	0.064	0.007

Bold numbers to be noted from Fig. 3 that blocks 4, 5 and 6 serve as foundation for Piers 1, 2 and 3, that support radial gates for spillways. Observations indicate that notable levels of vibration have been restricted to this section of the dam body

Traffic-induced vibration levels at various locations of the dam body were found to be insignificant with a maximum PPV of 0.064 mm/s. However, few locations of the structure in the spillway zone on Blocks 5 and 6 recorded a relatively higher PPV in the range of 0.254–2.858 mm/s. These are lower than the range of 5–12 mm/s of PPV, safe vibration level based on criteria adopted. On the other hand, a maximum acceleration level of 0.033 g has been observed at the top of Umiam Dam, which is very small and within acceptable limit. Continuous vibrations due to heavy traffic on top of the dam in the long run may induce internal cracking or increase the extent of cracking thus endangering structural safety of the dam. Moreover, heavy traffic movement on dams is not advisable as it may induce development of various distresses in the piers and dam body in the form of cracking, malfunctioning of gate operating mechanism and opening/expansion of lift/ block joints, etc., thus resulting in seepage through joints. Considering the importance of the Umiam Dam, it is suggested to carry out long-term vibration monitoring by installing vibration monitoring system at the dam site.

Acknowledgements The authors acknowledge the support and encouragement received from Director, CWPRS, Pune, Ministry of Jal Shakti, Government of India, to carry out and publish the present work.

References

1. Erkal A (2019) Impact of traffic-induced vibrations on residential buildings and their occupants in metropolitan cities. Promet Traffic Trans 31(3):271–285. https://doi.org/10.7307/ptt.v31i3.3000
2. Lozančić S, Penava D, Klečina MB, Jurić A (2019) A case study on influence of traffic-induced vibrations on buildings and residents, ActaTechnica Corviniensis Bull Eng 12(2):15–18
3. Gang W et al. (2019) Effect of vibration from highway vehicle load on adjacent buildings and its assessment. In: IWRED—2019, 3rd international workshop on renewable energy and development, Guangzhou, March 2019. Conf Ser Earth Environ Sci vol 267. Inst Phys Publ, Bristol, p 052048. https://doi.org/10.1088/1755-1315/267/5/052048
4. Shende VJ, Shirke RR, Varshikar NB, Ghodake VK, Govindan S (2012) Traffic vibration measurement studies on concrete gravity dam of Umiam Stage-I HEP, Me. E. C. L., Meghalaya. Technical Report No. 5009, Central Water and Power Research Station, Pune
5. Santhosh Kumar S, Ghodake VK, Prakash Palei, Rizwan Ali, and Bhajantri MR (2021) Traffic vibration measurement studies on concrete gravity dam of Umiam Stage-I HEP, Me. E. C. L., Meghalaya. Technical Report No. 5881, Central Water and Power Research Station, Pune
6. Whiffin AC, Leonard DR (1971) A survey of traffic induced vibrations. Laboratory Report No. 418, Transport and Road Research Laboratory (TRRL), Berkshire, UK
7. Swiss Norm 640 312A (1978) Vibration effects on buildings. Swiss Association for Standardization (SNV), Zurich
8. Siskind DE, Stagg MS, Kopp JW, Dowding CH (1980) Structure response and damage produced by ground vibration from surface mine blasting. Report of Investigations No. 8507, U.S. Bureau of Mines, Washington, DC.

Dam Safety Measures Against Earthquakes in Seismic Regions

S. Selvan, Suman Sinha, Sachin Khupat, Chaman Singh, K. Jerin Paul, and Rizwan Ali

Abstract Dams are important water resource projects because they provide water for irrigation, hydroelectric power, domestic and industrial needs, fisheries, navigation and recreation activities. Dams are generally constructed in hilly terrains. These dams are susceptible to be affected with earthquake forces, and hence, the safety of dams against earthquake loads is an important aspect during assessment of stability. Failing to consider the earthquake loads at design stage may result in under-safe dam construction which may cause damages in the dams during seismic activities. Dam failure may lead to loss of lives and properties resulting huge economical loss. The safety of dams is required to be ensured by applying the site-specific seismic design parameters during design of the dam. In this paper, the site-specific seismic design parameters obtained by deterministic and probabilistic seismic hazard assessments for Bhatsa dam, Maharashtra, lying in seismic Zone-III, are presented.

Keywords Dam safety · Earthquake load · Seismic design parameters · Bhatsa dam

1 Introduction

Seismic safety of hydroelectric projects is very important in view of their great socioeconomic significance. In India, a major portion of the water resources potential exists in the highly seismic Himalayan region. In the less seismically active central and southern India also, the seismic safety of hydroelectric projects is matter of concern due to the occurrence of irregular damaging earthquakes in the recent times and the apprehension regarding the effects on seismicity around formed reservoir. To ensure the safety of the dam, it is essential to have a realistic and reliable estimate of the

S. Selvan · S. Sinha · S. Khupat · C. Singh · K. Jerin Paul (✉) · R. Ali
Engineering Seismology Division, Central Water and Power Research Station, Pune, India
e-mail: jerinpaul@cwprs.gov.in

S. Sinha
e-mail: suman.sinha@cwprs.gov.in

P. V. Timbadiya et al. (eds.), *Flood Forecasting and Hydraulic Structures*, Lecture Notes in Civil Engineering 340, https://doi.org/10.1007/978-981-99-1890-4_50

expected earthquake potential and the resulting ground motion at the dam site. In the recent design practices, a dam needs to be safe against any forces due to earthquake ground motion under detailed dynamic response analysis using site-specific seismic design parameters. For a detailed dynamic analysis of dams, the interaction of dam with the foundation rock and hydrodynamic forces needs to be modelled in a systematic way. Recently, many advanced structural analysis methods, namely finite difference method, boundary integration method and finite element method, have been introduced to perform dynamic response analysis of dams. Dynamic response analysis results have to be standardized by examining the response of the structures to actual earthquakes and forced vibration experiments.

To perform detailed dynamic response analysis for earthquake-resistant design of important structures like dams, the input excitation needs to be described in the form of complete time-history of ground acceleration known as design accelerograms. In practical engineering applications, the design accelerograms are reproduced to be attuned with the response spectra having 5% damping ratio, termed as "target response spectra" for hydraulic structures. The target response spectra for a project site can be estimated using several different alternatives under "deterministic" and "probabilistic" approaches [1–5]. The preliminary design can, however, be based on simplified pseudostatic/dynamic analysis using site-specific design seismic coefficients, which would be described from the response spectra of the site-specific design accelerogram with a damping ratio equal to that of the dam. For this purpose, the response spectra for all the required damping ratios can be computed from the design accelerograms.

2 Brief Description of the Methodology

2.1 Deterministic Seismic Hazard Analysis (DSHA)

The design ground motion by DSHA is evaluated for a specific earthquake magnitude occurring at a closest distance from the project site of interest. Two different levels of earthquakes are considered for this purpose; one which represents a rare but possible event, and the other a more likely event during the life time of a project. These are considered as the Maximum Credible Earthquake (MCE) and the Design Basis Earthquake (DBE), respectively. The MCE is described as the biggest possible earthquake due to an active fault, or inside a geographically characterized tectonic regime. Each seismic source zone in a project area is characterized by its own MCE magnitude, which is presumed to occur at the closest possible distance to the project site. The MCE and DBE levels of ground motion are evaluated as shown in the Table 1 below as per the location of the site categorized under four seismic zones of India via, Zone-II, Zone-III, Zone-IV, and Zone-V. Seismic Zone-II corresponds to the region of low seismic activity and Zone-V corresponds to the region of high seismic activity.

Table 1 MCE and DBE levels of deterministic ground motion for various seismic zones

No.	Hazard level	Zone-II and Zone-III	Zone-IV and Zone-V
1	Maximum credible earthquake (MCE)	Median ground motion	Median plus one standard deviation ground motion
2	Design basis earthquake (DBE)	Median minus one standard deviation ground motion	Median ground motion

2.2 Probabilistic Seismic Hazard Analysis (PSHA)

In the probabilistic approach, the target response spectra (TRS) are evaluated by taking into account the effect of all the earthquakes with suitable spatial distribution in various seismic source zones (SSZ) during a specified exposure period. The PSHA is used to consider the random and uncertain nature of seismicity as well as the ground motion attenuation. This method considers the effect of total expected seismicity with appropriate spatial distribution to estimate the 5% damped target response spectra for a project site. The spectra obtained by PSHA approach have the property that, for a specified confidence level, the spectral amplitudes will not exceed due to any of the earthquakes expected to happen anywhere in the region within a specified exposure time. The probabilistic MCE level of ground motion is normally estimated with a confidence level of 98% during 50 years of exposure time [5]. The DBE level of probabilistic spectra is defined with 90% confidence level during an exposure period of 50 years. The composite probability distribution of the spectral amplitudes for a particular natural period used by the PSHA after McGuire [6]; Anderson and Trifunac [3] and Gupta [4] is described as

$$P[S(T)] = \exp\left\{ -Y \sum_{i,j} q[S(T)|M_j, R_i] \cdot \upsilon(M_j, R_i) \right\} \tag{1}$$

In this expression, $\upsilon(M_j, R_i)$ is the annual occurrence rate of earthquakes within small magnitude and distance ranges $(M_j - \delta M_j,\ M_j + \delta M_j)$ and $(R_i - \delta R_i,\ R_i + \delta R_i)$, and Y is the exposure time considered. Quantity $q[S(T)|M_j, R_i]$ is the probability of exceeding the spectral amplitude $S(T)$ due to earthquake magnitude M_j at distance R_i, which can be obtained from the probability distribution of Eq. (1). Thus, the main task to evaluate the distribution function of Eq. (1) is to estimate the occurrence rates $\upsilon(M_j, R_i)$, which is termed as the total design seismicity. Table 2 shows the MCE and DBE levels of probabilistic ground motion estimated for various seismic zones.

Table 2 MCE and DBE levels of probabilistic ground motion for various seismic zones

No.	Hazard level	All zones
1	Maximum credible earthquake (MCE)	2% of probability of exceedance in 50 years (Return period of 2475 years)
2	Design basis earthquake (DBE)	10% of probability of exceedance in 50 years (Return period of 475 years)

2.3 Ground Motion Prediction Equations (GMPE)

A GMPE is an empirical relation that quantifies the measures of ground motion caused by an earthquake. The results obtained from a GMPE are a probability distribution which describes the ground motion measure. The important output parameter of a GMPE is peak ground acceleration (PGA). However, GMPEs estimate few other parameters such as response spectral ordinates and peak ground velocity (PGV). GMPEs are developed from statistical regression of observed strong ground motion (SGM) data corresponding to wide range of magnitudes and distances and varying geological and geotectonic frameworks. They predict an expected ground motion and its intrinsic variability due to an earthquake. These ground motion relations estimate the distribution of expected ground motions as a function of a few independent parameters, such as magnitude, source-to-site distance and soil condition. The ground motions estimated by any one ground motion relation are given in terms of median spectral amplitudes and associated standard deviations. The GMPEs used in seismic hazard studies should ideally be formulated using the actually observed strong motion data in the region around the site of interest. However, due to scarcity of adequate strong motion data in India, such relations are unavailable for different parts of the country. Hence, few widely used GMPEs which are suitable for the region of interest have to be identified from published sources.

3 Bhatsa Dam, Maharashtra—A Case Study

The Bhatsa dam is located in Thane District, about 115 km from Mumbai. The dam contemplates water supply to Mumbai City and irrigation in the nearby area. The dam is of 88.5 m high gravity type built in uncoursed rubble masonry. The dam was built in 1983. The dam is located at latitude 19.52º N and 73.42º E. In recent times, Palghar district has experienced constant earthquake tremors. In order to facilitate the safety review through stress analysis, the site-specific seismic design parameters for the dam were estimated.

3.1 Local Geology and Seismo-Tectonic Features

The area surrounding the project site is made up of Deccan Basalt flows consisting of amygdaloidal basalt at some region, massive basalt and weathered basalt. At the dam site, variations of weathered basalt and amygdaloidal basalt and massive basalt are not exposed. In the river bed, weathered basaltic rocks are exposed, and on the right bank, rock is not exposed or under cover. In the spill channel downstream area, weathered basalt prone to erosion has been delineated from 120 to 420 m. This portion was suitably grouted. The geology of the dam site was considered as rock and assigned an average shear wave velocity (V_{s30}) of 1000 m/s for the estimation of seismic design parameters. The major seismo-tectonic features in the region of Bhatsa dam site are shown in Fig. 1 which is based on the sheet numbers 19, 20, 27, 28, 32 and 33 of seismo-tectonic atlas of India by Geological Survey of India [7].

The region of study includes features like faults, lineaments, folds, rifts and shear zones. In the area covered by Deccan Traps, major faults and lineaments trend NW–SE, a trend that corresponds to the tectonic grains of the adjacent Precambrian basement rocks. Some of the faults and lineaments traversing the trap rocks are found to continue in the peripheral older rocks. The major geofractures near the project sites are the West Coast, Ghod, Upper Godavari faults and Panvel flexure.

3.2 Preparation of Earthquake Catalogue

A distance of 300 km on all sides of the Bhatsa dam, i.e. a rectangle consisting of dimensions of 7° × 7.5°, has been drawn around the dam site. Therefore, the region from 16.5°N–23°N and 70°E–77°E has been considered for the present seismic hazard assessment study. The first step of hazard assessment is to prepare an earthquake catalogue. Earthquake database which contains details of each earthquake event, such as time of occurrence in terms of year, month, day, hour and minute; location of occurrence in terms of longitude, latitude and depth; magnitude of earthquake in terms of M_L, M_S, M_b and M_W is known as earthquake catalogue. The earthquake catalogue for the present analysis has been prepared from the data available from ISC, USGS and IMD. The catalogue has then been processed for homogenization (conversion of different magnitude scales into moment magnitude, M_W) and declustering (removal the foreshocks and aftershocks).

3.2.1 Catalogue Completeness

It is generally believed that earthquake catalogue is incomplete for smaller magnitude events in early times due to insufficient instrumentation. However, the occurrence rates for smaller magnitude events can be evaluated even from the most recent data, say about 15–20 years, for their short return periods. However, the data for a much

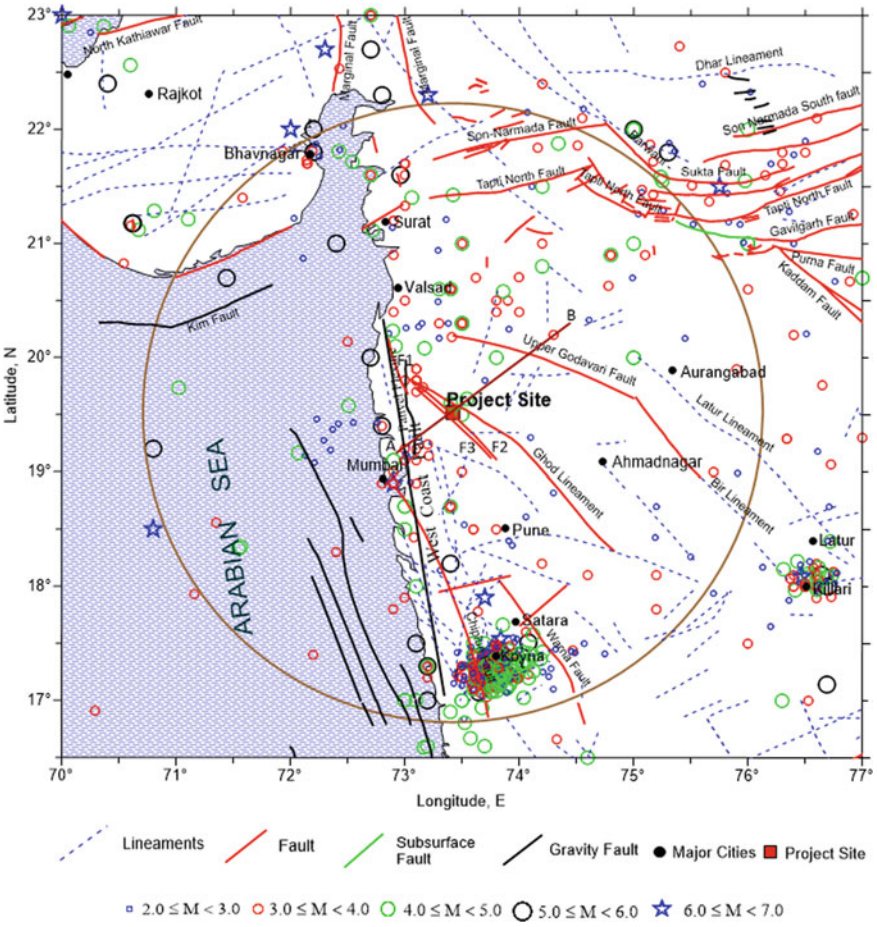

Fig. 1 Overlay of the past earthquakes with various tectonic features

longer period need to be considered to have a reliable estimate for the occurrence rates of larger magnitude earthquakes with long return periods, failing which may lead to underestimation of the mean rates of occurrence of earthquakes. The time period of complete data for pre-defined magnitude ranges has to be identified first, and then reliable mean rates of occurrence of earthquake for the said magnitude ranges have to be computed. Stepp [8] proposed a statistical method to compute the period of completeness, and the same has been followed in the present study to determine the period of completeness.

3.2.2 Estimation of Distribution of Past Seismicity

Figure 2 shows the histograms for the distribution of magnitude and epicentral distances for earthquakes within 300 km of the proposed project site for Bhatsa dam. It is evident from the histogram for magnitude that the relative numbers of earthquakes with magnitude greater than 5.2 M_W are not manifested in a consistent way. The limited period and the area covered by the catalogue may be attributed to this.

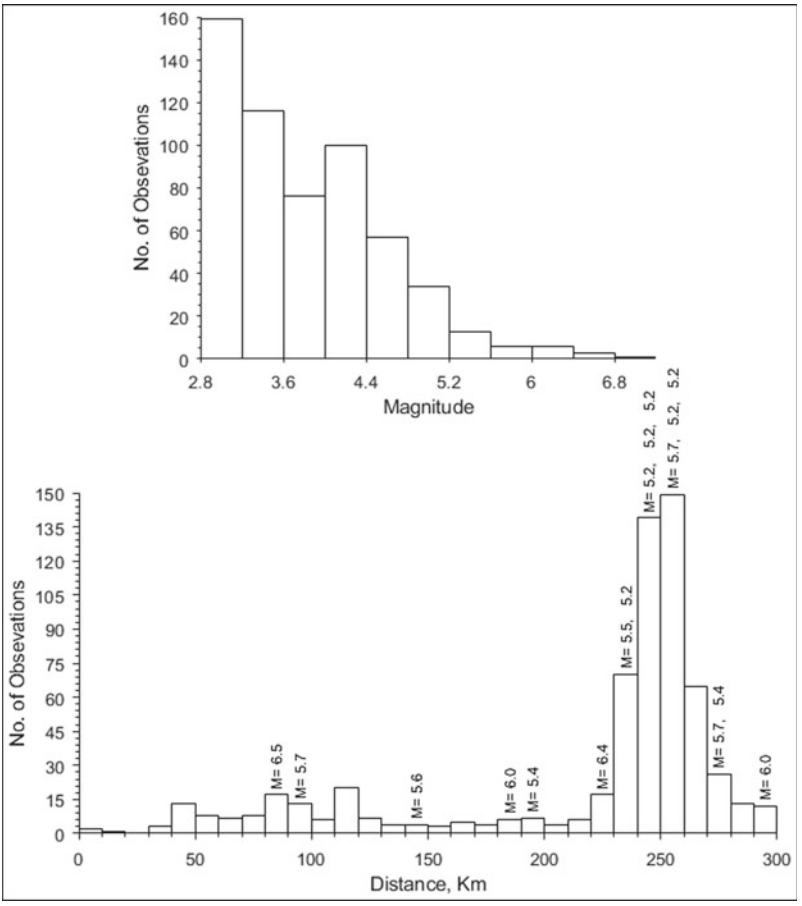

Fig. 2 Histograms showing the distribution of magnitude and epicentral distance of past earthquakes within 300 km from the Bhatsa dam site

Table 3 Details of MCE magnitude and closest distances from site to tectonic features

Sr No.	Name of tectonic feature	Type of faulting	Magnitude of MCE (M_W)	Closest distance from the dam site (Km)
1	F2	Unknown	5.5	2.1
2	F3	Unknown	5.5	5.6
3	Ghod fault	Strike slip	6.3	6.9
4	Panvel flexure	Strike slip	6.3	37.3
5	F1	Normal fault	5.5	45.0
6	West coast fault	Strike slip	6.3	48.6
7	Upper Godavari fault	Strike slip	6.3	72.5

3.3 Estimation of MCE Magnitudes and Distances for DSHA

The magnitude of MCE in the present study has been determined from an analysis of the available data on past earthquakes. To define the magnitude of MCE for plate boundary areas, the actually recorded largest magnitude was conventionally enhanced by 0.5–1 unit. The enhancement in the magnitude was made to account for the fact that the period of the available earthquake catalogue was not long enough to include the expected largest magnitude. Therefore, a magnitude of 6.3 MW for MCE can be expected on the Ghod, the Panvel flexure, the West Coast and the Upper Godavari faults, and a magnitude of 5.5 MW for MCE can be expected on F1, F2 and F3, respectively. These are the known significant tectonic features near the project site. The distances of the dam site from the significant tectonic features are given in Table 3. The 5% damped response spectra of horizontal and vertical ground motion have been evaluated with a confidence level of 0.50 for MCE magnitude 6.3 $\boldsymbol{M_W}$, associated with Ghod fault, at a closest distance of 6.9 km, MCE magnitude 5.5 $\boldsymbol{M_W}$, associated with F2 fault, at a closest distance of 2.1 km from the Bhatsa dam site. In the present case, the MCE magnitude 6.3 $\boldsymbol{M_W}$, associated with Ghod fault, is evidently the controlling MCE.

3.4 Estimation of Design Seismicity for PSHA

To implement the PSHA approach for obtaining the target response spectra for the Bhatsa dam site, the following form of Gutenberg–Richter's [9] relationship has been considered for each seismic source zone (SSZ) around the project site.

$$\log N(M) = a - bM \tag{2}$$

In the above equation, $N(M)$ is the annual number of earthquakes with magnitude M or greater, and 'a' and 'b' are the regression coefficients specific to the SSZ of interest. These constants are evaluated using the past earthquake data in each SSZ. The maximum likelihood method of Weichert [10] has been used to obtain the constants 'a' and 'b' in the present study. Once the values of 'a' and 'b' are determined for a SSZ, Eq. (3) is employed to obtain the total number $N(M_{\min})$ of earthquakes above a lower threshold magnitude $M_{\min}$ taken as 4.0 $\boldsymbol{M_W}$ in the present study. For engineering applications, it is necessary to put an upper bound magnitude $M_{\max}$ also. With the imposition of upper and lower threshold magnitudes, the expression for $N(M)$ is modified after Cornell and Van Marcke [11].

$$N(M) = N(M_{\min}) \frac{\exp(-\beta(M - M_{\min})) - \exp(-\beta(M_{\max} - M_{\min}))}{1 - \exp(-\beta(M_{\max} - M_{\min}))} \tag{3}$$

where $\boldsymbol{\beta = b}$ **ln 10**. The Eq. (3) defines an exponential decay of $N(M)$ with increase in M up to the upper threshold magnitude. It may not be suitable to describe the behaviour of very large magnitude earthquakes in some cases, where the largest earthquakes occur more periodically and frequently. In such cases, the characteristic earthquake model is found to describe the data better [12]. The characteristic model is obtained by fitting the relationship of Eq. (3) to the observed data up to some much lower magnitude than $M_{\max}$. In the range, $(M_{\max} - \Delta M_c,\ M_{\max})$ of the characteristic earthquake, a uniform occurrence rate is used with the probability density equal to that given by the distribution of Eq. (3) at a still lower magnitude, say one magnitude unit below $(M_{\max} - \Delta M_c)$. For a given SSZ, the occurrence rate of earthquakes within a small magnitude range $(M_j - \delta M_j,\ \ M_j + \delta M_j)$ around central magnitude M_j is obtained as

$$n(M_j) = N(M_j - \delta M_j) - N(M_j + \delta M_j) \tag{4}$$

In the present analysis, the magnitude range has been discretized into eleven intervals with central magnitude $M_j = 4.0, 4.4, 4.8, 5.2, \ldots, 8.0$ and $\delta M_j = 0.4$ for all the intervals. The number $n(M_j)$ for various SSZ is distributed uniformly to get the number within a small distance range $(R_i - \delta R_i, R_i + \delta R_i)$. The total number within the i^{th} distance range for all the SSZs provides the required design seismicity $\upsilon(M_j, R_i)$. By computing the probability distribution of Eq. (1) for each natural period, it is possible to estimate the spectral ordinate $S(T)$ for a desired confidence level at all the natural periods.

3.5 Target Response Spectra

The target response spectra (TRS) corresponding to DSHA and PSHA estimates were computed using the GMPE developed by Abrahamson and Silva [13]. The average of deterministic and probabilistic spectra has been considered to be the TRS for

horizontal and vertical components of ground motion for MCE condition following the NCSDP guidelines (2011, revised 2014) [14]. For DBE condition in seismic Zone III, the TRS shall be obtained as the envelope of the DSHA and PSHA estimates, and therefore, the envelope of the two has been taken to be the TRS for horizontal as well as vertical components of ground motion. The MCE and DBE levels of TRS for horizontal and vertical components are shown in Fig. 3.

3.6 Design Accelerogram and Response Spectra

The 5% damped TRS is used to generate the compatible design accelerograms by superposition of sinusoidal waves as follows:

$$a(t) = \sum_i C_i \cos(\omega_i t + \varphi_i) \tag{6}$$

where ω_i is the angular frequency and φ_i is the corresponding phase angle. Final design accelerograms compatible with the MCE and DBE conditions of TRS (for horizontal and vertical components) are shown in Fig. 4. The peak ground acceleration values of horizontal and vertical components of motion at MCE level are found to be 245.76 cm/sec^2 and 161.28 cm/sec^2 respectively. Similarly, the peak ground acceleration values of horizontal and vertical components for DBE level of motion are found to be 111.30 cm/sec^2 and 81.45 cm/sec^2 respectively. Using the accelerograms compatible to the 5% damped TRS for MCE and DBE conditions of design response spectra of horizontal and vertical components of motion are computed for damping values of 5%, 7%, 10% and 15% of critical. Figure 5 shows the design response spectra for the horizontal and vertical components for different damping values for the MCE and DBE conditions.

3.7 Seismic Coefficients

The site-specific estimates of the design horizontal seismic coefficient for initial design using simplified response analysis are obtained from the DBE level of horizontal response spectrum. As per NCSDP guidelines [14], the horizontal seismic coefficient (α_h) can be taken as two-thirds of DBE level of Effective PGA (EPGA). The EPGA is obtained by scaling down the DBE level of spectral amplitude of 5% damped design spectrum at 0.2 s by a factor of 2.5. The horizontal seismic coefficient is thus found to be 0.084. As this value is lower than the value 0.12 for seismic Zone-III as per the code IS 1893: 1984 (Part 1) [15], the horizontal seismic coefficient has to be taken as 0.12. The vertical seismic coefficient (α_v), taken as two-thirds of α_h, works out to be 0.08.

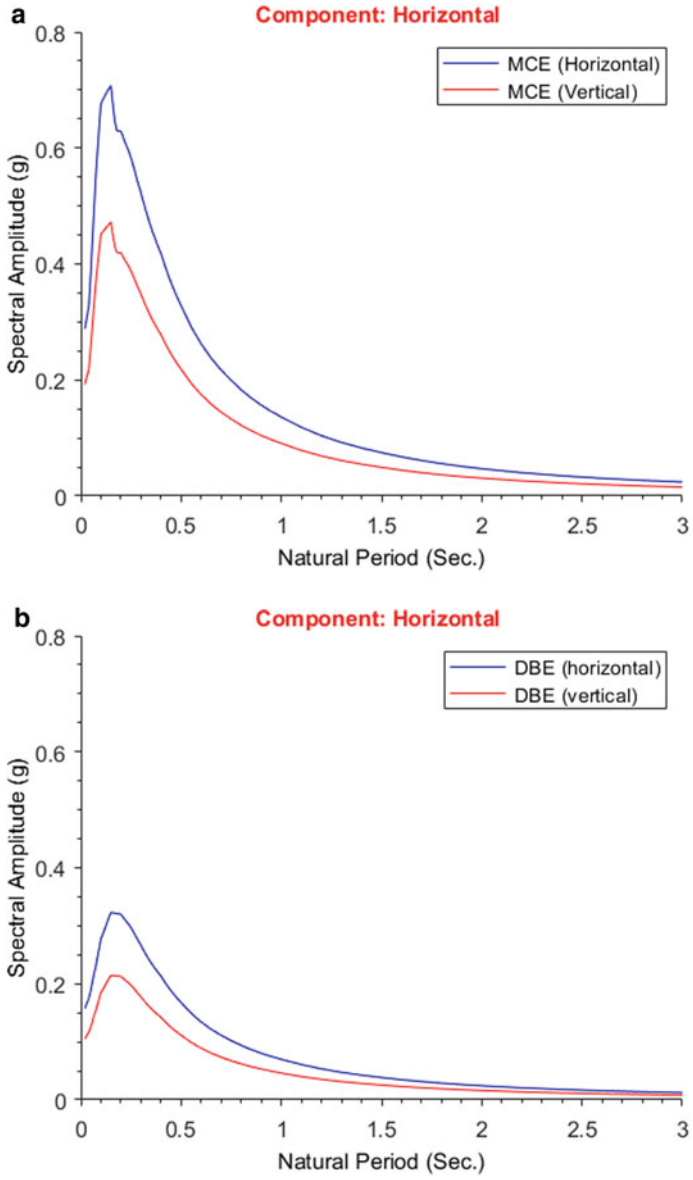

Fig. 3 MCE and DBE levels of TRS for horizontal and vertical components

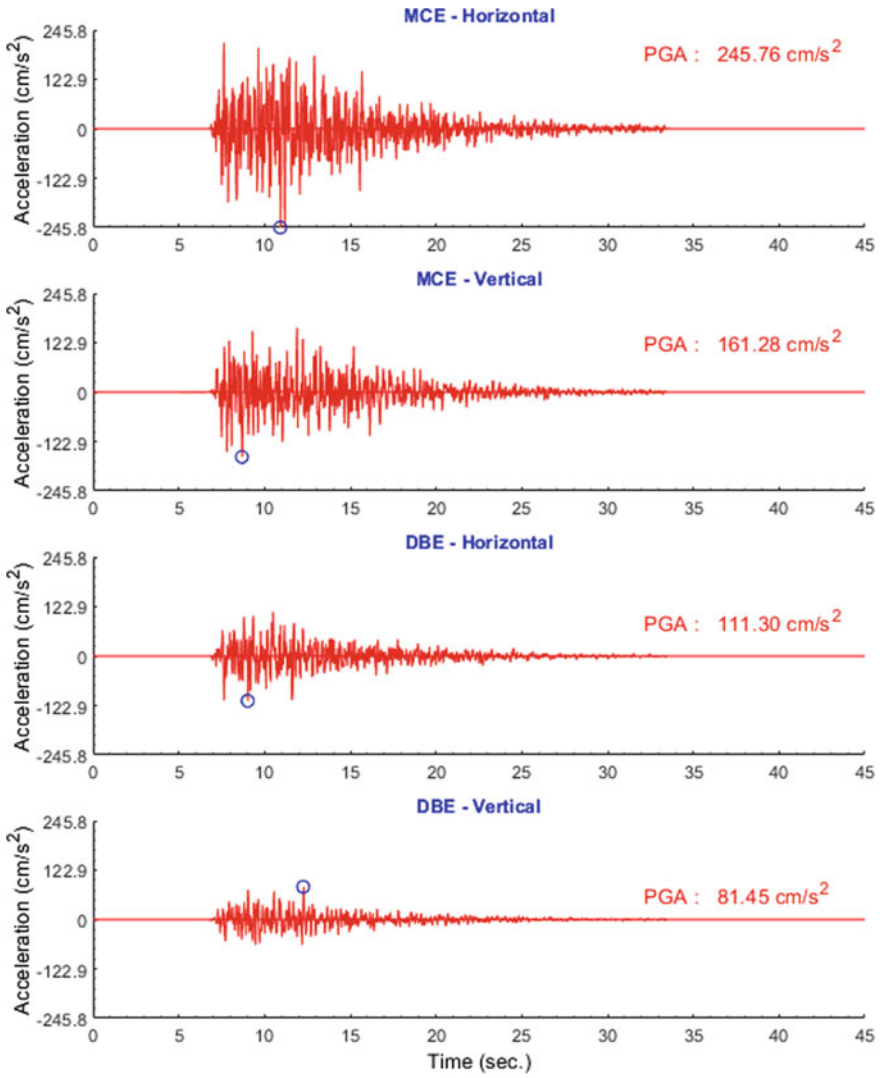

Fig. 4 MCE and DBE levels of design accelerogram

The natural period (T) of the structure is found to be 0.266 s for concrete portion of the dam. Therefore, the value of α_h, according to IS 1893: 2016 (Part 1) [16] for Zone-III with ratio of Importance Factor and Response Reduction Factor I/R as 1, works out to be 0.20 and the value of α_v (i.e. 2/3 of α_h) to be 0.13 for the concrete portion of the dam. With I/R as 0.6, α_{h} and α_{v} turn out to be 0.12 and 0.08, respectively. The values of α_{h} and α_{v} calculated from IS 1893: 2016 (Part 1) [16], being higher, are recommended to use for preliminary design purposes. The seismic coefficients computed from different criteria are given in Table 4.

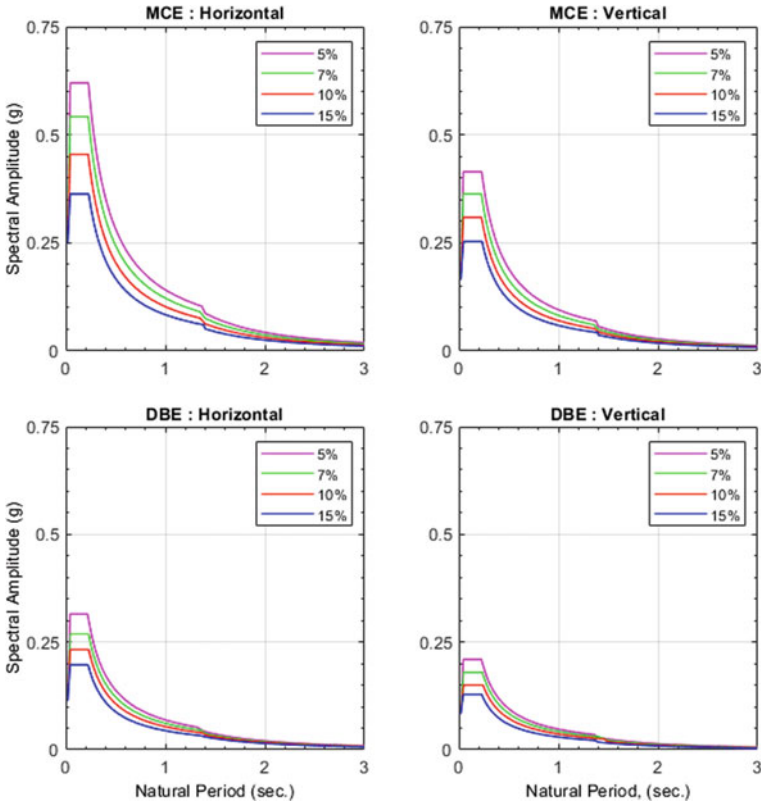

Fig. 5 MCE and DBE levels of design spectra

Table 4 Seismic coefficients computed using different criteria

Reference	α_h		α_v	
NCSDP (2011, revised 2014)	0.084		0.056	
IS 1893: 1984 (Part 1)	0.12		0.08	
IS 1893: 2016 (Part 1)	I/R = 1	I/R = 0.6	I/R = 1	I/R = 0.6
	0.20	0.13	0.12	0.08

3.8 Results and Recommendations

The values of the peak ground acceleration for horizontal and vertical components are found to be 0.25 g and 0.16 g for MCE; and 0.11 g and 0.08 g for DBE conditions, respectively. Smoothed design response spectra are computed for damping ratios of 5%, 7%, 10% and 15% of critical from the MCE and DBE levels of design accelerograms. The site-specific horizontal (α_h) and vertical (α_v) design seismic

coefficients for the Bhatsa dam are found to be 0.084 and 0.056, respectively. Since the present site falls under Zone-III, the values of α_h and α_v calculated from IS 1893: 2016 (Part 1) [16] are found to be higher than the values computed using other approaches. Therefore for preliminary analysis purposes, values of horizontal and vertical seismic coefficients found from IS 1893: 2016 (Part 1) [16] should be considered. For detailed dynamic analysis, site-specific acceleration time histories and response spectra under DBE condition should be used. The stress level under MCE condition should also be checked to estimate the probable extent of damage under MCE conditions. The MCE level of design accelerograms and response spectra are recommended to be used for testing the safety of a dam under extreme and rare earthquake load. Damages, which do not endanger the structural safety of the dam through catastrophic failures, are permitted under this load condition. The DBE level of design accelerograms are to be used for the detailed analysis purpose. Minor and easily repairable damages are permitted under DBE condition [14].

4 Conclusions

A reliable estimate of site-specific seismic design parameters is essential for the safe design of hydraulic structures to withstand earthquake forces. For the existing dams like Bhatsa Dam, Maharashtra, the estimated seismic design parameters help to assess the static and dynamic stability of the dams for taking up the strengthening measures. The horizontal and vertical seismic design coefficients are used for the preliminary analysis of hydraulic structures.

Acknowledgements The authors are thankful to Shri A.K. Agrawal, Director, Central Water and Power Research Station, Pune, for granting permission to present this paper.

References

1. ICOLD (1989). Selecting seismic parameters for large dams—guidelines and recommendations. ICOLD, Bulletin No. 72
2. US Army Corps of Engineers (1999) Response spectra and seismic analysis for concrete hydraulic structures. Engineer Manual EM 1110-2-6050
3. Anderson JG, Trifunac MD (1978) Uniform risk functionals for characterization of strong earthquake ground motion. Bull Seism Soc Am 68:1205–1218
4. Gupta ID (2002) State of the art in seismic hazard analysis. ISET J Earthq Eng 39(4):311–346
5. FEMA (2004) NEHRP recommended provisions for seismic regulations for new buildings and other structures (FEMA 450), Part 1: Provisions. 2003 edn
6. McGuire RK (1977) Seismic design spectra and mapping procedures using hazard analysis based directly on oscillator response. Earthq Eng Struct Dyn 5:211–234
7. GSI (2000) Seismotectonic Atlas of India and its environs. Geological Survey of India, Kolkata, India

8. Stepp JC (1973) Analysis of completeness of the earthquake sample in the Puget sound area. In: Seismic zoning (edited by ST Harding). NOAA Tech Report ERL 267-ESL30, Boulder, Colorado, USA
9. Gutenberg B, Richter CF (1944) Frequency of earthquakes in California. Bull Seism Soc Am 34(4):1985–1988
10. Weichert DH (1980) Estimation of the earthquake recurrence parameters for unequal observation periods for different magnitudes. Bull Seism Soc Am 70(4):1337–1346
11. Cornell CA, Van Marcke EH (1969) The major influence on seismic risk. In: Proceedings of 4th world conference on earthquake engineering, Santiago, Chile, A-1, pp 69–93
12. Youngs RR, Coppersmith KJ (1985) Implications of fault slip rates and earthquake recurrence models to probabilistic seismic hazard estimates. Bull Seism Soc Am 75(4):939–964
13. Abrahamson N, Silva W (2008) Summary of the Abrahamson & Silva NGA Ground-Motion Relations. Earthq Spectra 24(1):67–97
14. NCSDP (2011- Revised 2014) Guidelines for preparation and submission of site specific seismic study report of river valley project to National Committee on Seismic Design Parameters, CWC, pp 1–30
15. IS 1893:1984 (Part 1): Criteria for earthquake resistant design of structures. Bureau of Indian Standards, New Delhi
16. IS:1893-2016, Criteria for earthquake resistant design of structures. Bureau of Indian Standards, New Delhi, India

Analysis of Seismic Behavior of an Earthen Dam

Sandhya Joshi, Himanshu Pratap Singh, and Suprakash Biswas

Abstract The current research focuses on the dynamic study of the 260.5 m high Tehri dam, which spans the Bhagirathi River in India's Garhwal Himalayas. Since it was constructed in seismic zone-IV, there is a significant risk of an earthquake with a magnitude of 7–8.5 or more on the Richter scale in the area. Earthquakes with hypocentral distances of 50.6 km and 89.7 km from Tehri region occurred in the years 1991 (Uttarkashi earthquake) and 1999 (Chamoli earthquake), respectively, according to the data stored in Strong-Motion Virtual Data center (VDC). Hence, the repetition of such seismic activities in the Tehri region is highly probable. In this paper, numerical modeling is carried out using finite element analysis-based ABAQUS software to simulate a magnitude 7.8 earthquake in Nepal and calculated spectral accelerations. Response spectrum graphs are prepared using SEISMOMATCH, which are validated with IS: 1893:2016 (PART-1), and the spectral accelerations are scaled to 7.8 magnitude Nepal Earthquake in the Himalayan belt, with the help of which maximum acceleration is calculated. Finite element method and approximate methods are compared to obtain the crest acceleration in dam and give satisfactory results.

Keywords Seismic gap · Natural frequency · Shear wave velocity · Dynamic analysis

1 Introduction

Dams are huge structures comprising multi-purpose utility. When dams are built in seismically active regions, they are prone to earthquakes, which can have catastrophic consequences. While dam response during seismic activity has been extensively studied theoretically (using simplistic mathematical model), it is not well established

S. Joshi · H. P. Singh (✉) · S. Biswas
Department of Civil Engineering, DIT University, Dehradun 248009, India
e-mail: himanshu.pratap@dituniversity.edu.in

S. Biswas
e-mail: suprakash.biswas@dituniversity.edu.in

P. V. Timbadiya et al. (eds.), *Flood Forecasting and Hydraulic Structures*, Lecture Notes in Civil Engineering 340, https://doi.org/10.1007/978-981-99-1890-4_51

in practice since theoretical models do not always match real scenario. Seismic gap hypothesis considerably indicates high earthquake occurrence in the gap of long belt of earthquake seismicity where earthquake has already occurred [1]. According to [2], it is expected that earthquake repeats itself after 100 years, which is the estimated life of the Tehri dam. This seismic gap theory was initially studied by soviet and Japanese geophysicists [3–5]. Tehri dam is located between rupture zones of 1905 Kangra earthquake to 1934 Bihar and Nepal Earthquake according to [6], and this segment is known as central seismic gap or it can be defined as unruptured part of Himalayan region as shown in Fig. 2 [7]. After 1934, earthquakes (1991 Uttarkashi earthquake of magnitude 6.and 1999 Chamoli earthquake of magnitude 6) were recorded in the seismic gap-2 (central gap) as shown in Fig. 1. No earthquake has been recorded after that in seismic gap-2 but it is believed that the fault segment is capable of producing earthquakes on some other basis such as plate motion or strains.

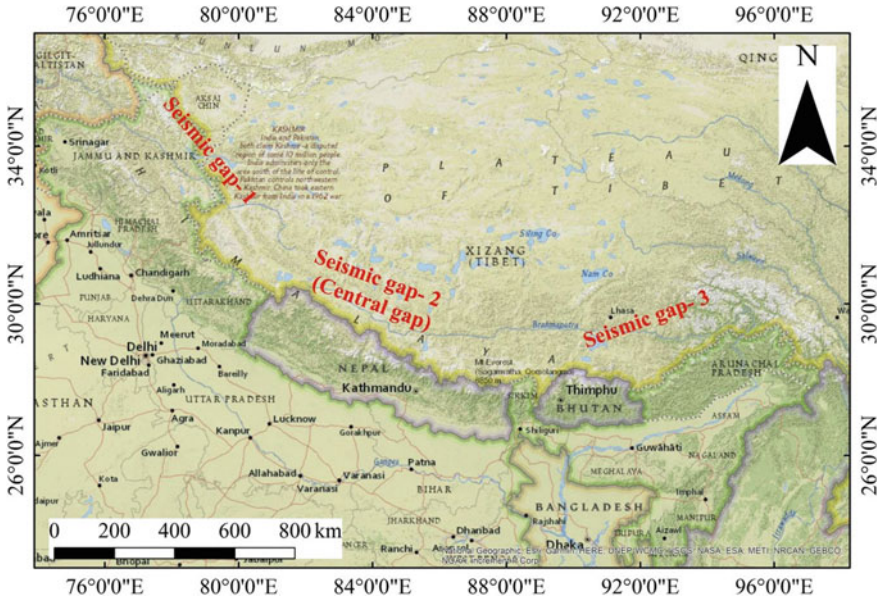

Fig. 1 Location of seismic gaps in Himalayan belt using ArcGIS

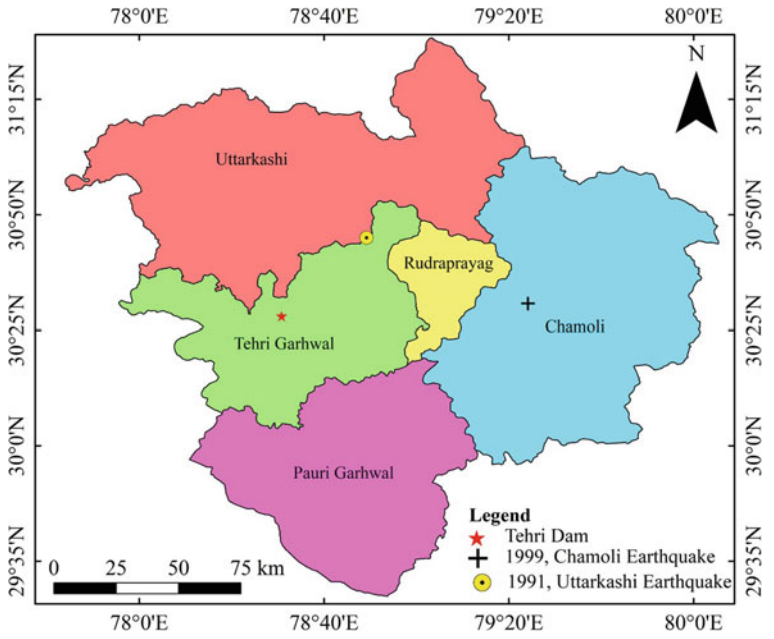

Fig. 2 Location of Tehri dam using ArcGIS

2 Study Area and Data Source

2.1 Seismic Zones in Himalayan Region

Region of Seismic gap-1 spans from Kashmir to Himachal Pradesh (Kangra), central gap from Himanchal Pradesh to Bihar and seismic gap-3 is from Bihar to Arunachal Pradesh [7]. Chopra et al. [8] performed the seismic analysis of Earthen dams. Lavania [9] explained the history of Tehri dam and its geological behavior and Sengupta [10] calculated permanent deformations of Tehri dam due to 7.0 and 8.5 magnitude earthquakes. Sengupta [11] tried to find permanent displacements of the Tehri dam in the Himalayas due to future strong earthquakes. In the present study, dynamic analysis of Earthen Dam has been performed to obtain the maximum acceleration and maximum displacement. Crest displacement is calculated and compared using finite element analysis and local slope failure mechanism.

2.2 Data Used

Tehri dam is one of the world's tallest dams. It is 260.5 m high and located at 30°28′ N latitude and 78°30′ E longitude. Thatte [12] gives a detailed account of the dam.

Table 1 Soil properties [16]

S. No.	Fill material of dam	Cohesion (C)	Friction angle (ϕ)	Shear wave velocity (m/s^2) Vs	Damping factor $\beta = \left(\frac{2\varepsilon}{\omega}\right)$
1	Shell	0.1	38	101.62	1.3386
2	Core	1.5	27	157.85	0.86169

The dam's construction resulted in the emergence of a massive reservoir (67 km) in the Bhagirathi and Bhilangana valleys as located in Fig. 2.

Salient features of Tehri dam have been taken from [12, 13], some of which are Tehri Earth-Rockfill Dam is situated in seismic zone-IV, seismic parameters include horizontal coefficient 0.4, having damping ratio of 10% which comes under zone factor of 0.24, also laboratory test results for shear modulus observed by Thatte [12] are 200 kg/cm^2 and 600 kg/cm^2 for clay and shell zone, respectively, and calculations of shear wave velocities and damping factor have been done as shown given in Table 1.

2.3 Dynamic analysis of Tehri Dam

Dynamic analysis of dam is done by using finite element method and approximate method. In finite element analysis, the structure is performed using Abaqus/CAE software and the meshing as shown in Fig. 3. And in approximate method, it is assumed that failure occurs on well-defined slip surface, where elastic behavior is seen in stress levels below failure and perfectly plastic above failure surface [14]. For given potential sliding mass, when the induced accelerations exceed the calculated yield accelerations, movements are assumed to occur along the direction of failure plane. Yield coefficient can be determined quickly once factor of safety (FS) of the potential sliding plane is known, and its FS can be calculated as follows:

$$\text{Factor of safety} = \left[\left\{\frac{C}{\gamma * h * \cos\alpha + \sin\alpha}\right\} + \left(\frac{\tan\emptyset}{\tan\alpha}\right)\right] \tag{1}$$

where C is the cohesion of soil material, α is the angle of failure plane, h is the height of sliding block mass, φ is the angle of internal friction. According to the [15], the yield coefficient of the sliding block is correlated to the static factor of safety (FS) of the block on the sliding surface, with the angle of α from the horizontal shown in equation below:

$$K_y = (\text{FS} - 1) * \sin\alpha \tag{2}$$

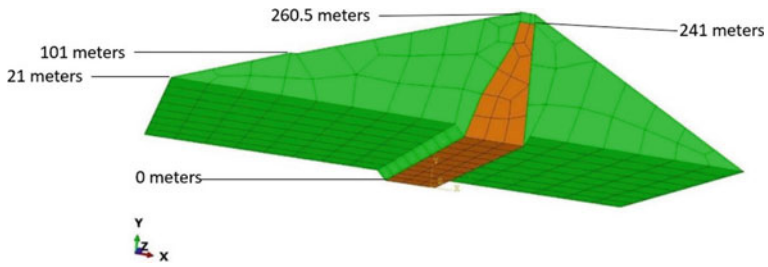

Fig. 3 Geometry of Tehri dam developed in Abaqus/CAE

3 Results and Discussion

Current work is based on finite element simulations performed for two shear wave velocities, viz. 101.62 m/s, 157.85 m/s and using spectrum of Nepal Earthquake (magnitude 7.8). Applying these three as input for seismic excitation in dam along the river flow, acceleration and displacements were obtained at upstream, downstream, base of dam, and crest level of the dam.

Figure 4 shows the deformed shape of dam on applying spectrum of acceleration-time by the calculated shear wave velocity of 101.62 m/s. Maximum acceleration obtained at crest is 1.4 g at time step of 3 s as shown in Fig. 5. Sinusoidal variation of acceleration in Fig. 6 explains that the acceleration here is smooth and periodic with maximum value of 4 g in time step of 2.0 s, which implies that at base of dam, if seismic forces act then it will balance itself by simple harmonic motion at that point but after that it will decrease and then become constant and Fig. 7 shows minimum accelerations at the max height of dam.

Figure 8 shows the deformable shape of dam model when applying the spectrum of 101.62 m/s, and when simulation is performed, maximum accelerations is found at maximum height of the dam as shown in Figs. 9 and 10, respectively.

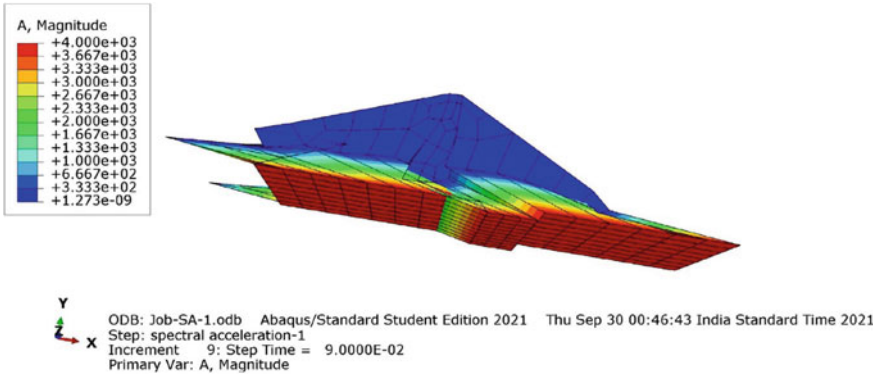

Fig. 4 Deformed shape of dam for shear wave velocity 101.62 m/sec core zone of the dam

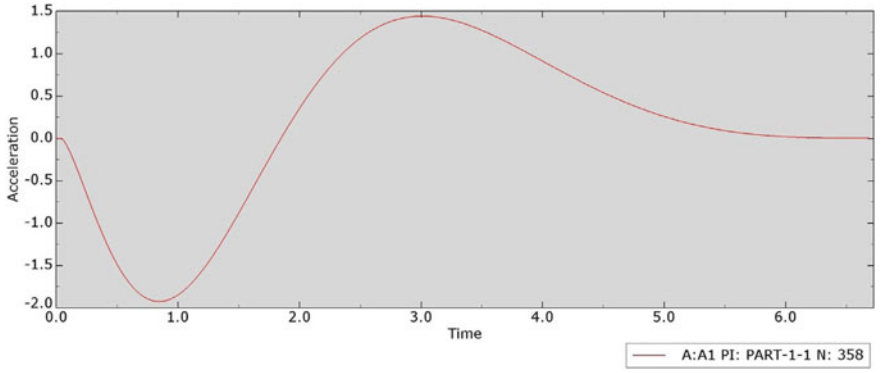

Fig. 5 Plot of spectral acceleration (g) versus time at 102 m of dam

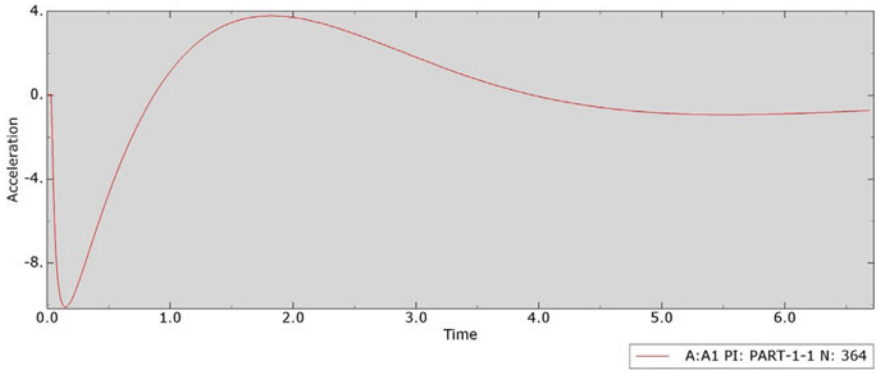

Fig. 6 Plot of spectral acceleration (g) at base of dam

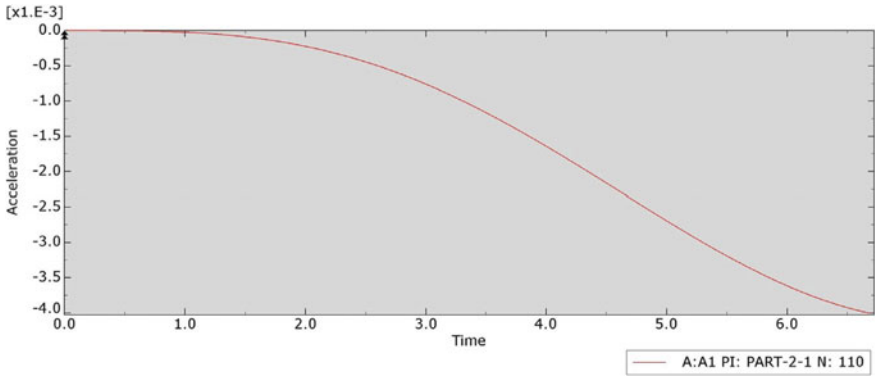

Fig. 7 Plot of spectral acceleration (g) versus time at 260.5 m of dam

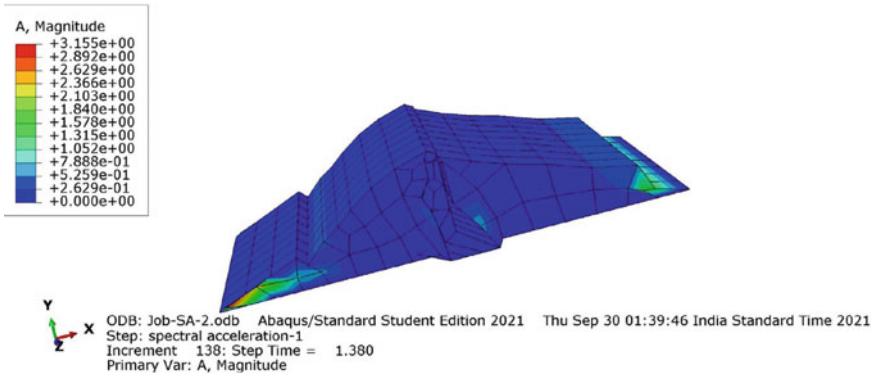

Fig. 8 Deformed shape of dam when applying spectra of shear wave velocity157.85 m/s

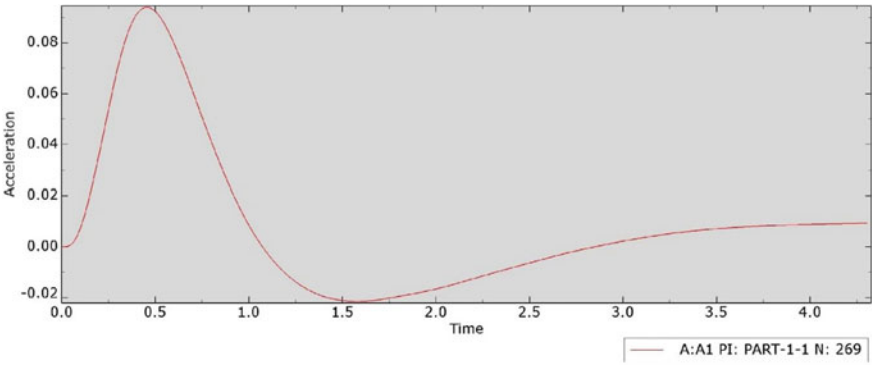

Fig. 9 Plot of spectral acceleration (g) with shear wave velocity 157.85 m/s at base of dam

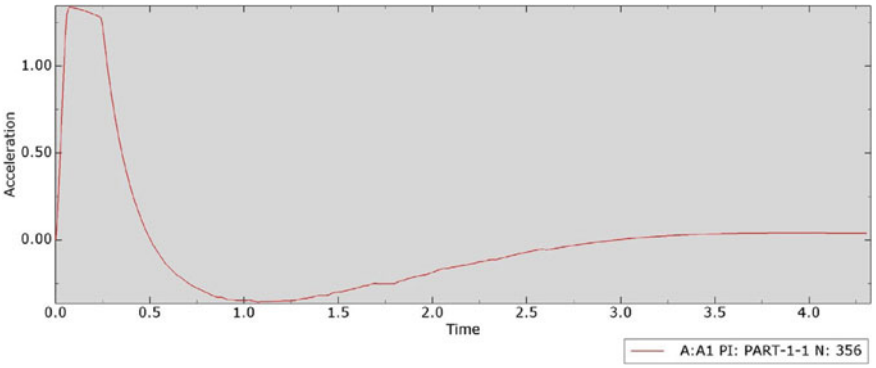

Fig. 10 Plot of spectral acceleration (g) with shear wave velocity 157.85 m/s at 260.5 m height of dam

Figure 11 shows the deformable shape of dam model when applying the spectrum of 101.62 m/s, and when simulation is performed, maximum accelerations is found at maximum height of the dam as shown in Figs. 12 and 13, respectively.

Dynamic analysis performed using finite element analysis from where displacement values are determined for upstream and downstream as given in Tables 3, 4, and 5, respectively, and displacements at crest level of the dam are given in Table 6. Maximum crest acceleration is highest for shear wave velocity of 101.62 m/s amongst the cases considered (Table 2).

Using the maximum value of crest acceleration (Kmax), Makdisi and Seed graphs are used to determine the displacements at different levels of upstream and crest of the dam for two spectral accelerations and Nepal Earthquake (magnitude 7.8) as shown in Tables 7, 8, and 9, respectively. Using the maximum value of crest acceleration (Kmax), Fig. 17 is used to determine the displacements at different levels of upstream

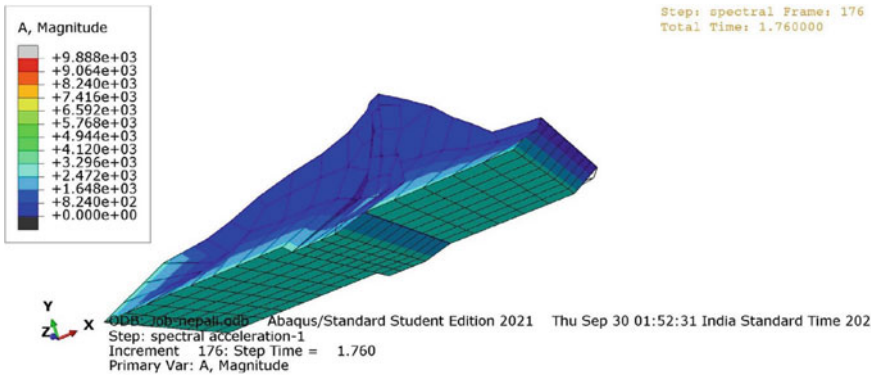

Fig. 11 Deformed shape of dam applying the spectrum of Nepal Earthquake magnitude 7.8

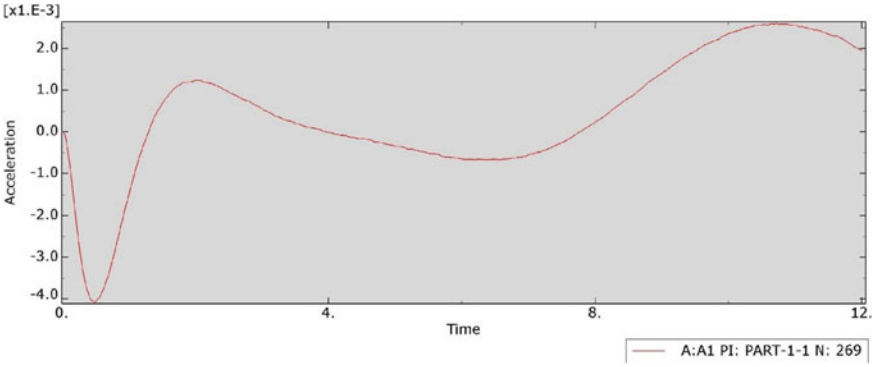

Fig. 12 Acceleration-time (g) plot with Nepal Earthquake time history of magnitude 7.8 at 260.5 m height of dam

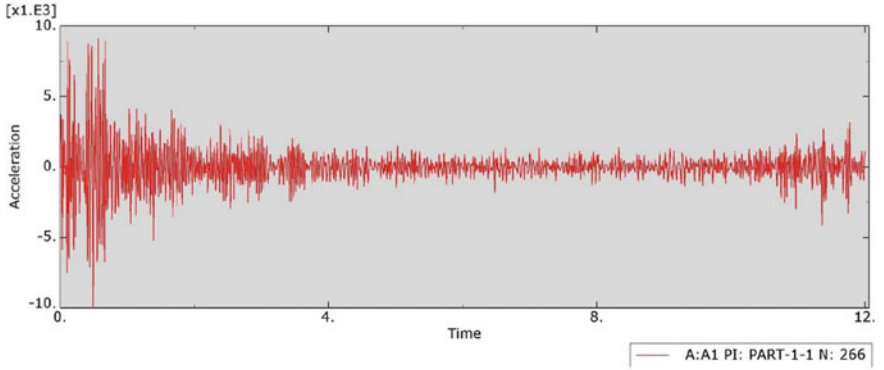

Fig. 13 Acceleration-time (g) plot with Nepal Earthquake time history of magnitude 7.8 at base of dam

Table 2 Results of maximum acceleration in Tehri dam from finite element analysis (ABAQUS)

S. No.	Input data	Maximum crest acceleration (g)
1	At shear wave velocity 101.62 m/s	1.4
2	At shear wave velocity 157.85 m/s	1
3	Nepal Earthquake magnitude 7.8	0.003

Table 3 Result from ABAQUS for Nepal Earthquake magnitude 7.8

S. No.	Input data	Maximum crest displacement (cm)
1	At shear wave velocity 101.62 m/s	19
2	At shear wave velocity 157.85 m/s	55
3	Nepal Earthquake magnitude 7.8	28

Table 4 Result from ABAQUS for shear wave velocity 101.62 m/s

Location	Upstream displacement U (cm)	Downstream displacement U (cm)
1/3 height of dam	10	20
2/3 height of dam	19.0	19.0
Crest of dam	18.96	17.94

Table 5 Result from ABAQUS for shear wave velocity 157.85 m/s

Location	Upstream displacement U (cm)	Downstream displacement U (cm)
1/3 height of dam	27	35
2/3 height of dam	25.0	55
Crest of dam	25.2	25.0

Table 6 Maximum crest displacement obtained from finite element analysis (ABAQUS)

Location	Upstream displacement U (cm)	Downstream displacement U (cm)
1/3 height of dam	0.5	0.6
2/3 height of dam	28	26
Crest of dam	25	27

and crest of the dam for two spectral accelerations and Nepal Earthquake (magnitude 7.8) as shown in Tables 7, 8, and 9, respectively.

The above results in Fig. 14 show that after applying the two methods of dynamic analysis, the crest of the dam is more susceptible to earthquake excitations when spectrums are applied, i.e., (a) spectral acceleration calculated from shear wave velocity 101.62 m/sec denoted by (SA-1), (b) spectral acceleration calculated from shear wave velocity 157.85 m/sec denoted by (SA-2), and (c) acceleration-time history of Nepal Earthquake magnitude 7.8. Approximate method is compared to finite element method, and it is found that FEM gives satisfactory results and dynamic analysis of Earthen Dams can also be performed using models as prepared in this study, and satisfactory results can be obtained to analyze and implement the precautions to actual model of dam.

Table 7 Displacement in dam due to shear wave velocity 101.62 m/s

Location	K_{max} (g)	K_y/K_{max}	U/Kmax.g.To	Displacement (U) (cm)
033H	1.4	0.0026	0.00083	7.62
0.66H	1.4	0.0043	0.0061	55.9
Full height of dam	1.4	0.0055	0.0048	44.05

Table 8 Displacement in dam due to shear wave velocity 157.85 m/s

Location	K_{max} (g)	K_y/K_{max}	U/Kmax.g.To	Displacement (U) (cm)
033H	1	0.00267	0.00083	3.5
0.66H	1	0.0053	0.0061	26
Full height of dam	1	0.0054	0.0048	47.04

Table 9 Displacement in dam due to spectrum of Nepal Earthquake magnitude 7.8

Location	K_{max}(g)	K_y/K_{max}	(U/Kmax.g.To)	Displacement (U) (cm)
033H	0.003	0.00267	0.00083	2.36
0.66H	0.003	0.0053	0.0067	19.11
Full height of dam	0.003	0.0054	0.0068	19.39

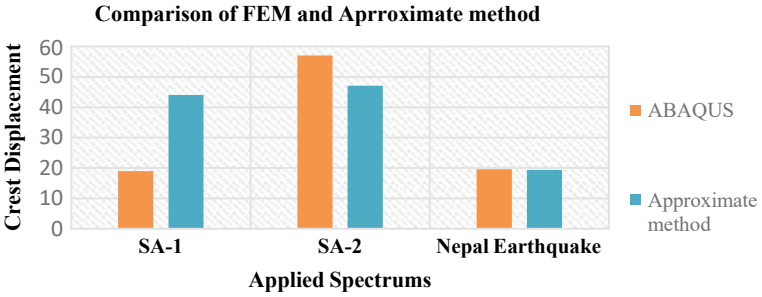

Fig. 14 Crest displacement comparison between finite element method (ABAQUS) and approximate method

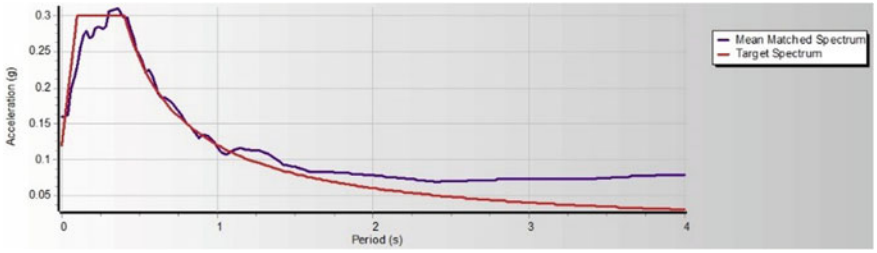

Fig. 15 Response spectra of shear wave velocity 157.85 m/sec. matched with response spectra, i.e., IS: 1893:2016

4 Validation

The above Figs. 15 and 16 show that 20 iterations and 15 iterations were done to match the response spectrums of IS: 1893:2016 Part-1, respectively, which implies that spectral accelerations calculated manually can be selected as the spectrum for dynamic analysis. Figures 17 and 18 show that after 14 and 30 iterations, scaling of spectral accelerations has been done to earthquake of magnitude 7.8, respectively. Scaling of magnitudes helps in getting the spectrum values to get correct values of spectral accelerations calculated.

5 Conclusions

The following conclusions are derived from the foregoing study:

- Maximum displacement due to lateral force like earthquake leads to deform the crest part of dam.

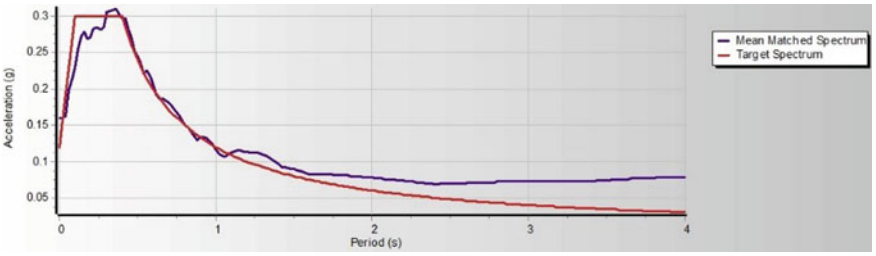

Fig. 16 Response spectra of shear wave velocity 101.62 m/sec. matched with response spectra, i.e., IS: 1893:2016

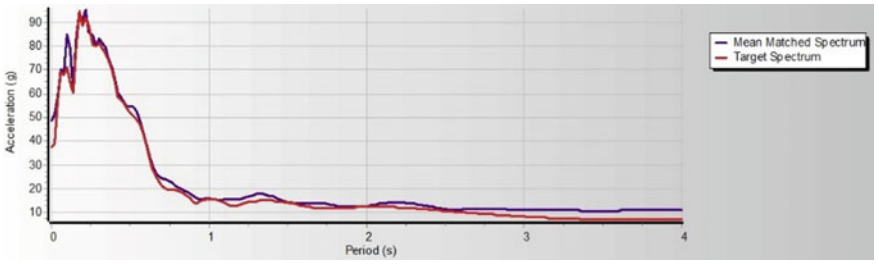

Fig. 17 Response spectra of shear wave velocity 101.62 m/sec. scaled to response spectra of Nepal Earthquake magnitude 7.8

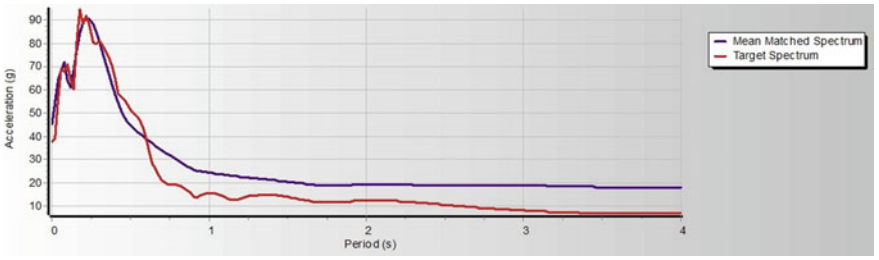

Fig. 18 Response spectra of shear wave velocity 157.85 m/sec. scaled to response spectra of Nepal Earthquake magnitude 7.8

- Considering the shear wave velocity of shell zone 157.85 m/s, maximum displacement is observed of 57 cm at crest of the dam, which is 1.2 times the displacement value by simplified method. As shell is major part of the dam, hence, the failure of distress can be seen in this part of dam.
- For acceleration-time history of Nepal Earthquake, crest displacement is 19.6 cm which is 1.01 times of displacement value by simplified methods.

- It has been suggested that core part of dam should be analyzed discretely so that the future problems like reservoir induced vibrations, and landslides near the dam happening could be taken care, because core part makes the dam composite, which can be affected by above problems in near future.

References

1. R Bilham (2019) Himalayan earthquakes: a review of historical seismicity and early 21st century slip potential. In: Geological society special publication, vol 483. Geological Society of London, pp 423–482. https://doi.org/10.1144/SP483.16
2. Murty CVR (2005) Learning earthquake design and construction. Resonance 10(11):89–92. https://doi.org/10.1007/bf02837649
3. Fedotov SA (1965) Upper mantle properties of the southern part of the Kuril island arc according to detailed seismological investigation data. Tectonophysics 2(2–3):219–225. https://doi.org/10.1016/0040-1951(65)90014-4
4. Mogi K (1968) Sequential occurrences of recent great earthquakes. Published online. https://doi.org/10.4294/jpe1952.16.30
5. Sykes LR (1971) Aftershock zones of great earthquakes, seismicity gaps, and earthquake prediction for Alaska and the Aleutians. J Geophys Res 76(32):8021–8041. https://doi.org/10.1029/jb076i032p08021
6. Brune JN (1993) The seismic hazard at Tehri Dam, vol 218. https://doi.org/10.1016/0040-1951(93)90274-N
7. Khattri KN (1987) Great earthquakes, seismicity gaps and potential for earthquake disaster along the Himalaya plate boundary. Tectonophysics 138(1):79–92. https://doi.org/10.1016/0040-1951(87)90067-9
8. Chopra AK, Dibaj M, Clough RW, Penzien J, Seed HB (1952) Earthquake analysis of earth dams. Published online, pp 55–72
9. Lavania BVK (1988) Assessment of non-recoverable deformations in tehri dam. Published online
10. Sengupta A (2009) Estimation of permanent deformations of Tehri Dam due to 7.0 and 8.5 magnitude earthquakes 40. https://doi.org/10.1061/40863(195)21
11. Sengupta A (2010) Estimation of permanent displacements of the Tehri Dam in the himalayas due to future strong earthquakes 35. https://doi.org/10.1007/s12046-010-0011-3
12. Thatte CD (1991) Earthquakes, Dam Design And Tehri Project
13. Shah AL, Mann PPS, Bharaj HL, Singh JN (2007) Quality control aspects in tehri dam. Published online
14. Makdisi FI, Seed HB (1977) A simplified procedure for estimating earthquake-induced deformations on dams and Embankbents
15. Newmark NM (1965) Effects of earthquakes on dams and Embankments 15. https://doi.org/10.1680/geot.1965.15.2.139
16. Sengupta A (2006) Estimation of permanent deformations of Tehri Dam due to 7.0 and 8.5 magnitude earthquakes. In Advances in earth structures: research to practice, pp 203–210